Bayesian Experimental Design Framework Applied To Complex Polymerization Processes

by

Afsaneh Nabifar

A thesis
presented to the University of Waterloo
in fulfillment of the
thesis requirement for the degree of
Doctor of Philosophy
in
Chemical Engineering

Waterloo, Ontario, Canada, 2012

Author's Declaration

I hereby declare that I am the sole author of this thesis. This is a true copy of the thesis, including any required final revisions, as accepted by my examiners.

I understand that my thesis may be made electronically available to the public.

Abstract

The Bayesian design approach is an experimental design technique which has the same objectives as standard experimental (full or fractional factorial) designs but with significant practical benefits over standard design methods. The most important advantage of the Bayesian design approach is that it incorporates prior knowledge about the process into the design to suggest a set of future experiments in an optimal, sequential and iterative fashion. Since for many complex polymerizations prior information is available, either in the form of experimental data or mathematical models, use of a Bayesian design methodology could be highly beneficial. Hence, exploiting this technique could hopefully lead to optimal performance in fewer trials, thus saving time and money.

In this thesis, the basic steps and capabilities/benefits of the Bayesian design approach will be illustrated. To demonstrate the significant benefits of the Bayesian design approach and its superiority to the currently practised (standard) design of experiments, case studies drawn from representative complex polymerization processes, covering both batch and continuous processes, are presented. These include examples from nitroxide-mediated radical polymerization of styrene (bulk homopolymerization in the batch mode), continuous production of nitrile rubber in a train of CSTRs (emulsion copolymerization in the continuous mode), and cross-linking nitroxide-mediated radical copolymerization of styrene and divinyl benzene (bulk copolymerization in the batch mode, with cross-linking). All these case studies address important, yet practical, issues in not only the study of polymerization kinetics but also, in general, in process engineering and improvement. Since the Bayesian design technique is perfectly general, it can be potentially applied to other polymerization variants or any other chemical engineering process in general.

Some of the advantages of the Bayesian methodology highlighted through its application to complex polymerization scenarios are: improvements with respect to information content retrieved from process data, relative ease in changing factor levels mid-way through the experimentation, flexibility with factor ranges, overall “cost”-effectiveness (time and

effort/resources) with respect to the number of experiments, and flexibility with respect to source and quality of prior knowledge (screening experiments versus models and/or combinations). The most important novelty of the Bayesian approach is the simplicity and the natural way with which it follows the logic of the sequential model building paradigm, taking full advantage of the researcher's expertise and information (knowledge about the process or product) prior to the design, and invoking enhanced information content measures (the Fisher Information matrix is maximized, which corresponds to minimizing the variances and reducing the 95% joint confidence regions, hence improving the precision of the parameter estimates).

In addition, the Bayesian analysis is amenable to a series of statistical diagnostic tests that one can carry out in parallel. These diagnostic tests serve to quantify the relative importance of the parameters (intimately related to the significance of the estimated factor effects) and their interactions, as well as the quality of prior knowledge (in other words, the adequacy of the model or the expert's opinions used to generate the prior information, as the case might be).

In all the case studies described in this thesis, the general benefits of the Bayesian design were as described above. More specifically, with respect to the most complex of the examples, namely, the cross-linking nitroxide-mediated radical polymerization (NMRP) of styrene and divinyl benzene, the investigations after designing experiments through the Bayesian approach led to even more interesting detailed kinetic and polymer characterization studies, which cover the second part of this thesis. This detailed synthesis, characterization and modeling effort, trigged by the Bayesian approach, set out to investigate whether the cross-linked polymer network synthesized under controlled radical polymerization (CRP) conditions had a more homogeneous structure compared to the network produced by regular free radical polymerization (FRP). In preparation for the identification of network homogeneity indicators based on polymer properties, cross-linking kinetics of nitroxide-mediated radical polymerization of styrene (STY) in the presence of a small amount of divinyl benzene (DVB; as the cross-linker) and N-tert-butyl-N-(2-methyl)-1-phenylpropyl)-O-(1-phenylethyl) hydroxylamine (I-TIPNO; as the unimolecular initiator) was investigated in detail and the

results were contrasted with regular FRP of STY/DVB and homopolymerization of STY in the presence of I-TIPNO, as reference systems. The effect of [DVB], [I-TIPNO] and [DVB]/ [I-TIPNO] were investigated on rate, molecular weights, gel content and swelling index. In parallel to our experimental investigations, a detailed mathematical model was developed and validated with the respective experimental data. Not only did model predictions follow the general experimental trends very well but also were in good agreement with experimental observations. Pursuing our investigations for a more reliable indicator for network homogeneity, corresponding branched and cross-linked polymers were characterized. Thermo-mechanical analysis was used as an attempt to investigate the difference between polymer networks synthesized through FRP and NMRP. Results from both Differential Scanning Calorimetry (DSC) and Dynamic Mechanical Analysis (DMA) showed that at the same cross-link density and conversion level, polymer networks produced by FRP and NMRP exhibit indeed comparable structures.

Overall, it was notable that a wealth of process information was generated by such a practical experimental design technique, and with minimal experimental effort compared to previous (undesigned) efforts (and associated, often not well founded, claims) in the literature!

Acknowledgements

First, a special thanks to my supervisor, Professor Alexander Penlidis, for his invaluable guidance and support in both my academic and personal life. Chapter 7 of this thesis is dedicated to him.

I would also like to express my appreciation to the department of Chemical Engineering at the University of Waterloo, and especially Professor Neil McManus, for the help and support. Many thanks go to my officemates for being understanding and patient with me during the course of writing my thesis. Special thanks go to Alison Scott for her help, and for being so dedicated and responsible.

I would also like to acknowledge the fruitful collaboration with Professor Eduardo Vivaldo-Lima and Julio C. Hernandez-Ortiz of UNAM, Mexico.

I wish to acknowledge the financial support from the Natural Sciences and Engineering Research Council (NSERC) of Canada, the Canada Research Chair (CRC) program, the Inter-American Materials Collaboration (IAMC) program of NSERC, and the Ontario Graduate Scholarship (OGS) program. Also, thanks go to OMNOVA Solutions/ United Way Worldwide (UWW), USA, for a special scholarship.

My sincere gratitude goes out to those friends I have made during the course of my studies in Waterloo, for making life in graduate school much more enjoyable.

I am extremely grateful for the support of my family. I would like to thank my brothers for their financial and moral support. Special thanks go to my dear sister, Azadeh Nabifar, and her husband, Hossien Shahkarami, without whose generosity and determination I wouldn't be able to come to Canada.

Finally, and most importantly, I would like to thank the dearest person in my life, my mom, for dedicating her life to us and being both a mother and a father to our family.

Table of Contents

List of Figures

List of Tables

Chapter 1. Introduction

For many polymerizations, experimental data may be available either from industrial or exploratory laboratory work. In addition, mathematical models usually do exist, albeit often with unreliable and/or highly correlated parameters, and sometimes even unverified mechanistic bases. In complex polymerization systems, these problems are even more prominent. Hence, ideas from the (statistical) design of experiments applied as early as possible can be very beneficial for the clarification of polymerization kinetics. Classical experimental design methods (for example, (fractional) factorial designs) have been used extensively and are useful in optimizing a wide variety of systems. However, these designs usually ignore the prior knowledge available and are often limited when the system digresses from linear behavior. Using more efficient experimental designs, which can accommodate both prior information and nonlinearities, could (hopefully) lead to optimal performance in fewer trials.

Bayesian design is a powerful and largely unstudied (in the polymerization area) experimental design methodology, which can accommodate practical limitations encountered in classical (fractional) factorial designs. This approach incorporates prior knowledge about a process into the design in order to suggest a set of future experiments in an optimal, sequential and iterative fashion. In addition, Bayesian design allows the use of a nonlinear (fully mechanistic) model along with experimental information (hence, it is essentially an optimal model-based design of experiments).

The approach is based on Bayes' theorem which is well established, especially among statisticians. Application of the Bayesian technique to chemical systems has been more practiced in the areas of drug and cell transport kinetics, pharmaceutical kinetics and analyses of catalytic systems, with the common characteristic of all these applications being that they are concerned with parameter estimation, but not with the issue of the design of experiments. The literature on the application of the Bayesian methodology to polymerization systems is scarce, with the exception of applications to emulsion terpolymerization kinetics and to particle size distribution studies in suspension polymerization, all in our group.

Looking at the last 15 years or so, whereas many advances have taken place in the area of polymer reaction engineering, Bayesian design of experiments has not been exploited extensively nor frequently in complex polymerization systems, which could benefit tremendously from its important traits. These observations motivated current work with the following objectives in mind:

1. Formalize the application of the Bayesian approach as a tool for the design of experiments
2. Shed light on the performance of the Bayesian design approach
3. Expand the implementation of the Bayesian design of experiments in polymer reaction engineering (PRE), which could lead to optimal performance in fewer trials, thus saving time and money
4. Exploit the Bayesian technique to guide one in addressing important practical issues in the study of polymerization processes

In order to meet our objectives, this thesis is organized into eleven chapters:

In *Chapter 2*, basic background on the Bayesian design of experiments is discussed and contrasted with standard experimental designs. A literature review is presented on applications of the Bayesian design approach to different general chemical engineering processes, but not on polymerization systems. Polymerization applications are the topic of the chapters that follow.

Details of the Bayesian design approach (including its principles, capabilities, benefits and different steps needed for its implementation) are discussed in *Chapter 3*. In order to visualize the inner workings of the approach and its superiority to the currently practiced (standard) design of experiments, the Bayesian design is then applied to a simple simulation bench-marking example.

With the purpose of further formalizing the application of the Bayesian approach as a tool for the design of experiments (objective #1), the Bayesian approach is implemented in *Chapter 4* to a more complicated system, namely, the nitroxide-mediated radical polymerization of

styrene. In this chapter several case studies are presented that clearly illustrate the benefits of the Bayesian method.

To shed light on the performance of the Bayesian design approach (objective #2), a series of statistical diagnostic tests can be carried out, which are discussed in *Chapter 5*. These diagnostic tests serve to quantify the relative importance of the parameters (intimately related to the significance of the estimated factor effects) and their interactions, as well as the quality of prior knowledge (in other words, the adequacy of the model or the expert's opinions used to generate the prior information, as the case might be). Different measures of information content are also presented in *Chapter 5* (e.g., the Fisher Information matrix is maximized, which corresponds to minimizing the variances and reducing the 95% joint confidence regions, hence improving the precision of the parameter estimates).

In order to satisfy objective # 3, expanding the implementation of the Bayesian approach to other polymerizations, case studies are drawn from representative complex polymerization processes, covering both batch and continuous processes. *Chapter 4* includes examples from bi- and uni-molecular nitroxide-mediated radical bulk homopolymerization of styrene in the batch mode. *Chapter 6* contains the application of the Bayesian approach to emulsion copolymerization of acrylonitrile/butadiene (nitrile rubber or NBR) in a continuous train of CSTRs. *Chapter 8* shows the implementation of the Bayesian design to cross-linking bulk copolymerizations (of styrene (STY) and divinyl benzene (DVB) under controlled radical polymerization conditions in batch). All these case studies, drawn from different polymerization processes, will clearly illustrate that what is novel in the Bayesian approach is the simplicity and the natural way with which it follows the logic of the sequential model building paradigm, taking full advantage of the researcher's expertise and information (knowledge about the process or product) prior to the design.

In pursuit of addressing further interesting process questions related to the cross-linking polymerization of STY/DVB under controlled radical polymerization (and in parallel, objective #4), *Chapter 9* includes polymer synthesis, kinetic and mathematical modeling of this polymerization system. The techniques used to characterize the corresponding branched and cross-linked polymers are presented in *Chapter 10*.

Finally, *Chapter 11* presents the main conclusions from the current work. In this chapter, the most significant research contributions from this thesis and recommendations for future research steps are also discussed. Several appendices complement the material in the chapters of this thesis. These appendices represent essentially "offsprings" from the research covered in the chapters and address peripheral but closely related issues. Figure 1.1 shows a flow chart for the overall thesis organization.

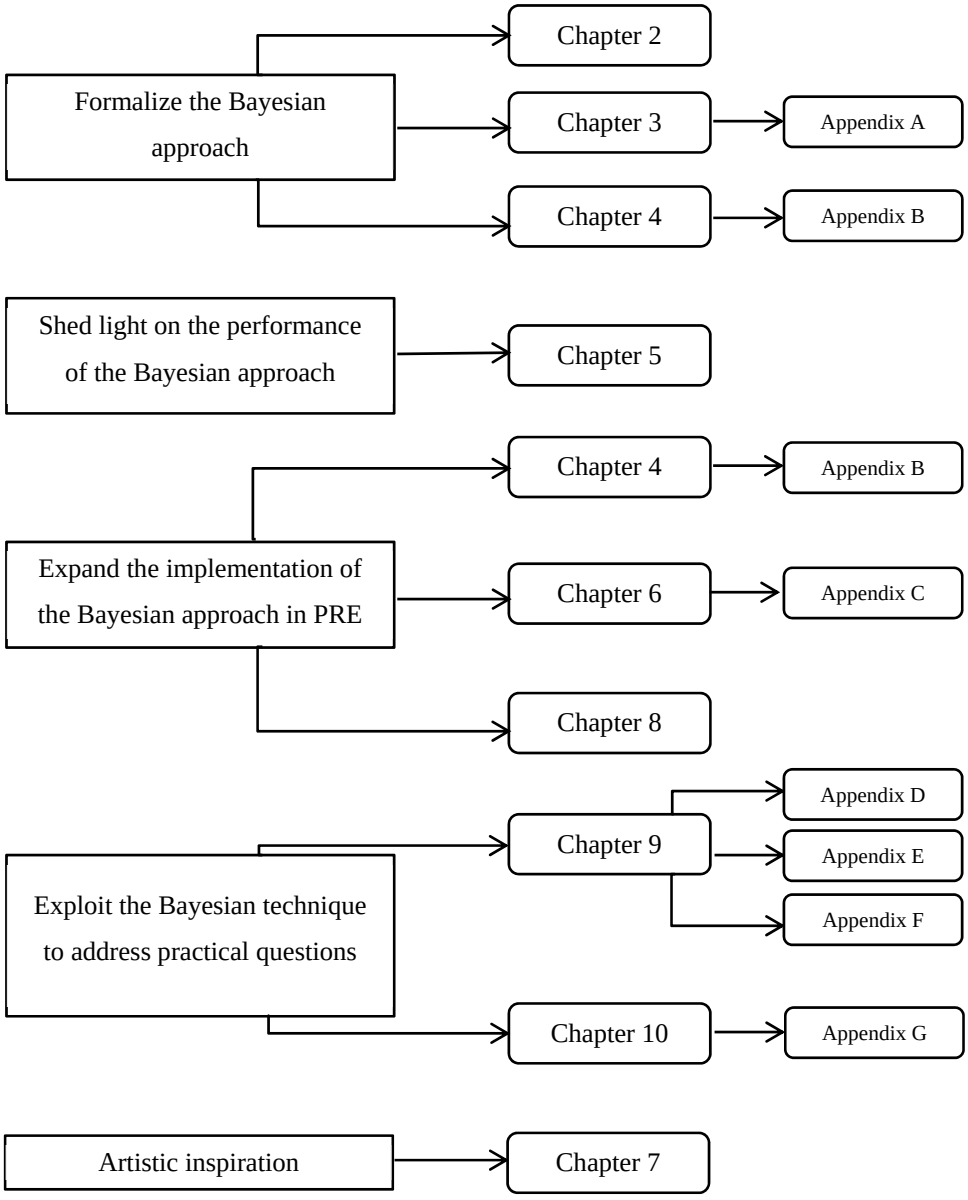

Figure 1.1 Flow chart of PhD thesis

Chapter 2. Background and Literature Review on Bayesian Design of Experiments

Some basic background and literature review on the Bayesian design of experiments is discussed in this chapter. Since this thesis has touched upon many different topics (several polymerization processes), specific literature review and related references for each polymerization process will be presented at the beginning of each relevant chapter and not repeated here for the sake of brevity. First, a brief overview of the characteristics and benefits of the classical (standard) design of experiments (i.e., mainly referring to the (fractional) factorial designs) is presented. Subsequently, the standard design of experiments is contrasted to the Bayesian design of experiments, since the latter approach is pursued further in our research. Bayes' theorem is then discussed and a literature review on the application of the Bayesian design approach to different chemical engineering processes is presented.

It should be mentioned up front that the purpose of this chapter is not a literature review on applications of Bayesian theory (versus frequentist statistics). For that large area of statistics, there are many reference books one can consult (e.g., see Meyer and Collier (1970) or Bolstad (2007)), and this is not in the scope of this research. Rather, our purpose is to make use of a specific tool from Bayesian statistics, as applied to the design of experiments as an alternative approach.

2.1 Classical (Standard) Design of Experiments: Brief Overview

Usually, experiments are performed to obtain (or confirm) some knowledge about a particular process or system. An experiment, in general, can be defined as a test (or series of tests) in which, purposeful changes are made to the input variables of a process or system, and the changes observed in the output response are recorded (tracked) (Montgomery, 2005). The results and conclusions that can be drawn from the analysis of an experiment depend to a large extent on the manner in which the data were collected. Essentially, in every experiment the aim of the researcher/scientist is to maximize the information content about the process. However, without carefully designed experiments, there will be little information content to maximize (Box et al., 2005). Thus, a suitable experimental design should be implemented in advance

(since it is referred to as “design”, it should be accomplished in advance at the “design stage”!), in order to collect appropriate experimental data which could result in valid and objective conclusions.

Statistical design of experiments, probably introduced and formalized for the first time by R. A. Fisher (Fisher, 1926), refers to the process of planning the experiment in a way that appropriate data, which could be analyzed by formal statistical methods, will be collected, resulting in unbiased conclusions. To use the statistical approach in designing and analyzing an experiment, it is necessary for everybody involved in the experiment to have a clear idea in advance of exactly what is to be studied, how the data are to be collected, and at least a qualitative understanding of how these data are to be analyzed (Montgomery, 2005).

Figure 2.1 outlines the recommended flow chart to follow when designing an experiment. The first step is to state the problem and set the objectives of experimentation, evidently. Although this might seem like a rather obvious point, in practice, usually, the objectives of the experiment (and a clear expression of the problem at hand) are rarely specified (clearly) at the outset. It is important to keep the overall objective in mind, as the specific questions to be addressed during experimentation are related directly to the overall objective chosen. For example, is the objective *characterization* or *factor screening*, as in a new process or system, or is it *optimization* or *stability*, as in a mature or well-understood system? (Montgomery, 2005)

The next step (as shown in Figure 2.1) is selecting the response(s) and the factors with their related levels or ranges. In selecting the responses, the experimenter should be certain that these responses will really provide useful information about the process under study. The potential design factors that the experimenter may wish to vary in the experiment should also be specified from the beginning. It is important to investigate all factors that may be of importance and this is where process knowledge, which is combination of practical experience and theoretical background, is necessary. Once the design factors are chosen, one should choose the ranges over which these factors will be varied or the specific levels at which runs will be made. When the objective of the experiment is *factor screening*, it is usually best to keep the number of levels low (generally, two levels work well), and the range, over which the

factors are varied, relatively broad. As more information is gathered about importance of factors and the levels which produce the best results, the region of interest will usually become narrower.

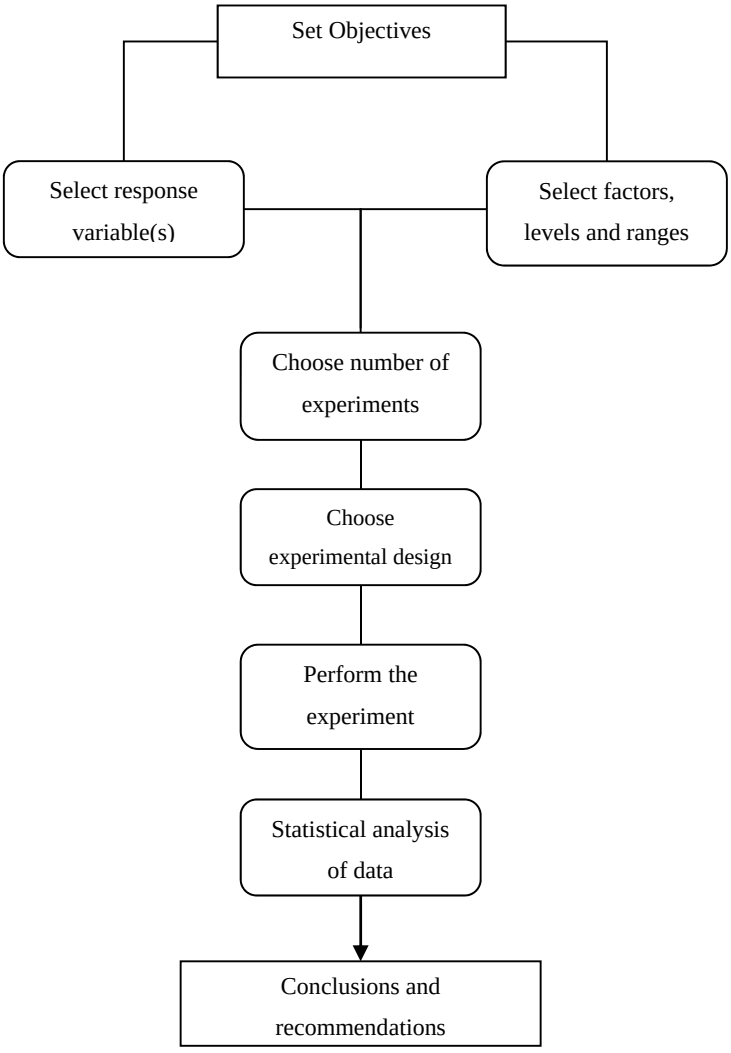

Figure 2.1 Guidelines for designing an experiment (Montgomery, 2005)

One should know from the outset, based on the resources and the time available, how many experiments could be afforded during experimentation. Based on the number of experiments that could be carried out, one can then choose the appropriate experimental design to follow. In selecting the design, it is important to keep the experimental objectives in mind. After the appropriate design is chosen, the next step is performing the chosen experiments in the lab

(refer again to Figure 2.1). When running the experiments, it is vital to monitor the process carefully to ensure that everything is being done according to plan. Error in experimental (and the related characterization) procedures at this stage can often destroy the whole validity of the experimental design (Montgomery, 2005).

After running the experiments (which is the most time-consuming stage), statistical methods should then be used to analyze the data so that results and conclusions are objective (and quantitative) rather than judgmental (and qualitative) in nature. If the experiment has been designed correctly and if it has been performed according to the design, the statistical methods required are not elaborate (Montgomery, 2005). In the last stage, by coupling the statistical analysis with good engineering or process knowledge and common sense, a sound conclusion could be derived.

Throughout the entire process, it is important to keep in mind that experimentation should be looked at as an important part of a learning process, where a tentative hypothesis is formulated about a process, experiments are then carried out to investigate this hypothesis and based on the results collected, a new, improved hypothesis could then be articulated. One of the most common and rather major mistakes is to design a single, large, comprehensive experimentation phase at once. In other words, an appropriate experimental design is one that is carried out in an iterative fashion. In addition, as experiments progress, more information is obtained which could lead to dropping some input variables, adding others, changing the region of exploration for some factors, or add new responses. Consequently, besides being iterative, an experimental design is best to be sequential, in order to accommodate possible changes in the design that might occur during experimentation. As a general rule of thumb, no more than about 25 percent of the available resources should be invested in the first sequence of the experiments (Box et al., 2005; Montgomery, 2005). This is to ensure that sufficient resources are available to accommodate the runs with the altered settings, or perform confirmation runs, and ultimately, accomplish the final objective of the experimentation without running out of resources.

There are several experimental designs available to choose from. One strategy of experimentation that is used extensively in practice (especially in chemistry, biology and

materials science, ironically three areas that are in most need of a good statistical design of experiments!) is the “one-factor-at a-time” (OFAT) approach. This method involves varying one factor while keeping the other factors constant. Although this approach seems like a simple method to follow, it often requires a considerable amount of experimental work. In addition, it fails to consider any possible interaction between the factors. An interaction is the failure of one factor to produce the same effect on the response at different levels of another factor. Interactions between factors are very common, and if they occur, the OFAT strategy will usually produce poor results. Many scientists do not recognize this, and, consequently, OFAT experiments are run frequently in practice (Montgomery, 2005).

The alternative to the OFAT methodology is the so-called factorial experimentation. This approach is one of the main approaches to the statistical design of experiments and has proven to be much more efficient than OFAT and with many advantages over it (Box et al., 2005; Montgomery, 2005). A factorial experiment is an experiment whose design involves two or more factors, each with discrete possible values or "levels", and whose experimental units take on all possible combinations of these levels across all such factors (Montgomery, 2005). A factorial design may also be called a fully-crossed design. Such an experiment allows studying the effect of each factor on the response variable, as well as the effects of interactions between factors on the response variable. The most widely used design is the 2^k factorial design, in which the effects of k factors are studied, while each factor has only two levels. These levels could be quantitative, such as two temperature or pressure levels, or qualitative, such as two machines, two operators or perhaps, presence or absence of a factor.

Clearly, as the number of factors of interest increases, the number of runs required increases rapidly; for instance, a 10-factor experiment with all factors at two levels would require 2^{10}= 1024 runs. This quickly becomes infeasible from a time and resource viewpoint (of course, if the process studied involves electronics and signal processing, in which each trial has a duration of a few seconds or minutes only, then a 2^{10} full factorial is not only feasible but imperative). Hence, considering typical process engineering scenarios involving long experiment durations and even longer product characterization stages, if there are four to five or more factors, it is usually unnecessary to run all possible combinations of factor levels since high order interactions are usually negligible. A fractional factorial experiment is thus a

variation of the basic full factorial design in which only a subset of the runs is used. This design will provide good information about the main effects as well as some information about how these factors interact. A 2^{k-p} fractional factorial design, consisting of 2^{k-p} runs, is a $\frac{1}{2^p}$ fraction of the 2^k full factorial design. For the above case of a 10-factor experiment, as an example, a $\frac{1}{2^2}$ fraction of 2^{10} will have $2^{10-2} = 256$ runs, a considerable reduction in the number of trials.

Full or fractional factorial designs are probably the most frequently used statistical design techniques for planning experiments in science and engineering (these factorial-type designs will be referred to from here on as "conventional" (but not in a derogatory sense) or "standard" experimental designs). However, quite often, these elegant and very useful techniques have several limitations and cannot satisfy several practical needs, as listed in Table 2.1. For instance, most of the experiments are strictly limited in the time and material resources that are available. A conventional experimental design does provide fractional factorial experiments to economize on effort but often the resources available do not match the number of trials which must be made for a specific fraction. Further practical difficulties involve impractical treatment combinations, experiments which go astray because of missing observations, redefinition of factor levels as the experiment proceeds, factors which require different number of levels, and dropping/ adding factors.

Table 2.1 Typical limitations encountered in standard designs

Issues
Available resources do not match the number of trials that can be designed
Handling of impractical treatment combinations
Handling of situations with missing observations
Factor levels change in the middle of experimentation
Factors with several (or combination of) levels
Dropping/adding factors
Not a sequential and iterative approach
Nonlinearities
Incorporation of prior knowledge

Although some of the issues with standard designs cited in Table 2.1 have solutions (with varying degrees of effort), these are usually known only to experts in the design of experiments. Hence, it often happens that the practicing scientist or engineer is not aware of the solutions, cannot easily handle the issues faced and, as a result, gives up on the use of statistical designs altogether. Therefore, using efficient experimental designs which can accommodate these restrictions could (hopefully) lead to optimal performance in fewer trials, thus saving time and money.

Finally, and more importantly, in the standard experimental designs minimal amount of prior knowledge is used/exploited. Most of the time there is some prior knowledge available about the process under study and the purpose of the experimentation is to strengthen/clarify an opinion already present (Bolstad, 2007). Ignoring this prior information, which is usually translated into a waste of time, materials and other experimental resources, does not sound like a reasonable thing to do! As prior information is already available within existing data, it is logical that it should be used in order to contribute to the optimality of the designed experiments, and hence to improved models and performance of the process in question (Bolstad, 2007).

2.2 Bayesian Design of Experiments

Bayesian design is a powerful and efficient experimental design methodology, which can accommodate practical limitations encountered in classical (fractional) factorial designs (as in Table 2.1). This design offers some distinct advantages that make it particularly attractive from both an industrial and theoretical perspective (Bolstad, 2007).

The most significant advantage of the Bayesian approach is that it incorporates prior knowledge about a process into the design in order to suggest a set of future experiments in an optimal, sequential and iterative fashion. The exercise of casting prior knowledge about a process into a mathematical form (as will be shown in later chapters) forces the experimenter to brainstorm/hypothesize and perhaps come to a clearer understanding of the process or even anticipate/solve some of the problems that triggered the specific questions about the process even before starting the experiments. Prior information can be updated in a sequential manner,

thus allowing, in parallel, the optimal update of key unknown parameters. In addition, prior information involves contributions from both the prior experimental region and a (usually non-linear) mathematical model for the process, thus making use of both experimental information and mechanistic models (in a way similar to optimal filtering techniques). Hence, Bayesian design could be essentially called an optimal model-based design of experiments.

Another advantage of the Bayesian design of experiments involves experimental flexibility. Unlike factorial designs, the number of experiments is unrestricted. As mentioned in section 2.1, in standard factorial designs one must perform a number of trials equal to an integer power of 2. When applying a Bayesian scheme, one can use as many experiments as he/she wants. In addition, dealing with common (often problematic) issues present in factorial designs, such as missing observations or design factors and levels needing to be added, dropped, or altered during the experimentation phase, is easier in the Bayesian design approach.

The Bayesian approach can be used to determine the relative importance of different operating factors and also to identify the "best" operating conditions. This design can shed light on the most uncertain parts of our process understanding, identify the least reliable (less well-known) parameters, e.g., uncertain values of kinetic rate constants, and further guide sensitivity analysis studies focusing on key uncertain parameters in one's model.

2.2.1 Bayes' Theorem

The main idea of Bayesian methodology comes from Bayes' rule:

$$P(\theta|y) = \frac{P(y|\theta)\,P(\theta)}{P(y)} \qquad \text{Eq. 2.1}$$

where θ is a vector of unknown parameters of interest and y is a vector of n observations whose probability distribution $P(y|\theta)$ depends on the values of these parameters. $P(\theta)$ is the prior distribution of θ which tells us what is known about θ before the collection (hence, knowledge) of the data. Correspondingly, $P(\theta|y)$ is the Bayesian posterior distribution of θ which tells us what is known about θ given the knowledge of the data. $P(y)$ is referred to as the sampling distribution (or data distribution) for fixed parameters θ.

When the data y are known and the parameters θ are unknown, $P(y|\theta)$ may be regarded as a function not of y but of θ. When so regarded, it is called the likelihood function of θ for given y and can be written as $l(\theta|y)$. $P(y) = \int P(y|\theta)\, P(\theta)\, d\theta$ is constant and acts as a normalizing factor to ensure that the Bayesian posterior integrates to unity (Box and Tiao, 1973). We can thus write Bayes' formula as

$$P(\theta|y) \propto l(\theta|y)\, P(\theta) \qquad \text{Eq. 2.2}$$

In other words, Bayes' theorem tells us that the probability distribution for θ posterior to the data y is proportional to the product of the likelihood for θ given y, $l(\theta|y)$, and the distribution for θ prior to the data, $P(\theta)$ (Box and Tiao, 1973).

The prior distribution of θ is interpreted as a "degree of belief", which is subjective. Each person can have his/her prior, which contains the relative weights that the person gives to every possible parameter value. It measures how "plausible" the person considers each parameter value to be, before observing the data (Bolstad, 2007). After data (y) are collected, the person's belief about the parameters ($P(\theta)$) is revised through the Bayes' theorem. The likelihood function, $l(\theta|y)$, is the function through which the data y modify the prior knowledge of θ. It can therefore be regarded as representing the information about θ coming from the data (Bolstad, 2007). The posterior distribution, $P(\theta|y)$, is then our modified belief about the parameters, after analyzing the data; hence, it contains information from both prior distribution and the observed data (experimental measurements).

Bayes' theorem is appealing because it provides a mathematical formulation of how previous knowledge may be combined with new knowledge (and hence, updates). It allows us to continually update information about a set of parameters θ as more observations are taken (Box and Tiao, 1973). Bayes' theorem has been implemented, in many different fields, to develop algorithms for parameter estimation and adaptation, model discrimination, or design of experiments. The following section touches upon some of the applications of the Bayesian approach in the chemical engineering field. However, since this work is more focused on polymerization processes and the aim has been more on the design of experiments, this

literature review is by no means a comprehensive one over the whole general chemical engineering field, but rather a selective one with more emphasis on polymerization processes.

2.3 Representative Applications of Bayesian Approach in Chemical Engineering: A review of recent literature

Certainly, Bayesian methods are well established, especially among statisticians. Although the Bayesian approach does not seem like a standard kit for chemical engineers, there have been many applications relevant to chemical and process engineering appearing in the literature over the years. Some classical applications of Bayesian design in chemical engineering date back to the early 1960s (for example, the work by Box and co-workers (Box and Draper, 1965; Box and Tiao, 1965 and Box and Tiao, 1968). Over the years, applications of the Bayesian technique have evolved, from being used only in catalytic (reaction) chemical engineering, to various other specialized branches of chemical engineering.

Duran and White (1995) applied the Bayesian framework to estimate model parameters for heat transfer in a packed bed using data from ill-controlled experiments. They showed that the Bayesian approach was superior to the standard estimation techniques, as it not only accounted for several important error sources (that could not be considered in the standard approaches), but also provided a probability distribution for these errors. The alternative solution to using the Bayesian approach would be to perform the experiments again under better controlled conditions, which would be a far more costly alternative.

The Bayesian technique has been also applied to microbial systems (Bois et al., 1997; Pouillot et al., 2003; and Coleman and Block, 2006). In all these applications, Bayesian statistical inference was used to model the development of a microbial system, and estimate the parameters of the related model. For example, Boise et al. (1997) modeled the development of biofilm in an industrial pilot drinking-water network by using a Bayesian approach, and derived statistical distributions for the model parameters, based on experimental data.

Another area where the Bayesian methodology had been applied is drug and cell transport. Murphy et al. (2004) developed a systematic and iterative Bayesian scheme and sets of rules

for the design of enzyme kinetic experiments. By using the Bayesian approach, they selected the optimum design to collect data suitable for accurate modeling and parameter estimation. Later, they used this algorithm to study other important kinetic systems, including drug transport, receptor binding, microbial culture and cell transport kinetics. They showed that by implementing the Bayesian technique, they could reduce the error in estimating the parameters of their models, and at the same time increase the overall efficiency and cost-effectiveness of the process (because of reducing the necessary amount of experiments and data points measured).

The Bayesian approach has traditionally been suggested for building models (among many alternative mechanisms) for catalytic reaction systems. Reilly and Blau (1974) and Froment (1975) summarized earlier efforts in this area. However, at the time, the computational challenges associated with the implementation of the Bayesian scheme made its adaptation prohibitive among the wider catalytic reaction community. Recent advances in high speed computation have made it possible for researchers to exploit the Bayesian method. For example, Blau and co-workers recently revisited the Bayesian approach in order to build kinetic models for catalytic systems (Blau et al., 2008; Hsu et al., 2009). In their work, the Bayesian methodology was used to estimate model parameters, discriminate between rival models and design new experiments to improve both model discrimination and fidelity of the parameter estimates.

The Bayesian approach has also been applied to pharmaceutical kinetics. For example, Hermanto et al. (2008) used Bayesian methodology to estimate the kinetic parameters of a model for polymorphic crystallization of L-glutamic acid. The kinetic model was developed from batch experiments with in situ measurements, including ATR-FTIR spectroscopy, to infer the solute concentration and provide crystal size information. In their work, a marginal probability distribution for each parameter was determined, which could give insight regarding uncertainties in the parameters, and also be of significant value in developing robust control strategies for the crystallization process.

More recently, Omidbakhsh et al. (2010) applied the Bayesian methodology to a disinfectant formulation process. Hydrogen peroxide was used as the basic chemical in formulating new

disinfectants; however, this chemical is not very stable and loses its antibacterial activity very quickly. Therefore, developing a model which could accurately predict peroxide loss in future formulations was desirable. The Bayesian approach was used to design the least possible number of trials which could then be used to obtain a robust model for prediction of peroxide loss. The prior information was based on historical data.

Although the Bayesian methodology has been used widely in many different chemical engineering fields, the literature on the application of Bayesian approaches to polymerization systems is scarce. Dube et al. (1996) were the first to present a systematic study of emulsion terpolymerization using the Bayesian design of experiments technique. The Bayesian experimental design was used to design 18 trials, in three sequences of 4-, 4- and 10- trials, in order to study the effect of seven different factors on four different responses. The seven factors studied were temperature, initiator, monomer, emulsifier, chain transfer and impurity concentrations, and type of initiator used. The responses collected from batch emulsion terpolymerization were batch time, terpolymer composition, weight-average molecular weight, and total number of particles. Subsequently, Vivaldo-Lima et al. (2006) used the Bayesian design to determine the relative importance of process factors in suspension copolymerization. They designed two sequences of 4-trials each to study the effect of six different factors ([CTA], [stabilizer], speed of agitation, dispersed phase hold-up, and two factors from impeller geometry) on mean particle size and coefficient of variation of the particle size distribution.

Scrutinizing all the Bayesian framework applications (including the ones mentioned above as well as others from the scientific literature not cited herein for the sake of brevity), one can see that the common characteristic is that they are concerned with admittedly very important, (multi)parameter estimation questions (of kinetic rate constants), but not so often with the issue of the design of experiments. Apart from Dube et al. (1996), Vivaldo-Lima et al. (2006) and Hsu et al. (2009), who dealt with the design of experiments both theoretically and experimentally (i.e., the design stage and how this can aid further decisions about optimizing process operation and product performance), there are not many cases where Bayesian ideas have been formally applied to the design of an actual scientific experiment, followed by conducting the experiments, analyzing the data, updating the information, and conducting the next (optimal) trial(s). Most often, based on the scientific literature on the topic, data already

collected are subjected to Bayesian analysis, with suggestions as to how the scenario could possibly have improved, had Bayesian design of experiments been applied at the outset.

In addition, looking at the last 15 years or so, whereby many advances have taken place in polymerization systems, Bayesian design of experiments has not been exploited extensively nor frequently in complex polymerization systems, which could benefit tremendously from its important traits. Complex polymerization processes are directly amenable/conducive to analysis following Bayesian approaches. In most polymerization processes mathematical models do exist, albeit often with unreliable parameter values and/or even unverified mechanistic bases (i.e., reaction mechanisms). In the cases of complex, new and emerging technologies, this problem is even more prominent. Hence, using ideas from the design of experiments (applied statistical methodology) to clarify polymerization kinetics seems beneficial. The Bayesian design of experiments combines, by definition, experimental data and prior modeling information, thus leading naturally to mathematical model updates and the identification of optimal operating (experimental) conditions (regions) in order to achieve certain polymer property targets.

In order to illustrate the principles and capabilities/benefits of the Bayesian design approach and its superiority to the currently practiced (standard) design of experiments (and, certainly, to the still dominant lack of practice of using designed experiments!), case studies are presented in this thesis, drawn from different complex polymerization processes. These case studies address important, yet practical, issues in not only the study of polymerization kinetics but also, in general, in process engineering and improvement. A preview of the important process issues and, accordingly, topics that can be handled efficiently by the Bayesian design approach are listed in Table 2.2. Before presenting results from the implementation of Bayesian design to different polymerization processes, the general Bayesian experimental design framework developed by Reilly (1993) is presented in Chapter 3 and applied to a simple case study for demonstration purposes.

Table 2.2 Overview of issues handled by the Bayesian design approach

Issue
Sources of prior knowledge (screening experiments vs. models)
Effect of informative vs. non-informative priors
Accommodating factor level and range changes and/or extra trial(s) mid-way through experimentation
Designing n-trial experiments vs. sequences of fewer trials
Diagnostic criteria for the quality of prior knowledge and significance of estimated effects
Single vs. multi-response scenarios
Handling process constraints and impractical treatment combinations
Increase of information content, flexibility and cost effectiveness

Chapter 3. Bayesian Design Framework

Standard experimental design methods, e.g., (fractional) factorial designs, have been employed extensively and are useful in optimizing a wide variety of systems. However, these designs usually suffer from several limitations and cannot handle certain situations, as listed in Table 2.1 of Chapter 2. In addition, these approaches do not take direct advantage of the considerable prior knowledge that is available about the reaction system to design experiments. As prior information is already available within existing data, it is logical that it should be used in order to contribute to the optimality of the designed experiments, and hence to improved models and performance of the process in question. Using a more efficient experimental design which can accommodate restrictions encountered in the standard experimental designs could (hopefully) lead to optimal performance in fewer trials, thus saving time and money.

Such efficient designs can be found in the family of Bayesian approaches. Bayesian design is a powerful and largely unstudied (in the polymerization area) experimental design methodology, which can accommodate practical limitations encountered in standard (fractional) factorial designs. The other significant advantage of the approach is that it incorporates prior knowledge about a process into the design in order to suggest a set of future experiments in an optimal, sequential and iterative fashion. In addition, Bayesian design allows the use of a nonlinear (fully mechanistic) model along with experimental information (hence, it is essentially an optimal model-based design of experiments). The approach can shed light on the most uncertain parts of our process understanding, identify the least reliable (less well known) parameters (e.g., uncertain values of kinetic rate constants), and further guide sensitivity analysis studies focusing on key uncertain parameters in one's model.

Details about the Bayesian design approach to experimentation are discussed in this chapter and in order to visualize the inner workings of the approach and its superiority to the currently practiced (standard) design of experiments, the Bayesian design is applied to a simple simulation bench-marking example.

3.1 Bayesian Approach to Experimentation: Algorithmic Steps

As discussed in section 2.2, the Bayesian methodology is based on Bayes' theorem which states that:

$$\underset{\text{distribution}}{\text{posterior parameter}} \propto \underset{\text{function}}{\text{parameter likelihood}} \times \underset{\text{distribution}}{\text{prior parameter}}$$

The prior distribution captures what is known about the parameters (or a process) before the collection (hence, knowledge) of the data. Prior knowledge may be based on the subjective opinion of the "expert", some exploratory literature data, or could be provided from a nonlinear/mechanistic model of the process under study or of a similar process. The likelihood function is the function through which the observed data points modify the prior knowledge about the parameters. It can therefore be regarded as the contribution about the parameters coming from the data. The posterior distribution reflects one's belief about the parameters after the data have been generated. Bayes' theorem basically quantifies the improvement in our knowledge about the parameters by weighing prior knowledge with the new information generated by the experimental data (Hsu et al., 2009). The Bayesian approach has a sequential nature and provides a mathematical formulation of how previous knowledge may be combined with new knowledge. It basically allows one to continually update information about a set of parameters as more observations are collected.

The Bayesian approach to experimentation requires a model for the process response(s) as a function (denoted as f in Eq. 3.1) of the factors or variables under study, and a distribution function which contains the prior knowledge about the process (parts of this theoretical background on the Bayesian approach to experimentation is based on Reilly (1993)).

$$\underline{y} = f(\underline{X}, \underline{\theta}) \pm \underline{\varepsilon} \qquad \text{Eq. 3.1}$$

In our study, we will use a linear regression model (Eq. 3.2), for simplicity, and a multivariate normal distribution for the prior knowledge (Eq. 3.3). Using a linear regression model is not only extremely common but will also serve to illustrate the basic steps in a relatively simple way, easy to follow and visualize. Consider the linear regression model:

$$\underline{y} = \underline{X\theta} + \underline{\varepsilon} \qquad \text{Eq. 3.2}$$

where $\underline{y}$ is an $n \times 1$ vector of observations with y_i representing the i^{th} observation. $\underline{X}$ is an $n \times p$ design matrix, with its elements having the values of +1 and -1, corresponding to the high and low levels of the design factors, respectively (these experiments and the methodology in general are by no means restricted to two levels but two levels were again chosen in order to reduce the number of trials required, for the sake of simplicity in these illustrative stages). A row of the $\underline{X}$ matrix corresponds to an experimental trial (treatment). n is the number of trials and p is the number of parameters or effects (p includes the mean, the main effects, and all of the interactions; for a 2^m factorial experiment, p is 2^m). $\underline{\theta}$ is the $p \times 1$ vector of true, yet unknown, values of parameters, with each parameter identified by its subscripts (e.g., θ_{37} is the parameter for the two-factor interaction between factor 3 and factor 7). Finally, $\underline{\varepsilon}$ is the error vector which is assumed to be normally distributed with mean $\underline{0}$ and variance matrix $\underline{I}\sigma^2$ ($\underline{I}$ is the identity matrix). σ^2 is the variance of the response(s).

The prior knowledge of θ can be represented by:

$$\underline{\theta} : N\,[\underline{\alpha};\, \underline{U}] \qquad \text{Eq. 3.3}$$

that is, the knowledge held about $\underline{\theta}$ before the experiment can be expressed by the multivariate normal distribution with mean $\underline{\alpha}$ and variance/covariance matrix $\underline{U}$, where $\underline{\alpha}$ is a $p \times 1$ known vector of the parameter means and $\underline{U}$ is a positive definite $p \times p$ known matrix of the variances (covariance(s) if they exist) of the parameter means. At first glance, it may seem strange that in order to use the Bayesian design approach, one must initially have estimates of the parameters; after all, it is the purpose of the experiment to obtain such estimates! However, as mentioned by Box and Hunter (1965), this paradox is merely an example of the fact that any experimental design uses the experimenter's beliefs about the situation being studied. In fact, the exercise of casting prior knowledge about a process into a mathematical form (as will be shown later) forces the experimenter to brainstorm/hypothesize and perhaps come to a clearer understanding of the process or even anticipate/solve some of the problems that triggered the specific questions about the process even before starting the experiments.

Prior knowledge can have different shapes and forms; it may simply be some advance knowledge, however vague, of the parameters in a linear model underlying a factorial experiment. In other situations, an engineer/scientist with expert knowledge of the system may be able to mentally estimate values, i.e., arrive at sufficiently good "guesses" of the response variable(s) for known values of the factors. Another situation where prior knowledge is available is when the kinetic parameters to be used in a nonlinear/mechanistic model are possibly available from literature information. However, in many cases they cannot be used as "the values" for the kinetic parameters of the system/model under consideration because maybe a different experimental approach has been used in order to determine/ calculate/ measure/ estimate them. On the other hand, ignoring them totally does not sound like a reasonable thing to do either!

After the prior knowledge is stored in the form of $\underline{\alpha}$ and $\underline{U}$, Bayes' theorem may be applied to give the posterior distribution of the parameter values (details behind the derivation of Eq. 3.4 are discussed in section A. 1 of Appendix A):

$$\left(\underline{\theta}\middle|\underline{y}\right) : N\left\{\left[\underline{U}^{-1} + \left(\frac{1}{\sigma^2}\right)\underline{X'X}\right]^{-1}\left[\underline{U}^{-1}\underline{\alpha} + \left(\frac{1}{\sigma^2}\right)\underline{X'}\underline{y}\right]; \left[\underline{U}^{-1} + \left(\frac{1}{\sigma^2}\right)\underline{X'X}\right]^{-1}\right\} \qquad \text{Eq. 3.4}$$

The design problem is therefore that of choosing the "best" n-trial fraction of a factorial experiment. One can search for the best set of trials by maximizing the determinant in Eq. 3.5. Hence, the optimality problem is reduced to that of choosing $\underline{X}$ in order to maximize H (additional remarks about Eq. 3.5 are presented in section A.2 of Appendix A):

$$H = \left|\underline{I} + \left(\frac{1}{\sigma^2}\right)\underline{XUX'}\right| \qquad \text{Eq. 3.5}$$

The optimality criterion of maximizing the determinant H reduces to the well-known D-optimality criterion of maximizing $\left|\underline{X'X}\right|$ in the special case when there is no prior knowledge about the parameters. After the completion of a set of experiments (design sequence), the vector of parameter means ($\underline{\alpha}$) and variance/covariance matrix ($\underline{U}$) are updated using Eq. 3.6

and Eq. 3.7, respectively (note that the updated $\underline{\alpha}$ is now defined (renamed) as $\underline{\theta}$, the posterior means of the parameters).

$$\underline{\theta} = \left[\underline{U}^{-1} + (\frac{1}{\sigma^2})\underline{X'X}\right]^{-1}\left[\underline{U}^{-1}\underline{\alpha} + (\frac{1}{\sigma^2})\underline{X}'\underline{y}\right] \quad \text{Eq. 3.6}$$

$$\underline{U} = \left[\underline{U}^{-1} + (\frac{1}{\sigma^2})\underline{X'X}\right]^{-1} \quad \text{Eq. 3.7}$$

The next sequence of experiments can then be chosen, once more following the optimality criterion of maximizing determinant H (Eq. 3.5). One can make a decision at some point during the course of the experimentation to halt the experimentation based on the corresponding variance of the parameters. That is, once the values of all of the parameters of interest are known with an acceptable degree of certainty, the experimentation can be stopped.

Implementation of the Bayesian design of experiments requires several steps. Table 3.1 gives a summary of the different steps (of the algorithm) that have to be taken in order to design experiments through the Bayesian approach. Going through the general steps of Table 3.1 might be straightforward at first glance, however, considerable time/effort/sophistication is needed starting with step 4, and then at every update (e.g., steps 7 and 8). The combination of extended/meaningful "brainstorming" (steps 1 and 2) and detailed experimental response characterization (steps 4 to 7) as linked by the optimality step 3, will hopefully lead to not only a more flexible design/experimentation scheme but also a much more informative posterior. As one can see from scrutinizing the steps (1-8) of Table 3.1, the Bayesian design approach is optimal, sequential and iterative.

Table 3.1 Summary steps for implementing the Bayesian design approach

1) Select the design factors and their levels; select response(s).
2) Cast the prior knowledge into a vector of prior parameter estimates ($\underline{\alpha}$) and a prior variance/covariance matrix ($\underline{U}$)
3) Select the "best" experiment using the search algorithm described by Eq. 3.5
4) Run and analyze the experiments (which have been selected using Eq. 3.5)
5) Update vector of parameter means ($\underline{\theta}$) and variance/covariance matrix ($\underline{U}$) using Eq. 3.6 and Eq. 3.7
6) Given the new variance/covariance matrix ($\underline{U}$), use Eq. 3.5 to select the next sequence of trials
7) Analyze the experiments and update $\underline{\theta}$ and $\underline{U}$; repeat steps 5 to 7.
8) Stop the experimentation once the values of parameters of interest are known with an accepted degree of certainty. Update the vector of parameters for the last time, after the analysis of the final sequence of experiments

3.2 Simple Case Study

The steps of Table 3.1 are "visualized" using a simple simulation "bench-marking" example herein. This example tackles the selection of twelve runs in two sequences of 8- and 4-trials each, with a single response and five independent variables. We begin with a linear model for the process, as follows:

$$y=\theta_0+\theta_1x_1+\theta_2x_2+\theta_3x_3+\theta_4x_4+\theta_5x_5+\theta_{12}x_1x_2+\theta_{13}x_1x_3+\theta_{14}x_1x_4+ \quad \text{Eq. 3.8}$$
$$\theta_{15}x_1x_5+\theta_{23}x_2x_3+\theta_{24}x_2x_4+\theta_{25}x_2x_5+\theta_{34}x_3x_4+\theta_{35}x_3x_5+\theta_{45}x_4x_5+$$
$$\theta_{123}x_1x_2x_3+\theta_{124}x_1x_2x_4+\theta_{125}x_1x_2x_5+\theta_{134}x_1x_3x_4+\theta_{135}x_1x_3x_5+\theta_{145}x_1x_4x_5+$$
$$\theta_{234}x_2x_3x_4+\theta_{235}x_2x_3x_5+\theta_{245}x_2x_4x_5+\theta_{345}x_3x_4x_5+\varepsilon$$

where y is the response and θ_i are the parameters. For a five-factor factorial design, with two levels per factor, the model would have $p=2^k=2^5=32$ parameters corresponding to a constant term (θ_0), $k=5$ main factor effects, $\binom{k}{2}=\binom{5}{2}=5!/[2!(5-2)!]=10$ two-factor

interactions, and similarly, 10 three-factor interactions, 5 four-factor interactions and 1 five-factor interaction. In this example, the effects of four- and five-factor interactions are assumed to be highly unlikely and are not included, hence, we end up with $p' = 2^k - \binom{k}{4} - \binom{k}{5} = 26$ parameters in the model. x_i represents the *i*th factor (setting) or coefficient of parameter *i*. In a typical two-level design of experiments scenario, the x_is assume the values of +1 and - 1, signifying the upper and lower level of the factor (independent variable), respectively. ε is the error, assumed to be normally distributed with mean $\underline{0}$ and known covariance matrix $\underline{I}\sigma^2$. σ^2, the variance of the response, is assumed to be known and equal to 2 for our example calculations. The true values of the parameters (θ_i^*), i.e., the values used to simulate the experiments, are shown in the second column of Table 3.2.

The next step is to cast our prior knowledge of the process into $\underline{\alpha}$ and $\underline{U}$ (see step 2 in Table 3.1). The prior parameter values (guessed or generated from the true parameter values to simulate a situation when we have reasonable starting estimates of the parameters and their associated uncertainties) are shown in the third column of Table 3.2. Note that only two of the interaction effects (θ_{12} and θ_{34}) are expected to be nonzero in the opinion of the "expert". "Expert" opinion is again used to make a calculated guess about the prior elements of the variance/covariance matrix (U_{ii}) for each parameter (see fourth column of Table 3.2), i.e., the "expert" is expressing how certain he/she is about the prior parameter values. In general, $\underline{U}$ is a $p \times p$ matrix, however, in our case it is $p' \times p' = 26 \times 26$. The diagonal elements (U_{ii}) of the prior $\underline{U}$ are shown in the fourth column of Table 3.2 (the off-diagonal elements are assumed to be zero initially).

Table 3.2 Prior knowledge about the parameters

Parameter	**True** θ_i^*	**Prior** α_i	**Prior** U_{ii}	**Prior standard deviation**	**Prior 2 standard deviations**
θ_0	200	180	100	10	20
θ_1	20	15	10	3.162	6.32
θ_2	1	0	5	2.236	4.47
θ_3	10	20	10	3.162	6.32
θ_4	-15	-10	10	3.162	6.32
θ_5	1	0	5	2.236	4.47
θ_{12}	10	8	5	7.071	4.47
θ_{13}	0	0	3	1.732	3.46
θ_{14}	0	0	3	1.732	3.46
θ_{15}	0	0	3	1.732	3.46
θ_{23}	0	0	3	1.732	3.46
θ_{24}	0	0	3	1.732	3.46
θ_{25}	0	0	3	1.732	3.46
θ_{34}	10	14	5	2.236	4.47
θ_{35}	0	0	3	1.732	3.46
θ_{45}	0	0	3	1.732	3.46
θ_{123}	0	0	1.5	1.225	2.46
θ_{124}	0	0	1.5	1.225	2.46
θ_{125}	0	0	1.5	1.225	2.46
θ_{134}	0	0	1.5	1.225	2.46
θ_{135}	0	0	1.5	1.225	2.46
θ_{145}	0	0	1.5	1.225	2.46
θ_{234}	0	0	1.5	1.225	2.46
θ_{235}	0	0	1.5	1.225	2.46
θ_{245}	0	0	1.5	1.225	2.46
θ_{345}	0	0	1.5	1.225	2.46

Considering the prior 2 standard deviations (last column of Table 3.2), one can see that all of the true parameter values are within the 95% confidence interval of the prior parameter values, except parameter three (θ_3). A deliberate discrepancy is introduced for θ_3 (the level of uncertainty is underestimated for this factor) in order to check the behavior of Bayesian methodology in the presence of false prior information. The variance/covariance matrix ($\underline{U}$) will have an effect on the design of experiments, as seen in Eq. 3.5. Herein lies one advantage of the Bayesian technique: small elements in the variance/covariance matrix will make a particular factor less important in the design, while larger elements will "steer" the design in

the direction of obtaining more information about the lesser known variables. In other words, the Bayesian technique will help one avoid generating unnecessary information about factors that are already well known. One can notice from the 4th column of Table 3.2 that the main parameters (and, hence, effects) and two-factor interactions have larger variances than three-factor interactions. In addition, we are expecting to gain more information about the main effects, the interaction between factors 1 and 2 (θ_{12}), and also the interaction between factors 3 and 4 (θ_{34}) during the sequential Bayesian updates, as higher U_{ii} have been allocated to these parameters in the variance/covariance matrix.

Next, optimal experiments are selected by employing the design criterion (see Eq. 3.5). Let's assume that $\underline{F}$ is the $p \times p$ matrix of coefficients for the full factorial experiment. Then $\underline{X}$ would be the n rows of $\underline{F}$, which are chosen as the next trials to be run (n<p). Hence, the design problem becomes that of choosing $\underline{X}$ ($n \times p$) from $\underline{F}$ to maximize our criterion (the determinant H of Eq. 3.5). Since in this specific example we have assumed that higher than three-factor interactions are negligible, $\underline{F}$ is a $p' \times p' = 26 \times 26$ matrix and $\underline{X}$ is a $n \times p'$ submatrix of F. Let's say that 8 trials are desired to be selected for the first sequence of experiments ($n = 8$); hence, $\underline{X}$ is a 8×26 matrix. There are $\binom{26}{8}$= 1,562,275 possible 8-trial sequences to choose from. Out of all the possible 8-trial sequences, eight happen to yield the maximum value for the determinant (H= 2.92×10^{14}). Since no initial conditions are specified, one of the eight "optimal" 8-trial sequences is chosen at random and the chosen levels (+1's and -1's) for the main factors are shown in Table 3.3, along with the simulated response, y, "obtained" for each trial (the whole 8×26 $\underline{X}$ matrix, containing interaction terms is not shown for the sake of brevity). The simulated responses are obtained by substituting the coded values of the factors (+1's and -1's) into the model using the true values of the parameters (see second column of Table 3.2), and subsequently adding normally distributed error (of variance σ^2 equal to 2, as discussed earlier) to the results in order to simulate process variability.

Table 3.3 8 trials of the **first** sequence of the simulated example

Trial	x_1	x_2	x_3	x_4	x_5	**Simulated process response**
1	-1	-1	-1	-1	1	207.32
2	-1	-1	1	1	-1	196.59
3	-1	1	-1	1	1	134.11
4	-1	1	1	-1	-1	183.72
5	1	-1	-1	1	-1	174.97
6	1	-1	1	-1	1	224.91
7	1	1	-1	-1	-1	246.03
8	1	1	1	1	1	237.75

Next, the posterior variance/covariance matrix is calculated using Eq. 3.7 and the corresponding 26×26 matrix is shown in Table 3.4 (since $\underline{U}$ is symmetric, only the lower diagonal elements are shown). One can now observe the presence of nonzero off-diagonal elements in the (updated) posterior variance/covariance matrix $\underline{U}$ of Table 3.4. This updated matrix can now be used back in Eq. 3.5 to design (in an iterative sequential fashion) the next sequence of trials.

Eq. 3.6 is then employed to calculate the posterior $\underline{\theta}$, using the prior $\underline{\alpha}$ (third column of Table 3.2), the prior $\underline{U}$ (a diagonal matrix with diagonal elements shown in the 4th column of Table 3.2), the responses $\underline{y}$ (last column of Table 3.3) and the $\underline{X}$ matrix (part of which is shown in Table 3.3).

To improve the parameter estimates and further decrease uncertainty (i.e., decrease the $\underline{U}$ elements), let's say that a second sequence of 4 trials is desired. The updated $\underline{U}$ from the first sequence of 8 trials (Table 3.4) can now be used as the prior variance/covariance matrix for the design of this new 4-trial experiment. Eq. 3.5 is employed again and out of all possible 4-trial sequences, two happened to yield the maximum value for the determinant (H= 2.44×10^6). One of these "optimal" 4-trial sequences is chosen and is shown in Table 3.5 along with the simulated response, y, for each trial. The updated variance/covariance matrix is shown in Table 3.6. Comparing Table 3.4 with Table 3.6, one can see that after the second sequence of experiments, the uncertainties about the parameters (diagonal elements of the $\underline{U}$ matrix) have

decreased. Eq. 3.6 can be employed again to calculate the posterior $\underline{\theta}$ after the second sequence of 4 trials. The calculations are the same as for the first sequence and the final results are shown in the 5th column of Table 3.7 (the superscript in $\theta_i^{(\ )}$ denotes the sequence of trials).

Table 3.4 Posterior variance/covariance matrix U after the **first** sequence of experiments

3.15																									
0	3.22																								
0	0	2.44																							
0	0	0	3.22																						
0	0	0	0	3.22																					
0	0	0	0	0	2.78																				
0	0	0	0	0	0	3.11																			
0	0	0	0	0	-1.33	0	2.2																		
0	0	0	0	0	0	0	0	2.03																	
0	0	0	-2.03	0	0	0	0	0	2.39																
0	0	0	0	0	0	0	0	-0.97	0	2.03															
0	0	0	0	0	-1.33	0	-0.8	0	0	0	2.2														
0	0	0	0	-2.03	0	0	0	0	0	0	0	2.39													
0	0	0	0	0	0	-1.89	0	0	0	0	0	0	3.11												
0	-2.03	0	0	0	0	0	0	0	0	0	0	0	0	2.39											
0	0	-1.54	0	0	0	0	0	0	0	0	0	0	0	0	2.08										
0	0	0	0	-1.02	0	0	0	0	0	0	0	-0.31	0	0	0	1.35									
0	0	0	-1.02	0	0	0	0	0	-0.31	0	0	0	0	0	0	0	1.35								
0	0	0	0	0	0	0	0	-0.49	0	-0.49	0	0	0	0	0	0	0	1.26							
0	0	-0.77	0	0	0	0	0	0	0	0	0	0	0	0	-0.46	0	0	0	1.27						
-1.45	0	0	0	0	0	0	0	0	0	0	0	0	0	0	0	0	0	0	0	1.48					
0	0	0	0	0	0	-0.57	0	0	0	0	0	0	-0.57	0	0	0	0	0	0	0	1.33				
0	-1.02	0	0	0	0	0	0	0	0	0	0	0	0	-0.31	0	0	0	0	0	0	0	1.35			
0	0	0	0	0	0	-0.57	0	0	0	0	0	0	-0.57	0	0	0	0	0	0	0	-0.17	0	1.33		
-1.45	0	0	0	0	0	0	0	0	0	0	0	0	0	0	0	0	0	0	0	-0.02	0	0	0	1.48	
0	0	0	0	0	0	0	0	-0.49	0	-0.49	0	0	0	0	0	0	0	-0.24	0	0	0	0	0	0	1.26

Table 3.5 4 trials of the **second** sequence of the simulated example

Trial	x_1	x_2	x_3	x_4	x_5	Simulated process response
1	-1	-1	-1	-1	-1	204.25
2	-1	1	1	-1	1	189.49
3	1	-1	-1	1	1	172.46
4	1	1	1	1	-1	237.25

Table 3.6 Posterior variance/covariance matrix U after the **second** sequence of experiments

1.35																									
0	2.31																								
0	0	1.88																							
0	0	-0.74	2.24																						
0	-0.91	0	0	2.31																					
0	0	0	0	0	1.35																				
0	0	0	0	0	0.62	2.84																			
0	0	0	0	0	-0.61	-0.31	1.84																		
-0.60	0	0	0	0	0	0	0	1.83																	
0	0	0.83	-0.94	0	0	0	0	0	1.17																
-0.60	0	0	0	0	0	0	0	-1.17	0	1.83															
0	0	0	0	0	-0.61	-0.31	-1.16	0	0	0	1.84														
0	1.02	0	0	-1.02	0	0	0	0	0	0	0	1.25													
0	0	0	0	0	0.62	-2.16	-0.31	0	0	0	-0.31	0	2.84												
0	-1.02	0	0	1.02	0	0	0	0	0	0	0	-1.13	0	1.25											
0	0	-0.83	0.94	0	0	0	0	0	-1.05	0	0	0	0	0	1.17										
0	-0.14	0	0	-1.15	0	0	0	0	0	0	0	-0.15	0	0.15	0	1.33									
0	0	-0.11	-1.16	0	0	0	0	0	-0.14	0	0	0	0	0	0.14	0	1.33								
0.59	0	0	0	0	0	0	0	-0.29	0	-0.29	0	0	0	0	0	0	0	1.06							
0	0	-0.94	-0.22	0	0	0	0	0	0.25	0	0	0	0	0	-0.25	0	-0.03	0	1.22						
-0.59	0	0	0	0	0	0	0	0.29	0	0.29	0	0	0	0	0	0	0	-0.28	0	1.06					
0	0	0	0	0	-0.60	-0.31	0.30	0	0	0	0.30	0	-0.31	0	0	0	0	0	0	0	1.08				
0	-1.15	0	0	-0.14	0	0	0	0	0	0	0	0.15	0	-0.15	0	-0.02	0	0	0	0	0	1.33			
0	0	0	0	0	-0.60	-0.31	0.30	0	0	0	0.30	0	-0.31	0	0	0	0	0	0	0	-0.42	0	1.08		
-0.59	0	0	0	0	0	0	0	0.29	0	0.29	0	0	0	0	0	0	0	-0.28	0	-0.44	0	0	0	1.06	
0.59	0	0	0	0	0	0	0	-0.29	0	-0.29	0	0	0	0	0	0	0	-0.44	0	-0.28	0	0	0	-0.28	1.06

A series of statistical diagnostic tests can now be carried out in addition to the previous steps. These diagnostic tests serve to quantify the relative importance of the parameters (i.e., factor effects) and their interactions, as well as the quality of prior knowledge (in other words, the adequacy of the model used to generate the "prior knowledge", as the case might be).

Results from these statistical diagnostic tests for our example are also shown in Table 3.7. The second column shows the true values of the parameter means, the third column presents the initial values of the parameter means ($\underline{\alpha}$), and the fourth and fifth columns contain the updated estimates of the parameter means after the first and second sequence, respectively. Test 1 (column six of Table 3.7) is defined as the ratio of the prior mean (3rd column of Table 3.7) to the prior standard deviation of the mean $[\alpha_i/(U_{ii})^{1/2}]$, where $(U_{ii})^{1/2}$ is shown in the fifth column of Table 3.2. This test checks the null hypothesis that $\alpha_i = 0$ purely in the opinion of the ''expert'' (the person who assigned the values for the prior effects and variances). It is essentially a measure of the uncertainty of the ''expert''. A value greater than 2 or less than -2 is considered significant (this is equivalent to a 95.44% confidence interval). Test 2 is a measure of the actual significance of an effect. For instance, the test 2 value after the second sequence of experiments (7th column of Table 3.7) is equal to the second updated estimate of the effect, $\theta_i^{(2)}$ (see fifth column of Table 3.7), divided by the square root of the corresponding diagonal element of the last posterior variance/covariance matrix (see Table 3.6; $[\theta_i^{(2)}$

/($U_{post(ii)}$)$^{1/2}$]). Once again, a value greater than 2 or less than -2 implies significance. Finally, test 3 is a measure of the quality of the expert's opinion. For instance, test 3 after the second sequence of experimentation (8th column of Table 3.7) is equal to ($\theta_i^{(2)}$ - α_i) divided by the square root of the diagonal element of the last posterior variance/covariance matrix (see again Table 3.6; [($\theta_i^{(2)}$ - α_i) /($U_{post(ii)}$)$^{1/2}$]). A significant value greater than 2 or less than -2 implies that portion(s) of the mechanistic model related to the response(s) and the effects in question may need further refinement. As explained in Dube et al. (1996) and Vivaldo-Lima et al. (2006), caution should be exercised in the interpretation of this test, since correlation and nonlinearity in the model equations could also cause the results of test 3 to become significant/insignificant. The numerical results for tests 2 and 3 after the first sequence (of eight trials), have also been included in columns 9 and 10 in Table 3.7, for the reader to appreciate the evolution of the output from these test values.

A careful analysis of the summary results of Table 3.7 can lead to several interesting remarks. Comparing the true values of the parameters (θ_i^* in Table 3.7), the prior estimates of the parameters (α_i in Table 3.7), and the estimates of the parameters after the first and second sequence, one observes that the parameter estimates have improved in the direction of the true values. For example, Figure 3.1a illustrates the evolution for parameter 3 from the prior value (α_3) towards the true value (θ_3^*) throughout the experimentation. As one can see, initially the value for parameter 3 had been estimated by the "expert" to be 20, while the posterior estimate after the second sequence ($\theta_3^{(2)}$) has been updated to be 12.88, a value much closer to the true value of 10. Comparing the corresponding variance values (see Figure 3.1b), one can observe that the Bayesian design moves in the direction of minimizing the variance in the parameters. Figure 3.1 is just one way of "visualizing" and demonstrating the improvements achieved by the Bayesian methodology.

Table 3.7 Summary results of diagnostic tests

Parameter	**True** θ_i^*	**Prior** α_i	$\theta_i^{(1)}$	$\theta_i^{(2)}$	**Test 1**	**Test 2 (after 2nd seq.)**	**Test 3 (after 2nd seq.)**	**Test 2 (after 1st seq.)**	**Test 3 (after 1st seq.)**
θ_0	200	180	200.024	200.425	**18**	**172.4089**	**17.5702**	**112.742**	**11.2865**
θ_1	20	15	18.553	18.284	**4.7434**	**12.0325**	**2.1613**	**10.3384**	1.9797
θ_2	1	0	-0.140	-0.432	0	-0.3153	-0.3153	-0.0895	-0.0895
θ_3	10	20	13.266	12.880	**6.3246**	**8.6028**	**-4.7554**	**7.3925**	**-3.7525**
θ_4	-15	-10	-13.268	-13.537	**-3.1623**	**-8.9082**	**-2.3274**	**-7.3935**	-1.8210
θ_5	1	0	0.154	0.613	0	0.5283	0.5283	0.0927	0.0927
θ_{12}	10	8	7.716	7.517	1.1314	**4.4569**	-0.2863	**4.3731**	-0.1609
θ_{13}	0	0	0.093	-0.137	0	-0.1014	-0.1014	0.0625	0.0625
θ_{14}	0	0	0.086	0.220	0	0.1631	0.1631	0.0604	0.0604
θ_{15}	0	0	-2.020	-1.589	0	-1.4688	-1.4688	-1.3068	-1.3068
θ_{23}	0	0	0.086	0.220	0	0.1631	0.1631	0.0604	0.0604
θ_{24}	0	0	0.093	-0.137	0	-0.1014	-0.1014	0.0625	0.0625
θ_{25}	0	0	-0.980	-0.680	0	-0.6071	-0.6071	-0.6342	-0.6342
θ_{34}	10	14	13.716	13.517	**6.2610**	**8.0144**	-0.2863	**7.7736**	-0.1609
θ_{35}	0	0	1.066	1.366	0	1.2193	1.2193	0.6894	0.6894
θ_{45}	0	0	-0.084	0.287	0	0.2655	0.2655	-0.0582	-0.0582
θ_{123}	0	0	-0.490	-0.530	0	-0.4604	-0.4604	-0.4223	-0.4223
θ_{124}	0	0	-1.010	-1.068	0	-0.9276	-0.9276	-0.8702	-0.8702
θ_{125}	0	0	0.043	-0.089	0	-0.0860	-0.0860	0.0383	0.0383
θ_{134}	0	0	-0.042	-0.130	0	-0.1174	-0.1174	-0.0372	-0.0372
θ_{135}	0	0	0.300	0.107	0	0.1039	0.1039	0.2470	0.2470
θ_{145}	0	0	-0.085	0.108	0	0.1044	0.1044	-0.0739	-0.0739
θ_{234}	0	0	0.533	0.493	0	0.4277	0.4277	0.4591	0.4591
θ_{235}	0	0	-0.085	0.108	0	0.1044	0.1044	-0.0739	-0.0739
θ_{245}	0	0	0.300	0.107	0	0.1039	0.1039	0.2470	0.2470
θ_{345}	0	0	0.043	-0.089	0	-0.0860	-0.0860	0.0383	0.0383

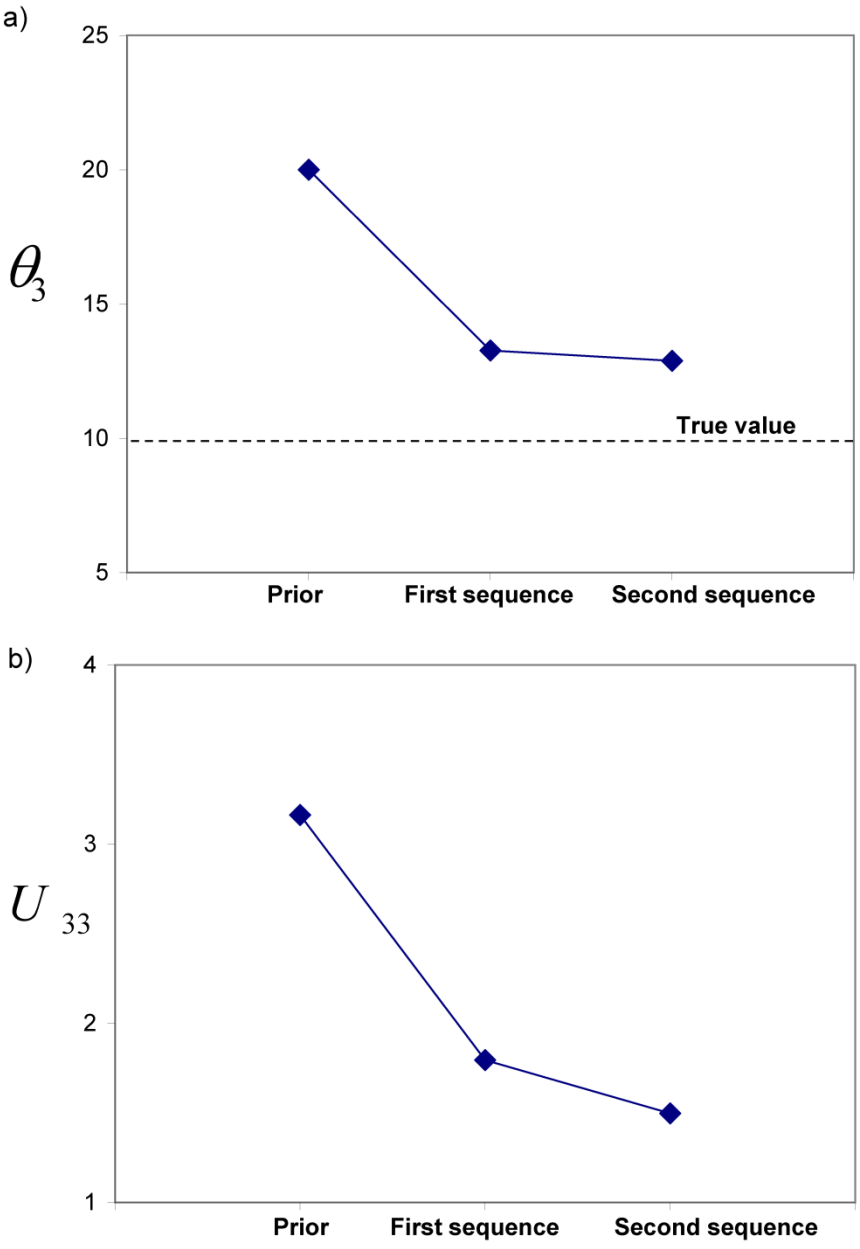

Figure 3.1 Evolution of mean of parameter 3 ($\boldsymbol{\theta_3}$) and the corresponding variance ($\boldsymbol{U_{33}}$) through the course of experimentation

Based on the results of test 1 (6th column of Table 3.7**)**, the significant parameters purely in the opinion of the "expert" (highlighted entries in Table 3.7 indicate a value greater than $|2|$) are θ_0, θ_1, θ_3, θ_4 and θ_{34}. The results of test 2 (7th column of Table 3.7**)** reveal that the actual

significant parameters, based on the new observations, are θ_0, θ_1, θ_3, θ_4, θ_{12} and θ_{34}. Finally, test 3 (8th column of Table 3.7) shows that the "expert's" opinion in the cases of θ_1, θ_3, θ_4 is questionable. The values of test 3 for θ_1 and θ_4 are arguably very close to $|2|$ but what is interesting is the result for θ_3. In the incorporation of prior knowledge stage, we had deliberately decided to give a very false initial value for θ_3 in order to check whether the Bayesian analysis can "spot" that. The result of test 3 indicates that the Bayesian design has indeed "spotted" this and identified that the expert's opinion is not valid about θ_3, yet another of the implicit advantages of the Bayesian design.

In fact, the results of tests 2 and 3 immediately after the first sequence of 8 trials (see columns 9 and 10 of Table 3.7) show that basically the same conclusions can be drawn from the diagnostic tests even after the first 8 trials. Hence, if one is interested solely in determining the relative importance of process factors (significant parameters), the first sequence of 8 trials is sufficient to address that. However, depending upon the intended target, if one is more focused on parameter estimation and on increasing parameter precision, then the second sequence of 4 trials is desirable in order to decrease parameter uncertainty (translated into lower parameter variances, vis á vis compare Table 3.4 and Table 3.6).

If a standard fractional factorial design was chosen to be carried out in this example (5 factors while being limited to only 12 runs), a ¼ fraction (8 experiments) would have been chosen. Another flexible trait of the Bayesian approach is that it allows one to easily run an experiment with a non-standard number of trials (for example, 12 runs, as in this example). This can only result in a more efficient use of resources, while providing acceptable parameter estimates.

Now that the basic details about the Bayesian design framework have been discussed in this chapter and implemented to a simple case study, the application of this technique to different case studies, drawn from various polymerization processes, will be presented in the next chapters and more light will be shed on its significant benefits over the standard design of experiments.

Chapter 4. Bayesian Design of Experiments Applied to Nitroxide-Mediated Radical Polymerization (NMRP)

After the development of the general framework for the Bayesian design of experiments (Chapter 3), the method was then used to design experiments for nitroxide-mediated radical polymerization (NMRP), in order to enhance our understanding of the important process characteristics. In this chapter, a brief background on NMRP is first presented, along with a summary of the modeling effort for NMRP of styrene. Then, various case studies are described which illustrate the significant benefits of the Bayesian design approach via its application to both bimolecular and unimolecular NMRP.

4.1 Brief Background on NMRP

In order to improve the performance of polymeric materials and broaden their application ranges, synthesis of polymers with controlled composition/molecular architecture (and for some specific applications, narrow molecular weight distribution) has become an attractive area in polymer research. Well defined polymeric materials with controlled microstructure (architecture) are accessible by controlled radical polymerizations (CRP). Its versatility and ability to produce novel polymer structures (block and gradient copolymers; star, comb, and hyperbranched architectures) are perhaps the main reasons for the increased academic (and potentially industrial) interest. The future for CRP seems bright, and it is anticipated that new products will be introduced in the market within the next several years (Rutsch and Cech, 2007).

There are several approaches to controlled radical polymerization. All of these approaches employ some sort of dynamic equilibrium between growing free/active radicals and various types of dormant species (see Figure 4.1). Nitroxide-mediated radical polymerization is one of the three most popular approaches towards CRP. Polymeric materials synthesized by NMRP have the potential for uses as coatings, adhesives, lubricants, gels, thermoplastic elastomers, as well as materials for biomedical applications (Matyjaszewski and Spanswick, 2005). The success of this technically simple approach can be related to the ability of stable nitroxide free radicals (X• in Figure 4.1) to react with the carbon-centered free radical of the growing

polymer chain end (R_n• in Figure 4.1), in a reversible process. This dramatically lowers the concentration of active (free) radicals in the polymerization system and, coupled with the inability of the nitroxide free radicals to initiate new chain growth, leads to controlled polymerization (Moad and Solomon, 2006).

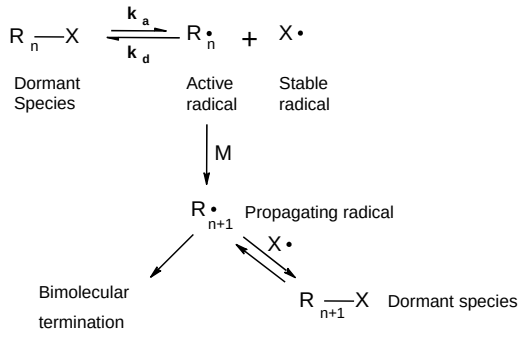

Figure 4.1 A general CRP equilibrium between dormant and active species

The main features of NMRP are:

i) Linear kinetic plot in semi-logarithmic coordinates (ln $[M]_0$/ [M] vs. time) for an isothermal batch reactor ($[M]_0$: concentration of monomer at time 0; [M]: concentration of monomer at time t). With instantaneous initiation and negligible termination, the total radical concentration remains (almost) constant during polymerization, and this results in a linear trend in ln $[M]_0$/ [M] vs. time, as shown in Figure 4.2. Curvature indicates deviation from the ideal situation caused by slow initiation, loss of radicals by termination, or other side reactions.

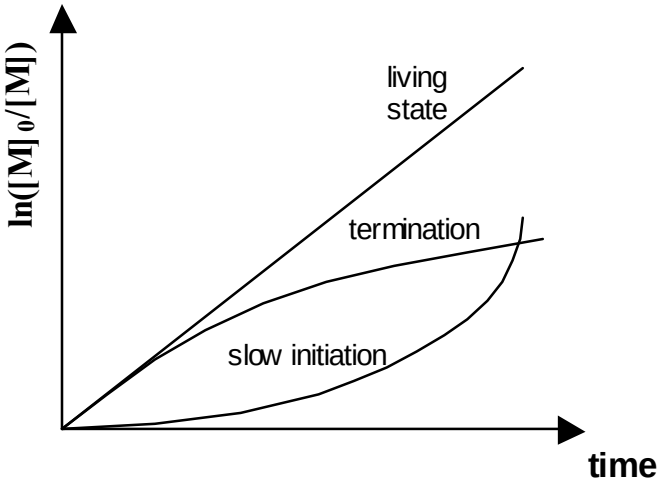

Figure 4.2 First order kinetic plot for NMRP

ii) Linear increase in average molecular weights with conversion. This is quite different from regular free radical polymerization (FRP), in which high molecular weights are produced right from the outset (see Figure 4.3). Ideally, NMRP produces polymers with degrees of polymerization (DP: number of monomer repeat units in a chain) predetermined by the ratio of the concentration of consumed monomer to the introduced initiator ($DP_n = \Delta[M]/ [I]_0$).

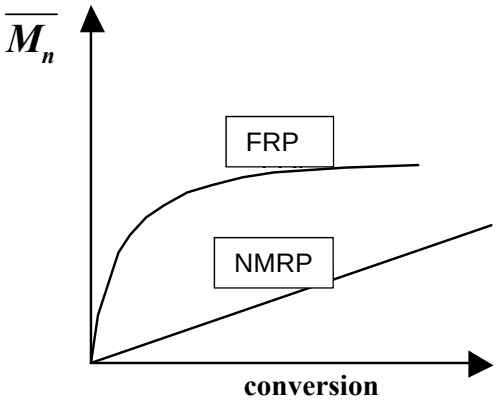

Figure 4.3 Comparison of the molecular weight behaviour vs. conversion for NMRP and FRP

iii) Low polydispersity values (PDI, the ratio of the weight-average to number-average molecular weight (M_w/M_n)), which results in narrow molecular weight distributions (MWD).

PDI values are typically in the range of 1.1 to 1.4, which are well below the lowest limit for FRP. Figure 4.4 (drawn from our experimental work) compares as an example size exclusion chromatography (SEC) data of polystyrene made by NMRP (Curve C) to polystyrene made by anionic polymerization (Curve B) and regular free radical polymerization (FRP; Curve A). As can be seen in Figure 4.4, the polystyrene made by NMRP has a much narrower MWD than the sample made by FRP and the MWD from this sample is very close to the one made by anionic polymerization (chromatography "standard").

iv) Having reactive polymer chain ends which allow the re-initiation of the polymerization.

In general, these characteristics are the prominent features of ionic polymerization. However, these features are now also accessible by the more robust and versatile radical polymerization (controlled radical polymerization), under less stringent conditions.

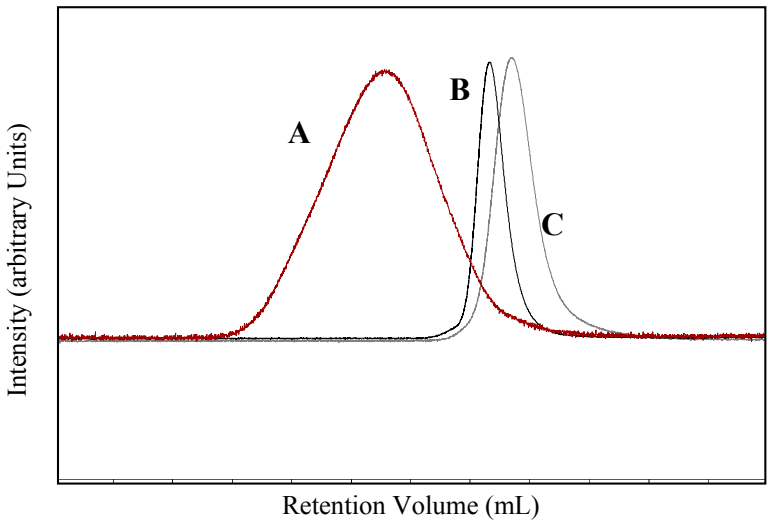

Figure 4.4 Size exclusion chromatographs of polystyrene samples. Curve A: polystyrene made by FRP (PDI= 2), Curve B: a SEC 'standard' polystyrene made by anionic polymerization (PDI = 1.1), Curve C: polystyrene made by NMRP (PDI = 1.2)

In NMRP, two initiating approaches can be used. In the first, a nitroxide radical (such as 2,2,6,6-tetramethyl-1-piperidinyloxy (TEMPO)), along with a primary free radical initiator such as benzoyl peroxide (BPO) or azobisisobutyronitrile (AIBN) are used as the initiation system. This approach is called bimolecular initiation. In this method, the initiator decomposes to primary radicals of high reactivity, which initiate the polymerization of monomer. The nitroxide radical then forms a labile bond (C–O) with the radical chain, leading to the formation of alkoxyamines in situ. The C–O bond is weak enough to reversibly dissociate at higher temperatures (for example, greater than 100°C for TEMPO), thus establishing the activation-deactivation equilibrium between dormant and active chains. Figure 4.5 illustrates the nitroxide radical polymerization of styrene through the bimolecular approach with TEMPO as nitroxide, and benzoyl peroxide as initiator. This approach was first used by Georges et al. (1993).

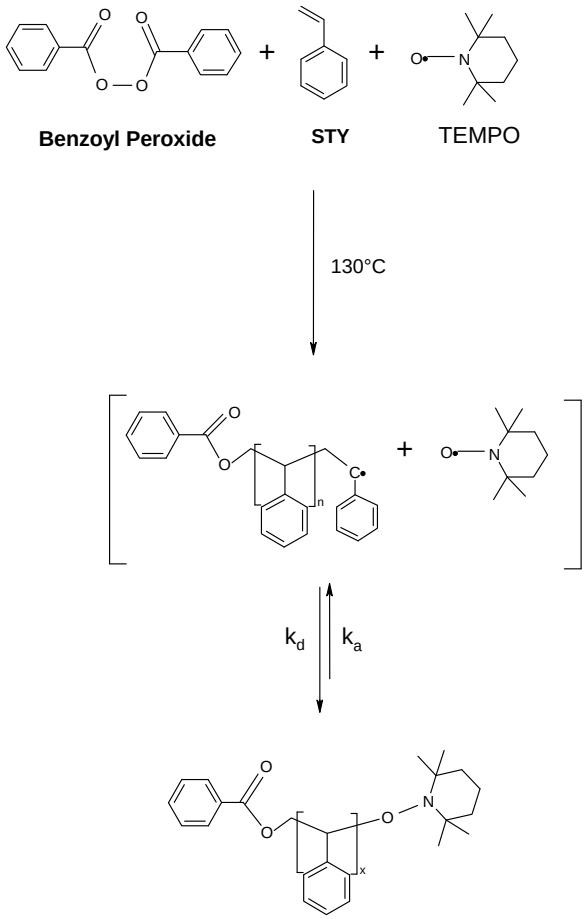

Figure 4.5 Bimolecular NMRP of styrene with TEMPO as the controller and benzoyl peroxide as initiator

The second option to NMRP is unimolecular initiation. This approach was first illustrated by Fukuda et al. (1996) and Greszta and Matyjaszewski (1996), almost at the same time. In the unimolecular NMRP, a single molecule initiator is used, which on dissociation generates two radicals. One of the radicals should be of high reactivity to initiate the polymerization, while the second one should be a low reactivity, stable nitroxide radical. The structure of these initiators is usually based on the alkoxyamine functionality. The C–O bond of the small-molecule alkoxyamine derivative is thermolytically unstable and decomposes on heating to give an initiating radical as well as the stable nitroxide radical. Following initiation the polymerization proceeds as described previously for the bimolecular case. Figure 4.6 shows the mechanism for the unimolecular NMRP of styrene using a TEMPO-based alkoxyamine.

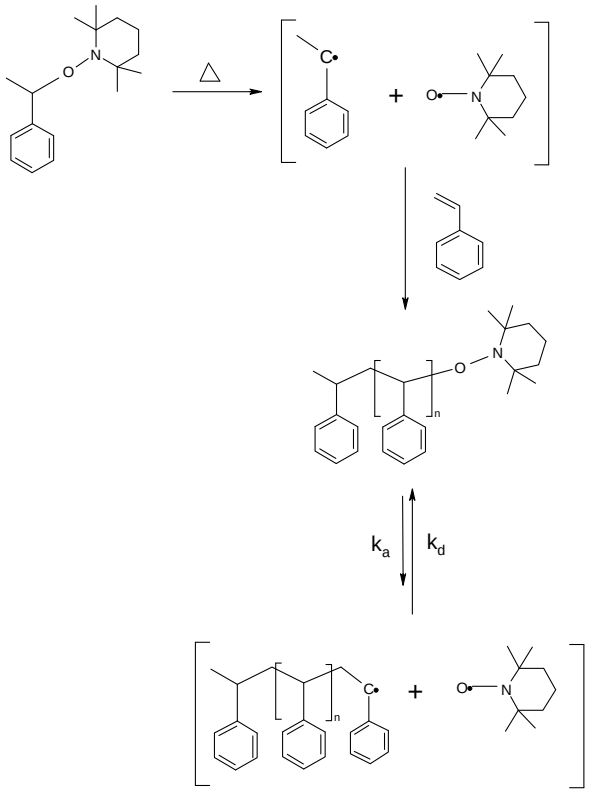

Figure 4.6 Unimolecular NMRP of styrene using a TEMPO-based alkoxyamine as the unimolecular initiator

NMRP was first discovered by Solomon et al. (1986), however, it received significant attention only after the influential work of Georges et al. (1993) on bimolecular NMRP, and subsequent work of Fukuda et al. (1996) and Greszta et al. (1996) on unimolecular NMRP. Since then, the literature on NMRP has developed in several directions. Representative examples of reviews on chemistry and mechanistic aspects can be found in the literature (Hawker et al., 2001; Fischer, 2003; Goto and Fukuda, 2004; Shipp, 2005; Braunecker and Matyjaszewski, 2007; Bertin et al., 2011; Grubbs, 2011). Although at first glance the NMRP seems relatively well-studied, there is still considerable amount of effort needed to better understand this system, from both a mechanistic point of view and also its use as a tool for the construction of useful new polymer architectures (Bertin et al., 2011; Grubbs, 2011).

Looking critically at the literature, one can make the following observations: i) Systematic modeling efforts are sporadic and, usually, very specific over a narrow experimental region/recipe. Parameter estimates are usually unreliable, as most of them are often guessed. ii) Detailed /reliable experimental results are still rare, and experimental runs are usually carried out in non-systematic ways (making the mathematical modeling stage even more complicated, with added uncertainties with respect to important parameter values). For instance, conversion vs. time data points reported in the past only capture the first few hours of the experiment and low to medium conversion, whereas average molecular weight data are usually not readily available and, if available, are presented at a limited number of conversion levels. In addition, checks for reproducibility and independent replication are almost non-existent. iii) Design of experiments and systematic, concerted approaches are lacking. Hardly any group has tried to combine the available information from both experimental observations and mathematical models in an experimental design scheme.

Essentially, these general observations are a confirmation that such a system would be readily amenable to (and could potentially benefit tremendously from) analysis using model-based experimental design schemes, namely a Bayesian approach. The development of the mathematical model for NMRP is briefly discussed in the next section, as this model is one of the “tools” used in the model-based Bayesian method.

4.2 Mathematical Modeling for NMRP of Styrene

The kinetic model for NMRP of styrene used is based on Bonilla et al. (2002) and the summary of the modeling effort presented here draws heavily from the work of Belincanta-Ximenes et al. (2007) and Roa-Luna et al. (2007b). The reaction mechanism used, as the basis for the derivation of the model, is summarized in Table 4.1. The model was based on mole balances for the main recipe ingredients. As an example, the mole balances for initiator, monomer, polymeric radicals and dead polymer species are shown in Eq. 4.1 to Eq. 4.4; for the list of all molar balances, refer to Belincanta et al. (2007). In order to track molecular weight development, the method of moments was used. Three polymer populations were considered in the system: polymer radicals, dead polymer, and dormant polymer. As shown by Roa-Luna et al. (2007a), diffusion-controlled (DC) effects did not influence the NMRP systems significantly, therefore, they were not considered in the model. Overall, the model consisted of 22 ordinary differential equations. All the kinetic rate constants were assumed to be independent of chain length and are cited in Table 4.2, presented as Arrhenius functions of activation energies and temperature.

$$\frac{d[I]}{dt} = -k_d[I] \qquad \text{Eq. 4.1}$$

$$\frac{d[M]}{dt} = -2k_{dim}[M]^2 - k_{ia}[M][D] - k_p[M]\left(\left[D^\bullet\right] + \left[M^\bullet\right] + \left[R_{in}^\bullet\right]\right) - k_p[M]\left[R^\bullet\right] - k_{fM}[M]\left[R^\bullet\right] + k_{decomp}[MNO_x] \qquad \text{Eq. 4.2}$$

$$\frac{d\left[R^\bullet\right]}{dt} = +k_p[M]\left(\left[M^\bullet\right] + \left[D^\bullet\right] + \left[R_{in}^\bullet\right]\right) - (k_{tc} + k_{td})\left(\left[R^\bullet\right]\right)^2 - k_{da}\left[NO_x^\bullet\right]\left[R^\bullet\right] + k_a\left[R_rNO_x\right] - k_{fM}\left[R^\bullet\right][M] - k_{fD}\left[R^\bullet\right][D] \qquad \text{Eq. 4.3}$$

$$\frac{d[P]}{dt} = +k_{fM}\left[R^\bullet\right][M] + k_{fD}\left[R^\bullet\right][D] + k_t\left[R^\bullet\right]^2 \qquad \text{Eq. 4.4}$$

Table 4.1 General mechanism for NMRP kinetics (Roa-Luna et al., 2007b)

Description	**Step**
Chemical initiation	$I \xrightarrow{k_d} 2R_{in}^{\bullet}$
Nitroxyl ether decomposition	$NO_E \underset{k_{d2}}{\overset{k_{a2}}{\leftarrow\!\!\rightarrow}} R_{in}^{\bullet} + NO_x^{\bullet}$
Mayo dimerization	$M + M \xrightarrow{k_{dim}} D$
Thermal initiation	$M + D \xrightarrow{k_{ia}} D^{\bullet} + M^{\bullet}$
First propagation (primary radicals)	$R_{in}^{\bullet} + M \xrightarrow{k_p} R_1^{\bullet}$
First propagation (monomeric radicals)	$M^{\bullet} + M \xrightarrow{k_p} R_1^{\bullet}$
First propagation (dimeric radicals)	$D^{\bullet} + M \xrightarrow{k_p} R_1^{\bullet}$
Propagation	$R_r^{\bullet} + M \xrightarrow{k_p} R_{r+1}^{\bullet}$
Dormant living exchange (monomeric alkoxyamine)	$M^{\bullet} + NO_x^{\bullet} \underset{k_{da}}{\overset{k_a}{\leftarrow\!\!\rightarrow}} MNO_x$
Dormant living exchange (polymeric alkoxyamine)	$R_r^{\bullet} + NO_x^{\bullet} \underset{k_{da}}{\overset{k_a}{\leftarrow\!\!\rightarrow}} R_r NO_x$
Alkoxyamine decomposition	$MNO_x \xrightarrow{k_{decomp}} M + HNO_x$
Rate enhancement reaction	$D + NO_x^{\bullet} \xrightarrow{k_{h3}} D^{\bullet} + HNO_x$
Termination by combination	$R_r^{\bullet} + R_s^{\bullet} \xrightarrow{k_{tc}} P_{r+s}$
Termination by disproportionation	$R_r^{\bullet} + R_s^{\bullet} \xrightarrow{k_{td}} P_r + P_s$
Transfer to monomer	$R_r^{\bullet} + M \xrightarrow{k_{fM}} P_r + M^{\bullet}$
Transfer to dimer	$R_r^{\bullet} + D \xrightarrow{k_{fD}} P_r + D^{\bullet}$

Table 4.2 Kinetic rate constants for the monomolecular and bimolecular NMRP processes (T [K] and R [cal mol^{-1} K^{-1}]) (Belincanta-Ximenes et al., 2007)

Variable	Unit	Bimolecular	Unimolecular
k_d(BPO)	s^{-1}	$1.7\times10^{15}\exp\left(-\frac{30000}{RT}\right)$	-
f_0		0.54-0.55 [a)]	-
k_{dim}	L mol^{-1} s^{-1}	$188.97\exp\left(-\frac{16185.1}{RT}\right)$	$188.97\exp\left(-\frac{16185.1}{RT}\right)$
k_{ia}	L mol^{-1} s^{-1}	$6.359\times10^{12}\exp\left(-\frac{36598.55}{RT}\right)$	$6.359\times10^{12}\exp\left(-\frac{36598.55}{RT}\right)$
k_{p0}	L mol^{-1} s^{-1}	$4.266\times10^{7}\exp\left(-\frac{7769.17}{RT}\right)$	$4.266\times10^{7}\exp\left(-\frac{7769.17}{RT}\right)$
k_{t0}	L mol^{-1} s^{-1}	$2.002\times10^{10}\exp\left(-\frac{3081.84}{RT}\right)$	$2.002\times10^{10}\exp\left(-\frac{3081.84}{RT}\right)$
k_{td}/k_{t0}		0.0	0.0
k_{fM}	L mol^{-1} s^{-1}	$9.376\times10^{6}\exp\left(-\frac{13372}{RT}\right)$	$9.376\times10^{6}\exp\left(-\frac{13372}{RT}\right)$
k_{fD}	L mol^{-1} s^{-1}	50	50
k_{a2}	s^{-1}	0.0	$2.0\times10^{13}\exp\left(-\frac{29683}{RT}\right)$
k_{d2}	L mol^{-1} s^{-1}	0.0	$5.03\times10^{9}\exp\left(-\frac{3722}{RT}\right)$
k_{da}	L mol^{-1} s^{-1}	$5.03\times10^{9}\exp\left(-\frac{3722}{RT}\right)$	$5.03\times10^{9}\exp\left(-\frac{3722}{RT}\right)$
k_a	s^{-1}	$2.0\times10^{13}\exp\left(-\frac{29683}{RT}\right)$	$2.0\times10^{13}\exp\left(-\frac{29683}{RT}\right)$
k_{decomp}	s^{-1}	$5.7\times10^{14}\exp\left(-\frac{36639.6}{RT}\right)$	$5.7\times10^{14}\exp\left(-\frac{36639.6}{RT}\right)$
k_{h3}	L mol^{-1} s^{-1}	0.001	0.001

[a)] Initiator efficiency (f) range depending on reaction temperature.

A comparison between model predictions and experimental data for conversion, number-average molecular weights and polydispersity values are shown in Figure 4.7, Figure 4.8, and Figure 4.9, respectively. As can be seen, the model predicts the general trends perfectly. The agreement between model predictions and experimental data is fairly good for conversion and

polydispersity values, however, the model underpredicts the experimental data for number-average molecular weights.

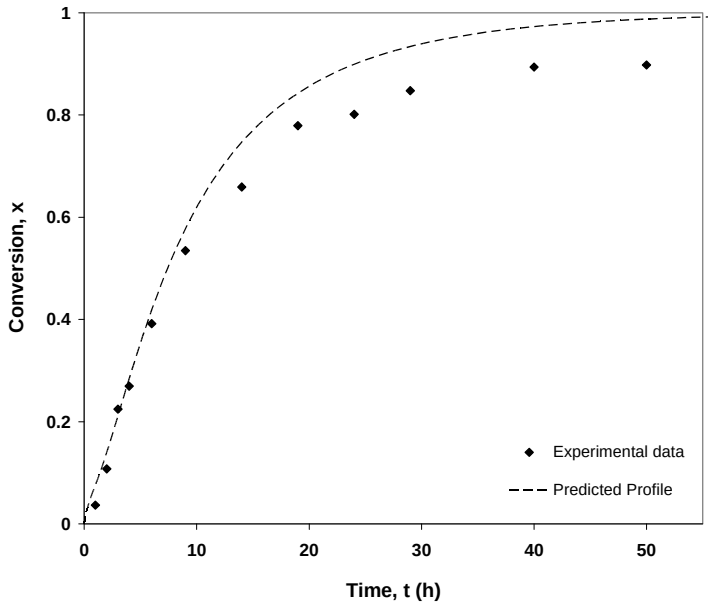

Figure 4.7 Comparison of experimental data and model predictions for conversion vs. time, at 120 °C and [TEMPO]/[BPO] = 1.1

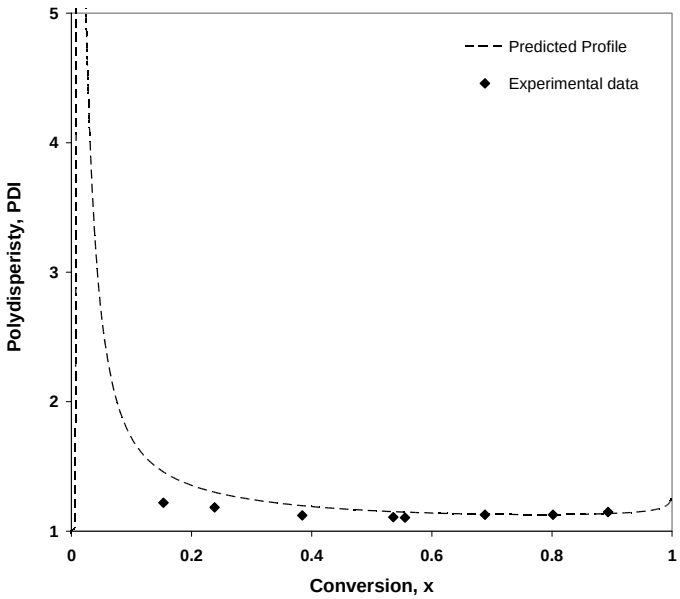

Figure 4.8 Comparison of experimental data and model predictions for polydispersity vs. conversion, at 120 °C and [TEMPO]/[BPO] = 1.1

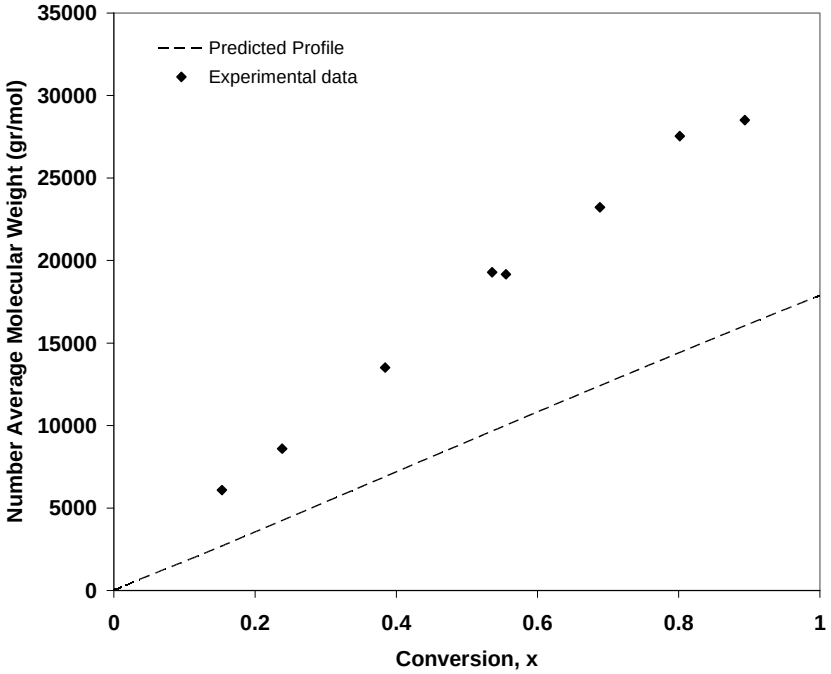

Figure 4.9 Comparison of experimental data and model predictions for number-average molecular weight vs. conversion, at 120 °C and [TEMPO]/[BPO] = 1.1

The model was also capable of simulating concentrations of intermediate species like nitroxyl radicals, dead, dormant and living species. This was extremely useful, as it offered additional insight in the polymerization behavior, and was used in formulating viable explanations for the behavior of many variables. As an example, Figure 4.10 shows the simulated profiles for nitroxyl radicals, active radicals, dormant species, and dead polymer versus conversion for different [TEMPO]/[BPO] ratios at 120°C; in this figure, R stands for [TEMPO]/ [BPO] molar ratio.

As illustrated in this section, the mathematical model already developed for NMRP of styrene looks quite reasonable and the predicted profiles for different responses were in satisfactory agreement with experimental data. This model was a good starting point and, since in principle the mechanistic model contained a good deal of prior information about the process, it could be employed in the Bayesian model-based design scheme.

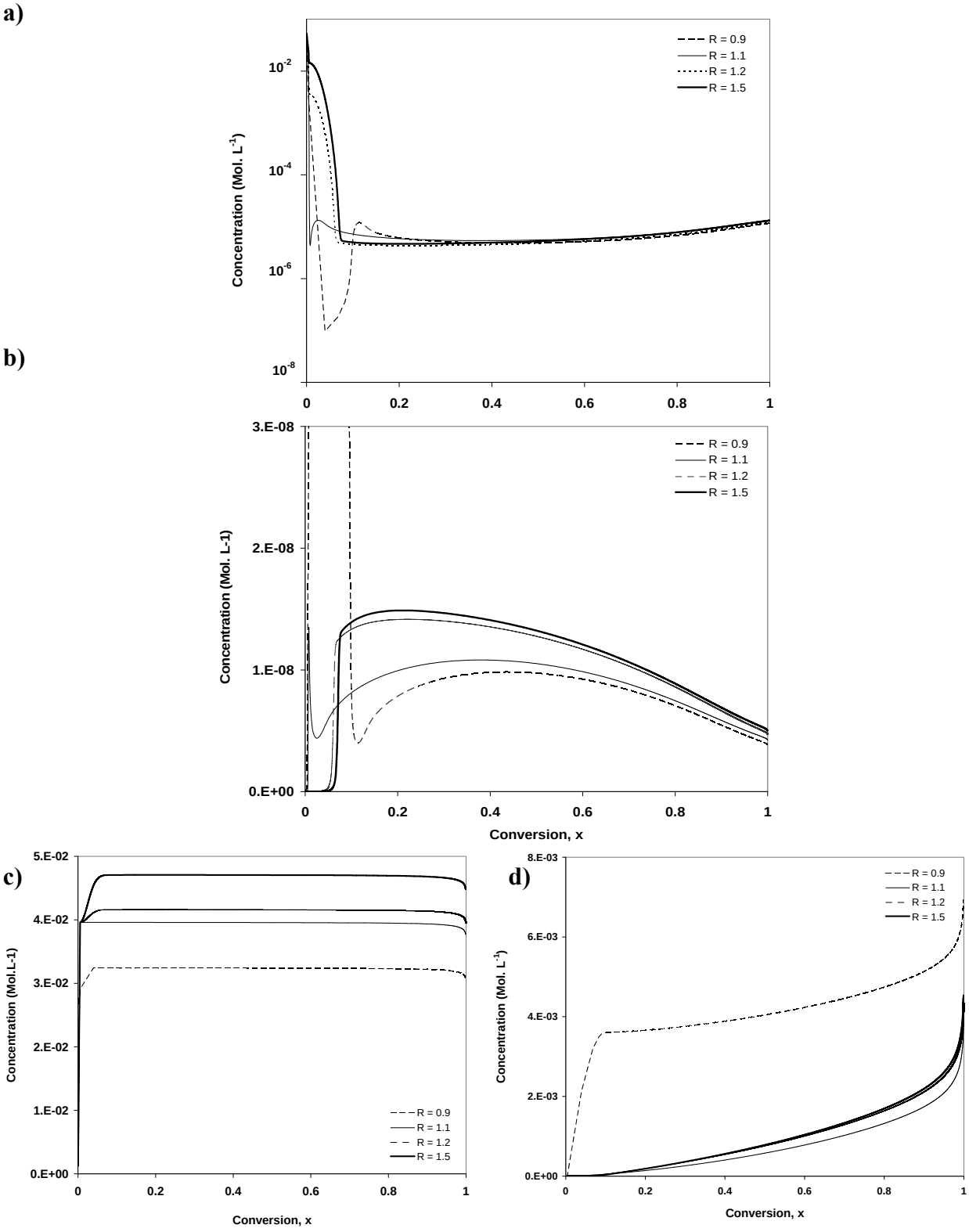

Figure 4.10 Effect of [TEMPO]/[BPO] on simulated profiles of a) nitroxyl radicals, b) active radicals, c) dormant species, and d) dead polymer for NMRP of styrene at 120°C

4.3 Results and Discussion: Case Studies with Bayesian Design in NMRP

The Bayesian design of experiments is now implemented to controlled radical polymerization (CRP) and more specifically to the nitroxide-mediated radical polymerization (NMRP) of styrene, as a first example of a complex polymerization process. The case studies drawn from both bimolecular (Case Studies 1 to 4) and unimolecular NMRP (Case Studies 5 and 6) are presented herein in order to demonstrate some of the many benefits of Bayesian methodology, outlined in Table 2.2 (see section 2.3 in Chapter 2).

4.3.1 Case Study 1: Design of Two Optimal Experiments

To demonstrate how the Bayesian approach works, two experiments were initially designed in Case Study 1. In this case study the Bayesian method was implemented to bimolecular NMRP.

Selection of Design Factors and Levels: As mentioned previously in Table 3.1, the first step in implementing the Bayesian design of experiments is choosing the design factors and their levels. Three factors have been chosen and are shown (with their initial levels) in Table 4.3.

Table 4.3 Selected factors and their levels (bimolecular NMRP)*

Ingredient	Amount (Low)	Amount (High)
T (°C)	120 °C	130 °C
$[I]_0$ (M)	0.036	0.072
$[N]_0$ (M)	0.058	0.086

* T = temperature, $[I]_0$ = initial initiator concentration, $[N]_0$ = initial nitroxide concentration

The selection of factors and their low and high level values were based on a detailed and critical analysis of the literature (Veregin et al., 1995; Veregin et al., 1996a, b; Goto and Fukuda, 1997b; Zhang and Ray, 2002), combined with some of our previous experience about bimolecular NMRP (Roa-Luna et al., 2007; Nabifar et al., 2008). In the case of temperature, low and high levels chosen were 120 and 130 °C because values of kinetic rate constants were readily available for these two temperatures. However, later in this chapter (see case study 3), results for an expanded range are also presented (e.g., low level: 110 °C and high level: 140 °C), in order to illustrate how the Bayesian design scheme can easily accommodate an expanded factor range, if so desired. 1 wt% (with respect to monomer) was chosen for the low

level values of both initiator and nitroxide; for the high level value of initiator, 2 wt% was chosen. It was decided not to select 2 wt% for the high level of nitroxide since the nitroxide would act as inhibitor instead of mediator with this amount (0.116 M). Investigating the literature (Goto and Fukuda, 1997a), it was found that the system would still act as a controlled polymerization if 0.086 M nitroxide was added to 2 wt% (0.072M) of initiator. A two-level design was chosen in order to reduce the number of experiments and also to have a simpler case for step-by-step demonstration purposes.

Selection of Response(s): There are no restrictions on the number of responses that can be chosen in the Bayesian design technique. For example, Dube et al. (1996) looked at applications of Bayesian design to emulsion terpolymerization having four responses, while Vivaldo-Lima et al. (2006) implemented the Bayesian design to suspension copolymerization with two responses. In this case study, the Bayesian design was implemented to a single response. Application of the approach to case studies with multiple responses is going to be discussed in Case Study 5 and also in later chapters. Reaction time or batch time (in hrs) to reach 75% conversion was chosen as the single response. The reason that batch time (the time needed to reach a specific conversion level) was picked as the response first is that it is one of the most important features in any polymerization process and it is usually desirable to minimize it, especially in the case of CRP/NMRP. It was chosen to measure the batch time at the 75% conversion level because based on experience with the NMRP of styrene (Roa-Luna et al., 2007; Nabifar et al., 2008), usually after this point there was a plateau in the profiles of conversion vs. time. In addition, at higher conversion levels (>80%), the profiles of conversion vs. time for different operating conditions usually overlapped.

The variance of the batch time response was calculated from previous sets of experiments (Roa-Luna et al., 2007; Nabifar et al., 2008). It was felt (based on process information and experience) that due to various sources of error in the experiments such as sampling error, evaporation of ingredients, conversion measurement error, etc., the time for a batch to reach 75% conversion would vary by ± 1 hr about 95% of the time, thus, the variance was $\sigma^2 = 1$.

Incorporation of Prior Knowledge: Having chosen the factors (and their levels) and the response(s) of interest, casting prior information into the vector $\underline{\alpha}$ and the matrix $\underline{U}$ was the

next step (see Table 3.1). $\underline{\alpha}$, the vector of the parameter means, and $\underline{U}$, the matrix of the variance/covariance of the means, can be considered as the storehouse of prior knowledge. Prior knowledge can have different shapes and forms; in this case study, to generate the prior information about the parameters and the variances of the effects, the general mechanistic model developed for bimolecular NMRP (discussed in section 4.2) was used to obtain the responses for a 2^3 conventional factorial design (8 trials). As explained in section 4.2, this model was a good starting point because in principle a mechanistic model contains a good deal of prior information (by definition) about the process in question. The computer simulations were run and the corresponding responses were recorded for each of the $2^3 = 8$ trials. $\underline{\alpha}$ (the vector of parameter means) was obtained by performing linear regression on the data and is shown in the second column of Table 4.4.

The parameters were then multiplied by 2 (except for the mean) to represent the effect of going from the low level to the high level of the design factor. In order to determine the variances of the effects, each effect was then examined separately and, based on our knowledge of the process, a 'guess' of the maximum/minimum value of the effect was made. This stage was where most of the brainstorming takes place. In the cases where the parameter was considered to be well known, a smaller interval of uncertainty was given, i.e., a smaller fluctuation about the mean was tolerated. The difference between the effect and its maximum or minimum was taken to be 2σ on a normal distribution curve. Dividing this value by 2 and squaring it gave the variance of the effect. Recognizing that the parameters were multiplied by 2 to give the effects, dividing the variances of the effects by 4 gave the diagonal elements of the prior variance/covariance matrix ($\underline{U}$), which are shown in the last column of Table 4.4. The off-diagonal elements were initially all set to zero.

For more clarity, an example is now given on how prior variances were calculated. Consider the case of the effect of temperature on batch time. As shown in Table 4.4, the value obtained from the 2^3 standard factorial design of experiments (using the mechanistic model) for the parameter was -5.129. Multiplying the parameter by 2 gave the effect of going from the low temperature level to the high level (i.e., -10.258). Assuming a normal distribution for the effect, it was decided that the effect could vary from -12.258 to -8.258 (that is, ± 2 hrs, in a worst case scenario) about 95% of the time. In other words, $2\sigma = 2$ and $\sigma^2 = 1$. As mentioned

above, this was the variance of the effect, so in order to obtain the variance of the parameter, the variance of the effect (σ^2= 1) was divided by 4. Thus, the diagonal element of the prior variance/covariance matrix, $\underline{U}$, was $U_2 = 0.25$, as shown in Table 4.4.

Table 4.4 Elements of prior $\underline{\alpha}$ and $\underline{U}$ for batch time

Effect	α_i	U_i
Mean	11.346	0.01
T	-5.129	0.25
[I]	-0.563	0.0625
[N]	0.079	0.0443
T×[I]	0.251	0.0039
T×[N]	-0.107	0.0056
[I]×[N]	0.032	0.0625
T× [I]×[N]	-0.043	0.0156

Selection of Experimental Designs: As mentioned in section 3.1, the basic idea for the design of experiments was to choose the set of conditions ($\underline{X}$) in order to maximize the determinant H (see Eq. 3.5 in chapter 3). Following the metric for designing experiments, four 2-trial experiments were found that corresponded to a maximized H (H = 2.106); the results, showing the level of each factor are shown in Table 4.5. An interesting point to notice in this table was that all sets of 2-trials chosen by the Bayesian design followed a similar pattern. For example, if we look at set # 1, the first trial was chosen with all factors at the low level; the second run was suggesting to keep the same settings and just change the temperature level from low to high. In a similar way, for instance with set # 3, the first experiment was chosen with temperature and nitroxide set at low level while the initiator concentration was at high level. The second trial was suggesting the same settings but again changing the temperature level from low to high. Overall, in all the 2-trial sets, the only factor that was changing sign, when going from the first to the second suggested run, was temperature. Checking the last column of Table 4.4 (remembering that it shows the diagonal elements of $\underline{U}$), one can see that the largest variance belongs to temperature (U_2 = 0.25). Hence, in a logical way, the Bayesian methodology was assigning more importance to temperature and choosing to change its sign (level) only.

Table 4.5 Four possible 2-trial experiments in Case Study 1

No.	T	$[I]_0$	$[N]_0$
1	-1	-1	-1
	1	-1	-1
2	-1	-1	1
	1	-1	1
3	-1	1	-1
	1	1	-1
4	-1	1	1
	1	1	1

Now to verify this pattern, let's assume that more importance was allocated to nitroxide concentration, by assigning a variance of 0.25 to it (Table 4.6 shows the corresponding U matrix). The experiments suggested by the Bayesian design (Table 4.7) were different. The pattern in all these 2-trial experiments was to keep the temperature and initiator concentration constant and change the sign of nitroxide concentration only. In conclusion, the Bayesian design considers the experimenter's prior knowledge about the system; if more knowledge is available about a specific parameter before the experiment, a smaller initial variance for that parameter is assigned. If, on the other hand, it is desired to find out more information about a specific parameter, higher initial variances can be allocated in the U matrix.

Table 4.6 Alternative prior U for batch time

Effect	$\mathbf{U_i}$
Mean	0.01
T	0.0443
[I]	0.0625
[N]	0.25
T×[I]	0.0625
T×[N]	0.0056
[I]×[N]	0.0039
T× [I]×[N]	0.0156

Table 4.7 Four possible 2-trial experiments (with altered U)

No.	T	$[I]_0$	$[N]_0$
1	1	-1	-1
	1	-1	1
2	-1	-1	1
	-1	-1	-1
3	-1	1	-1
	-1	1	1
4	-1	1	1
	-1	1	-1

Now, going back to our initial case, since all of the four 2-trial experiments of Table 4.5 yielded the same H, one of them was chosen randomly (say, set # 3). The corresponding visual illustration of the design is shown in Figure 4.11. As can be seen in Trial 1, the suggestion was to run an experiment at 120 °C, with initiator concentration of 0.072 M and nitroxide concentration of 0.058 M. The initiator and nitroxide concentrations for Trial 2 were the same as in Trial 1 (0.072 and 0.058 M, respectively), but the suggestion was to change the temperature to 130 °C.

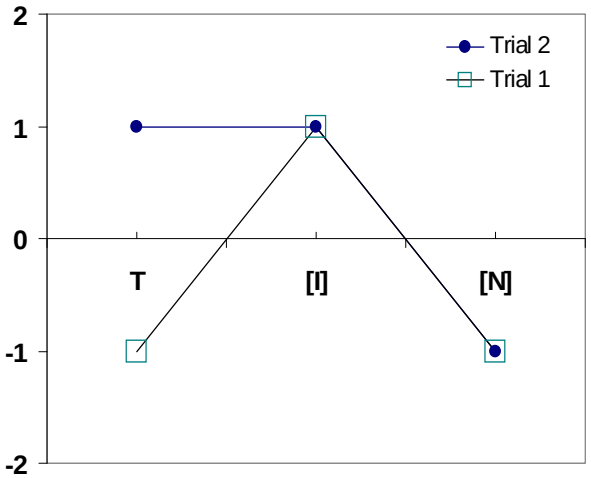

Figure 4.11 Visual illustration of the 2-trial experiment chosen for Case Study 1

As shown in Table 3.1, the next step in the Bayesian design framework is to update the posterior vector of the parameters ($\underline{\theta}$) and the (updated) posterior variance/covariance matrix ($\underline{U}$). Eq. 3.6 was employed to calculate $\underline{\theta}$ (shown in Table 4.8), using the prior vector of parameter means ($\underline{\alpha}$) and the prior $\underline{U}$s (both shown in Table 4.4), along with the responses $\underline{y}$ (also reported in the last two lines of Table 4.8) and the $\underline{X}$ matrix (set # 3 in Table 4.5). Comparing Table 4.4 and Table 4.8, one can see that initiator concentration, nitroxide concentration and the interaction between initiator and nitroxide were the only parameter coefficients that have changed significantly. Eq. 3.7 can then be used to obtain the posterior variance/covariance matrix ($\underline{U}$); the results are shown in Table 4.9. One can now observe the presence of non-zero off-diagonal elements in the (updated) posterior variance/covariance matrix. This updated $\underline{U}$ can now be used back in Eq. 3.5 to design (in an iterative sequential fashion) the next set of experiments (results shown in Case Study 2).

Table 4.8 Posterior vector of parameters for Case Study 1

Parameter Coefficient	$\theta_i^{1\dagger}$ *for batch time*
Mean	11.360
T	-5.129
[I]	-0.470
[N]	0.0137
T×[I]	0.251
T×[N]	-0.107
[I]×[N]	-0.060
T× [I]×[N]	-0.043
Batch time response (hr)- Trial 1	16.40
Batch time response (hr)- Trial 2	6.94

† θ_i^1 is the updated vector of parameter means after the first sequence

Table 4.9 Posterior variance/covariance matrix, U, for Case Study 1

0.009853	0	-0.00092	0.000652	0	0	0.00092	0
0	0.169371	0	0	-0.00126	0.001814	0	0.005039
-0.00092	0	0.05675	0.004077	0	0	0.00575	0
0.000652	0	0.004077	0.04142	0	0	-0.00408	0
0	-0.00126	0	0	0.003887	2.83E-05	0	7.87E-05
0	0.001814	0	0	2.83E-05	0.005584	0	-0.00011
0.00092	0	0.00575	-0.00408	0	0	0.05675	0
0	0.005039	0	0	7.87E-05	-0.00011	0	0.01531

4.3.2 Case Study 2: Design of Four Optimal Experiments (n-trial Experiments vs. Sequences of Fewer Trials)

The "chronology" of events to design four optimal experiments for bimolecular NMRP still with batch time as response is documented in Case Study 2. This case study is connected to Case Study 1, hence the factors chosen and their levels are as in Table 4.3. The "*sequential approach*" looked at two sequences of 2-trials each. The first sequence of 2-trials was the one designed in Case Study 1 (see set # 3 in Table 4.5). In Case Study 2, the updated $\underline{\theta}$ and the posterior $\underline{U}$ from the first sequence (reported in Case Study 1; see Table 4.8 and Table 4.9) were then used to arrive at the second sequence of 2-trials. This approach was contrasted to the design of a "*single 4-trial experiment",* in which four experiments were designed at once. For further illustration purposes, the results from these two variations of Bayesian design were compared to the corresponding 4-trial experiment designed through a conventional fractional factorial design.

Sequential approach (two sequences of 2-trials each): As explained in Table 3.1, the updated $\underline{U}$ after the first sequence is used as the prior $\underline{U}$ in Eq. 3.5, to design the set of experiments for the second sequence. Here, the 2-trial experiment chosen in Case Study 1 (set # 3 in Table 4.5) was picked as the first sequence of the experimentation (visual illustration in Figure 4.11). Then, the updated $\underline{U}$ matrix (shown in Table 4.9) was used in Eq. 3.5 to design the second sequence of 2-trials. The only 2-trial run that gave the highest H is illustrated in Figure 4.12 (with H = 1.9114). Contrasting with Figure 4.11, one can see that the Bayesian design is suggesting to run both trials at the high levels of initiator and nitroxide (0.072 and 0.086M) and just change the temperature from low to high.

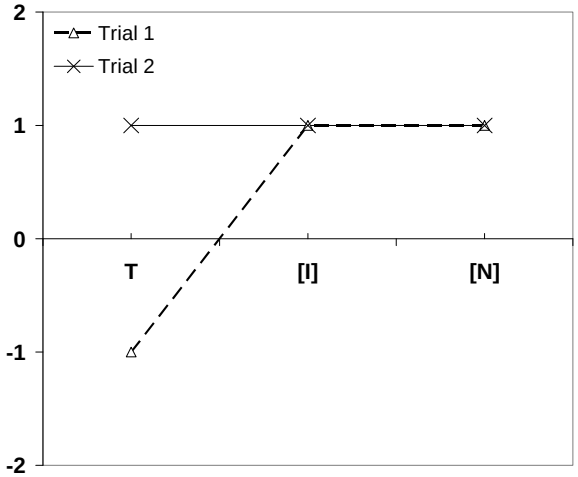

Figure 4.12 Illustration of the second sequence of 2-trials (Case Study 2)

The decision to use the sequential approach (run two sequences of 2-trials each), instead of running a single 4-trial sequence, was made to accommodate cases where the experimenter might not be certain that the chosen factor levels were the most adequate. However, the sequential approach may not necessarily yield the "optimum" choice (highest H) (Dube et al., 1996; Omidbakhsh et al., 2010). In order to check and confirm this, in the next attempt, a single 4-trial experiment was designed and the results were compared with the corresponding sequential approach.

Single 4-trial experiment: In this approach, the prior $\underline{\alpha}$ and prior $\underline{U}$ (from Table 4.4) were used directly to design four experiments at once. The Bayesian design suggested two sets of 4-trial experiments, shown in Table 4.10. For comparison purposes, the two sequences of 2-trials (i.e., a total of four trials) designed through the sequential approach are also cited along with the corresponding H value (see Figure 4.13 for the corresponding illustrations). Comparing the H values one can see that both single 4-trial experiments were only slightly better than the sequential approach. Keeping in mind the flexibility that the sequential approach offers (e.g., changing the level of factors, adding/dropping factors, etc.) and due to the fact that the single 4-trial approach was not producing a significantly higher H value, the sequential approach was deemed a better way of designing a total of four runs.

Table 4.10 Two possible sets of 4-trial experiments along with the four trials of the "sequential approach" (Case Study 2)

No.	T	$[I]_0$	$[N]_0$	H-value
1	-1	-1	-1	4.065
	-1	-1	1	
	-1	1	-1	
	-1	1	1	
2	1	-1	-1	4.065
	1	-1	1	
	1	1	-1	
	1	1	1	
Sequential Approach	-1	1	-1	4.026
	1	1	-1	
	-1	1	1	
	1	1	1	

Figure 4.13 illustrates our options in a clearer way; as can be seen, experiments 1 and 2 (Figure 4.13a and Figure 4.13b, chosen by the single 4-trial strategy) are "mirror" images of each other with respect to factor T. In each of these single 4-trial experiments, the level of temperature was kept constant in all trials (in Figure 4.13a at the low and in Figure 4.13b at the high level), while the levels for [I] and [N] were changing. In the sequential approach (Figure 4.13c) on the other hand, the levels of T and [N] were changing, while [I] was set at the high level. Based on our U matrix (see again Table 4.4), and due to the fact that temperature had the highest variance, changing the temperature level seemed like the appropriate thing to do in order to reveal more information about the T factor.

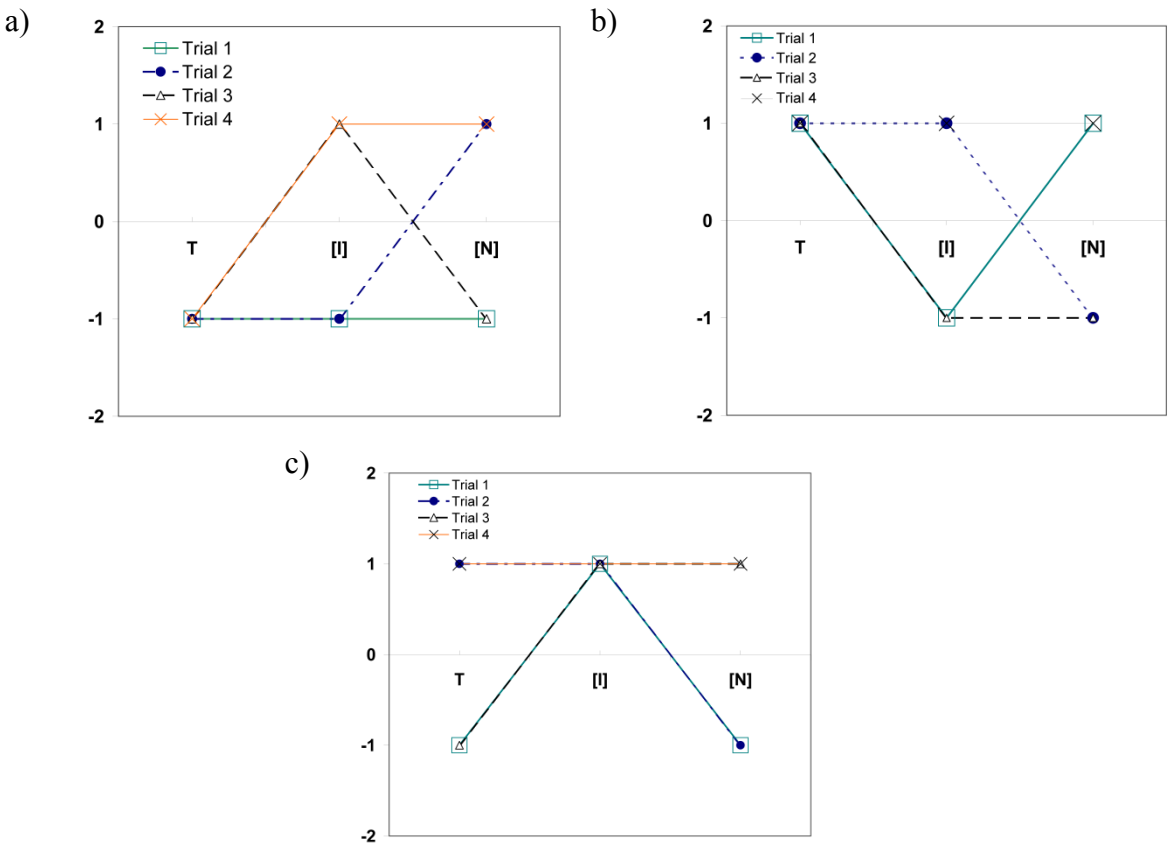

Figure 4.13 Illustration of 4-trial experiments in Case Study 2, a) first single 4-trial experiment, b) second single 4-trial experiment, c) two sequences of 2-trials

Comparison with standard fractional factorial design: Several qualitative statements were made in section 2.2, regarding the superiority of the Bayesian design with respect to the standard factorial designs. A quantitative measure is now presented in order to reinforce the previous statements. Recall that the algorithm used to find the "best" design in the Bayesian framework attempts to maximize the determinant H (see Eq. 3.5 section 3.1), hence, a design with the highest value of determinant H is recognized as the "optimal" one. The two half-fractions recommended by a regular fractional factorial design are shown in Table 4.11 along with their H values. It can be seen that in all cases, the experiments designed through the Bayesian approach were better than the ones designed through fractional factorials (compare the H values of Table 4.10 and Table 4.11). Hence, H calculations showed that Bayesian-designed experiments were superior in the D-optimal sense.

Table 4.11 Two half-fractions from standard fractional factorial design (Case Study 2)

No.	T	$[I]_0$	$[N]_0$	H-value
1	-1	-1	1	3.884
	1	-1	-1	
	-1	1	-1	
	1	1	1	
2	-1	-1	-1	3.765
	1	-1	1	
	-1	1	1	
	1	1	-1	

The corresponding plot for the fraction of Table 4.11 with higher H is shown in Figure 4.14. As can be seen, the 4-trial experiment chosen by the fractional factorial design was completely balanced with respect to all factors (the levels of all factors are changing). Altering the levels of all factors is desirable if there was no knowledge available prior to the experiment and the experimenter wanted to find information about all factors. However, if one is more interested in the effect of, say, one or two factors only, changing the level of all factors at the same time is superfluous. The 4-trial experiment suggested by the fractional factorial could be a special case in the Bayesian design when the variances of all the effects are equally high (non-informative prior) or equally low (informative prior). In that scenario the Bayesian design will allocate equal importance to all of the factors and alter the levels for all.

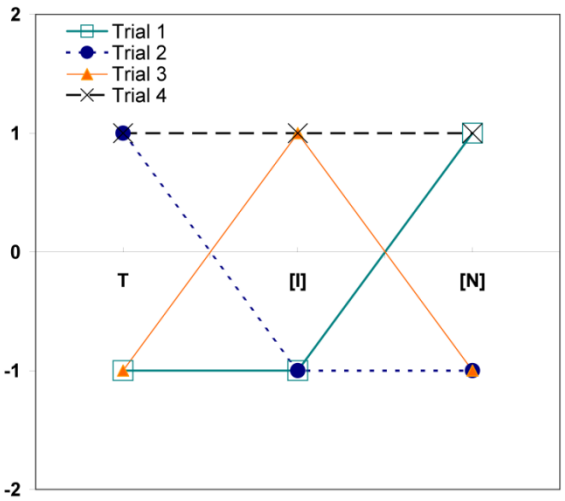

Figure 4.14 Illustration of 4-trial experiment suggested by fractional factorial design (Case Study 2)

4.3.3 Case Study 3: Expanding the Range of a Factor after the First Sequence

This case study demonstrates yet another advantage of the Bayesian design which is flexibility to change the factor levels in the middle of experimentation. Let's assume that after designing the first 2-trial sequence with the low and high temperature levels at 120 and 130 °C (see Case Study 1), the experimenter decides to change the temperature levels to 110 and 140 °C in the second sequence in order to expand the range of temperature. While impossible to do so in (fractional) factorial designs, it is shown here that using the Bayesian design approach one can accommodate the change in temperature range following fairly straightforward steps (the same steps can be taken if the range of more factors is changed). This case study is again in a way connected to Case Study 1, where the Bayesian design approach was implemented on to the bimolecular NMRP, with batch time as the single response. Table 4.3 summarizes the selected factors; the levels for all factors are the same, except for temperature, as explained above.

Due to the expanded range, the coding for the temperature levels in the first sequence had to be changed (from the original -1 and +1). Based on the new coding system (110 °C assigned to low level (-1) and 140 to high level (+1)), the design levels for the first sequence of experiments (set # 3 in Table 4.4) were revised and are shown in Table 4.12.

Table 4.12 Sequence 1: Revised coding of factor levels in Case Study 3

T	$[I]_0$	$[N]_0$
-0.33	1	-1
0.33	1	-1

Since the range between high and low levels was changed, other revisions were necessary. Initially, the difference was 130 - 120 =10 °C but after the modification, the difference is 140 – 110 = 30 °C. This change affected the values of the prior parameters (second column, Table 4.4), as well as the prior variances (elements of the $\underline{U}$ matrix; third column, Table 4.4). Thus, the values for the prior parameters and variances had to be modified; the updated Table 4.4 is shown in Table 4.13.

Table 4.13 Updated elements of initial $\underline{\alpha}$ and $\underline{U}$ for Case Study 3

Effect	$\boldsymbol{\alpha_i}$	$\mathbf{U_i}$
Mean	11.346	0.01
T	-15.387	7.562
[I]	-0.563	0.078
[N]	0.079	0.04
T×[I]	0.754	0.25
T×[N]	-0.321	0.0625
[I]×[N]	0.032	0.000225
T× [I]×[N]	-0.129	0.0025

Among the changes to adjust for the expanded temperature range, the $\underline{U}_{posterior}$ matrix (calculated after the first sequence) had to be updated using Eq. 3.7 (see section 3.1). The corresponding $\underline{X}$ matrix to be used in this equation included the design levels shown in Table 4.12; the corresponding prior $\underline{U}$ was a diagonal matrix with diagonal elements shown in the last column of Table 4.13. The updated $\underline{U}_{posterior}$ (not shown here for the sake of brevity) was then used in the design generating program to find the next "best" 2-trial sequence following the same procedure as for the first sequence, that is, to find designs that were optimal by comparing values of the determinant H. Two 2-trial sequences were found that had the highest H, shown in Table 4.14.

Table 4.14 2-trial experiments suggested in sequence 2 (expanded rage)

No.	**T**	$\mathbf{[I]_0}$	$\mathbf{[N]_0}$
1	-1	-1	-1
	1	-1	-1
2	-1	1	1
	1	1	1

One of the sets in Table 4.14 was chosen randomly and its visual illustration is given in Figure 4.15, along with the trials from the first sequence. The change in coding of the temperature levels after the first sequence resulted in temperature attaining more than two levels (i.e., effectively "exposed" more process information which leads naturally to studying nonlinearities!). Again, the flexibility to allow changes of the levels of the factors

with relative ease is another advantage of the Bayesian design that is not easily achieved in conventional factorial designs.

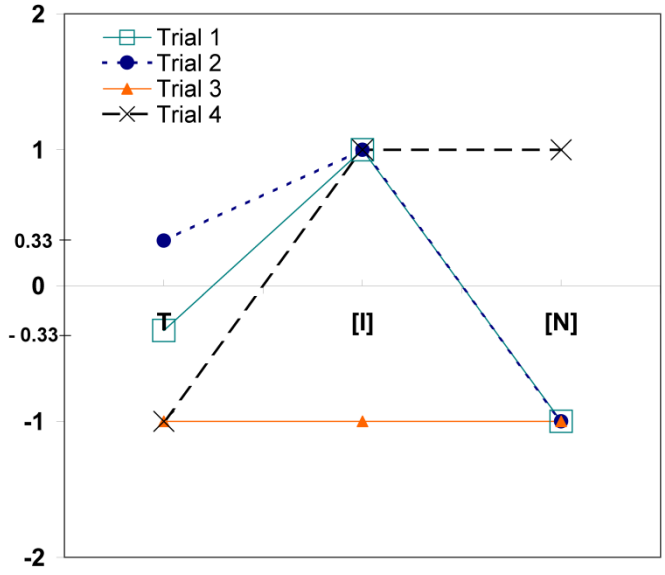

Figure 4.15 Illustration of the two sequences of 2-trial experiments (expanded range)

4.3.4 Case Study 4: Design of Five Optimal Experiments (with a Different Response)

As shown in Case Study 2, one of the advantages of the Bayesian approach is that one can design and proceed with several (smaller) optimal sequences of fewer trials per sequence. Another advantage of the Bayesian method, as mentioned in section 2.2, is that this approach is flexible with respect to the number of experiments that can be designed; when applying a Bayesian scheme, one can use as many experiments as he/she wants. This is unlike the standard fractional designs, where the number of trials designed can only be equal to an integer power of 2. In order to demonstrate this additional flexibility of the Bayesian design and reinforce the benefit of having a sequential nature, in Case Study 4, two sequences of 3- and 2-trials each were considered through the Bayesian design, and this design was then compared with the corresponding single 5-trial experiment.

In this case study, the Bayesian design was again applied to the bimolecular NMRP with the same three factors (and their levels) considered in Case Study 1 (therefore, for the selected factors and their levels see Table 4.3). However, the single response chosen for this case study was weight-average molecular weight (number-average could be chosen in an equivalent way). Molecular weight was selected to be measured at 50% conversion, first of all because 50% was the mid-point of the process, so the molecular weight behaviour was well established by then. In addition, prior experimental information (Roa-Luna et al., 2007; Nabifar et al., 2008) advised that molecular weight measurements show more scatter at higher conversion levels (80-95%) for NMRP of styrene. Replicates of molecular weight measurements available from prior experimental work gave a good idea about the expected variability in the response. In our case, it was calculated from independent replicates that molecular weight values varied by $\sim \pm 916$ gr/mol, leading to a variance of 840,000.

Following the framework offered in Table 3.1, after the design factors (and their levels) and responses were selected, the next step would be casting the prior knowledge into the vector of prior parameter means ($\underline{\alpha}$) and the prior variance/covariance matrix ($\underline{U}$). To generate the initial values for the parameter means, a 2^3 standard factorial design was used and the corresponding molecular weight responses were obtained again from the general mechanistic model developed for NMRP of styrene (see Section 4.2). The vector of prior parameter means ($\underline{\alpha}$), shown in the second column of Table 4.15, was obtained via conducting linear regression on the results. In order to determine the variances of the parameters, each parameter was again multiplied by two to give the magnitude of the effect, then effects were examined separately and based on our knowledge of the process, a reasonable estimate of the maximum/minimum value was made. This stage was where most of the brainstorming took place. In cases where the effect (or the parameter) was considered to be well known, a smaller interval of uncertainty was given, i.e., a smaller fluctuation about the mean was tolerated. The difference between the effect and its maximum or minimum was taken to be 2σ on a normal distribution curve. Dividing this value by 2 and squaring it gave the variance of the effect. Recognizing that a parameter is multiplied by 2 to give the effect, dividing the variance of the effect by 4 gave the diagonal element of the prior variance/covariance matrix ($\underline{U}$) (third column of Table 4.15); the off-diagonal elements were initially all set to zero.

Table 4.15 Elements of prior $\underline{\alpha}$ and $\underline{U}$ for Case 4

Parameter	α_i	U_{ii}
Mean	7007	1,934,392
T	160	2,500
[I]	-552	62,500
[N]	-1125	1,562,500
T×[I]	-183	7,656
T×[N]	107	15,625
[I]×[N]	-175	7,656
T× [I]×[N]	140	156

For more clarity, a sample of calculations for the prior variances is given here. Let's look at the interaction effect between temperature and nitroxide concentration (T×[N]). This interaction was considered to have an effect on molecular weight but the magnitude of the effect was in question. It was expected to likely obtain a negative overall value for this interaction effect (considering that nitroxide concentration had a large negative effect on molecular weight), while the value obtained from the linear regression was positive. At this point, we decided to stick to the regression estimate and assign a larger variability to the value. Another option would be to alter the value of the effect somewhat based on one's more informed opinion, if possible. The parameter value was 107.0975, the effect was therefore 214.195, and the variability was assigned to be ± 500 about 95% of the time. Thus, $\sigma = 250$, $\sigma^2 = 62{,}500$ and $U_{13} = \sigma^2/4 = 15{,}625$.

Sequential approach (sequences of 3- and 2-trials each): Again, considering the optimality criterion of maximizing the determinant H (see Eq. 3.5 in Section 3.1), there were eight 3-trial experiments which corresponded to the same maximum H (H = 59.1403); the results, containing the levels for each factor, are shown in Table 4.16. Since all the experiments gave the same H value, one can be chosen randomly (say, set # 4) and the related pattern is illustrated in Figure 4.16. As can be seen, the suggestion was to run the first trial with all the factors at the low level; the third run was exactly the other extreme, having all the factors at the high level, while trial 2 set temperature and initiator concentration at the high, and nitroxide concentration at the low level.

After the U matrix was updated (not shown here for the sake of brevity), the next optimal 2-trial experiment was designed, again using Eq. 3.5 in Section 3.1. The 2-trial experiment that corresponds to the highest value of H is shown in Table 4.17, along with the 3-trial experiment from the first sequence. The corresponding molecular weight responses (shown in the last column of Table 4.17) were calculated via adding a random error to the response generated from the mechanistic model.

Table 4.16 Set of eight possible 3-trial experiments in Case 4

No.	T	$[I]_0$	$[N]_0$
1	-1	-1	-1
	-1	-1	1
	1	1	1
2	-1	-1	-1
	-1	-1	1
	1	1	-1
3	-1	-1	1
	1	1	-1
	1	1	1
4	-1	-1	-1
	1	1	-1
	1	1	1
5	-1	1	-1
	1	-1	-1
	1	-1	1
6	-1	1	-1
	-1	1	1
	1	-1	1
7	-1	1	-1
	-1	1	1
	1	-1	-1
8	-1	1	1
	1	-1	-1
	1	-1	1

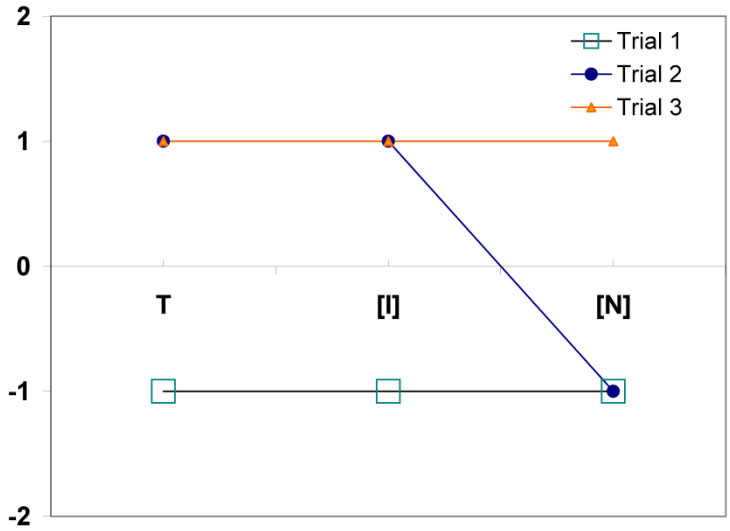

Figure 4.16 Visual illustration of the 3-trial experiment chosen by Bayesian design (Case 4)

Table 4.17 Five experiments via "sequential" choice in Case 4

	T	$[I]_0$	$[N]_0$	Molecular weight response (g/mol)
First sequence (3-trials)	-1	-1	-1	7243
	1	1	-1	6300
	1	1	1	6107
Second sequence (2-trials)	-1	-1	1	8048
	1	-1	1	7593

Single 5-trial experiment: In designing five trials in one batch, the Bayesian algorithm resulted in eight optimal sets with H =197.4, cited in Table 4.18. As can be seen by scrutinizing the entries of Table 4.17 and Table 4.18Table 4.18, the 5-trial experiment chosen by the "sequential" approach was actually among the best 5-trial experiments (set # 4) resulting from the single 5-trial ("batch") choice, hence leading to the same H value (H = 197.4). So again, given that there was no difference in the H value, and considering the fact that in many circumstances it is highly desirable to use a sequential procedure (flexibility being the obvious advantage along with minimization of wasted resources), the sequential approach seemed to be the superior choice. Furthermore, a comparison of conventional fractional factorial designs

with the Bayesian design performed in this case study was not straightforward, since the number of trials (equal to 5) did not correspond to any fractional factorial design (these designs require 2^n trials). This highlights yet another advantage of the Bayesian design, i.e., no restrictions in the number of experiments that can be performed.

Table 4.18 Eight sets of possible 5-trial experiments (Case 4)

	T	$[I]_0$	$[N]_0$
1	-1	-1	-1
	-1	-1	1
	-1	1	-1
	1	1	-1
	1	1	1
2	-1	-1	-1
	-1	-1	1
	1	-1	-1
	1	1	-1
	1	1	1
3	-1	-1	-1
	-1	1	-1
	-1	1	1
	1	-1	-1
	1	-1	1
4	-1	-1	-1
	-1	-1	1
	1	-1	1
	1	1	-1
	1	1	1
5	-1	-1	-1
	-1	-1	1
	-1	1	1
	1	1	-1
	1	1	1
6	-1	1	-1
	-1	1	1
	1	-1	-1
	1	-1	1
	1	1	-1
7	-1	1	-1
	-1	1	1
	1	-1	-1
	1	-1	1
	1	1	1
8	-1	-1	1
	-1	1	-1
	-1	1	1
	1	-1	-1
	1	-1	1

4.3.5 Case Study 5: Single- vs. Multi-response Scenarios

In order to show the flexibility of the Bayesian design in handling multi-response scenarios, this case study is applied to unimolecular NMPR of styrene with both batch time at 75% conversion, and weight-average molecular weight at 50% conversion as responses. As explained in Section 4.1, the unimolecular approach uses a single molecule (usually an alkoxyamine) that upon dissociation generates a propagating and a stable nitroxide radical.

The details of Case Study 5 are cited in Appendix B, since the basic steps of the procedure are the same as in other case studies of this chapter. In addition, several multi-response scenarios will be handled in case studies of the chapters that follow in this thesis.

4.3.6 Case Study 6: Source of Prior Knowledge

Yet another flexibility of the Bayesian design approach is related to the source of prior knowledge. As mentioned previously in Chapter 3, the prior knowledge can have different shapes and forms. In the case studies presented up to now, the prior knowledge was provided from a mechanistic model developed for NMRP of styrene. In Case Study 6, however, a different source is used to generate the prior information.

In this case study, the Bayesian approach was implemented to the unimolecular NMRP of styrene to design three experiments. The same three factors chosen for Case Study 5 were used in this case study (temperature, initial concentration of the unimolecular initiator, and number-average molecular weight of the unimolecular initiator), as listed with their initial levels in Table 4.19. The number-average molecular weight at 50% conversion was chosen as the single response. Molecular weight was again selected to be measured at 50% conversion (the reason explained in Case Study 4). The variance of the molecular weight response was calculated from replicated molecular weight measurements available from prior experimental work, giving a good idea about the variability in average molecular weight. From replicated results, it was calculated that molecular weight values vary by $\sim \pm 916$ gr/mol, leading to a variance of 840,000.

Table 4.19 Selected factors and their levels in Case 6 (unimolecular NMRP, T = temperature, [I]0 = initial unimolecular initiator concentration, = average molecular weight of the unimolecular initiator)

Level	T (°C)	$[I]_0$ (M)	$\overline{M}_n(I)$ (g/mol)
low	120	0.03	2,200
high	140	0.05	6,200

In order to demonstrate that the source of prior knowledge in the Bayesian design approach could be altered depending on one's choices, in this case study a different model, shown in Eq. 4.5, was used to generate prior knowledge. It is well known that the number-average molecular weight (M_n) for any living polymerization (including CRP) can be mechanistically related to the ratio of the concentration of consumed monomer to the introduced initiator (Matyjaszewski, 1997):

$$M_n = \frac{[M]_0 - [M]}{[I]_0} \cdot M_{mon} \qquad \text{Eq. 4.5}$$

where $[M]_0$ is the initial concentration of monomer, $[M]$ is the concentration of monomer at any time t, $[I]_0$ is the initial concentration of unimolecular initiator, and M_{mon} is the molecular weight of the monomer (in our case, styrene). Responses for the 2^3 standard factorial design were provided using Eq. 4.5 and the calculated values for the prior $\underline{\alpha}$ and $\underline{U}$ are shown in Table 4.20; calculations were carried out in the same way as in previous case studies.

Table 4.20 Elements of initial $\underline{\alpha}$ and $\underline{U}$ for Case Study 6

Effect	α_i	U_i
Mean	9213	6,250,000
T	-98	12,656
[I]	-2686	202,500
M_n[I]	-730	250,000
T×[I]	30	225
T×M_n[I]	11	15,625
[I]×M_n[I]	-3	22,500
T×[I]×M_n[I]	-0.25	5,625

Let's look at a hypothetical scenario where initially it was decided to run only two experiments. There were four 2-trial experiments all corresponding to a maximized H (H = 33.88); one was again chosen randomly and is shown in Figure 4.17. Carefully checking Figure 4.17, one can see that all factors are changing sign from one trial to the next in the design chosen. Since it was assumed that this case study had a non-informative prior (not a lot of information was known about any of the effects), large variances were allocated to each factor (see Table 4.20), and hence the Bayesian design suggested to change the sign of all factors to investigate their effects.

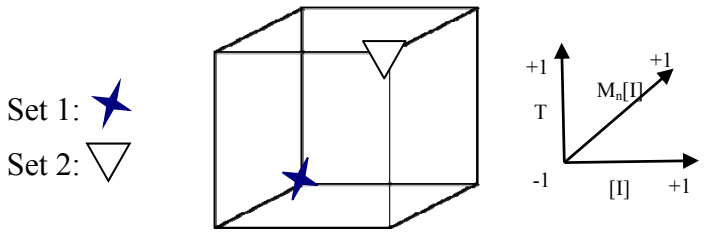

Figure 4.17 Visual illustration of experiments chosen for Case Study 6

Now, let's assume that after the first two trials were carried out in the lab, the experimenter was informed that an extra run could be afforded. Here is an illustration of another advantage of the Bayesian design, namely, the ability to incorporate an extra run (or runs) in the design and thus gain additional information from performing it (as will be discussed shortly, it was found that the amount of information obtained was 119.6% greater when the extra trial was run). After running the first two experiments in the lab (the corresponding molecular weight responses are shown in Table 4.21), Eq. 3.6 (shown in Section 3.1) was used to update the vector of parameter means and the corresponding values are shown in Table 4.21. Then the covariance matrix was updated (using Eq. 3.7 in Section 3.1) and based on the new $\underline{U}$ (shown in Table 4.22), the next single trial was designed. Comparing Table 4.20 and Table 4.22, one can see the presence of off-diagonal elements in the $\underline{U}$ matrix. Figure 4.18 illustrates all three runs suggested by the Bayesian design for this case study; one can see that the extra trial was suggested to be run with all factors at the high level.

Table 4.21 Posterior vector of parameters after the first 2-trial experiment in Case Study 6

Parameter Coefficient	$\underline{\theta}_1$ [§]
Mean	10,361
T	-118
[I]	-3,007
M_n[I]	-333
T×[I]	30
$T \times M_n[I]$	8.206
[I]× M_n [I]	-7.145
T× [I]× M_n [I]	8.67
Molecular weight response- Trial 1	13,935
Molecular weight response- Trial 2	7,000

[§] $\underline{\theta}_1$ is the updated vector of parameter means after the first sequence

Table 4.22 Posterior variance/covariance matrix, U, for Case Study 6 (first two trials)

427,033	0	0	0	-210	14,557	20,963	0
0	12,476	-2,877	3,552	0	0	0	80
0	-2,877	156,466	56,832	0	0	0	1,279
0	3,552	56,832	179,837	0	0	0	-1,579
-210	0	0	0	225	0.524	0.754	0
14,557	0	0	0	0.524	15,589	-52	0
20,963	0	0	0	0.754	-52	22,424	0
0	80	1,279	-1,579	0	0	0	5,589

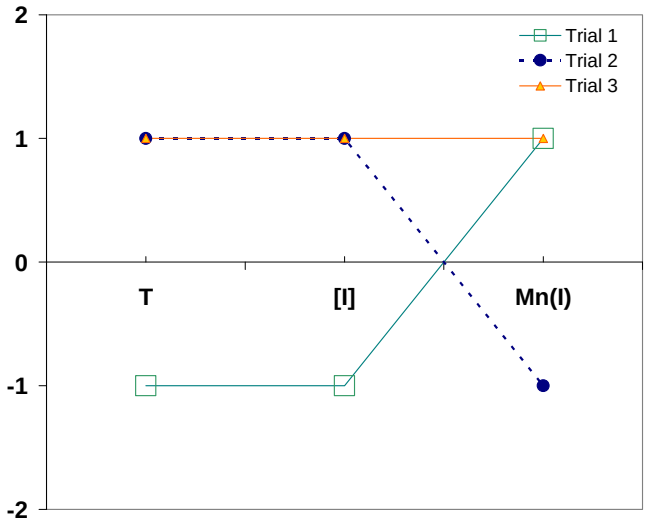

Figure 4.18 Visual illustration of the three runs suggested for Case Study 6

One can always check whether or not it was worth running the single extra trial and here we demonstrate the incremental gain for this. The major objective in the Bayesian design approach is to minimize the (hyper)volume of the posterior joint confidence region (JCR) of the parameter values. Hence, the percentage decrease in the (hyper)volume of the JCR can be the criterion to quantify the improvement of a design over another. As the (hyper)volume of the posterior JCR of the parameters is proportional to the inverse of the determinant H, one can simply calculate the percentage increase in the determinant H to quantify the improvement obtained in performing an extra trial. Thus, the benefit of running the extra trial is determined by comparing the H value of the first 2-trial sequence with the 3-trials (i.e., the first two trials plus the addition of the extra run). The percentage improvement of the H value is 119.6%. As a result, running an extra trial indeed increased the information content of the process. Not being able to use this extra run in (fractional) factorial designs is another shortcoming of the standard designs.

4.4 Statistical Diagnostic Tests

In addition to all the analysis in the case studies conducted so far, a series of statistical diagnostic tests can be carried out. These diagnostic tests serve to quantify the relative importance of the parameters and their interactions, as well as the quality of prior knowledge (in other words, the adequacy of the model used to generate the "prior knowledge", as the case might be). For the sake of brevity, we will only describe these tests for the last case study (Case Study 6), since results for the other cases are analogous.

Results from these statistical diagnostic tests for Case Study 6 are shown in Table 4.23. The second column shows the initial values of the means of the parameters ($\underline{\alpha}$) (as shown in Table 4.20), whereas the third column contains the final updated estimates of the means of the parameters ($\underline{\theta}$; after the third trial). Test 1 (column 6 of Table 4.23) is defined as the ratio of the prior means to the prior standard deviations of the means $[\alpha_i/(U_{ii})^{1/2}]$, where U_{ii}s are shown in the fourth column of Table 4.23. This test checks the null hypothesis that $\alpha_i = 0$ purely in the opinion of the ''expert'' (the person who assigned the values for the prior effects and variances). It is essentially a measure of the uncertainty of the ''expert''. A value greater than 2 or less than -2 is considered significant (this is equivalent to a 95.44% confidence interval).

Test 2 is a measure of the actual significance of an effect. It is equal to the last updated estimate of the effect, $\underline{\theta}$ (see third column of Table 4.23), divided by the square root of the diagonal element of the last posterior variance/covariance matrix (shown in the fifth column of Table 4.23). Once again, a value greater than 2 or less than -2 implies significance. Finally, Test 3 (last column of Table 4.23) is equal to ($\underline{\theta}_i$ - $\underline{\alpha}_i$) divided by the square root of the diagonal element of the last posterior variance/covariance matrix. Test 3 is a measure of the quality of the expert's opinion. A significant value, a value greater than 2 or less than -2, for Test 3 implies that portion(s) of the mechanistic model related to the response(s) and the effects in question may need refinement. As explained in Dube et al. (1996) and Vivaldo-Lima et al. (2006), caution should be exercised in the interpretation of this test, since correlation and nonlinearity in the model equations could also cause the results of Test 3 to become significant/insignificant.

Table 4.23 Results of diagnostic tests for Case Study 6

Effect	α_i	θ_i	Prior U_{ii}	U_{ii}^2	*Test 1*	*Test 2*	*Test 3*
Mean	9213.19	10576.19	6,250,000	311,156	**3.685**	**18.960**	**2.443**
T	-98.46	-112.38	12,656	12,382	-0.875	-1.010	-0.125
[I]	-2686.15	-2908.92	202,500	132,172	**-5.969**	**-8.001**	-0.613
M_n[I]	-730.03	-222.40	250,000	148,965	-1.460	-0.576	1.315
T×[I]	30.28	30.33	225	225	**2.019**	**2.022**	0.003
T×M_n[I]	11.08	22.21	15,625	15,098	0.089	0.181	0.091
[I]×M_n[I]	-3.01	13.02	22,500	21,407	-0.020	0.089	0.110
T×[I]×M_n[I]	-0.25	11.17	5,625	5,574	-0.003	0.150	0.153

The results from Test 1 in Table 4.23 indicate that in the "expert's opinion", initiator concentration ([I]) and the interaction between temperature and initiator (T×[I]) are influential factors on the molecular weight response. Temperature (T) and initiator molecular weight (M_n[I]) are not affecting the molecular weight response (within the considered operating conditions). The results from Test 2 verify the actual significance of an effect; as can be seen in Table 4.23, the results are in agreement with the expert's opinion. Lastly, Test 3 implies that the expert's opinion is valid and the model used seems reliable.

An extremely important point worth mentioning here is that for the results of Case Study 6 and of Table 4.23 related to the diagnostic tests, we were able to confirm the exact trends based on experimental results from a recent kinetic investigation with a unimolecular initiator in the literature (Zhou et al., 2010). What is even more important is that the literature experimental study reaches certain conclusions after performing twelve runs. Case Study 6 and Table 4.23 basically arrive at the same conclusions (via the Bayesian scheme) after only three runs! This is yet another confirmation of how powerful an approach the Bayesian design is, leading to considerable savings in experimental time, effort, resources and hence cost, by focusing on the most essential changes of factor settings, based on minimum prior information about the system from either very few preliminary experimental runs or a reasonable mechanistic model.

4.5 Concluding Remarks

The Bayesian approach is a powerful, largely unstudied (in the polymerization area) experimental design methodology which offers several distinct advantages over standard experimental designs that make it particularly attractive from both an industrial and theoretical perspective. This chapter highlights numerous advantages of the Bayesian design over standard (fractional) factorial design via presentation of several case studies drawn from the NMRP of styrene.

As shown in Case Study 2, the Bayesian design is an improvement from the point of view of *information content* retrieved from process data compared to conventional designs. The approach allows for *flexibility to changing levels of factors* with relative ease (as shown in Case Study 3). Bayesian design is flexible and "cost"-effective with respect to the *number of experiments* that can be designed (see Case Studies 4 and 6). The inherent *sequential nature* of the design methodology with any number of runs is another powerful feature (Case Studies 2 to 6). In addition, this approach can be also applied to cases with *multiple-responses* (see Case Study 5 in Appendix B).

The most distinguished feature of the Bayesian methodology is its ability to *incorporate the prior knowledge* into the design (as demonstrated in all case studies). This is in contrast to standard (admittedly important) design methods, which try to generate process data without

any input from the “expert” other than the specification of the model and (often set incorrectly) operating ranges for the factors involved. The exercise of casting the prior knowledge about a process into a mathematical form (estimating prior parameter means and prior variance matrix) forces the experimenter to brainstorm/define clearer objectives for the overall experimentation and perhaps come to a better understanding of the process or even anticipate/solve some of the problems that triggered the specific questions about the process, even before starting the experiments. Prior information can come from a variety of sources, including both empirical or other simpler models (see Case Study 6) and fully mechanistic models (case studies 1 to 5).

Finally, the method is amenable to formal statistical diagnostic tests, which can eventually shed more light on the quality of prior knowledge and the significance of the estimated effects (relative importance of factors), and through these on some of the most uncertain parts of out process understanding (model). Since the technique is perfectly general, it can be potentially applied to other complex polymerization variants and chemical engineering processes, with uncertain models/parameters, especially in industrial settings.

Chapter 5. Diagnostic Checks and Measures of Information in the Bayesian Design of Experiments

5.1 Introduction

A Bayesian approach to the design of experiments has the same objectives as standard experimental (full or fractional factorial) designs but with significant practical benefits over standard design methods. The ability of the Bayesian approach to incorporate prior process knowledge (which is available in most of the cases but usually discarded) into the design (prior knowledge coming from a variety of sources) is a distinct advantage. This and other advantages of the Bayesian methodology (improvements with respect to information content retrieved from process data, relative ease in changing factor levels in the middle of experimentation, flexibility with factor ranges and overall "cost"-effectiveness (time and effort/resources) with respect to the number of experiments) were highlighted in Chapter 4, with examples from complex polymerization scenarios drawn specifically from the nitroxide-mediated radical polymerization (NMRP) of styrene, under both bimolecular and unimolecular initiating options.

Table 5.1 gives a compendium of experimental design issues that can effectively be handled by the Bayesian design approach (and hence pose typical limitations for standard experimental designs). Most of these issues along with the more superior performance of the Bayesian approach in handling them were demonstrated via the case studies presented in Chapter 4. Table 5.2 summarizes all the case studies discussed in Chapter 4 along with the case studies drawn from other polymerization processes, studied previously in our group (the last two entries of Table 5.2 summarize the work by Dube et al. (1996) and Vivaldo-Lima et al. (2006)). An "identifier letter" in Table 5.1 cross-references the entries (design issues) of Table 5.1 with the corresponding case studies in Table 5.2, where the issues have been addressed. A few explanations/remarks for the entries of Table 5.2: (a) T, [I] and [N] stand for polymerization temperature, initiator concentration (I represents initiator, in general) and controller (for example, TEMPO) concentration, respectively (b) $\overline{M}_n(I)$ represents the average molecular weight of the unimolecular initiator (c) CTA is chain transfer agent (d) Comparisons

of the number of Bayesian trials are made (see first column of Table 5.2) with either full factorial trials (2^k, k = number of experimental factors considered in the design) or fractional factorial trials (usually, half fraction of a full factorial design); observe how much fewer the Bayesian runs are with respect to both full and fractional factorial trials (e) The column of responses (third column of Table 5.2) gives a feel about the many different measured variables that can be employed (single- and multi-response scenarios).

Table 5.1 Overview of issues handled by the Bayesian design approach

Issue	**Identifier**
Flexible wrt number of trials that can be designed	A
Changing factor level/range in the middle of experimentation	B
Accommodating extra trial(s) mid-way through experimentation	C
Sequential nature (n-trials vs. sequences of fewer trials)	D
Process constraints (and impractical treatment combinations)	E
Situations with missing observation(s)	F
Increase of information content	G
Possible detection of nonlinearities	H
Incorporation of prior knowledge	I
Flexible wrt source of prior knowledge (screening experiments vs. models and/or combinations)	J
Flexible wrt quality of prior knowledge (informative vs. non-informative priors)	K
Factors with several (or combination of) levels	L
Dropping/adding factors	M
Iterative fashion	N
Single vs. multi-response scenarios	O

Two typical questions that often arise in Bayesian design implementations have to do with how effectively one can make statements about the quality of prior knowledge and the significance of the estimated effects (from the designed experiments), and about the gain in information content. These two important questions were not addressed in detail in earlier parts of the thesis and hence they are the topic of the present chapter. In other words, the following questions, intimately related to the Bayesian experimental design technique, will be addressed in what follows: (1) What statistical diagnostic criteria can one use in order to shed light on the quality of prior knowledge and the significance of estimated effects? (2) What measures of information (content) are available and what different aspects of the design procedure can they emphasize? Addressing questions (1) and (2) above not only clarifies the design steps further

but also could only make one more confident in the effectiveness and practicality of the Bayesian design of experiments procedure.

In order to address the above questions, a case study from the bimolecular NMRP of styrene is presented in this chapter, where the Bayesian approach is implemented to design two sequences of 2-trials each. The results from the Bayesian approach are compared with a standard fractional factorial design. The improved effectiveness of the Bayesian design is demonstrated through a discussion of diagnostic criteria (on the quality of prior knowledge and the significance of estimated effects) and enhanced information content measures.

Table 5.2 Case studies/examples with Bayesian design implementations on complex polymerization scenarios

Case study	Process details	Responses	Identifier
Design 2 experiments (Full factorial experiment (exp) = 8)	Bimolecular NMRP Three factors (T, [I], [N]) Prior knowledge: mechanistic model	Single: batch time	A, I, K, N
Design 4 exp (two sequences of 2-trials each vs. 4-trials; comparison with fractional factorial) (Full factorial exp = 8; half fraction of full factorial = 4)	Bimolecular NMRP Three factors (T, [I], [N]) Prior knowledge: mechanistic model	Single: batch time	A, D, G, I, K, N
Design 4 experiments (expanded T range in the middle of experimentation) (Full factorial exp = 8)	Bimolecular NMRP Three factors (T, [I], [N]) Prior knowledge: mechanistic model	Single: batch time	A, B, D, H, I, L, N
Design 3 experiments (accommodating extra trial to gain new information) (Full factorial exp = 8)	Unimolecular NMRP Three factors (T, [I], $\overline{M}_n(I)$) Prior knowledge: empirical model	Single: number-average molecular weight	A,C, D, G, I, J, K, N
Design 5-trial experiment vs. two sequences of 3- and 2- trials each (Full factorial exp= 8)	Bimolecular NMRP Three factors (T, [I], [N]) Prior knowledge: mechanistic model	Single: weight-average molecular weight	A, D, G, I, N
Two sequences of 2-trials each (design experiments that are nearly optimal for all responses) (Full factorial exp= 8)	Unimolecular NMRP Three factors (T, [I], $\overline{M}_n(I)$) Prior knowledge: reduction of mechanistic model from bimolecular to unimolecular	Two: batch time and weight-average molecular weight	A, D, G, I, N, O
Three sequences of 4-, 4- and 10-trials each (Full factorial exp = 128)	Emulsion terpolymerization Seven factors (T, [I], [monomer], [CTA], [impurity], [emulsifier], I type) Prior knowledge: mechanistic model	Four: batch time, terpolymer composition, weight-average molecular weight, total # of particles	A, B, C, D, E, F, I, L, M, N, O
Two sequences of 4-trials each (Full factorial exp = 64)	Suspension polymerization Six factors ([CTA], [stabilizer], speed of agitation, dispersed phase hold-up, two factors from impeller geometry Prior knowledge: mechanistic model	Two: mean particle size, coefficient of variation of the particle size distribution	A, E, F, I, N, O

5.1 Design Stage

As mentioned in Table 3.1 of Chapter 3, the first step in implementing the Bayesian approach is selection of the design factors with their levels, and the responses. Three factors were chosen for this case study and are shown (with their initial levels) in Table 5.3. The selection of factors and their low and high levels were based on a detailed and critical analysis of the literature, combined with some of our previous experience about the process (Roa-Luna et al., 2007; Nabifar et al., 2008), as discussed in detail in Chapter 4. Reaction (batch) time (in hrs) to reach 60% conversion was chosen as the single response in this case study. It was felt (based on process information and experience) that due to various sources of experimental error, the time for a batch to reach 60% conversion would vary by $\pm$ 1 hr about 95% of the time.

Table 5.3 Selected factors and their levels (T = temperature, [I] = initiator concentration, [N] = nitroxide concentration)

Level	T (°C)	[I] (M)	[N] (M)
low	120	0.0305	0.0324
high	130	0.036	0.0396

Casting the prior knowledge into the vector of parameter means ($\underline{\alpha}$) and the variance/covariance matrix ($\underline{U}$) was the next important step (see Table 3.1 in Chapter 3). To generate the initial values for the parameter means, a 2^3 standard factorial design was used and the corresponding batch times were obtained from a general mechanistic model developed for NMRP of styrene (details of the modeling effort have been discussed in Section 4.2). The vector of parameter means ($\underline{\alpha}$), shown in the second column of Table 5.4, was obtained via conducting a linear regression on the results (see Eq. 3.2 in Chapter 3). In order to determine the variances of the parameters, each parameter was examined separately and based on our knowledge of the process, a reasonable estimate of the variance was made. This stage was where most of the brainstorming took place. In cases where the parameter (or the effect) was considered to be well known, a smaller interval of uncertainty was given, i.e., a smaller fluctuation about the mean was tolerated. Since in the bimolecular NMRP of styrene nitroxide concentration plays an important role, it was genuinely desired to find out more information about the model term involving this factor. Hence, higher initial variances were allocated to the parameters related to nitroxide concentration ([N]) and its interactions. The diagonal elements

of the prior variance/covariance matrix (U) are shown in the third column of Table 5.4; the off-diagonal elements were initially all set to zero.

Table 5.4 Elements of prior $\underline{\alpha}$ and $\underline{U}$

Parameter	α_i	U_{ii}
Mean	7.795	11.95
T	-3.189	0.25
[I]	-0.295	0.25
[N]	0.250	6.25
T×[I]	0.167	0.0068
T×[N]	-0.178	1.562
[I]×[N]	-0.239	0.562
T× [I]×[N]	0.144	0.016

The next step is selection of the "best" experiments using the search algorithm. As an example, it was decided to run a total of four experiments in two sequences of 2-trials each (as shown in Chapter 4, the Bayesian technique allows one to design any number of trials per sequence, and any number of sequences). Following the metric for designing experiments, i.e., maximizing the determinant H (Eq. 3.5 of Chapter 3), four 2-trial experiments were found that corresponded to a maximized H (H= 460.77), as shown in Table 5.5.

Now let's make a few practical remarks, in order to demonstrate the efficiency of the design procedure and the importance of the interplay between Bayesian steps and "process" sense. If this case study were examined blindly, somebody could have picked one of the four experiments of Table 5.5 completely randomly. However, combining knowledge about the bimolecular NMRP of styrene with the suggested results from the Bayesian design, we can now make a more judicious choice of the appropriate experiment, which is optimal from both a statistical and process sense. For instance, from previous experience with the bimolecular NMRP of styrene we know that the ratio of concentrations of nitroxide to initiator ([N]/[I]) is important. Experiments 1 and 3 (and experiments 2 and 4) in Table 5.5 lead to trials with the same nitroxide to initiator ratio at two different temperatures. It was decided to choose the lower temperature (120 °C), as it was the most common temperature used in bimolecular NMRP. Hence, running experiments 1 and 2 would be preferable. Between experiments 1 and 2, experiment 1 would appear even more preferable, as in this experiment a wider range of

[N]/[I] was examined (1.06-1.3 vs. 0.9-1.1). Hence, experiment 1 was conducted for the first sequence of 2 trials and the corresponding batch time responses are shown in Table 5.5. Here we demonstrated the importance of a parallel correct scientific/practical decision, not a statistical one, which might not be apparent, if not for the added emphasis of the Bayesian methodology on prior information.

Table 5.5 Four possible 2-trial experiments for the first sequence

No.	T	[I]	[N]	[N]/[I]	Batch time response
1	-1	-1	-1	1.06	9.63
	-1	-1	1	1.30	13.26
2	-1	1	-1	0.9	-
	-1	1	1	1.1	-
3	1	-1	-1	1.06	-
	1	-1	1	1.30	-
4	1	1	-1	0.9	-
	1	1	1	1.1	-

For the next step, Eq. 3.7 of Chapter 3 was employed to calculate the posterior variance/covariance matrix (shown in Table 5.6; one can now observe the presence of non-zero off-diagonal elements, i.e., covariance elements, in the updated $\underline{U}$ matrix). The updated variance/covariance matrix was then used back in Eq. 3.5 (of Chapter 3) to design (in an iterative sequential fashion) the next sequence that maximizes the determinant H. Only one 2-trial experiment corresponded to the highest value of H (H= 78.73) this time. The corresponding levels for the factors are shown in Table 5.7, along with the batch time responses obtained from conducting experiments in the lab. Scrutinizing again Table 5.5 and Table 5.7, one can see that the Bayesian design is choosing the second sequence at a higher temperature level (130°C) and different ratios of [N]/[I]. Therefore, in a very succinct way, the total of 4 runs (two sequences of 2-trials) covered both temperatures and all four different [N]/[I] ratios.

Table 5.6 Posterior variance/covariance matrix U after the first sequence of experiments

0.9286	0.2306	0.2306	0	-0.0063	0	0	0
0.2306	0.2452	-0.0048	0	0.0001	0	0	0
0.2306	-0.0048	0.2452	0	0.0001	0	0	0
0	0	0	1.8563	0	1.0984	0.3954	-0.0110
-0.0063	0.0001	0.0001	0	0.0068	0	0	0
0	0	0	1.0984	0	1.2879	-0.0989	0.0027
0	0	0	0.3954	0	-0.0989	0.5269	0.0010
0	0	0	-0.0110	0	0.0027	0.0010	0.0156

Table 5.7 The second sequence of 2 trials

T	[I]	[N]	[N]/[I]	Batch time response (hrs)
1	1	-1	0.9	3
1	1	1	1.1	5

The updated variance/covariance matrix is shown in Table 5.8. Comparing Table 5.6 with Table 5.8, one can see that after the second sequence of experiments, the uncertainties about the parameters (diagonal elements of the U matrix) have decreased. Also, most of the covariances (off-diagonal elements of the U matrix; measures of the strength of the correlation between parameters) appearing in the first sequence (Table 5.6) were zero in the second sequence (Table 5.8). Eq. 3.6 of Chapter 3 was then employed to calculate the posterior $\underline{\theta}$ after each sequence of 2-trials (results are shown in the 3rd and 4th column of Table 5.9; the superscript in $\theta_i^{(\ )}$ denotes the sequence of trials).

Table 5.8 Posterior variance/covariance matrix U after the second sequence of experiments

0.2514	0	0	0	-0.0067	0	0	0
0	0.1667	-0.0833	0	0	0	0	0
0	-0.0833	0.1667	0	0	0	0	0
0	0	0	0.2548	0	0	0	-0.0150
-0.0067	0	0	0	0.0068	0	0	0
0	0	0	0	0	0.5345	-0.3701	0
0	0	0	0	0	-0.3701	0.4293	0
0	0	0	-0.0150	0	0	0	0.0156

5.2 Statistical Diagnostic Tests: Discussion

A series of statistical diagnostic tests can now be carried out in addition to the analysis presented so far. These diagnostic tests serve to quantify the relative importance of the parameters (i.e., factor effects) and their interactions, as well as the quality of prior knowledge (in other words, the adequacy of the model used to generate the "prior knowledge", as the case might be). Results from these statistical diagnostic tests for our example are shown in Table 5.9. The 2nd column presents the initial values of the parameter means ($\underline{\alpha}$); the 3rd and 4th columns contain the updated estimates of the parameter means after the first and second sequence, respectively. Test 1 (5th column of Table 5.9) is defined as the ratio of the prior mean (2nd column of Table 5.9) to the prior standard deviation of the mean $[\alpha_i/(U_{ii})^{1/2}]$, where (U_{ii}) is shown in the third column of Table 5.4. This test checks the null hypothesis that $\alpha_i = 0$ purely in the opinion of the ''expert'' (the person who assigned the values for the prior effects and variances). It is essentially a measure of the uncertainty of the ''expert''. A value greater than 2 or less than -2 is considered significant (this is equivalent to a 95.44% confidence interval). Test 2 is a measure of the actual significance of an effect. For instance, the test 2 value after the second sequence of experiments (6th column of Table 5.9) is equal to the second updated estimate of the effect, $\theta_i^{(2)}$, divided by the square root of the corresponding diagonal element of the last posterior variance/covariance matrix (see Table 5.8; $[\theta_i^{(2)}/(U_{post(ii)})^{1/2}]$). Once again, a value greater than 2 or less than -2 implies significance. Finally, test 3 is a measure of the quality of the expert's opinion. For instance, test 3 after the second sequence of experimentation (7th column of Table 5.9) is equal to $(\theta_i^{(2)} - \alpha_i)$ divided by the square root of the diagonal element of the last posterior variance/covariance matrix (see again Table 5.8; $[(\theta_i^{(2)} - \alpha_i)/(U_{post(ii)})^{1/2}]$). A significant value greater than 2 or less than -2 implies that portion(s) of the mechanistic model related to the response(s) and the effects in question may need further refinement.

Table 5.9 Summary results of diagnostic tests

Parameter	Prior α_i	$\theta_i^{(1)}$	$\theta_i^{(2)}$	Test 1	Test 2 (after 2nd seq.)	Test 3 (after 2nd seq.)
Mean	7.795	7.795	7.561	**2.255**	**15.079**	-0.466
T	-3.189	-3.189	-3.269	**-6.378**	**-8.006**	-0.195
[I]	-0.295	-0.295	-0.374	-0.589	-0.917	-0.195
[N]	0.250	0.953	1.220	0.100	**2.417**	1.921
T×[I]	0.167	0.167	0.167	**2.021**	**2.020**	-0.002
T×[N]	-0.178	-0.354	-0.170	-0.142	-0.233	0.010
[I]×[N]	-0.239	-0.302	-0.236	-0.318	-0.360	0.004
T× [I]×[N]	0.144	0.146	0.147	1.155	1.176	0.019

A careful analysis of the summary results of Table 5.9 can lead to several interesting remarks. Based on the results of test 1, the influential factors on the batch time response, purely in the opinion of the "expert", were temperature (T) and the interaction between temperature and initiator concentration (T×[I]). The results of test 2 revealed that the actual significant parameters, based on the new observations, are T, [N], and T×[I]. Initiator concentration ([I]) was not affecting the batch time response (within the considered operating conditions). This result explained why in kinetic studies of bimolecular NMRP, most of the time the concentration of initiator was kept constant while the concentration of nitroxide was varied to study the effect of [N]/[I] (Veregin et al., 1996a, b; Nabifar et al., 2008; Zhang and Ray, 2002). Finally, test 3 showed that the results were in agreement with the expert's opinion. However, the value of test 3 for [N] was arguably very close to 2 and thus indicates that the expert's opinion about the nitroxide concentration might not be overly accurate. The result of test 3 indicated that the Bayesian design has indeed "spotted" this and identified that the expert's opinion was not valid about [N], yet another of the implicit advantages of Bayesian design.

5.3 Measures of Information Content: Discussion

In order to "visualize" and demonstrate the improvement achieved by the Bayesian methodology (compared to a standard fractional factorial design), various possible measures of information (content) are discussed next. The Fisher information is a way of measuring the amount of information that an experiment carries about an unknown parameter θ. The Fisher information and the estimated variance are reciprocal, thus minimizing the variance

corresponds to maximizing the information. In the case of multi-parameter scenarios, the means of the parameters form a vector and their variances are included in a variance/covariance matrix. The inverse of the variance/covariance matrix is called the "information matrix". Since the Fisher information is now in the form of a matrix, this matrix could be compressed using a real-valued summary statistic (like the determinant or trace of the matrix). Being real-valued functions, these "information criteria" can now be maximized.

In the Bayesian design of experiments, the information matrix is the reciprocal of the posterior variance/covariance matrix (Eq. 3.7 of Chapter 3). The summary statistic used in our approach is the determinant. Hence, Fisher information (FI) = $|\underline{U}^{-1} + (1/\sigma^2)\underline{X}'\underline{X}|$. Scrutinizing the determinant H (Eq. 3.5 of Chapter 3), one can see that our experimental criterion to arrive at optimal experiments is indeed a function of the Fisher information. For our example case study presented here, FI after two sequences of 2-trials each is 8.42×10^7. The Fisher information would be 6.65×10^7 in the case of a half fraction of a full factorial design. Therefore, the Bayesian design is an improvement with respect to information content.

Another advantage of the Bayesian design is that it moves in the direction of minimizing the variance of the parameters. For example, Figure 5.1 illustrates the evolution of the variances for the nitroxide concentration effect (corresponding to element U_{44} of the variance/covariance matrix) throughout the experimentation. As one can see, this value has dropped from 6.25 in the prior (Table 5.4) to 1.85 (Table 5.6) to 0.25 after the second sequence (Table 5.8), thus demonstrating that the Bayesian design in its sequential nature minimizes the uncertainty in the parameter values (translating uncertainty into variance of the effects and the related parameters).

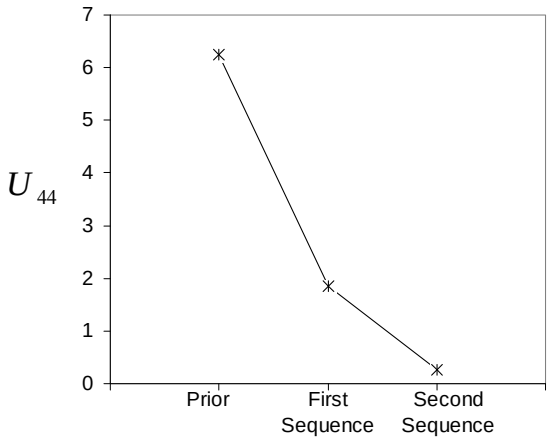

Figure 5.1 Evolution of variance ($\boldsymbol{U_{44}}$) through the course of experimentation

Another indication that the Bayesian approach is an improvement over the corresponding standard fractional factorial design can be visualized through the estimated response from the regression model (Y_{model}), where $Y_{model} = \underline{X}\underline{\theta}$. Figure 5.2 illustrates an example of the evolution of the estimated response for the conditions of the first trial of the second sequence (the 1st row of Table 5.7) through the course of experimentation and compares the corresponding estimated response with the actually observed value (Y_{exp}; solid line in Figure 5.2). The estimated response from the fractional factorial experiment is also shown for comparison (dashed line in Figure 5.2). As one can see, Y_{model} after the second sequence of the Bayesian experiments is very close to the actually observed Y_{exp}, while the corresponding Y_{model} calculated for the fractional factorial experiment is farther away from the actually observed value. Once more, in the Bayesian steps, Y_{model} moves in the direction of minimizing its difference with Y_{exp}.

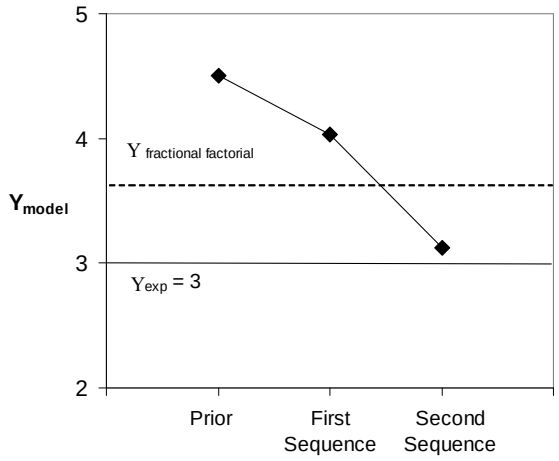

Figure 5.2 Evolution of Y_{model} through the course of experimentation

Finally, Figure 5.3 illustrates yet another measure of information content, as expressed by the 95 % joint confidence region (JCR). It can be seen in Figure 5.3a, b and c that the areas of the joint confidence regions are significantly reduced from prior to the first sequence, and then from the first sequence to the second sequence of experimentation. The reduction indicates that the precision in parameter estimates has increased. These figures also contain the JCRs for the corresponding standard fractional factorial design and they all demonstrate that the novel Bayesian approach is indeed significantly more effective than the standard fractional factorial (much smaller JCRs for the Bayesian designed experiments).

The joint confidence region for the T-[I] parameters is slightly tilted after the second sequence (see Figure 5.3a), indicating that the T and [I] related parameters are moderately correlated. Going back to the results of Table 5.6 and Table 5.8, translating covariances into the corresponding correlation values (Covariance (i, j) / [Variance (i) $\times$ Variance (j)]$^{0.5}$), one would see that most of the correlation coefficients are considerably smaller in absolute value than 1. In theory, the magnitude of the correlation values is the factor that would affect the orientation of the final joint confidence regions of the parameters. For instance, in Table 5.8, U_{32} shows the covariance between [I] and T. U_{32} being non-zero will give rise to a joint confidence region that is tilted. The negative covariance (U_{32} = - 0.0833) implies that initiator concentration effect, [I], tends to decrease as the temperature effect, T, increases (see Figure 5.3a). The JCRs in Figure 5.3b and Figure 5.3c are completely horizontal, representing completely uncorrelated parameters (which again confirms the results of Table 5.6 and Table 5.8).

a)

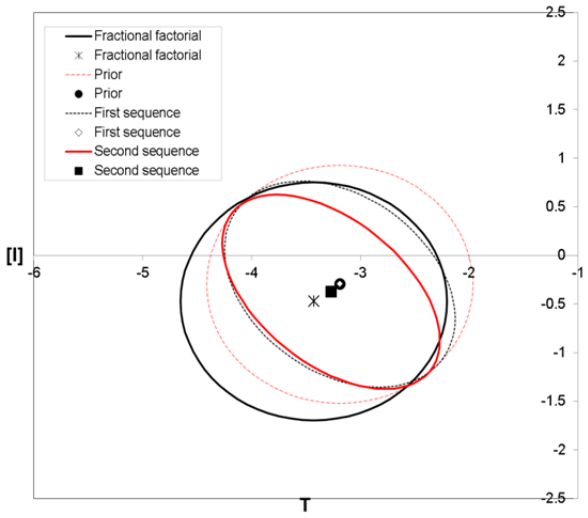

b)

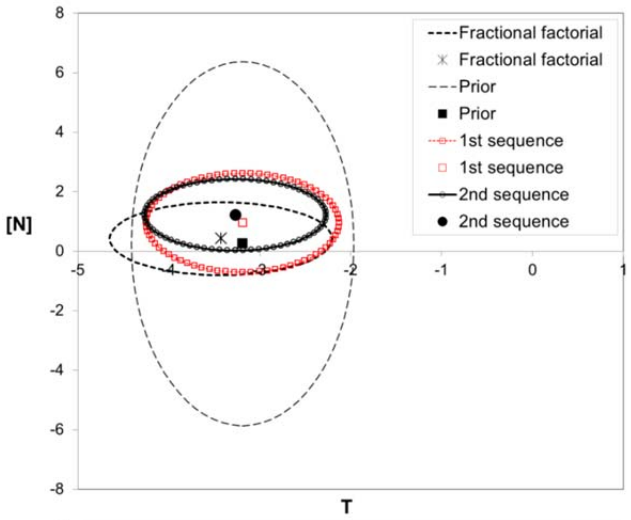

C)

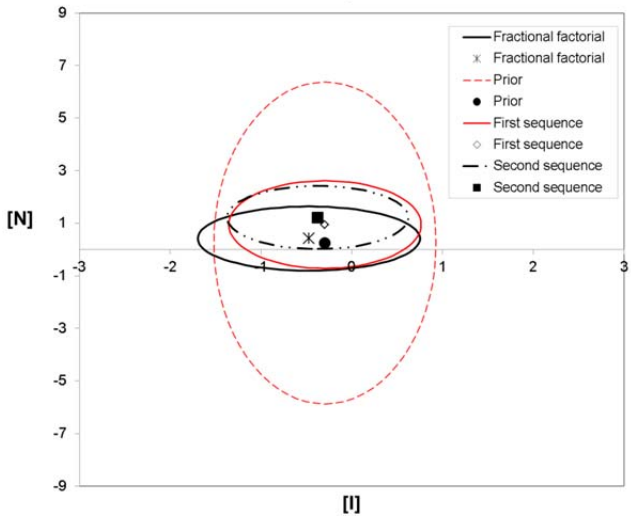

Figure 5.3 95% joint confidence regions (JCRs) for parameters, a) T-[I], b) T-[N], and c) [I]-[N]

5.4 Concluding Remarks

Two important questions, intimately related to the Bayesian design of experiments, were addressed via implementing this technique to NMRP of styrene. The first had to do with statistical diagnostic criteria that one can use in order to make statements about the quality of prior knowledge and the significance of estimated factor effects. These statistical diagnostic checks can "spot" and identify situations when the expert's opinion (prior knowledge) is not valid about certain parameters (hence, factor effects). The second question was concerned with enhanced information measures (obtained from the Bayesian procedure versus a standard design of experiments), as another illustration of the effectiveness and practicality of the approach. It was shown that the Fisher Information matrix is maximized in the Bayesian approach, which corresponds to minimizing the variances and reducing the 95% joint confidence regions (JCR), hence improving the precision of the parameter estimates.

Chapter 6. Bayesian Design of Experiments Applied to the Continuous Production of Nitrile Rubber in a Train of CSTRs

In the previous chapters, the general framework for the Bayesian design of experiments was presented in detail and the application of this technique to bulk homopolymerization of styrene in unimolecular and bimolecular nitroxide-mediated radical polymerization (NMRP) in batch mode was discussed. In this chapter, the Bayesian technique is applied to a more complex system, namely, emulsion copolymerization of acrylonitrile (AN) and butadiene (Bd) in a train of CSTRs. In Chapter 8, the Bayesian design of experiments will be implemented to an even more complex system, the bulk cross-linking NMRP of STY/DVB in the batch mode.

In this chapter, a brief introduction to nitrile rubber is initially presented followed by a summary of recent modeling efforts conducted in our group (Washington et al., 2010; Madhuranthakam and Penlidis, 2011 and 2012). This section is not a detailed explanation of the modeling work, but rather a short summary to convince the reader that the model developed in our group is capable of predicting the correct trends and behavior and can thus be reliably used to provide the prior knowledge in implementing the Bayesian design approach to the continuous production of NBR rubber. Finally, results from implementing the Bayesian design of experiments are discussed in Section 6.3.

6.1 Introduction

Nitrile-butadiene (or, simply, nitrile) rubber (NBR) is produced through emulsion copolymerization of acrylonitrile (AN) and butadiene (Bd). The main indicators for product quality are the polymer molecular weight, degree of branching and the level of bound AN in the copolymer (AN copolymer composition). The average molecular weights usually range from 2.5×10^5 to 6×10^5 with varying degrees of polydispersity and branching. AN copolymer composition can vary between 15% to 50% depending on desired product properties and final uses Although the physical and chemical properties of the rubber vary depending on copolymer composition, NBR rubber is generally resistant to oil, fuel, and other chemicals (the more nitrile within the polymer, the higher the resistance to oils but the lower the flexibility of the material).

By selecting the appropriate acrylonitrile content in balance with other molecular structure properties (e.g., molecular weight, branching and polydispersity), NBR rubber can be used in a wide variety of application areas requiring oil, fuel, and chemical resistance. Its ability to withstand a range of temperatures from -40 °C to +108 °C makes it an ideal material for aeronautical applications as well. NBR rubber is used in the automotive and aeronautical industry to make fuel and oil handling hoses, seals, O rings, gaskets, as well as transmission belts. It is also used to create moulded goods, footwear, adhesives, pigment binder, sealants, sponges, expanded foams, and floor mats.

The emulsion latexes can be produced using batch/semibatch or continuous reactor modes based on demand and quality requirements. On an industrial scale, a continuous process is used to produce nitrile rubber in large volumes while a batch process is typically used for smaller quantities of specialty products. In the continuous process, many stirred tank reactors (CSTRs) are connected in series to form a train with the outflow from the previous reactor entering the next reactor as an inflow. The train of CSTRs mimics plug flow behavior so that polymer characteristics similar to those obtained in a batch reactor can be obtained in addition to the advantage of higher production and output over batch production.

In the production of nitrile rubber, depending on the temperature at which the copolymerization takes place, the terms ’cold’ and ’hot’ recipe are used. Cold recipes are those that use a redox radical initiation mechanism with temperatures in the range of 5°C to 15°C. Hot recipes employ persulfate initiators that thermally decompose to free radicals in the range of 30°C to 50°C. A typical example of both recipe types can be seen in Table 6.1. The ratio of AN to Bd can vary depending on the desired final rubber properties. The amount of water can also vary; however, this is primarily dependent on the desirable “solids content” level to be obtained and, secondarily, on the heat generated by polymerization and the available heat transfer capacity of the reactor cooling system. Electrolytes are often used to help control and maintain the colloidal stability of the polymer particles. Polymerization initiator systems used are mainly water soluble and designed to generate a continuous supply of free radicals. The choice of emulsifier is dependent on the monomers, polymerization conditions (i.e., temperature, latex stability), and the influence on the final product. Typically, more than one emulsifier with differing functionalities may be used to control and stabilize particle formation

and growth. A detailed discussion on the functionality of each recipe ingredient can be found in the extensive and by now classical source by Hofmann (1964).

Table 6.1 Typical nitrile rubber polymerization recipes (Washington et al., 2010)

		Parts per Hundred Monomer (pphm)	
Material	**Typical Chemical**	**Cold recipe**	**Hot recipe**
Acrylonitrile		30 - 35	30 - 35
Butadiene		65 - 70	65 - 70
Water		170 - 200	170 - 200
Electrolyte	Na_2CO_3, K_2CO_3	0.3 - 0.5	0.3 - 0.5
Peroxide Initiator	PMHP, DIBHP[a]	0.04 - 0.2	-
Metal Ion	Iron chelate[b]	0.005 - 0.1	-
Reducing Agent	SFS[c]	0.04 - 0.2	-
Persulfate Initiator	KPS, SPS, APS[d]	-	0.2 - 0.4
Primary Emulsifier	Tamol, Daxad, SDS[e]	1.0 - 5.0	1.0 - 5.0
Secondary Emulsifier	Dresinate, Potassium oleate, Emersol	0.1 - 5.0	0.1 - 5.0
Chain Transfer Agent	Mercaptan [f]	0.2 - 0.6	0.2 - 0.6
Temperature		5 – 15°C	30 – 50°C

[a] para-menthane (PMHP) or di-isobutyl hydroperoxide (DIBHP); [b] e.g. $FeSO_4.7H2O$; [c] Sodium formaldehyde sulfoxylate (SFS); [d] Potassium (KPS), sodium (SPS), or ammonium persulfate (APS); [e] Sodium dodecyl sulfate (SDS); [f] e.g., tert-dodecyl mercaptan (t-DDM)

6.2 NBR Rubber Model Development

A mathematical model for the emulsion copolymerization of AN and Bd has recently been developed in our group by Washington et al. (2010) and further modified by Madhuranthakam and Penlidis (2011, 2012). The purpose of this modeling effort was to simulate the industrial production of NBR in batch, semi-batch, continuous and trains of continuous reactors, using a cold recipe, and evaluate the model with (whatever limited) sets of experimental data and process property trends could be found either in the literature or based on industrial practice.

The final target would be to use the model for the derivation of optimal scenarios for reactor train start-ups and other operational or grade change policies.

The mechanistic aspects considered in this model were: initiation, propagation, termination, transfer to monomer, polymer and CTA, reactions with impurities (both water and monomer soluble), and reactions with internal and terminal double bonds. Appropriate reactions were considered in both the aqueous and particle phases. Table 6.2 summarizes the reaction mechanism considered.

Table 6.2 Reaction mechanism for the emulsion copolymerization of NBR rubber (Washington et al., 2010)

Mechanism	**Reaction/Event**
Redox decomposition	$S_2O_8^{2-} + Fe^{2+} \xrightarrow{k_1} SO_4^{-\cdot} + Fe^{3+} + SO_4^{2-}$
	$Fe^{3+} + SFS \xrightarrow{k_2} Fe^{2+} + SFS^{+}$
Thermal decomposition	$S_2O_8^{2-} \xrightarrow{k_d} 2SO_4^{-\cdot}$
Radical initiation	$SO_4^{-\cdot} + M_j \xrightarrow{k'_{p_{ja}}} R_{1,j}^{\cdot}$
Propagation	$R_{n,i}^{\cdot} + M_j \xrightarrow{k_{pij}} R_{n+1,j}^{\cdot}$
Termination	$R_{n,i}^{\cdot} + R_{m,j}^{\cdot} \xrightarrow{k_t} P_{(m+n)}$ or $P_n + P_m$
Transfer to monomer	$R_{n,i}^{\cdot} + M_j \xrightarrow{k_{fm_{ij}}} P_{n,i} + M_j^{\cdot}$
Transfer to polymer	$R_{n,i}^{\cdot} + P_{m,j} \xrightarrow{k_{fp_{ij}}} P_{n,i} + R_{m,j}^{\cdot}$
Transfer to CTA	$R_{n,i}^{\cdot} + (CTA)_j \xrightarrow{k_{fcta_{ij}}} P_{n,i} + CTA_j^{\cdot}$
Reaction with internal double bonds	$R_{n,i}^{\cdot} + P_m^{i=} \xrightarrow{k^{**}_{pij}} R_{n+m,i}^{\cdot}$
Reaction with terminal double bonds	$R_{n,i}^{\cdot} + P_m^{t=} \xrightarrow{k^{*}_{pij}} R_{n+m,i}^{\cdot}$

Reaction with water-soluble impurities	$R_{n,i}^{\cdot} + WSI_j \xrightarrow{k_{fwsi_{ij}}} P_i$
Reaction with monomer-soluble impurities	$R_{n,i}^{\cdot} + MSI_j \xrightarrow{k_{fmsi_{ij}}} P_i$
Micellar nucleation	$R_{n,i}^{\cdot} + \text{Micelle} \xrightarrow{k_{cm}} \text{Particle}$
Homogeneous nucleation	$R_{j_{cr},i}^{\cdot} + M_j \xrightarrow{k_h} \text{Particle}$
Capture of radical by particle	$R_{n,i_a}^{\cdot} \xrightarrow{k_{cp}} R_{n,i_p}^{\cdot}$
Desorption of radical from particle	$R_{1,i_p}^{\cdot} \xrightarrow{k_{des}} R_{1,i_a}^{\cdot}$

The model was cast in a dynamic form using 32 ordinary differential equations that track the changes in recipe ingredient moles, number of particles, polymer volume, temperature, and the first three molecular weight moments (along with tri- and tetra-functional branching averages) over time. Appendix C contains an overview of the most important mathematical model equations. The particle generation was modeled considering both micellar and homogeneous nucleation, the latter included due to the high water solubility of AN. Radical desorption was initially included in the model according to Asua et al. (1989), however, later simulations by Madhuranthakam and Penlidis (2011) showed that desorption is negligible in NBR emulsion polymerization and the polymerization follows Case II emulsion kinetics. The pseudo-kinetic rate constant method was employed to capture the dependency of overall rate constants not only on temperature but also on composition, polymer weight fraction, monomer conversion and radical chain length. The model predictions included monomer conversion, copolymer composition (as bound AN level in the copolymer, $\bar{F}_{AN}$), number- and weight-average molecular weights ($\bar{M}_n$, $\bar{M}_w$), tri- and tetra-functional branching frequencies ($\overline{BN}_3$, $\overline{BN}_4$), and the number and average size of polymer latex particles (number of particles (N_p) and particle diameter ($\bar{d}_p$)). Model parameters were obtained from the open literature or arrived at after sensitivity analysis or, occasionally, parameter estimation based on (limited) experimental data.

Washington et al. (2010) compared model simulations to industrial data for NBR emulsion carried out in a batch reactor. Figure 6.1 illustrates the comparison between model predictions and experimental data for conversion, copolymer composition, particle diameter and molecular weight; the overall picture is quite satisfactory and good results were obtained. It was also found that both monomer and water soluble impurities had a profound impact on model predictions and they were necessary aspects to model in order to obtain a good fit to industrial data. The influence of emulsifier and initiator concentration on particle nucleation have been studied in both batch and continuous reactors and it was shown that the NBR model developed behaved according to the experimental findings of other similar Case II systems (Washington et al., 2010).

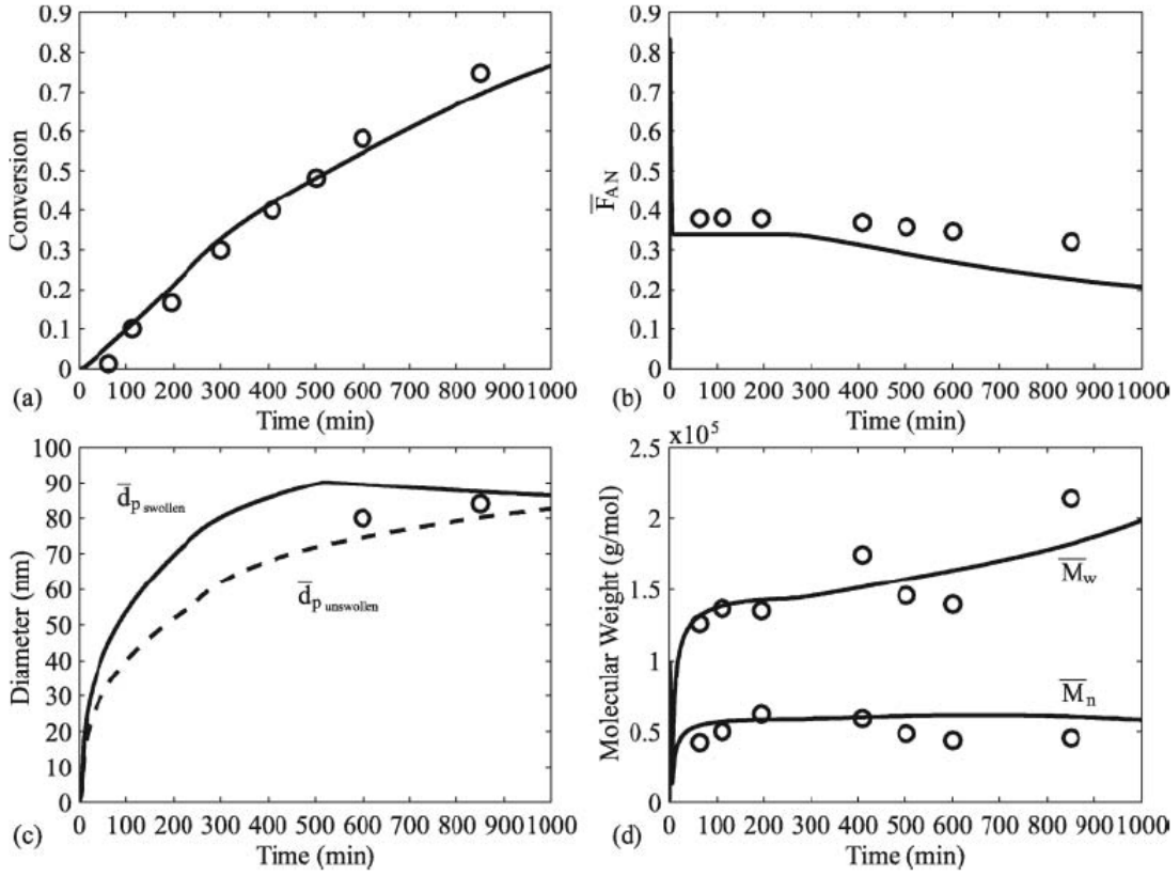

Figure 6.1 NBR batch reactor simulation and comparison to industrial data for (a) conversion, (b) cumulative copolymer composition, (c) average particle diameter, and (d) molecular weight averages (Washington et al., 2010)

With a multiphase system like emulsion polymerization, it is necessary to determine the concentration of each component in each phase. There are two important partitioning methods that have been used to calculate the concentration of components in different phases: the constant partition coefficient approach (PCA) used by Washington et al. (2010), and the thermodynamic approach (TDA) employed by Madhuranthakam and Penlidis (2011). In the PCA option, the ratio of the concentrations of a reaction species in two different phases is assumed to be constant over the course of polymerization. These constants, otherwise referred to as partition coefficients, are often simply guessed or adjusted to fit process data, or at best, obtained empirically from experiments using parameter estimation techniques. On the other hand, in the thermodynamic option, thermodynamic equations that describe the equilibrium among different phases are used. In this method the monomers are assumed to be distributed among different phases corresponding to a dynamic equilibrium and hence, the partial molar free energies (ΔG) of monomer j in the different phases are equal. Madhuranthakam and Penlidis (2011) compared the model simulations obtained for NBR emulsion polymerization using the PCA and the TDA partitioning options and showed that the profiles for different process variables (conversion, cumulative copolymer composition of AN, average particle diameter, average molecular weights and average tri- and tetra-functional branching frequencies) are very similar, if not identical, for both batch and continuous reactors. However, the profiles corresponding to the volume of polymer particles (V_p), volume of monomer droplets (V_d) and average number of radicals per particle ($\bar{n}$) with respect to time showed much more significant differences for the different approaches used for partitioning. Madhuranthakam and Penlidis (2011) explained that major differences between the two approaches were due to how the monomer concentrations in the particles and in the aqueous phase were estimated after the monomer droplets disappeared. In PCA, a constant coefficient is used to estimate the concentration of monomer in the corresponding phases, while in TDA, the estimation of monomer in the particle phase after the droplets disappear is also a function of particle size in addition to the different monomer-monomer and monomer-polymer interactions. In order to compensate for this in the PCA option, Madhuranthakam and Penlidis (2011) used a different value of the partition coefficient after the monomer droplets disappear and showed that using modified coefficients in PCA would make the estimates comparable to those obtained using the TDA option. They hence concluded that both PCA and TDA

approaches work equally satisfactorily and the choice of adopting one over the other is based on the information available and the selection/preference with respect to the general modeling framework.

The model also has the capability to simulate different properties for a train of CSTR reactors. Figure 6.2 illustrates typical simulation results for a train of 10 reactors each with a volume of 20,000L and a mean residence time of 60 min. The reactor start up procedure used was to have all the reactors initially full of water before the material was fed to the first reactor. Simulation profiles for conversion, copolymer composition, particle number and size, weight-average molecular weight and tri-functional branching frequency are presented in Figure 6.2. Operating the reactor train with a residence time of 60 minutes per reactor yields a gradual increase in conversion which reaches a steady-state of approximately 77% in the final reactor at around 26.6 hours (Figure 6.2a). A similar time is required for copolymer composition (Figure 6.2b), particle size (Figure 6.2c) and particle number (Figure 6.2d), while the molecular properties (i.e., $\bar{M}_w$, $\overline{BN_3}$, in Figure 6.2e and Figure 6.2f, respectively) require approximately 30 hours to achieve steady-state in the final reactor. Copolymer composition begins to drift in the fourth reactor (Figure 6.2b), and the monomer droplet phase vanishes in the sixth reactor, which is evident from a decrease in the swollen particle diameter (Figure 6.2c). From Figure 6.2d it can be seen that particle nucleation occurs only in the first reactor followed by a long transient period where the steady-state is initially preceded by a large overshoot. The distinct "double-hump" in Np in the first reactor is a result of the startup procedure and the use of two emulsifiers in the recipe, which are initially below their critical micelle concentration. From Figure 6.2e the weight-average molecular weight appears to increase starting in the fifth reactor. The tri-functional chain branching frequency profile (Figure 6.2f) reveals a sharp increase beyond the sixth reactor, which indicates the onset of gel formation.

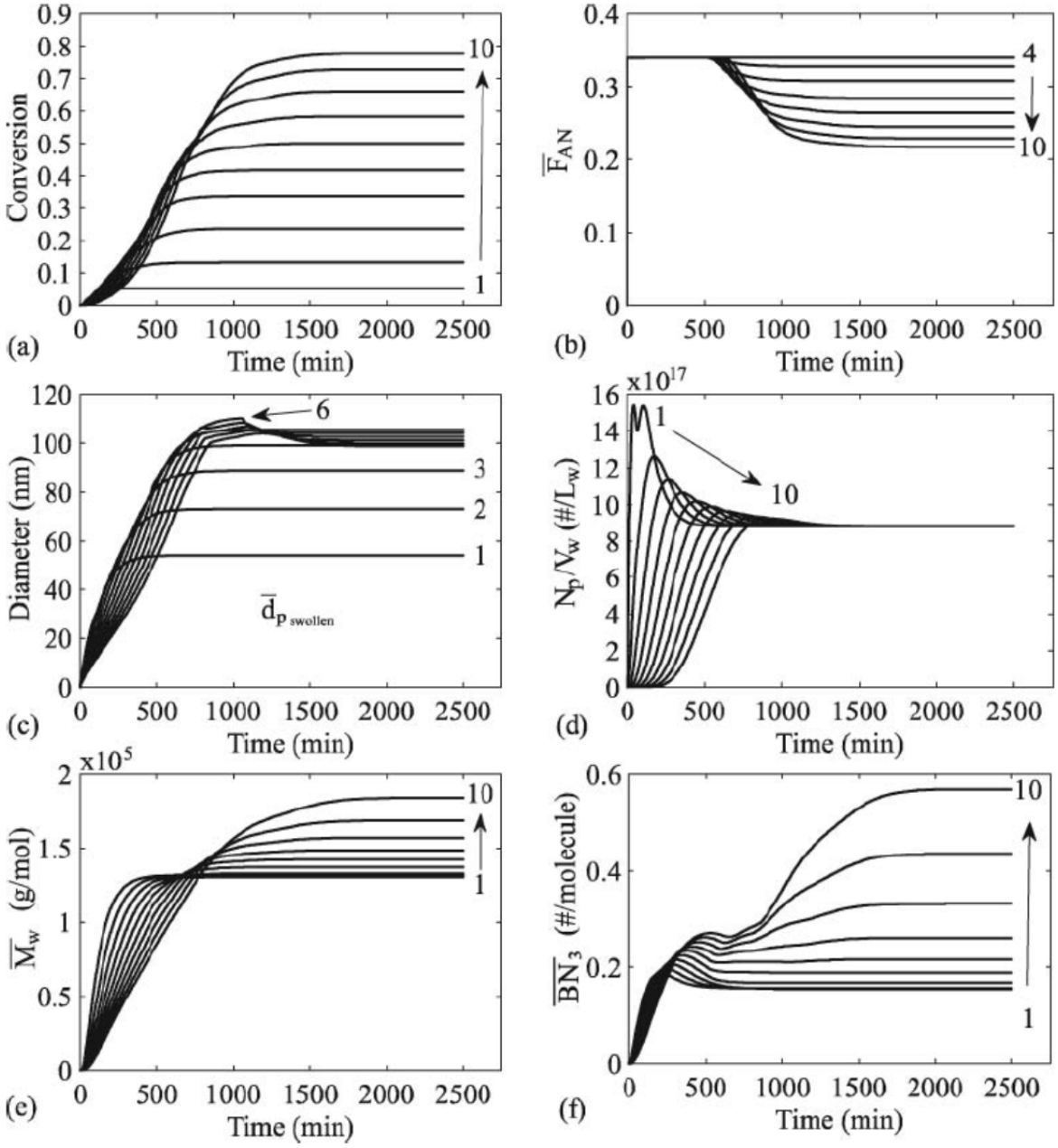

Figure 6.2 Continuous reactor train simulation for conversion (a), copolymer composition (b), average particle diameter (c), particle number (d), weight-average molecular weight (e) and tri-functional branching frequency (f) (Washington et al., 2010)

The mathematical model was also used to simulate different start-up policies in a single CSTR and in a train of CSTR reactors (Washington et al., 2010; Madhuranthakam and Penlidis, 2011). The transient behavior typically seen upon reactor start-ups is very important for the efficient production of NBR emulsion and can be used to minimize off-spec product, and optimize flow rates of various ingredients. Four different types of start-up procedures were investigated, and these included starting the reactor full of "batch recipe" (i.e., all ingredients charged in the same proportions as in batch operation), full of water (i.e., have all reactors initially full of water before material was fed to the first reactor), empty and half full of water. The simulations showed that using a reactor initially full of "batch recipe" results in an initial overshoot in conversion due to the large initial burst in particle nucleation, as the emulsifier and initiator concentrations are also at high level. Conversion reaches the steady state around five to six residence times, which is expected in a CSTR operation. In addition, number- and weight-average molecular weights converged quickly to their steady-state values. On the other end, starting the reactor up initially full of water shows a much longer transient period in each of the reactor variables, which is to be expected since the concentration levels of all the reaction species build up gradually and rather slowly. The profiles for various polymerization variables with empty start-up were found to be lying between those obtained with the full of "recipe" and full of water start-ups, while the profiles corresponding to half full of water start-up were very similar to those of empty start-up. A full of "recipe" start-up results in "off-spec" product that would be a waste, if not controlled. In contrast, reactor full of water or empty results in suppressed transients and smooth/gradual profiles for different polymer properties. However, start-up of the reactor train with full of "recipe" would yield lower time periods (settling times) to reach the target compared to the times obtained with either empty or full of water start-ups. In addition to the time periods, the monomer droplets would disappear, for example, in the fifth reactor with "full of recipe" start-up, while this happens in the sixth reactor (or later) with other start-ups. If the droplets disappear early in a reactor train, the remaining reactors can be used merely for polymerization in the particle phase. Hence, Madhuranthakam and Penlidis (2011) concluded that depending on the manufacturing policies, different start-ups can be applied and the model developed can be used for prediction purposes as it gives a very good insight into the transient behavior, steady state time, and effect on the level of the final properties of the polymer.

Washington et al. (2010) and Madhuranthakam and Penlidis (2012) also used the model to discuss miscellaneous operating procedures for a train of eight reactors to target desired properties of the NBR emulsion and at the same time reduce the amount of off-spec material during the transient period before reaching steady state. It was shown that the total number of particles can be increased by increasing the molar flow of initiator and surfactant. Also, in order to have a constant copolymer composition, the AN flow can be split between the first two reactors or the molar flow of AN can be increased, with the latter procedure being superior. Further, it was concluded that CTA could be added intermittently along the reactor train to control the average molecular weights and branching frequencies that would otherwise become extremely high, especially in the last few reactors of the train.

All in all, the current model is a detailed mechanistic model that has the ability to handle different start-up scenarios and different feed policies and operating procedures, in addition to options such as including desorption, monomer and water soluble impurities, and even using different monomer partitioning approaches. The aim of this introduction was to give a summary of the capabilities of the model and also to set the stage for using the model in implementing the Bayesian design of experiments on emulsion NBR. More details on this model and its features can be found in Washington et al. (2010), and Madhuranthakam and Penlidis (2011, 2012). This model is used to generate the prior knowledge during the implementation of the Bayesian design approach to the continuous production of NBR rubber. Case studies are discussed and experiments designed through the Bayesian approach are compared to experiments suggested by other standard statistical designs. Effectively, one could view the Bayesian design approach under the same context as Evolutionary Operation (EVOP). EVOP has been specifically developed in aid of continuous processes and production (Hunter and Kittrell, 1966; Box and Draper, 1969), essentially as a way to experiment with a continuous process (and involving only a small number of operating factors, say, two or three, at a time) without disrupting production.

6.3 Results and Discussion: Implementation of Bayesian design to the continuous production of nitrile rubber

A detailed discussion on the inner workings of the Bayesian design procedure has been presented in Chapter 3 and will not be repeated herein for the sake of brevity. Instead, an overview of the different steps for implementing the Bayesian design is given in a point form in Table 6.3. The steps of this methodology are illustrated in detail for the continuous production of nitrile rubber in a train of 8 CSTRs in this section.

Table 6.3 Summary steps for implementing the Bayesian design of experiments

1. Select the design factors and their levels; select response(s).
2. Incorporation of prior knowledge: cast the prior knowledge into a vector of prior parameters estimates ($\underline{\alpha}$) and a prior variance/covariance matrix ($\underline{U}$)
3. Select the "best" experimental setting ($\underline{X}$) by maximizing determinant H: $H = \left\lvert \underline{I} + (1/\sigma^2)\underline{XUX'} \right\rvert$ Eq. 6.1
4. Run and analyze the experiments to obtain response(s) ($\underline{y}$)
5. Apply Bayes' theorem to obtain the posterior distribution and update $\underline{\alpha}$ and $\underline{U}$ using the following equations: $\underline{\hat{\theta}} = [\underline{U}^{-1} + (1/\sigma^2)\underline{X'}\underline{X}]^{-1}[\underline{U}^{-1}\underline{\alpha} + (1/\sigma^2)\underline{X'}\underline{y}]$ Eq. 6.2 $\underline{U} = [\underline{U}^{-1} + (1/\sigma^2)\underline{X'}\underline{X}]^{-1}$ Eq. 6.3
6. Given the new $\underline{U}$, use Eq. 6.1 to select the next sequence of trials
7. Analyze the experiments and update $\underline{\theta}$ and $\underline{U}$; repeat steps 3 to 8
8. Stop the experimentation once the values of parameters of interest are known with accepted degree of certainty. Update the vector of parameters, after the analysis of the final sequence of experiments.

Three different case studies with respect to the responses were initially investigated. In the first case, responses after the last reactor (8th reactor) were studied, i.e., when the train had reached operational steady state. In the second case study, responses were considered at the output of the 2nd reactor, while in the third scenario, responses were considered just after the monomer droplets had disappeared (output of 4th reactor). Only the results of the first case study are discussed herein, since the trends in the other two case studies were similar to the first one and hence not repeated here for the sake of brevity.

Two sequences of 4-trials each are designed, and contrasted with an 8-trial optimal design. Comparisons are offered with fractional factorial and Plackett–Burman designs. Several diagnostic checks are presented that shed light on the quality of prior knowledge and the significance of estimated effects.

Selection of Design Factors and Levels: As shown in Table 6.3, the first step in implementing the Bayesian design is choosing the design factors and their levels. Four factors were chosen and shown with the corresponding low and high levels in Table 6.4. When selecting factors and their low and high level values, it was tried to keep the settings as close to the real industrial production as possible. We based our study on an already existing industrial set up, with a train of 8 CSTR reactors, each having a volume of 20,000 L. The existing production line functions with a mean residence time (θ) of 60 min for each reactor. Recipe ingredients similar to the ones shown in Table 6.1 for polymerization of nitrile rubber with the cold recipe were implemented and the start-up procedure used was the "full of recipe" one. Starting the train with all reactors full of the "batch recipe" means that all polymerization ingredients (except for the initiator or redox initiator part) were added in each reactor, so initially, the concentration and ingredient proportions were equal to those of a "typical batch reactor recipe". In Table 6.4, the low level settings of the factors represent the current operation setting in the industrial set up with a residence time of 60 min. Since the reactors have the same volume, the residence time had to be changed in order to change the ingredient flow rates. The high level of factors corresponds to a residence time of 45 min.

After brainstorming with the process experts, it was felt that the important factors to study were related to initiator, emulsifier, monomer, water, and chain transfer agent flow rates. Using the cold recipe for the production of NBR rubber, peroxide initiator (I) is not the only component in charge of starting the initiation stage; reducing agent (RA) and iron (metal) compound (IMC) also play a role. However, since they are not independent from each other to be considered as separate factors (since they have to satisfy certain proportions), all of them were lumped together as factor (RA/ IMC/ I), referred to from now on as initiation factor (INT) throughout this chapter. Essentially, INT accounts for the redox initiation package components.

The ratio of monomer to latex ($\frac{M}{(M+W)}$) is an important factor related to the total solids content of the finally produced NBR latex. The typical ratio used in industrial continuous production of NBR rubber is about 0.6. It is important to keep this ratio the same, if there is a need to change both monomer and water levels during plant-wide experimentation. Hence, once more, monomer and water could not be presented as separate factors, and they were hence combined in one factor, referred to as WM throughout the chapter. In both low and high levels of WM, the ratio ($\frac{M}{(M+W)}$) is kept at 0.6.

Table 6.4 Selected factors and their levels for implementing Bayesian design to continuous production of nitrile rubber

Factor	**Name**	**(Low) level**[†] **θ = 60 min**	**(High) level**[†] **θ = 45 min**
INT: RA/ IMC/ I	RA: Sodium formaldehyde sulfoxylate (SFS) Iron (metal) compound (IMC): $FeSO_4.7H2O$ I: p-menthane hydroperoxide (PMHP)	0.046/ 0.004/ 0.165	0.062/ 0.005/ 0.220
E	Tamol (primary emulsifier)/ Dresinate (secondary emulsifier)	1.670/ 0.890	2.228/ 1.183
WM: (M_1, M_2)/ W	(AN, Bd)/ W	(48.6, 160.3)/ 121.36	(64.8, 213.7)/ 161.81
CTA	tert-dodecyl mercaptan	0.33	0.44

[†] Volumetric flow rate (L/min); θ : residence time; INT: initiation factor, composed of reducing agent (RA), Iron(metal)compound (IMC) and peroxide initiator (I); E: emulsifier flow rate, including both primary and secondary emulsifier; WM: latex flow rate, comprised of monomer 1 (M_1, acrylonitrile(AN)), monomer 2 (M_2, butadiene (Bd)) and water (W); CTA: chain transfer agent

Selection of Responses: There are no restrictions on the number of responses that can be accommodated by the Bayesian design technique. Responses chosen here were based on practical considerations and measurements so as to mimic as much as possible what could ideally be done in industry. Responses chosen were conversion (x), the cumulative amount of acrylonitrile (AN) bound in the copolymer (cumulative copolymer composition of acrylonitrile, $\bar{F}_{AN}$), and weight-average molecular weight ($\bar{M}_w$). Variances of responses were estimated from previous sets of experiments and are summarized in Table 6.5. It was felt (based on process information and experience) that due to various sources of error in the experiments, the standard error associated with the conversion measurement was around 5% (σ = 0.05), hence, $\sigma^2 = 2.5 \times 10^{-3}$. The typical H-NMR spectroscopy error is around 5% (Dube et

al., 1996), therefore, the variance for $\bar{F}_{AN}$ is also $\sigma^2 = 2.5 \times 10^{-3}$. From experience with emulsion polymerization, the error in measuring molecular weights is $\sigma = 25{,}000$ (Dube and Penlidis, 1996); hence, the variance for $\bar{M}_w$ is $\sigma^2 = 6.25 \times 10^8$. These are essentially the default values of the response variances. If, at any specific stage, variances other than the ones indicated in Table 6.5 were used, this will be stated up front.

Table 6.5 Variance of the responses

Response	**Variance**
Conversion (x)	2.50×10^{-3}
Cumulative copolymer composition ($\bar{F}_{AN}$)	2.50×10^{-3}
Weight-average molecular weight ($\bar{M}_w$)	6.25×10^{8}

Incorporation of Prior Knowledge: As shown in Table 6.3, casting the prior knowledge into the vector of parameter means ($\underline{\alpha}$) and the variance/covariance matrix ($\underline{U}$) is the next important step. To generate the initial values for the parameter means, a 2^4 standard factorial design was used, and the corresponding conversion, copolymer composition and molecular weight responses were obtained from the mechanistic model developed in our group (Madhuranthakam and Penlidis, 2011). As explained in the previous section, this model, based on the reaction mechanism and consisting of mole balances for the main recipe ingredients and detailed population balances for the molecular weight part, eventually leads to the development of 32 ordinary differential equations. This model is a good starting point as in principle a mechanistic model contains a good deal of prior information about the process.

In all the cases studies, vectors of parameter means ($\underline{\alpha}$) were obtained via conducting linear regression on the results. In order to determine the variances of the parameters ($\underline{U}$), each parameter was examined separately and based on our knowledge of the process, a reasonable estimate was made. This stage was where most of the brainstorming took place. In cases where the parameter was considered to be well-known, a smaller interval of uncertainty was given, i.e., a smaller fluctuation about the mean was tolerated. The estimated variances occupy the diagonal elements of the prior variance/covariance matrix; off diagonal elements (covariances) are initially set to zero.

Selection of Experimental Design: As illustrated in Table 6.3, the basic idea for the design of experiments in the Bayesian design approach is to choose $\underline{X}$ in order to maximize the determinant H (see Eq. 6.1 in Table 6.3). Three case studies were initially investigated in order to demonstrate how the Bayesian design scheme works when applied to the continuous production of nitrile rubber. Results from one of these three case studies (practically speaking, the most important one) are cited and discussed in detail in this chapter, whereas results from the other two case studies are not discussed here for the sake of brevity. The results from the other two case studies (output from the 2nd and 4th reactor) are in agreement with the results from the major one, and exhibit the same (or very similar) trends. The major case study shown herein tackles data from a train of 8 CSTRs, the way they would be available in practice, under steady state operation of the CSTR train, hence it is more realistic.

6.3.1 Case Study 1: Responses after the 8th reactor

In this case study, responses after the last reactor (8th reactor) are considered. Two sequences of 4-trials each are designed, and contrasted with an 8-trial optimal design. For further illustration purposes, the experiments design through the Bayesian approach are compared to the corresponding 8-trial experiments designed through fractional factorial and Plackett–Burman designs. Steps 1 and 2 of the procedure cited in Table 6.3 have been explained above. See Table 6.4 for factors and their levels, and Table 6.5 for the variances of the responses. The prior vector of parameter means ($\underline{\alpha}$) and the diagonal elements of the variance/covariance matrix ($\underline{U}$) (shown in Table 6.6, Table 6.7 and Table 6.8 for conversion, copolymer composition and molecular weight responses, respectively) have been calculated following the framework explained under *'Incorporation of Prior Knowledge'*.

Table 6.6 Elements of **prior** α and U after the **8th** reactor for **conversion**

Parameter	α_i	U_{ii}
Mean	5.93E-01	2.50E-03
INT	1.12E-02	4.00E-06
E	3.85E-02	5.63E-05
WM	-1.44E-01	3.03E-03
CTA	-5.00E-05	1.60E-09
INT × E	-5.25E-04	1.00E-08
INT × WM	2.35E-03	1.00E-06
INT × CTA	1.25E-05	1.00E-10
E× WM	-1.12E-04	2.50E-09
E × CTA	6.94E-18	1.00E-34
WM × CTA	-6.94E-18	4.90E-35
INT × E × WM	1.75E-04	6.40E-07
INT × E × CTA	-1.25E-05	6.40E-09
INT × WM × CTA	-1.25E-05	6.40E-09
E × WM × CTA	6.94E-18	1.00E-34

Table 6.7 Elements of **prior** α and U after the **8th** reactor for **copolymer composition**

Parameter	α_i	U_{ii}
Mean	2.73E-01	2.50E-03
INT	2.62E-03	8.10E-07
E	6.53E-03	1.00E-06
WM	-2.94E-03	8.10E-07
CTA	-6.25E-06	1.60E-11
INT × E	-3.12E-05	1.69E-10
INT × WM	3.94E-04	2.25E-08
INT × CTA	6.25E-06	2.50E-11
E× WM	-5.94E-04	2.25E-08
E × CTA	-6.25E-06	2.50E-11
WM × CTA	-6.25E-06	2.50E-11
INT × E × WM	-1.06E-04	1.00E-08
INT × E × CTA	6.25E-06	6.40E-11
INT × WM × CTA	6.25E-06	6.40E-11
E × WM × CTA	-6.25E-06	6.40E-11

Table 6.8 Elements of **prior** α and U after the **8th** reactor for **weight-average molecular weight**

Parameter	α_i	U_{ii}
Mean	113,160	6.25E+08
INT	3,306	2.25E+06
E	14,030	2.50E+07
WM	-43,676	1.44E+08
CTA	-14,777	1.23E+07
INT × E	-156	1.00E+04
INT × WM	-223	4.00E+04
INT × CTA	-403	3.24E+04
E× WM	-5,141	7.29E+06
E × CTA	-1,768	5.63E+05
WM × CTA	5,090	4.00E+06
INT × E × WM	476	1.60E+05
INT × E × CTA	3	4.00E+00
INT × WM × CTA	-9	6.40E+01
E × WM × CTA	588	2.50E+05

6.3.1.1 Sequential Approach (Two Sequences of 4-Trials Each)

The prior variances (U) were fed to the Bayesian design algorithm, and the best 4-trial experiments (X in Eq. 6.1) that maximized the determinant H were chosen for each response, separately. There happen to be four optimal 4-trial designs detected for each of x, $\bar{F}_{AN}$ and M_w, with the determinant H equal to 32.09, 5.02, and 13.0, respectively. Since we were dealing with a multi-response case, it was important to check whether an optimal design for one response was nearly optimal for the other two. Hence, the optimal trials for one response were combined with the U matrices and σ^2 from the other responses in order to re-evaluate the determinant H for the other two responses. For example, the optimal designs for the conversion response were each used along with the variance/covariance matrix (U) and σ^2 for copolymer composition in order to recalculate the determinant H for copolymer composition. In each case, the overall optimality criterion was calculated, which was the summation of the H determinants for the three responses (D = H(x) + H ($\bar{F}_{AN}$) + H (M_w)). It was observed that using the four 4-trial designs from M_w decreased the overall optimality criterion less (D (M_w) = 50.12 vs. D ($\bar{F}_{AN}$) = 49.52 and D (x) = 50. 06). Hence, one of the 4-trial designs from the M_w response had to be chosen as the optimal design for the first sequence of experiments.

To choose the best 4-trial design out of the 4 optimal options of M_w, considerable brainstorming had to be carried out. With respect to the output levels of the CSTR train, one usually aims at sufficiently high levels of conversion (for productivity reasons) and molecular weight averages (for product quality and final rubber property balance), at the same time trying to achieve a range of copolymer composition content to be as narrow as possible (for improved copolymer chain compatibility) around 25%. In doing so and keeping in mind the above CSTR train general output specifications, we decided to favor experimental trials with higher levels of INT and E flow rates and lower WM levels. These choices were made in order to produce polymer particles with smaller particle size (E effect) and reduce the probability of extremely high chain lengths and branching/cross-linking levels (INT effect), while trying to maintain production rate at high levels (low WM and high INT). After applying the above logic, the first sequence of 4-trial experiments was chosen and is shown in Table 6.9. The corresponding x, $\bar{F}_{AN}$ and M_w responses are also shown in Table 6.9 and were calculated via adding a random error to the response generated from the mechanistic model.

Table 6.9 **First** 4-trial sequence

INT	E	WM	CTA	x	$\bar{F}_{AN}$	M_w
-1	-1	-1	1	0.788	0.367	166,430
-1	1	1	1	0.574	0.173	114,552
1	-1	1	-1	0.325	0.168	22,240
1	1	-1	-1	0.683	0.386	151,480

Next, Eq. 6.3 in Table 6.3 can be employed to calculate the posterior variance/covariance matrices. The prior vector of parameter means ($\underline{\alpha}$) and the prior $\underline{U}$s, shown in the second and third columns of Table 6.6, Table 6.7 and Table 6.8, are used along with the $\underline{X}$ matrix (shown in Table 6.9) and responses (reported in the last three columns of Table 6.9) in order to calculate posterior variance/covariance matrices. The corresponding matrices for conversion, copolymer composition, and weight-average molecular weight responses are shown in Table 6.10, Table 6.11, and Table 6.12, respectively. One can now observe the presence of nonzero off-diagonal elements, i.e., covariance elements, in the updated $\underline{U}$ matrices.

The updated variance/covariance matrix can now be used back in Eq. 6.1 to design (in an iterative sequential fashion) the next 4-trial sequence that maximizes the determinant H. In the second sequence, only one optimal 4-trial design for each x, $\bar{\bar{F}}_{AN}$ and M_w was found to maximize the determinant H. In order to find a design that was nearly optimal for all responses, the designs from one response were used in the H recalculations for the other two responses and the overall optimality criterion (D) was calculated in the same way as discussed for the first sequence. For example, the optimal design from conversion was used in the H recalculation for copolymer composition and molecular weight (using $\underline{U}_{posterior}$ from copolymer composition and molecular weight, respectively) and vice versa (the designs from copolymer composition and molecular weight were used in the H recalculations for conversion). Again, upon scrutinizing the overall optimality criterion (D), the 4-trial sequence designed through molecular weight decreased the overall D less dramatically. Table 6.13 shows the design that was chosen along with the corresponding responses shown in the last columns, calculated as explained earlier. Comparing Table 6.9 and Table 6.13, one can see that levels for INT, E and CTA are the same in both sequences and the only difference between the two sequences is in the levels of WM.

Table 6.10 Posterior variance/covariance matrix U after the **first** 4-trial sequence for **conversion** response

5.00E-04														
0	3.97E-06													
0	0	5.16E-05												
0	0	0	5.18E-04											
0	1.02E-11	0	0	1.60E-09										
0	0	0	8.29E-09	0	1.00E-08									
0	0	8.24E-08	0	0	0	9.99E-07								
8.00E-11	0	0	0	0	0	0	1.00E-10							
0	1.59E-11	0	0	-6.36E-15	0	0	0	2.50E-09						
0	0	0	-8.29E-35	0	2.74E-40	0	0	0	1.00E-34					
0	0	-4.04E-36	0	0	0	7.18E-38	0	0	0	4.90E-35				
5.12E-07	0	0	0	0	0	0	-2.05E-14	0	0	0	6.40E-07			
0	0	5.28E-10	0	0	0	-9.38E-12	0	0	0	4.60E-40	0	6.40E-09		
0	0	0	5.30E-09	0	-1.75E-14	0	0	0	1.75E-40	0	0	0	6.40E-09	
-8.00E-35	0	0	0	0	0	0	3.20E-42	0	0	0	2.05E-38	0	0	1.00E-34

Table 6.11 Posterior variance/covariance matrix U after the **first** 4-trial sequence for **cumulative copolymer** response

5.00E-04														
0	8.09E-07													
0	0	9.98E-07												
0	0	0	8.09E-07											
0	2.07E-14	0	0	1.60E-11										
0	0	0	2.19E-13	0	1.69E-10									
0	0	3.59E-11	0	0	0	2.25E-08								
2.00E-11	0	0	0	0	0	0	2.50E-11							
0	2.91E-11	0	0	-5.75E-16	0	0	0	2.25E-08						
0	0	0	-3.24E-14	0	6.75E-18	0	0	0	2.50E-11					
0	0	-3.99E-14	0	0	0	8.99E-16	0	0	0	2.50E-11				
8.00E-09	0	0	0	0	0	0	-8.00E-17	0	0	0	1.00E-08			
0	0	1.02E-13	0	0	0	-2.30E-15	0	0	0	2.56E-18	0	6.40E-11		
0	0	0	8.28E-14	0	-1.73E-17	0	0	0	2.56E-18	0	0	0	6.40E-11	
-5.12E-11	0	0	0	0	0	0	5.12E-19	0	0	0	2.05E-16	0	0	6.40E-11

Table 6.12 Posterior variance/covariance matrix U after the **first** 4-trial sequence for **weight-average molecular weight** response

1.25E+08														
0	2.22E+06													
0	0	2.16E+07												
0	0	0	7.51E+07											
0	1.55E+05	0	0	1.14E+07										
0	0	0	4.79E+03	0	1.00E+04									
0	0	5.40E+03	0	0	0	4.00E+04								
2.59E+04	0	0	0	0	0	0	3.24E+04							
0	9.21E+04	0	0	-5.02E+05	0	0	0	6.99E+06						
0	0	0	-2.69E+05	0	1.87E+01	0	0	0	5.61E+05					
0	0	-5.40E+05	0	0	0	8.64E+02	0	0	0	3.91E+06				
1.28E+05	0	0	0	0	0	0	-6.63E+00	0	0	0	1.60E+05			
0	0	5.40E-01	0	0	0	-8.64E-04	0	0	0	8.64E-02	0	4.00E+00		
0	0	0	3.06E+01	0	-2.13E-03	0	0	0	1.20E-01	0	0	0	6.40E+01	
-2.00E+05	0	0	0	0	0	0	1.04E+01	0	0	0	5.12E+01	0	0	2.50E+05

Table 6.13 **Second** 4-trial sequence

INT	E	WM	CTA	x	$\overline{F}_{AN}$	M_w
-1	-1	1	1	0.497	0.361	99,702
-1	1	-1	1	0.867	0.181	101,240
1	-1	-1	-1	0.607	0.371	109,770
1	1	1	-1	0.401	0.179	143,091

The updated variance/covariance matrices are shown in Table 6.14, Table 6.15, and Table 6.16. Comparing variance/covariance matrices after the first and second sequence for each response (for example, compare Table 6.10 and Table 6.14 for conversion), one can see that after the second sequence of experiments, the uncertainties about the parameters (diagonal elements of the U matrix) have decreased. Also, most of the covariances (off-diagonal elements of the U matrix; measures of the strength of the correlation between parameters) appearing in the first sequence (Table 6.10) are zero in the second sequence (Table 6.14). This trend is the same for the other two responses. Eq. 6.2 of Table 6.3 can now be employed to calculate the posterior vector of parameters ($\underline{\theta}$) after each sequence of 4-trials for each response. Further remarks about these results are presented in the *Statistical Diagnostic Tests* section.

Table 6.14 Posterior variance/covariance matrix U after the **second** 4-trial sequence for **conversion** response

2.78E-04														
0	3.95E-06													
0	0	4.77E-05												
0	0	0	2.83E-04											
0	2.02E-11	0	0	1.60E-09										
0	0	0	0	0	1.00E-08									
0	0	0	0	0	0	9.97E-07								
8.89E-11	0	0	0	0	0	0	1.00E-10							
0	0	0	0	0	0	0	0	2.50E-09						
0	0	0	0	0	3.20E-39	0	0	0	1.00E-34					
0	0	0	0	0	0	1.56E-37	0	0	0	4.90E-35				
0	0	0	0	0	0	0	0	0	0	0	6.39E-07			
0	0	9.76E-10	0	0	0	0	0	0	0	0	0	6.40E-09		
0	0	0	5.80E-09	0	0	0	0	0	0	0	0	0	6.40E-09	
0	0	0	0	0	0	0	0	0	0	0	2.04E-37	0	0	1.00E-34

Table 6.15 Posterior variance/covariance matrix U after the **second** 4-trial sequence for **cumulative copolymer** response

2.78E-04														
0	8.08E-07													
0	0	9.97E-07												
0	0	0	8.08E-07											
0	4.14E-14	0	0	1.60E-11										
0	0	0	0	0	1.69E-10									
0	0	0	0	0	0	2.25E-08								
2.22E-11	0	0	0	0	0	0	2.50E-11							
0	0	0	0	0	0	0	0	2.25E-08						
0	0	0	0	0	1.35E-17	0	0	0	2.50E-11					
0	0	0	0	0	0	1.80E-15	0	0	0	2.50E-11				
0	0	0	0	0	0	0	0	0	0	0	1.00E-08			
0	0	2.04E-13	0	0	0	0	0	0	0	0	0	6.40E-11		
0	0	0	1.65E-13	0	0	0	0	0	0	0	0	0	6.40E-11	
0	0	0	0	0	0	0	0	0	0	0	2.05E-15	0	0	6.40E-11

Table 6.16 Posterior variance/covariance matrix U after the **second** 4-trial sequence for **weight-average molecular weight** response

6.95E+07														
0	2.20E+06													
0	0	1.89E+07												
0	0	0	5.06E+07											
0	2.98E+05	0	0	1.06E+07										
0	0	0	0	0	1.00E+04									
0	0	0	0	0	0	4.00E+04								
2.88E+04	0	0	0	0	0	0	3.24E+04							
0	0	0	0	0	0	0	0	6.67E+06						
0	0	0	0	0	7.15E+01	0	0	0	5.58E+05					
0	0	0	0	0	0	1.95E+03	0	0	0	3.81E+06				
0	0	0	0	0	0	0	0	0	0	0	1.60E+05			
0	0	9.70E-01	0	0	0	0	0	0	0	0	0	4.00E+00		
0	0	0	4.15E+01	0	0	0	0	0	0	0	0	0	6.40E+01	
-2.00E+05	0	0	0	0	0	0	1.04E+01	0	0	0	5.12E+01	0	0	2.50E+05

6.3.1.2 Single 8-Trial Experiment

The sequential approach is now contrasted to the design of a "single" 8-trial experiment, in which eight experiments are designed at once. In this approach, the prior vector of parameter means ($\underline{\alpha}$) and the prior $\underline{U}$s (see Table 6.6, Table 6.7, and Table 6.8 for conversion, copolymer composition and weight-average molecular weight, respectively) are used directly to design eight experiments at once. The Bayesian design suggested two sets of 8-trial experiments for each response and again, the analysis showed that the experiments designed for molecular weight decrease the overall D less; hence, one of the 8-trial experiments was chosen as the optimal 8-trial experiment and is shown in Table 6.17. For comparison purposes, the values of the H determinant and overall optimality criterion (D) of the sequential approach are shown in Table 6.18 along with the corresponding values for the single 8-trial experiment. It can be seen from the overall D that the single 8-trial experiment is only slightly better than the sequential approach. Keeping in mind the flexibility that the sequential approach offers (e.g., changing the level of factors, adding/dropping factors, etc.) and due to the fact that the single 8-trial approach is not producing a significantly higher D value, the sequential approach is deemed a better way of designing a total of eight runs.

Table 6.17 **"Single"** 8-trial experiment along with the responses

INT	E	WM	CTA	x	$\bar{F}_{AN}$	M_w
-1	-1	-1	-1	0.588	0.167	100,580
-1	-1	1	1	0.497	0.161	99,702
-1	1	-1	1	0.667	0.181	101,240
-1	1	1	-1	0.374	0.374	35,391
1	-1	-1	1	0.807	0.371	173,880
1	-1	1	-1	0.325	0.368	122,240
1	1	-1	-1	0.883	0.186	151,480
1	1	1	1	0.601	0.379	120,461

Table 6.18 Comparison of sequential approach with single 8-trial experiment

	Determinant H			
Experiment	**x**	$\overline{F}_{AN}$	M_w	**Overall D**
2 sequences of 4-trials	115.48443	9.07728	46.63024	171.19411
Single 8-trial	115.48448	9.07728	46.80732	171.36907

6.3.1.3 Comparison with Standard Statistical Designs

Several qualitative statements have been made in the previous sections regarding the superiority of the Bayesian design with respect to standard factorial designs. In order to reinforce these previous statements, a quantitative measure is presented, where experiments designed through the Bayesian approach are compared with 8-trial experiments designed through fractional factorial and Plackett–Burman designs.

The 8-trial experiment designed through the Bayesian approach was compared with a 2_{IV}^{4-1} fractional factorial design. The comparison was made based on the value of the determinant H. The 2_{IV}^{4-1} design is a $\frac{1}{2}$ fraction of a full 2^4 factorial experiment and consists of a total of 8 runs. The two half-fractions recommended by a regular fractional factorial design are shown in Table 6.19. It can be seen that Fraction 1 is exactly the same as the 8-trial experiment designed through the Bayesian design (compare Table 6.17 and Table 6.19), hence giving exactly the same H values. Fraction 2 also gives the same H values for all responses. Therefore, one can say that the Bayesian suggestion for the 8-trial experiment is at least as good as the standard fractional factorial design experiment in the D-optimal sense. Therefore, overall, the Bayesian design is superior, since it offers the extra flexibility of designing sequences of fewer trials with the related benefits, as discussed earlier herein and also in earlier chapters.

Table 6.19 Two half-fractions from standard **fractional factorial** design

Fraction 1				Fraction 2			
INT	**E**	**WM**	**CTA**	**INT**	**E**	**WM**	**CTA**
-1	-1	-1	-1	-1	-1	-1	1
-1	-1	1	1	-1	-1	1	-1
-1	1	-1	1	-1	1	-1	-1
-1	1	1	-1	-1	1	1	1
1	-1	-1	1	1	-1	-1	-1
1	-1	1	-1	1	-1	1	1
1	1	-1	-1	1	1	-1	1
1	1	1	1	1	1	1	-1

Next, the 8-trial experiment designed through the Bayesian approach was compared with an 8-trial experiment designed through a Plackett–Burman (PB) design. PB designs are economical designs with the run number a multiple of four rather than a power of 2. The number of runs for typical Plackett-Burman designs are 4, 8, 12, 16, 20 and so on. PB designs allow the estimation of k main effects using k + 1 runs. These designs are very efficient screening designs when only main effects are of interest. PB designs are resolution III, meaning that main effects are, in general, heavily confounded with two-factor interactions. Therefore, these designs are very useful for economically detecting large main effects, only when one can assume that all interactions are negligible compared to the important main effects (Montgomery, 2005).

In our case, we were looking for designing 8 runs for 4 factors. 8 runs could be designed using a 2^3 full factorial. A 2^3 design could accommodate up to 7 factors in the PB context. To construct a PB design for 4 factors, 3 columns of a 2^3 design should be dropped. Table 6.20 presents the corresponding PB designs along with their overall optimality criterion (D). Design No. 1 is only slightly better than the 8-trial sequence from the Bayesian design, when comparing the overall optimality criterion values (D) ($D_{Bayesian}$ = 171.36907 vs. D_{PB} = 171.36912). Designs No. 2 and 3 both give D values much lower than the D value from the Bayesian design. Design No. 4 is exactly the same as the 8-trial from the Bayesian design, hence, has the same D. Once again, one can conclude that the Bayesian design experiment is better than or as good as the PB design experiments in the D-optimal sense.

Table 6.20 8-trial runs from **Plackett–Burman** (PB) designs

No	INT	E	WM	CTA = INT × E	Overall D
1	-1	-1	-1	1	171.36912
	-1	-1	1	1	
	-1	1	-1	-1	
	-1	1	1	-1	
	1	-1	-1	-1	
	1	-1	1	-1	
	1	1	-1	1	
	1	1	1	1	
	INT	**E**	**WM**	**CTA = INT × WM**	**Overall D**
2	-1	-1	-1	1	171.30833
	-1	-1	1	-1	
	-1	1	-1	1	
	-1	1	1	-1	
	1	-1	-1	-1	
	1	-1	1	1	
	1	1	-1	-1	
	1	1	1	1	
	INT	**E**	**WM**	**CTA = E × WM**	**Overall D**
3	-1	-1	-1	1	169.96154
	-1	-1	1	-1	
	-1	1	-1	-1	
	-1	1	1	1	
	1	-1	-1	1	
	1	-1	1	-1	
	1	1	-1	-1	
	1	1	1	1	
	INT	**E**	**WM**	**CTA = INT × E × WM**	**Overall D**
4	-1	-1	-1	-1	171.36907
	-1	-1	1	1	
	-1	1	-1	1	
	-1	1	1	-1	
	1	-1	-1	1	
	1	-1	1	-1	
	1	1	-1	-1	
	1	1	1	1	

6.3.2 Statistical Diagnostic Tests

A series of statistical diagnostic tests can now be carried out in addition to results discussed in subsection 6.3.1. These diagnostic tests serve to quantify the relative importance of the parameters (i.e., factor effects) and their interactions, as well as the quality of prior knowledge (in other words, the adequacy of the model used to generate the "prior knowledge", as the case might be).

Results from these statistical diagnostic tests are shown in Table 6.21, Table 6.22, and Table 6.23 for conversion, copolymer composition, and molecular weight responses, respectively. The 2nd column in all tables presents the initial values of the parameter means ($\underline{\alpha}$); the 3rd and 4th columns contain the updated estimates of the parameter means after the first and second sequence, respectively. The 5th column shows the estimates of parameter means after the "single" 8-trial experiment. Test 1 (10th column of Table 6.21, Table 6.22, and Table 6.23) is defined as the ratio of the prior mean to the prior standard deviation (Std) of the mean $[\alpha_i/(U_{ii})^{1/2}]$. For example, in the case of conversion response (Table 6.21), test 1 is the ratio of the 2nd column, divided by the sixth column of Table 6.21. This test is essentially a measure of the uncertainty of the ''expert''.

Test 2 is a measure of the actual significance of an effect. For instance, the test 2 values after the second sequence of experiments for conversion response (12th column of Table 6.21) is equal to the second updated estimate of the effect, $\theta_i^{(2)}$ (4th column in Table 6.21), divided by the square root of the corresponding diagonal element of the last posterior variance/covariance matrix (8th column of Table 6.21), $[\theta_i^{(2)}/(U_{post(ii)})^{1/2}]$. There is another test (test 3) that measures the quality of the expert's opinion. For instance, test 3 after the second sequence of experimentation is equal to $(\theta_i^{(2)} - \alpha_i)$ divided by the square root of the diagonal element of the last posterior variance/covariance matrix, $[(\theta_i^{(2)} - \alpha_i)/(U_{post(ii)})^{1/2}]$. Test 3 is not shown here, since none of the values were significant which implies that the expert's opinion was valid, and the model used seemed reliable.

Table 6.21 shows the main effects and two factor interactions for the conversion response. Based on the results of test 2, among main factors, WM had the strongest effect followed by E and INT. WM had a large and negative effect on conversion. At first glance one might argue that this does not make sense, since we are increasing monomer flow rate and hence the rate of polymerization should increase. However, this was not the case here. In emulsion processes, the rate of polymerization is proportional to the concentration of monomer in the particles ($[M]_p$); see Eq. 6.4. The concentration of monomer in the particles is fixed in emulsion polymerization and is only affected by the thermodynamics of the system. Therefore, a higher flow rate of monomer will not affect $[M]_p$, it will just dilute the system and hence decrease conversion. In addition, a higher WM level has a higher water flow rate, and that also adds to the dilution effect.

$$R_p = k_p [M]_p \frac{N_p \bar{n}}{N_A} \qquad \text{Eq. 6.4}$$

R_p: Rate of polymerization
k_p : Propagation rate constant
$[M]_p$: Monomer concentration in particles
N_p : Number of particles
$\bar{n}$: Average number of radicals per particle
N_A: Avogadro's number

Both emulsifier (E) and initiator (INT) flow rates had a positive and relatively large effect on conversion. This is as expected; both effects influence the number of particles (N_p) and increasing N_p will increase the rate of polymerization, according to Eq. 6.4. Addition of more emulsifier creates more micelles, which could eventually lead to generation of more particles (higher N_p), and hence, a higher rate of polymerization. Addition of more initiator increases the number of radicals in the reaction mixture, which again results in generating more particles and increasing the rate of polymerization. Chain transfer flow rate (CTA) showed no significant effect on conversion response in our operating region (conversion range of 0.32 to 0.86), as expected. Among 2-factor interactions, INT × E, INT × WM and E × WM were significant. This was straightforward; as all three main factors were significant, the 2-factor interactions between them would be important too. Based on test 2, the most important 2-factor interaction influencing the conversion response was INT × E. Comparing tests 1 and 2 for the

conversion response, one can see that the expert's opinion has been valid in all cases and has predicted the significant effects correctly.

Results of the diagnostic tests for the copolymer composition response are cited in Table 6.22. Test 2 results showed that E, WM and INT were important effects, with the order of importance as cited here. Again, CTA did not show a significant effect on the copolymer composition response. The important 2-factor interactions were E× WM, INT × WM and E × WM.

Table 6.21 Summary results of diagnostic tests for **conversion** response

Parameter	**Prior** α_i	$\theta_i^{(1)}$	$\theta_i^{(2)}$	$\theta_i^{8-trial}$	**Prior Std**	**Std (after 1st seq.)**	**Std (after 2st seq.)**	**Std (after 8 trials)**	**Test 1**	**Test 2 (after1st seq.)**	**Test 2 (after 2nd seq.)**	**Test 2 (after 8 trials)**
Mean	5.93E-01	5.93E-01	5.93E-01	5.93E-01	5.00E-02	2.24E-02	1.67E-02	1.67E-02	11.86	26.50	35.57	35.57
INT	1.12E-02	1.06E-02	9.94E-03	1.18E-02	2.00E-03	1.99E-03	1.99E-03	1.99E-03	5.60	5.30	5.00	5.95
E	3.85E-02	3.85E-02	3.85E-02	3.85E-02	7.50E-03	7.18E-03	6.90E-03	6.90E-03	5.13	5.35	5.57	5.57
WM	-1.44E-01	-1.44E-01	-1.44E-01	-1.44E-01	5.50E-02	2.28E-02	1.68E-02	1.68E-02	-2.61	-6.31	-8.54	-8.54
CTA	-5.00E-05	-4.97E-05	-4.95E-05	-4.97E-05	4.00E-05	4.00E-05	4.00E-05	4.00E-05	-1.25	-1.24	-1.24	-1.24
INT × E	-5.25E-04	-5.25E-04	-5.25E-04	-5.23E-04	1.00E-04	1.00E-04	1.00E-04	1.00E-04	-5.25	-5.25	-5.25	-5.23
INT × WM	2.35E-03	2.35E-03	2.35E-03	2.19E-03	1.00E-03	9.99E-04	9.98E-04	9.98E-04	2.35	2.35	2.35	2.19
INT × CTA	1.25E-05	1.25E-05	1.25E-05	1.25E-05	1.00E-05	1.00E-05	1.00E-05	1.00E-05	1.25	1.25	1.25	1.25
E× WM	-1.12E-04	-1.12E-04	-1.13E-04	-1.12E-04	5.00E-05	5.00E-05	5.00E-05	5.00E-05	-2.25	-2.24	-2.25	-2.25
E × CTA	6.94E-18	6.94E-18	6.94E-18	6.94E-18	1.00E-17	1.00E-17	1.00E-17	1.00E-17	0.69	0.69	0.69	0.69
WM × CTA	-6.94E-18	-6.94E-18	-6.94E-18	-6.94E-18	7.00E-18	7.00E-18	7.00E-18	7.00E-18	-0.99	-0.99	-0.99	-0.99

Table 6.22 Summary results of diagnostic tests for **copolymer composition** response

Parameter	**Prior** α_i	$\theta_i^{(1)}$	$\theta_i^{(2)}$	$\theta_i^{8-trial}$	**Prior Std**	**Std (after 1st seq.)**	**Std (after 2st seq.)**	**Std (after 8 trials)**	**Test 1**	**Test 2 (after1st seq.)**	**Test 2 (after 2nd seq.)**	**Test 2 (after 8 trials)**
Mean	2.73E-01	2.73E-01	2.73E-01	2.73E-01	5.00E-02	2.24E-02	1.67E-02	1.67E-02	5.47	12.22	16.40	16.40
INT	2.62E-03	2.62E-03	2.62E-03	2.75E-03	9.00E-04	8.99E-04	8.99E-04	8.99E-04	2.91	2.91	2.91	3.06
E	6.53E-03	6.53E-03	6.37E-03	6.53E-03	1.00E-03	9.99E-04	9.98E-04	9.98E-04	6.53	6.54	6.38	6.54
WM	-2.94E-03	-3.07E-03	-3.07E-03	-2.81E-03	9.00E-04	8.99E-04	8.99E-04	8.99E-04	-3.27	-3.42	-3.42	-3.13
CTA	-6.25E-06	-6.25E-06	-6.25E-06	-6.25E-06	4.00E-06	4.00E-06	4.00E-06	4.00E-06	-1.56	-1.56	-1.56	-1.56
INT × E	-3.12E-05	-3.12E-05	-3.12E-05	-3.13E-05	1.30E-05	1.30E-05	1.30E-05	1.30E-05	-2.40	-2.40	-2.40	-2.41
INT × WM	3.94E-04	3.94E-04	3.90E-04	3.94E-04	1.50E-04	1.50E-04	1.50E-04	1.50E-04	2.63	2.63	2.60	2.63
INT × CTA	6.25E-06	6.25E-06	6.25E-06	6.25E-06	5.00E-06	5.00E-06	5.00E-06	5.00E-06	1.25	1.25	1.25	1.25
E× WM	-5.94E-04	-5.94E-04	-5.94E-04	-5.90E-04	1.50E-04	1.50E-04	1.50E-04	1.50E-04	-3.96	-3.96	-3.96	-3.93
E × CTA	-6.25E-06	-6.25E-06	-6.25E-06	-6.25E-06	5.00E-06	5.00E-06	5.00E-06	5.00E-06	-1.25	-1.25	-1.25	-1.25
WM × CTA	-6.25E-06	-6.25E-06	-6.25E-06	-6.25E-06	5.00E-06	5.00E-06	5.00E-06	5.00E-06	-1.25	-1.25	-1.25	-1.25

Table 6.23 Summary results of diagnostic tests for **weight-average molecular weight** response

Parameter	**Prior** α_i	$\theta_i^{(1)}$	$\theta_i^{(2)}$	$\theta_i^{8-trial}$	**Prior Std**	**Std (after 1st seq.)**	**Std (after 2st seq.)**	**Std (after 8 trials)**	**Test 1**	**Test 2 (after1st seq.)**	**Test 2 (after 2nd seq.)**	**Test 2 (after 8 trials)**
Mean	1.13E+05	1.13E+05	1.13E+05	1.13E+05	2.50E+04	1.12E+04	8.33E+03	8.33E+03	4.53	10.11	13.58	13.58
INT	3.31E+03	2.67E+03	2.70E+03	4.00E+03	1.50E+03	1.49E+03	1.48E+03	1.48E+03	2.20	1.79	1.82	2.71
E	1.40E+04	1.40E+04	1.40E+04	7.97E+03	5.00E+03	4.65E+03	4.35E+03	4.35E+03	2.81	3.02	3.22	1.83
WM	-4.37E+04	-4.37E+04	-2.75E+04	-2.75E+04	1.20E+04	8.66E+03	7.12E+03	7.12E+03	-3.64	-5.04	-3.86	-3.86
CTA	-1.48E+04	-1.13E+04	-1.15E+04	-1.14E+04	3.50E+03	3.38E+03	3.26E+03	3.25E+03	-4.22	-3.36	-3.52	-3.50
INT × E	-1.56E+02	-1.56E+02	-1.53E+02	-1.56E+02	1.00E+02	1.00E+02	1.00E+02	1.00E+02	-1.56	-1.56	-1.53	-1.56
INT × WM	-2.23E+02	-2.23E+02	-2.23E+02	-2.23E+02	2.00E+02	2.00E+02	2.00E+02	2.00E+02	-1.12	-1.12	-1.12	-1.12
INT × CTA	-4.03E+02	-4.03E+02	-4.03E+02	-4.03E+02	1.80E+02	1.80E+02	1.80E+02	1.80E+02	-2.24	-2.24	-2.24	-2.24
E× WM	-5.14E+03	-3.09E+03	-3.00E+03	-5.14E+03	2.70E+03	2.64E+03	2.58E+03	2.58E+03	-1.90	-1.17	-1.16	-1.99
E × CTA	-1.77E+03	-1.77E+03	-1.95E+03	-1.77E+03	7.50E+02	7.49E+02	7.47E+02	7.47E+02	-2.36	-2.36	-2.61	-2.37
WM × CTA	5.09E+03	5.09E+03	5.09E+03	5.09E+03	2.00E+03	1.98E+03	1.95E+03	1.95E+03	2.54	2.57	2.61	2.61

Table 6.23 summarizes the diagnostic checks for the weight-average molecular weight response. The significant factors affecting weight-average molecular weight were WM, CTA and E. WM had the highest and negative effect. Based on a simplified version of the relationship between some average molecular weight and the relevant rates of initiation, transfer and polymerization, as given by Eq. 6.5 (this equation will do for the purposes of our discussion and analysis, even if simplified), as R_p decreases, so does the average molecular weight of the polymer produced. Let's call this average molecular weight MW. As explained previously, the WM factor has a negative effect on R_p due to dilution, hence the same effect on MW (and, eventually, we would expect the same effect on number- and weight-average molecular weights). The strongly significant effect of CTA is an important demonstration of why CTAs are widely used for molecular weight control, especially in rubber production. The CTA effect manifested itself in the rate of transfer (R_{tr}) in Eq. 6.5. The transfer of a radical center from a growing polymer radical to the CTA stops the growth of the polymer radical and thus lowers the molecular weight and that is why R_{tr} is inversely proportional to MW in Eq. 6.5. Emulsifier flow rate (E) affects molecular weight through R_p; as discussed previously, increasing E, increases R_p and therefore MW increases with increasing E (see Eq. 6.5). An interesting point to note here is that the INT flow rate is not detected as an important factor in the diagnostic tests for average molecular weight. The reason could be that increasing INT will affect both R_I and R_p and, as can be seen in Eq. 6.5, these two could have the tendency to cancel out and that might explain the reason why the effect of INT does not appear significant in test 2 of Table 6.23. As for the effect of 2-factor interactions on MW all the 2-factor interactions involving CTA were deemed important (E× CTA, INT× CTA and WM × CTA).

$$\frac{1}{MW} = \frac{R_I}{R_p} + \frac{R_{tr}}{R_p} \qquad \text{Eq. 6.5}$$

MW: some average molecular weight

R_I: Initiation Rate

R_{tr}: Rate of transfer reactions

R_p: Propagation rate

In all the diagnostic check tables above, test 2 is reported after the first 4-trials (after 1st seq.), after the second 4-trials (after 2nd seq.), and after the single 8-trial (see columns 11th, 12th and 13th in Table 6.21, Table 6.22, and Table 6.23). The results show that in most cases, basically

the same conclusions can be drawn from the diagnostic tests, even after the first 4-trial experiment. Hence, if one is interested solely in determining the relative importance of process factors (significant parameters), one sequence of 4-trials is sufficient to address that. However, depending upon the intended target, if one is more focused on parameter precision, then the second sequence of four trials or a "single" 8-trial may be desirable in order to decrease parameter uncertainty (translated into lower parameter variances). However, in this specific case, there is not much difference between the variances from the 1st sequence, 2nd sequence and 8-trials (compare columns 7th, 8th and 9th of Table 6.21, Table 6.22, and Table 6.23, respectively). In conclusion, one can run only 4 trials and obtain the same trends as the ones after 8 trials and this is, once again, yet another demonstration of the benefits of the sequential approach and the Bayesian approach, in general.

6.4 Concluding Remarks

The Bayesian design technique, previously shown to be a valuable approach in the study of batch homopolymerization of styrene in bulk, was also proven to be a practical tool in designing experiments for the emulsion copolymerization of AN/Bd in a continuous train of CSTRs. This was the first time that the Bayesian design of experiments was implemented to a continuous process. The motivation behind this study was to investigate the potential of the Bayesian design of experiments in relation to the Evolutionary Operation (EVOP) in a continuous process.

It was shown that designing 8 experiments in two sequences of 4-trials each was almost as good an option as designing a single 8-trial experiment. The sequential nature of the Bayesian approach offers the flexibility to change the conditions with relative ease. Comparison with standard experimental designs, namely, fractional factorial and Plackett-Burman designs showed that the Bayesian design is better than or as good as the standard experimental design techniques in the D-optimal sense. Therefore, overall, the Bayesian design is superior, since it offers the extra flexibility of designing sequences of fewer trials with the related benefits, as discussed earlier herein and also in earlier chapters.

Finally, the Bayesian approach is amenable to formal statistical diagnostic tests, which can eventually shed more light on the quality of prior knowledge and the significance of the estimated effects (relative importance of factors), and through these on some of the most uncertain parts of out process understanding (model). The results of these statistical tests revealed that the model used was indeed valid and confirmed many established kinetic theories. In addition, it was shown that INT, E and WM were significant factors for conversion and copolymer composition, while CTA did not have any significant effect. The factors influencing molecular weights were INT, WM and CTA.

Chapter 7. Gazing into the Abyss

Both experience and educational research have indicated over many years that almost all PhD students go through ups and downs during their PhD program. Therefore, the corresponding PhD trajectory would look like a typical oscillatory behavior, with satisfaction as the positive part of the graph, and frustration as the negative part of it. This graph (satisfaction and frustration curves versus the different stages of the PhD program) has a horizontal line at zero, so one may see satisfaction as positive 'bursts', followed by frustration as negative 'dips'. Of course, if one is learning something, the frustration curves may dominate, whereas the satisfaction curves will become more apparent when the experimental or modeling work produces good results. My supervisor had explained these aspects by going over a talk that he had given on the subject in the late 1980s.

Not surprisingly, my own PhD trajectory followed this typical behavior. I was certainly elated when I passed my PhD comprehensive exam successfully, in Jan. 2009, but shortly after that, I hit the frustration part of the curves, as nothing wanted to work or produce the expected results! During this frustrating period, my supervisor had several long discussions with me, in which he explained what was happening to me, and in fact managed to anticipate most of the situations and emotions that I was going through. He indicated that at some point after the PhD comprehensive exam, the PhD candidate can obtain a very good appreciation of the concept of infinity or the 'abyss' ahead of her/him, and that was exactly what I was going through. I tried many different ways to get out of the quagmire and get on with the program, however, nothing seemed to work! To cut a long story short, finally, in Dec. 2010, I decided to pay a visit to some friends in Chile as an immediately-acting and strong medication (my supervisor was very supportive of me taking that break in order to recharge my batteries).

While in Chile, I saw a very interesting painting that depicted a small Aymara (the indigenous ethnic group in the Andes and Altiplano regions of South America) family, taking a mid-day rest, with their water gourds on the side, at the edge of a hill in the Andean Altiplano (a high plateau in the Andes). The painting stayed with me and when I came back to Canada, well rested and eventually cured from the 'frustration malady', I decided to paint my own rendition of the Chilean painting in watercolor media.

My painting is shown in Figure 7.1. It is based on the Chilean painting that I came across during my travels, but it is my own interpretation. It is entitled ‘Gazing into the Abyss’, and shows two people, gazing down at the abyss of the high planes of the Andes, with their water gourds on the side. This painting is, of course, metaphorical and depicts me and my supervisor, while gazing at the abyss of my PhD research. Indeed, with my supervisor always on my side, willing not only to offer technical opinions and guidance at any time, but also willing to admit and accept that sometimes he also could just sit along with me and gaze at the abyss himself, my job became less daunting.

This painting is dedicated to my supervisor and mentor, and many times a “father-figure”, and always a good friend, Professor Alexander Penlidis, with many thanks for his willingness to be supportive in different ways, matching my different learning needs, at every step along the PhD “Altiplano Pass”, always full of challenging (and rather tempting) ideas in long tea sessions!

Figure 7.1 Gazing into the Abyss (Nabifar A., Feb 2010)

Chapter 8. Bayesian Design Applied to Cross-liking NMRP of Styrene with Divinyl Benzene

Cross-linked polymers (polymer networks) are very important in technology, medicine, biotechnology, agriculture, and other areas. They are used as construction materials, paints and coatings, polymer glasses with high mechanical strength and high thermal stability, rubbers, ion-exchange resins and sorbents, insoluble polymer supported reagents, controlled drug-release matrices, electronics and cables, food packaging, sensors, ‘‘smart’’ materials, artificial organs, implants, superabsorbent materials, etc. In order to obtain an optimal performance in most of these applications, a uniform structure of the polymer network is desirable.

Usually, cross-linked polymers are produced via regular free-radical polymerization (FRP). The polymerization is very fast and leads to polymer networks with high gel content at fairly low conversion levels. This makes cross-linking through FRP not a well-controlled process and the networks that are formed are not homogeneous. That means that within one sample, some sections may be very tightly cross-linked (high crosslink density), while other sections could exhibit a very loose network. This poses a problem, since a varying property distribution at the molecular level (i.e., heterogeneity) can lead to a polymer having inconsistent macroscopic properties. While the high density crosslinks will likely form a glassy substance, the lower density crosslinks will form a more amorphous gel. The non-uniformity of network morphology within cross-linked polymers makes consistent production challenging and limits their marketability. Therefore, it would be desirable to search for a synthetic route to produce polymer networks with homogenous structure (morphology).

Recently, the claim has been made that cross-linking under controlled radical polymerization (CRP) conditions might result in a more homogeneous network. Therefore, synthesis, characterization and modeling of polymer networks by CRP have received considerable attention in the last decade and production of cross-linked polymer by controlled radical copolymerization of vinyl and divinyl monomers has already been addressed in the open literature. The relevant literature review will be discussed in detail in Chapter 9 (the experimental chapter) and not repeated here for the sake of brevity. However, the main

conclusion, based on the comprehensive literature review of Chapter 9 is as follows: although the research conducted in the literature points to the direction that production of a more homogeneous polymer network is possible through CRP techniques, the hard evidence is only indirect and based on rather theoretical speculations of how polymer networks are produced. Perhaps, a more detailed and comprehensive study is required to clarify many existing conflicting statements encountered in the literature, and also find a more formal, direct, and reliable way (if such a way exists) of characterizing the cross-linked polymer network with respect to homogeneity (and the closely related cross-link density distribution).

These observations motivated our work on cross-linking nitroxide-mediated radical polymerization (NMRP) of styrene (STY) in the presence of small amounts of a common cross-linker, divinyl benzene (DVB). The cross-linked copolymer of STY/DVB is used for chromatographic applications and as a precursor for ion-exchange resins. It is also a system well studied under regular free radical polymerization conditions, hence an excellent system for the fundamental comparison between networks synthesized through CRP and FRP, and also for addressing the quest to identify a more formal indicator for network homogeneity.

An experimental study of the cross-linking NMRP of STY with DVB was first carried out in our group following a bimolecular NMRP approach, where a popular nitroxide controller, 2,2,6,6-tetramethyl-1-piperidinyloxy (TEMPO), was added to the mixture of monomers and (a typical) initiator, such as benzoyl peroxide (BPO) (Tuinman et al., 2006). The results on monomer conversion, molecular weights, gel fraction, and swelling index were compared against a STY/DVB copolymer synthesized through FRP. No significant auto-acceleration effect was detected in the early and intermediate conversion ranges. It was observed that the gelation point was significantly delayed. However, based on the experimental data collected, it was not possible to offer any statements related to the homogeneity of the network synthesized through NMRP.

Later on, a detailed mechanistic model for cross-linking NMRP of STY with DVB was developed in our group (Hernandez-Ortiz et al., 2009). Performance of the model was validated using the experimental data available from Tuinman et al. (2006). The agreement between model predictions and experimental data for polymerization rate, molecular weights,

gelation point and sol consumption was fairly good. However, the experimental data available were focused on only one nitroxide concentration, and molecular weight and gel content data were not collected over the whole conversion range. Hence, supplementary experimental information was required in order to:

- Fully verify the validity of the trajectories predicted by the model
- Develop the ability of the model further to use nitroxides other than TEMPO
- Address our question of whether a network synthesized through NMRP is more homogeneous than the network produced through FRP

Since considerable prior knowledge related to cross-linking NMRP of styrene with DVB was already available from previous experimental and modeling efforts, application of the Bayesian design of experiments seemed like a perfect approach. By using the Bayesian design technique, the valuable prior knowledge would be practically incorporated into the design. This would help to come up with the "best" settings, to be carried out in the laboratory, to collect meaningful experimental data that could satisfy the needs mentioned above. In addition, using the Bayesian design would, in principle, result in running fewer experiments, hence saving considerable time and resources (since a typical polymerization trial, and especially a cross-linking polymerization one, may take more than a month, to plan, prepare, execute, and subsequently fully characterize the resulting polymer product).

For the above reasons, it was decided to apply the Bayesian design of experiments to cross-linking NMRP of styrene with DVB. Implementation of the Bayesian design to this system is discussed in this chapter. Information about the model developed and further detailed literature background will be presented, at length, in Chapter 9 and not repeated here for the sake of brevity.

8.1 Bayesian Design Preliminaries

As explained in Chapter 3 and summarized in Figure 8.1, implementation of the Bayesian design of experiments requires several steps. A step by step discussion on the application of the Bayesian design methodology to cross-linking NMRP of STY with DVB is presented in this

chapter. The related experimental parts (e.g., polymerization method, characterization techniques, etc.) are presented in detail in Chapter 9.

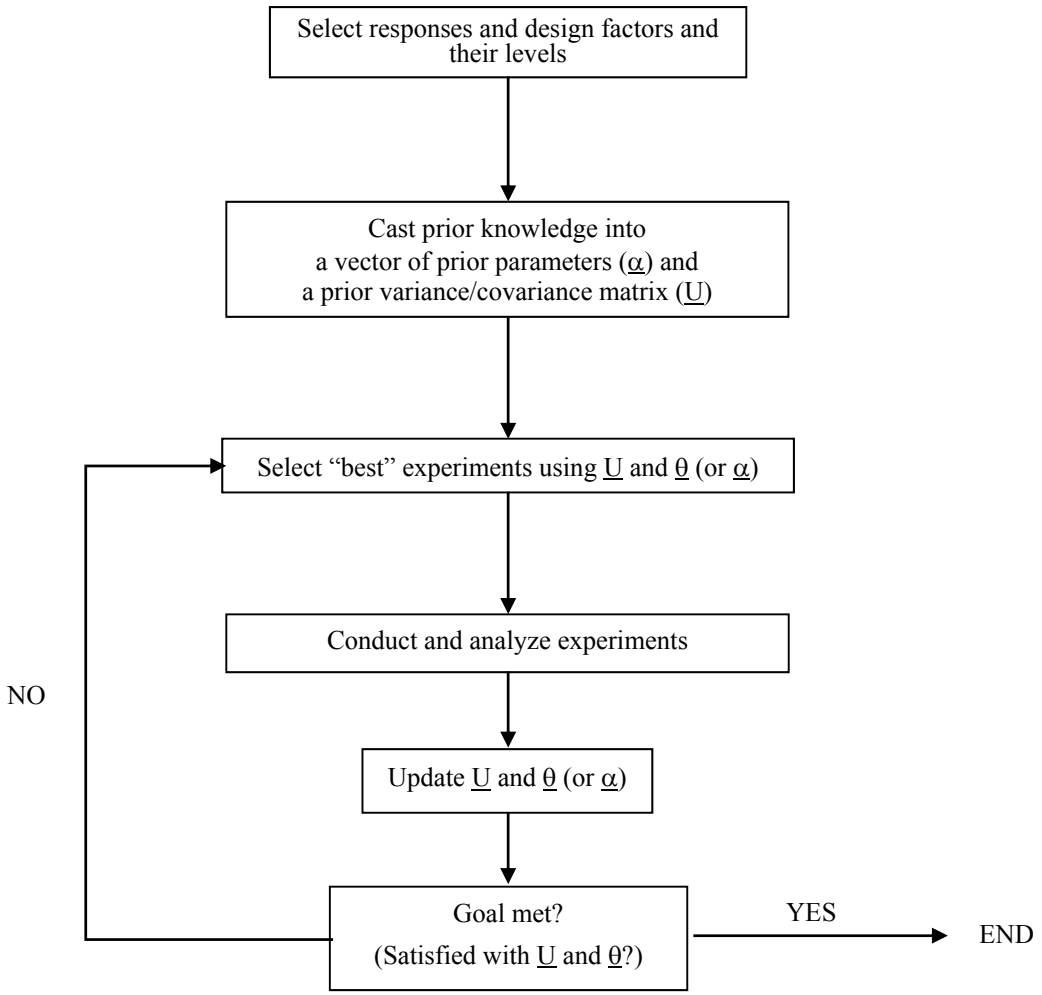

Figure 8.1 Procedure for the Bayesian design of experiments

Selection of Design Factors and Levels: As can be seen in Figure 8.1, the first step in the Bayesian procedure is selecting design factors and their levels. Three factors were chosen and are shown (with their initial levels) in Table 8.1. Selection of factors and their low and high level values were based on a detailed and critical analysis of the literature (Ide & Fukuda, 1999; Drache et al., 2007; Zhou et al., 2010), combined with some of our previous experience with cross-linking NMRP (Tuinman et al., 2006; Hernandez-Ortiz et al., 2009). Based on our

prior information, it was felt that temperature (T), concentration of alkoxyamine initiator ([N]) and concentration of the cross-linker ([DVB]) could be influential factors in the cross-linking polymerization of STY and DVB.

Table 8.1 Selected factors and their levels (cross-linking NMRP; T = temperature, [N] = alkoxyamine concentration, [DVB] = cross-linker concentration)

Level	T (°C)	[N] (wt%)	[DVB] (wt%)
low	120	1	1
high	130	2	1.5

In the case of temperature, low and high levels chosen were 120 and 130 °C because these were common temperatures used in NMRP polymerization of styrene and values of kinetic rate constants were readily available for these two temperatures. Divinyl benzene (DVB) was used as the cross-linker. The cross-linked copolymerization of STY/DVB is a system well studied under regular free radical polymerization conditions, and also some research has already been carried out on the cross-linking NMRP of STY/DVB in our group (Tuinman et al., 2006; Hernandez-Ortiz et al., 2009) and in the literature (e.g., Ide & Fukuda, 1997; Ide & Fukuda, 1999; Zetterlund et al., 2005; Zetterlund et al., 2006).

It was decided to use an alkoxyamine unimolecular initiator as opposed to using a nitroxide and a bimolecular approach. An alkoxyamine can act as both initiator and nitroxide upon decomposition. By using a unimolecular approach one can avoid the complications that occur because of the side reactions between nitroxide and the (peroxide) initiator in the bimolecular approach, as discussed by Moad et al. (1981), Georges et al. (2002) and Fu et al. (2007). A unimolecular initiator based on TEMPO was synthesized in our lab and a comprehensive kinetic study on the polymerization of styrene with this unimolecular initiator was carried out by Zhou et al. (2010). Based on this experience, it was decided to use a commercially available alkoxyamine initiator, as it would eliminate the difficulties involved in making the unimolecular initiator consistently. After a complete survey of the commercially available alkoxyamine initiators, N-tert-butyl-N-(2-methyl-1-phenylpropyl)-O-(1-phenylethyl)hydroxylamine (TIPNO-based alkoxyamine) was chosen, since based on previous research, relatively faster rates could be achieved using this alkoxyamine (Benoit et al., 1999;

Drache et al., 2007). When decomposing, this alkoxyamine produces 2,2,5-trimethyl-4-phenyl-3-azahexane-3-nitroxide which is known as a TIPNO nitroxide. TIPNO and its alkoxyamine were first synthesized by Benoit et al. (1999), where a series of acyclic α-hydrogen-bearing nitroxides and their corresponding alkoxyamines were synthesized to be used for the controlled radical polymerization of a wide range of monomers.

One wt% (with respect to monomer) was chosen for the low level values of both alkoxyamine initiator and cross-linker. For the high level value of alkoxyamine initiator, 2 wt% was chosen; based on Drache et al. (2007), polymerization of styrene with 2 wt% TIPNO-based alkoxyamine had the characteristics of controlled-radical polymerization and gave acceptable rates, without TIPNO slowing the reaction considerably or acting as an inhibitor. Based on our previous experience with cross-linking polymerization of STY with DVB (Tuinman et al., 2006), it was noted that handling the polymerization mixture was very difficult with 3 wt% DVB, as the system gelled very quickly and the polymer mixture became very viscous; hence, 1.5 wt% was chosen as the high level for the cross-linker.

Selection of Responses: It was decided that three responses satisfied our objectives of controlling the polymer production rate and product quality. The responses chosen were: conversion at gel point, gel content at 85% conversion, and weight-average molecular weight at 45% conversion. Conversion at gel point gave information on the extent of reaction at the gel point and how much the presence of TIPNO-based alkoxyamine had affected the cross-linking reaction. Gel content and weight-average molecular weight were specified to be measured at particular conversion levels. Gel content was chosen to be measured at 85% conversion because of the interest in obtaining a well-developed polymer network for further characterization. From previous experience by Tuinman et al. (2006), it was known that the presence of the controller (i.e., nitroxide) would delay gelation and a well-developed network was achieved only towards the end of the reaction, therefore, measuring gel content at 85% conversion seemed suitable. Weight-average molecular weight was selected to be measured at 45% conversion because again, based on Tuinman et al. (2006), copolymer of STY with DVB would gel at higher conversion levels and therefore, it would be impossible to have reliable molecular weight measurements.

The prior variances for the responses, calculated from previous experience, are shown in Table 8.2. The error associated with conversion is usually considered around 3-5% (Dube et al. (1996); Roa-Luna et al. (2007); Nabifar et al. (2008)). However, since in cross-linking polymerization of STY with DVB we are dealing with gels, which means that there might be higher error associated with the conversion measurement, 6% error was considered for conversion, resulting in a prior variance of 3.60×10^{-3}. The error in gel content was estimated from experimental data from Tuinman et al. (2006). Later in our study, a detailed replicated study of the gel content measurement was carried out, which is presented in Appendix D. The error estimated from this replication was in good agreement with Tuinman et al. (2006). The variance of the molecular weight response was calculated from replicated molecular weight measurements available from prior experimental work, which gave a good idea about the variability in weight-average molecular weight. From replicated results, it was calculated that molecular weight values vary by ≈ 5000 gr/mol in the current range of molecular weights, leading to a variance of 2.50×10^{7}.

Table 8.2 Prior variances of the responses of interest

Response	Prior Variance
Conversion at gel point	3.60×10^{-3}
Gel content	7.05×10^{-4}
Molecular weight (weight-average)	2.50×10^{7}

Incorporation of Prior Knowledge: Having chosen the factors (and their levels) and the response(s) of interest, as illustrated in Figure 8.1, casting prior information into the vector $\underline{\alpha}$ and the matrix $\underline{U}$ was the next step. $\underline{\alpha}$, the vector of the parameter means, and $\underline{U}$, the variance/covariance matrix of the means, can be considered as the storehouse of prior knowledge. To generate the prior information about the parameters and their variances, a general mechanistic model developed for cross-linking NMRP of styrene by Hernandez-Ortiz et al. (2009), was used to obtain the responses for a 2^3 standard factorial design (8 trials). Details about this mechanistic model and the related predicted profiles will be presented in Chapter 9. The computer simulations were run and the corresponding responses were recorded for each of the $2^3 = 8$ trials. $\underline{\alpha}$ (the vector of parameter means) was obtained

by performing linear regression on the data and is shown in the second columns of Table 8.3, Table 8.4, and Table 8.5, for conversion, gel content and weight-average molecular weight responses, respectively. It was decided that the three-factor interaction (T × [N] × [DVB]) was not important; hence, it was not included in the results.

In order to determine the variances of the parameters, each parameter was examined separately and, based on our knowledge of the process, a 'guess' of the maximum/minimum value of the parameter was made. This stage was where most of the brainstorming took place. In the cases where the parameter was considered to be well known, a smaller interval of uncertainty was given, i.e., a smaller variance. The diagonal elements of the prior variance/covariance matrices (U) for conversion, gel content and molecular weight responses are shown in the third columns of Table 8.3, Table 8.4, and Table 8.5, respectively. The off-diagonal elements were initially all set to zero.

Table 8.3 Elements of prior α and U for **conversion at gel point** in cross-linking NMRP

Effect	α_i	U_{ii}	**Test 1**
Mean	0.663	1.00E-04	66.30
T	0.004	4.00E-06	1.97
[N]	0.091	2.03E-03	2.03
[DVB]	-0.052	6.25E-04	-2.07
T × [N]	0.001	4.90E-07	0.79
T × [DVB]	0.001	8.10E-07	1.40
[N] × [DVB]	-0.005	6.25E-06	-2.06

Table 8.4 Elements of prior α and U for **gel content at 85% conversion** in cross-linking NMRP

Effect	α_i	U_{ii}	**Test 1**
Mean	0.664	8.10E-05	73.73
T	-0.005	6.76E-06	-1.87
[N]	-0.227	4.00E-04	-11.33
[DVB]	0.139	4.00E-04	6.95
T × [N]	-0.006	9.00E-06	-1.86
T × [DVB]	0.003	9.00E-06	1.16
[N] × [DVB]	0.079	9.00E-04	2.62

Table 8.5 Elements of prior $\underline{\alpha}$ and $\underline{U}$ for **molecular weight at 45%** in cross-linking NMRP

Effect	α_i	U_{ii}	**Test 1**
Mean	34,607	1.23E+07	9.89
T	-3,898	4.00E+06	-1.95
[N]	-22,643	4.90E+07	-3.23
[DVB]	12,215	2.50E+07	2.44
T × [N]	3,802	4.00E+06	1.90
T × [DVB]	-3,656	4.00E+06	-1.83
[N] × [DVB]	-11,173	9.00E+06	-3.72

Scrutinizing the 2nd columns of Table 8.3, Table 8.4, and Table 8.5, one can observe that the values of prior parameters for the temperature effect (for all three responses) were the smallest among the parameters values of the main factors and were closer to the values for the two-factor interactions. Although it was expected that temperature, in fact, shows a significant effect on our responses, it was decided to keep the related parameters as they were first arrived at and also assign relatively smaller variances for the temperature effects at the same time. The reason was that the effect of temperature on our responses was considered to be well known. At the same time, we were interested in finding more information about the effects of the TIPNO-based alkoxyamine, the cross-linker and the interaction between them (if there were any present). Therefore, relatively higher initial variances were allocated to these parameters (see the 3rd columns in Table 8.3, Table 8.4, and Table 8.5). The corresponding values for test 1 are shown in the last columns of Table 8.3, Table 8.4, and Table 8.5. This test checked the null hypothesis that $\alpha_i = 0$ purely in the opinion of the ‘‘expert’’ (the person who assigned the values for the prior effects and variances). It was essentially a measure of the uncertainty of the ‘‘expert’’. A value greater than 2 or less than -2 was considered significant (this is equivalent to a 95.44% confidence interval). Test 1 was defined as the ratio of the prior mean (α_i) to the prior standard deviation (Std) of the mean $(U_{ii})^{1/2}$. As can be seen in Table 8.3, Table 8.4, and Table 8.5, based on the expert’s opinion, [N], [DVB] and [N] × [DVB] were considered important factors that would influece all three responses.

8.2 Selection of Experimental Designs and Discussion

It was decided to run a total of 3 experiments in two sequences, 2-trials first followed by 1-trial. As illustrated in Figure 8.1, the next step is using the prior variances (U) in the Bayesian design algorithm to choose the design conditions (X), in order to satisfy the optimality criterion (maximizing the determinant H) for each response. There happen to be four optimal 2-trial designs detected for each response. The optimal experiments from the conversion response were the same as the ones for the molecular weight response. Since two out of the three responses were optimal with the experiments designed for conversion, one of the 2-trial designs from this response was chosen as the 'best' 2-trial for the first sequence.

Table 8.6 shows the four possible 'optimal' 2-trial experiments. It can be seen that all sets of 2-trial experiments chosen by the Bayesian design follow a similar pattern, and the only setting being changed from the first trial to the second one within the first sequence is the level of [N]. For example, if we look at set No. 1, the first trial is chosen with all the factors at the low level; the second is suggesting to keep the same settings and just change the [N] level from low to high. From our previous experience with the cross-linking NMRP of styrene (Tuinman et al. (2006)), we know that it is easier to handle samples at lower levels of cross-linker and temperature. Hence, set No. 1 is chosen as the first sequence of 2-trials. This is, once again, a demonstration of one of the benefits of Bayesian design, whereby combining our process knowledge with the Bayesian design approach, we could make a judicious choice of the appropriate experiment, which may be optimal in both statistical and process senses. As the next step of the procedure (see Figure 8.1), these experiments were run in the lab and the responses were collected, as shown in Table 8.7. The related experimental details and the profiles of conversion, molecular weights, and gel content versus time are discussed in detail in Chapter 9 and not shown here for the sake of brevity.

Table 8.6 Four possible 2-trial experiments for the **first** sequence in cross-linking NMRP

No.	T	[N]	[DVB]
1	-1	-1	-1
	-1	1	-1
2	1	-1	-1
	1	1	-1
3	-1	-1	1
	-1	1	1
4	1	-1	1
	1	1	1

Table 8.7 Experimental responses for the **first** sequence in cross-linking NMRP

T	[N]	[DVB]	Conversion @ gel point	Gel content @ x = 85%	Molecular weights @ x = 45%
-1	-1	-1	0.617	0.915	53,889
-1	1	-1	0.834	0.484	14,756

For all the responses, the posterior variance/covariance matrix was calculated using the prior vector of parameter means ($\underline{\alpha}$), and the prior $\underline{U}$ (shown in the second and third columns of Table 8.3, Table 8.4, and Table 8.5, respecively), along with the $\underline{X}$ matrix (part of it shown in Table 8.7), and the responses collected via experimentation (reported in the last three columns of Table 8.7). The updated variance/covariance matrices were then used back into the Bayesian procedure to design (in an iterative sequential fashion) the next sequence of 1-trial that maximized the determinant H for all three responses. This time was one set of experimental conditions that maximized the determinant H for all responses. Hence, it was chosen as the second sequence and was carried out in the laboratory.

The settings along with the corresponding responses collected from the single trial are shown in Table 8.8. As can be seen, the Bayesian design is suggesting to keep the temperature at the low level, while running the experiment at the high levels of [N] and [DVB]. The design

suggested by the Bayesian approach made process sense. We ran both trials in the first sequence with low levels of [DVB], hence it made sense to run the experiment in the second sequence at the high level of [DVB], as we were interested in finding more information about [DVB] (by changing the level of this factor, we could gather more information). Although the temperature level was also kept constant at -1 in the first sequence, since we were relatively certain about T, it was more convenient experimentally to keep T at the low level, and that was also what was suggested by the Bayesian approach. The level suggested by the Bayesian design for [N] also made process sense. As we would be running the experiment at the high level of [DVB], having a higher level for [N] would make it easier to control the gelation and avoid a very viscous polymerization mixture, which would be difficult to handle.

Table 8.8 Experimental responses for the **second** sequence in cross-linking NMRP

T	[N]	[DVB]	**Conversion @ gel point**	**Gel content @ x = 85%**	**Molecular weights @ x = 45%**
-1	1	1	0.723	0.774	23,682

Figure 8.2 shows the visual illustration of all three runs suggested by the Bayesian design for cross-linking NMRP of STY with DVB. As can be seen in trial 1, the suggestion was to run an experiment at 120 °C, with 1 wt% alkoxyamine and 1 wt% cross-linker. The temperature and the cross-linker concentration for trial 2 were the same as in trial 1 (120 °C and 1 wt%, respectively), but the suggestion was to change the alkoxyamine concentration to 2 wt%. Finally, trial 3 was suggested to be run at low temperature (120 °C) and high levels of both alkoxyamine and cross-linker (2 wt% and 1.5 wt%, respectively).

The smallest number of experiments that could be designed through a standard fractional factorial design was four experiments, which is the $\frac{1}{2}(2^3)$. The 4-trial experiment chosen by the fractional factorial design would be completely balanced with respect to all the factors (the level of all the factors would be changing). Altering the levels of all the factors would be desirable if there were no knowledge available a priori, and the experimenter was equally interested in finding more information about all three factors. However, in our case, since the interest was more focused on finding more information about the effects of the alkoxyamine

and the cross-linker on our three responses, changing the level of all factors at the same time would be superfluous. Once again, some of the advantages of the Bayesian design approach were illustrated. There were no restrictions in the number of experiments that could be performed in the Bayesian design method (3 in the Bayesian vs. 4 in the standard fractional factorial). In addition, runs could be 'tailored' to the experimenter's interest in the Bayesian design, where more emphasis could be given to one or two factors only.

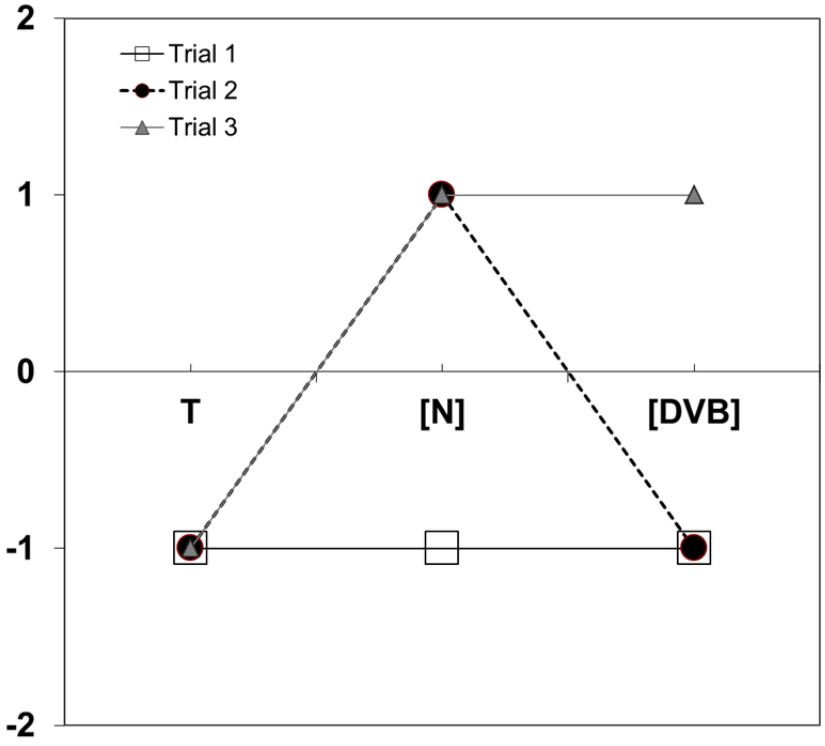

Figure 8.2 Visual illustration of the three runs suggested by the Bayesian design for cross-linking NMRP of STY and DVB

8.3 Diagnostic Tests and Further Discussion

In addition to the analysis presented above, a series of diagnostic tests can be carried out. A detailed discussion about these tests was presented in Chapter 3, however, whenever necessary, explanations are repeated here to remind the reader. These diagnostic tests serve to quantify the relative importance of the parameters (i.e., factor effects) and their interactions, as well as the quality of prior knowledge (in other words, the adequacy of the model used to generate the "prior knowledge).

Results from these statistical diagnostic tests are shown in Table 8.9, Table 8.10, and Table 8.11 for conversion, gel content, and molecular weight responses, respectively. The 2nd columns in all the tables present the initial values of the parameter means ($\underline{\alpha}$), while the 3rd columns contain the updated estimates of the parameter means after the second sequence. The prior standard deviations assigned to each parameter are shown in column 4, while column 5 exhibits the updated values for the standard deviations after the second sequence. Test 1 is shown in the 6th columns of these tables. As mentioned before, this test is a measure of the uncertainty of the ''expert'' and is defined as the ratio of the prior mean to the prior standard deviation (Std) of the mean $[\alpha_i/(U_{ii})^{1/2}]$. A value greater than 2 or less than -2 is considered significant (this is equivalent to a 95.44% confidence interval). Results for test 2 after the second sequence are shown in the 7th column. Test 2 is a measure of the actual significance of an effect and can be calculated after each sequence. It is equal to the updated estimate of the effect, $\underline{\theta}$, divided by the square root of the diagonal element of the posterior variance/covariance matrix (which is equal to the standard deviation of the diagonal elements). Once again, a value greater than 2 or less than -2 implies significance.

Results of the diagnostic tests for the conversion response, shown in Table 8.9, indicate that the TIPNO-based alkoxyamine ([N]) had the highest positive effect on this response. This trend was expected; as [N] was increased, the gel point was delayed to a higher conversion. For example, in the first sequence of our experiments (see Table 8.7), conversion at gel point was shifted from 62% to 83%, when [N] was increased from low to high (i.e., from 1 wt% to 2 wt%). The cross-linker concentration had the second highest effect on conversion; however, this effect was negative, meaning that by increasing [DVB], conversion at gel point was lower.

Again, this trend was anticipated; as we increased the amount of cross-linker, the polymer mixture would get more viscous and therefore, would gel sooner (at lower conversions). For example, if the conversion at gel point for the second run in the first sequence (see last row in Table 8.7) was compared with this response in the second sequence (see Table 8.8), it could be seen that while keeping T and [N] at the same levels, going from low to high [DVB], would shift (decrease) the conversion at gel point from 83% to 72%.

Our results show that the interaction between [N] and [DVB] was also among the factors influencing the conversion at gel point. (For confirmation purposes, a fourth run was carried out in the laboratory with low level of [N] and high level of [DVB] (complementing the run in the second sequence; see the first settings in run No. 3 of Table 8.6). Details about this run will be discussed in Chapter 9). The corresponding interaction plot for [N] and [DVB], based on our experimental data, is shown in Figure 8.3. As can be seen, at both levels of [N], the cross-linker concentration ([DVB]) had a strong negative effect on conversion at gel point. However, the effect of [DVB] at the low level of [N] (blue line) was not as strong as this effect at the high level of [N] (red line). Figure 8.3 illustrates that there was interaction present between [N] and [DVB] (revealed by the nonparallel lines) and this confirmed that our result from test 2 about the [N] × [DVB] parameter was indeed valid (see Table 8.9), hence the Bayesian design had correctly spotted this interaction. It can also be seen that results from test 1 and test 2 were in good agreement, therefore the expert's opinion was valid, and the model used gave reliable trends for the conversion at gel point response.

Table 8.9 Summary results of diagnostic tests for **conversion at gel point** response in cross-linking NMRP

Parameter	**Prior** α_i	$\theta_i^{(2)}$	**Prior Std**	**Std (after 2st seq.)**	**Test 1**	**Test 2 (after 2nd seq.)**
Mean	0.663	0.664	1.00E-02	9.66E-03	66.30	68.80
T	0.004	0.004	2.00E-03	2.00E-03	1.97	1.95
[N]	0.091	0.102	4.50E-02	2.79E-02	**2.03**	**3.65**
[DVB]	-0.052	-0.052	2.50E-02	2.06E-02	**-2.07**	**-2.52**
T × [N]	0.001	0.001	7.00E-04	7.00E-04	0.79	0.78
T × [DVB]	0.001	0.001	9.00E-04	9.00E-04	1.40	1.40
[N] × [DVB]	-0.005	-0.005	2.50E-03	2.49E-03	**-2.06**	**-2.04**

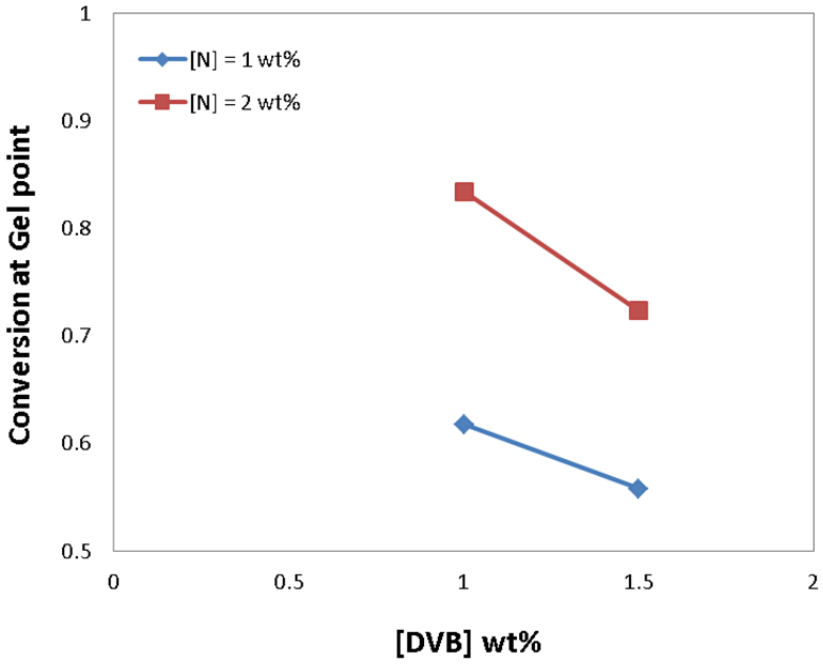

Figure 8.3 Interaction plot for [DVB] and [N]: conversion at gel point response

Table 8.10 summarizes the diagnostic tests for the gel content response (at 85% conversion). As can be seen, concentration of the TIPNO-based alkoxyamine ([N]) had the highest effect on gel content as well; however, this factor had a negative effect on the response. This trend made sense; the presence of the alkoxyamine controller ([N]) slows down the reaction and delays the gelation in NMRP, hence, the amount of gel (gel content) produced at 85% conversion will be lower for the run with higher concentration of the alkoxyamine. This trend was observed in our experiments; in the first sequence of our experiments (see Table 8.7), gel content changed from 0.91 to 0.48 when [N] was increased from the low to the high level (i.e., from 1 wt% to 2 wt%).

On the other hand, [DVB] had a significant positive effect on the gel content, as would have been expected. When the concentration of the cross-linker increases, there would be more gel produced, resulting in higher gel content at 85% conversion. For example, if the gel content at 85% for the second run in the first sequence (see last row in Table 8.7) is compared with the gel content of the second sequence (see Table 8.8), it can be seen that while keeping T and [N] at the same level, going from low to high [DVB], shifts (increases) the gel content from 0.48 to 0.77. Again, the interaction between [N] and [DVB] appeared as significant for the gel content response in Table 8.10. The same as for the conversion response, the interaction plot is shown in Figure 8.4. Once more, the interaction between [N] and [DVB] was obvious in the nonparallel lines (see blue and red lines in Figure 8.4). At both levels of [N], the cross-linker concentration ([DVB]) had a strong positive effect on gel content. However, the effect of [DVB] at the low level of [N] (blue line) was not as strong as this effect at the high level of [N] (red line). This confirmed that the test 2 result about the [N] × [DVB] parameter (shown in Table 8.10) was indeed valid, and once more the Bayesian design had correctly spotted this interaction.

Comparing the results of test 1 and test 2 in Table 8.10, it can be seen that although based on expert's opinion it was decided to consider temperature and its interactions not important (see Test 1 in Table 8.10), results from test 2 (which is an indicator of the actual significance of an effect) in Table 8.10 indicate that T and T × [N] could also be important factors influencing gel content. This result may be pointing to the direction that the mechanistic model's

predictions of the gel content response with respect to T might need some correction. However, this could as well be an artifact; as previously mentioned by Dube et al. (1996) and Vivaldo-Lima et al. (2006), caution should be exercised in the interpretation of the results of the diagnostic tests, as correlation and nonlinearity in the model equations could also cause the results of these tests to become significant. At this point, since we do not have any experimental clarification of the trend recognized by the Bayesian design, we cannot make any comments. Hence, one of the future recommendations will be to run an experiment at the high temperature level (130 °C), and contrast the results obtained for gel content response with the results from the low T level.

Table 8.10 Summary results of diagnostic tests for **gel content at 85% conversion** response in cross-linking NMRP

Parameter	**Prior** α_i	$\theta_i^{(2)}$	**Prior Std**	**Std (after 2st seq.)**	**Test 1**	**Test 2 (after 2nd seq.)**
Mean	0.664	0.690	9.00E-03	8.23E-03	73.73	83.80
T	-0.005	-0.007	2.60E-03	2.58E-03	-1.87	**-2.72**
[N]	-0.227	-0.160	2.00E-02	1.36E-02	**-11.33**	**-11.82**
[DVB]	0.139	0.083	2.00E-02	1.36E-02	**6.95**	**6.12**
T × [N]	-0.006	-0.007	3.00E-03	2.98E-03	-1.86	**-2.37**
T × [DVB]	0.003	0.005	3.00E-03	2.98E-03	1.16	1.59
[N] × [DVB]	0.079	0.092	3.00E-02	1.53E-02	**2.62**	**6.04**

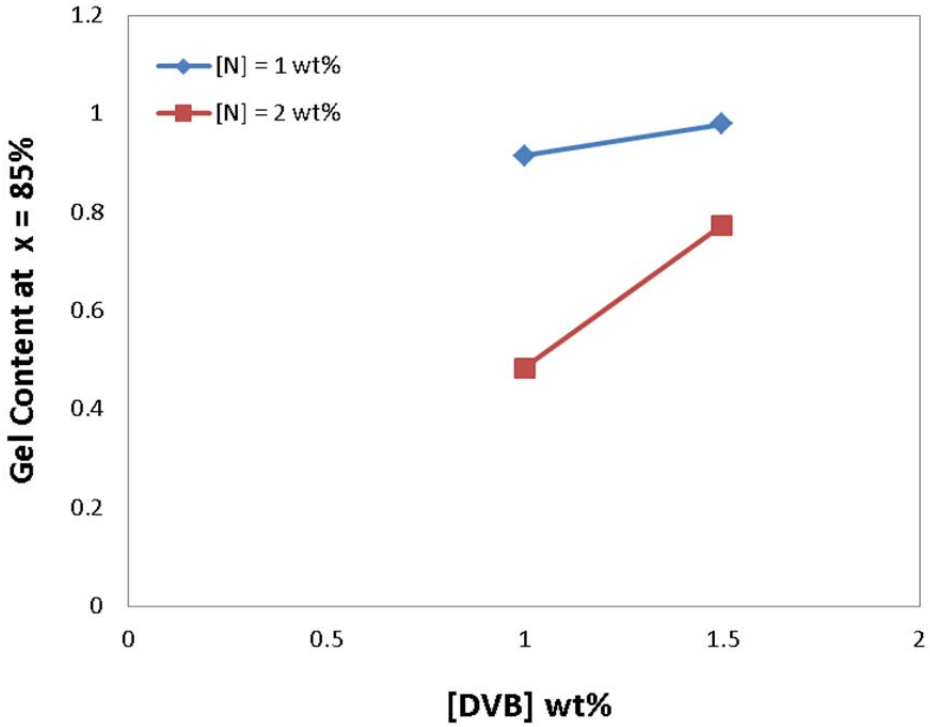

Figure 8.4 Interaction plot for [DVB] and [N]: gel content at 85% conversion response

Finally, Table 8.11 illustrates the corresponding diagnostic tests for the molecular weight response (at 45% conversion). Again, [N] had the highest negative effect. As [N] increased, the weight average molecular weight at 45% conversion decreased. This is as expected; the inverse relationship between molecular weight and concentration of alkoxyamine initiator has been noted previously and is one of the characteristics of an ideal controlled radical polymerization (Matyjaszewski, 2002). On the other hand, [DVB] had a positive effect, meaning that by increasing the cross-linker concentration, molecular weight also increased, which was also expected. Based on the results of test 2 in Table 8.11, the [N] × [DVB] parameter was also spotted as a significant factor influencing the weight average molecular weight. The interaction plot of [DVB] and [N] for the molecular weight response, shown in Figure 8.5, offers a visual illustration of this interaction. Although at both levels of [N], the cross-linker concentration ([DVB]) had a strong positive effect on the molecular weight response, the effect of [DVB] at the high level of [N] (blue line) was slightly more significant than this effect at the low level of [N] (red line).

Table 8.11 Summary results of diagnostic tests for **molecular weight at 45% conversion** response in cross-linking NMRP

Parameter	**Prior** α_i	$\theta_i^{(2)}$	**Prior Std**	**Std (after 2st seq.)**	**Test 1**	**Test 2 (after 2nd seq.)**
Mean	34,607	39,349	3.50E+03	2.77E+03	9.89	14.20
T	-3,898	-5,446	2.00E+03	1.87E+03	-1.95	**-2.91**
[N]	-22,643	-23,925	7.00E+03	3.65E+03	**-3.23**	**-6.56**
[DVB]	12,215	10,102	5.00E+03	3.29E+03	**2.44**	**3.07**
T × [N]	3,802	3,906	2.00E+03	1.94E+03	1.90	**2.01**
T × [DVB]	-3,656	-3,318	2.00E+03	1.91E+03	-1.83	-1.74
[N] × [DVB]	-11,173	-8,214	3.00E+03	2.52E+03	**-3.72**	**-3.26**

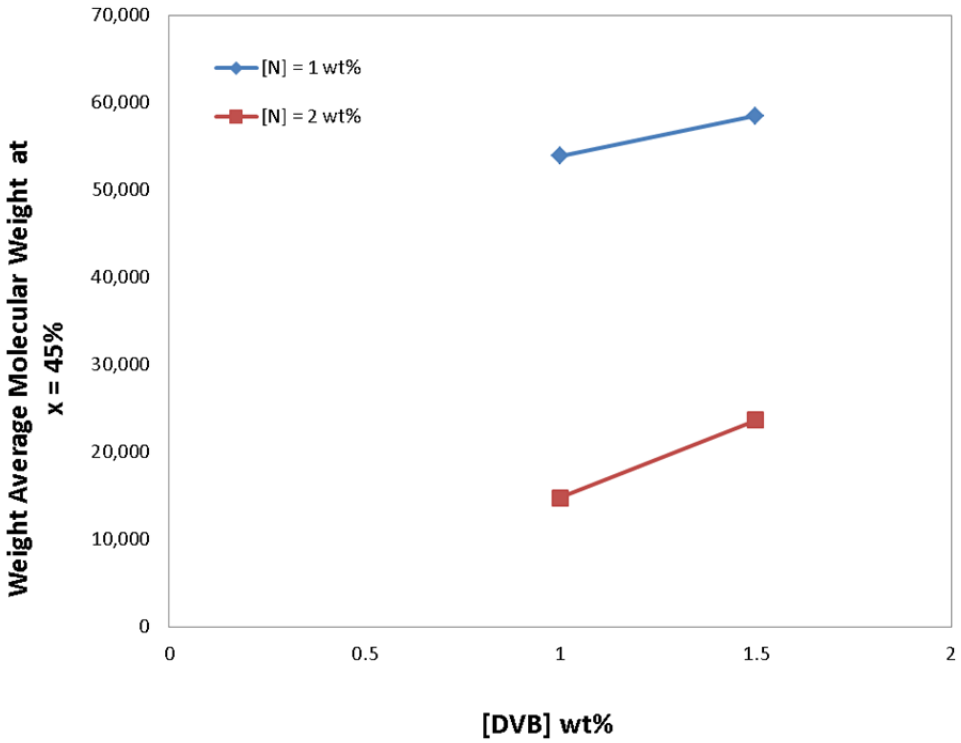

Figure 8.5 Interaction plot for [DVB] and [N]: molecular weight at 45% conversion response

Although based on expert's opinion (test 1), temperature and its interactions were considered insignificant factors for the molecular weight response, test 2, which demonstrates the actual significance of an effect, was again significant for T and (borderline significant) for T × [N] (see Table 8.11). Temperature was expected to have a relatively significant effect on molecular weight, however, the T parameter calculated from the linear (regression) model based on the molecular weight response, as predicted by the non-linear mechanistic model, was smaller compared to the [N] and [DVB] parameters (see α_i for T in Table 8.5 and Table 8.11). It is interesting to see that the Bayesian design, in fact, had picked this up and the analysis showed that indeed temperature could be an important effect on the molecular weight response. Therefore, either the mechanistic model's predictions of the molecular weight response need some correction, or there could be some nonlinearities or correlations present that had caused the test 2 results to be simply an artifact, as indicated earlier by Dube et al. (1996) and Vivaldo-Lima et al. (2006). At this point, since we do not have any experimental evidence of the effect of temperature on the molecular weight response, we cannot make any further comments. Hence, one of the future recommendations will be to run an experiment at the high temperature level, and compare the results obtained for molecular weight with the results at the low T level.

8.4 Concluding Remarks

The Bayesian design of experiments was successfully implemented to the cross-linking nitroxide-mediated radical copolymerization of styrene and divinyl benzene. The prior knowledge, generated from a mechanistic model already developed for cross-linking NMRP, was used in the Bayesian approach to design three 'optimal' experiments. After conducting these experiments in the laboratory and analyzing the results, we were able to determine the relative importance of the factors in the cross-linking nitroxide-mediated radical copolymerization of styrene and divinyl benzene. This was found to be in agreement with the experimental trends presented in Chapter 9. The combination of the mechanistic nature of the model used as the prior knowledge generator, the versatility of the Bayesian technique, and our process sense, allowed us to obtain valuable information about the effects of different factors via running a minimal number of experiments!

Our initial speculation that both alkoxyamine concentration and cross-linker concentration were significant factors on the responses of conversion at gel point, gel content at 85% conversion and molecular weight at 45%, was confirmed via the diagnostic tests that are part of the Bayesian design approach. Results from our diagnostic checks also determined that there were interactions present between [N] and [DVB] for all three responses. The interaction plots also corroborated the findings from our diagnostic tests and visually illustrated the interaction between [N] and [DVB]. However, when it came down to the temperature effect, the expert's opinion was not always in agreement with the actual significance of the effect picked up through the diagnostic checks. Hence, further investigations are needed in order to determine whether this discrepancy was indeed true (i.e., the mechanistic model needs improvement with respect to the temperature effect), or simply an artifact caused by nonlinearities and possible correlations induced by the equations, which might have caused these slightly anomalous results. The trends observed here from the Bayesian analysis (diagnostic checks) will be experimentally verified in Chapter 9.

Chapter 9. Cross-linking NMRP of Styrene with Divinyl Benzene

Results from the cross-linking kinetics of nitroxide-mediated radical polymerization (NMRP) of styrene (STY) in the presence of a small amount of divinyl benzene (DVB) are presented in this chapter. The experimental conditions used in this study were arrived at through the Bayesian design of experiments of Chapter 8. First, a brief introduction on the concept of cross-linking is offered, followed by a selective review of literature studies on cross-linking under controlled radical polymerization (CRP) and, more specifically, nitroxide-mediated radical polymerization (NMRP). Subsequently, the experimental and characterization techniques used to study cross-linking NMRP of STY/DVB are described. Then, a summary of the mechanistic mathematical model (including the reaction scheme and other general considerations) developed for cross-linking NMRP of STY/DVB is given in the modeling section. This section relies heavily on the mechanistic model development efforts of Hernandez-Ortiz et al. (2009 and 2012).

In the results and discussion section, the performance of styrene polymerization with N-tert-butyl-N-(2-methyl-1-phenylpropyl)-O-(1-phenylethyl) hydroxylamine (referred to as TIPNO-based alkoxyamine or I-TIPNO) is first examined to see if the system exhibits controlled behavior. Then, typical profiles for cross-linking NMRP of STY/DVB in the presence of this alkoxyamine (as controller) are presented and contrasted with cross-linking under regular free radical polymerization, and NMRP of styrene (in the absence of cross-linker). Subsequently, the performance of cross-linking NMRP is evaluated based on rate of polymerization, molecular weights, polydispersity values and gel content under different operating conditions (different cross-linker and nitroxide concentrations). Finally, prediction profiles from the mathematical model are contrasted with experimental data to check the validity of the developed model with respect to both NMRP and cross-linking NMRP of STY/DVB with this TIPNO-based alkoxyamine.

9.1 Introduction and Selective Literature Review

A cross-linked polymer can be defined as a macromolecule in which essentially all units are connected to each other. A highly cross-linked polymer results in a polymer network which is characterized by having an "infinite" molecular weight. Cross-linked polymers exhibit completely different properties when compared to linear polymers with identical chemical compositions. Figure 9.1 shows various typical structures for polymers. Degree of branching/cross-linking influences polymer properties such as density, melt viscosity, and crystallinity; it also determines the flow behavior of the material. Non-cross-linked polymers are in general thermoplastic, they can be melted and cast, extruded, or (injection) molded, while highly cross-linked polymers become thermoset, and they do not flow when heated.

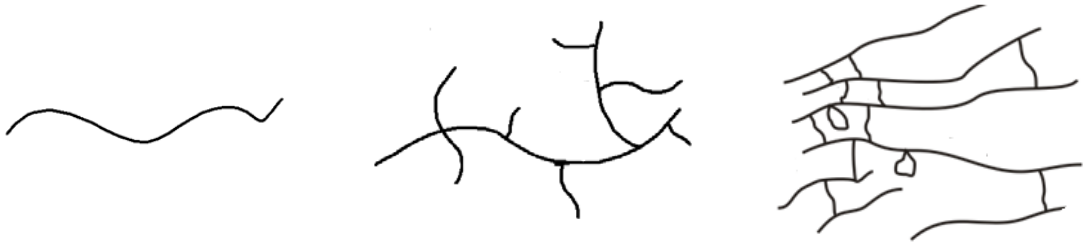

a) b) c)

Figure 9.1 Various polymer molecular architectures: a) linear, b) randomly branched, c) cross-linked

Cross-linking is especially important from a commercial point of view. Production of cross-linked polymer may be undesirable for some applications; in such cases, chain transfer agents can be used to prevent or delay gelation. On the other hand, many commercial polymers owe their value to their cross-linked structures, which can range from slightly cross-linked materials (as in the case of elastomers), to highly cross-linked materials (as in the case of thermosets). Cross-linked polymers are very important in several areas, like medicine, biotechnology and agriculture, with multiple applications, such as super absorbent materials, chromatography packings, ion-exchange resins, dental restorative materials, and additives in surface coatings. They are also used in cosmetics and pharmaceuticals, drug-delivery systems, artificial organs, sensors, optics and electronics (Patrickios, 2010).

Cross-linking can be achieved via physical or chemical routes. Chemical cross-linking can either ensue as part of the polymerization process (step growth polymerization and free radical polymerization), or as a post-processing stage (vulcanization and end linking prepolymers) (Odian, 2004). Cross-linked polymers can be obtained by step-growth polymerization when the functionality of one of the monomers is greater than two. Many thermoset polymers of major commercial importance, like unsaturated polyesters, polyurethanes, melamines, phenolic and urea formaldehyde resins, epoxy resins, and silicones, are synthesized by step-growth polymerization. In these systems, the cross-linking process, which leads to a polymer network formation, is usually referred to as curing. Vulcanization is a post-processing chemical technique where linear polymer chains become cross-linked by the action of certain agents that attack some active functional groups present in the polymer backbone, thus improving the mechanical properties of the resultant polymer structure. Vulcanization by sulfur bonding is one of the main techniques employed for cross-linking of polymer chains with diene groups, like natural rubber, styrene-butadiene rubber and polybutadiene. In end-linking cross-linking, two *f*-functional reactive groups are attached to each end of the linear pre-polymer and the cross-link step is then performed by bonding of the end groups (*f*: average functionality of cross-links, i.e., the number of effective elastic chains of the network attached to one given branch point). Anionic polymerization is among the techniques used for the synthesis of well-defined macromolecules by the end-linking route (Odian, 2004).

The regular free radical (FRP) copolymerization of a vinyl monomer with a small amount of a divinyl monomer is another method for the preparation of polymer networks, and offers one of the simplest routes. In these systems, the divinyl monomer acts both as a co-monomer and as a cross-linker. The reaction between vinyl and divinyl monomers leads to the formation of macromolecules with pendant vinyl groups. Depending on the reaction conditions, the pendant vinyl group from one polymer molecule can either react with the propagating radical center of a different chain, forming a single new macromolecule with an increased chain length (intermolecular cross-linking reaction), or with the radical center on the same polymer molecule, causing connective loops or cycles within the macromolecule (intramolecular cross-linking). In the case of intramolecular cross-linking, if the two reacting sites are attached to the same primary chain, a primary cycle results; on the other hand, if the two reacting sites are

attached to two different primary chains (which have already experienced cross-linking), a secondary cycle is formed. Figure 9.2 shows a schematic of different types of cross-linking in FRP. Intramolecular reactions, in contrast to intermolecular ones, do not contribute to the growth of the molecular structure during polymerization and, therefore, they do not affect the molar mass distribution of the polymer population. However, these reactions manifest themselves by a shift to a higher value of the critical conversion for onset of gelation, and by a reduced amount of gel content during the formation of the polymer network.

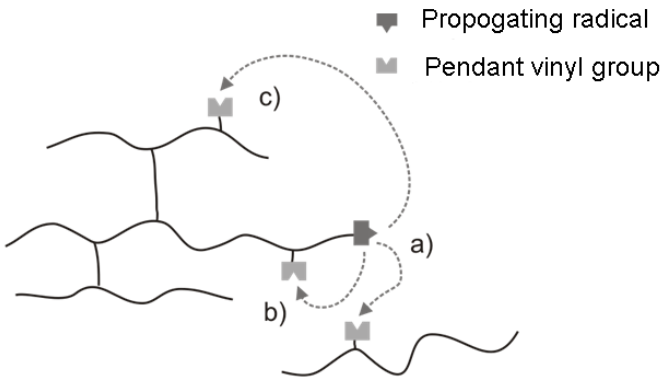

Figure 9.2 Different types of cross-linking: a) intermolecular, b) intramolecular, yielding a primary cycle, c) intramolecular, yielding a secondary cycle

Intermolecular and intramolecular cross-linking tend to occur simultaneously because both reactions involve the same functional groups. The relative reaction rates are determined by polymer concentration and chain length. Thus, at very low polymer concentrations, intramolecular cross-linking dominates, yielding highly cross-linked particles (usually referred to as microgels) as product, whereas at higher polymer concentrations, intermolecular cross-linking is the dominant route, leading to a polymer network (Gao et al., 2007). The presence of microgels in the network structure brings about an extremely restricted segmental mobility, while other regions of the polymer network experience a more mobile local environment, resulting in a heterogeneous distribution of segmental mobilities and broader relaxation time distributions.

Although regular free radical polymerization (FRP) has been extensively used for copolymerization of monovinyl monomers and divinyl cross-linkers, and has many advantages

over other polymerization mechanisms (including mild experimental conditions and various applicable monomer species), the network synthesized through this route is rather heterogeneous in structure. This heterogeneity in the structure is mainly ascribed to several inherent features of FRP, including slow initiation, fast chain propagation and high termination rates (Gao et al., 2007). The slow initiation results in gradual and continuous production of primary radicals, while the fast chain propagation and unavoidable termination allow the presence of dead polymer molecules with high molecular weights and numerous pendant vinyl groups per chain, from the beginning of the reaction. However, at the early stages of reaction, the environment is very dilute (because of the presence of a lot of monomer) and under dilute conditions, polymer chains hardly ever overlap with each other to produce a cross-linked network. Therefore, initially most of the pendant double bonds are consumed through intramolecular cross-linking which results in highly cross-linked nanodomains (microgels). As the reaction proceeds and the polymer concentration increases, these nanodomains further react with each other by intermolecular reaction and agglomerate. The agglomeration process will continue until the onset of gelation is eventually reached, when all these microgels are interconnected (see Figure 9.4). Therefore, gel formation by means of conventional free radical copolymerization is the result of a continuous association of microgels, where each one could experience a different crosslink history, and as a result, these gels are intrinsically heterogeneous. This mechanism have been experimentally confirmed via the studies of Soper et al. (1972), Holdaway et al. (1978), Mrkvicìkova and Kratochvil (1981) and Landin and Macosko (1988). They showed that significant amounts of vinyl groups were doubly reacted even at zero conversion, when, clearly, no intermolecular reactions were possible. Hence, the initial stage of the reaction was dominated by intramolecular x-linking and most of the consumed cross-linker was used to make small rings.

Most applications of cross-linked polymers (especially in pharmaceuticals, bioengineering or biomedicine) require a structural perfection for optimal performance (Patrickios, 2010). Figure 9.3 illustrates schematic representations of three polymer networks with different degrees of structural perfection. On the left is depicted a perfect (or ‘‘model’’) network, where the length of the polymer chains between the cross-linking nodes (elastic chain length) and the number of polymer chains emanating from each cross-linking node (core functionality) are both well-

defined (Hild, 1997). An imperfect network is drawn on the right. In this network, both the elastic chain lengths and the core functionality are broadly distributed. Furthermore, this last network bears other defects, such as dangling chains, loops and totally unattached chains. In between these two extremes is the structure of an almost-perfect (‘‘quasi-model’’) network, shown in the middle of the figure and exhibiting only a small number of defects (Patrickios, 2010). The majority of polymer networks produced and studied to date, through regular free radical copolymerization, are imperfect networks and have rather a heterogeneous structure (as discussed above). Therefore, it would be desirable to have a synthetic route to produce model or quasi-model networks that have homogeneous structures.

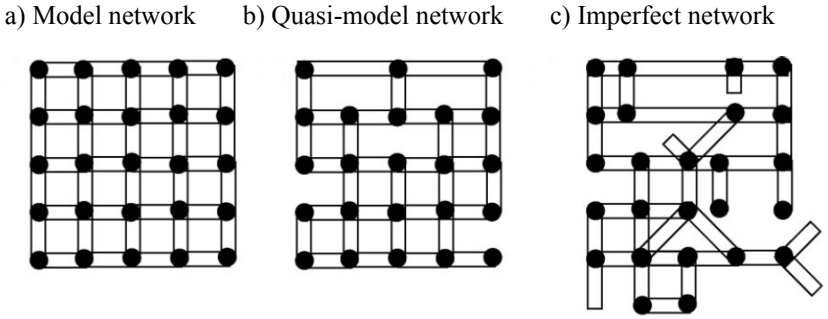

Figure 9.3 Polymer networks of different degrees of perfection (Patrickios, 2010)

Recently, the claim has been made that copolymerizing vinyl and divinyl monomers under controlled radical polymerization (CRP) might result in a more homogeneous network compared to FRP. The difference between the synthesized networks through CRP and FRP is attributed to having a rather different cross-linking mechanism. In CRP, due to fast initiation and almost negligible termination, all polymer chains are initiated at approximately the same time, and the number of primary growing chains is nearly constant throughout the polymerization. In addition, the fast activation/deactivation equilibrium causes slow and controlled growth of the polymer chains in CRP, where only a few monomer units are incorporated into the chains in every activation/deactivation cycle. During the dormant periods, the polymer chains cannot propagate but they have enough time for chain relaxation and diffusion, which increases the chance of radical centers randomly reacting with the available pendant double bonds from other molecules and hence, favoring more the intermolecular cross-linking. These characteristics, which seem to reduce the intramolecular cyclization,

might encourage the production of a less heterogeneous structure and a polymer network closer to a model or quasi-model one. Figure 9.4 shows a schematic of the assumed differences between networks synthesized through FRP and CRP.

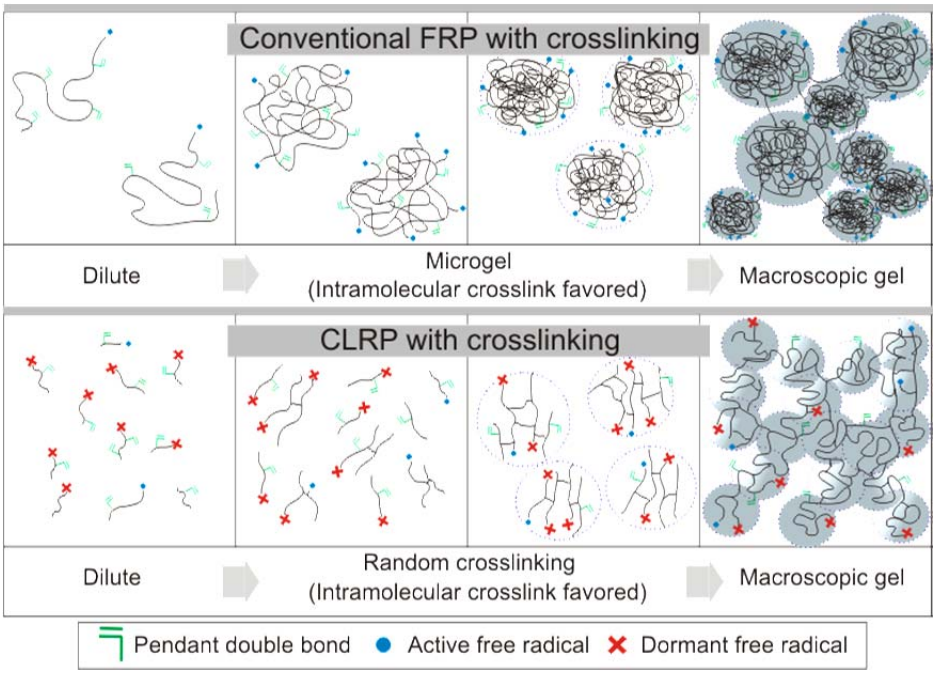

Figure 9.4 Assumed differences between the network formation mechanism through FRP and CRP

Based on these speculations, synthesis, characterization and modeling of polymer networks by CRP have received considerable attention in the last decade or so. Probably the first group reporting the use of CRP to prepare cross-linked networks was Solomon and coworkers (Abrol et al., 1997 and 2001) and thereafter, more research has been carried out in this area. Table 9.1 captures the essence of the relevant work carried out in the literature on the cross-linking NMRP process. (Of course, parallel to the progress in cross-linking NMRP, there also have been developments in both ATRP and RAFT. For instance, Wang and Zhu (2005) and Yu et al. (2001, 2008) have reported on the ATRP of methacrylates with divinyl monomers, whereas Gao et al. (2007, 2008a and 2008b) have studied the copolymerization of acrylate monomers with diacrylate as cross-linkers in ATRP. For representative work in RAFT one can refer to Norisuye et al. (2005) and Dong et al. (2008). However, since the focus of this work is cross-linking NMRP, no detailed literature review on the other CRP techniques is offered here; for a

comprehensive summary of the work in RAFT, ATRP and INIFERTER see Hernandez-Ortiz et al. (2009)).

Although at first glance the cross-linking polymerization under CRP seems relatively well studied in the literature, with the production of a more homogeneous polymer network under CRP an "accepted" concept, our observation after a comprehensive literature review is as follows: although the research conducted in the literature points to the direction that production of a more homogeneous polymer network is possible through CRP techniques, "concrete" evidence is only indirect and based on rather theoretical speculations of how polymer networks are produced (e.g., conversion of pendant double bonds in the initial stages of the reaction, theory of gelation, swelling ratios, etc.). Perhaps, a more detailed and comprehensive study is required to clarify many existing conflicting statements encountered in the literature, and also find a more formal, direct, and reliable way (if such a way exists) of characterizing the cross-linked polymer network with respect to homogeneity (and the closely related cross-link density distribution).

Table 9.1 Relevant literature on cross-linking NMRP

Group	Main studies	Comments
Solomon and coworkers (Abrol et al., 1997 and 2001)	• Synthesized statistical and star microgels of TBS/DVB via NMRP, using a unimolecular initiator (TBS: t-butylstyrene); solution polymerization with benzene • Multimodal distribution observed in the DRI detector • Displayed a considerably higher molecular weight through SEC-MALLS than that determined with SEC using polystyrene standards for calibration	• First group to report NMRP to prepare cross-linked networks • No trajectory for conversion or MWs. • No mention of homogeneity • Just mentioned that attempts to prepare microgels using AIBN (instead of the alkoxyamine), at the same concentrations of reactants used in their study, gave extensive gelation • Impossible to make star microgels via FRP as there are no functionalities at the ends of the chain to facilitate the formation of such molecular architecture
Fukuda and coworkers (Ide and Fukuda, 1997 and 1999)	• Copolymerization of styrene with small amount of 4,4´-divinylbiphenyl, in the presence of an oligomeric polystyryl adduct (PS-TEMPO), at 125°C • Evaluated pendant vinyl reactivity before the gel point o The pendant vinyl concentration before the gel point (C_p) was determined using UV spectroscopy; the plot of C_p vs. styrene polymerization (C_1) for NMRP showed an almost linear behavior; in contrast, the same plot for FRP showed high values of C_p at relatively low C_1, which indicates the consumption of pendant double bonds via intramolecular (cyclization) reactions • Evaluated gelation behaviour o Determined swelling ratio, gel content and molecular weights between cross-links (M_c) according to Flory and Rehner o Showed that the polymer synthesized under NMRP swells more and the gelation is delayed. In addition, M_c is claimed to be much higher for NMRP samples. However, M_c values are shown for low conversions only!	• Study almost at the same time as Solomon and coworkers above • Conclusions about network homogeneity are made based on the pendant vinyl concentration before the gel point! • M_c is an average value and does not give any information about the distribution, which basically dictates the homo- or hetero-geneity of the network! • Made a sweeping statement in the conclusions that NMRP will be more homogenous than FRP based on DMA studies, but no experimental evidence offered
Fréchet and coworkers (Peters et al., 1999; Viklund et al., 2001)	• Solution copolymerization of styrene and divinyl benzene, in the presence of different NMRP controllers to produce porous poly(styrene-co-divinyl benzene) monoliths for chromatographic applications	• They showed that the unique porous structure resulted not from the controlled free radical nature of the polymerization but rather from the effect of the elevated reaction temperature on the solvency of the specific porogen employed

Zetterlund and coworkers (Alam et al., 2006; Saka et al., 2007; Tanaka et al., 2007; Zetterlund et al., 2005, 2009a and 2009b)	• STY/DVB (f2= 0.01) with PS-TEMPO initiator at T = 125 °C in both bulk and miniemulsion o Pendant double bond conversion determined from combination of NMR and GC o Higher cross-link density and rate of polymerization in bulk compared to miniemulsion o Detailed analysis of inter- and intra-molecular pendant conversion with monomer conversion carried out for bulk/solution and miniemulsion o Comparison of experimental gelation points with theoretical predictions based on Flory-Stockmayer (FS) gelation theory for solution and miniemulsion • STY/DVB copolymerization via NMRP (with TEMPO) at 125 °C compared to STY/DVB copolymerization via FRP at 70 °C, in micro-suspension o Mechanical properties of individual micron-sized particles were compared o X-linked polymer particles prepared by NMRP exhibit different mechanical properties than X-linked particles prepared by FRP at low to intermediate conversion: compressive strength, deformation at break and breaking energy remain approximately constant from low to high conversion in FRP, while in NMRP these quantities increase linearly with conversion	• Relatively high pendant conversion even at low polymer content in bulk could be indicative of intramolecular cross-linking • No comparison with FRP presented in bulk • Showed that although at low to intermediate conversion X-linked particles synthesized through NMRP exhibited different mechanical characteristics than particles synthesized through FRP, at higher conversions (>70%) both systems exhibited very similar mechanical properties
Sato and coworkers (Hirano et al., 2005)	• Polymerization of DVB in the presence of nitrobenzene as a retarder, using an excess of dimethyl 2,2`-azobisisobutyrate (MAIB) to promote the formation of hyperbranched structures, at 70 and 80°C o Based on the initial polymerization rate equation, they found, at 70°C, that the radicals coming from the nitro group of nitrobenzene behave as a NMRP controller, forming dormant polymer molecules.	• No comparison with FRP presented in bulk • No mention of homogeneity
Dias and coworkers (Goncalves et al., 2010)	• Modeling work on STY/DVB copolymerization in the presence of TEMPO	• Modeling predictions offered only for molecular weights, and rate of polymerization; no prediction for cross-link density • No discussion of homogeneity • Limited experimental data

The observations of Table 9.1 motivated our work on cross-linking NMRP of styrene (STY) in the presence of small amounts of a common cross-linker, divinyl benzene (DVB). The cross-linked copolymer of STY/DVB is used for chromatographic applications and as a precursor for ion-exchange resins. It is also a system well studied under regular free radical polymerization conditions, hence an excellent system for a meaningful comparison between networks synthesized through CRP and FRP, and also for addressing the quest to identify a more formal indicator for network homogeneity.

As discussed in Chapter 8, prior work had already been carried out in our group on cross-linking NMRP in both experimental (Tuinman et al., 2006) and modeling (Hernandez-Ortiz et al., 2009) fronts. However, the experimental data available were focused on only one nitroxide concentration, and molecular weight and gel content data were not collected over the whole conversion range. In addition, based on the experimental data collected, it was not possible to offer any statements related to the homogeneity of the network synthesized through NMRP. Hence, supplementary experimental information was required in order to:

- Fully verify the validity of the trajectories predicted by the model
- Develop the ability of the model further to use nitroxides other than TEMPO
- Address our question of whether a network synthesized through NMRP is more homogeneous than a network produced through FRP

Since considerable prior knowledge related to cross-linking NMRP of styrene with DVB was already available from previous experimental and modeling efforts, it was felt that the area would be an excellent application of the Bayesian design of experiments, especially in order to save considerable time and resources. The details on the implementation of the Bayesian design to cross-linking NMRP were already discussed in Chapter 8. This chapter is dedicated to the experimental details of the runs suggested by the Bayesian approach. The kinetic study described here was carried out in preparation for the identification of network homogeneity indicators, the topic of Chapter 10.

9.2 Experimental

9.2.1 Reagent Purification

Styrene (STY) and divinyl benzene (DVB) were both obtained from Sigma Aldrich. DVB was a technical grade (> 80% DVB, 18% Ethylstyrene, < 0.5 % Diethylbenzene, and < 0.12% 4-tert-butylpyrocatechol). STY was washed three times with a 10 w/v % sodium hydroxide solution, washed three times with distilled water, dried over calcium chloride and distilled under vacuum to remove the inhibitor and impurities. Solvents such as ethanol, dichloromethane, tetrahydrofuran, and acetone, used during the course of the experiments, and both di-tert-butyl peroxide (Trigonox B) and N-tert-Butyl-N-(2-methyl-1-phenylpropyl)-O-(1-phenylethyl) hydroxylamine (TIPNO-based alkoxyamine) were used as received from suppliers (AKZO chemicals, and Sigma Aldrich, respectively). For detailed discussion of experimental methods see the ampoule polymerization manual (McIsaac et al., 1993).

9.2.2 Polymer Synthesis

The homo- and co-polymerizations were completed in borosilicate glass ampoules (capacity ~ 4 mL). Reagents were weighed, mixed and pipetted into ampoules. Ampoules were then degassed by several vacuum-freeze-thaw cycles, sealed under vacuum with a gas/oxygen torch and immersed in a silicone oil bath having a temperature control of ±0.1 °C. Ampoules were removed at selected time intervals to ensure a well-defined conversion versus time plot. Once removed from the bath, the ampoules were placed in liquid nitrogen to stop the polymerization. Ampoules were then thawed, weighed, and opened. The contents were dissolved in dichloromethane, and poured into a flask containing ethanol to precipitate the polymer. The polymer samples were air-dried to remove the solvent and vacuum-dried for three days at approximately 60°C until a constant weight was reached (McManus and Penlidis, 1996).

9.2.3 Polymer Characterization

Conversion levels were determined by gravimetry. Gravimetry involved comparing the weight of the isolated dried polymer to the weight of the monomer initially added in the ampoule as shown below:

$$conversion\% = \frac{mass\ of\ polymer}{initial\ mass\ of\ monomer\ in\ ampoule} \times 100 \qquad \text{Eq. 9.1}$$

Polymer products were then characterized for molecular weight (averages and molecular weight distribution) by using size exclusion chromatography (SEC). SEC was also used for branching detection and characterization of the branched polymers. The general concept of SEC characterization is discussed below in subsection 9.2.3.1 (a more detailed discussion about the usage of SEC for branching detection will be given in Chapter 10). Gel content and swelling index for the samples were determined using a Soxhlet extraction setup, following ASTM D2765-01. Toluene was used as the reflux solvent. Subsection 9.2.3.2 contains more details about Soxhlet extraction.

9.2.3.1 Size Exclusion Chromatography

Size exclusion chromatography (SEC), also referred to as gel permeation chromatography (GPC), is the most popular and convenient method for determining average molecular weights and molecular weight distribution (MWD) of a polymer. As its name implies, SEC works on the principle of size exclusion. A very dilute polymer solution is passed through a column of porous particles. The molecules that are large cannot enter the pores of the packing and as such, they elute faster. Smaller molecules that can penetrate or diffuse into the pores are retained in the column and elute at a later time. Thus a sample is fractionated by molecular hydrodynamic volume and the resulting profile describes the molecular weight distribution. A concentration detector (e.g., differential refractometer (DRI) or UV detector) is placed downstream of the columns to measure the polymer concentration of each fraction as a function of time. The actual method for determining molecular weight averages and the MWD depends upon the presence of any accompanying detectors. For comprehensive information on SEC refer to" Size Exclusion Chromatography" by Mori and Barth (1999).

The SEC setup used in this study consisted of a Waters solvent delivery system and autosampler followed by Viscotek's quad detector equipped with a UV detector, low- and right-angle laser light scattering detectors (LALLS/RALLS), differential refractometer (DRI) and viscometer in series. The setup was maintained at 30 °C with tetrahydrofuran as the mobile phase flowing at a rate of 1.0 mL/min. One PLgel 5 μm guard column (50 × 7.5 mm) and three

PLgel 5 μm Mixed-C columns (300 × 7.5 mm) from Varian (now Agilent) were used with the detectors. The laser operated at 670 nm and the light-scattering intensity was measured at 7° (LALLS) and 90° (RALLS). Data analysis for this system was performed using OmniSEC software version 3.0 (Viscotek). The polymer was dissolved in THF to obtain concentrations of ~0.2 wt% and the injection volume varied between 100 and 200 μL (Scorah et al., 2004). Prior to injection, polymer solutions were filtered through a 0.2 μm filter to remove any insoluble materials, if present.

The second virial coefficient for the light-scattering equation was assumed to be negligible as very low concentrations of polymer were employed. A replicated study was carried out to determine the values of the specific refractive index increment (dn/dc) for both homo- and co-polymerization of styrene in NMRP (to be used in the light scattering analysis in SEC). The dn/dc values were determined using a Brookhaven BI-DNDC Differential Refractometer and the results were independently replicated to establish the error associated with this instrument (calculated error was ~ 0.004 mL/g). All the dn/dc values determined for our samples were within the 95% confidence interval for the value of 0.185mL/g (0.185 ± 0.008 mL/g). Hence, it was decided to simply use the value of 0.185mL/g as the specific refractive index increment in the light scattering analysis for all the polystyrene samples.

Since we were dealing with a cross-linking system, which is difficult to deal with in the laboratory due to the presence of gel material, presence of a considerable amount of error in experimentation and subsequent analyses was expected. As a result, when determining the molecular weights, higher (than normal) experimental errors were involved in addition to the typical instrumental error. To properly identify the sources and magnitudes of errors in determining molecular weights, a replicated experiment was conducted and subjected to extensive characterization using a hierarchical design (Box et al., 2005). This design was used to separate the total variation in the molecular weight measurement into parts assignable to three sources: error associated with the SEC measurement itself (analytical error), error related to the polymerization process/reactor, and the variability in the measurements corresponding to different sampling times. Results from this detailed study are presented in Appendix D. Our analysis showed that the error associated with the GPC (analytical error) was much lower than

the error associated with the other two (higher) levels. Also, the error related with the weight-average molecular weight was higher than that of the number-average molecular weight.

9.2.3.2 Soxhlet Extraction

In the characterization of cross-linked polystyrene samples, Soxhlet extraction was used to separate the insoluble (gel) fraction from the soluble one (sol). Figure 9.5 provides a schematic typical of a Soxhlet extraction setup. A small amount of polymer is placed in a cellulose thimble and then the thimble is positioned inside the extraction chamber, as shown in Figure 9.5. The solvent reservoir is heated such that a suitable amount of vapour can be condensed overhead of the thimble, in the condenser. The warm solvent then flows over the polymer in the thimble dissolving and extracting the soluble fraction of the polymer sample. Once enough vapour has been condensed, and the extraction chamber is almost full, the solvent drains through the siphon arm and back into the solvent reservoir. This process can be repeated and continued for several hours.

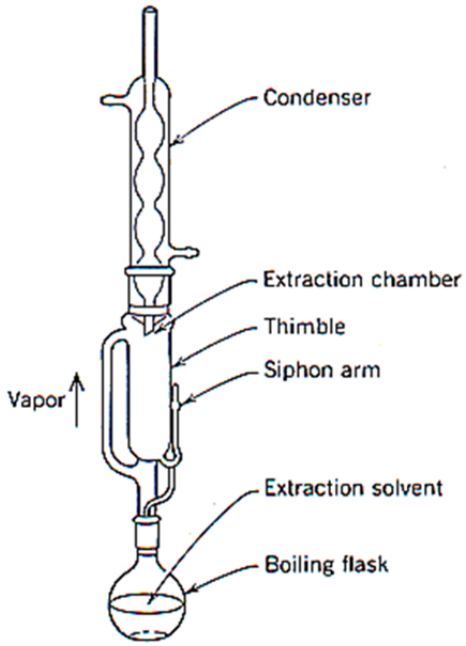

Figure 9.5 Soxhlet extraction apparatus

Due to the fact that low amounts of polymer were used, losses in the weight of the thimble during the procedure hindered the determination of reliable values for gel content. For this

reason, prior to the extraction process, the cellulose thimbles were placed inside the apparatus, refluxed with toluene for one hour and half, dried under vacuum and then weighed. In the extraction procedure, toluene was refluxed over approximately 20 mg of polymer for 12 hrs (for confirmation purposes, the extraction procedure was carried out at 6, 12 and 24 hrs for several samples, in order to check if 12 hrs was sufficient to obtain reliable gel content and swelling index results. The outcome of the exercise showed that both gel content and swelling index values were the same for 12 and 24 hrs, hence 12 hrs was chosen for our extraction procedure). The thimbles containing insoluble polymer were removed from the setup, pat dried to remove the excess solvent, and then weighed. After that, the thimbles containing the insoluble polymer were placed inside a vacuum oven for a week at 60 °C to dry. Finally, the dried thimbles were weighed to allow for the calculation of the gel content and swelling index. For some of the samples, the soluble fraction of the polymer was recovered from the solvent reservoir to be analyzed with SEC.

Gel content is defined as the mass fraction of the cross-linked polymer that is insoluble in a specific solvent after extraction under specific conditions, and can be determined using the following equation:

$$Gel\ content\ = \frac{Mass\ of\ the\ dried\ polymer}{Mass\ of\ the\ original\ sample} \qquad \text{Eq. 9.2}$$

Swelling index is a measure of the type of gel. Gel with a low swelling index is referred to as "hard" or "tight" gel and usually indicates the presence of material that does not break easily. A high swelling index normally indicates the presence of a "loose" gel. Swelling index can be determined using:

$$Swelling\ Index\ = \frac{Mass\ of\ the\ swollen\ gel}{Mass\ of\ the\ dried\ gel} \qquad \text{Eq. 9.3}$$

Determining the gel content and swelling index by Soxhlet extraction is prone to considerable error because of the nature of the procedure (although not always appreciated and even more rarely quantified). In our case, the error was even higher since very small amounts of polymer were used. To obtain an estimate of the error for the Soxhlet extraction setup, independent

replicates were conducted. The variance calculated from the error analysis for the gel content was 7.05×10^{-4} (corresponding to $\pm$ 1.23 % error), while the variance for the swelling index was 12.23% (corresponding to $\pm$1.62 % error). Details of the error analysis are presented in Appendix E.

The molecular weight between cross-links (M_c) was calculated according to the Flory and Rehner approach (for tetrafunctional cross-linking):

$$M_c = \frac{\rho}{\upsilon_e} \qquad \text{Eq. 9.4}$$

where ρ is the density of the polymer, and υ_e is the number of cross-links per unit volume (Hild, 1997):

$$\upsilon_e = \frac{-[ln(1 - V_r) + V_r + \chi V_r^2]}{\left[V_1 (V_r^{\frac{1}{3}} - \frac{V_r}{2})\right]} \qquad \text{Eq. 9.5}$$

V_r is the volume fraction of polymer in a swollen gel and can be calculated as (Okay, 1988):

$$V_r = \left[1 + (swelling\ index - 1) \times \frac{\rho}{d}\right]^{-1} \qquad \text{Eq. 9.6}$$

ρ and d are the densities of polymer and solvent, respectively (in our case, X-linked polystyrene and toluene). The values of ρ and d used are 1.08 g/ml and 0.867 g/ml (at 20 °C), respectively. V_1 is the molar volume of the solvent; for toluene, V_1 is 106.3 ml/mol (Okay, 1988). χ is the polymer-solvent interaction parameter. The required value of χ for the polystyrene-toluene system was obtained from (Okay, 1988):

$$\chi = 0.455 - 0.155 \times V_r \qquad \text{Eq. 9.7}$$

After calculating the values of V_r and χ from Eq. 9.6 and Eq. 9.7, respectively, one can then calculate υ_e from Eq. 9.5 and subsequently, calculate M_c from Eq. 9.4.

9.2.3.3 Nuclear Magnetic Resonance Spectroscopy

The fractions of unreacted pendant double bonds in the nitroxide-mediate copolymerization of STY/DVB (before the gelation point) were determined by ^{1}H-NMR using a Bruker AVANCE 500 NMR spectrometer. Deuterated methylene chloride was used as the solvent and the measurements were taken at room temperature. The relative amounts of total double bonds reacted (this included both STY and DVB) and residual double bonds (from unreacted DVB; the final sample was purified, so there was no unreacted STY or DVB present) in the copolymer were estimated from absorption peaks of the spectra. In the case of reacted double bonds from both STY and DVB, the five protons in the –C6H5 group were taken at 6.5-7.5 ppm (integrated area under the curve: A)), while for the unreacted pendant double bonds, one of the protons of the =CH2 group was found at δ = 5.2 ppm (integrated area under the peak: B). Hence, the fraction of unreacted pendant double bonds was calculated by $\frac{B}{A/5}$. Figure 9.6 shows a typical spectrum for the cross-linking NMRP of STY/DVB.

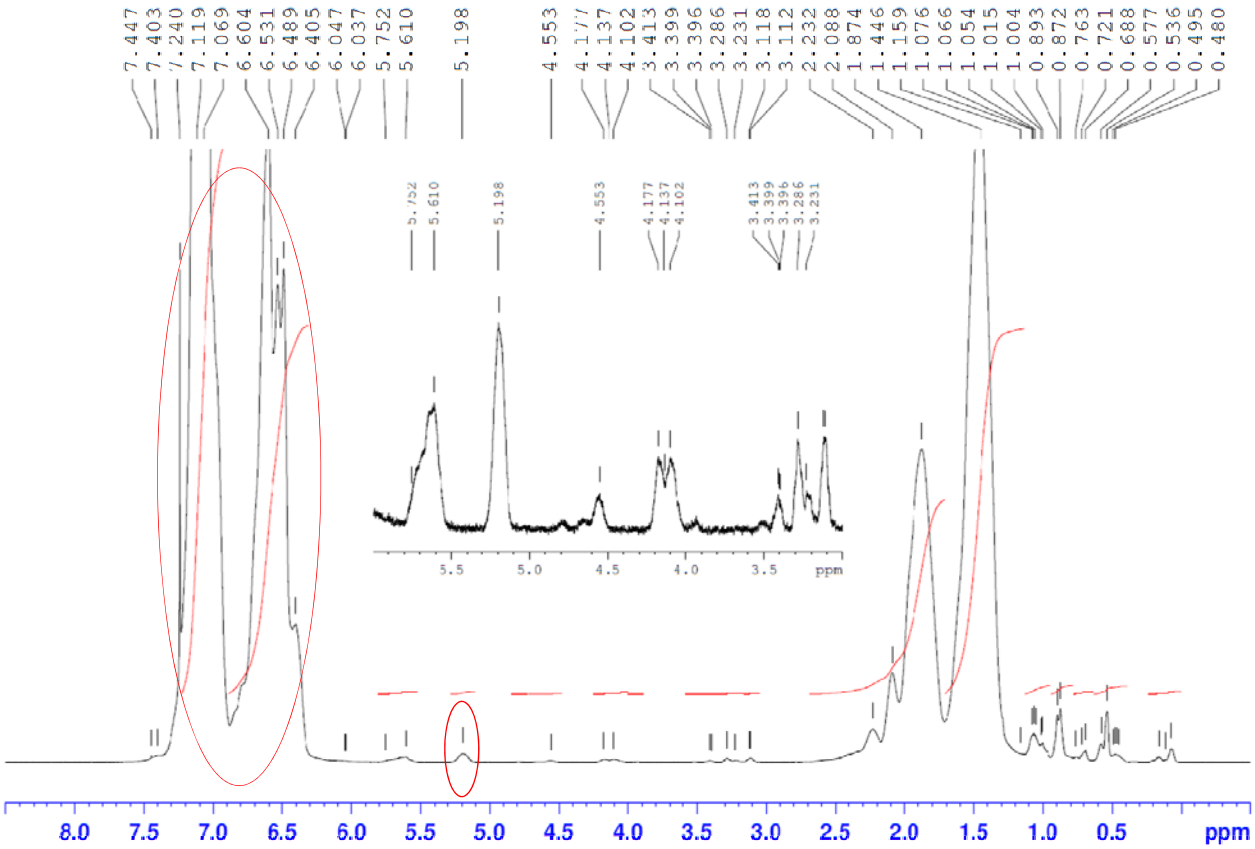

Figure 9.6 H-NMR spectra for cross-linked NMRP of STY with 1wt% DVB and 1 wt% I-TIPNO at 33% conversion

9.2.4 Experimental Summary and Design

In an attempt to determine the importance of different factors influencing the cross-linking NMRP of STY, the Bayesian approach was utilized to design three experiments in two sequences. As discussed in Chapter 8, three main factors were identified (concentration of the TIPNO-based alkoxyamine, DVB concentration and temperature) and high and low levels were chosen for each, as can be seen in Table 9.2. Experiments #4 and #5 in Table 9.2 show the experimental settings suggested by the Bayesian approach for the first sequence, while the single trial of the second sequence is experiment # 7. Experiment #6 was carried out for confirmation purposes and to complement experiment # 7.

Results from these four designed experiments were contrasted with homopolymerization of STY in the presence of I-TIPNO and regular FRP of STY/DVB, as reference systems. Experiments # 1 and 2 in Table 9.2 show the homopolymerization of styrene with low and high levels of I-TIPNO, respectively, while experiment # 3 is the regular free radical polymerization of styrene with 1 wt% DVB and 0.0053 M Trigonox B (as initiator).

In order to check the reproducibility of the experimental data obtained, completely independent replicates were conducted for some of the runs. Reliability of molecular weight measurements was also checked by running GPC replicates at different times.

Table 9.2 Summary of experiments designed for the kinetic study of cross-linked NMRP of STY

Experiment #	**Temperature (°C)**	**[I-TIPNO]**		**[DVB]**	**[DVB]/[I-TIPNO] (molar ratio)**
		wt%	M	wt%	
1	120	1.0	0.028	--	--
2	120	2.0	0.058	--	--
3	120	--	--	1.0	--
4	120	1.0	0.027	1.0	2.50
5	120	2.0	0.055	1.0	1.25
6	120	1.0	0.028	1.5	3.75
7	120	2.0	0.056	1.5	1.87

9.3 Mathematical Modeling

The mathematical modeling for cross-linking NMRP of STY/DVB is presented in this section and is heavily based on Hernandez-Ortiz et al. (2009 and 2012). This kinetic model was based on a detailed reaction mechanism. The reactions considered in the polymerization mechanism included reversible deactivation of alkoxyamine, dimer formation, thermal initiation, monomer propagation, reversible deactivation of polymer radicals, propagation through pendant double bonds (cross-linking and cyclization reactions), bimolecular termination and transfer reactions (transfer to monomer, dimer, polymer and other small molecules). Alkoxyamine decomposition was considered as a side reaction in the polymerization scheme (Li et al., 1995; Nilsen et al., 2006; Aldabbagh et al., 2008), while the reaction between dimer and nitroxide and the addition of nitroxide to monomer double bonds typically present during NMRP in the presence of TEMPO, were neglected. The detailed polymerization scheme can be found in Hernandez-Ortiz et al. (2009). A more simplified summary version is presented in Table 9.3. In this table, M is the monomer (in the current copolymerization system, two different types of monomers were involved, styrene and divinyl benzene). NO_E, $R_{in}^{\bullet}$, ${}^{\bullet}NO_X$, D, $R_r^{\bullet}$, $R_r NO_X$, P_s^*, $R_s^* NO_X$, P_r, and HNO_X in Table 9.3 are the alkoxyamine, primary free radical, nitroxyl stable free radical, dimer, polymer radical of size *r*, dormant polymer of size r, polymer molecule of size s which participates in cross-linking, dormant polymer of size s with deactivated radical which participates in cross-linking, dead polymer of size r and hydroxylamine.

In order to make the mathematical treatment tractable, it was assumed that every polymer radical contained only one active center (monoradical assumption), and that every dormant polymer molecule contained only one nitroxyl capping unit (monofunctional assumption). These assumptions implied that a polymer molecule could only be living, dormant or dead at once, and it was considered that when an active polymer molecule attacked the double pendant bond of a dormant polymer, a new polymer radical was formed. Pseudo-rate constants are listed in the third column of Table 9.3.

Table 9.3 Simplified polymerization scheme for cross-linking NMRP with alkoxyamine as unimolecular initiator

Process	**Reaction**	**Rate constant**
Alkoxyamine deactivation (unimolecular initiation)	$NO_E \underset{\leftarrow}{\rightarrow} R^{\bullet}_{in} + {}^{\bullet}ON_X$	k_{a2}, k_{d2}
Dimerization	$M + M \rightarrow D$	k_{dim}
Thermal initiation	$D + M \rightarrow D^{\bullet} + R^{\bullet}_1$	k_{thi}
First propagation		
• Primary radicals	$M + R_{in}^{\bullet} \rightarrow R^{\bullet}_1$	k_i
• Dimeric radicals	$M + D^{\bullet} \rightarrow R^{\bullet}_1$	k_i
Propagation	$R^{\bullet}_r + M \rightarrow R^{\bullet}_{r+1}$	k_p
Reversible deactivation of polymeric radicals	$R^{\bullet}_r + {}^{\bullet}ON_X \underset{\leftarrow}{\rightarrow} R_rON_X$	k_{da}, k_a
Cross-linking		
• Living to dead polymer	$R^{\bullet}_r + P_s^{*} \rightarrow R^{\bullet}_{r+s}$	k_p^{*}
• Living to dormant polymer	$R^{\bullet}_r + R^{*}_s ON_X \rightarrow R^{\bullet}_{r+s}$	k_p^{*}
Termination		
• Disproportionation	$R^{\bullet}_r + R^{\bullet}_s \rightarrow P_r + P_s$	k_{td}
• Combination	$R^{\bullet}_r + R^{\bullet}_s \rightarrow P_{r+s}$	k_{tc}
Chain Transfer to:		
• Monomer	$R^{\bullet}_r + M \rightarrow P_r + R^{\bullet}_1$	k_{fm}
• Dimer	$R^{\bullet}_r + D \rightarrow P_r + D^{\bullet}$	k_{fD}
• Polymer	$R^{\bullet}_r + P_s \rightarrow P_r + R^{\bullet}_s$	k_{fp}
Termination		
• Disproportionation	$R^{\bullet}_r + R^{\bullet}_s \rightarrow P_r + P_s$	k_{td}
• Combination	$R^{\bullet}_r + R^{\bullet}_s \rightarrow P_{r+s}$	k_{tc}
Alkoxyamine decomposition		
• Nitroxyl ether decomposition	$NO_E \rightarrow M + HON_X$	k_{decomp}
• Polymeric alkoxyamine	$R_rON_X \rightarrow P_r + HON_X$	k_{decomp}

Based on the kinetic mechanism, species balance equations were derived. The complete set of these equations is given in Hernandez-Ortiz et al. (2009). Balances for monomer and nitroxyl radical are shown in Eq. 9.8 and Eq. 9.9, as examples of the balance equations for small molecules, while the mass balance for dead polymer radicals is shown in Eq. 9.10, as representative for polymer molecules (living, dormant, and dead polymer).

Monomer conversion

$$\frac{dx}{dt} = 2k_{\dim}(1\text{-}x)^2 + k_{thi}[D](1\text{-}x) + k_i\left[D^\bullet + R_{in}^\bullet + T^\bullet\right](1\text{-}x) + \left(k_p + k_{fm}\right)(1\text{-}x)\,Y_0 - k_{decomp}[NO_E] + k_{iNO}\left[^\bullet NO_X\right](1\text{-}x) \qquad \text{Eq. 9.8}$$

Nitroxyl radicals

$$\frac{1}{V}\frac{d\left(V\left[^\bullet ONX\right]\right)}{dt} = k_a[S_0] - k_{da}\left[^\bullet ONX\right]Y_0 + k_{a2}\left[NOE\right] - k_{d2}\left[R_{in}^\bullet\right]\left[^\bullet ONX\right] + k_{a3}\left[DONX\right] - k_{d3}\left[^\bullet ONX\right]\left[D^\bullet\right] + k_{a3}\left[TONX\right] - k_{d3}\left[^\bullet ONX\right]\left[T^\bullet\right] - k_{h3}\left[D\right]\left[^\bullet ONX\right] - k_{pr}\left[I\right]\left[^\bullet ONX\right] - k_{iNO}\left[^\bullet NO_X\right][M] \qquad \text{Eq. 9.9}$$

Dead polymer

$$\frac{d[D_r]}{dt} = k_{td}[P_r][P] + k_{fT}[T][P_r] + \frac{1}{2}k_{tc}\sum_{s=1}^{r-1}[P_s][P_{r-s}] - \left(k_{fP} + k_p^*\right)Y_0\,r[D_r] + k_{fP}[P_r]Q_1 + k_p^*\sum_{s=1}^{r-1}[P_{r-s}]s[D_s] \qquad \text{Eq. 9.10}$$

In order to follow the molecular weight development, in terms of number and weight averages, the method of moments was used. There were three polymer populations in this system: "living" polymer radicals, dead polymer molecules, and dormant species. The number-average molecular weight was the ratio of the first moments of all the species to their zeroth moment, while the weight-average molecular weight was the ratio of their second moments to their first moments. The model also included equations for the average cross-link density, divinyl monomer consumption and accumulated copolymer composition. All in all, the model for the cross-linking NMRP consisted of twenty three ordinary differential equations (ODEs); twelve of them were balance equations for small molecules, nine were moment equations for the

molecular weight development, one equation accounted for the calculation of average crosslink density, and the other one the calculated divinyl monomer consumption. The system of ODEs was solved and the predicted profiles were generated. The criterion for gel formation was weight-average molecular weight reaching a value greater or equal to 10^7.

This kinetic model was originally developed for cross-linking NMRP of STY/DVB with TEMPO (Hernandez-Ortiz et al. (2009)), therefore it was altered to be applicable to the TIPNO-based alkoxyamine as well. Most of the kinetic parameters used in the simulations were the same as the ones presented in Hernandez-Ortiz et al. (2009) and are not cited here for the sake of brevity. The activation rate constant, $k_{a2} = 3.3 \times 10^{-3}$ s^{-1} (Marque et al., 2000), the deactivation rate constant, $k_{d2} = 8.2 \times 10^{6}$ L. mol^{-1}. s^{-1} (Sobek et al., 2001), and the decomposition rate constant, $k_{decomp} = 6.2 \times 10^{-5}$ s^{-1} (Aldabbagh et al., 2008), were used for I-TIPNO at 120 °C. Although the model was originally developed for the cross-linking NMRP of vinyl and divinyl monomers, its validity was also tested by reducing the model to check if it showed an acceptable prediction ability for NMRP homopolymerization of styrene. The predicted profiles from the model for conversion, molecular weights and polydispersity were contrasted to our experimental data for NMRP of styrene with I-TIPNO; results are presented in Subsection 9.4.1.2. Comparison results for cross-linking NMRP of styrene with DVB and I-TIPNO are presented in Subsection 9.4.2.5.

9.4 Results and Discussion

9.4.1 Kinetic Investigation of NMRP of Styrene with TIPNO-based Alkoxyamine

As explained earlier, NMRP of styrene in the presence of a nitroxide controller was carried out in our investigations to serve as a reference for comparison with the cross-linking copolymerization of STY/DVB in the presence of a nitroxide controller. It was decided to use NMRP in the unimolecular approach as opposed to the bimolecular approach, since by using the former approach one could avoid the complications that occur because of side reactions between the nitroxide and the initiator in the latter approach, which affects both nitroxide concentration and the initiator efficiency factor (see Moad et al. (1981), Georges et al. (2002) and Fu et al. (2007)).

A unimolecular initiator based on TEMPO was synthesized in our lab and a comprehensive kinetic study of polymerization of styrene with this unimolecular initiator was carried out by Zhou et al. (2010). However, there were several chemistry steps involved related to the careful synthesis and characterization of this unimolecular initiator. Based on this experience, it was decided to use a commercially available unimolecular initiator, as it would eliminate the difficulties involved in making the unimolecular initiator and also save a lot of time.

Given prior experience we have had with a Ciba nitroxide, Irgatec CR76 (described in Psarreas et al. (2007) but for a totally different application) and its availability in our lab, it was decided to investigate the potential replacement of the commonly used nitroxide (TEMPO) with this nitroxide in our study. However, thorough kinetic investigations on styrene polymerization using Ciba's Irgatec CR76 (NOR) over several temperature levels showed that there was no controlled radical polymerization behavior; the system behaved rather like regular thermal polymerization of styrene (Nabifar et al., 2010). Results from this detailed investigation are presented in Appendix F.

In pursuit of finding a proper unimolecular initiator, and after a complete survey of the commercially available alkoxyamine initiators, N-tert-butyl-N-(2-methyl-1-phenylpropyl)-O-(1-phenylethyl) hydroxylamine (called TIPNO-based alkoxyamine or I-TIPNO from hereon) was chosen to be used in our study. When it decomposes, this alkoxyamine produces 2,2,5-

trimethyl-4-phenyl-3-azahexane-3-oxyle, which is commonly referred to as TIPNO nitroxide. TIPNO and its alkoxyamine (shown in Figure 9.7) were first described by Benoit et al. (1999), where a series of acyclic α-hydrogen- bearing nitroxides and their corresponding alkoxyamines were synthesized to be used for the controlled radical polymerization of a wide range of monomers. This alkoxyamine is commercially available and can be purchased from Sigma Aldrich.

a) b)

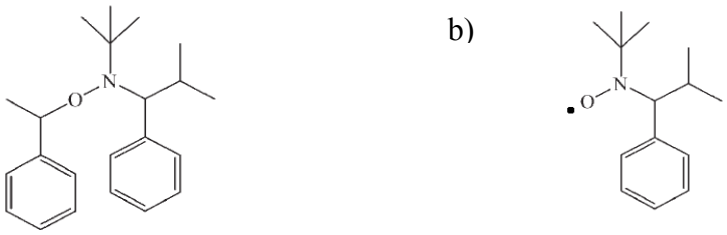

Figure 9.7 Structures of a) N-tert-butyl-N-(2-methyl-1-phenylpropyl)-O-(1-phenylethyl) hydroxylamine (TIPNO-based alkoxyamine), and b) 2,2,5-trimethyl-4-phenyl-3-azahexane-3-oxyle (TIPNO)

9.4.1.1 Comparison with NMRP of STY with TEMPO-based Unimolecular Initiator

The results of styrene polymerization in the presence of TIPNO-based alkoxyamine are presented in this subsection. The polymerizations were carried out at 120 °C with different concentrations of the alkoxyamine under bulk conditions. Figure 9.8a shows the conversion vs. time plot of styrene polymerization with 1 and 2 wt % TIPNO-based alkoxyamine (corresponding to 0.0.28 and 0.058 molar concentration (M), respectively, and shown as [I-TIPNO] in the figure). As can be seen, the results for both concentrations are relatively close to each other and also close to the experimental data presented by Drache et al. (2007) (for styrene polymerization with 0.05 M TIPNO-based alkoxyamine at 123 °C). The corresponding ln ($[M]_0/[M]$) vs. time plots are illustrated in Figure 9.8b; a linear relationship can be observed for the first 15 hrs of the reaction. This is typical behavior for controlled radical polymerization (as discussed in Chapter 4), which suggests that TIPNO is acting as a suitable unimolecular initiator. The rate of polymerization is only imperceptibly higher for the run with higher alkoxyamine concentration; the effect of alkoxyamine concentration is not

significant on the rate of polymerization, as observed previously for other nitroxides (Fukuda et al., 1996).

a)

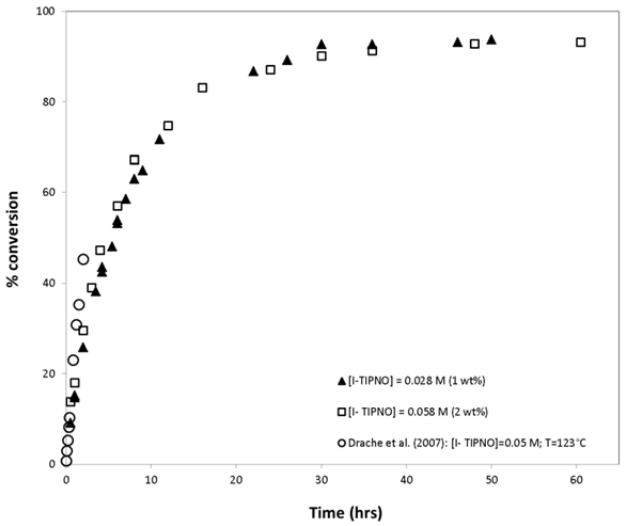

b)

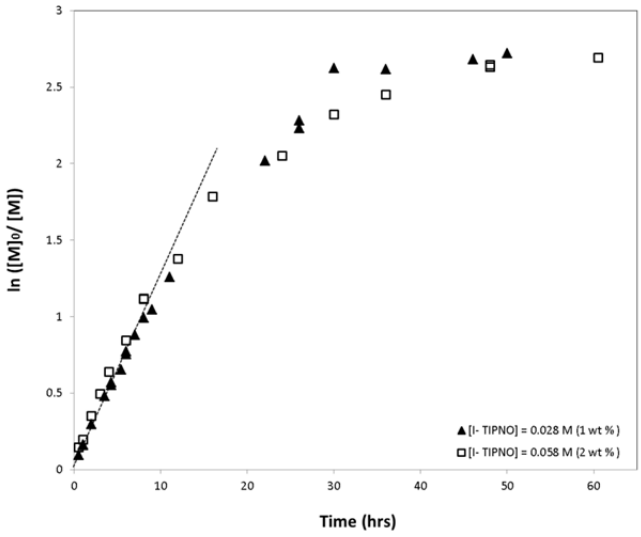

Figure 9.8 a) Conversion vs. time, b) ln ($[M]_0/[M]$) vs. time, for styrene polymerization at 120 °C, with TIPNO-based alkoxyamine

Figure 9.9 presents a comparison between the data from our experimental run (styrene polymerized with [I-TIPNO] = 0.028 M), and the data obtained by Zhou et al. (2010) (styrene polymerization with [I-TEMPO] = 0.03 M). It is apparent that the polymerization rate of the styrene polymerization in the presence of TIPNO-based unimolecular initiator (I-TIPNO) is higher than in the case of I-TEMPO; this behaviour was also observed by Benoit et al. (1999)

and Drache et al. (2007). A complementary replicate run was also carried out, shown in Figure 9.9, to collect more data and also check the reproducibility of the data. As can be seen, the experimental data are very reproducible.

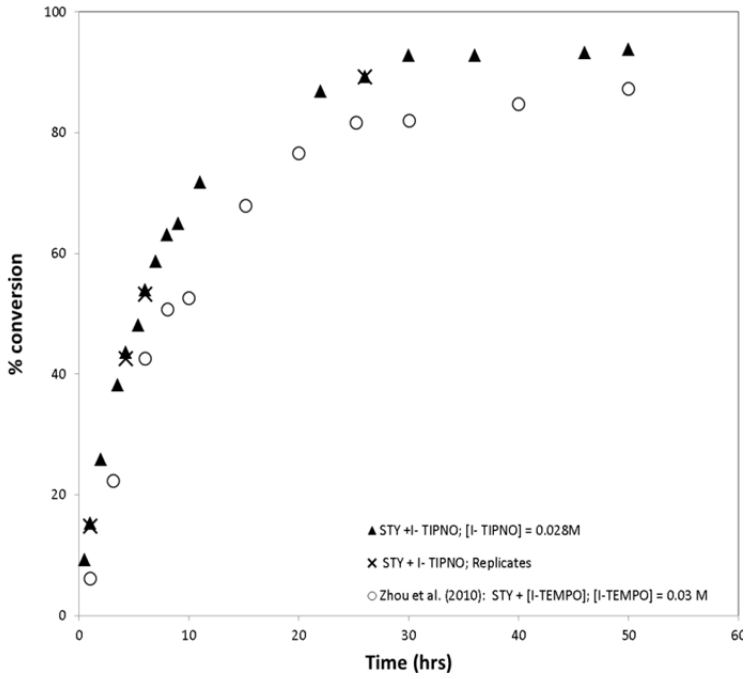

Figure 9.9 Rate comparison for STY polymerization with TIPNO-based and TEMPO-based unimolecular initiators, at 120 °C

The corresponding average molecular weight vs. conversion data are shown in Figure 9.10a. Both number- and weight-average molecular weights increase linearly with conversion, which serves as another indicator of controlled behaviour of styrene polymerization with TIPNO. The run with higher alkoxyamine concentration (I- TIPNO) has lower average molecular weights, as expected based on Eq. 9.11, which shows the theoretically calculated number-average molecular weight (the factor 104.5 in Eq. 9.11 is the molecular weight of styrene monomer). Polydispersity (PDI) vs. conversion data are shown in Figure 9.10b. PDI values are below 1.3, well below typical PDI values for regular free radical polymerization. The average molecular weights and PDI values for styrene polymerization with [I-TIPNO] = 0.05 M at 123 °C determined by Drache et al. (2007) are also illustrated alongside our experimental data; as can be seen, there is good agreement between the two experimental data sets.

$$M_n = [Sty]_0 \times conversion_{sty} \times \frac{104.15}{[I - TIPNO]}$$ Eq. 9.11

Figure 9.11a compares the molecular weight results from our experiment (with 0.028 M [I-TIPNO]) to the results of Zhou et al. (2010) (with [I-TEMPO] at 0.03 M). It can be seen that the molecular weight data for the TEMPO-based unimolecular initiator are lower than the molecular weights for the TIPNO-based one. Also, it seems that the TIPNO-based initiator offers better control of the polymerization reaction at higher conversions, i.e., a linear correlation between average molecular weights and conversion is maintained even at higher conversions, which is not the case for the TEMPO-based initiator. The corresponding PDI values are shown in Figure 9.11b; both polymerizations showed PDI values well below 1.3.

a)

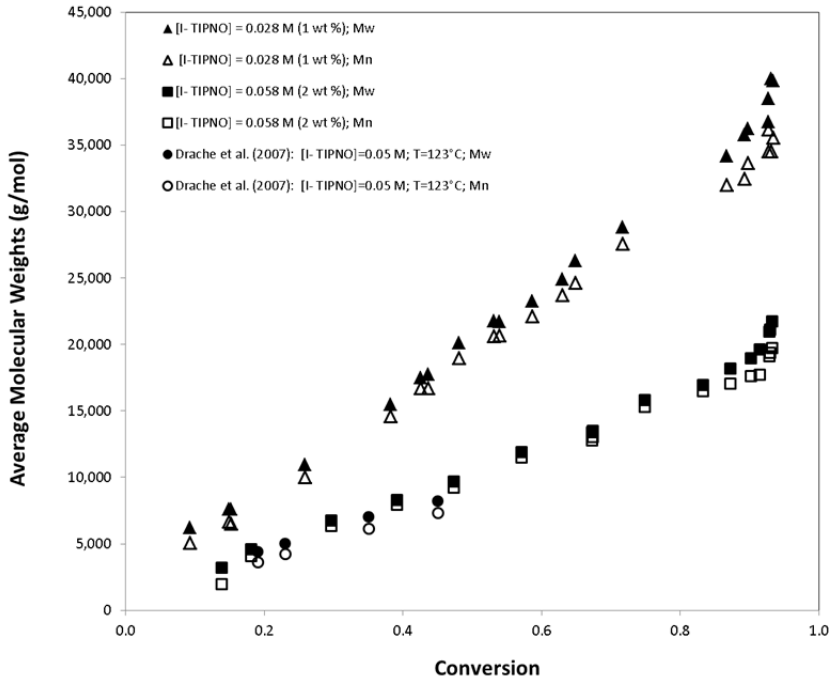

b)

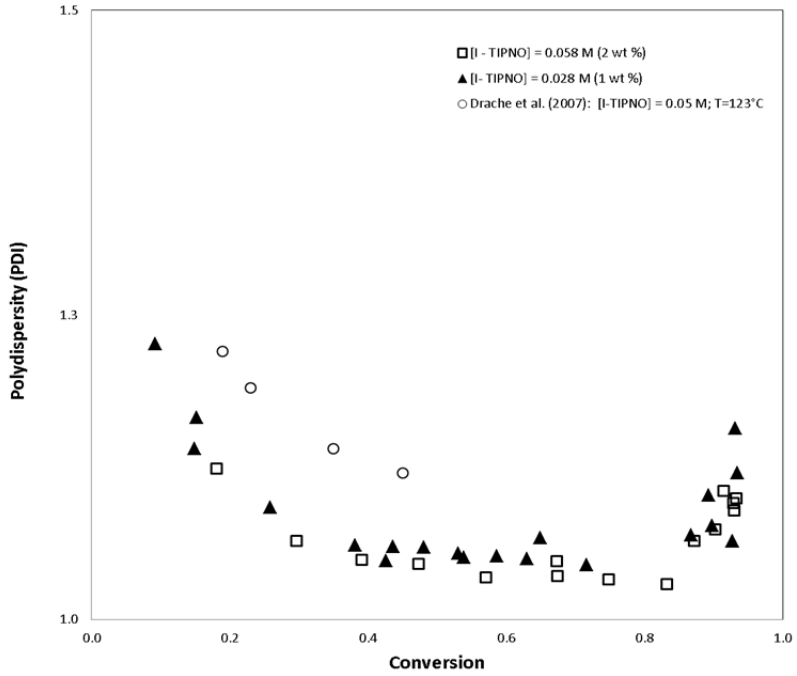

Figure 9.10 Molecular weights (a) and polydispersity (b) vs. conversion, for styrene polymerization at 120 °C, with TIPNO-based alkoxyamine

a)

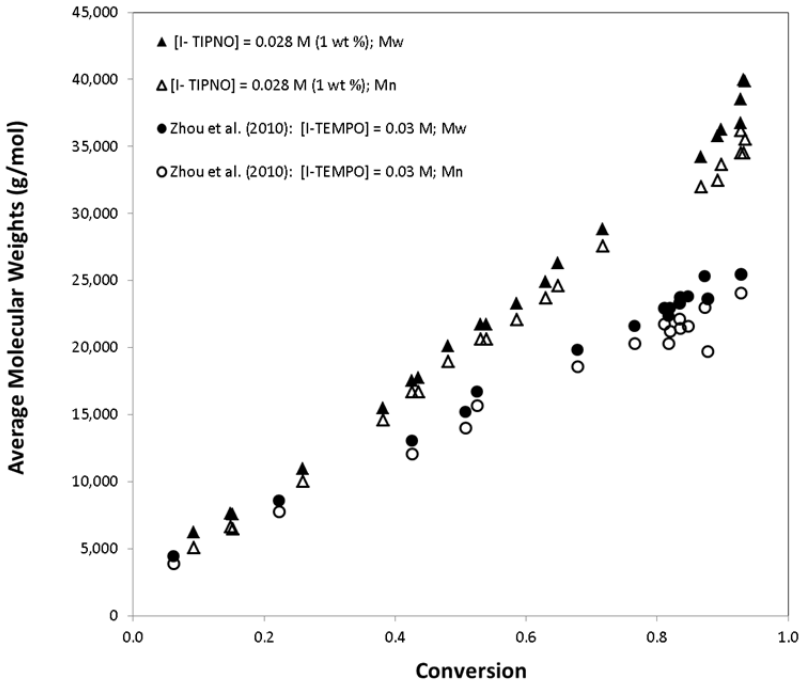

b)

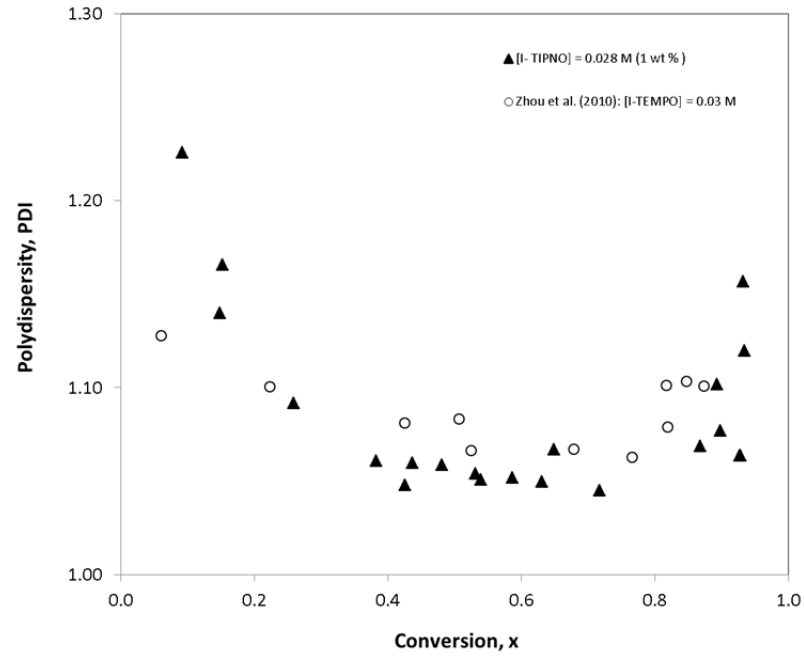

Figure 9.11 Molecular weights (a) and polydispersity (b) vs. conversion comparisons, for STY polymerization with TIPNO-based and TEMPO-based unimolecular initiators, at 120 °C

9.4.1.2 Comparison of Model Predictions with Experimental Data

Figure 9.12 shows a comparison of model predictions and experimental data of conversion versus time, for the NMRP of STY with TIPNO-based unimolecular initiator at 120 °C. It is observed in Figure 9.12a, b (for both concentrations of [I- TIPNO]) that the model captures the trends perfectly and the agreement between model predictions and experimental data is good. The corresponding comparisons for average molecular weights versus conversion are shown in Figure 9.13. It can be seen that the model captures the linear relationship between molecular weights and conversion perfectly; however, it underestimates the values of the molecular weights. This qualitative disagreement between model predictions and experimental data is more pronounced for the higher concentration of TIPNO-based initiator (see Figure 9.13b). The agreement in the polydispersity index (PDI) versus conversion profile is very good for both concentrations of the TIPNO-based initiator, as can be seen in Figure 9.14a and b. Again the model captures the behaviour of PDI perfectly, i.e., initially high values of PDI, lower than 1.5 values during most of the polymerization, and then slight increase in the values towards the end of the reaction.

In conclusion, the model captures well the controlled-radical polymerization features, such as linear increase of molecular weights with conversion and low PDI values. However, the quantitative agreement in the molecular weight versus conversion profiles is still not completely satisfactory, in spite of the inclusion of some known side reactions. Further investigation is required to find the reason for this discrepancy.

a)

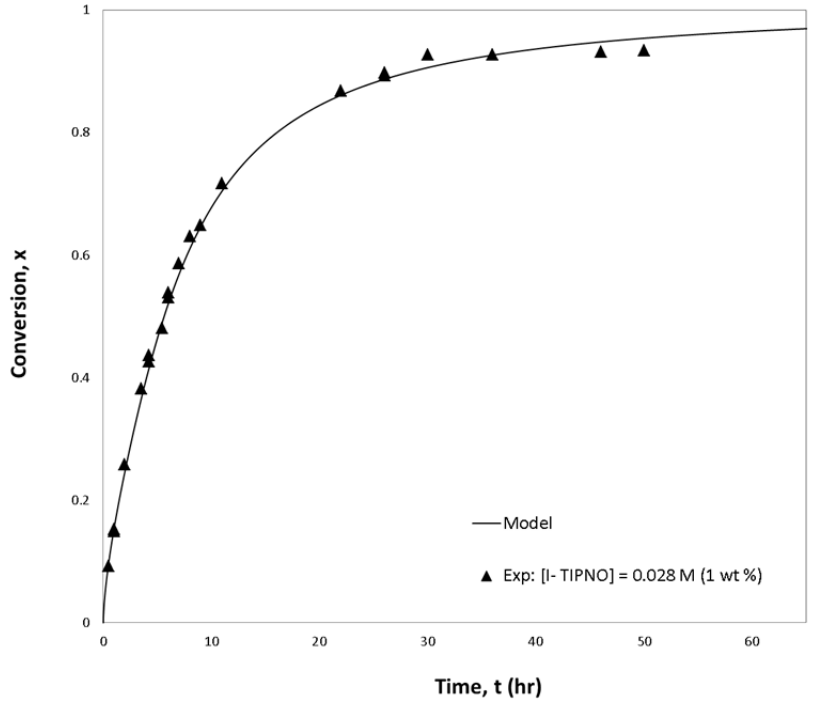

b)

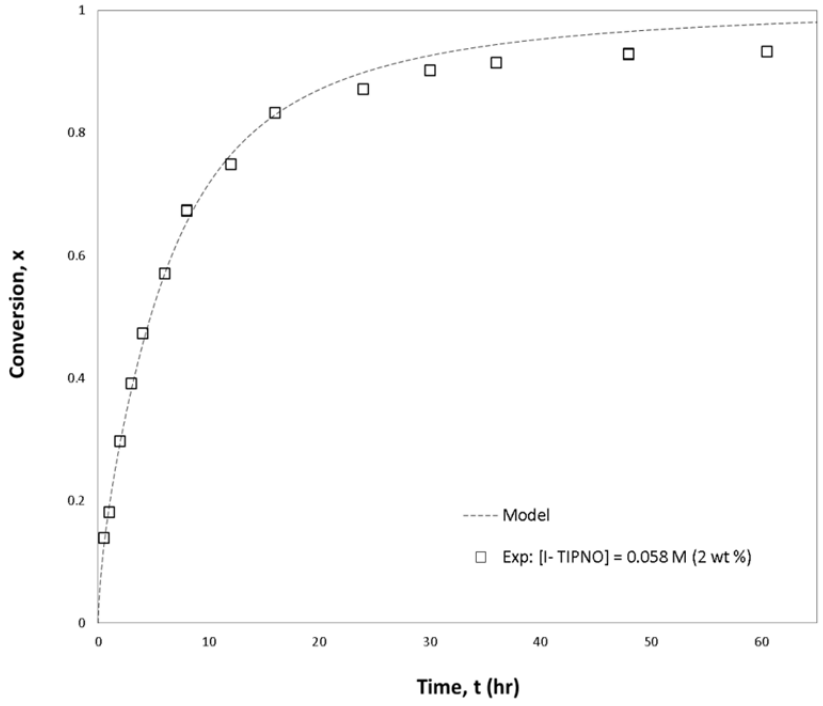

Figure 9.12 Comparison of model predictions and experimental data of conversion vs. time, for styrene polymerization at 120 °C with TIPNO-based alkoxyamine, a) [I-TIPNO] = 0.028 M (1 wt%), b) [I- TIPNO] = 0.058 M (2 wt%)

a)

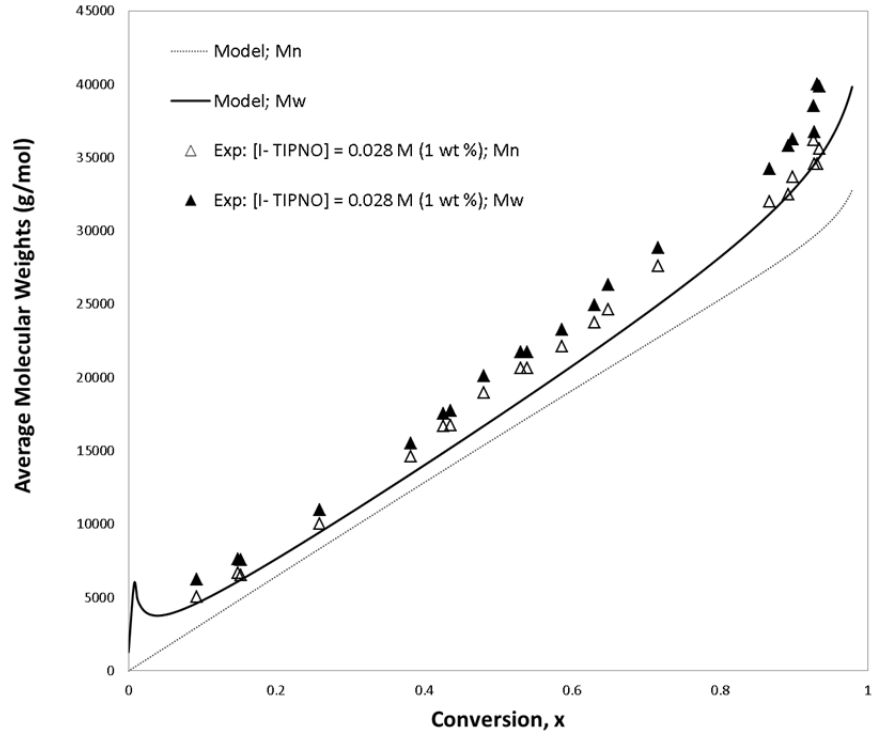

b)

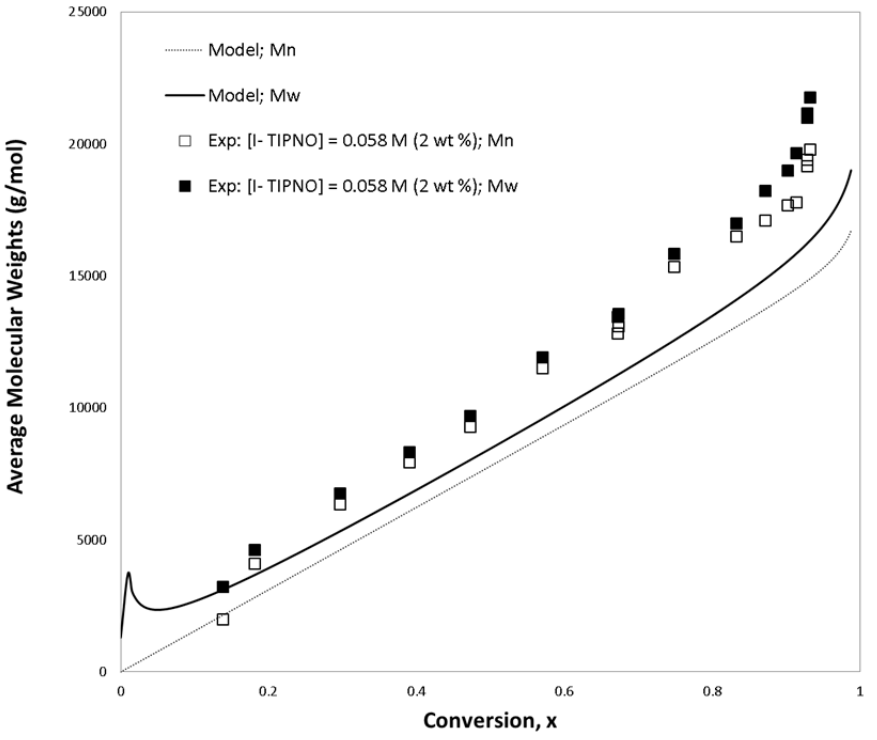

Figure 9.13 Comparison of model predictions and experimental data of average molecular weights vs. conversion, for styrene polymerization at 120 °C with TIPNO-based alkoxyamine, a) [I- TIPNO] = 0.028 M (1 wt%), b) [I- TIPNO] = 0.058 M (2 wt%)

a)

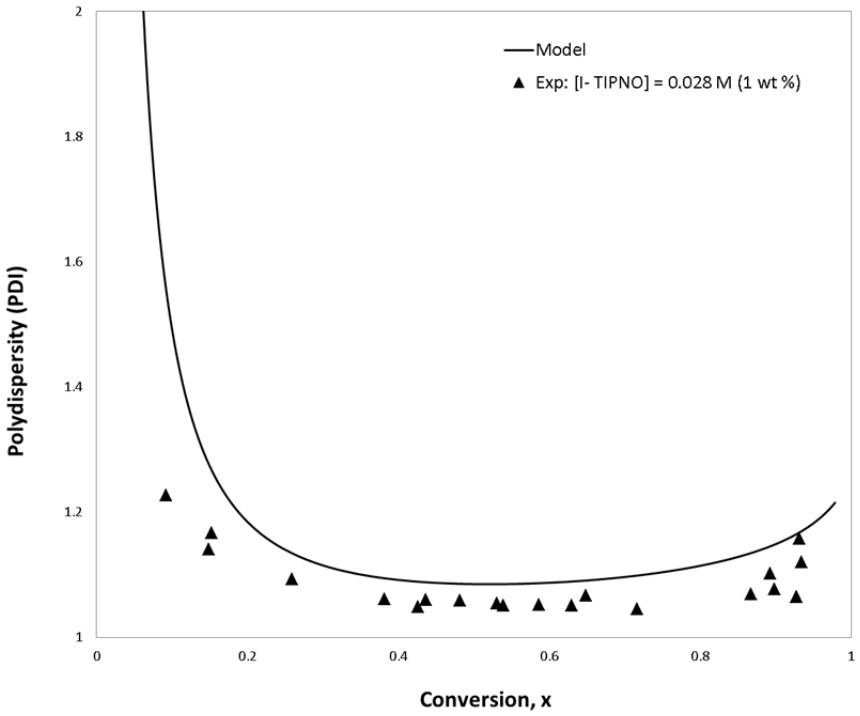

b)

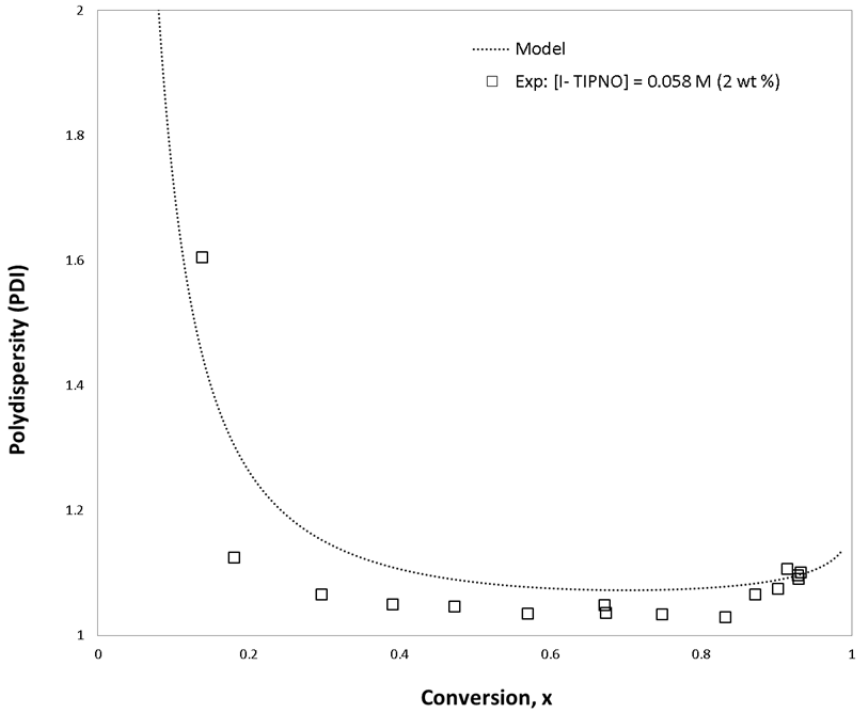

Figure 9.14 Comparison of model predictions and experimental data of PDI vs. conversion, for styrene polymerization at 120 °C with TIPNO-based alkoxyamine, a) [I- TIPNO] = 0.028 M (1 wt%), b) [I- TIPNO] = 0.058 M (2 wt%)

9.4.2 Kinetic Investigation for NMRP of STY/DVB with TIPNO-based Alkoxyamine

Now that it is well-established that styrene polymerization in the presence of TIPNO-based alkoxyamine exhibits controlled-radical polymerization characteristics, results from the cross-linking kinetics of NMRP of STY/ DVB with this unimolecular initiator are presented in this subsection. As mentioned earlier, this kinetic study is carried out in preparation for the identification of network homogeneity indicators based on polymer properties (which will be discussed in Chapter 10). Results are contrasted with regular FRP of STY/DVB and homopolymerization of STY in the presence of I-TIPNO, as reference systems. The effect of cross-linker concentration and I-TIPNO concentration and subsequently the [DVB]/ [I-TIPNO] molar ratio are investigated on rate, molecular weights, gel content and swelling index. In order to build more confidence in the observed data from such a complex, noisy and experimentally uncertain system, careful independent replication was carried out for most of the runs. In parallel to our experimental investigations, a detailed mathematical model has been developed. Comparisons between experimental data and model predictions will also be discussed in this subsection.

9.4.2.1 Comparison with NMRP of STY with I-TIPNO and with FRP of STY/ DVB

Conversion versus time for styrene copolymerization with 1 wt% DVB, in the presence of [I-TIPNO] = 0.028 M (1 wt %) (Experiment # 4 in Table 9.2; chosen as the base case for our study) is presented in Figure 9.15 (see open rhombic symbols). As can be seen, the rate of polymerization is slower than the regular styrene copolymerization with 1 wt% DVB (see open circles in Figure 9.15; this was conducted in the absence of TIPNO-based alkoxyamine), and is almost identical to the conversion versus time profile for styrene homopolymerization with [I-TIPNO] = 0.028 M (1 wt %) (also shown in Figure 9.15; see black triangles). This experiment was replicated to check for reproducibility; the replicated conversion levels were very close to the original data, confirming the reliability of our data (compare crosses and open rhombic symbols in Figure 9.15). Our experimental data points were also compared to the data for bimolecular NMRP of STY/DVB in the presence of BPO as initiator and TEMPO as controller, collected by Tuinman et al. (2006). It can be seen in Figure 9.15 that the cross-linking NMRP of styrene with TEMPO as controller is slower than this reaction with the

TIPNO-based unimolecular initiator; this observation is in agreement with the comparison of homopolymerization of styrene for these two nitroxides (see Figure 9.9).

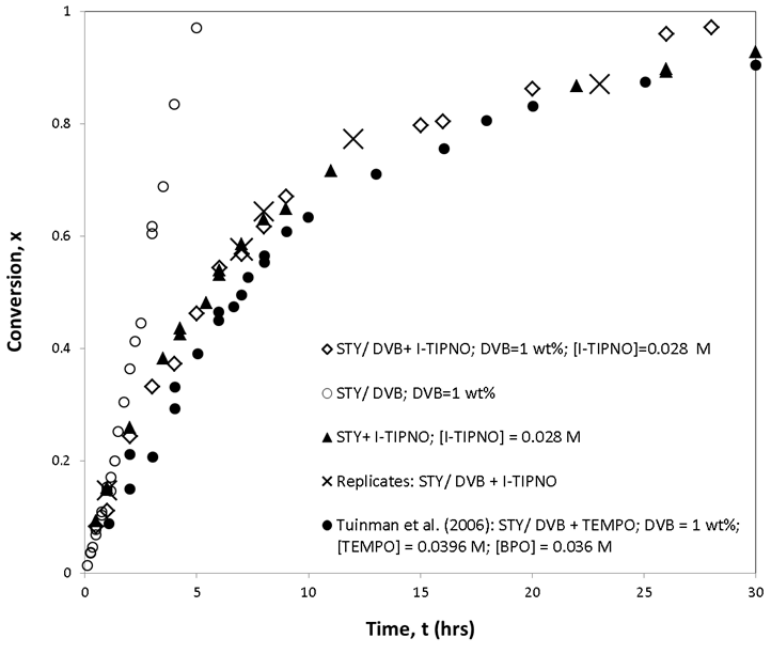

Figure 9.15 Conversion vs. time for STY/DVB with [I-TIPNO] = 0.028 M (1 wt %) and [DVB] = 1 wt % at 120 °C; comparison with FRP, NMRP and STY/DVB with TEMPO

Figure 9.16 shows the corresponding average molecular weights. The insert in the figure shows the molecular weight values just before the gelation point. The molecular weights for styrene homopolymerization with I-TIPNO are also illustrated in this insert for comparison purposes. As can be seen in the insert, both number- and weight-average molecular weights increase linearly with conversion until about 33% conversion, and these values are very close to the ones from NMRP of styrene with I-TIPNO. However, just after the 33% conversion, average molecular weights start deviating from linearity (with M_w increasing more rapidly compared to M_n), which could be an indication of branching in the system (as will be discussed in more detail in Chapter 10). Around the 60% conversion level (approximately 8 hrs), there is a sudden jump in M_w, which is an indirect indication that the system had gelled. Due to the presence of DVB, the system had become viscous and had lost the 'controlled' behavior. After the gelation point, there is a drop in the average molecular weights. The reason is that only the soluble fraction of the produced polymer (sol) is analyzed via GPC and typically this sol fraction has lower molecular weight.

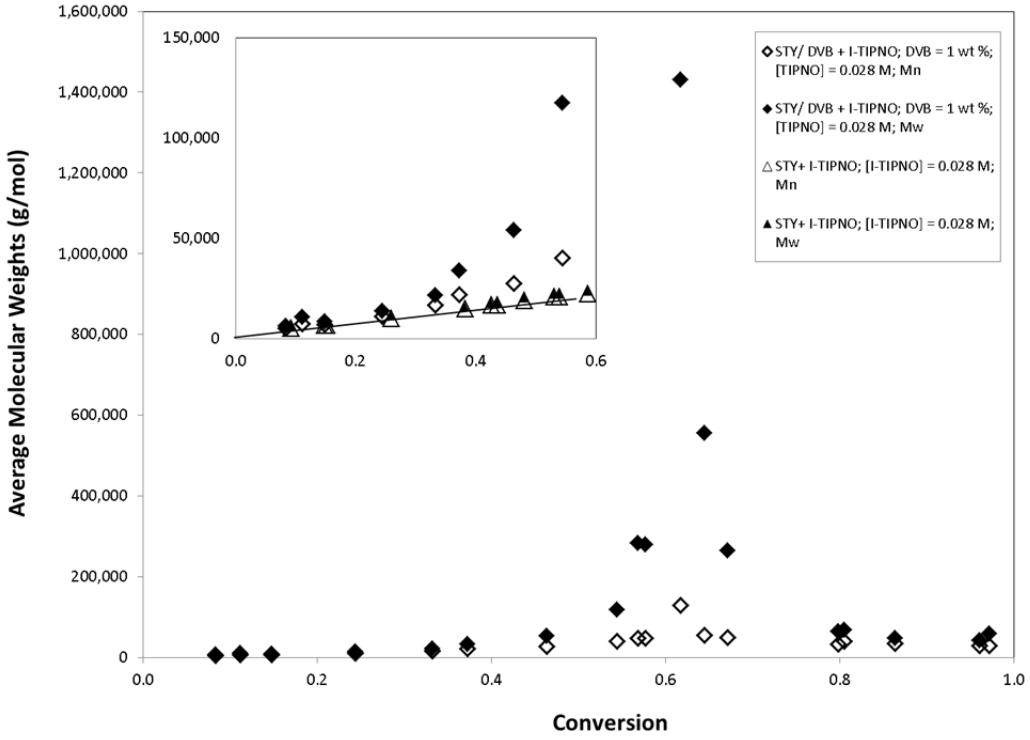

Figure 9.16 Molecular weights vs. conversion for STY/DVB with [I-TIPNO] = 0.028 M (1 wt %) and [DVB] = 1 wt % at 120 °C; comparison with NMRP of STY

Molecular weights vs. conversion for NMRP of STY/DVB with TEMPO (carried out by Tuinman et al. (2006)) are shown in Figure 9.17, for comparison purposes. As can be seen, the general trends are almost the same as STY/DVB with I-TIPNO (illustrated in Figure 9.16). However, in the case of NMRP with TEMPO, the system is not as well behaved as NMRP with I-TIPNO (there is a lot of error in the molecular weight measurements), and the system had gelled around 55% conversion.

The behavior observed for cross-linking STY/DVB under NMRP conditions was entirely different from that of cross-linking in free radical polymerization. Figure 9.18 shows the molecular weights vs. conversion for cross-linking polymerization of styrene with 1 % DVB, in the absence of nitroxide controller. It can be observed that the mixture gels in much earlier stages of the polymerization (almost around 7% conversion, corresponding to 30 min polymerization time) and there is no controlled features as was observed for the cross-linking NMRP (compare Figure 9.18 with Figure 9.16).

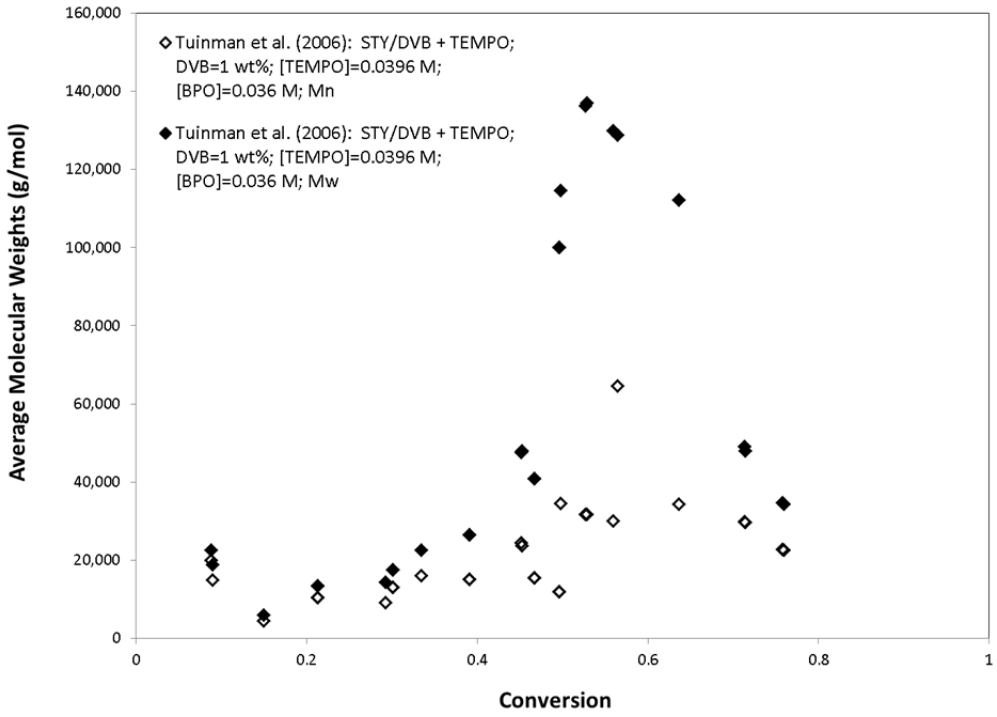

Figure 9.17 Molecular weights vs. conversion for STY/DVB with [TEMPO] = 0.0396 M and [DVB] = 1 wt % at 120 °C (Tuinman et al. (2006)

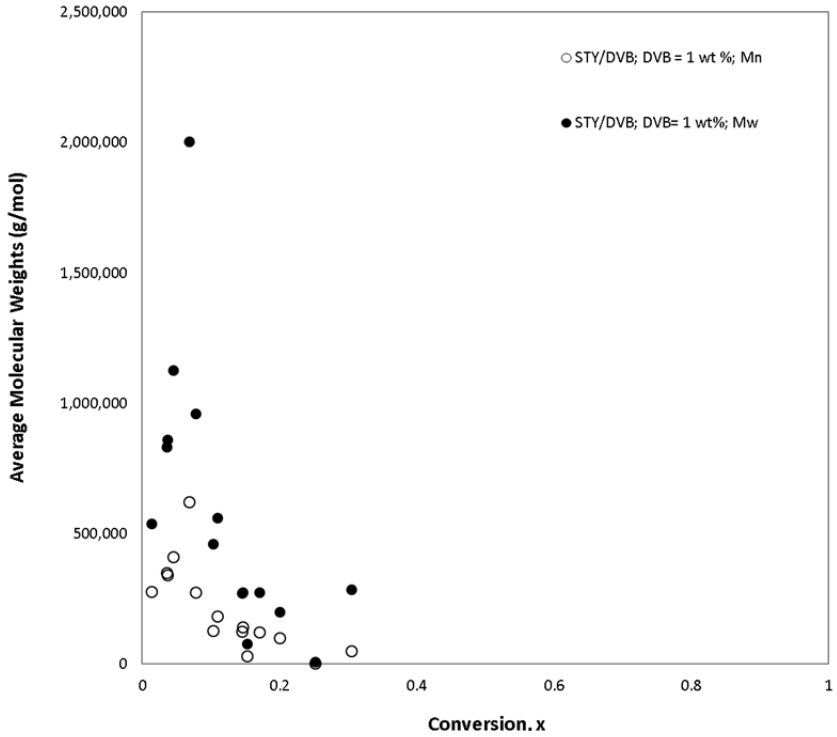

Figure 9.18 Molecular weights vs. conversion for STY/DVB at 120 °C with [TrigB] = 0.0053 M, [DVB] = 1 wt %

Polydispersity values follow the same trend, as shown in Figure 9.19. For cross-linking NMRP with I-TIPNO (see open rhombic symbols in Figure 9.19), the PDI values are well below 2 and close to the values of NMRP of styrene with I-TIPNO (see black triangles in Figure 9.19) up to 33% conversion, after which the PDI values start to increase until reaching a high value of 11 at the gelation point (which is around 60% conversion). The behavior for the cross-linked styrene under regular radical polymerization is totally different; the gel point is shifted to a much lower conversion (see the jump in PDI around 7% conversion) and also the magnitude of the PDI at the gelation point is not as high as the ones in NMRP systems. The corresponding PDI values for cross-linking NMRP with TEMPO show the same trends as the one with I-TIPNO, however, same as with the molecular weight trends, the jump in PDI value, corresponding to the gelation point, is shifted to a lower conversion (around 55% conversion) in this case.

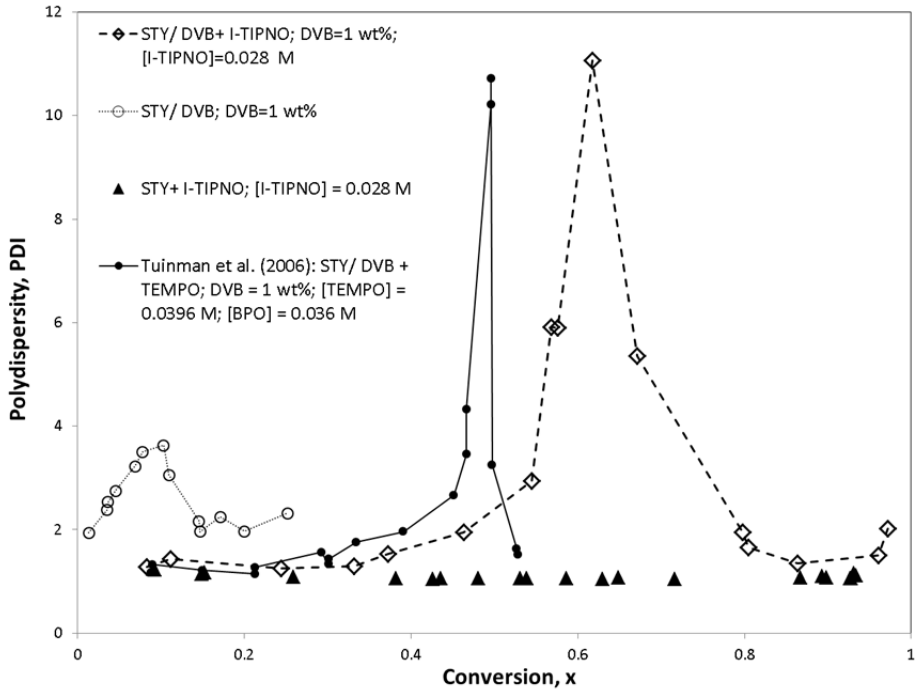

Figure 9.19 PDI vs. conversion for STY/DVB with [I-TIPNO] = 0.028 M (1 wt %) and [DVB] = 1 wt % at 120 °C; comparison with FRP, NMRP and STY/DVB with TEMPO

Gel content and swelling index for our samples from cross-linked NMRP were measured in toluene, following the technique discussed in Subsection 9.2.3.2, and are shown in Figure 9.20a and b, respectively. The gel content increased very rapidly after the gelation point (see open rhombic symbols in Figure 9.20a), while the swelling index decreased from a maximum at the gelation point to a plateau lower value at high conversions (see open rhombic symbols in Figure 9.20b). The decrease in the swelling index suggests that the polymer network is loose at the onset of the gelation point and it becomes more compact, as the polymerization proceeds. Compared to the corresponding gel content and the swelling index for the copolymerization of STY/DVB using free radical polymerization (shown by the open circles in Figure 9.20a and b), the gelation point in NMRP is shifted to a significantly higher conversion (7% in FRP vs. 60% in NMRP). In addition, the swelling index at the gelation point for the cross-linked polystyrene under FRP is much lower than the one for the cross-linked NMRP (35% vs. 54%; see Figure 9.20b), suggesting that the corresponding network for cross-linked FRP starts much tighter than the one for NMRP. However, it seems that as polymerization proceeds, the swelling index plateau at high conversions for both polymerizations emerges (see Figure 9.20b), suggesting that at high conversions, when both polymerizations are well developed, the swelling indices for both polymerization are almost similar. This behaviour can be observed more clearly in Figure 9.21, which exhibits swelling index vs. gel content for both FRP and NMRP cross-linked samples. It can be seen that when the polymerization is well developed for both systems, and at almost the same gel content, the swelling indices are identical (both systems swell 10% at around 90% gel content).

The gel content and swelling index values for cross-linking NMRP of styrene with TEMPO (determined by Tuinman et al. (2006)) are also shown in Figure 9.20 for comparison purposes (see filled circles). As can be seen, the gelation point is shifted from 60% to around 55% conversion for Tuinman et al. (2006). Apart from this difference, both gel content and swelling index behaviors are identical to our cross-linked polystyrene samples in the presence of TIPNO-based alkoxyamine.

The comparison of the molecular weight between cross-links (M_c) versus conversion for FRP and NMRP is shown in Figure 9.22. M_c was calculated following the Flory-Rehner equation, as discussed in Subsection 9.2.3.2. The M_c determined for FRP is not strongly dependent on

conversion (if one excludes the initially high values) and is smaller than the M_c determined for NMRP, showing that the network synthesized through FRP seems tighter than the one synthesized through NMRP. It is worth noticing that towards the end of the reaction, at high conversions, the M_c values for FRP and NMRP are relatively very close together.

Now that the general trends for conversion, average molecular weights and gel content are established for cross-linking NMRP of styrene, and the trajectories have been compared with the ones of homopolymerization of styrene with I-TIPNO and regular free radical polymerization of styrene and DVB as reference systems, the following subsections will document the effects of cross-linker and alkoxyamine concentrations in this system.

a)

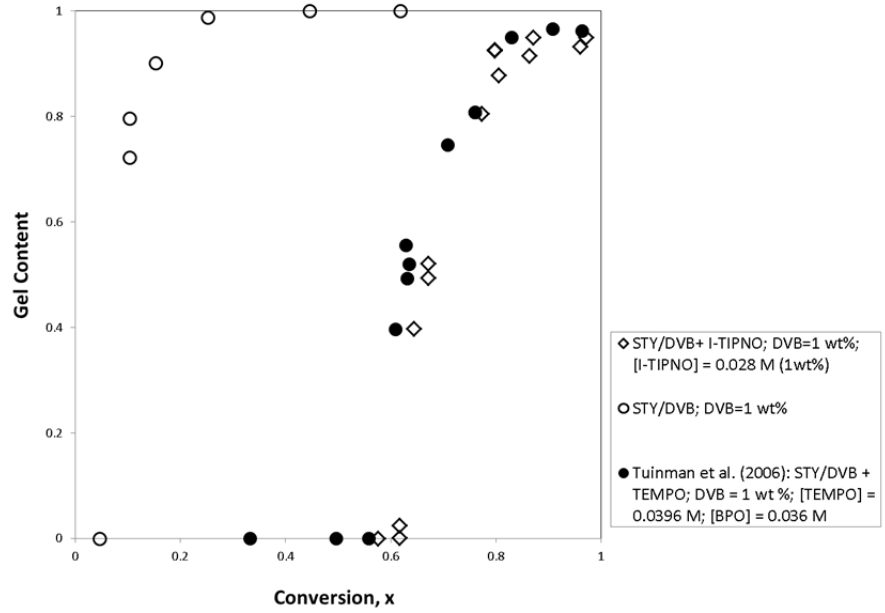

b)

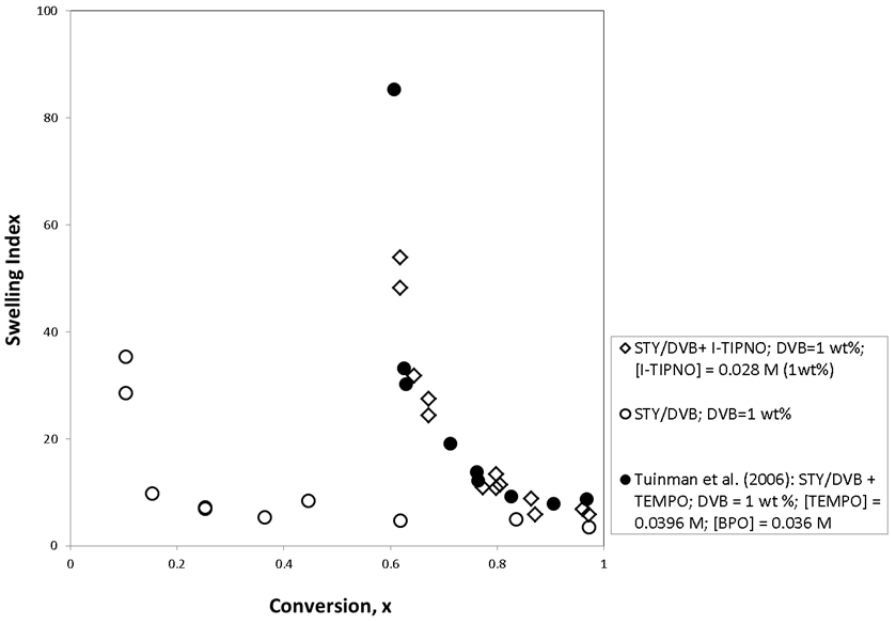

Figure 9.20 a) gel content, b) swelling index, vs. conversion for STY/DVB with [I-TIPNO] = 0.028 M (1 wt %) and [DVB] = 1 wt % at 120 °C; comparison with FRP, NMRP and STY/DVB with TEMPO

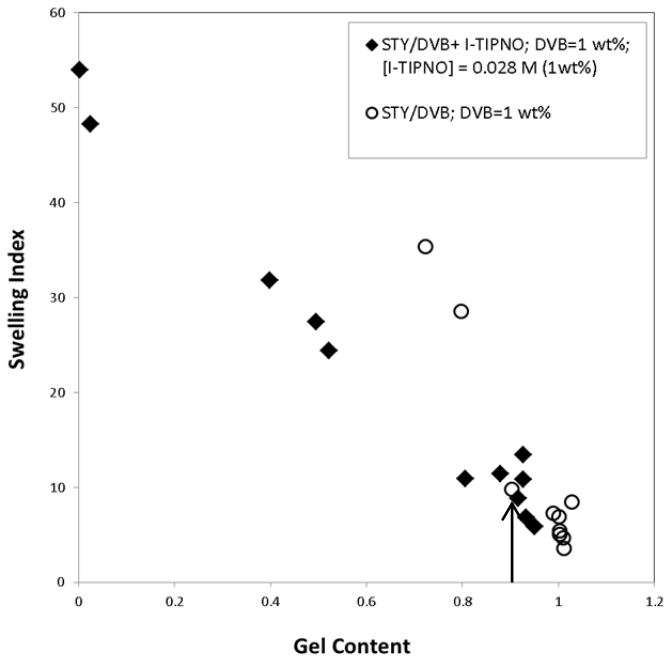

Figure 9.21 Comparison of the swelling index vs. gel content for STY/DVB network cross-linked under NMRP and FRP

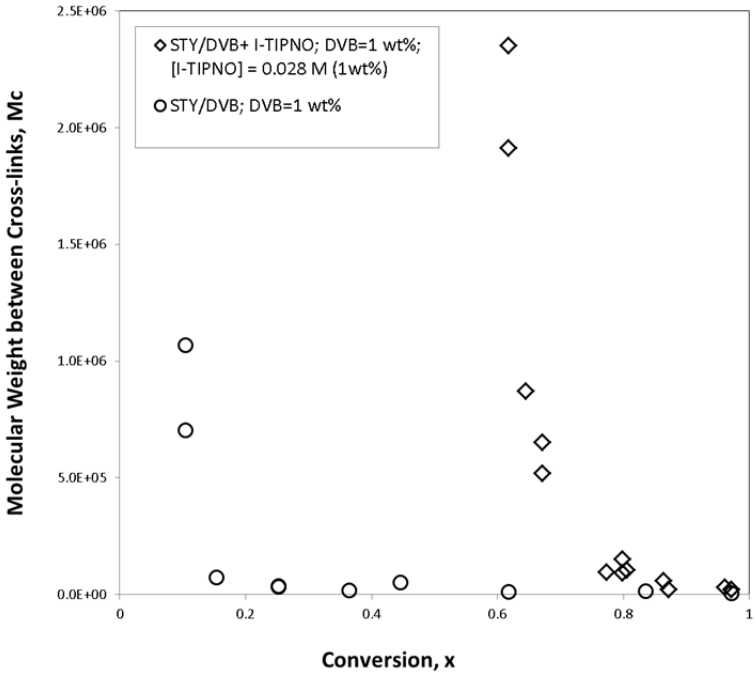

Figure 9.22 M_c vs. conversion for STY/DVB with [I-TIPNO] = 0.028 M (1 wt %) and [DVB] = 1 wt % at 120 °C; comparison with FRP and NMRP

9.4.2.2 Effect of I-TIPNO Concentration

As outlined in Table 9.2, two levels of alkoxyamine concentration were chosen for our study (see Experiments #4 to #7 in Table 9.2). Therefore, it was possible to study the effect of alkoxyamine concentration on the rate of polymerization, molecular weights and gel content. Our base case (Experiment #4) is compared with Experiment # 5, displaying the effect of [I-TIPNO] at the low level of DVB, while Experiment #6 is compared to Experiment #7, illustrating the effect of [I-TIPNO] at the high level of DVD.

Figure 9.23a shows the effect of the alkoxyamine concentration on conversion vs. time at the low level of DVB. As can be seen, the rate of polymerization was independent of the alkoxyamine concentration, as observed previously for nitroxide-mediated homopolymerization of styrene with I-TIPNO (see Figure 9.8) and other nitroxides (Fukuda et al., 1996). Although it seems that above 25 hrs, the conversions tend to be higher for the run with [I-TIPNO]= 1%, our speculation is that this discrepancy between the two runs was due to the higher level of error at high conversions (due to a very viscous, and difficult to handle polymerization mixture). Our speculations were confirmed with the runs at higher [DVB], as shown in Figure 9.23b. As can be seen, although these two runs had different levels of alkoxyamine, their rates of polymerization were almost identical.

a) b)

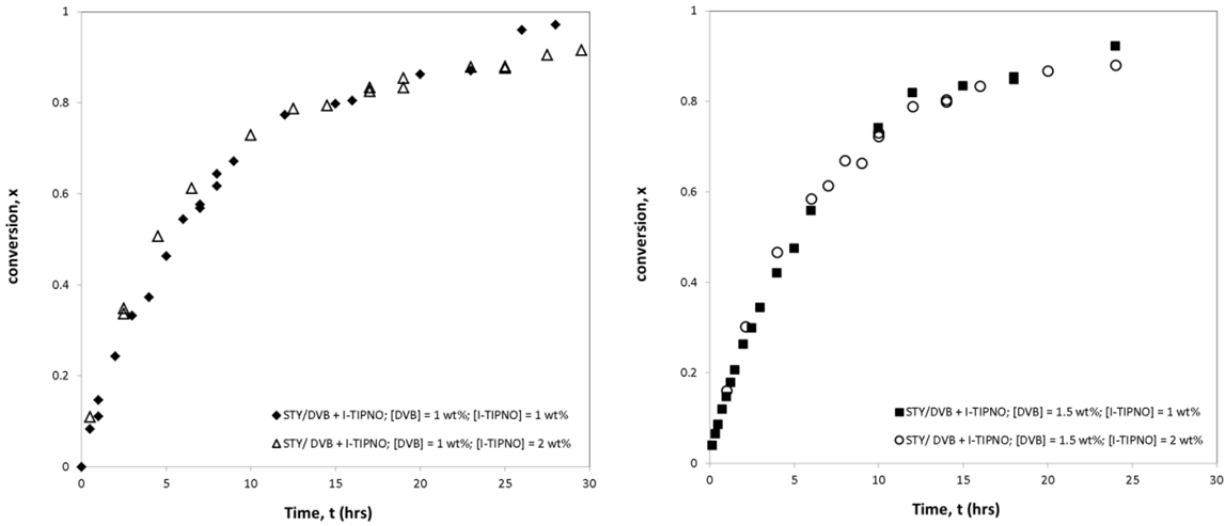

Figure 9.23 Effect of [I-TIPNO] on conversion vs. time at, a) low [DVB] and b) at high [DVB]

The corresponding molecular weight averages for low and high [DVB] are shown in Figure 9.24 and Figure 9.25, respectively. As can be seen, at both low and high [DVB], the runs with the lower alkoxyamine concentration had gelled earlier and the molecular weights at the gelation point were higher. For example, in Figure 9.24, the polymer synthesized with 1 wt % alkoxyamine gelled around 60% conversion (with M_w @ gelation point = 1,430,000 g/mol), whereas the polymer made with 2 wt% alkoxyamine gelled closer to 80% conversion (with M_w @ gelation point = 1, 216,000 g/mol).

The inserts in both figures show the trends of the molecular weights at conversions below the gelation point. It is obvious in both inserts that runs with higher I-TIPNO had lower molecular weights. This is again in agreement with our previous observations for homopolymerization of styrene with I-TIPNO (see Figure 9.10) and with a unimolecular initiator based on TEMPO (Zhou et al., 2010), and also in agreement with the theory that the molecular weights are inversely proportional to the alkoxyamine concentration in NMRP systems (see Eq. 9.11).

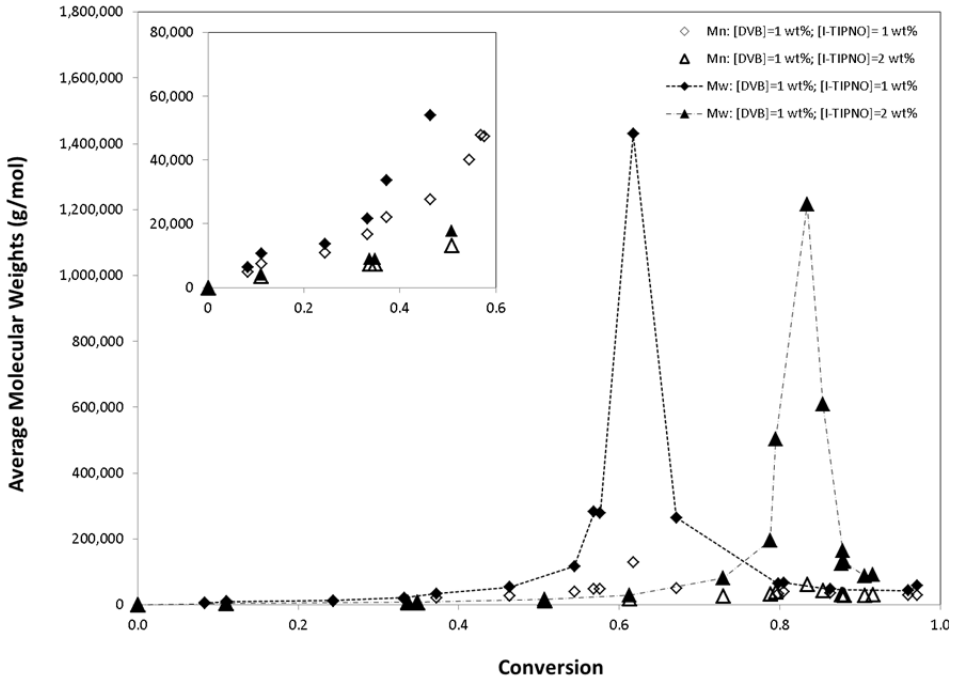

Figure 9.24 Effect of [I-TIPNO] on molecular weights at low [DVB]

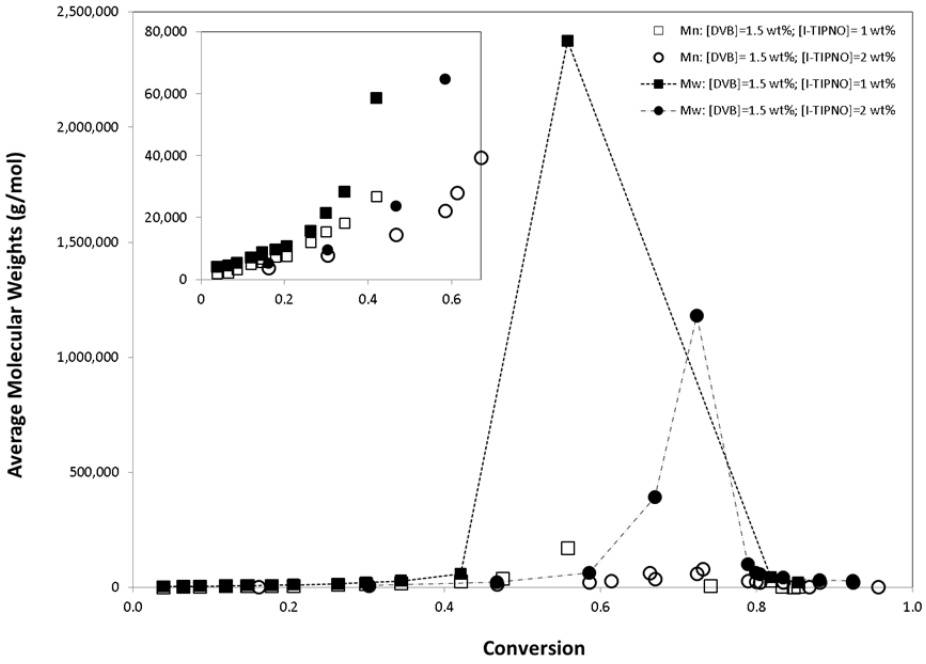

Figure 9.25 Effect of [I-TIPNO] on molecular weights at high [DVB]

The trends in gel content confirmed our experimental data for average molecular weights. As can be seen in Figure 9.26, at both low and high levels of DVB, the runs with the lower alkoxyamine concentration not only gelled earlier but also had higher gel content at the same conversion level.

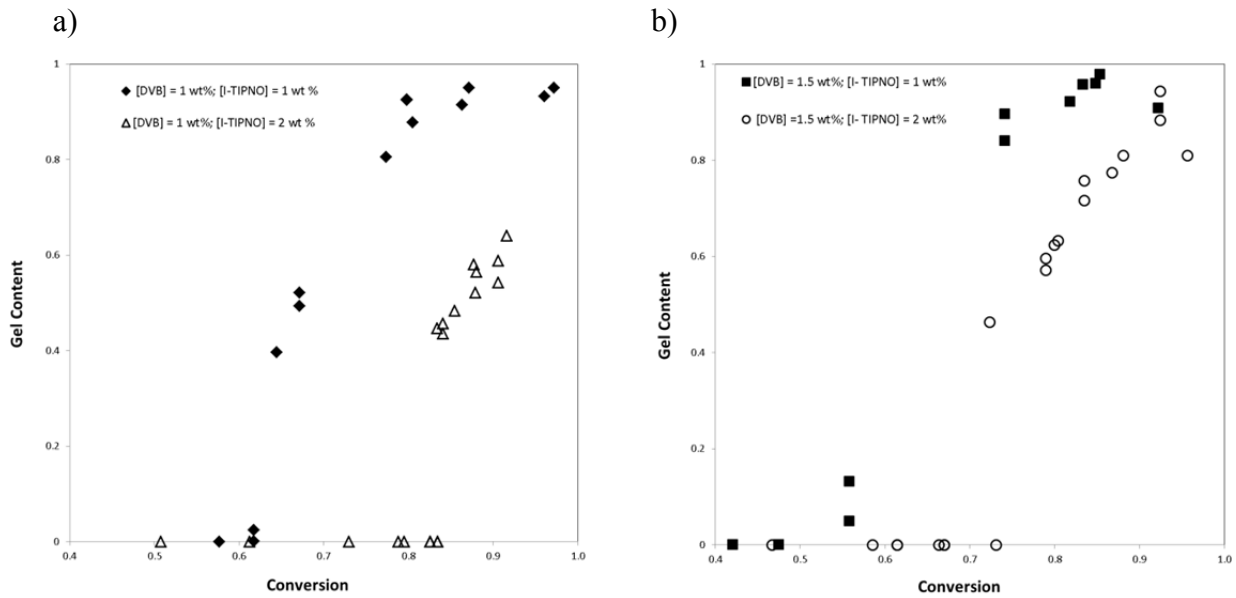

Figure 9.26 Effect of [I-TIPNO] on gel content vs. conversion at, a) low [DVB] and b) high [DVB]

9.4.2.3 Effect of DVB Concentration

The next factor studied was DVB concentration. Referring back to Table 9.2, in this subsection, Experiment # 4 (our base case) is compared with Experiment #6 (effect of [DVB] at low alkoxyamine concentration), while Experiment # 5 is compared with Experiment #7 (effect of [DVB] at high alkoxyamine concentration). According to Tuinman et al. (2006), concentration of DVB did not have any effect on the polymerization rate in cross-linking NMRP of STY/ DVB with TEMPO. This behavior was also observed for our experiments in cross-linking NMRP of STY/ DVB with the TIPNO-based alkoxyamine. As can be seen in Figure 9.27, the conversion vs. time profiles are almost identical for both low and high [DVB], at both low alkoxyamine concentration (Figure 9.27a) and high alkoxyamine concentration (Figure 9.27b).

a) b)

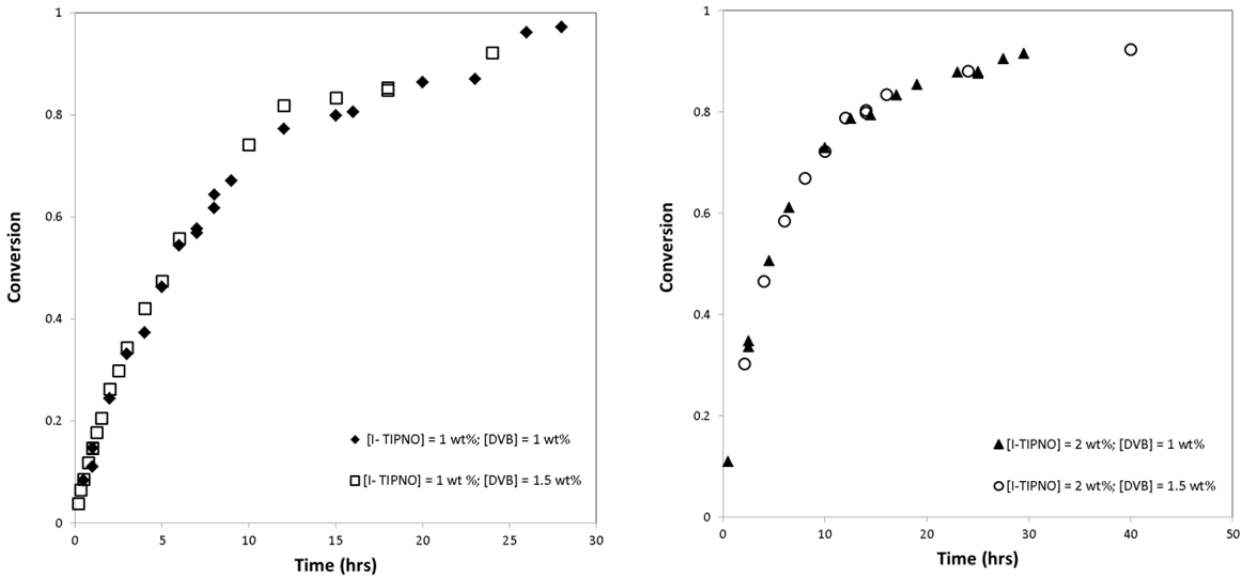

Figure 9.27 Effect of [DVB] on conversion vs. time at, a) low [I-TIPNO], b) at high [I-TIPNO]

Figure 9.28 and Figure 9.29 illustrate the corresponding comparisons for molecular weights. At both low and high levels of alkoxyamine, the run with the higher DVB concentration gelled earlier (at a lower conversion), however, the difference between the conversion levels (at the gelation point) was more significant at the higher level of alkoxyamine. That is, at [I-TIPNO] = 1 wt%, $X_{@\text{gel point (1 wt\%)}} = 0.617$ and $X_{@\text{gel point (1.5 wt\%)}} = 0.558$ (see Figure 9.28), while at [I-TIPNO] = 2 wt%, $X_{@\text{gel point (1 wt\%)}} = 0.824$ and $X_{@\text{gel point (1.5 wt\%)}} = 0.723$ (see Figure 9.29).

This is consistent with our finding from the implementation of the Bayesian design, as was observed in Figure 8.3. The inserts in both Figure 9.28 and Figure 9.29 compare the molecular weights before the gelation point. As can be seen, the effect of [DVB] on the molecular weights is more pronounced at the higher level of alkoxyamine, i.e., the difference between molecular weights is higher in Figure 9.29 compared to Figure 9.28. This observation is again in agreement with our Bayesian design study of the cross-linking system, as observed in Figure 8.5.

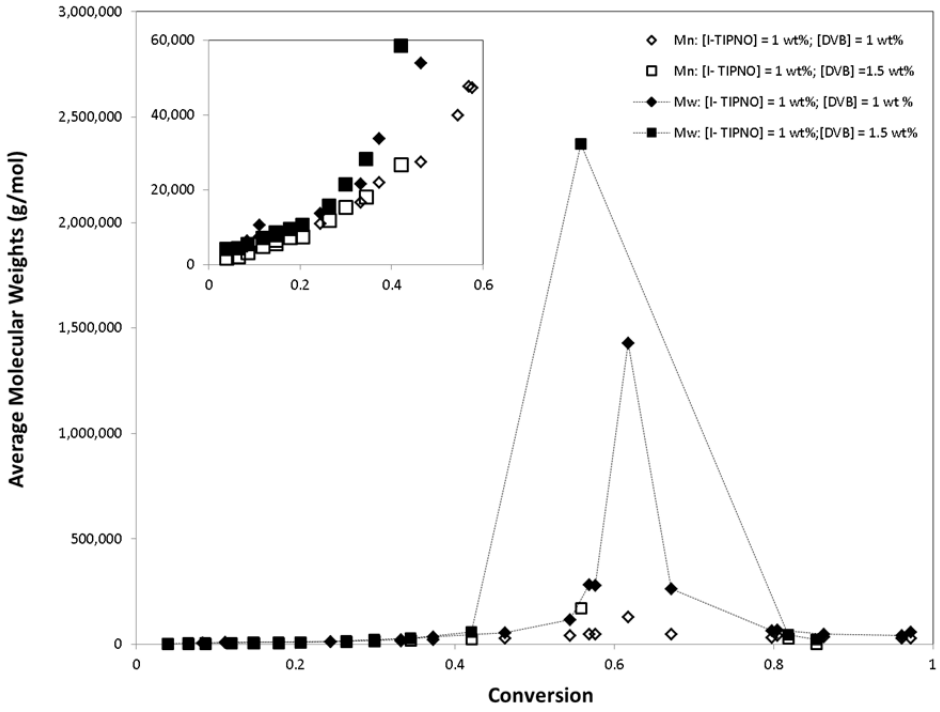

Figure 9.28 Effect of [DVB] on molecular weights at low [I-TIPNO]

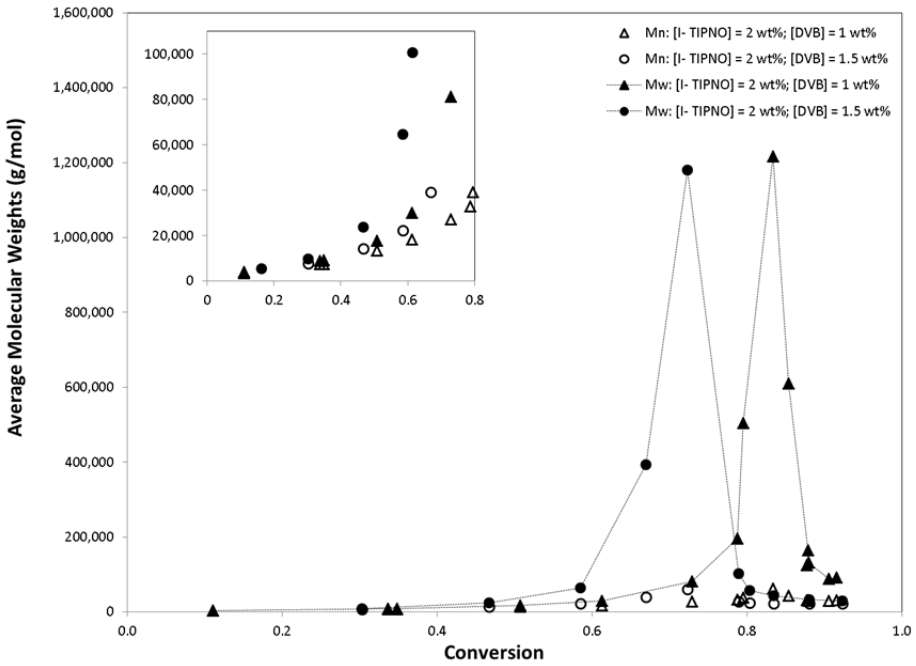

Figure 9.29 Effect of [DVB] on molecular weights at high [I-TIPNO]

The trends in gel content confirmed our experimental data for average molecular weights. As can be seen in Figure 9.30, at both low and high concentrations of alkoxyamine, the runs with the higher DVB concentration not only gelled earlier but also had higher gel content at the same conversion level. This trend is again consistent with the trend observed in our Bayesian approach for the cross-linking system, as observed in Figure 8.4.

a) b)

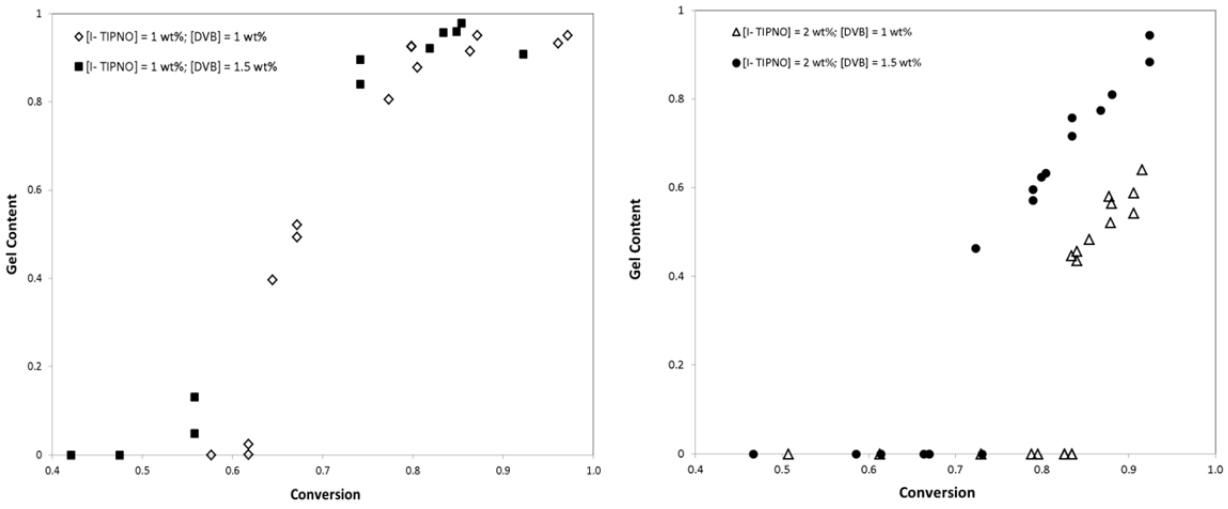

Figure 9.30 Effect of [DVB] on gel content vs. conversion at, a) low [I-TIPNO] and b) high [I-TIPNO]

9.4.2.4 Effect of [DVB]/ [I-TIPNO] Molar Ratio

Using two concentration levels for each I-TIPNO and DVB resulted in four different molar ([DVB]/ [TIPNO]) ratios. The effect of this molar ratio is investigated on conversion, molecular weights and gel analysis data. As can be observed in Figure 9.31, the [DVB]/ [I-TIPNO] molar ratio does not affect the rate of polymerization, at least at the DVB levels employed. The non-significant effect of controller concentration (I-TIPNO) was as expected and has been observed for other systems as well (Tuinman et al., 2006).

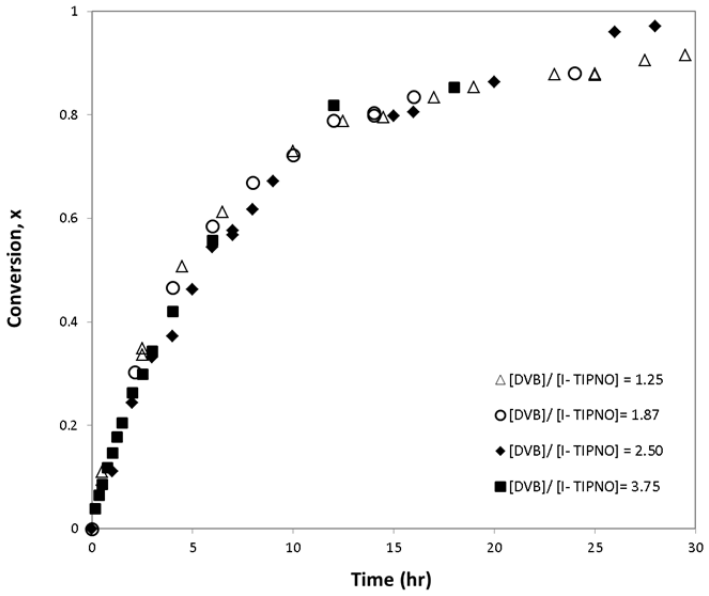

Figure 9.31 Effect of [DVB]/ [I- TIPNO] on conversion vs. time

Contrary to what was observed for rate of polymerization, the effect of [DVB]/ [I-TIPNO] was significant on average molecular weights, and polydispersity, as can be seen in Figure 9.32 and Figure 9.33, respectively. The combination of high DVB concentration and low I-TIPNO concentration (i.e., maximizing the [DVB]/ [I-TIPNO] ratio) resulted in the earliest gelation point and hence, fastest loss of 'livingness'. As the [DVB]/ [I-TIPNO] ratio decreased, the gel point was observed at higher conversion levels. For all the different ratios, before the vicinity of the gelation point, the average molecular weights increased linearly with conversion, and the polydispersity values were lower than 1.5. However, when closer to the gelation point, the "controlled" or "livingness" behavior was lost and one could observe a jump in average molecular weights and polydispersity values at the gelation point.

a)

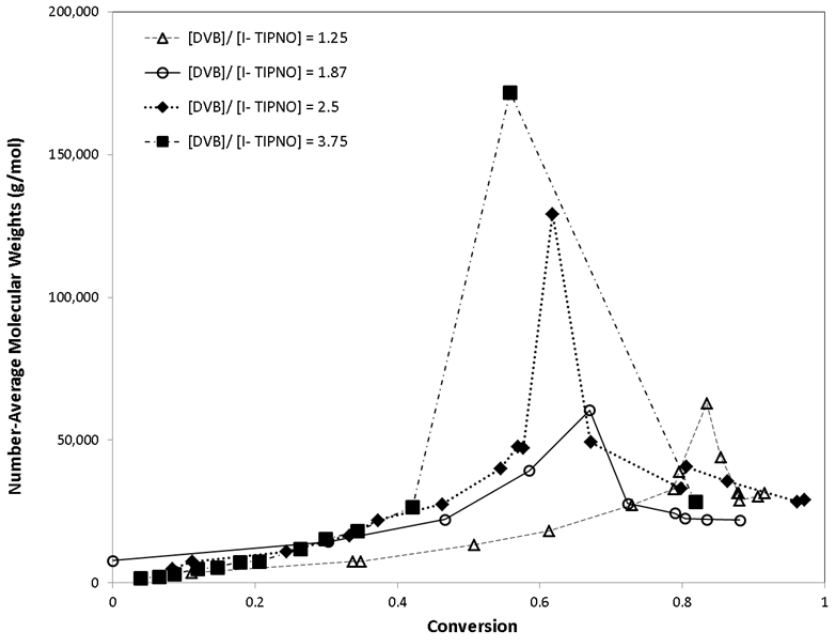

b)

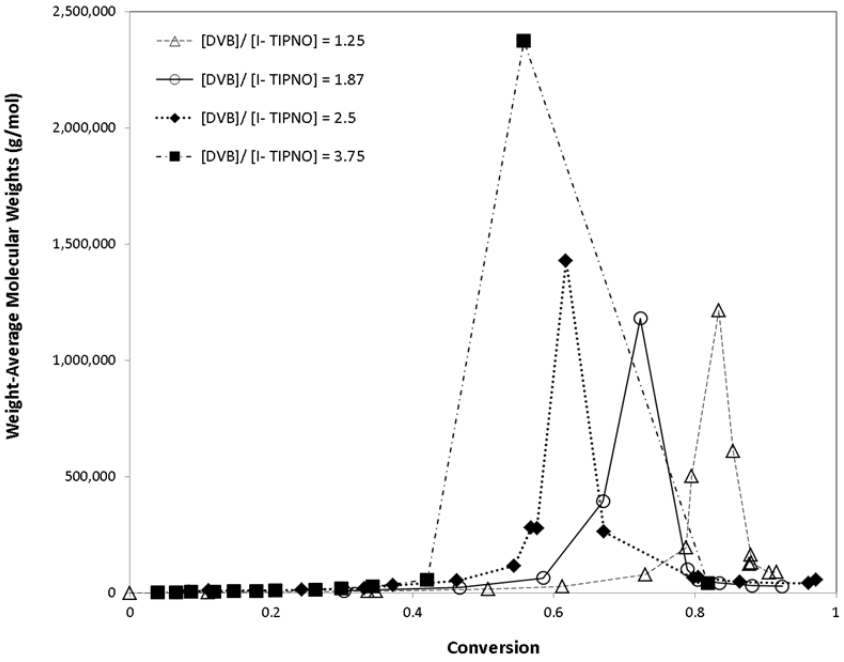

Figure 9.32 Effect of [DVB]/ [I- TIPNO] on a) number-average molecular weight, b) weight-average molecular weight, vs. conversion

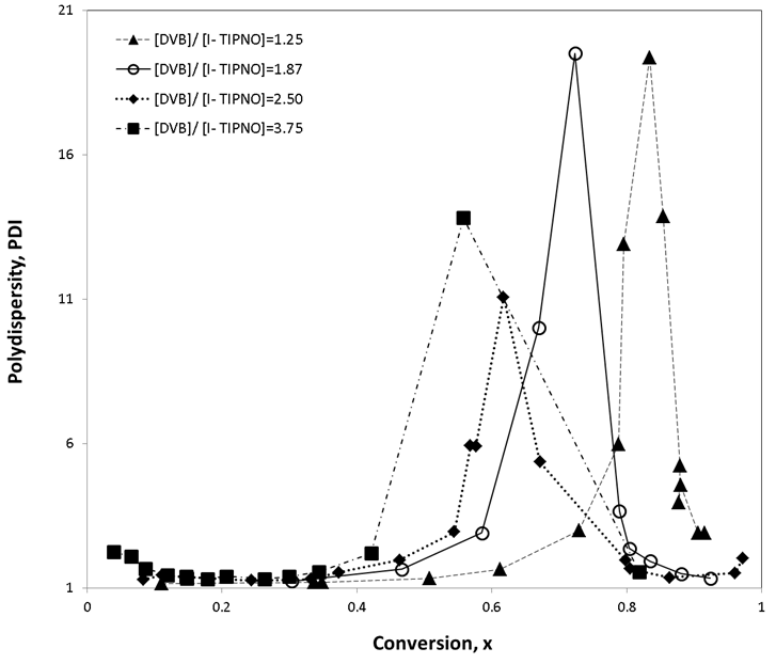

Figure 9.33 Effect of [DVB]/ [I- TIPNO] on polydispersity vs. conversion

These observations, based on the jump in average molecular weight values versus conversion data, were confirmed also through more direct steps measuring the gel content using a Soxhlet extraction setup. As can be seen in Figure 9.34a, the largest [DVB]/ [I-TIPNO] resulted in the earliest gelation point (around 56% conversion) and as this ratio decreased the gelation was delayed towards higher conversion (e.g., gelation happened around 83% conversion for [DVB]/ [I-TIPNO] = 1.25). Furthermore, our swelling index results, shown in Figure 9.34b, indicated that the lower the [DVB]/ [I-TIPNO] ratio, the 'looser' the polymer network was at higher conversions, which resulted in higher molecular weight between cross-links (M_c), as corroborated in Figure 9.35.

a)

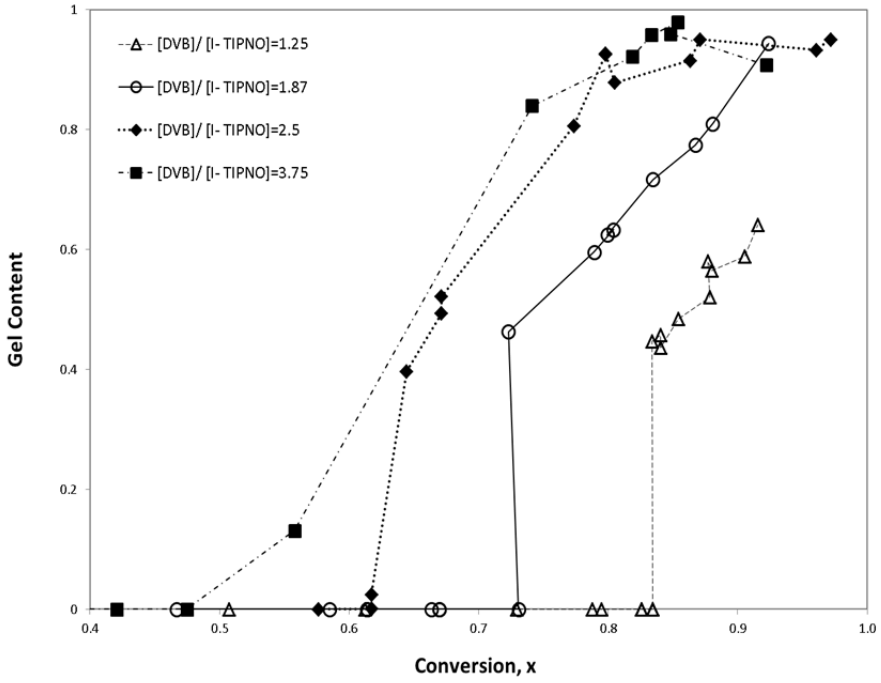

b)

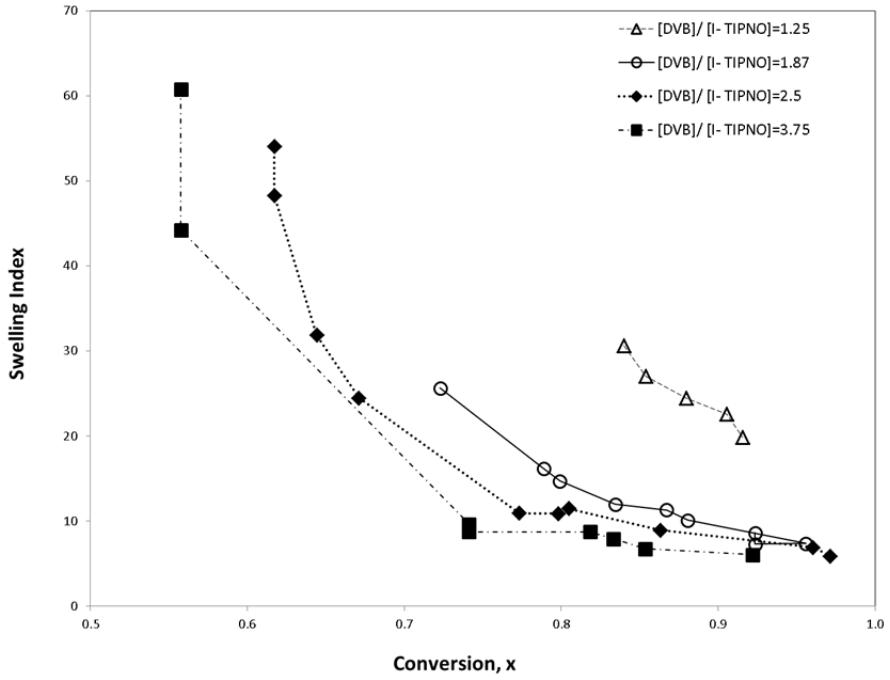

Figure 9.34 Effect of [DVB]/ [I- TIPNO] on a) gel content, b) swelling index

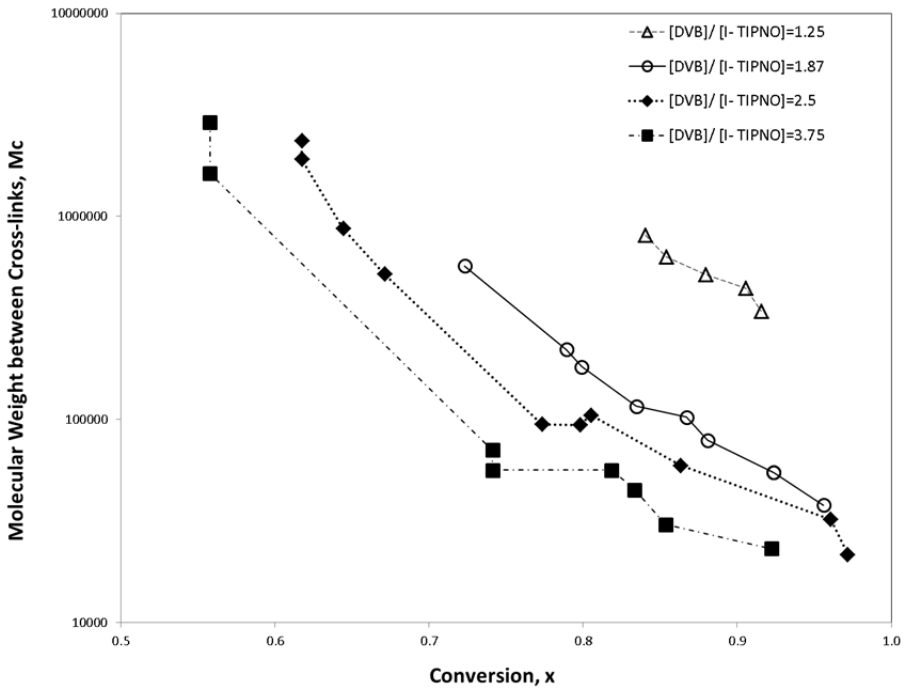

Figure 9.35 Effect of [DVB]/ [I- TIPNO] on molecular weight between cross-links vs. conversion

In Figure 9.36, the gel content, swelling index and molecular weight between cross-links (M_c) values for different [DVB]/[I-TIPNO] ratios are contrasted at 85% conversion level, as an example. As the [DVB]/ [I-TIPNO] ratio increases, the gel content at 85% conversion increases (see Figure 9.36a), while the swelling index decreases (see Figure 9.36b); this in turn indicates a tighter network and as a result a lower Mc is obtained (see Figure 9.36c).

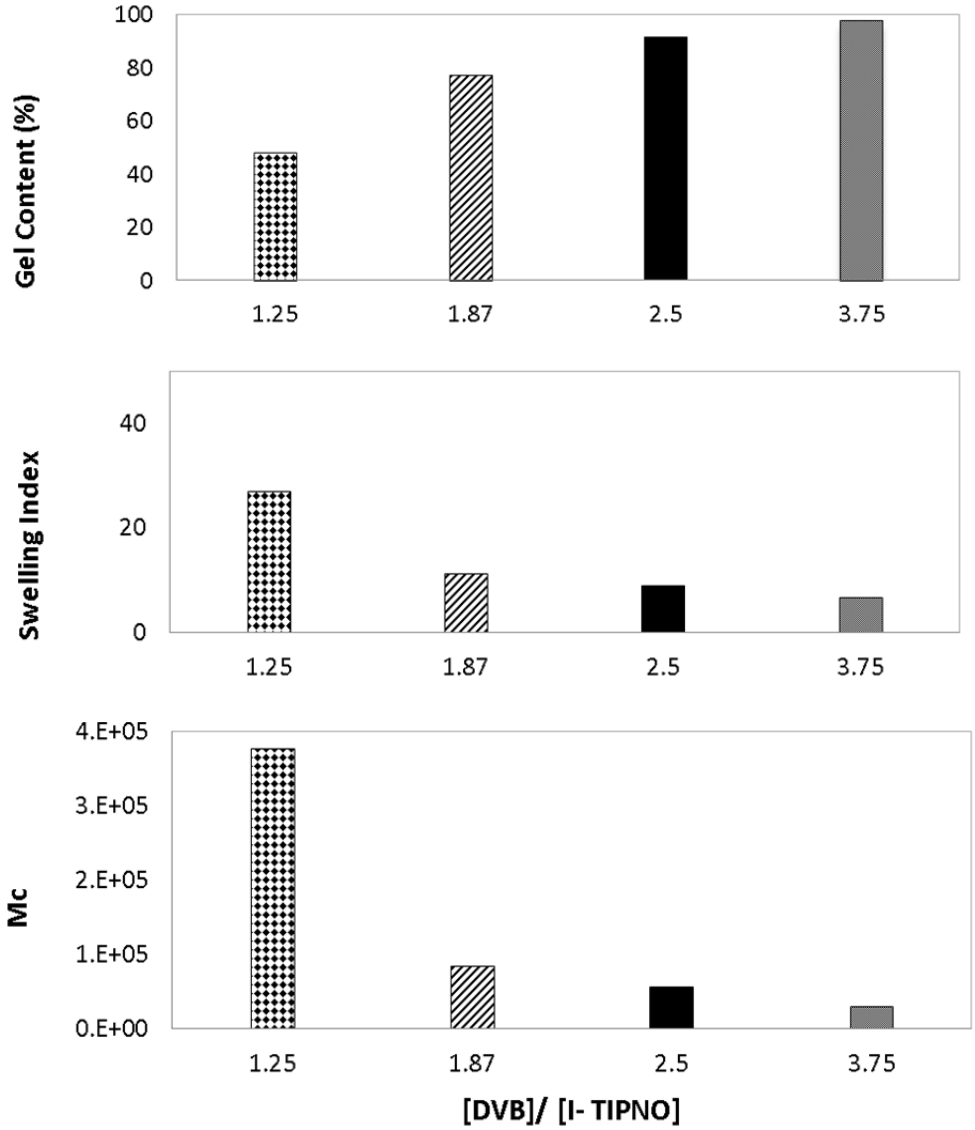

Figure 9.36 Effect of [DVB]/ [I- TIPNO] on a) gel content, b) swelling index, c) Mc, at 85% conversion

9.4.2.5 Comparison of Model Predictions versus Experimental Data

In parallel to our experimental investigations, a detailed mathematical model for the copolymerization kinetics of STY/ DVB in the presence of nitroxide-type controllers has been developed (Hernandez-Ortiz et al., 2009 and 2012). In this subsection, the predicted profiles for polymerization rate, molecular weight averages and gel content are validated with the respective experimental data for NMRP copolymerization of STY/ DVB in the presence of TIPNO-based alkoxyamine. These validations took place independently (between two different research groups in two universities in two countries), without additional parameter fitting (thus indirectly confirming the validity and generality of the developed mathematical model and accompanying database of kinetic and physical/ chemical characteristics and parameters).

Figure 9.37 shows a comparison of model predictions of conversion versus time for all the different levels of [DVB]/ [I-TIPNO]. As can be seen, the model captured the trends extremely well and there is good agreement between experimental data and model predictions. For [DVB]/ [I-TIPNO] = 2.5 and 3.75, the model seems to imperceptibly underpredict the experimental data at a couple of spots along the full trajectory, but that is certainly related to the error associated with the experimental data, as explained earlier.

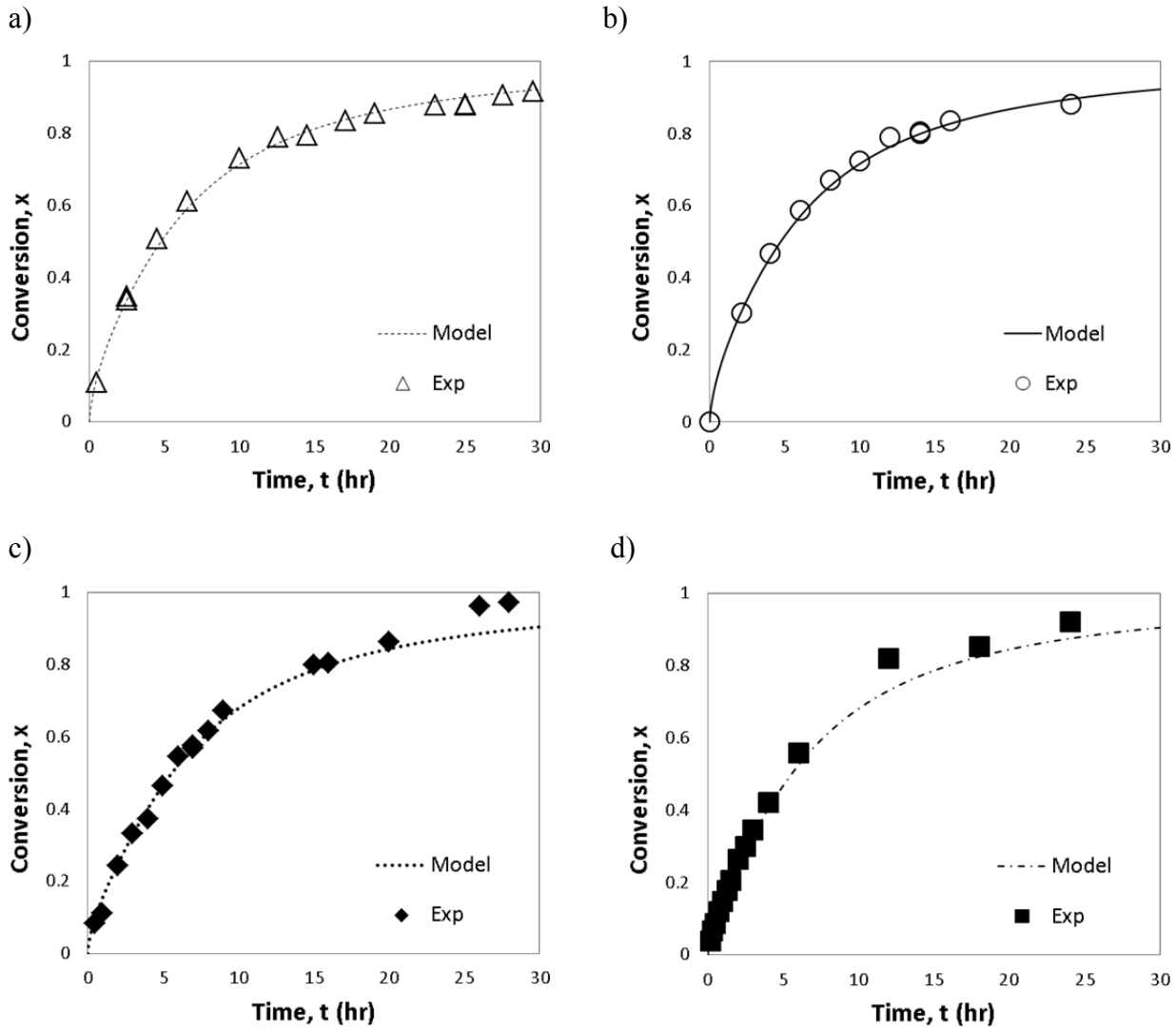

Figure 9.37 Comparison of model predictions and experimental data of conversion vs. time for a) [DVB]/ [I- TIPNO] = 1.25, b) [DVB]/ [I- TIPNO] = 1.87, c) [DVB]/ [I- TIPNO] = 2.5, d) [DVB]/ [I- TIPNO] = 3.75

The corresponding comparisons for molecular weights versus conversion are shown in Figure 9.38. The model captured well the slow and linear increase of molecular weights with conversion during the pre-gelation period up to very close to gelation point. Also, the indirect indication of the gelation point (the jump in weight-average molecular weight vs. conversion) predicted by the model was in fairly good agreement with the experimental data for all attempted conditions. After the gelation point, the values of molecular weight averages are for the sol fraction. Given that no attempt was made at fitting the data, the agreement can be deemed impressive.

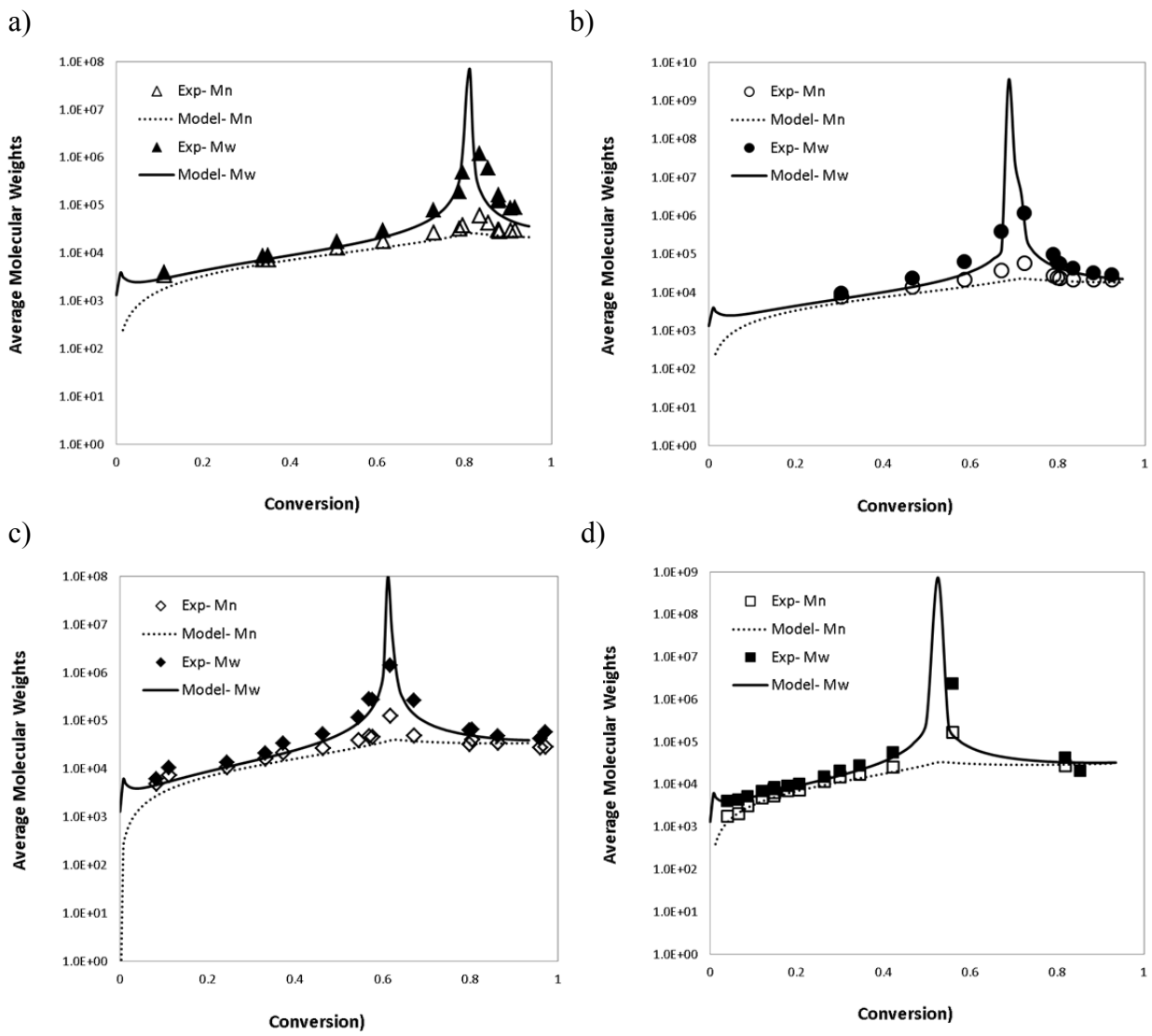

Figure 9.38 Comparison of model predictions and experimental data of molecular weights vs. conversion for a) [DVB]/ [I- TIPNO] = 1.25, b) [DVB]/ [I- TIPNO] = 1.87, c) [DVB]/ [I- TIPNO] = 2.5, d) [DVB]/ [I- TIPNO] = 3.75

Comparisons between experimental and predicted profiles of gel content versus conversion are shown in Figure 9.39. The model predicted the trajectories for the gel content well. Given that there is considerable amount of error present in the Soxhlet measurements, the agreement between experimental data and the model predictions are indeed impressive.

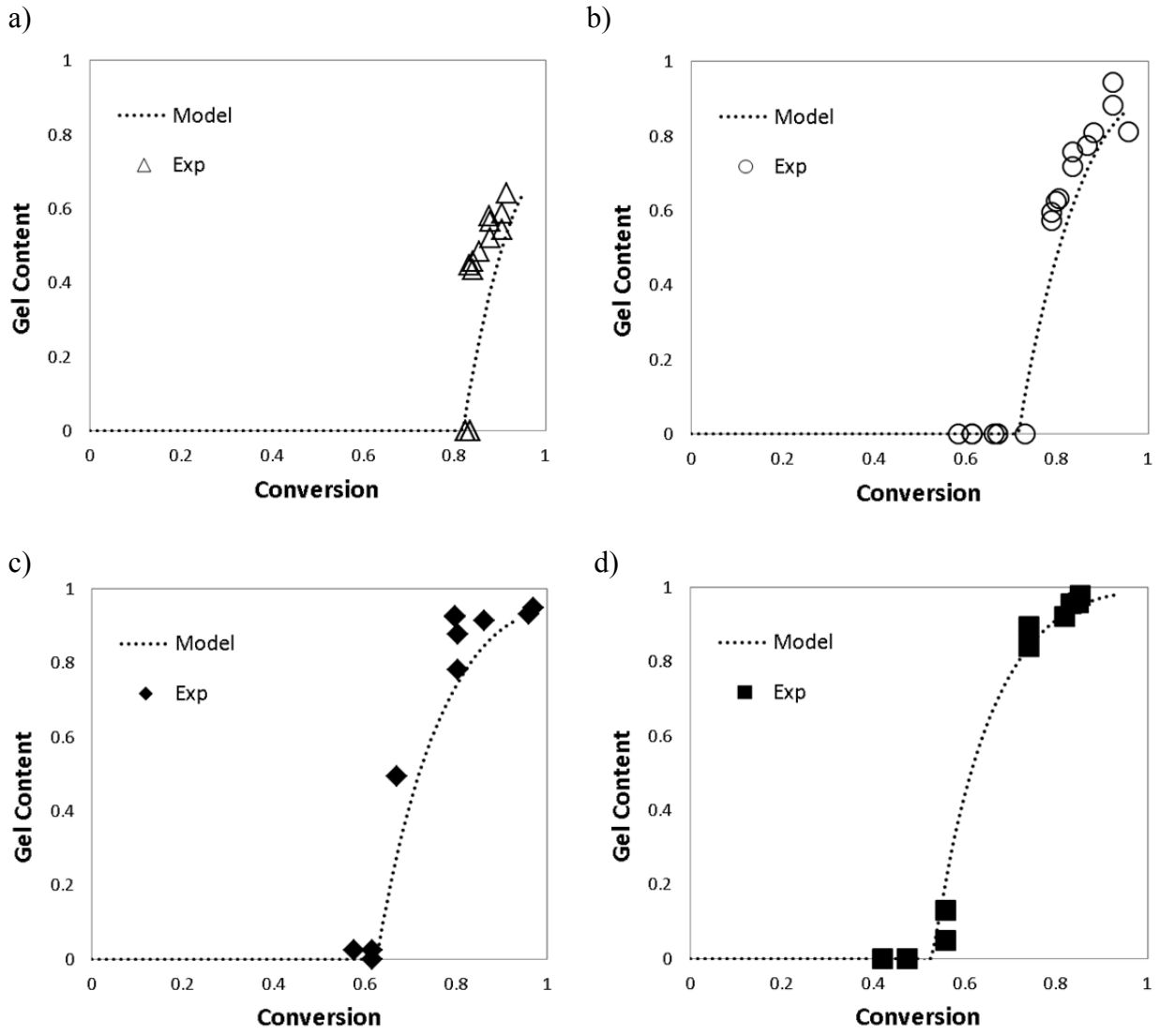

Figure 9.39 Comparison of model predictions and experimental data of gel content vs. conversion for a) [DVB]/ [I- TIPNO] = 1.25, b) [DVB]/ [I- TIPNO] = 1.87, c) [DVB]/ [I-TIPNO] = 2.5, d) [DVB]/ [I- TIPNO] = 3.75

The model is also capable of predicting the amount of the average fraction of reacted and unreacted pendant double bonds (PDB) in divinyl benzene. Figure 9.40a shows the profiles of the reacted PDB for all the different [DVB]/ [I-TIPNO] ratios. As the ratio increases, so does the amount of reacted PDB, which results in higher gel content, as was observed in Figure 9.34a. On the other hand, the profiles of unreacted PDB for different ratios do not follow the same trend (see Figure 9.40b). It can be seen that the profiles of unreacted PDB are actually only affected by DVB concentration and are almost independent of alkoxyamine concentration; this means that the profiles for [DVB]/ [I- TIPNO] = 1.25 and [DVB]/ [I-

TIPNO] = 2.5 are close together, whereas the profiles for [DVB]/ [I- TIPNO] = 1.87 and [DVB]/ [I-TIPNO] = 3.75 are almost identical (see Table 9.2 for a reminder about the levels of [DVB] and [I-TIPNO]). The initial amount of unreacted PDB at zero percent conversion is equal to $2f_{20}$ (f_{20}: the initial concentration of the cross-linker). As the initial amount of cross-linker increases, so does the amount of unreacted PDB. However, towards the end of the reaction (i.e., at high conversions), the profiles for the unreacted PDB merge and hence, the amount of unreacted PDB is the same for all runs and independent of the initial cross-linker concentration (see Figure 9.40b).

NMR spectroscopy was used to determine the experimental values for the unreacted pendant double bond fraction for some samples before the gelation point (see Subsection 9.2.3.3). Figure 9.41 illustrates the comparison between model predictions and experimental values. As can be seen, the model predictions overpredict the experimental data only slightly and this discrepancy is within the error associated with NMR measurements (observe that the $y = x + 0.005$ in Figure 9.41; i.e., assuming 0.5% error in NMR measurements). When reacted, both styrene and divinyl benzene showed identical peaks in the NMR spectrum, hence it was not possible to differentiate between the two, in order to determine the experimental values for the reacted double bonds of divinyl benzene.

a)

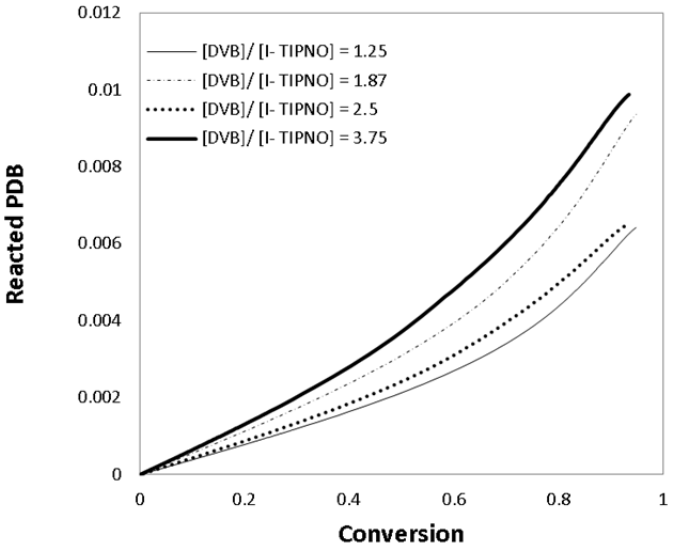

b)

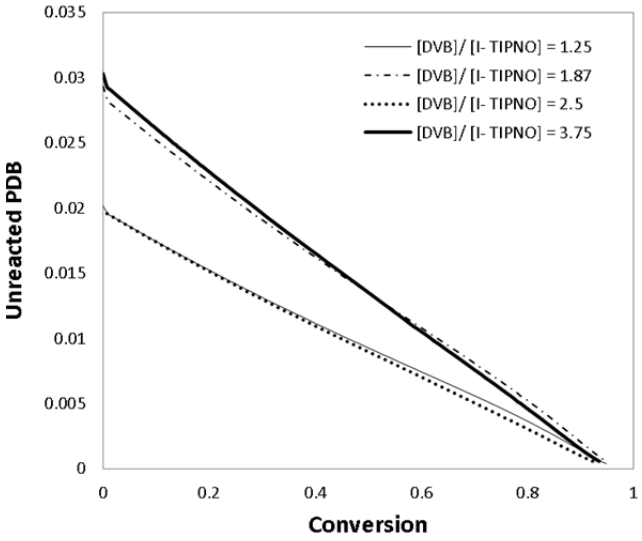

Figure 9.40 Effect of [DVB]/ [I- TIPNO] on a) reacted PDB, b) unreacted PDB, versus conversion

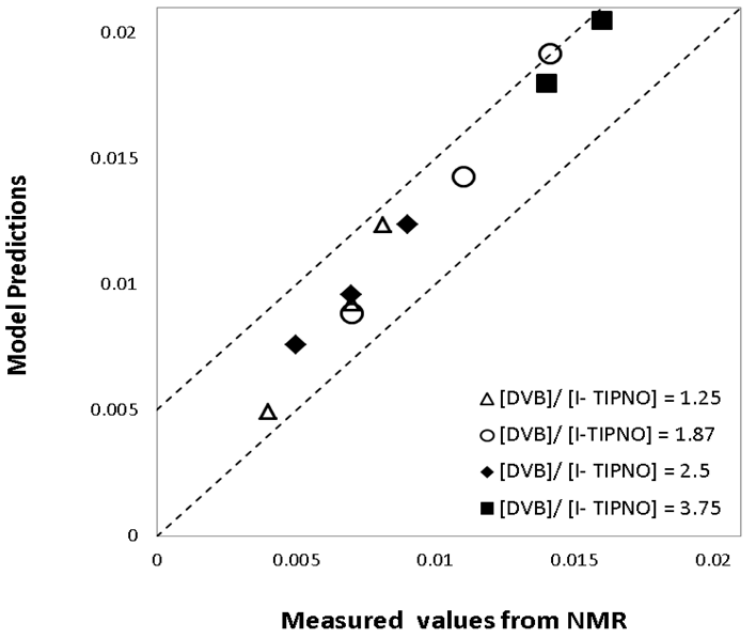

Figure 9.41 Comparison of model predictions and experimental data for unreacted double bonds (mole fraction)

9.5 Concluding Remarks

Results on the cross-linking kinetics of nitroxide-mediated radical polymerization of styrene with divinyl benzene in the presence of TIPNO-based alkoxyamine were presented in this chapter, in preparation for the identification of network homogeneity indicators based on polymer properties, which will be discussed in Chapter 10.

Results were contrasted with regular FRP of STY/DVB and homopolymerization of STY in the presence of I-TIPNO, as reference systems. Our investigations showed that the presence of I-TIPNO as a mediator in the copolymerization of STY/ DVB slowed down the rate of polymerization, delayed the onset of gelation, yielded lower average molecular weights and polydispersities, and produced a 'looser' polymer network compared to the regular free radical copolymerization of the two monomers. The copolymerization reaction exhibited controlled behaviour up to the vicinity of the gelation point (i.e., linear increase of average molecular weights with conversion, and low polydispersity values (well below typical PDI values in regular free radical polymerization). However, after the gelation point, and due to the presence of the cross-linker (DVB), the polymerization mixture became very viscous, and this led to the loss of 'livingness' of the NMRP process at higher conversion levels.

The effects of I-TIPNO concentration, DVB level and the corresponding [DVB]/ [I-TIPNO] molar ratio were investigated on polymerization rate, average molecular weights (number- and weight-average, and polydispersity), gel content, swelling index and molecular weight between cross-links. The experimental results (which were independently replicated, in order to build more confidence in the observed data from such a complex, noisy and experimentally uncertain system) showed that I-TIPNO and DVB concentrations do not affect the rate of polymerization (at least at the DVB levels employed; the non-significant effect of I-TIPNO concentration was as expected). On the other hand, their effects on average molecular weights, gel content and network morphology were noticeable. Using a higher I-TIPNO concentration, while keeping the same DVB concentration, delayed the gelation point. In contrast, using a higher DVB concentration, while keeping the same I-TIPNO concentration, accelerated the formation of gel. All in all, our studies revealed that combinations of high DVB concentration and low I-TIPNO concentration (i.e., maximizing the [DVB]/ [I-TIPNO] ratio) resulted in the earliest gelation point and hence, fastest loss of 'livingness'. As the [DVB]/ [I-TIPNO] ratio decreased, the gelation point was observed at higher conversion levels. These observations were confirmed both indirectly, based on the jump in average molecular weight values versus conversion data, and also through more direct steps measuring the gel content and swelling index using a Soxhlet extraction setup. Furthermore, our Soxhlet results indicated that the lower the [DVB]/ [I-TIPNO] ratio, the 'looser' the polymer network (observed through both swelling index and molecular weight between cross-links).

In parallel to our experimental investigations, a detailed mathematical model has been developed and validated with the respective experimental data. These validations took place independently (between two different research groups in two universities in two countries), without additional parameter fitting (thus indirectly confirming the validity and generality of the developed mathematical model and accompanying database of kinetic and physical/ chemical characteristics and parameters). Not only did model predictions follow the general experimental data trends but also were in good agreement with experimental observations. After this sound kinetic study, the results of our investigations for a more reliable and comprehensive indicator for network homogeneity will be discussed in Chapter 10.

Chapter 10. Characterizing Branched and Cross-linked Polymers Synthesized under NMRP

Characterization of branched and cross-linked polystyrene samples, synthesized via nitroxide-mediated radical polymerization (NMRP) in the presence of a small amount of divinyl benzene (DVB), is presented in this chapter. Results are compared with cross-linked polystyrene samples synthesized through regular free radical polymerization (FRP). The kinetic data of both NMRP and FRP systems have been discussed in detail in Chapter 9. Initially, a detailed review is presented on efforts in the literature to address the homogeneity of the network synthesized through CRP. Characterization of branched polystyrene samples (before the gelation point) using size exclusion chromatography (SEC) is then discussed in the results and discussion section, followed by characterization of cross-linked (X-linked) polystyrene samples with thermo-mechanical analysis, as a tool for determining the homogeneity or heterogeneity of the network. Finally, a discussion about several other potential techniques to determine homogeneity or heterogeneity of a cross-linked network is offered.

10.1 Introduction and Literature Review

The structure of a polymer network can simply be depicted as a three dimensional "mesh" formed by polymer chains interconnected by crosslink points. A homogeneous "mesh" would be obtained if a uniform distribution of functional groups took place with the absence of structural defects. The resulting cross-linked network would have little variation in the molecular weight between cross-links (M_c). However, usually the actual structure of this "mesh" is not regular and the distribution of polymer chain length between joining points is unequal throughout the whole network. So, a polymer network represents an ensemble of regions (domains) of different structures with different crosslink densities, resulting in a heterogeneous structure.

This heterogeneity in the polymer network affects properties such as swelling, elasticity, transparency and permeability. In addition, the structural heterogeneity results in a dramatic reduction in the strength of the cross-linked material. There are many applications where these

material properties are required (e.g., super absorbents, contact lenses). Hence, production of a more uniform network is desirable.

Polymer networks are often synthesized through regular free radical polymerization. However, due to rather complex reaction kinetics originating from the difference in reactivity between monomers and formation of intramolecular cross-linking (cyclization), the structures of these networks are rather heterogeneous, which results in a wide distribution of M_c in the network (Okay, 1988; Bastide et al., 1990; Elliott and Bowman, 1999; Matsumoto et al., 1999; Gundogan et al., 2004). Recently, the claim has been made that copolymerizing vinyl and divinyl monomers under controlled radical polymerization (CRP) conditions will result in a homogeneous network. The claim is based on the premise that the slow and simultaneous growth of the primary chains in CRP could potentially result in a more homogeneous distribution of the pendant vinyl compared to FRP, which in return results in favoring intermolecular crosslinking over intramolecular crosslinking (cyclization), which could then lead to the formation of a more homogenous polymer network. Since the first study of cross-linking under CRP by Ide and Fukuda et al. (1997), a lot of effort has been put into addressing the question of homogeneity of the polymer network synthesized through CRP; Table 10.1 summarizes all the work carried out so far (in the last column of Table 10.1, Q stands for "question on network homogeneity").

Table 10.1 Summary of literature work addressing the homogeneity of network synthesized through CRP

Group	Proof	Exp. Tech.	Comments	Addressed our Q?
Fukuda and co-workers (Ide and Fukuda, 1997 and 1999)	Theory	--	• Copolymerization of styrene with small amount of 4,4´-divinylbiphenyl, in the presence of an oligomeric polystyryl adduct (PS-TEMPO), at 125°C o For more details, see the second entry in Table 9.1	• No, no experimental results offered to measure the morphology of the network! • Conclusion about network homogeneity drawn only from kinetic data!
Bowman and co-workers (Kannurpatti et al., 1997 and 1998)	Exp.	DMA	• INIFERTER controlled radical polymerization used to study the mechanical properties of networks formed by dimethacrylates • DMA measurements used to glean information regarding structural heterogeneity o Distribution of relaxation times of the cross-linked polymers characterized by performing frequency scan experiments o Structural heterogeneity measured by the width of the distribution of relaxation times of the networks	• No, but informative
Peppas and co-workers (Ward and Peppas, 2000; Ward et al., 2002)	Model (2000) Exp. (2002)	DMA	• Percolation (random walk) modeling technique was applied to model INIFERTER controlled radical polymerization o Presence of INIFERTER-based initiator resulted in more primary cycles at the beginning of the reaction: more heterogeneous network! o Gelation was delayed in the case of INIFERTER polymerization, correlated to the formation of more primary cycles (more primary cycles, resulting in more microgel regions; system not growing, thus delaying the gel point) o For high cross-linking concentration, no difference between CRP and FRP detected! o Pendant double bond reactivity the same in FRP and CRP • Experimental work focused on dimethacrylates o From DMA measurements, concluded that the presence of the controller had no effect on the heterogeneity of the polymer network (the width of tan δ peaks for CRP and FRP almost identical), because the pendant double bond reactivity is not affected by the presence of the controller	• Yes, with some evidence, but no replication!

Crescenzi et al. (Crescenzi et al., 2002)	Exp.	Rheology and SEM	• Comparison of the structures of methacrylated compounds cross-linked with FRP and RAFT • Network formed via RAFT swelled to a greater extent than the one via FRP, with a more pronounced difference at lower conversion • SEM showed that the porosity of the gels could be more effectively regulated with RAFT	• No direct solid evidence! No replication!
Wang et al. (Wang and Zhu, 2005a and b)	Theory	--	• ATRP of dimethacrylates-branching • Pregel cross-link density agreed with Flory's gelation theory, and from that concluded that the network was homogeneous! • Number of branches per molecule was estimated from a molecular weight versus conversion regression	• No! No analytical technique exists to fully characterize branched or cross-linked polymers!
Norisuye and co-workers (Norisuye et al., 2005)	Exp.	Static/dynamic light scattering (SLS/DLS)	• RAFT copolymerization of STY/DVB • Different scattering intensity behavior observed for FRP and RAFT	• Evidence from light scattering analysis showed different behavior, but does that mean a more homogenous network for CRP?
Bannister et al. (Bannister et al., 2006)	Theory and modeling	--	• ATRP copolymerization of dimethacrylates -branching • Analysis of the branching statistics suggested that the network formation is almost perfectly fitted by the classic Flory-Stockmayer model for gelation!	• No! Leap from kinetics to morphology
Zetturlund and co-workers (Zetterlund et al., 2005; Alam et al., 2006; Saka et al., 2007; Tanaka et al., 2007; Zetterlund et al., 2009a and b)	Theory and Exp.	SEM and Micro-compression testing	• STY/DVB with PS-TEMPO initiator at T = 125 °C in miniemulsion o Comparison of the experimental gel points with the theoretical prediction based on FS gelation theory for bulk/solution and miniemulsion o X-linked polymer particles prepared by NMRP exhibit different mechanical properties than X-linked particles prepared by FRP at low to intermediate conversion o Compressive strength, deformation at break and breaking energy remain approximately constant from low to high conversion in FRP; while in NMRP these quantities increase linearly with conversion	• Yes, but in miniemulsion (not applicable to our case)

Zhu and co-workers ATRP: (Yu et al., 2007 and 2009); RAFT: (Yu et al., 2008)	Exp.	DMA	• ATRP and RAFT of dimethacrylates o Kinetic evolution followed by DSC o Structural evolution followed by DMA o Comparison of DMA results for CRP and FRP showed that samples from FRP produced narrower peak width of the tan δ curve, suggesting a more homogeneous network o Gelation process followed by both rheological measurements and solvent extraction o Micro-gelation occurred much earlier than macro-gelation in FRP, however, for ATRP their occurrence overlapped	Yes, with evidence, however no replicates! It is not indicated if the comparison is at the same conversion level or at the same X-link densityt!
Matyjaszewski and co-workers (Gao et al., 2007, 2008a ,b and 2009; Gao and Matyjaszewski, 2009; Li et al., 2009; Van Camp et al. 2010)	Theory and Modeling	--	• ATRP of different acrylate monomers and diacrylate cross-linkers • Studied the kinetics of the reaction o Including the effects of initial molar ratio of cross-linker to initiator, the concentration of reagents, the relative reactivity of cross-linker compared to monomer, the initiator efficiency, and polydispersity of the primary chains on gelation o An example of a group that still uses OFAT to study the effect of different factors! • Predici and Monte Carlo simulations to model the kinetics of the reaction o Experimental gel points were approximately equal to gel points predicted by simulator	No! Leap from kinetic data to structural homogeneity!

Our extensive literature review shows that the methods that have been used so far for analysis of network structure in CRP (and in FRP, in general) can be subdivided into different categories:

1. *Analysis of chemical conversion:* Several techniques such as spectroscopy (UV, IR, FTIR, and NMR) or wet chemistry (titration, such as bromination) have been used to monitor the amount of reacted and unreacted pendant double bonds. However, no exact quantitative information on the network structure can be obtained from these techniques, since reacted groups can form not only chemical cross-links but also cycles and loops. Furthermore, side reactions, which can easily cause additional cross-links, complicate data interpretation due to overlapping of signals from different types of chemical groups in complex mixtures (Litvinov and Dias, 2001). Ironically, the first group that has made claims about homogeneity of networks in CRP had used UV spectroscopy to make their claims (Fukuda et al, 1997).

2. *Flory-Stockmayer theory:* In this approach, the theoretical conversion at the gelation point, calculated through Flory-Stockmayer theory (x_g theo.), is compared to the experimental or actual one (x_g act.). If the actual conversion at the gelation point is only one to two orders of magnitudes larger than the theoretical one (x_g act./ x_g theo.~ 1-2), then the conclusion is drawn that the network formed follows the Flory-Stockmayer theory, which has been developed for an ideal network, hence the network should be homogeneous. However, Flory- Stockmayer theory is developed for an "ideal network" in which no defects are present and the network should obey some simplified assumptions (equal reactivity of double bonds, no intramolecular cross-linking and independent reaction of all groups). There is a considerable debate about the validity and applicability of this theory to networks synthesized through CRP, as one cannot guarantee that CRP could fall under the simplified assumptions made for an "ideal network"! Oddly, the majority of work on network homogeneity in CRP has concentrated on this approach (see again Table 10.1).

3. *Characterization of physical properties:* In this category, some common methods like equilibrium swelling and mechanical measurements (stress-strain or elastic modulus) have been used to draw conclusions about the network structure. Although these methods

provide valuable information (such as modulus, stress-strain behavior, and glass transition temperature) that is desirable for practical applications, they are based on rubber elasticity theory, which is related to an average cross-link density and not the distribution of cross-links in the network (Litvinov and Dias, 2001).

4. *Analysis of molecular mobility of polymer chains:* Dynamic mechanical analysis (DMA) is among the techniques under this category which has been used by several groups to make inferences regarding the structural heterogeneity of polymer networks formed. This method provides information about the mobility of polymer chains and since chain motion is strongly coupled to the length of network chains, information on network structure and network homogeneity could be potentially obtained in this way.

   It has been observed that in highly cross-linked networks, the transition (T_g) does not take place at a unique temperature and occurs over a wide range of temperatures. This broad distribution of relaxation times was related to the heterogeneous structure of the corresponding networks, as they contained very highly cross-linked regions (i.e., microgels) as well as less densely cross-linked regions connecting the microgels. The distribution of relaxation times in the various microregions of the polymers is reflected in the mechanical behaviour of these cross-linked materials and has been used in the past by several researchers as a measure of the structural heterogeneity (Kannurpatti et al., 1997). Qualitatively, this structural heterogeneity was observed by measuring the peak width of tan δ curves. The broader the distribution, the more heterogeneous the network is.

   A couple of groups have tried using DMA for determining the homogeneity of a network in CRP; however, contradictory results have been reported. With one group, reporting on a more homogeneous network in CRP (see the entry for Zhu and co-workers in Table 10.1), while others either found that the presence of the controller had no effect on the heterogeneity of the polymer network (see the entry for Peppas and co-workers in Table 10.1) or concluded that the results were difficult to interpret (see the Kannurpatte and co-workers entry in Table 10.1).

5. *Scattering techniques*: Since the gel heterogeneity is closely connected to spatial concentration fluctuations, scattering methods such as static or dynamic light scattering could potentially be used to investigate this spatial "inhomogeneity" (Norisuye et al., 2003). The gel "inhomogeneity" can be manifested by comparing the scattering intensities from the gel and from a semi-dilute solution of the same polymer at the same concentration. The scattering intensity from the gel is always larger than that from the polymer solution. The excess scattering over the scattering from the polymer solution is related to the degree of "inhomogeneity" in the gels.

   Norisuye et al. (2005) had been the only group so far that investigated the potential of using light scattering techniques for comparing networks in CRP and FRP. They have used different curve fitting techniques to come up with model functions to describe the data collected from the light scattering measurements. Although differences have been observed between components of the total scattering intensity for CRP and FRP, the connection between these observations and the network morphology is not clearly stated. Hence, the jury is still out with respect to further investigating whether the scattering techniques could in fact be useful techniques in providing information about the morphology or structure of the network.

Most of the approaches that have been used so far for characterizing networks synthesized through CRP (i.e., see comments 1 to 3 above) are in fact indirect macro-indicators that give some idea about the degree and kinetics of cross-linking and no information about the morphology of the network. Researchers have used these indicators to make claims about network homogeneity (see the literature review in Table 10.1). However, this jump from, essentially, kinetic data and gel average characteristics is based on very speculative arguments. Although other more practical techniques such as DMA and scattering techniques have been attempted to give an answer to the question of homogeneity of the network in CRP, these efforts are rather incomprehensive and highly unreliable because of lack of reproducibility (see comments 4 and 5 above).

In addition, most of the researchers agreed that no matter what behavior they were following (mechanical analysis (Kannurpatti et al., 1997; Tanaka et al., 2007) or light scattering

(Norisuye et al., 2005) or swelling behavior (Ide and Fukuda, 1999)), the behaviors observed for FRP and CRP were actually similar towards the end of the reaction! Of course, since the gelation is delayed in CRP, it would be expected that less gel is developed at the earlier stages of the reaction compared to FRP, hence, could it be that the different behavior observed for the two systems was caused by different levels of cross-link density?

These observations motivated us to look for a more formal, direct, and reliable way (if such a way exists) of characterizing the cross-linked polymer network. We knew that in order to make inferences about the structure or morphology of a polymer network and clarify many existing conflicting statements encountered in the literature, the ultimate target is the cross-link density distribution, albeit a very difficult distribution to obtain. Looking for such techniques in the more general network and cross-linked literature (e.g., cross-linking in rubber, or hydrogels) we found a couple of techniques that could possibly give indirect information about the cross-link density distribution. Among those techniques we managed to conduct thermo-mechanical analysis. Results from this investigation are presented below. Other potential techniques that might give information about the cross-link density distribution are also presented towards the end of this chapter.

Before the discussion about the characterization of cross-linked polystyrene, one subsection is dedicated to the characterization of branched polystyrene samples using SEC. During the early stages of copolymerization of STY and DVB, branched primary macromolecules are formed at the DVB repeat units. The branched polystyrene samples synthesized through NMRP are compared to the ones synthesized through FRP.

10.2 Background and Experimental Methods

10.2.1 Branching Detection with SEC

Branched polymers are macromolecules containing three or more long chains that are attached together. Branched polymers lie between linear polymers and cross-linked polymers. Branching can result from the synthesis method or from post-synthesis modification of the polymer. Polymers may have a wide variety of branching structures depending on how they have been made or modified. Figure 10.1 shows different types of branching.

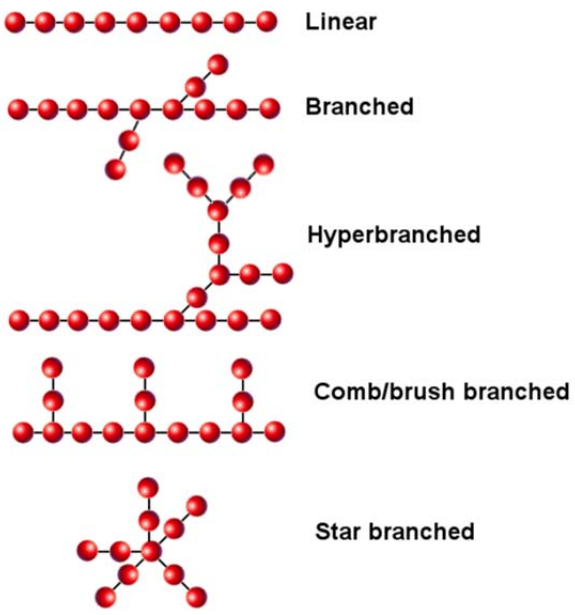

Figure 10.1 Various polymer molecule architectures

Occurrence of branching (even in small amounts) can influence polymer properties considerably. Long-chain branching (LCB) can influence both dilute solution and melt properties. A comprehensive literature survey and a good review of different techniques to detect long chain branching is provided by Scorah et al. (2007). In this work, our focus will be solely on the effect of branching on polymer solution properties and whenever referring to branching we mean long chain branching (LCB).

Studies have shown that a branched chain is more compact compared to a linear chain with the same number of units. As a result, branching decreases the size of a polymer chain in a dilute

solution (see Figure 10.2). If we can measure the density or size of a branched molecule and compare it to a linear molecule of similar chemistry, we might be able to get information on the nature of the branching. Various contraction factors can be used to quantify the reduction of molecule's size because of branching.

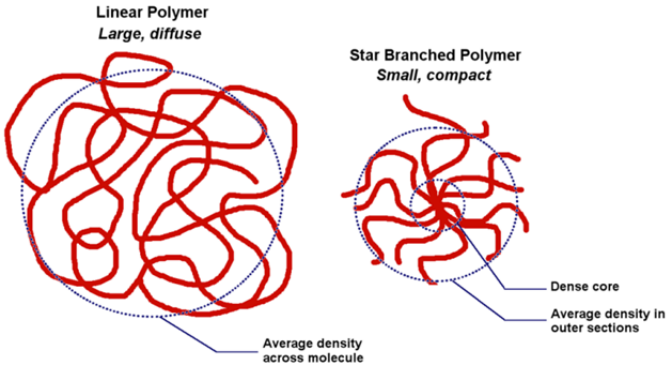

Figure 10.2 Schematic diagram illustrating difference in size for a branched and linear molecule

One way to represent the size of a polymer chain is radius of gyration which is simply the square root of the mean-square radius:

$$R_g = \langle S^2 \rangle^{1/2} \qquad \text{Eq. 10.1}$$

where the mean-square radius is given by Eq. 10.2:

$$\langle S^2 \rangle = \langle \sum_{i=1}^{N} \frac{r_i^2}{N} \rangle \qquad \text{Eq. 10.2}$$

The polymer molecule is considered to be comprised of N small elements of identical mass and r_i is the distance of the i^{th} unit from the polymer molecule's center of gravity. To assess the decrease in size due to branching, the radius of gyration of a branched polymer is compared to the radius of gyration for a linear analog at the same molecular weight:

$$g = \left. \frac{\langle S^2 \rangle_{br}}{\langle S^2 \rangle_l} \right|_M = \left. \frac{R_{g\,br}^2}{R_{g\,l}^2} \right|_M \qquad \text{Eq. 10.3}$$

g is called branching or contraction factor. The subscript *M* indicates that both branched (*br*) and linear (*l*) chains have the same molecular weight. Since branched polymers are more compact than linear polymers, g will always be less than unity, with smaller values indicating a higher degree of branching.

R_g and eventually g can be obtained experimentally using multi-angle laser light scattering (MALLS), where the particle size can be determined by measuring the angular dependence of the intensity of the scattered radiation between polymer particles and the probing radiation. Light scattering experiments provide a z-average estimate of the radius of gyration ($R_{g(z)}$). For samples with a narrow molecular weight distribution, this does not pose a problem as R_g= $R_{g(z)}$. However, when the sample is polydisperse, $R_{g(z)}$ will increase and is no longer equivalent to R_g. In this situation, the influence of branching can be completely masked by a large polydispersity. Hence, some fractionation method must be used in order to obtain monodisperse fractions. Coupling a light scattering device with gel permeation chromatography (GPC) is a method to overcome this problem. GPC will fractionate the polymer sample, therefore, the light scattering detector cell contains monodisperse fractions at any particular time and a distribution of the radius of gyration as a function of molecular weight can be obtained.

Another indicator of the size of a polymer molecule in solution is hydrodynamic volume. Hydrodynamic volume is a volume of a hypothetical impenetrable sphere that would display the same properties as the polymer coil (Painter and Coleman, 2009). Hydrodynamic volume depends upon the nature of the polymer-solvent pair, chain architecture and temperature. A branched polymer with the same number of segments as a linear sample occupies a smaller hydrodynamic volume, at the same temperature and solvent. Hydrodynamic volume, V_h, is related to the intrinsic viscosity of a dilute solution:

$$[\eta] = 2.5\, V_h \left[\frac{A}{M}\right] \qquad \text{Eq. 10.4}$$

where *A* is Avogadro's number and *M* is the molecular weight of the polymer. Hence, intrinsic viscosity is a property also influenced by branching and based on Eq. 10.4, presence of branching leads to smaller intrinsic viscosity values.

By measuring the solution viscosity as a function of polymer concentration, the intrinsic viscosity can be calculated using a viscometer, which leads to useful information about the polymer's molecular properties:

$$[\eta] = \lim_{c \to 0} \frac{1}{c} \left(\frac{\eta}{\eta_0} - 1 \right) \qquad \text{Eq. 10.5}$$

c is the concentration of polymer in solution, η the solution viscosity and η_0 the viscosity of the pure solvent. A branching or contraction factor can also be defined using intrinsic viscosity, in a way analogous to Eq. 10.3:

$$g' = \left. \frac{[\eta]_{br}}{[\eta]_l} \right|_M \qquad \text{Eq. 10.6}$$

Since intrinsic viscosity is easier to measure compared to radius of gyration, considerably more experimental work can be found that has reported intrinsic viscosity for branched molecules. Thus, it is desirable to relate the two contraction factors. Simple theoretical relationships between g and g' have not been developed and the analysis has been based on empirical equations, the most common one being:

$$g' = g^{\varepsilon} \qquad \text{Eq. 10.7}$$

where ε is the so-called structure factor, which typically varies in the range of 0.5 for low branching to 1.5 for high branching, with 0.75 for medium branching. In general, the value of the structure factor is affected by experimental conditions and the type of branching. In styrene/divinylbenzene copolymers, ε has been observed to be 0.65 for low conversion and 1.41 at high conversion (Ambler & McIntyre, 1977).

Long chain branching can be detected using different characterization techniques. Most common ones are: spectroscopic methods like nuclear resonance spectroscopy (NMR), chromatographic methods like gel permeation chromatography (GPC) and rheological methods like zero-shear viscosity. The method we focused on in this work is branch detection using GPC.

GPC separates polymer molecules based on their hydrodynamic volume, which is found to be proportional to the product of intrinsic viscosity and molecular weight (see Eq. 10.4):

$$V_h \propto [\eta]\, M \qquad \text{Eq. 10.8}$$

This relationship has become the basis for molecular weight determination in GPC. Detection of branching using GPC depends on the type of detectors available and the type of information collected. For linear and branched polymer molecules with the same molecular weight, it is known that the branched molecule has a smaller intrinsic viscosity, so will elute later than the linear molecule with the same molecular weight. As a result, using GPC with only a concentration detector will underestimate the molecular weight of branched polymers. In order to use GPC for branch detection, another detector is needed in addition to a concentration detector.

GPC with a MALLS detector can be used to determine the radius of gyration as a function of molecular weight. Radius of gyration can be related to molecular weight by the following equation:

$$R_g = K_{R_g} M^{\upsilon} \qquad \text{Eq. 10.9}$$

where K_{R_g} and υ are constants which are affected not only by the experimental conditions (solvent, temperature) but also by the polymer structure. For randomly branched polymers υ has been found to be close to 0.5 and in some cases much lower. In plots of R_g- M, presence of branching is detected by a decrease in slope compared to a linear sample (see Figure 10.3). Using a MALLS detector allows for the determination of g directly and calculation of branching parameters such as branching number and frequency using an appropriate Zimm-Stockmayer expression. The Zimm-Stockmayer equations are a series of expressions that depend on polymer shape (e.g., star, comb, etc.), polydispersity, and number of the arms per branching point. These expressions relate branching number to the contraction factor g. Scorah et al. (2007) illustrated a detailed table summarizing all the theoretical equations for calculating the contraction factor for various types of branched polymers. For instance, STY/ DVB branched polymer is a randomly branched, monodisperse molecule and the number of arms per

branching point is three (tri-functional); the related Zimm-Stockmayer equation is shown below (Scorah et al., 2007):

$$g = \left[(1 + \frac{\bar{n}}{7})^{\frac{1}{2}} + \frac{4\bar{n}}{9\pi}\right]^{-\frac{1}{2}} \quad \text{Eq. 10.10}$$

where $\bar{n}$ is (number average) number of branch points per molecule. In addition, a branching frequency (λ) defined as the average number of branch points per molecule per molecular weight, can also be determined from Eq. 10.11:

$$\lambda = \frac{\bar{n}\, F_R}{M} \quad \text{Eq. 10.11}$$

where M is molar mass of each chromatograph slice and F_R is the molar mass of the repeating factor, defined as the mass of 100 repeat units. For STY/DVB copolymer, F_R is equal to 10400, which is the mass of 100 units of STY.

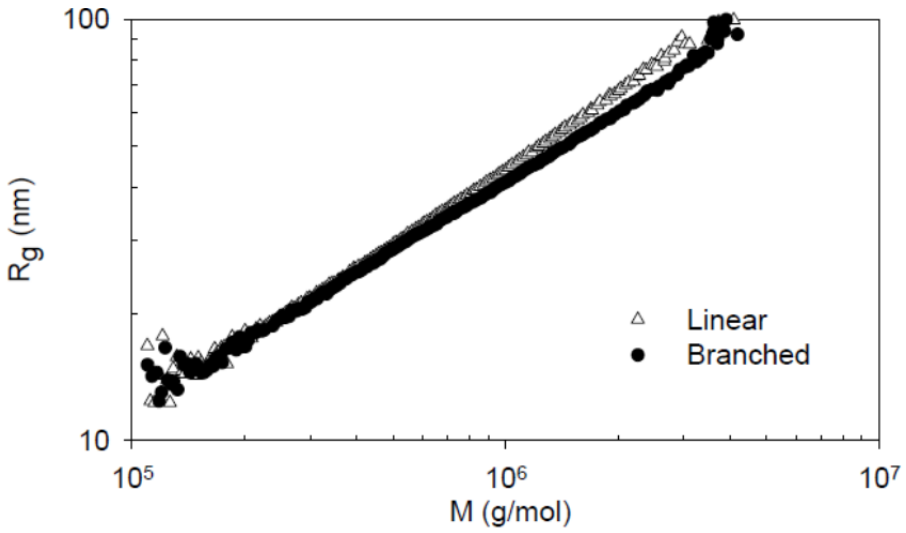

Figure 10.3 Radius of gyration as a function of molecular weight for polystyrene (GPC at 30 °C with 1 ml/min of tetrahydrofuran) (Scorah et al., 2007)

Another GPC detector which is very common for determining branching is an online viscometer. Using an online viscometer, the intrinsic viscosity of a branched polymer can be measured. The intrinsic viscosity can be related to molecular weight using the Mark-Houwink-Sakurada (MHS) equation:

$$[\eta] = K_{[\eta]} M^{\alpha} \qquad \text{Eq. 10.12}$$

$K_{[\eta]}$and α are the so-called MHS constants. For a randomly branched polymer molecule, α is smaller compared to that for a linear molecule. In general, α decreases with increasing molecular weight for randomly branched polymers. From the molecular weight and intrinsic viscosity data collected, the MHS plot can be constructed for branched molecules and comparison can be made to linear polymers. In order to measure the degree of branching, the same polymer with a linear structure needs to be available or the MHS parameters for the linear polymer must be known. Figure 10.4 shows an example of MHS plot for branched polystyrene compared with a linear sample obtained using GPC. As the level of branching increases, the log$[\eta]$ vs. log M plot deviates more and more from linearity.

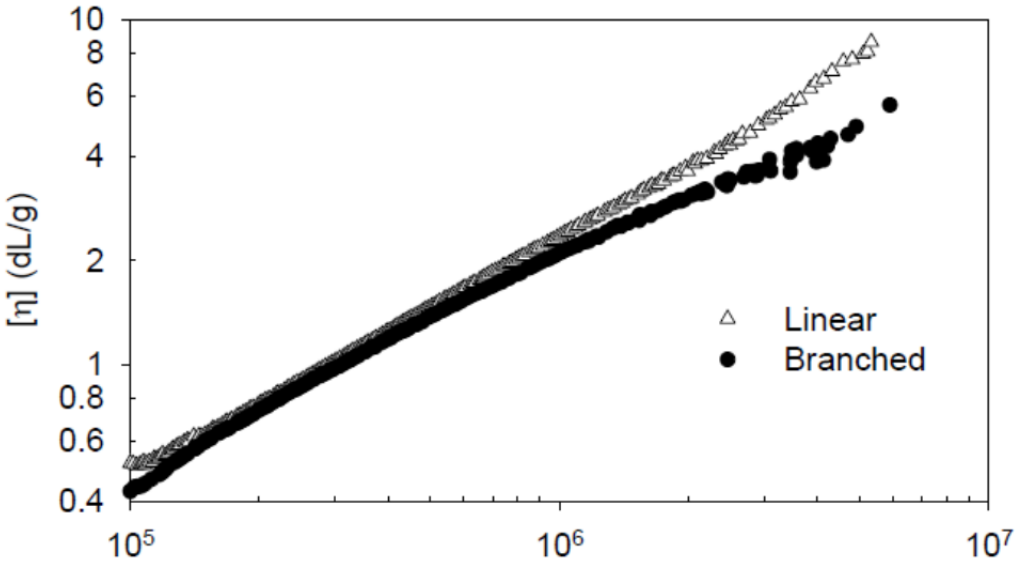

Figure 10.4 Intrinsic viscosity vs. molecular weight for polystyrene (GPC at 30 °C with 1 ml/min of tetrahydrofuran) (Scorah et al., 2007)

Having the measured intrinsic viscosity of the branched polymer, one can determine g' (see Eq. 10.6). It is expected that g' decreases with molecular weight. At low molecular weights, the amount of branching is almost zero and hence, intrinsic viscosity of the branched molecule is the same as the linear and $g' = 1$. As molecular weight increases so does branching, and this will lead to a decrease in g'. In order to calculate branching parameters, Eq. 10.7 should be used to obtain g, while applying a reliable value for the contraction factor (ε). The branching number and branching frequency can then be determined from the known value of g, using the appropriate Zimm-Stockmayer expression.

10.2.2 Differential Scanning Calorimetry (DSC)

Thermal properties of a polymer can give insight into its molecular structure. Differential Scanning Calorimetry (DSC) is a thermo-analytical technique often used for studying phase transitions in polymers (Mathot, 1993). DSC measures the temperature and heat flow associated with phase transitions in materials. With this technique a sample and an inert reference are heated and cooled in a controlled environment. The reference pan is subjected to a chosen heating/cooling program, e.g., 20°C/min. The heat flow to the sample is adjusted in such a way that at all times the temperature of the sample is equal to that of the reference. If a heat-related change takes place in the sample (glass transition, melting, crystallization), the sample either absorbs or emits heat. In order to keep the temperature of both sample and reference the same, more or less heating power is needed. The heating power difference between sample and reference from such a heat change is directly related to the heat flow, which is tracked by the DSC curves. DSC measurements provide thus quantitative and qualitative information about physical and chemical changes that involve endothermic or exothermic processes, or changes in heat capacity (Mathot, 1993). Figure 10.5 gives an example of how the heat flow curve would look like for a few typical phase transition events for a polymer. Exothermic behaviour (crystallization) shows up as increase on the heat flow curve, thus resulting in a concave peak. On the other hand, an endothermic event (glass transition or melting) shows up as decrease in the heat flow curve, thus as a drop or a convex peak.

DSC can be used to measure glass transition temperature (T_g) for amorphous polymers like polystyrene. Amorphous polymers are hard, rigid and glassy below T_g, while at temperatures above the glass transition temperature they are soft and flexible. Many physical and mechanical properties show profound changes in the region of the glass transition. These properties include the coefficient of thermal expansion, heat capacity, refractive index, mechanical damping, elastic modulus, and tensile strength (Nielsen and Landel, 1994). DSC determines the glass transition temperature based on changes in heat capacity. Many points on the DSC curve can be used to determine T_g, and Figure 10.6 shows various points on the heat capacity vs. temperature curve. Point A shows the onset of transition, while point C marks the end of the change in heat capacity, C_p. The width ΔT_g is defined by $\Delta T_g = T_C - T_A$. Point B is where half the specific heat increment has occurred ($1/2\ \Delta C_p$) and it is the typical point mostly used to show glass transition temperature.

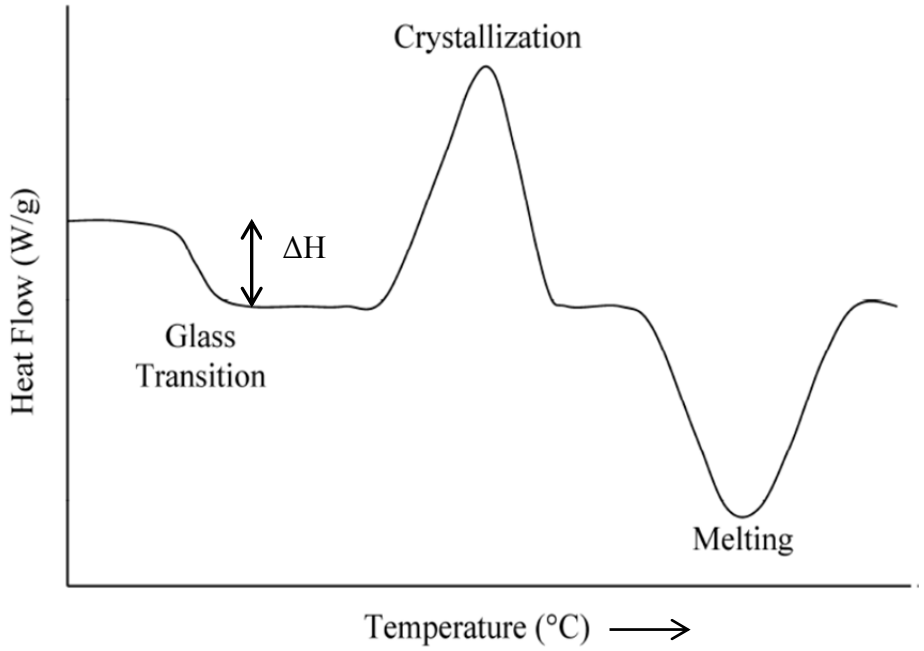

Figure 10.5 Schematic representation of thermal events recorded by DSC (Mathot, 1993)

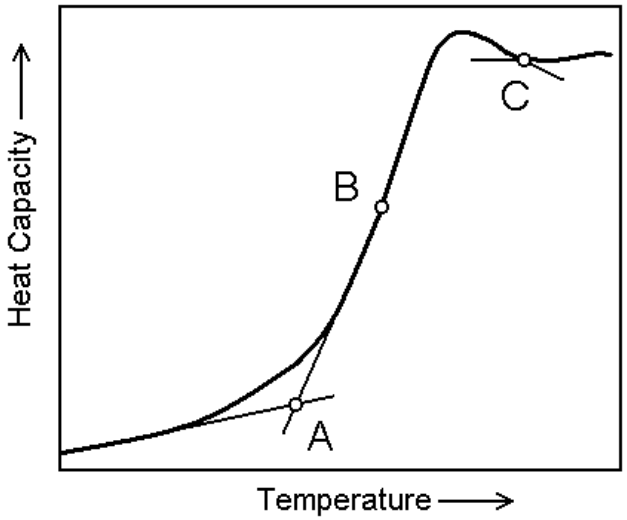

Figure 10.6 The glass transition region showing some commonly used definitions of T_g. A: onset, C: end, and B is the point where half the specific heat increment has occurred (Mathot, 1993)

Several factors related to chemical structure are known to affect the glass transition temperature. The glass transition temperature increases with number-average molecular weight to a limiting asymptotic value of T_g^0 for infinite molecular weight (Nielsen & Landel, 1994) and is given by:

$$T_g = T_g^0 - \frac{K}{M_n} \qquad \text{Eq. 10.13}$$

where K is a constant characteristic of each polymer. For polystyrene (PS) K = 1.75 X 10^5, so its T_g value increases from about 83 °C for a molecular weight of 10^4 to 100 °C for infinite molecular weight (Nielsen & Landel, 1994). Another factor affecting T_g is cross-linking; by introducing restrictions on the molecular motion of a chain, cross-linking increases the glass transition of a polymer. Low degrees of cross-linking increase T_g only slightly above that of the uncross-linked polymer. However, it is well established that an increase in the degree of crosslinking in a polymer network results in an increase in T_g (provided copolymerization effects are relatively small). The incremental thermal property at T_g such as ΔC_p decreases as the degree of crosslinking increases (see Figure 10.7 and Table 10.2). At a very high degree of crosslinking, ΔC_p becomes practically unobservable (Ellis et al., 1983).

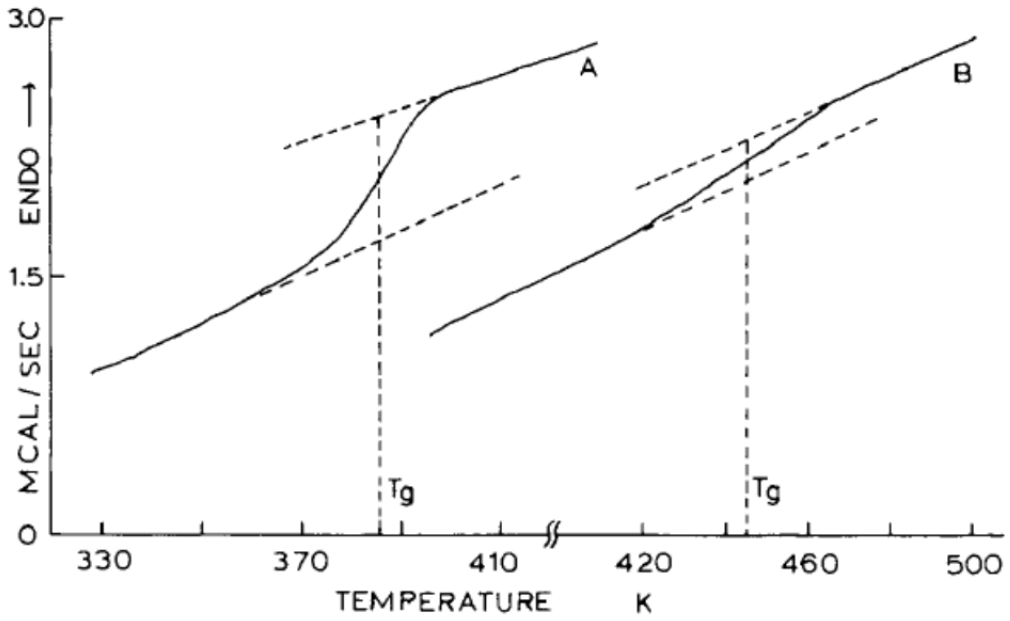

Figure 10.7 Typical DSC traces for A (PS), B (PS cross-linked with 35% DVB) (Ellis et al., 1983)

Table 10.2 DSC results of PS compared to cross-linked PS with different levels of DVB (Ellis et al., 1983)

Sample	% DVB (w/w)	Onset (TA)	TB (Tg)	ΔCp (J/g.C)
PS	0	105	112	0.283
PS-T1	5	111.7	117	0.252
PS-T4	21	130	142	0.2
PS-T5	35.7	145	171.9	0.095

T_A: onset of transition; T_B (T_g): point where half of the specific heat increment has occurred, used as indicator of T_g (as a reminder, refer to Figure 10.6); Tc: end of transition; ΔC_p: change in heat capacity

It is well known that T_g is a result of relaxed segmental motions (Harrison, 1985). In a cross-linked polymer, there is a considerable range of molecular weights between crosslinks (M_c) and it is expected that longer chains between crosslink points (i.e., higher molecular weight between crosslinks) will be activated and relax at lower temperatures compared to the very short chain segments between crosslink points (resulting from a tighter network) (Ellis et al., 1983). Therefore, a transition plot obtained from a DSC scan represents the glass transition of a

spectrum of chains and it is expected that a more heterogeneous network (broader distribution of M_c values) should produce a broader T_g range. The slope of the transition line could also be an acceptable indicator for the degree of network uniformity. It is expected that a more uniform polymer network (narrower distribution of M_c values) will exhibit a sharper transition, which translates into a larger slope.

In conclusion, in order to use DSC to obtain information related to network uniformity (or homogeneity), additional pieces of information such as ΔT_g, ΔH, ΔC_p and the slope of the transition line are useful. In our pursuit of finding a proper technique to differentiate between cross-linked polystyrene synthesized through nitroxide-mediated radical polymerization and regular radical polymerization, samples from both polymerization processes have been characterized using DSC and the related results are presented in section 10.3.2.1.

10.2.2.1 Experimental

DSC analysis was carried out on a TA Instruments DSC Q2000 module. The heating method used was the following:

Equilibrate at 40°C
Cycle 1: 20°C/min ramp from 40°C to 180°C; Isothermal for 5 min @ 180°C
Cycle 2: 10°C/min ramp from 180°C to 40°C; Isothermal for 5 min @ 40°C
Cycle 3: 10°C/min ramp from 40°C to 180°C

Each DSC sample size used per run was about 5 - 7 mg. Three cycles were used to clear the thermal history of the sample. The data collected for the third cycle was used for the analysis. In order to check the reproducibility of the data, two DSC samples were prepared and each sample was run twice. All data points reported here are the average of four readings.

10.2.3 Dynamic Mechanical Analysis

Polymers have unique viscoelastic properties which combine the characteristics of elastic solids and viscous fluids. A perfectly elastic solid acts as an ideal spring and all the energy given to it will be stored in the material. On the other hand, the energy given to a purely viscous fluid will be used to deform the material and the energy will be lost into heat. Since polymers have the characteristics of both elastic solids and viscous fluids, a certain fraction of the energy given to them can be stored in the material (storage modulus, related to the elastic part), while the rest will be dissipated into heat (loss modulus, related to the viscous part) (Nielsen & Landel, 1994).

Dynamic Mechanical Analysis (DMA) is used for studying the viscoelastic behavior of polymer materials. An oscillatory or pulsing force (sinusoidal stress) is applied to a sample and the response (strain) of the material is measured. Stress (σ) applied is described by Eq. 10.14, while the resulting strain (ε) is described by Eq. 10.15. As can be seen, both stress and strain have a sinusoidal shape with frequency ω, however, strain lags behind stress by a phase angle difference δ (see also Figure 10.8). For a perfectly elastic solid, the resulting strain and the applied stress will be perfectly in phase. For a purely viscous fluid, there will be a 90 degree phase lag of strain with respect to stress. Since viscoelastic polymers have the characteristics in between the two extremes, there will be some phase lag δ between 0 and 90 degrees during DMA tests and stress will have a component in phase with strain and a component exactly 90 degrees out of phase with strain (Nielsen & Landel, 1994), as seen in Eq. 10.14.

$$\sigma = \sigma_0 \sin(\omega t + \delta) = \underbrace{(\sigma_0 \cos\delta)}_{\text{in phase with } \varepsilon} \sin\omega t + \underbrace{(\sigma_0 \sin\delta)}_{\text{90 degrees out of phase with } \varepsilon} \cos\omega t \qquad \text{Eq. 10.14}$$

$$\varepsilon = \varepsilon_0 \sin(\omega t) \qquad \text{Eq. 10.15}$$

t: time
σ_0 : stress at t = 0
ε_0 : strain at t = 0

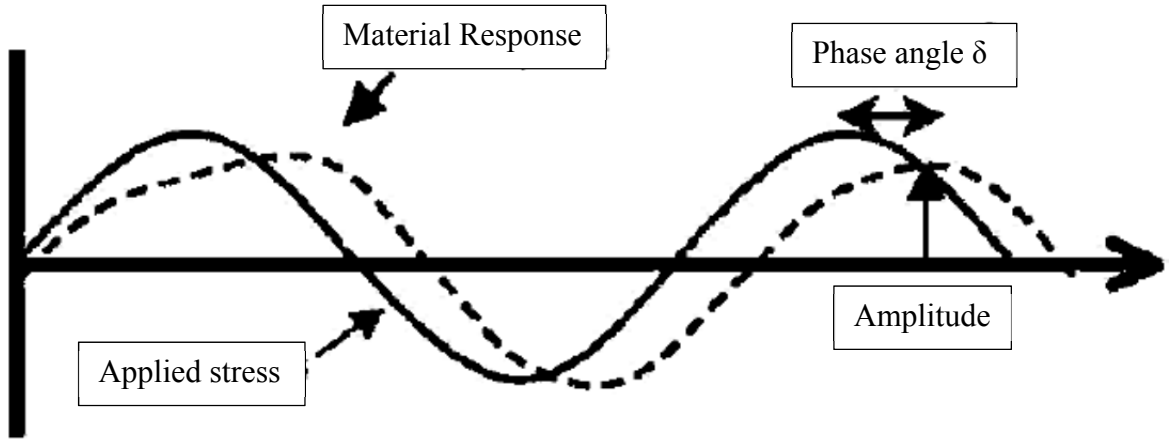

Figure 10.8 Schematic representation of stress and strain curves in DMA (Cheng, 2008)

Stress and strain are related through the modulus, with modulus being the ratio of stress to strain. The modulus measured in a DMA test is a complex modulus (E^*), which consists of a storage modulus (E') and a loss modulus (E''), as shown in Eq. 10.16. Storage modulus measures the stored energy, representing the elastic portion, while loss modulus measures the energy dissipated as heat, representing the viscous portion (Nielsen & Landel, 1994). Therefore, E' is the component of stress in phase with strain divided by the maximum strain (ε_0) (Eq. 10.17), while E'' is the ratio of the component of stress 90 degrees out of phase with strain to ε_0 (Eq. 10.18). The ratio of loss modulus to storage modulus is called the loss tangent (tan δ) or damping factor and is shown in Eq. 10.19.

$$E^* = E' + iE'' \qquad \text{Eq. 10.16}$$

$$E' = \frac{\sigma_0 \cos \delta}{\varepsilon_0} \qquad \text{Eq. 10.17}$$

$$E'' = \frac{\sigma_0 \sin \delta}{\varepsilon_0} \qquad \text{Eq. 10.18}$$

$$\tan \delta = \frac{E''}{E'} \qquad \text{Eq. 10.19}$$

The damping term is a measure of the ratio of energy dissipated as heat to the maximum energy stored in the material during one cycle of oscillation. The dynamic mechanical properties, especially tan δ, are sensitive to all kinds of molecular motions that are going on in a material, even in the solid state. Hence, DMA testing can be used to detect transitions, relaxation processes, structural heterogeneities, and even determine indirectly molecular weights, molecular weight distributions (MWD), the composition of copolymers, and the degree and heterogeneity of crosslinking (Nielsen & Landel, 1994).

Two major kinds of test modes can be used to probe the viscoelastic properties of polymers with DMA: temperature sweep and frequency sweep tests. In a temperature sweep, the complex modulus is measured at low constant frequency while varying the temperature. On the other hand, in the frequency sweep, the sample is held at a fixed temperature and the complex modulus is measured at varying frequency. Peaks observed in $E^{"}$ and tan δ and the dramatic change in E' with respect to both frequency and temperature can be associated with the glass transition, which corresponds to the ability of chains to move past each other.

Figure 10.9 shows typical viscoelastic regions seen in the storage modulus obtained from DMA. At lower temperatures (below T_g), the sample is in the glassy plateau where it is hard or rock- like. Localized bending and stretching of bonds is occurring and tan δ is below 0.01. As temperature increases, the sample reaches the glass transition region, where the sample becomes less hard and the storage modulus decreases while tan δ peaks. As temperature increases and passes the glass transition region, the sample enters the rubbery plateau, where it is springy. Main backbone chains exhibit gradual slippage and tan δ starts to decrease. Next is a viscous region where the sample is like a viscous fluid and flows as temperature increases. Large scale main chain mobility occurs. Finally, the fluid region (often treated as part of the viscous region) is where the sample is flowing, water-like. Free chain movement and inter-chain slipping occur (Menard, 2008).

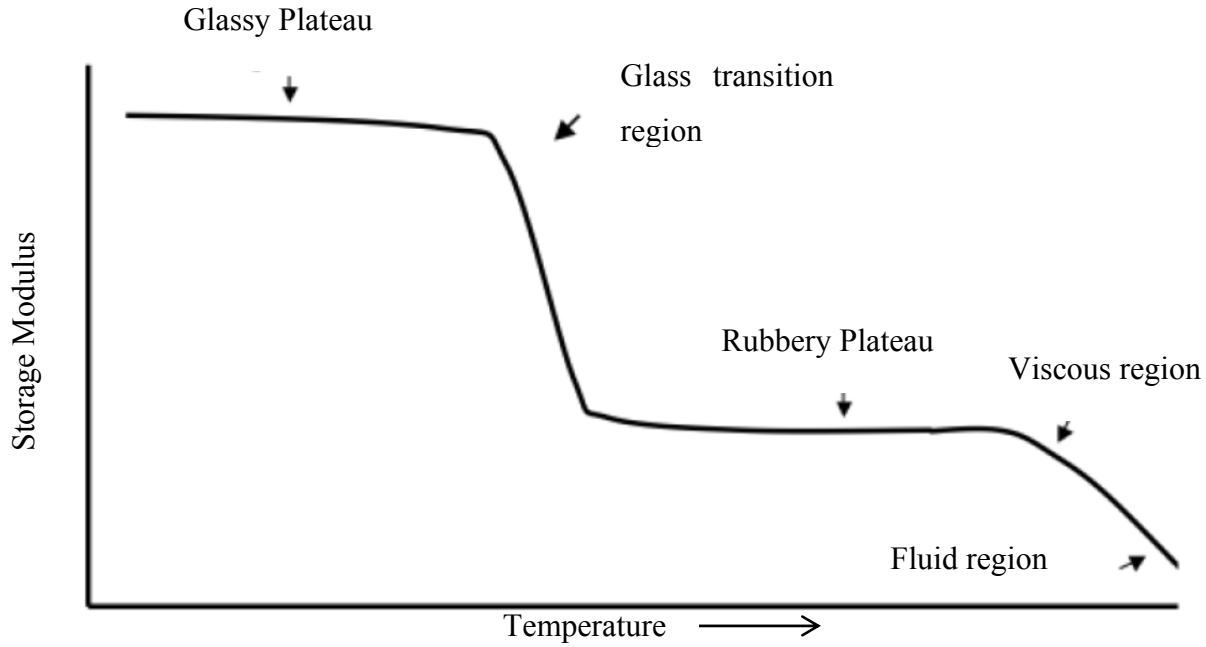

Figure 10.9 Regions of viscoelastic behavior (Menard, 2008)

Figure 10.10 shows temperature sweep data (storage modulus and tan δ) collected in our lab for polystyrene using a frequency of 1 Hz. It can be observed that the storage modulus decreases steadily with temperature; according to Nielsen & Landel (1994), this is mostly due to thermal expansion. The drop in storage modulus by several decades around 105 °C corresponds to the glass transition region and it is accompanied by an increase in the value of tan δ, which is at a maximum around 120 °C. At temperatures above the glass transition, the storage modulus drops sharply to zero and tan δ also decreases. After the glass transition, the sample becomes too soft to support itself as a rectangular bar in the DMA set up, hence, the data points after around 130 °C are not meaningful, and eventually the run had to be stopped before being able to observe the viscous region, which should occur around 240°C.

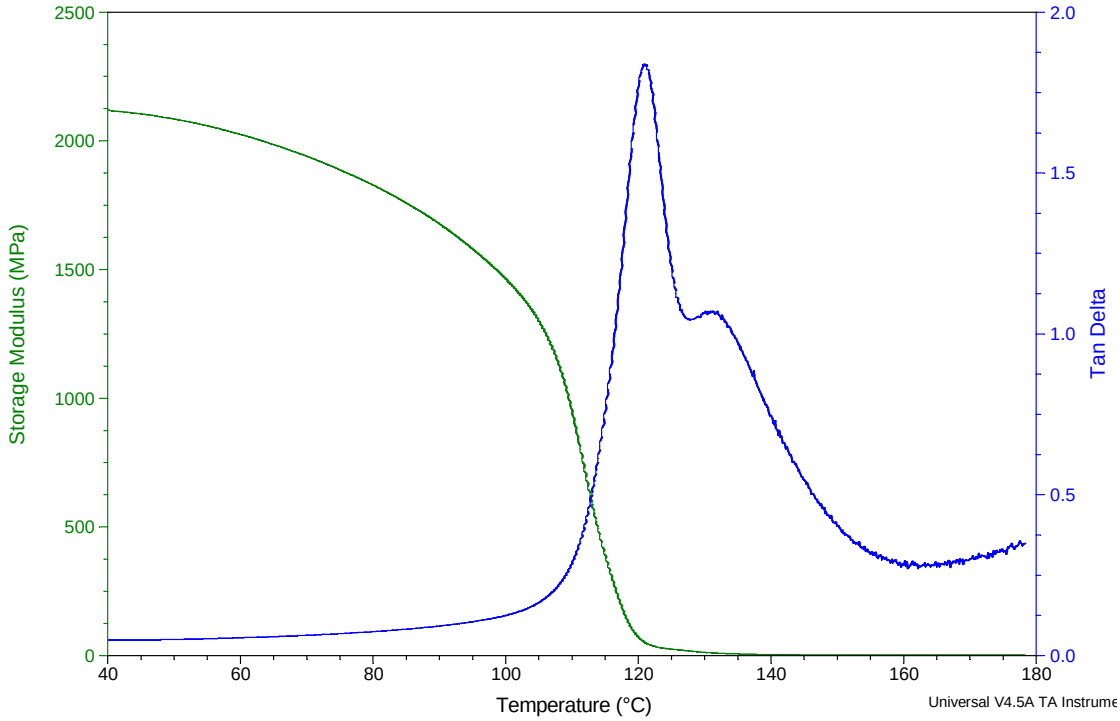

Figure 10.10 Dynamic mechanical properties for polystyrene as a function of temperature (data collected in this work)

When the polymer is cross-linked, the maximum of the tan δ peak shifts to higher temperatures and the dramatic drop in storage modulus and the increase in loss modulus, happening at the glass transition, also shift to higher temperatures. As the degree of crosslinking increases, both the maximum in tan δ and the drop in storage modulus shift to higher temperatures (Nielsen & Landel, 1994). Our results for a typical linear polystyrene (PS) are compared to the ones for cross-linked polystyrene with 1% DVB in Figure 10.11, where the shift of tan δ, E' and E'' to higher temperatures can clearly be observed. It is also observable that the storage modulus starts at higher values for cross-linked polystyrene, while the starting value for the loss modulus is actually lower for cross-linked polystyrene. Therefore, according to Eq. 10.19, the initial values of tan δ will be lower for the cross-linked PS (as observed in Figure 10.11). This is due to the fact that cross-linking increases the ability of the polymer material to store more energy. Although not clearly seen in Figure 10.11, it is a fairly well-known fact that the value of storage modulus after the glass transition is higher for a cross-linked polymer compared to a linear polymer (Flory, 1953). In addition, as the degree of cross-linking increases, so does the

value of E' after the glass transition (Mark et al., 1985). This is reasonable, since as % cross-linking increases, the molecular weight between cross-links (M_c) decreases, and based on Eq. 10.20 (Mark et al., 1985), the storage modulus is inversely proportional to M_c:

$$E' = \frac{\rho RT}{M_c} \qquad \text{Eq. 10.20}$$

ρ: Polymer density
R: Gas constant
T: Absolute temperature

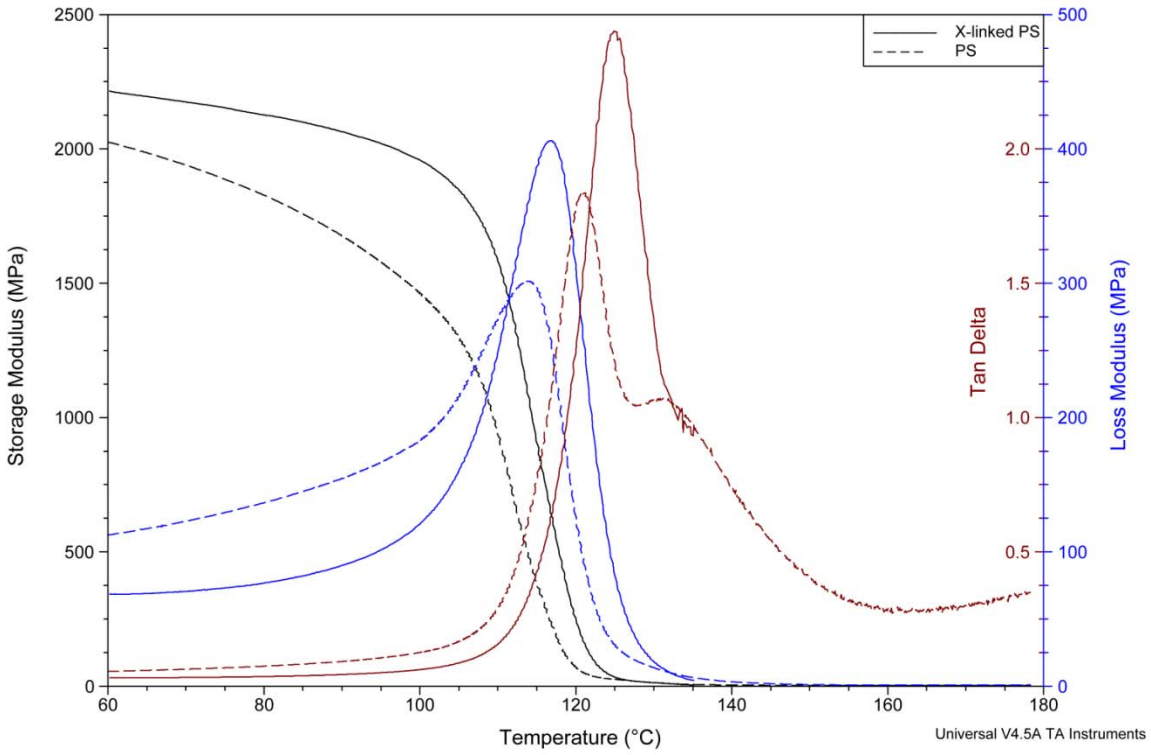

Figure 10.11 Effect of cross-linking on dynamic mechanical data of polystyrene; polystyrene cross-linked with 1% divinyl benzene (data collected in this work)

As can be seen in Figure 10.11, although the initial values of loss modulus were lower for cross-linked polystyrene, this trend is reversed after the glass transition temperature, and in addition, the peak of loss modulus becomes higher, which results in observing a higher maximum (peak) for the tan δ of the cross-linked polystyrene (see also Eq. 10.19).

As mentioned previously, according to Nielsen & Landel (1994), dynamic mechanical properties, especially tan δ, are sensitive to all kinds of molecular motions that are going on in a material. There have been several studies in the literature investigating homogeneity or heterogeneity of polymer networks by means of dynamic mechanical analysis, where the broadening of tan δ has been attributed to a broader distribution of the molecular weights between cross-links or to heterogeneity in the network structure (Simon et al., 1991; Tieghi et al., 1992; Zosel, 1995; Kannurpatti et al., 1998; Rey et al., 2004). Ide and Fukuda (1999) had alluded to the fact that mechanical characteristics can be used to show the homogeneity of the network in NMRP of styrene and divinyl benzene, but never showed any evidence or experimental data to corroborate their claim. (In fact, several papers in the literature have since referred to the paper by Ide and Fukuda (1999), basically accepting the statement (which was made in passing at the very end of the 1999 paper), and, furthermore, reporting it as if Ide and Fukuda "had shown" unambiguous experimental evidence on the homogeneous vs. heterogeneous network topic). Later on, Yu et al. (2007) compared a network prepared by conventional free radical polymerization to one produced through Atom Transfer Radical Polymerization (ATRP) and showed that the product synthesized through ATRP was more homogeneous, documented by a narrower peak width of the tan δ curve. Based on these literature statements, it was decided that DMA testing could be a potential technique to indicate the heterogeneity of a cross-linked network. Hence, dynamic mechanical analysis was carried out on our cross-linked polymers and the results of samples synthesized through regular free radical polymerization were compared to samples from nitroxide-mediated radical polymerization (NMRP).

10.2.3.1 Experimental

The dynamic mechanical measurements were carried out in a Q800 dynamic mechanical analyzer from TA Instruments in a multi-strain mode. After trying several clamps, a single cantilever clamp was used, as it is a good general purpose mode for evaluating thermoplastics and highly damped materials (e.g., elastomers). A sinusoidal stress of 1 Hz frequency was applied. A stress-strain experiment was carried out prior to formal testing to establish the linear viscoelastic region (LVR) and also to find test conditions that give optimal results. LVR is the linear part of a stress–strain curve where an increase in stress is accompanied by a proportional

increase in strain, that is the modulus is constant and the change in dimensions is reversible. Figure 10.12a shows storage modulus for different amplitudes (μm). As can be seen, storage modulus is constant up to an amplitude of about 6 μm, after which there is a slight decrease in storage modulus. From Figure 10.12a, it seems safe to pick an amplitude of 5 μm. Figure 10.12b shows that an amplitude of 5 μm corresponds to a strain of about 0.05% and the stress vs. strain curve (Figure 10.12c) shows that the 0.05% value of strain lies in the linear part of the stress-strain curve. A temperature sweep mode was used to record changes in storage modulus, loss modulus and tan δ with temperature over a range of 60 °C to 160 °C with a ramping rate of 2 ºC/min. Two specimens were prepared from each polymer sample and an independent DMA test was carried out for the specimens in order to check the reproducibility of the results (which is infrequently done in the literature, if at all!).

The specimens examined were thin rectangular sheets of 0.6 mm thickness and 20 mm × 5 mm area. The samples were compression molded at 190 ± 10 °C following the procedure below, tailored from ASTM method D4703-10a: The stainless steel mold was preheated between two ferrotype plates to 190 °C, then enough material was poured in the mold, distributing it evenly in the cavity. The set up was then placed in the preheated press. The material was preheated for 5 min by applying only a contact pressure. Two cycles of 2 min pressure-30 sec release were applied, with 10,000 lb_f. At the last stage, the material was cooled down under pressure to 80 °C using compressed air. The pressure- release cycles were applied to make sure there were no bubbles trapped in the sample. When the temperature of the press was around 80 °C, it was opened and the mold was quench-cooled to room temperature and the specimen was taken out of the mold and examined to make sure it had a smooth surface and there were no bubbles trapped in it or any cracks on the surface.

a)

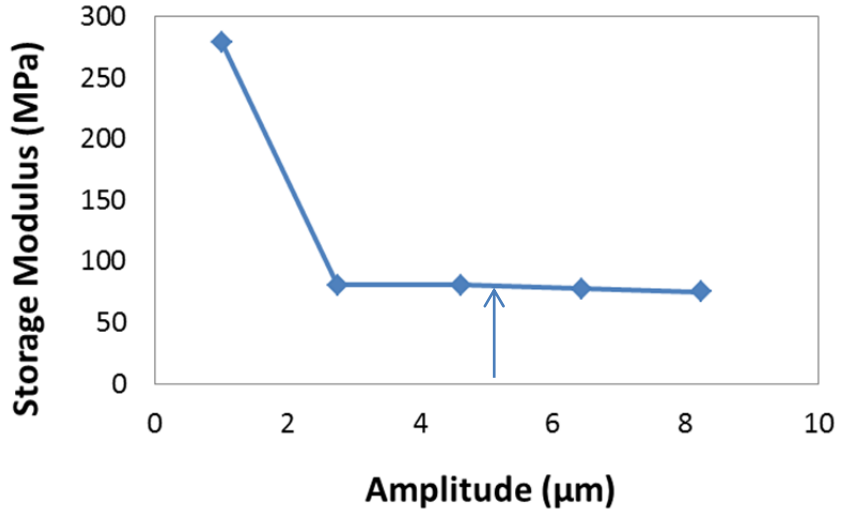

b)

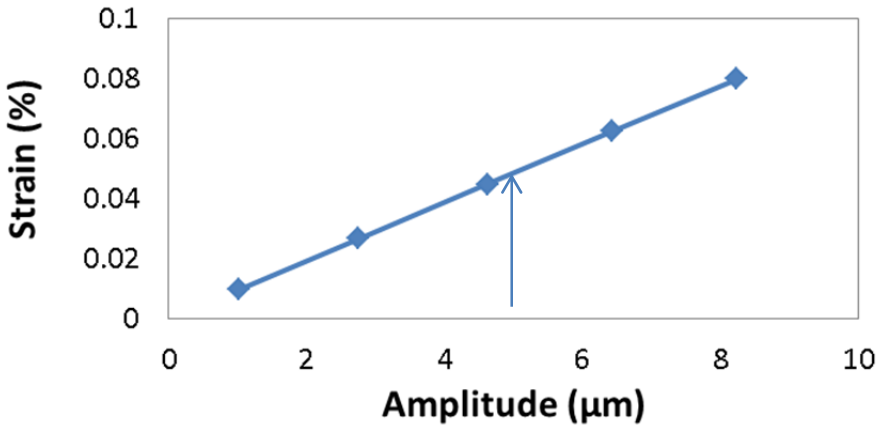

c)

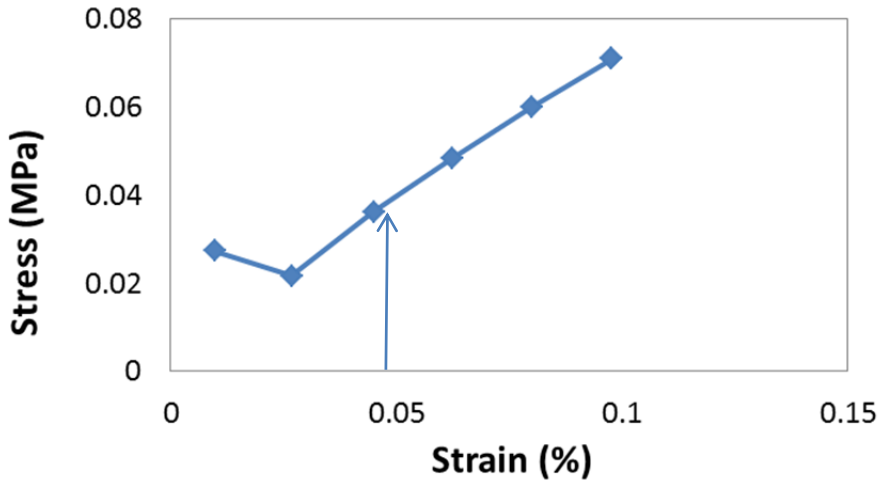

Figure 10.12 Strain and frequency sweep for PS sample; a) Storage Modulus vs. Amplitude, b) Strain vs. Amplitude, c) Stress vs. Strain

10.3 Results and Discussion

10.3.1 Long Chain Branching in NMRP of STY/DVB

Presence of a di-functional monomer (DVB) in radical copolymerization of STY/DVB could lead to production of branched polystyrene before the formation of cross-linked polystyrene at the gelation point. In regular radical copolymerization of STY/DVB at high temperatures, the gelation point occurs at the very early stages of conversion (since the molecular weights are high from the beginning); hence, progression of branching with conversion is hard to detect before the gel point. For instance, crosslinking happens around 7% conversion for STY copolymerization with 1% DVB at 120 °C. Figure 10.13 shows intrinsic viscosity vs. molecular weight in logarithmic scale for polystyrene at different conversions. At 1.4% conversion, there is no sign of branching and log $[\eta]$ increases linearly with log M. This plot deviates slightly from linearity at higher molecular weights for the sample at 3.4% conversion, resulting in an average number of branch points per molecule equal to 10 ($\bar{n} = 10$). At 7% conversion the sample is highly cross-linked and the deviation from linearity is prominent in Figure 10.13, with $\bar{n} = 184$. The evidence of branching can also be observed in the shoulders or bimodality of the GPC chromatograms for different detectors. Figure 10.14 shows viscometer signals vs. retention volume. It can be seen that at 1.4% conversion there is no sign of shouldering in the viscometer signal. At 3.4% conversion there is a slight shoulder appearing at lower retention volume, which indicates small amounts of high molecular weight species produced by branching. At 7% conversion, the shoulder is prominent and the concentration of linear polystyrene (observed in the RI signal, not shown here for the sake of brevity) is almost negligible in comparison with the shoulder

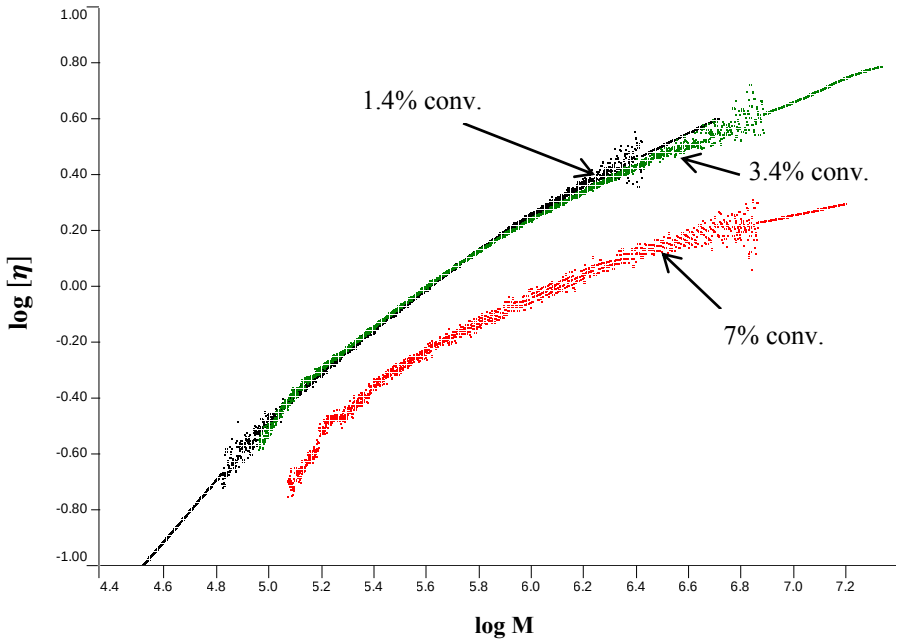

Figure 10.13 Intrinsic viscosity as a function of molecular weight for polystyrene at different conversions

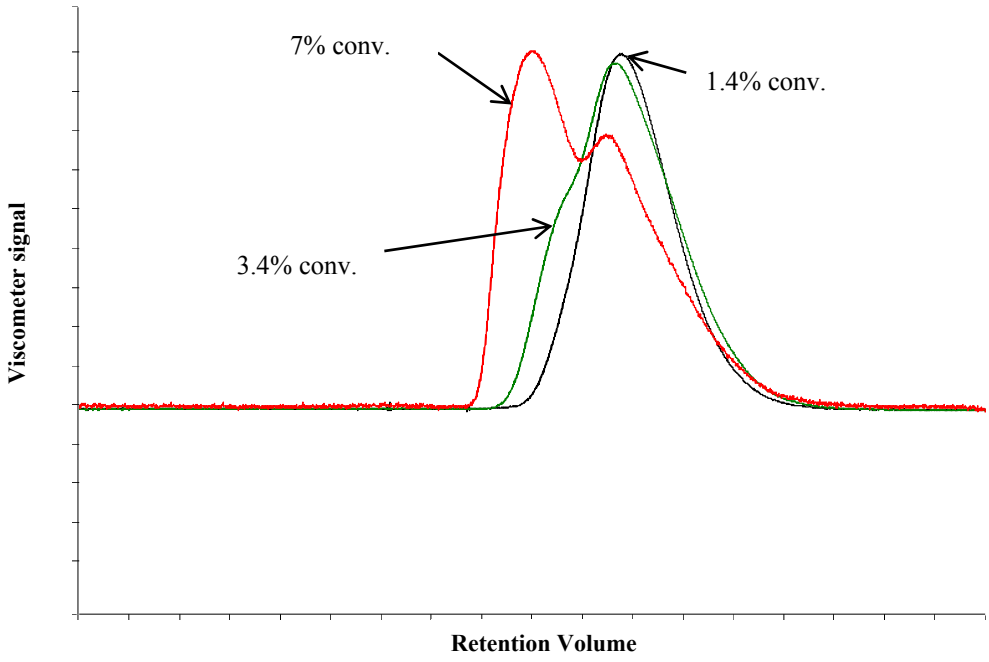

Figure 10.14 GPC chromatograms for polystyrene with 1% DVB at different conversions

In the case of controlled radical copolymerization of STY/DVB, presence of I-TIPNO delays the gelation point and branched polystyrenes are produced at higher conversions. Comparing the weight average molecular weight vs. conversion plot from this experiment with controlled radical polymerization of STY with I-TIPNO, one can see that, in the initial stages of the reaction, the copolymerization reaction follows the linear increase in molecular weights with conversion, however, at about 35% conversion, deviation from linearity emerges especially for weight average molecular weight, indicating the formation of high molecular weight chains by addition to branch points (see Figure 10.15). Figure 10.16 compares the corresponding GPC chromatograms for STY copolymerization with 1% DVB and 1% I-TIPNO and STY homopolymerization with 1% I-TIPNO. Figure 10.16a shows the chromatograms at 10% conversion; as can be seen, presence of DVB does not show any effect. However, at 35% conversion (see Figure 10.16b), one can see a shoulder at lower retention volumes which corresponds to the presence of high molecular weight polymer formed by branching of the controlled molecular weight chains.

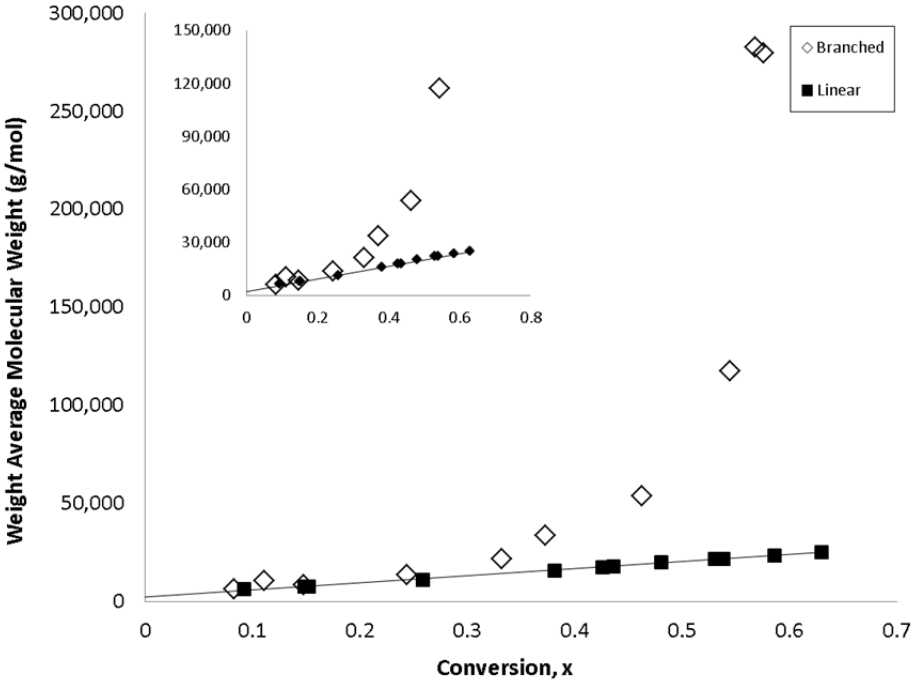

Figure 10.15 Weight average molecular weight vs. conversion for branched (1% DVB) and linear polystyrene synthesized through controlled radical polymerization with 1 % I-TIPNO

a)

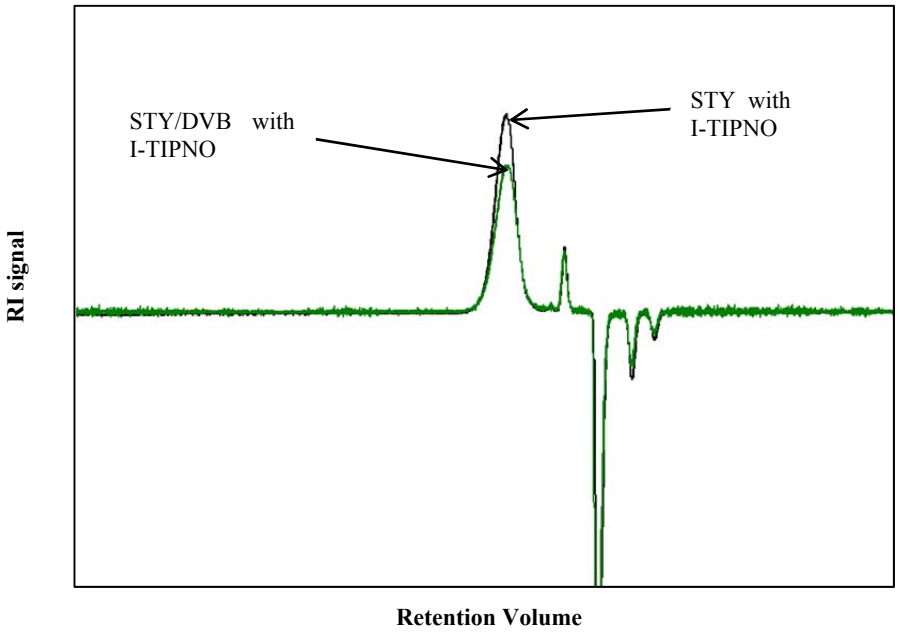

b)

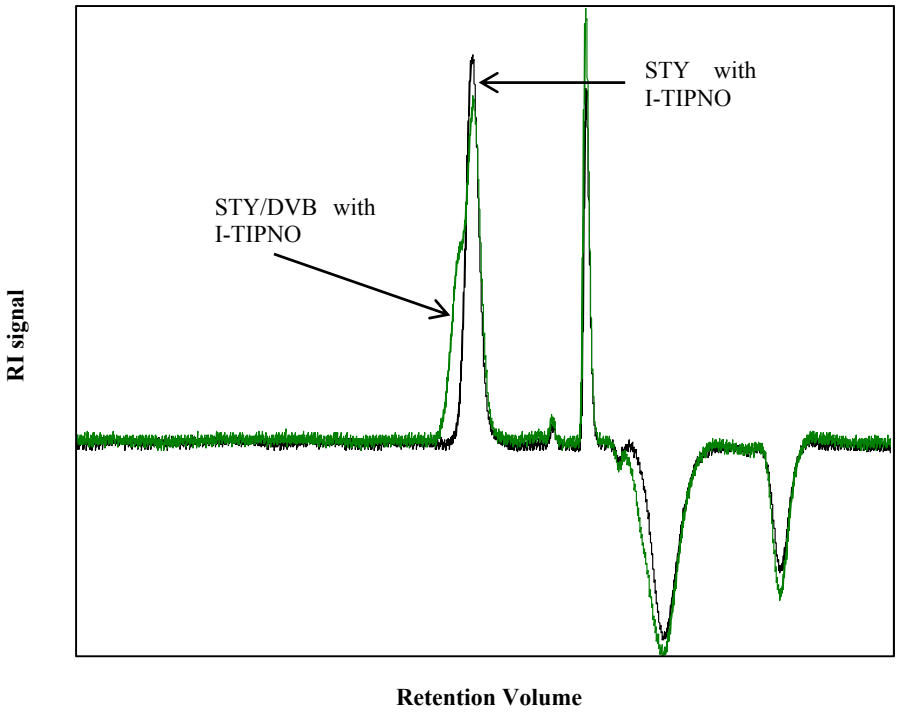

Figure 10.16 Comparison of GPC chromatograms of controlled copolymerization (1% DVB, 1% I-TIPNO) and controlled polymerization of styrene (1% I-TIPNO), a) at 10% conversion, b) at 35% conversion

As mentioned previously, the level of branching can be described by the contraction factors g and g'. The GPC set up used for characterizing our samples was equipped with a viscometer but not a multi-angle light scattering. Hence, it was only possible to experimentally determine intrinsic viscosity ([η]), shown in Table 10.3, for different conversion levels. In order to calculate g' from Eq. 10.6, the intrinsic viscosity of a linear analogue at the same molecular weight was required. Whenever available, the intrinsic viscosity of linear polystyrene synthesized through controlled radical polymerization with the same level of I-TIPNO was used. In cases where the linear analogue was not available from our experiments, the following Mark-Houwink equation, from the *Polymer Handbook (Brandrup et al., 1999)*, was used for linear polystyrene in tetrahydrofuran (THF)):

$$[\eta] = 1.1 \times 10^{-4} M^{0.725} \qquad \text{Eq. 10.21}$$

Eq. 10.7 was used to calculate g contraction factor values from g'. The value of the structure factor (ε) used was 0.75 (Ambler and McIntyre, 1977). The g and g' data for controlled radical copolymerization of STY with 1% DVB and 1% I-TIPNO are shown in Table 10.3, with g' in the range of 0.211-0.955 and g in the range of 0.126-0.941. The polymers with higher branching clearly give lower g and g' values, at the same molecular weights. Subsequently, to calculate branching number and frequency, Eq. 10.10 and Eq. 10.11 were used and the results are also shown in Table 10.3. Branch frequency per 100 STY units is plotted vs. conversion in Figure 10.17. It can be seen that branch frequency increases with conversion but is still low just before the gelation point, where the average number of branch points per 100 STY units jumps to 7 (value of λ for the last entry is not a meaningful value, since λ could not be higher than 1 for our case with 1 wt% DVB. However, qualitatively this value means that the macromolecule is not branched anymore, and it is cross-linked, hence not possible to find the branching number).

Table 10.3 Branching characteristics for controlled radical copolymerization of STY with 1% DVB and 1% I-TIPNO

Time (hr)	Conv.	Mn	Mw	PDI	$[\eta]$	g'	g	$\bar{n}$	λ
2	0.244	10,941	13,745	1.256	0.114	0.955	0.941	0.51	0.25
3	0.332	15,931	20,836	1.31	0.143	0.967	0.956	1.22	0.31
4	0.373	22,851	35,164	1.54	0.194	0.897	0.865	2.59	0.40
5	0.463	28,271	54,881	1.94	0.228	0.763	0.698	5.84	0.65
6	0.544	37,977	113,261	2.98	0.309	0.610	0.517	13.38	0.82
7	0.568	45,871	250,489	5.46	0.424	0.471	0.367	28.46	0.93
7	0.576	46,078	262,716	5.70	0.432	0.464	0.359	32.91	0.96
8	0.617	128,902	1.38E+06	10.73	0.656	0.211	0.126	354.04	7.06

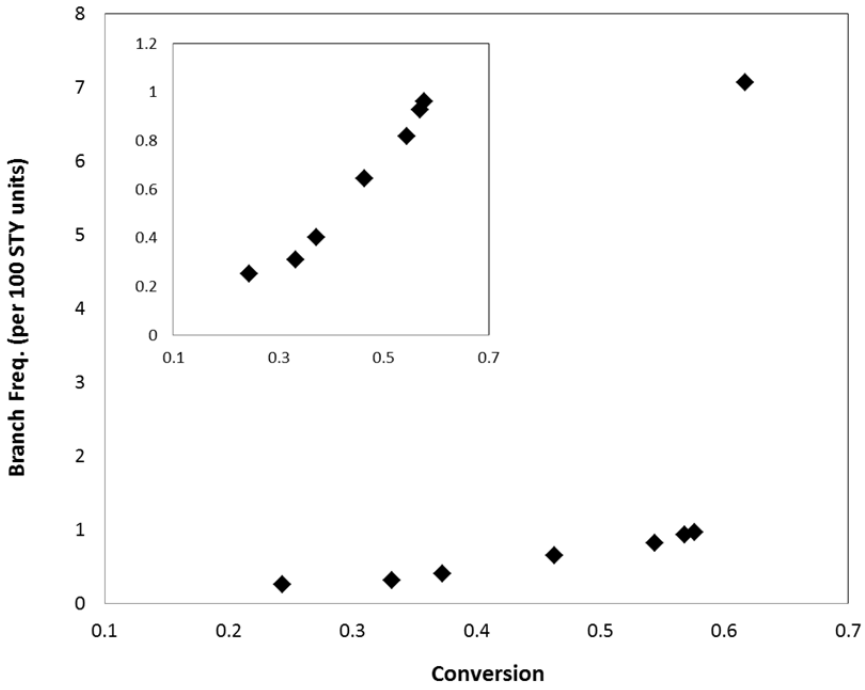

Figure 10.17 Branch frequency vs. conversion for controlled radical copolymerization of styrene with 1% DVB and 1% I-TIPNO

Figure 10.18 shows the progression of viscometer responses with retention volume for polystyrene samples, synthesized through controlled radical copolymerization of styrene with 1% DVB and 1% I-TIPNO. It can be seen that as conversion increases the chromatogram shifts towards lower retention volumes, which represents higher molecular weights, and there is the presence of a shoulder appearing in the peak that becomes broader and broader as conversion

increases. This shoulder is the widest at 60% conversion, which is the gelation point. After this point, we have cross-linked polystyrene which is not soluble in THF for GPC analysis.

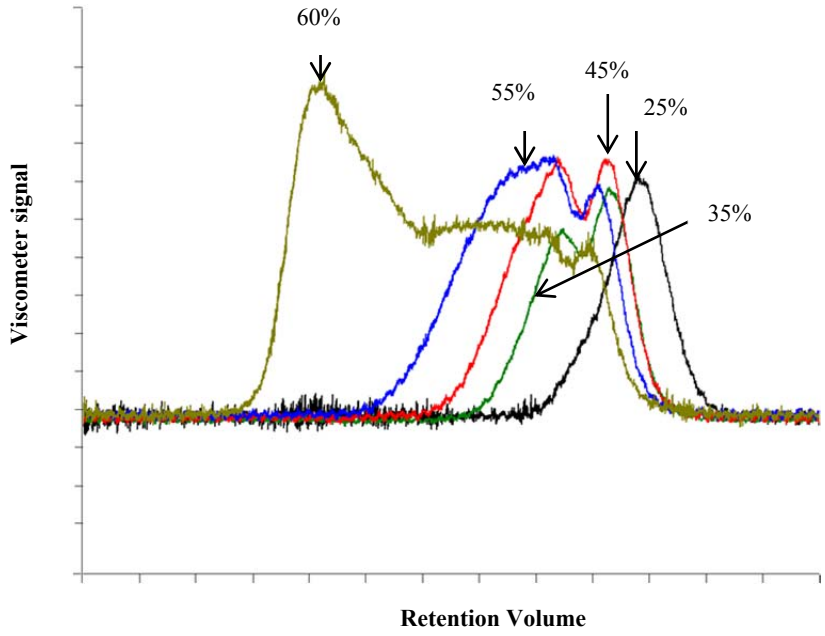

Figure 10.18 GPC chromatograms for polystyrene synthesized through controlled radical copolymerization with 1% DVB and 1% I-TIPNO, at different conversions

Effect of DVB concentration: Let's keep the case of 1% DVB and 1% I-TIPNO as our base case. Then for controlled radical copolymerization of styrene with the same level of I-TIPNO (1%) but higher level of DVB (1.5%), branching levels are higher, as expected (and also observed in Chapter 9; see subsection 9.4.2.3), due to the presence of more DVB. Table 10.4 shows the related branching information for this run. It can be seen that g' is in the range of 0.133-0.998 and g in the range of 0.068-0.998. At around 45% conversion, the run with higher percentage of DVB has lower g' and g values and hence, it is more branched resulting in a higher branching frequency (compare Table 10.3 and Table 10.4). Comparisons between the branch frequencies are shown in Figure 10.19. It can be seen that branch frequency increases with conversion for both runs; however, the run with higher percentage of DVB has higher branching frequencies at all conversion levels, and the branching parameters, ($\overline{n}$) and (λ), are higher at the gel point, which happens at lower conversion for the run with higher % DVB.

Again, the branching characteristics for the last entry of the table are not meaningful, as at gelation point the branching relationships become out of trend.

Table 10.4 Branching characteristics for controlled radical copolymerization of STY with 1.5% DVB and 1% I-TIPNO

Time (hr)	Conv.	Mn	Mw	PDI	$[\eta]$	g'	g	$\bar{n}$	λ
2	0.263	10,098	13,244	1.31	0.107	0.998	0.998	0.88	0.35
2.5	0.299	12,707	17,721	1.40	0.121	0.918	0.892	1.54	0.51
3	0.344	15,143	23,631	1.56	0.139	0.853	0.809	3.20	0.81
4	0.421	23,323	51,334	2.20	0.201	0.706	0.629	7.98	1.01
5	0.475	26,500	102,458	3.87	0.240	0.511	0.408	20.79	1.70
6	0.558	107,695	1.81E+06	16.80	0.502	0.133	0.068	1396.68	20.09

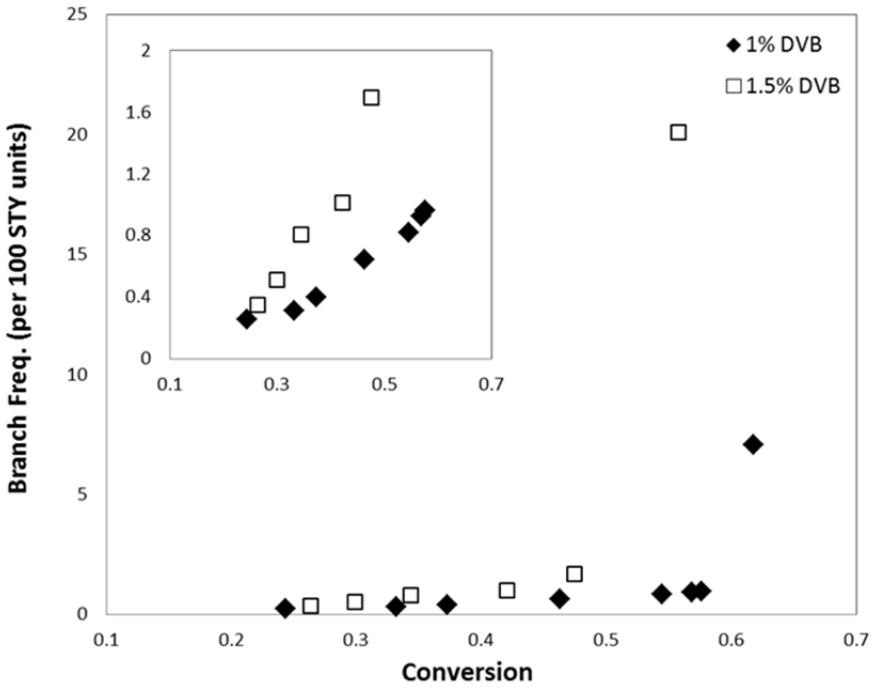

Figure 10.19 Effect of % DVB on branch frequency vs. conversion data for controlled radical copolymerization of styrene with 1% I-TIPNO

Effect of I-TIPNO concentration: In the case of controlled radical copolymerization of STY with the same level of DVB as the base case (1%) but higher level of I-TIPNO (2%), branches are produced at higher conversions (35% for 1% I-TIPNO vs. 50% for 2% I-TIPNO). Table 10.5 shows the corresponding branching information for this run. It can be seen that g' varies in the range of 0.189-0.991 and g in the range of 0.109-0.988. Effect of I-TIPNO percentage on branch frequency is shown in Figure 10.20. It can be seen that branch frequency increases with conversion for both runs; however, the run with higher percentage of I-TIPNO produces branched polystyrene with lower branching frequencies. The gelation is delayed for the case of higher I-TIPNO, as expected and was observed previously in Chapter 9 (see subsection 9.4.2.2). On the other hand, at gelation point, branching frequency and branching number are higher than in the case of 1% I-TIPNO. This could be due to the fact that at higher conversions, higher % of I-TIPNO also contributes to branching, as will be discussed in detail below.

Table 10.5 Branching characteristics for controlled radical copolymerization of STY with 1% DVB and 2% I-TIPNO

Time (hr)	Conv.	Mn	Mw	PDI	$[\eta]$	g'	g	$\bar{n}$	λ
4.5	0.507	12,050	16,982	1.41	0.127	0.991	0.988	0.51	0.20
6.5	0.612	17,677	30,479	1.72	0.164	0.838	0.790	2.96	0.62
10	0.729	26,686	83,046	3.11	0.245	0.606	0.513	10.83	1.06
12.5	0.788	31,931	191,048	5.98	0.337	0.456	0.351	24.59	1.27
14.5	0.795	40,813	497,367	12.19	0.509	0.344	0.241	67.35	1.29
17	0.834	70,160	1.07E+06	15.24	0.487	0.189	0.109	610.93	10.85

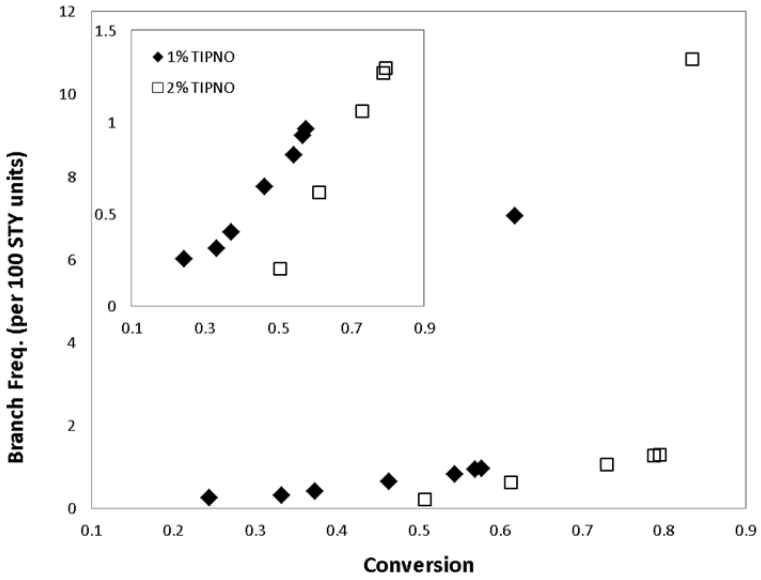

Figure 10.20 Effect of % I-TIPNO on branch frequency vs. conversion data for controlled radical copolymerization of styrene with 1% DVB

Figure 10.21 compares the weight average molecular weight vs. conversion plot from this experiment with controlled radical homopolymerization of STY with 2% I-TIPNO, one can see that, in the initial stages of the reaction, the copolymerization reaction follows the linear increase in molecular weights with conversion, however, at about 50% conversion, deviation from linearity emerges.

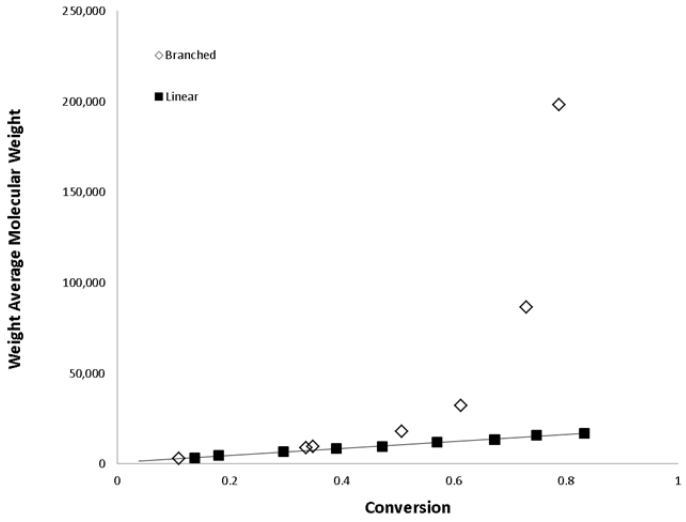

Figure 10.21 Weight average molecular weight vs. conversion for branched and linear polystyrene synthesized through controlled radical polymerization with 2 % I-TIPNO

The corresponding GPC chromatograms for STY copolymerization with 1% DVB and 2% I-TIPNO and STY homopolymerization with 2% I-TIPNO are shown in Figure 10.22. Figure 10.22a shows the chromatograms at 10% conversion; as can be seen, the presence of DVB does not show any effect on the Refractive Index (RI) signal. However, at 50% conversion (see Figure 10.22b), one can see a shoulder at lower retention volumes which corresponds to branching because of the presence of DVB. At around 85% conversion, the system with DVB is gelled, which results in a significant broadening in the RI signal (see Figure 10.22c).

It is interesting to notice that the RI signal for the system without DVB also shows a slight shoulder at this conversion, which could be an indication of low levels of branching. This shoulder was not observed in the case of homopolymerizaion of styrene with 1% I-TIPNO until around 93% conversion. It can be seen from Figure 10.23a that for 1% I-TIPNO, there is no evidence of branching at 92% conversion. There is a broadening in the signal at 93% conversion, and a more prominent shoulder at 95%. However, for 2% I-TIPNO (Figure 10.23b), there is a noticeable shoulder appearing at 87% conversion, which becomes very prominent (and a lot more relative to Figure 10.23a) as conversion increases.

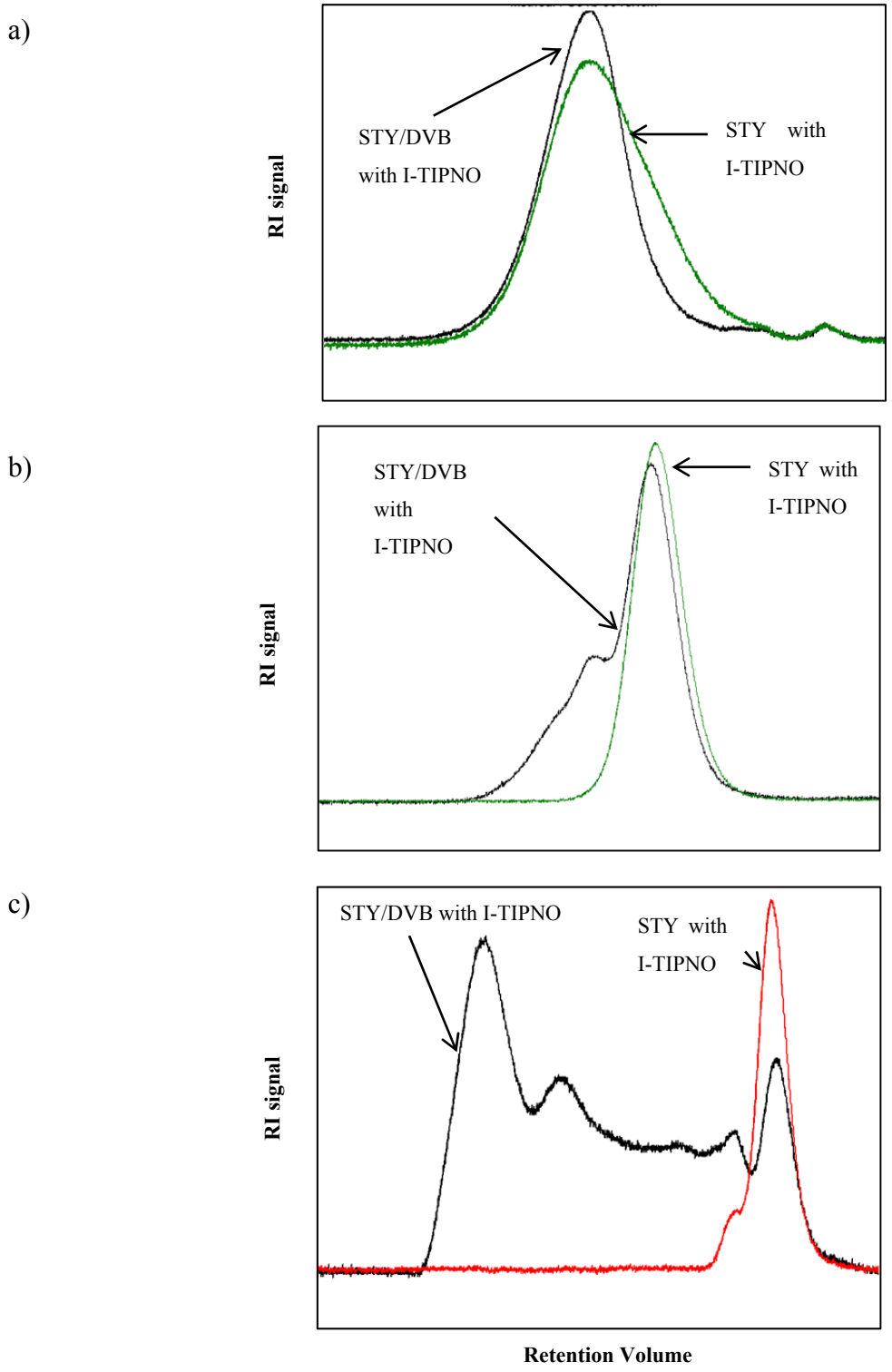

Figure 10.22 Comparison of GPC chromatograms of controlled copolymerization (1% DVB, 2% I-TIPNO) and controlled polymerization of styrene (2% TIPNO), a) at 10% conversion, b) at 50% conversion, and c) at 85% conversion

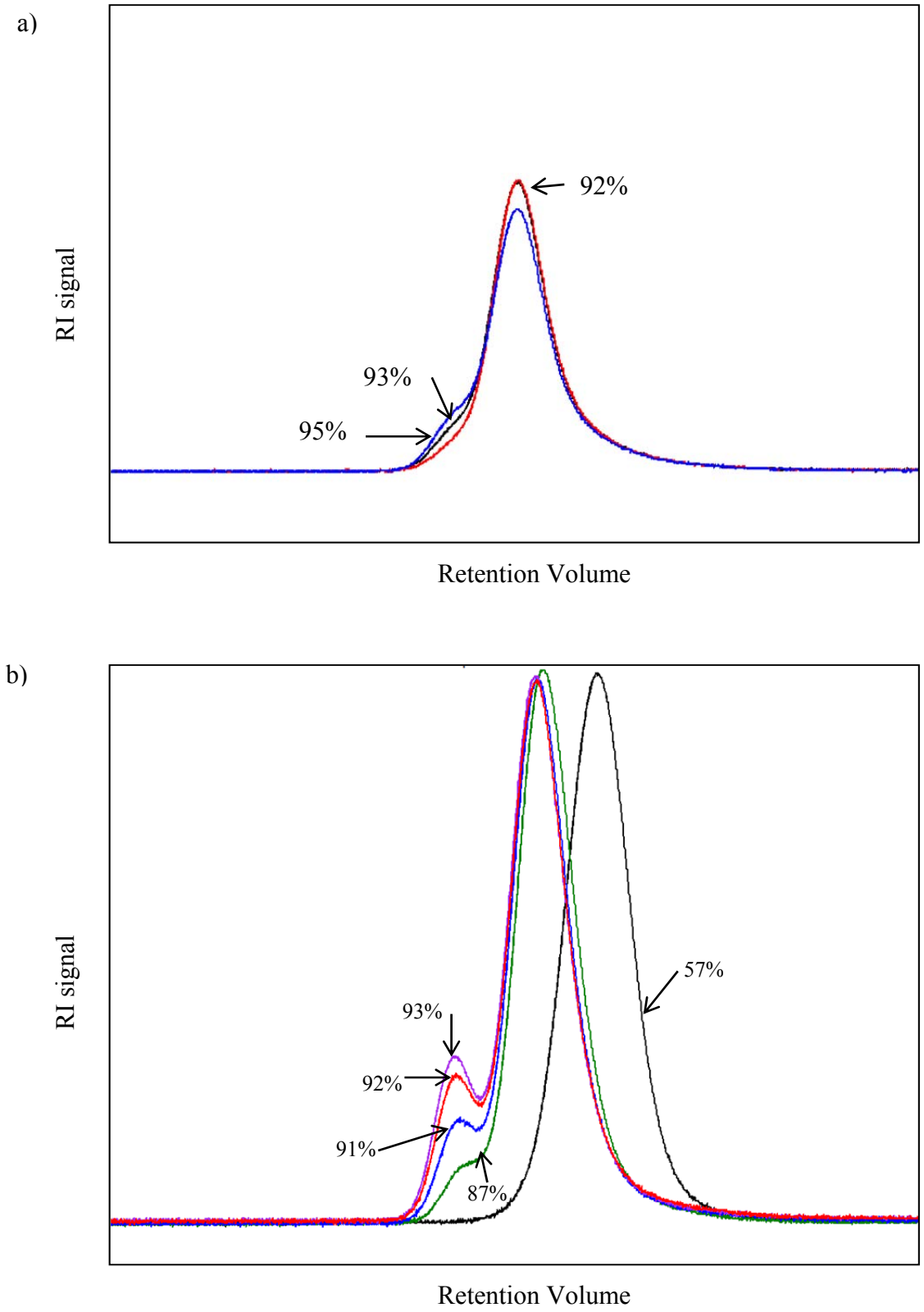

Figure 10.23 GPC chromatograms for polystyrene synthesized through controlled radical polymerization with a) 1% TIPNO, b) 2% TIPNO, at different conversions

Marx et al. (2009) synthesized different TIPNO-based alkoxyamines and showed that polymerizing styrene with a styrenic alkoxyamine (structure **(1)** in Figure 10.24) will result in branched polystyrene at conversions higher than 30%, as illustrated in Figure 10.24. Having first established the reproducibility of the obtained results in Figure 10.23 (i.e., the observed shoulders are not artifacts of error), our explanation is as follows. During polymerization of styrene with I-TIPNO, at low to moderate conversion levels, the preference is the addition of styrene units to the growing radical, due to the abundance of styrene vinyl bonds. Hence, structure **(1)**, even if present in nominal amounts (almost as impurity), might be transformed into linear TIPNO-end-capped styrenic macromolecules (structure **(2)** in Figure 10.24). However, at higher conversion levels (certainly higher than 70-80%, based on experience by analogy with other polymerizations), where the concentration of styrene monomer (and hence styrenic vinyl double bonds) is decreased, the concentration of terminal double bonds of structure **(2)** will be relatively higher, to the point that these terminal double bonds will become competitive for radicals, and hence the presence of structure **(2)** might start producing branched polystyrene molecules. This could certainly explain the appearance of a growing shoulder at higher molecular weights in the GPC traces (at very high conversion levels, above 92% for 1% I-TIPNO, as in Figure 10.23a, and at lower conversion levels, around 85%, as seen in Figure 10.23b for 2% I-TIPNO). In the next step, we tried to check with the I-TIPNO supplier, Sigma Aldrich, who could not enlighten us further but did not deny the fact that there might be very low levels or traces of other reactive admixtures in such a chemical (e.g., the purity is reported as 99+%, with the possibility of the remaining 0.5-1% to be reactive, very much so as admixtures of 0.5-1% of diacrylates or dimethacrylates that might be present in 99+% pure butyl acrylate on a regular basis).

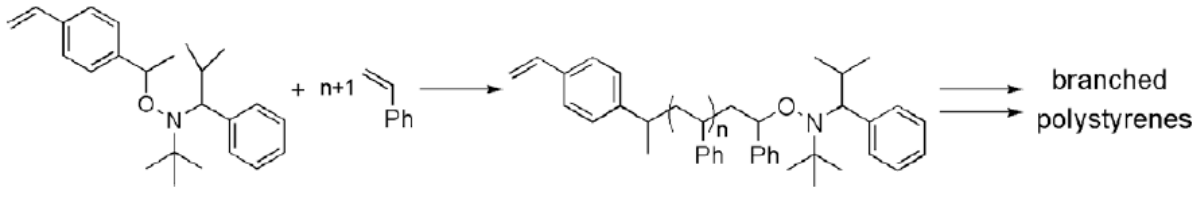

(1) **(2)**

Figure 10.24 Synthesis of branched polystyrene with styrenic TIPNO-based alkoxyamine (Marx et al., 2009)

In the next step, we tried to see if we could find any corroborating evidence from the TIPNO literature at large. In all the research conducted previously in the literature, polymerization had been stopped before high conversions were reached and that could explain why production of branched polystyrene with TIPNO (or I-TIPNO) at higher conversions was never reported or observed before. Hence, in our next forensic step, we decided to resort to NMR. Figure 10.25 shows the NMR spectrum of TIPNO in deuterated chloroform. The insert in the middle magnifies the region between 4.6 to 6.2 ppm. As can be seen in the insert, there is a double peak appearing around 5.6 ppm along with the multiplet at ~ 5.2 ppm, which correspond to the presence of two of the vinylic protons in structure **(1)** of Figure 10.24 (the third proton appearing around 6.6 ppm in the NMR spectrum is not evident in the insert of Figure 10.24 but magnifying the figure one can observe it). Hence, one can postulate/speculate with more certainty now that the purchased TIPNO from Sigma Aldrich did indeed contain small amounts of structure **(1)** of Figure 10.24. Therefore, one can conclude that shoulders observed at higher conversions, in the GPC traces for polymerization of styrene with TIPNO, could be attributed to branched polystyrene produced due to the presence of small amounts of structure **(1)**, present in the TIPNO mixture.

What is left as a confirmation exercise in future work is the further purification of TIPNO (following typical purification methods such as precipitation/recrystallization, or chromatography). GPC chromatograms from polymerization using purified TIPNO can then be compared to the high conversion results of Figure 10.23 (with TIPNO as received). We are in contact with Sigma Aldrich in order to coordinate such a comparison.

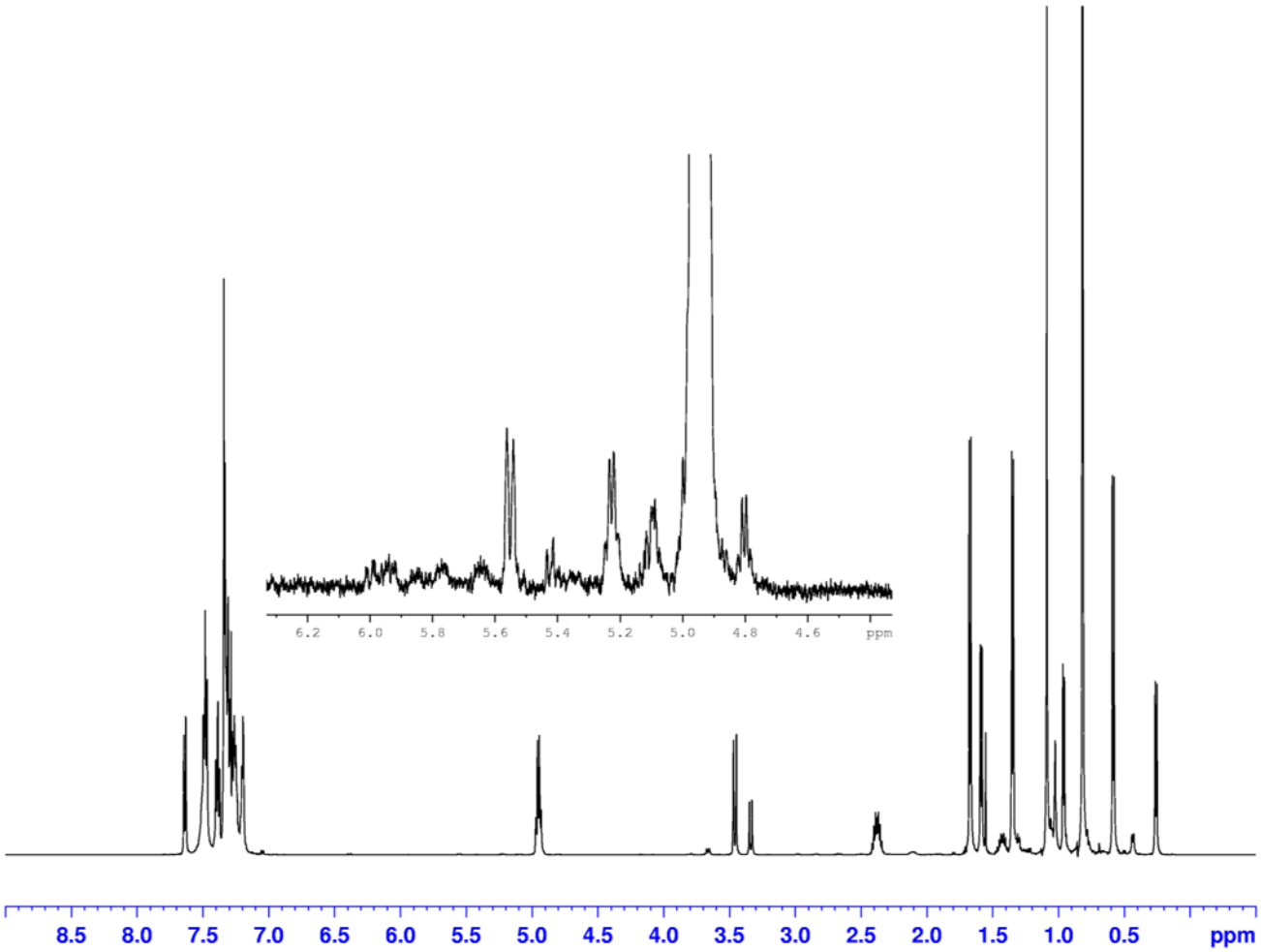

Figure 10.25 H-NMR spectrum of I-TIPNO recorded in deuterated chloroform (performed by the author)

The results discussed so far indicate that both I-TIPNO and DVB percentages have significant effects on the branching characteristics. At 1% I-TIPNO, branching increased with the higher percentage of DVB. Figure 10.26 illustrates the same trend at 2% TIPNO; higher percentage of DVB results in higher branching frequencies and earlier gelation. Table 10.6 shows the branching information for controlled radical copolymerization of STY with 1.5% DVB and 2% I-TIPNO. It can be seen that g' varies in the range of 0.162-0.791 and g in the range of 0.108-0.731.

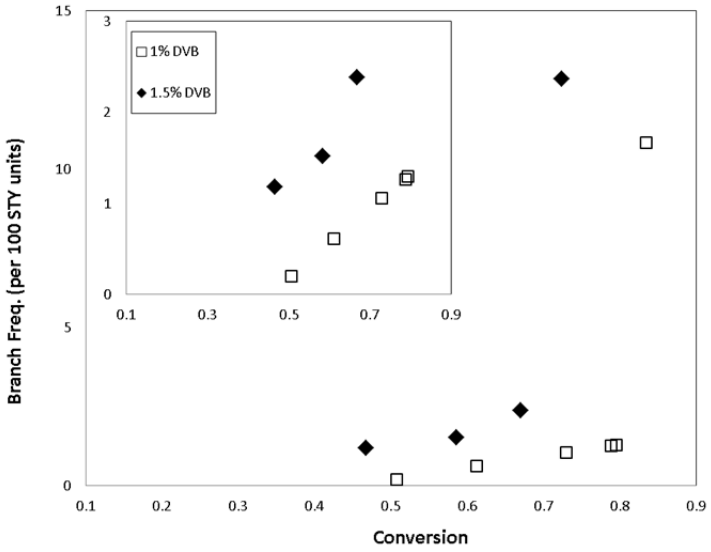

Figure 10.26 Effect of % DVB on branch frequency vs. conversion data for controlled radical copolymerization of styrene with 2% I-TIPNO

Table 10.6 Branching characteristics for controlled radical copolymerization of STY with 1.5% DVB and 2% I-TIPNO

Time (hr)	Conv.	Mn	Mw	PDI	$[\eta]$	g'	g	$\bar{n}$	λ
4	0.467	11,416	18,527	1.62	0.108	0.791	0.731	3.74	1.19
6	0.585	18,700	54,452	2.91	0.181	0.610	0.517	10.78	1.52
8	0.670	30,699	348,115	11.34	0.366	0.320	0.219	69.03	2.38
10	0.723	34,714	1.09E+06	31.51	0.424	0.162	0.088	232.96	12.85

Figure 10.27 illustrates the effect of I-TIPNO percentage at 1.5% DVB. In the same way as for the case of 1% DVB, gelation is delayed for the higher percentage of I-TIPNO. However, due to lack of lower conversion data for the run with higher I-TIPNO, it is difficult to state whether

the trends are the same as in the case of 1% DVB. What is evident is that at 50% conversion, the run with lower I-TIPNO produces polystyrene with higher branching frequencies. The run with 1% I-TIPNO illustrates higher branching frequency at the gel point, compared to the run with 2% TIPNO ($\lambda_{(1\%\ \text{I-TIPNO})} = 20.09$ vs. $\lambda_{(2\%\ \text{I-TIPNO})} = 12.85$, in Figure 10.27 around the gel point). This trend is reversed when comparing the branching frequencies at the gelation point with 1% DVB ($\lambda_{(1\%\ \text{I-TIPNO})} = 7.06$ vs. $\lambda_{(2\%\ \text{I-TIPNO})} = 10.85$, in Figure 10.20 around the gelation point). The reason could be that the gel point for 1% DVB and 2% I-TIPNO occurred at 85% conversion, which is around the conversion level where I-TIPNO itself also contributes to branching (see Figure 10.22c and Figure 10.23b). On the other hand, the gel point for 1.5% DVB and 2% I-TIPNO occurred around 72% conversion, which is below the conversion level at which TIPNO itself contributes to branching.

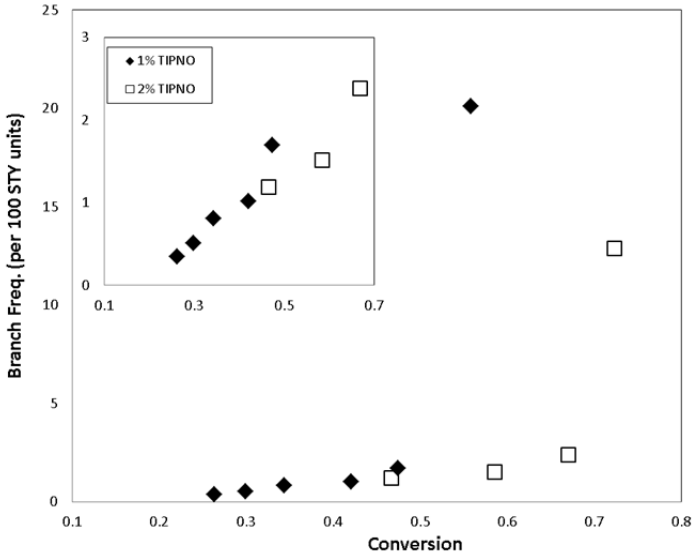

Figure 10.27 Effect of % TIPNO on branch frequency vs. conversion data
for controlled radical copolymerization of styrene with 1.5 % DVB

Table 10.7 shows a summary of the runs with different combinations of low and high % TIPNO and % DVB. Figure 10.28 summarizes the branching frequency vs. conversion data for all the runs. The red window in Figure 10.28 looks at all the runs at 50% conversion. Branching frequency for run 6 is the highest, followed by run 7, run 4 and then run 5 (see also the last column in Table 10.7). As for the gelation point, run 6 gels earliest (higher DVB and lower I-TIPNO), followed by run 4, run 7 and run 5 (lower DVB and higher I-TIPNO) (see the

4th column of Table 10.7). This is in agreement with observations presented in Chapter 9 (see Subsection 9.4.2.4). However, the branching frequency at the gelation point (5th column in Table 10.7) does not follow the exact order of the gelation point occurrence. Runs with higher % DVB produce higher branching frequency at the gel point (run 6 followed by run 7), the next high branching frequency belongs to run 5 (1% DVB and 2% I-TIPNO), and finally the lowest branching frequency at gelation belongs to run 4.

Table 10.7 Summary of runs

Run	% DVB	% TIPNO	[DVB]/[TIPNO] molar ratio	x @ gelation	λ @ gelation	λ @ x= 50%
4	1	1	2.5	0.617	7.06	0.82
5	1	2	1.25	0.834	10.85	0.20
6	1.5	1	3.75	0.558	20.09	1.70
7	1.5	2	1.87	0.723	12.85	1.19

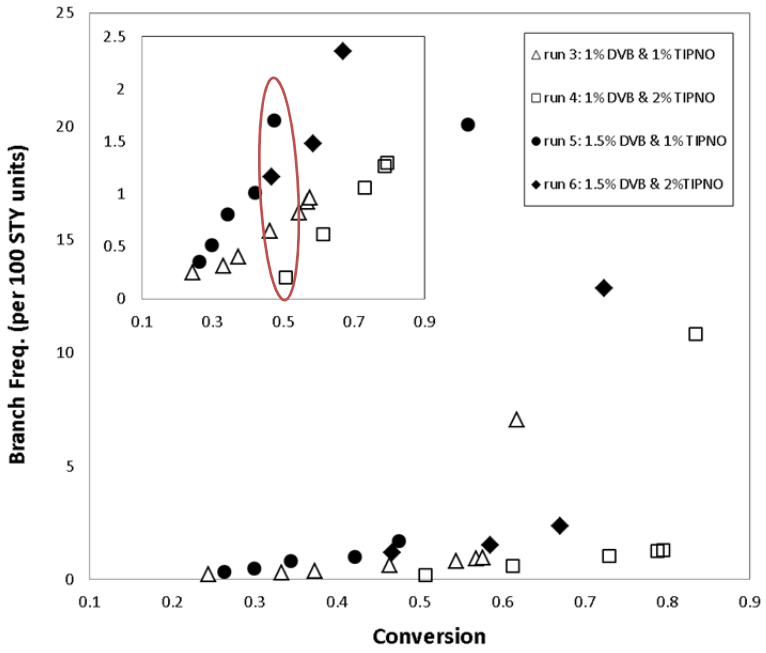

Figure 10.28 Branch frequency vs. conversion data for controlled radical copolymerization of styrene with different levels of I-TIPNO and DVB

10.3.2 Thermo-Mechanical Analysis

In this subsection thermal and mechanical properties of polymer networks synthesized through nitroxide-mediated radical polymerization (NMRP) are compared to networks synthesized through regular free radical polymerization (FRP). Both thermal and mechanical properties of a polymer can give insight into its molecular structure. The first part covers discussion on the results of Differential Scanning Calorimetry (DSC) tests on our polymer samples while the second part discusses the results of Dynamic Mechanical Analysis (DMA).

10.3.2.1 Differential Scanning Calorimetry (DSC)

DSC is used to differentiate between cross-linked polystyrene (PS) synthesized through nitroxide-mediated radical polymerization (NMRP) and PS cross-linked through regular free radical polymerization. Table 10.8 summarizes the DSC results; Runs 3 and 3B are synthesized through NMRP with 1% I-TIPNO and 1% DVB, whereas run 2B is synthesized through regular radical polymerization with 1% DVB only. Comparisons are carried out at two different conversion levels, namely, around 65% (2B-10 vs. 3B-2 and 3-11) and 96% conversion level (2B-12 vs. 3-15 and 3-16). Samples at lower conversion levels have different % gel, whereas samples at higher conversion have almost the same amount of gel. It was decided that the comparisons would be more meaningful at about the same gel level. It can be seen that using a nitroxide in the copolymerization of styrene (STY) with divinyl benzene (DVB) resulted in a shift of T_g to lower temperatures. At around 65% conversion level, T_g has shifted from 107.83 °C for 2B-10 to 103.62°C for 3B-2 and 3-11. On the other hand, at 97% conversion, T_g has shifted from 106.80 °C for 2B-12 to 96.43°C and 97.58 °C for 3-15 and 3-16, respectively.

Table 10.8 DSC results of PS cross-linked with 1% DVB; comparison between NMRP cross-linking (Run 3 and 3B; 1% TIPNO) and regular radical cross-linking (Run 2B)

Sample	% I-TIPNO	x	% Gel	T_B (T_g) ºC	ΔT_g ºC	ΔH (W/g)	ΔC_p (J/ºC.g)	Slope (W/g. ºC)
2B-10	-	0.62	100	107.83	5.17	0.0564	0.3408	-9.58E-03
3B-2	1	0.64	40	103.63	5.56	0.0562	0.3390	-8.97E-03
3-11	1	0.67	50	103.62	4.79	0.0544	0.3273	-1.00E-02
2B-12	-	0.97	100	106.80	5.36	0.0563	0.3400	-9.45E-03
3-15	1	0.96	93	96.43	10.93	0.0510	0.3056	-4.04E-03
3-16	1	0.97	95	97.58	10.75	0.0538	0.3224	-4.78E-03

x: conversion;; T_B (T_g): point where half of the specific heat increment has occurred, used as indicator of T_g (as a reminder, refer to Figure 10.6); $\Delta T_g = T_C - T_A$, where T_A is onset and Tc is the end of transition; ΔH: change in heat flow; ΔC_p: change in heat capacity; Slope: slope of the transition line.

Additional information such as ΔT_g, ΔH, ΔC_p and slope of the transition line have also been calculated from the DSC curves in order to obtain information related to network uniformity. Figure 10.29 shows typical results extracted from DSC (sample 2B-12). The top curve shows heat capacity behavior, while the lower curve captures the heat flow. T_g is determined from the heat flow plot and the slope of the transition and the range of T_g are indicated on the plot. It can be seen in Table 10.8 that at 97% conversion the slope of the transition line is almost twice in the case of regular radical polymerization (e.g., FRP: -9.45×10^{-3} vs. NMRP: -4.78×10^{-3}). This is also confirmed by the ΔT_g results, with ΔT_g for 2B-12 being almost half of the ones for samples 3-15 and 3-16. These results indicate that the transition is sharper for 2B-12 and occurs in a narrower temperature range, which suggests a more uniform polymer network when compared to 3-15 and 3-16. In the cases of the data for ΔH and ΔC_p, the values for all three samples are fairly close to each other and it is difficult to make a comment just by looking at the numbers. However, by running statistical tests (discussed below), it was concluded that there was indeed no difference between the data for ΔH and ΔC_p.

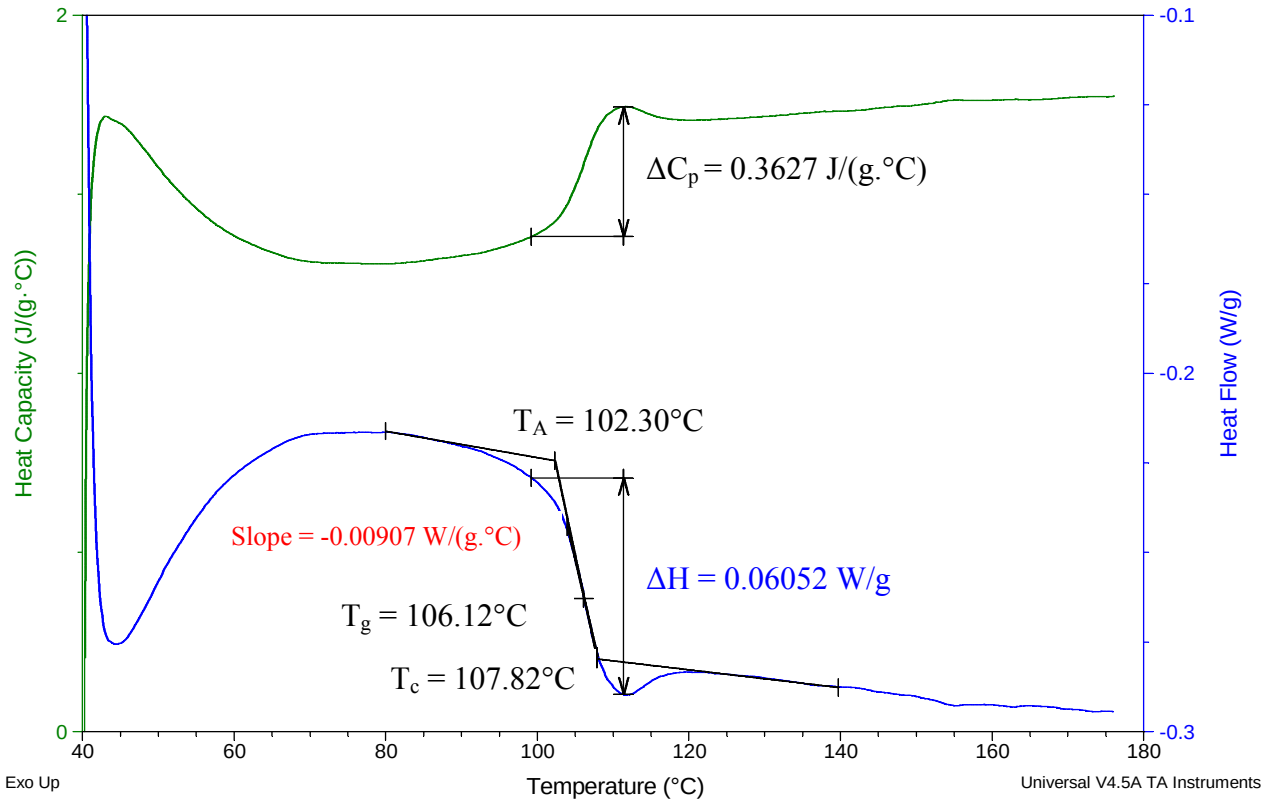

Figure 10.29 Typical results extracted from a DSC run (2B-12)

For samples around 65% conversion, it is not possible to visually distinguish the differences between values of ΔT_g, ΔH, ΔC_p and slope of the transition line. Hence, formal statistical hypothesis testing has been carried out to make an inference for differences in the values of Table 10.8. Table 10.9 summarizes the statistical hypothesis testing carried out to compare if the values of ΔT_g, ΔH, ΔC_p and slope of the transition line for sample 2B-10 are different from the values of sample 3B-2. The four readings from DSC for each sample are shown in Table 10.9 along with the sample average and variance. For example, to compare the ΔT_g values of 2B-10 and 3B-2 (see column 3 of Table 10.9), the null hypothesis stated is $H_0 : \mu (\Delta T_{g\,(2B\text{-}10)}) - \mu (\Delta T_{g\,(3B\text{-}2)}) = 0$ and tested against the alternative hypothesis of $H_1 : \mu (\Delta T_{g\,(2B\text{-}10)}) - \mu (\Delta T_{g\,(3B\text{-}2)}) \neq 0$. In all the calculations it is assumed that the distribution variances are the same but unknown, hence two sample variances are pooled to form an estimate of distribution variance (S_p^2). For example, for ΔT_g:

$$S_p^2 = \frac{6.79E-02 + 2.19E-01}{2} = 1.43\text{E}-01 \quad \text{Eq. 10.22}$$

t_{obs} for the hypothesis testing is calculated as:

$$t_{obs} = \frac{\overline{X_1} - \overline{X_2}}{S_p\sqrt{\frac{1}{n_1}+\frac{1}{n_2}}} = \frac{5.17 - 5.56}{\sqrt{1.43E-01\,(\frac{1}{4}+\frac{1}{4})}} = -1.47 \quad \text{Eq. 10.23}$$

t_{obs} calculated is now compared to values read from the t distribution with $n_1 + n_2 - 2$ degrees of freedom. In our study, for a 95% confidence level, t_{obs} is contrasted against $t_{6,\,0.025} = 2.45$. If $|t_{obs}| > t_{6,0.025}$, reject the null hypothesis and conclude that the two values compared are different. On the other hand, if $|t_{obs}| < t_{6,0.025}$, we fail to reject the null hypothesis and conclude that the two values compared are the same. In the case of comparing ΔT_g values for samples 2B-10 and 3B-2, $|-1.47| < 2.45$, hence we failed to reject the null hypothesis and concluded that the two values are the same. The other hypothesis tests for ΔH, ΔC_p and slope of the transition line are also shown in Table 10.9. As can be seen, all the hypothesis tests fail to reject the null. Therefore, it is concluded that all the values are statistically the same, and it is not possible to conclude through DSC testing if 2B-10 has a more uniform network compared to 3B-2 (as seen for 2B-12 vs. 3-15 and 3-16). The only statement that can be made based on the DSC data is that sample 2B-10 has a higher T_g compared to 3B-2. The comparison table for 2B-10 and 3-11 is shown in Subsection G.1 in Appendix G and the conclusion is the same, i.e., again it is not possible to differentiate between 2B-10 and 3-11 through DSC measurements.

Table 10.9 Comparison of DSC data for 2B-10 and 3B-2 of Table 10.8

Sample	Stat. indicator	ΔT_g °C	ΔH (W/g)	ΔC_p (J/°C.g)	Slope (W/g.°C)
2B-10		5.53	0.0634	0.3862	-0.00989
		4.91	0.0531	0.3202	-0.00991
		5.1	0.0543	0.3258	-0.00888
		5.13	0.0549	0.3310	-0.00962
	average	5.17	0.0564	0.3408	-9.58E-03
	variance	6.79E-02	2.22E-05	9.36E-04	2.31E-07
3B-2		5.96	0.0582	0.3520	-0.00882
		5.97	0.0555	0.3366	-0.00792
		5.15	0.0569	0.3408	-0.00976
		5.16	0.0542	0.3266	-0.00936
	average	5.56	0.0562	0.3390	-8.97E-03
	variance	2.19E-01	3.00E-06	1.11E-04	6.35E-07
	S_p^2	1.43E-01	1.26E-05	5.23E-04	4.33E-07
	$\mathbf{t_{obs}}$	-1.47	0.09	0.11	-1.31
	$\mathbf{t_{6,\ 0.025}}$ **= 2.45**	Fail to reject	Fail to reject	Fail to reject	Fail to reject

In conclusion, DSC measurements showed that the presence of nitroxide in cross-linked polymerization of styrene with DVB shifts the glass transition to lower temperatures. This overall observation was expected. At around 65% conversion, there was no difference detected between FRP and NMRP for the values of ΔT_g, ΔH, ΔC_p and slope of the transition line. However, at 97% conversion, FRP samples exhibited lower ΔT_g, and sharper slope of transition line compared to NMRP samples, which could be an indicator of FRP samples having a more homogeneous polymer network. This was not as expected and, in fact, somewhat surprising.

10.3.2.2 Dynamic Mechanical Analysis (DMA)

To investigate the structure of the networks prepared through nitroxide-mediated radical polymerization (NMRP) and regular free radical polymerization (FRP), dynamic mechanical analysis was carried out on samples from both NMRP and FRP of styrene with 1% DVB. Table 10.10 summarizes the information of these samples. As can be seen, an attempt was made to compare samples at similar (practically speaking, the same) conversion levels; in the last comparison, 2B-12 with 3-15 and 3-16, all three samples were also at a similar % gel. To check the reproducibility of the results, a separate specimen was made for each polymer sample and independent measurements were carried out. Figure 10.30 shows tan δ and storage modulus data for two independent DMA measurements of sample 2B-10. Subsection G.2 in Appendix G contains additional figures showing the replicates for other samples.

Table 10.10 Summary of conversion and % gel for DMA samples

Sample	% I-TIPNO	x	% Gel
2B-10	-	0.62	100
3B-2	1	0.64	40
2B-12	-	0.97	100
3-15	1	0.96	93
3-16	1	0.97	95

Figure 10.30 shows the storage modulus and tan δ trends for cross-linked PS synthesized through FRP at 62% conversion (sample 2B-10). In order to eliminate the effect of sample geometry, storage modulus values were normalized by dividing each value with the starting storage modulus. As can be seen, both tan δ and storage modulus trends of two independent replicates are in good agreement. The modulus behavior was well captured over a temperature range of 60 to 140°C; both curves decreased from a glassy state value of $\sim 1.7 \times 10^9$ Pa to a rubbery state value of $\sim 1.8 \times 10^6$ Pa. The storage modulus in the rubbery region is an indication of the crosslinking density of the network. Tan δ distributions were also fully captured; width (breadth) at half maximum height (WHM) has been used as an indicator for

the breadth of the tan δ distribution. For sample 2B-10, WHM is 11.27 °C while WHM = 10.88 °C for the replicate; as observed, the WHM values are very close to each other and tan δ data are reproducible. The same agreement between replicates has also been shown in all independent determinations of Appendix G.

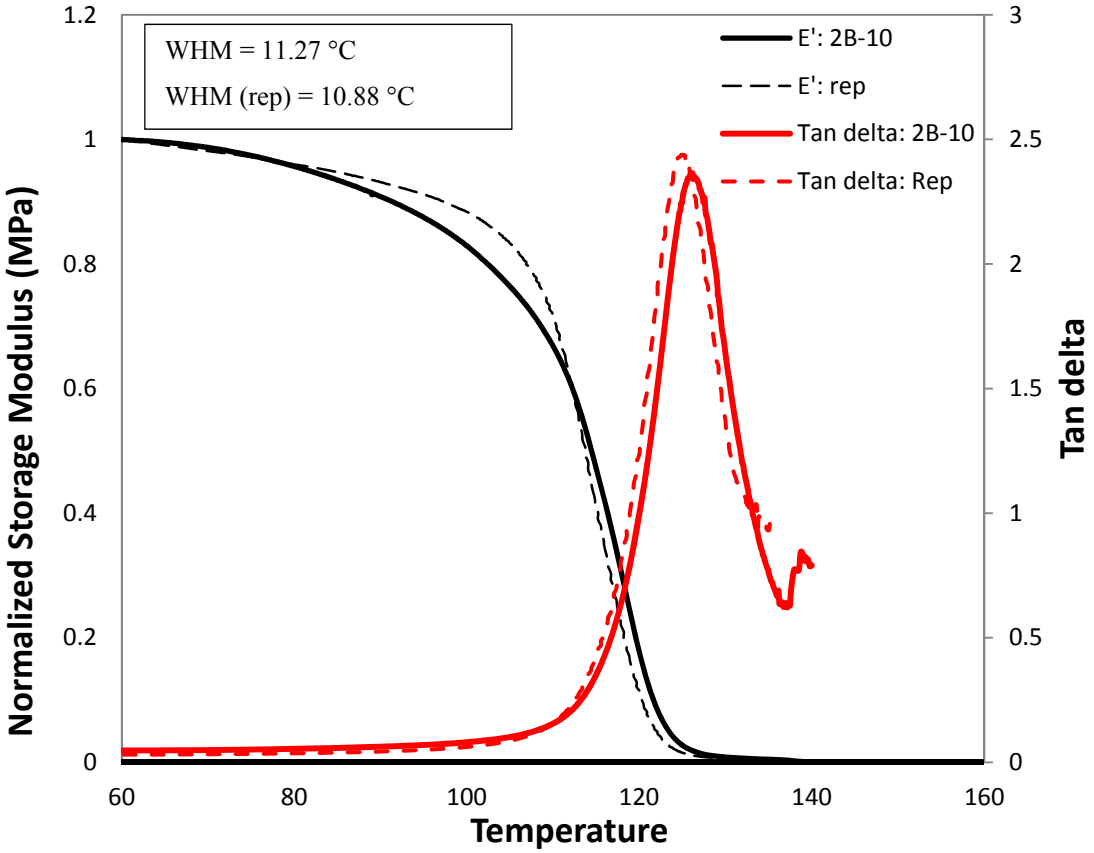

Figure 10.30 Storage modulus and Tan delta for cross-linked PS at 62% conversion, synthesized through regular radical polymerization with 1% DVB (sample 2B-10)

Figure 10.31a compares samples 2B-10 (regular free radical (FRP) with 1% DVB) and 3B-2 (a sample synthesized through NMRP at the same conversion level and DVB level, but with 1% I-TIPNO). FRP is much faster that NMRP, and gels earlier than NMRP; as a result, although the samples are at the same conversion level, they have different gel content (see Table 10.10). It can be seen from Figure 10.31a that the storage modulus for the NMRP sample (sample 3B-2), which has a lower % gel, is lower. This trend is as expected; as % cross-linking decreases, the molecular weight between cross-links (M_c) increases. For example, the molecular weight between cross-links for 2B-10 (higher % gel) is $M_c = 2.62 \times 10^4$, whereas for sample 3B-2

(lower % gel), $M_c = 4.52 \times 10^5$. Based on Eq. 10.20, storage modulus is inversely proportional to M_c, therefore since $M_{c\,(3B-2)} > M_{c\,(2B-10)}$, then $E'_{2B-10} > E'_{3B-2}$.

In addition to having a lower storage modulus, the dramatic drop in storage modulus corresponding to glass transition is also shifted to lower temperatures for the NMRP sample (sample 3B-2). This result is again in agreement with the DSC data (see column 5 of Table 10.8 for 2B-10 and 3B-2), although the glass transition temperature (T_g) determined through DMA is higher than the one from DSC data. This behavior is expected and has been mentioned before by Nielsen and Landel (1994). Figure 10.32a and b compare the glass transition temperature determined through DMA and DSC for samples 3B-2 and 2B-10, respectively. It can be seen that T_g determined through DMA is almost 10 °C higher than the one determined through DSC for both 3B-2 and 2B-10.

Figure 10.31a also shows tan δ peaks for samples 3B-2 and 2B-10. It can be seen that, as for the storage modulus, the tan δ peak is also shifted towards lower temperatures for the sample synthesized through NMRP (sample 3B-2). Figure 10.31b shows the superposition of the two tan δ distributions. It can be seen that the width at maximum height (WHM) is larger for 3B-2 (sample synthesized through NMRP); $WHM_{(NMRP)}$ = 13.01 °C vs. $WHM_{(FRP)}$ = 11.27 °C. At first glance, one might argue that the differences between the two distributions of Figure 10.31b are within the error of the dynamic mechanical analyzer. However, the error in WHM has been estimated from independent replication (see Figure 10.30, and G.1, G.2 and G.3 of Appendix G) and is around $\pm$0.8 °C (the estimate of σ is s = 0.4 °C). The difference between the WHM values from samples 3B-2 and 2B-10 is 1.74 °C, which is higher than the error associated with the DMA instrument. Hence, one can conclude that the sample synthesized through NMRP has a broader distribution compared to the sample from FRP and this could be an indicator that the former sample has a more heterogeneous polymer network compared to the latter. This was not as expected and, in fact, somewhat surprising, as the difference between samples 2B-10 and 3B-2 with respect to the homogeneity of the network was not detected through the DSC measurements (see Table 10.8). In addition, based on literature statements, we were expecting sample 3B-2 (NMRP) to show a more homogeneous network than 2B-10 (FRP).

a)

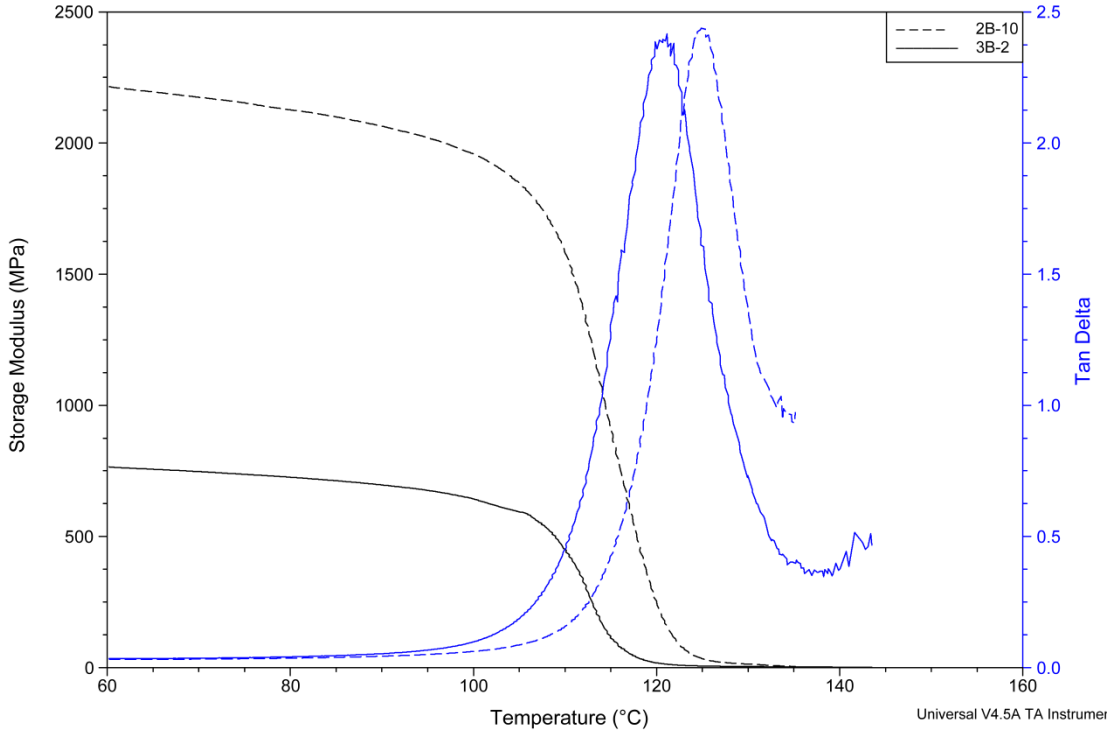

b)

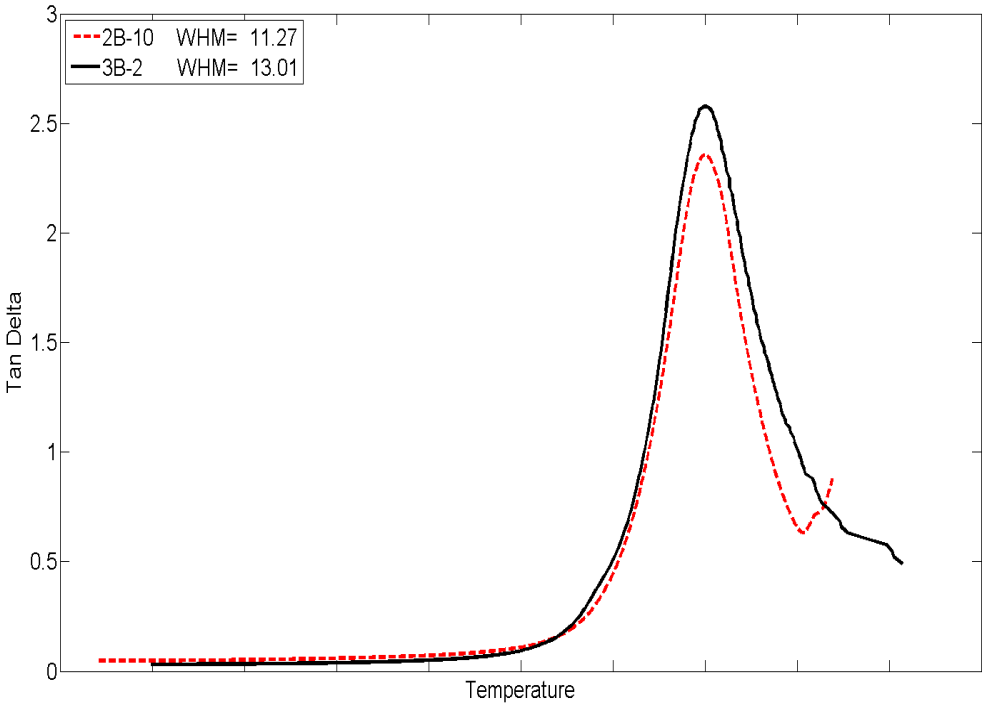

Figure 10.31 Storage modulus (a) and tan δ (b) versus temperature for samples prepared by NMRP (3B-2) and FRP (2B-10)

a)

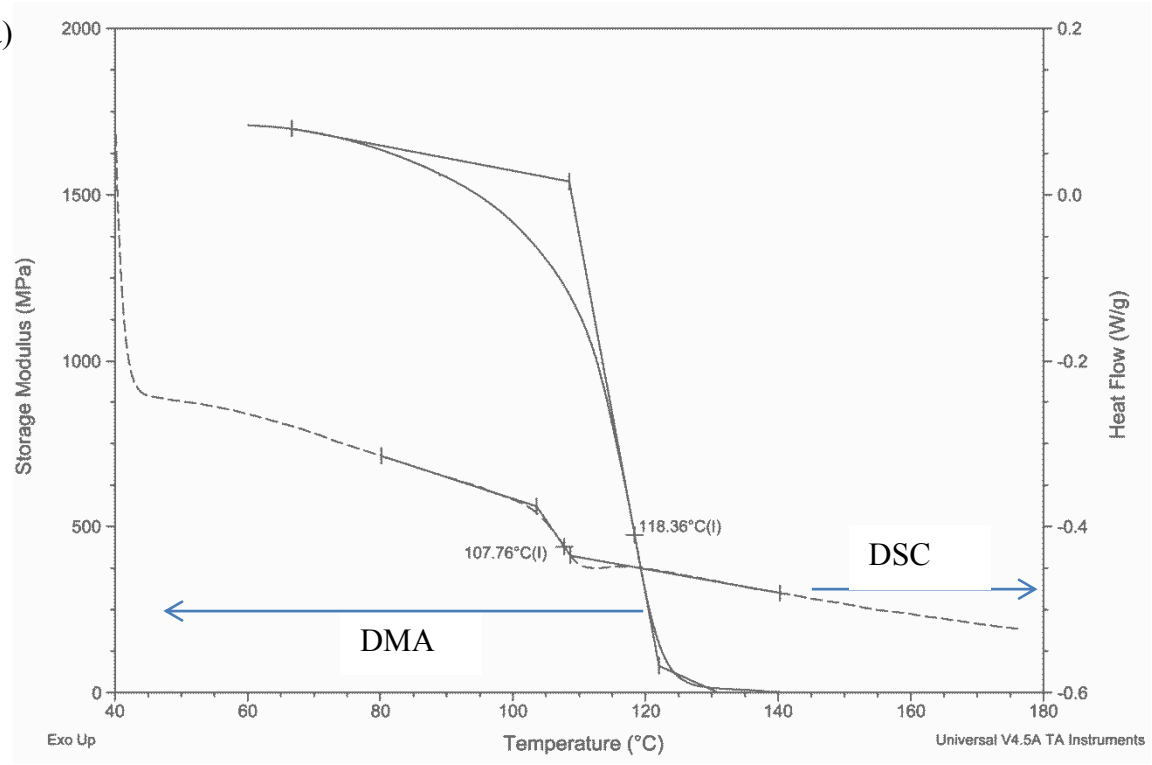

b)

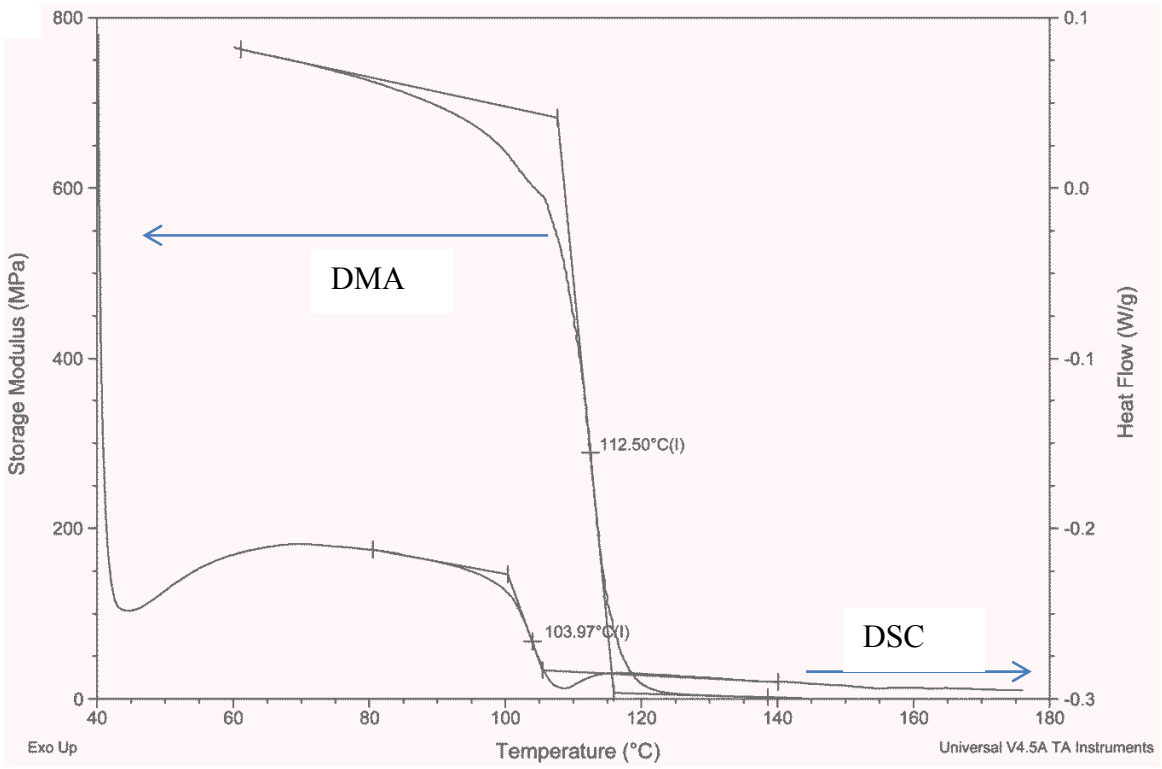

Figure 10.32 Comparison between glass transitions measured through DMA and DSC for a) 3B-2, b) 2B-10

Figure 10.33 shows the same comparison but between two samples that have the same conversion and the same gel content (see information for samples 2B-12 and 3-16 in Table 10.10). As can be seen in Figure 10.33a, the storage modulus is a bit higher for 3-16 but the difference between E's is not very significant, and one can argue that the difference is within the error for determining the storage modulus through DMA. This is a valid conclusion, as the two samples are at the same gel content and have fairly close M_c values ($M_{c(2B\text{-}12)} = 0.4 \times 10^4$ vs. $M_{c(3\text{-}16)} = 2 \times 10^4$), hence, based on Eq. 10.20, it is expected that they have almost the same E'. The same way as in the previous comparison (see Figure 10.31a), the drop in storage modulus due to glass transition is shifted to lower temperatures for the NMRP sample. This behavior was as expected and also observed in the DSC measurements; compare T_g values for 2B-12 and 3-16 in Table 10.8. Figure 10.33a also shows tan δ peaks for samples 3-16 and 2B-12. It can be seen that, as in Figure 10.31a, the tan δ peak for the sample synthesized through NMRP (sample 3-16) is also shifted towards lower temperatures. Figure 10.33b shows the superposition of the two tan δ distributions. It can be seen that, again as observed in Figure 10.31b, the width at maximum height (WHM) is larger for the sample synthesized through NMRP ($WHM_{(3\text{-}16)}$ = 14.39 °C vs. $WHM_{(2B\text{-}12)}$ = 11.85 °C). As discussed for Figure 10.31, a broader tan δ peak would be an indicator of a more heterogeneous polymer network (for the NMRP sample). These results are in agreement with the DSC measurements for samples 3-16 and 2B-12, where we measured a larger ΔT_g and a smaller slope of transition for the sample synthesized through NMRP (sample 3-16). The figure comparing samples 3-15 and 2B-12 is shown in Appendix G (see Figure G.4). The same trend and behavior as samples 3-16 and 2B-12 can be observed for samples 3-15 and 2B-12.

a)

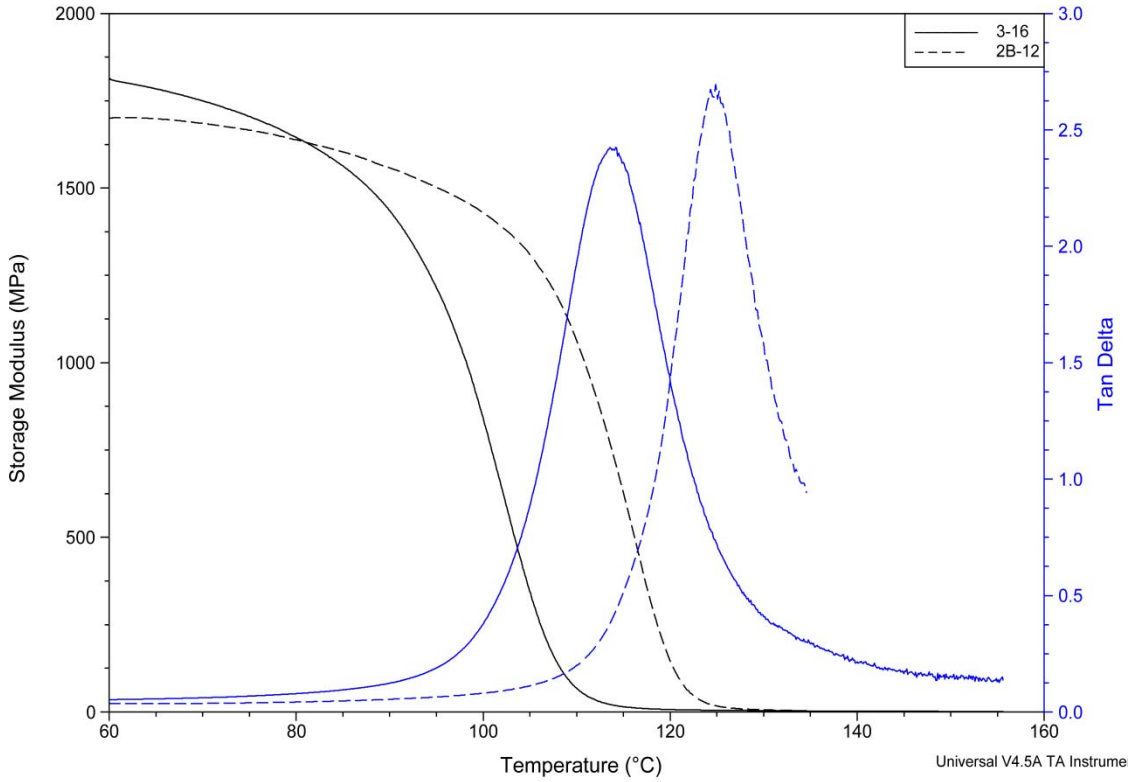

b)

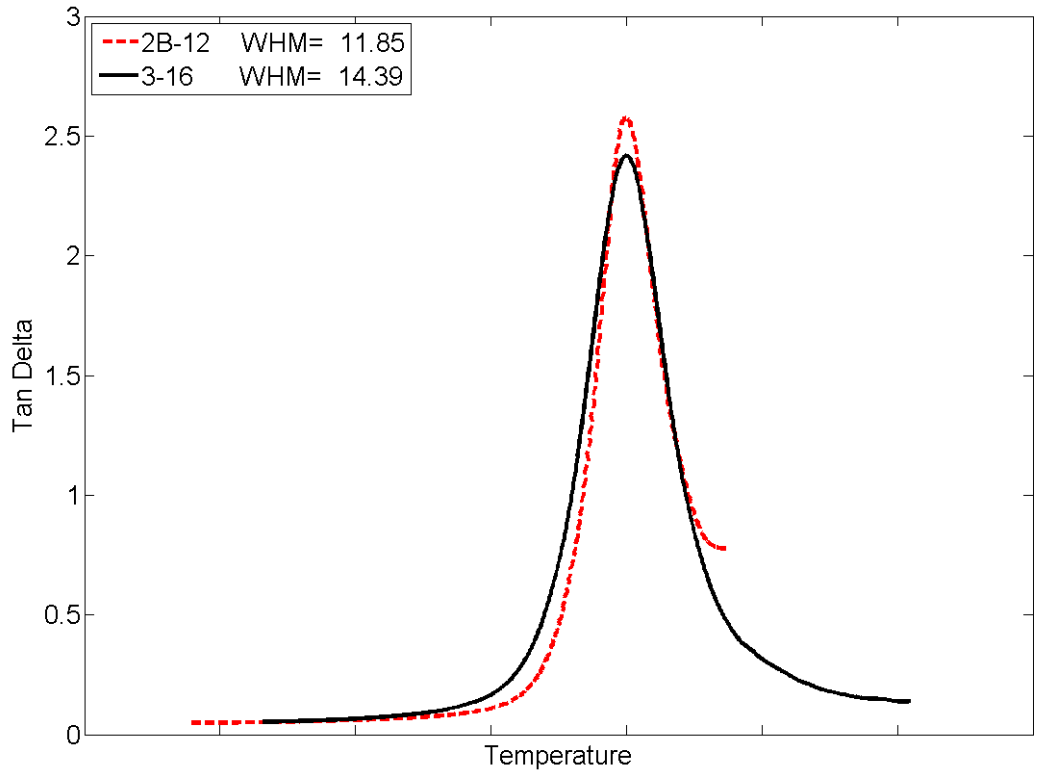

Figure 10.33 Storage modulus and tan δ versus temperature for samples prepared by NMRP (3-16) and FRP (2B-12)

10.3.2.3 Further Discussion and Concluding Remarks

Structural differences between samples synthesized through NMRP and FRP with 1% DVB have been investigated by means of thermo-mechanical measurements. A summary of our observations is cited in Table 10.11. Differential Scanning Calorimetry (DSC) is a reliable test to determine the glass transition temperature. Our DSC results showed that T_g values for NMRP samples were shifted to lower temperatures, compared to FRP samples (see the row of T_g(DSC) in Table 10.11for 64%, 97% and 96% conversions). The shift of T_g towards lower temperatures for NMRP samples was also observed by the Dynamic Mechanical Analysis (DMA) determinations. Both the drop in storage modulus and the maximum in the tan δ peak (corresponding to the glass transition region in DMA) were shifted towards lower temperatures (see "Drop in E'in glass transition region (DMA)" and "tan δ maximum (DMA)" entries in Table 10.11). This was as expected, since cross-linked samples under NMRP conditions should in principle have a looser network (higher M_c values) compared to cross-linked samples under FRP.

ΔT_g and the slope of the transition line in the heat flow curve measured in DSC reflect the fact that a polymer contains segments that could have different T_g values. A larger ΔT_g or a milder slope of the transition line are indicators for a broader glass transition region, hence revealing that the corresponding polymer could potentially have segments with low and high T_g values, and could thus be considered as a heterogeneous network (Nielsen and Landel, 1994). The measured ΔT_g values and the slopes of the transition lines for NMRP and FRP samples at lower conversions did not show any significant differences based on our formal statistical tests (see "ΔT_g (DSC)" entry for x~ 63 % in Table 10.11). However, for the samples at higher conversion levels that had the same gel content, the differences between ΔT_g values and the slopes of the transition lines for NMRP and FRP samples were remarkable and detected through the formal statistical tests (see "ΔT_g (DSC)" entries for x~ 97 % and x~ 96 % in Table 10.11). ΔT_g values measured through DSC for NMRP samples were twice the ΔT_g values measured for FRP samples, while the slope of transition for the former was half of the slope for the latter samples. These results could be an indicator that the networks synthesized through NMRP were in fact more heterogeneous than the networks synthesized through FRP, and this was not as expected!

The corresponding indicator in DMA determinations is the breadth of the tan δ peak. According to Nielsen and Landel (1994), the broadening of the tan δ peak is often assumed to be due to a broad distribution in molecular weights between cross-links or some other kind of heterogeneity in the network structure. Our results showed that the breadths of the tan δ peaks for the NMRP samples were larger (around 2 to 3 °C) than those of the tan δ peaks for the FRP samples (see "tan δ breadth-WHM (DMA)" entries in Table 10.11). Hence, our results are not in agreement with the results shown by Yu et al. (2007; 2009) and the claims by Ide and Fukuda (1999). Ide and Fukuda (1999) claimed that the DMA tests should show a narrower distribution for samples synthesized through NMRP. However, they never showed any experimental results to corroborate their claim. The results shown by Yu et al. (2007; 2009) were for samples synthesized through Atom Transfer Radical Polymerization (ATRP) but the authors never offered any replication or statistical analysis of their results!

As discussed previously, the glassy plateau in E' (determined by DMA) is higher for the FRP sample at 63% conversion. The reason was that the FRP sample had a higher gel content, compared to the NMRP sample. However, when the FRP and NMRP samples were at the same gel content, they exhibited the same glassy plateau in E'(see "Glassy plateau in E'" entries for 97% and 96% conversions in Table 10.11) and these trends were as expected.

Further investigation is required to address the observed discrepancies in the literature. First of all, additional replications of DMA results are needed to reinforce that the differences observed in the WHMs are truly differences between samples and not due to instrumental error. Secondly, according to Nielsen and Landel (1994), to carefully examine this trend, the temperature sweep results need to be complemented with frequency sweeps. However, since at this point we did not have enough polymer material to perform further tests, these become recommendations for immediate future work. If after further investigation, the results still indicate that networks synthesized through NMRP are more heterogeneous than the ones from FRP, one possible explanation could be that since the gel point is delayed in NMRP, these systems go through more branching before gelation than the FRP systems. Therefore, there might be molecules with various lengths of branched arms available in NMRP and when eventually transformed to a polymer network, the resulting structure could be more

heterogeneous. Certainly, further careful investigations are needed in order to clarify these speculative statements.

Table 10.11 Summary of DSC and DMA observations

	x ~ 63 %			x ~ 97 %			x ~ 96 %		
Observation	**2B-10 (FRP) (100 % gel)**	**3B-2 (NMRP) (40 % gel)**	**Q***	**2B-12 (FRP) (100% gel)**	**3-16 (NMRP) (95% gel)**	**Q**	**2B-12 (FRP) (100% gel)**	**3-15 (NMRP) (93% gel)**	**Q**
T_g (DSC)		Lower	Y		Lower	Y		Lower	Y
ΔT_g (DSC)		Same	N		Larger	N		Larger	N
Slope of transition line (DSC)	Same		N		Milder	N		Milder	N
Glassy plateau in E' (DMA)	Higher		Y	Same		Y	Same		Y
Drop in E' in glass transition region (DMA)		Earlier	Y		Earlier	Y		Earlier	Y
tan δ maximum (DMA)		Earlier	Y		Earlier	Y		Earlier	Y
tan δ breadth-WHM (DMA)		Broader	N		Broader	N		Broader	N

* Q is short for question and refers to the question, whether the expected trend was detected; Y is short for Yes, meaning that the trend detected by our results was as expected; N is short for No, meaning that the trend detected by our results was not expected.

10.3.3 Recommendation of Other Techniques for Detecting Homogeneity of the Network

10.3.3.1 Can Ultrasonics Provide an Indicator?

Ultrasonic waves are sound waves that are of higher frequency than the human audible range. These waves can be used for many different applications. Depending on their frequency and intensity, ultrasonic waves can either penetrate a medium and measure the reflection signature or supply focused energy. Table 10.12 shows different applications of ultrasonic waves categorized by different intensities (I) and frequencies.

High frequency (>1 MHz) and low intensity ultrasonic waves do not change the medium; instead, they are affected by the medium. Hence, using ultrasonic waves with high frequencies and low intensities gives us the ability to "see through" a solid material and detect surface or internal flaws (hence, internal "structure") without affecting the material in an adverse manner. This feature can be used for non-destructive testing and examination (NDT/NDE), medical diagnosis, chemical analysis and the study of material properties.

Table 10.12 Application of ultrasonic waves (Bruinewoud, 2005)

20 kHz- 500 kHz		*> 1 MHz*	
$I > 10$ W/cm^2	$I < 1$ W/cm^2	$I < 1$ W/cm^2	$I > 1$ W/cm^2
Welding Cleaning Cell disruption Sterilisation Lithotripsy Chemical reactions	Sonophoresis	Flaw detection Medical diagnosis Chemical analysis Material properties	Massage therapy Tumour treatment Surgery Drug delivery

Ultrasonic methods have been successfully used in polymer technology and industry and some examples are presented herein. Ultrasonics were used for in-line monitoring of the degree of mixing and the melt temperature in extrusion processes (Chen et al., 1998; Franca et al., 2000). Alig et al. (1994) used ultrasonic spectroscopy to measure longitudinal modulus and determine structural relaxation times during the curing of an epoxy. Ultrasonic methods were used to characterize glass transition temperature in epoxy resins (Nguyen et al., 1995); results were shown to be close to the measurements by Dynamic Mechanical Analysis (DMA). In addition,

influence of fillers on the thermal properties of the epoxy matrix in a composite material was also studied and characterized using ultrasonic techniques. Constable et al. (2003) used in-situ ultrasonic spectroscopy to study the ring-opening metathesis polymerization of dicyclopentadiene. Changes in the density, wave speed, acoustic modulus, and attenuation were all simultaneously monitored to determine the rate constant for the crosslinking reaction. The effects of binding various modifiers to polystyrene's aromatic ring were also investigated (Oral et al., 2011; 2012), where the elastic properties were determined using ultrasound. Recently, properties and internal structure (phase structure, morphology) of two devulcanized rubber blends were compared using ultrasonic waves (Zhu et al., 2011).

Ultrasonic Properties: The properties which are tracked in typical ultrasonic measurements are velocity, as inferred from an arrival time, and attenuation, as inferred from a rate of decay of the wave. Velocity is usually the easiest ultrasonic variable to measure. The speed of sound in a medium is directly related to both elastic modulus and density. Thus, changes in either elasticity or density will affect the wave's traveling time through a sample of a given thickness. Additionally, varying degrees of heterogeneity may have an effect on sound velocity. The velocity, V, at which sound travels in the sample is calculated by

$$V = \frac{d}{d - \Delta t \times V_w} \times V_w \qquad \text{Eq. 10.24}$$

where

V_w— the speed at which ultrasound travels in water (1500 m/s);

d— sample thickness;

Δt — the difference in the pulse arrival time with and without sample.

This velocity calculated by Zhu et al. (2011) is a wave group velocity, which includes both longitudinal wave velocity (V_L) and shear wave velocity (V_s). Using Fast-Fourier-transform (FFT) plots one can obtain V_L and V_s separately. Table 10.13 shows typical wave velocities for polystyrene (PS) samples measured by the pulse-echo ultrasound method at room temperature using 5 MHz transducers (Oral et al., 2011). As can be seen, a higher molecular weight corresponds to higher density and velocity in polystyrene samples.

Table 10.13 Variation of density (ρ), V_L and V_s (Oral et al., 2011)

Polymer	ρ (g/cm^3)	V_L (m/s)	V_s (m/s)
PS (Mw= 5 X 10^5)	1.051	2355±0.04	1155± 0.03
PS (Mw= 3.5 X 10^5)	1.043	2352±0.04	1153± 0.03

Attenuation of the ultrasonic wave traveling through a medium depends on the properties of the medium too. The reasons for attenuation are energy absorption (thermal energy) and/or reflection, refraction, diffraction and dispersion of the waves, particularly for heterogeneous media. Attenuation (Att, $^{dB}/_{cm}$) can be obtained from

$$Att = \frac{1}{d} \times 20\ log(\frac{A_0}{A}) \qquad \text{Eq. 10.25}$$

where d is the thickness, and readings A and A_0 are the gain reading values to maintain the pulse amplitude at 80% of the full scale; with (A) and without (A_0) samples in the path between the emitter and receiver ultrasonic sensors, respectively (Zhu et al., 2011). The weakening of the ultrasonic wave is usually characterized by the wave attenuation coefficient α ($^{dB}/_{cm.Hz}$), which determines the change of the acoustic pressure after the wave has traveled a unitary distance through the given medium. Table 10.14 gives an idea of typical attenuation values expected for some polymers. As can be seen, polystyrene has the lowest attenuation value; it is more than three times lower than the next lowest option, poly methylmethacrylate (PMMA). Having relatively low attenuation value, polystyrene has extensive application is industrial ultrasound. The trade name used in industry, associated with cross-linked polystyrene is “Rexolite”. “Rexolite” is a favorite material used for plastic wedges in ultrasound applications.

Table 10.14 Typical attenuation values for some polymers from Selfridge, Institute of Electrical and Electronics Engineers (IEEE), 1985 (in Ginzel, 1996)

Material	**Attenuation (dB/mm) @ 5 MHz**
ABS (acrylonitrile /butadiene / styrene copolymer)	1.11
PMMA - Acrylic (Plexiglas & safety glazing)	0.64
Delrin	3.03
Nylon(black)	1.60
Polystyrene	0.18
PVC (Polyvinyl chloride)	1.12
Styrene Butadiene	2.43

Ultrasonic Apparatus: Typically, the fluid-assisted ultrasonic apparatus consists of a pulser/receiver, a transducer, a water tank and a display device. A representative schematic of fluid-assisted transmission through an ultrasound apparatus is shown in Figure 10.34. The fluid-assisted ultrasonic method uses a fluid medium between the transducer and the sample. This is normally realized by setting the sample in a water tank that includes submerged transducers. A pulser/receiver is an electronic device that can produce electrical pulses. Driven by the pulser, the transducer generates high frequency ultrasonic oscillations. These oscillations, when coming in contact with a sample, produce waves at the surface of the sample that propagate into the material. In the case of the through transmission method, the wave is received by a second transducer positioned on the other side of the sample, and then acquired, saved, and possibly displayed by an oscilloscope (Landais, 2011). In this case, one transducer acts as a transmitter while the second acts as receiver. To receive all the ultrasonic energy sent by the transmitter and passed through the sample, the two transducers have to be well aligned and this is achieved by using the turntable (see Figure 10.34).

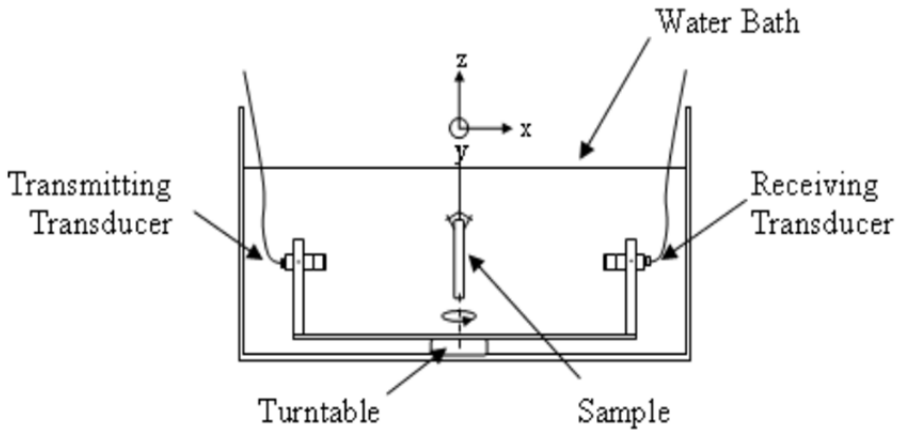

Figure 10.34 Principle of an ultrasonic apparatus (Landais, 2011)

*Possibility for STY/DVB Samples:*Based on this brief literature review on the subject of ultrasound measurements for polymers, it is evident that the ultrasound properties of polymers, such as wave velocity and attenuation, are strongly affected by their molecular structure (Nguyen et al., 1995; Oral et al., 2011, 2012; Zhu et al., 2011). Hence, measurements of wave velocity and attenuation for our cross-linked polystyrene samples might provide information related to the homogeneity or heterogeneity of the synthesized network.

In our study, for each STY/DVB sample, 3 specimens of 2 cm $\times$ 2 cm with different thicknesses (2 mm, 4 mm, and 6 mm) should be prepared; this translates roughly into 5 to 10 grs of polymer for each STY/DVB sample. However, with our ampoule polymerizations, at high conversion, each ampoule gives around 2 grs of polymer. Hence, to produce enough polymer material for the ultrasound measurements, multiple ampoules are needed to be prepared for a single STY/DVB sample (to provide 3 specimens). Care should be taken in preparing ultrasound samples with good surface quality, as the reflection levels of ultrasound waves at the surface are dependent upon surface roughness (Zhu et al., 2011).

The acoustic measurements can be conducted using an available apparatus in our laboratory, developed in collaboration with Eclipse Scientific Inc. and Materials Research Institute (MRI), Waterloo, Ontario, Canada. The apparatus consists of an immersion tank filled with deionized water and two ISA boards installed inside a PC. In the immersion tank, a rail sits at the bottom and two ultrasound sensors (one emitter and one receiver, interchangeable) are mounted on two

sliding blocks along the rail. A windowed sample mounting plate crosses the rail in the middle between the two detectors. The two detectors are connected by shielded cables to the ISA board, where ultrasonic signals are generated and received according to the control software Winspec (for more details about the apparatus, refer to (Zhu et al., 2011)).

Wave velocity and attenuation measurements should be conducted on samples with different thicknesses in the pulse-echo mode with a single wave frequency (suggested frequency 5 MHz) at room temperature. The pulse arrival time should be recorded for the wave velocity measurements, using Eq. 10.24. The wave amplitude is also recorded for calculating the attenuation using Eq. 10.25. Figure 10.35 shows typical qualitative trends expected. As the thickness of the sample increases, the velocity at which the 5 MHz ultrasound wave travels in the sample decreases, while the attenuation level increases. By changing the frequency of the ultrasound in the tuned tone-burst mode, the attenuation coefficient could be obtained for each polymer sample (Zhu et al., 2011). Figure 10.36 shows the attenuation levels (dB) at different sample thicknesses and ultrasonic frequencies. The expected qualitative trend is that a thicker sample and a higher frequency lead to a higher level of attenuation (Zhu et al., 2011).

a)

b)

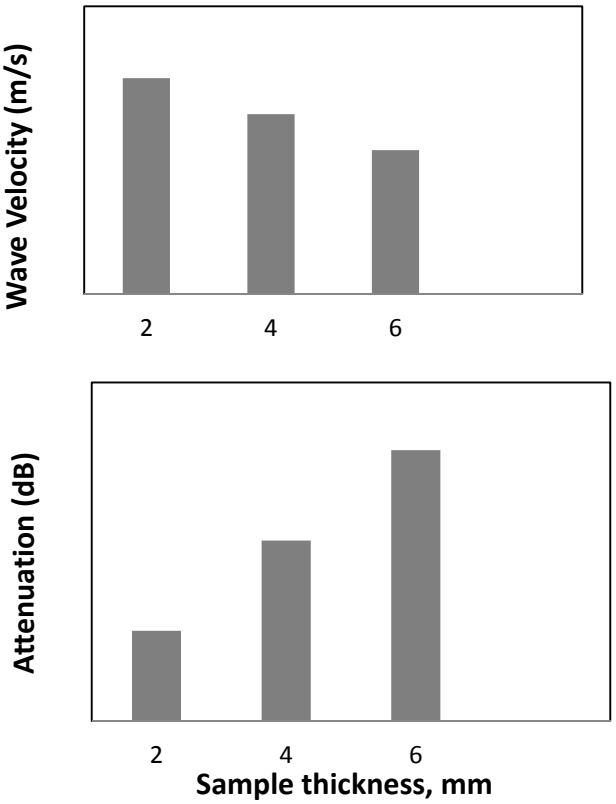

Figure 10.35 a) Velocity, b) Attenuation level, of 5 MHz ultrasound wave as a function of sample thickness

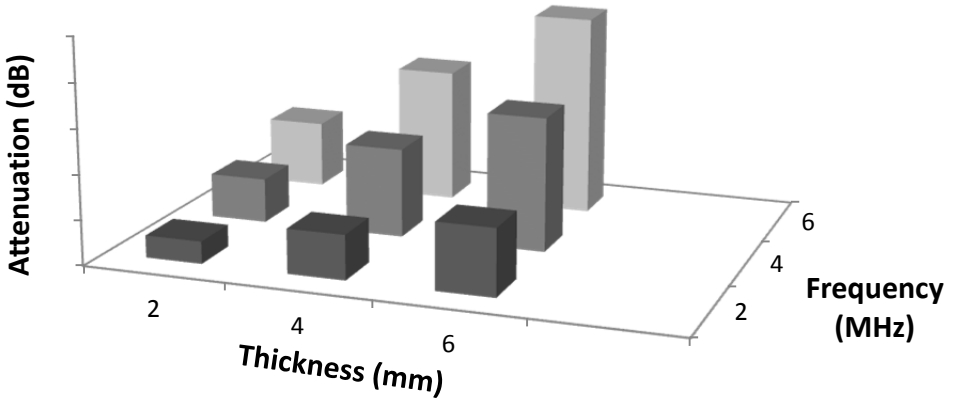

Figure 10.36 Attenuation level (dB) at different thickness and ultrasonic frequency

According to Zhu et al. (2011), the degree of crosslinking does not affect the wave velocity significantly and the velocity remains constant with sample thickness within a typical error of 5%. However, as the degree of crosslinking increases, higher attenuation levels are expected. Hence, attenuation can be used as an indicator for the degree of crosslinking in our STY/DVB samples. As the gel content (degree of crosslinking) increases, higher attenuation values are expected.

Based on the studies of Oral et al. (2011, 2012) and Zhu et al. (2011), polymers with different densities have different ultrasonic properties (both velocity and attenuation). Hence, it might be possible to detect different ultrasonic properties with STY/DVB samples synthesized through controlled radical polymerization (CRP) and samples synthesized through regular free radical polymerization (FRP), as they exhibit different cross-link densities (and, presumably, networks of different homogeneity).

Oral et al. (2011, 2012) have used the ultrasonic measurements to calculate characteristic elasticity constants (longitudinal modulus, shear modulus, Young's modulus). Another interesting aspect to explore in STY/DVB cross-linked samples could be the use of the ultrasonic characteristics in order to determine the viscoelastic properties of polymer samples and compare the results with results obtained from Dynamic Mechanical Analysis (DMA). Further study could measure the ultrasonic variables at different temperatures to calculate longitudinal moduli and tan delta. Figure 10.37 shows typical results from Nguyen et al. (1995).

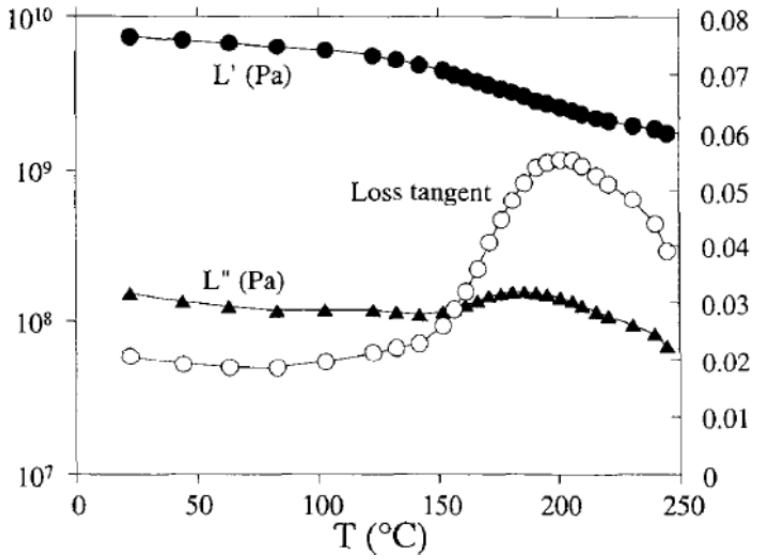

Figure 10.37 Longitudinal moduli and loss tangent calculated from the longitudinal velocity and attenuation (Nguyen et al., 1995)

Nguyen et al. (1995) also used the ultrasonic technique to characterize the influence of different fillers on the thermal properties of an epoxy matrix in a composite material. Experimental curves of longitudinal velocity and attenuation for pure epoxy and composites with different filler characteristics are shown in Figure 10.38. As can be seen, different microstructures result in different velocities and glass transition temperatures. In addition, the attenuation peak changes in both amplitude and width.

This brief literature review on the topic of ultrasonics reveals that ultrasonic measurements could potentially provide us with valuable information about STY/DVB polymer networks. Two more final remarks:

1) The discussion in this section, more so like an afterthought, is by no means meant to be exhaustive. It was rather triggered by parallel work in our labs on ultrasonic characteristics of rubber blends.
2) Whether ultrasound measurements could eventually reveal specific information about the homogeneity or heterogeneity of a cross-linked network is still debatable, however the overall idea is worth exploring further. In essence, this brief exposure to the topic is eventually a glorified recommendation (see Chapter 11), due to lack of time for further investigation during the course of this thesis.

a)

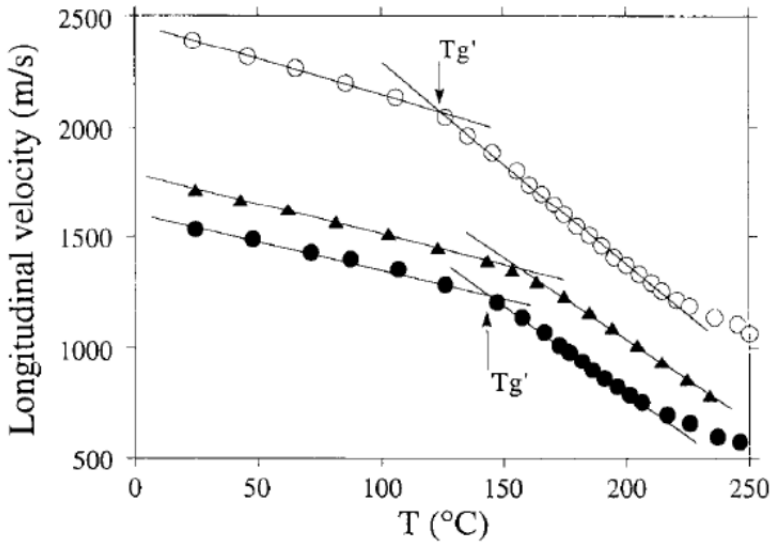

b)

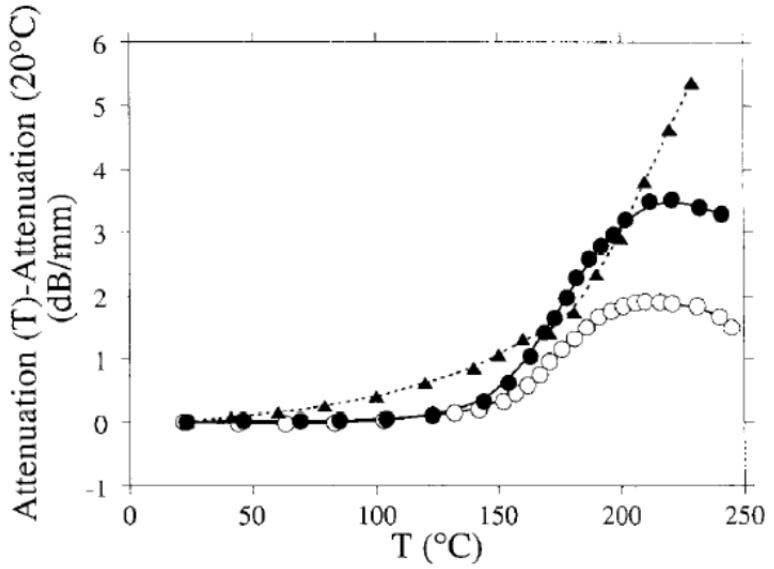

Figure 10.38 a) Longitudinal velocities, and b) attenuation, versus temperature of pure epoxy and composites at 2 MHz (○ pure epoxy, ▲composite made with 0.5pm tungsten particles in a volume fraction of 0.17, ● composite made with 5 pm tungsten particles in a volume fraction of 0.25) (Nguyen et al., 1995)

10.3.3.2 Nuclear Magnetic Resonance (NMR) Spectroscopy: Indicator for homogeneity?

One method that could potentially give some information regarding the homogeneity of a polymer network is NMR spectroscopy. NMR imaging or microscopy have been used previously in the literature for the determination of spatial heterogeneity of rubbery materials on the scale of 15-50 μm. Different types of NMR relaxation experiments have been used for analysis of local and long-range spatial mobility of polymer chains. Since chain motion is strongly coupled to the length of network chains, chemical information on network structure and network defects can be obtained in this way. Selective information on the mobility of polymer chain units of different chemical origins can be obtained by means of selective NMR relaxation experiments (Litvinov and Dias, 2001).

O' Connor et al. (1996) used ^{1}H NMR to determine the level of heterogeneity in domain sizes as small as 20 μm. In their study, the focus was on the solvent rather than the network. Their method utilized the differences in chemical shift between solvent absorbed into the cross-linked polymer and that of solvent outside the polymer. This chemical shift was then correlated to macroscopic swelling though a simple model which attempts to account for both the chemical cross-links and chain entanglements. One problem with their technique was that they needed a series of standard materials with known swelling characteristics for calibration.

Other groups like Litvinov and Dias (2001) and Saalwachter (2007) focused on analysis of chain mobility with respect to cross-link density using NMR relaxation experiments. NMR relaxation times, especially spin-spin relaxation time (T_2), are largely affected by local segmental mobility. In addition to the mean cross-link density, the analysis of T_2 relaxation can provide information on network defects and heterogeneous distribution of network junctions. The sensitivity of the T_2 experiments to the molecular scale heterogeneity is due to the local origin of the relaxation process, which is predominantly governed by the near-neighbor environment and intrachain effects for T_2 relaxation at temperatures well above the T_g (Litvinov and Dias, 2001). In a simplified picture, the total T_2 relaxation decay for a heterogeneous elastomer is a weighted sum of decays from the different submolecules which are defined as network chains between the chemical and the physical junctions, chain loops, and chain-end blocks. These submolecules possess different relaxation characteristics due to

differences in the large spatial scale mobility. The relative contribution of the submolecules to the total proton T_2 relaxation decay is proportional to the number of protons, which are attached to these chain fragments (Litvinov and Dias, 2001). A quantitative analysis of the decay shape is not always straightforward due to the complex origin of the relaxation function itself and the structural heterogeneity of the long chain molecules (Saalwachter, 2007).

10.3.3.3 How about Scattering Techniques?

Since gel homogeneity or heterogeneity is closely connected to spatial concentration fluctuations, scattering methods such as light scattering, or more recently developed microscopic techniques such as small-angle X-ray (SAXS) and neutron scattering (SANS), might be helpful in gaining information about the structure of the polymer network. So far the effectiveness of these techniques has been demonstrated mainly in networks formed by step growth polymerization and less densely cross-linked polymer.

Gundogan et al. (2004) studied the "inhomogeneity" of polymer gel via using static and dynamic light scatting. By comparing the scattering intensities from the gel and from a semi-dilute solution of the same polymer at the same concentration, they showed that the excess scattering over the scattering from the polymer solution is related to the degree of "inhomogeneity" in the gels. However, the drawback in their technique is that the concentration and/or density fluctuations also interfere with the scattering intensity. In addition, for the light scattering measurements, all glassware needs to be kept dust-free and should be carried out in a dust-free glove box.

Liu et al. (2006) used dynamic light scattering to characterize hydrogel structures. The scattering was separated into two parts: the frozen-in component, arising from spatial "inhomogeneity", and the liquid-like component due to thermal concentration fluctuations. Subtracting the scattering intensity arising from the thermal concentration fluctuations, from the ensemble-average scattering intensity, led to the intensity coming from the frozen-in spatial "inhomogeneity".

Some groups used SANS as a technique to characterize the structure of a polymer network (Horkay et al., 2000; Norisuye et al., 2003; Hammouda, 2010). However, the use of SANS as a

characterization technique is not very straightforward, as it usually needs a model function to be fitted to the collected data (and the choice of the model is still the subject of debate among physicists).

10.3.3.4 Other potential techniques?

Among other potential techniques that might provide some information about the homogeneity of a network is fluorescence. Leicht and Fuhrmann (1981) used 9-vinylanthracene as the fluorescence indicator and monitored the segmental density via a microstructure-sensitive fluorescence polarization method. The issue here is the efficiency of incorporation of fluorescence dyes (molecules).

10.4 Concluding Remarks

Production of cross-linked polymer with homogeneous structure is desirable for several applications. It has been widely acknowledged that structural "inhomogeneities" are especially present in systems with very low gelation point conversions and complexities that are specific to regular free radical polymerization (Kannurpatti et al., 1996). In parallel, it has been claimed that cross-linked polymers synthesized through controlled radical polymerization can produce a homogenous polymer network. However, a reliable characterization method to evaluate structural homogeneity in these systems is sorely absent in the literature. Hence, it is highly desirable to seek a reliable characterization technique to evaluate the structure of polymer networks synthesized through controlled radical polymerization (and other polymerizations).

The results of our study on the characterization of polymer structure via thermo-mechanical analysis (DMA and DSC) showed that there was no difference detected between the two networks synthesized through CRP and FRP. In order to reinforce our results further, a frequency sweep can be carried out to complement the results of our temperature sweep. Other potential techniques that one can investigate include SANS, SAXS, NMR and ultrasonics.

Chapter 11. Concluding Remarks, Main Contributions and Future Recommendations

11.1 Concluding Remarks

The Bayesian approach is a powerful, largely unstudied (in the polymerization area) design of experiments method that has the same objectives as the standard experimental designs but with significant practical benefits over standard design methods, which make it particularly attractive from both an industrial and theoretical perspective. Numerous advantages of the Bayesian design over standard (fractional) factorial designs have been highlighted in this thesis. The most distinct advantage of the Bayesian approach is its ability to incorporate into the design prior process knowledge, which is available in most of the cases but usually discarded. This and other advantages of the Bayesian methodology were highlighted in this thesis with examples drawn from complex polymerization scenarios, specifically from the nitroxide-mediated radical polymerization (NMRP) of styrene (under both bimolecular and unimolecular initiating options), emulsion copolymerization of acrylonitrile/butadiene (nitrile rubber or NBR) in a continuous train of CSTRs, and cross-linking NMRP of styrene and divinyl benzene.

Table 11.1 gives a compendium of experimental design issues that can effectively be handled by the Bayesian design approach. All of these issues along with the superior performance of the Bayesian approach (over standard experimental designs) in handling them were demonstrated via case studies discussed throughout this thesis, drawn from the three different complex polymerization scenarios mentioned above. The effort was to illustrate that the Bayesian design approach can be exploited in many different processes (bulk/emulsion), batch and continuous, and even more complex systems with cross-linking, and can lead to optimal performance in fewer trials, thus saving time and money. In addition, the novelty of the approach is the simplicity and the natural way with which it follows the logic of the sequential model building paradigm, taking full advantage of the researcher's expertise and information (knowledge about the process or product) prior to the design, and invoking enhanced information content measures (the Fisher Information matrix is maximized, which corresponds to minimizing the variances and reducing the 95% joint confidence regions, hence improving

the precision of the parameter estimates). The bottom line is that the Bayesian design is a balanced approach which is statistically correct and scientifically sound, and yet very practical!

Table 11.1 Overview of issues handled by the Bayesian design approach

Issues handled in Bayesian design
Incorporation of prior knowledge (screening experiments, models and/or combinations)
Flexible wrt quality of prior knowledge (informative vs. non-informative prior)
Sequential nature (n-trials vs. sequences of fewer trials)
Iterative fashion
Increase of information content
Statistical diagnostic tests
“Tailoring” runs to experimenter's intended target
Single vs. multi-response
Flexible wrt number of trials that can be designed
Process constraints (and impractical treatment combinations)
Changing factor level/range in the middle of experimentation
Possible detection of nonlinearities
Accommodating extra trial(s) mid-way through experimentation
Balance: statistically correct and scientifically sound, yet practical, decisions

In all the case studies described in this thesis, the general benefits of the Bayesian design were as described above. More specifically, with respect to the most complex of the examples, namely, the cross-linking nitroxide-mediated radical polymerization (NMRP) of styrene and divinyl benzene, the investigations after designing experiments through the Bayesian approach led to even more interesting detailed kinetic and polymer characterization studies, which cover the second part of this thesis (Chapters 9 and 10). This detailed synthesis, characterization and modeling effort, trigged by the Bayesian approach, set out to investigate whether the cross-linked polymer network synthesized under controlled radical polymerization (CRP) conditions had a more homogeneous structure compared to the network produced by regular free radical polymerization (FRP).

In preparation for the identification of network homogeneity indicators based on polymer properties, cross-linking kinetics of NMRP of STY in the presence of a small amount of DVB (as the cross-linker) and I-TIPNO (as the unimolecular initiator) was investigated in detail. In Chapter 9, the results were contrasted with regular FRP of STY/DVB and homopolymerization of STY in the presence of I-TIPNO, as reference systems. Our investigations showed that

NMRP copolymerization exhibited controlled behaviour up to the vicinity of the gelation point, after which 'livingness' was lost. Presence of I-TIPNO slowed down the rate, delayed the onset of gelation, yielded lower molecular weights, and produced a 'looser' polymer network compared to regular FRP of the two monomers.

In our designed experiments (with careful independent replication, in order to build more confidence in the observed data from such a complex, noisy and experimentally uncertain system), two concentration levels were used for I-TIPNO and DVB, which resulted in four different molar ratio ratios. The effects of [DVB], [I-TIPNO] and [DVB]/ [I-TIPNO] molar ratio were investigated on rate, molecular weights, gel content and swelling index. Results showed that the rate of polymerization was not affected by [I-TIPNO], [DVB], or [DVB]/ [I-TIPNO] (at least at the DVB levels employed; the non-significant effect of I-TIPNO concentration was as expected). On the other hand, the effect of these factors on molecular weights, gel content and network morphology were noticeable. Using a higher [I-TIPNO], while keeping the same [DVB], delayed the gel point. In contrast, using a higher [DVB], while keeping the same [I-TIPNO], accelerated the formation of gel. All in all, our studies revealed that maximizing the [DVB]/ [TIPNO] molar ratio resulted in the earliest gelation point and hence, fastest loss of 'livingness'. As the [DVB]/ [TIPNO] ratio decreased, the gel point was observed at higher conversion levels and the corresponding polymer network was 'looser'.

In parallel to our experimental investigations, a detailed mathematical model was developed. The predicted profiles for polymerization rate, molecular weight averages and gel content (or swelling index) were validated with the respective experimental data for NMRP copolymerization of STY/ DVB in the presence of TIPNO. These validations took place independently (between two different research groups in two universities in two countries), without additional parameter fitting (thus indirectly confirming the validity and generality of the developed mathematical model and accompanying database of kinetic and physical/ chemical characteristics and parameters). Not only did model predictions follow the general experimental trends very well but also were in good agreement with experimental observations.

Pursuing our investigations for a more reliable indicator for network homogeneity, Chapter 10 contained characterization of the corresponding branched and cross-linked polymers. Thermo-mechanical analysis was used to investigate the difference between polymer networks synthesized through FRP and NMRP. Results from both Differential Scanning Calorimetry (DSC) and Dynamic Mechanical Analysis (DMA) showed that at the same cross-link density and conversion level, polymer networks produced by FRP and NMRP exhibit indeed comparable structures.

Overall, it was impressive to see what a wealth of process information was generated by a such a practical experimental design technique, and with minimal experimental effort compared to previous (undesigned) efforts (and associated, often not well founded, claims) in the literature!

11.2 Main Contributions

The research in this thesis has made the following original contributions:

1. Although the basics of the Bayesian approach have been suggested in 1993 (Reilly, 1993), the technique has not been formalized and publicized as a practical tool that can be applied to various chemical engineering processes. Through work in this thesis (see Chapters 2 to 4), the application of the Bayesian approach as a tool for the design of experiments was formalized. In addition, the inner workings of the technique were investigated in detail.

2. Two typical questions that often arise in Bayesian design implementations have to do with how effectively one can make statements about the quality of prior knowledge and the significance of the estimated effects (from the designed experiments), and about the gain in information content. These two important questions were not addressed in earlier Bayesian design implementations (Dube et al., 1996; Vivaldo-Lima et al. 2006) and are among the main contributions of the present work (see Chapter 5). A quantitative comparison between the Bayesian approach and standard experimental designs was carried out via comparing different measures of information content. For example, it was shown that Fisher's information matrix was maximized in the Bayesian approach, which corresponds to minimizing the variances and reducing the 95% joint

confidence regions (JCR), hence improving the precision of the parameter estimates. All in all, these quantitative comparisons made one more confident in the effectiveness and practicality of the Bayesian design of experiments procedure.

3. Although Bayes' theorem is well established, especially among statisticians, and has been implemented to some chemical systems (for example drug and cell transport kinetics, pharmaceutical kinetics and analyses of catalytic systems), the practice of using the Bayesian approach (as described in this thesis) as a tool for designing experiments in polymerization processes has been sorely missing. The effort in this has been to expand the implementation of the Bayesian design of experiments in polymer reaction engineering (PRE), which could lead to optimal performance in fewer trials, thus saving time and money. Chapters 4, 6 and 8 illustrate applications of the Bayesian design to three complex polymerization processes.

4. The role of the Bayesian technique as an excellent tool to guide one in addressing important practical issues in the study of polymerization processes was clearly demonstrated by the application of this technique to the most complex polymerization system (out of three relatively complex ones), namely, the cross-linking NMRP of STY/DVB (see Chapters 8 to 10).

11.3 Recommendations for Future Steps

Bayesian Design Approach:

- Use a non-linear model in the Bayesian design to replace Eq. 3.2 in Chapter 3. Initially, and for practical purposes, one can start with a reduced non-linear model, in order to make things simpler. This has already been initiated in a MASc thesis (Mark Hazlett), essentially an offspring of this PhD thesis. In addition, comparisons with regular D-optimal designs are being conducted. The results will be forthcoming in September 2012.

- Combine Bayesian methodology with other statistical criteria to reduce parameter correlation (focus on parameter values) (e.g., combine with the work in Franceschini and Macchietto (2008a and b)).

- Design experiments for the cross-linking NMRP (in Chapter 8) to investigate the effect of temperature on polymerization properties (this has already been planned as the MASc project of a new student, Alison Scott).

Cross-linking NMRP:

- Adding chain transfer agent to a regular free radical cross-linking polymerization system to lower the average molecular weight of the primary chains to the level of the nitroxide-mediated radical polymerization, so that the two systems can be compared without significant effects of chain length differences.

- Further purification of TIPNO-based alkoxyamine (following typical purification methods such as precipitation/recrystallization, or chromatography). GPC chromatograms from polymerization using purified I-TIPNO can then be compared to the high conversion results of the I-TIPNO "as received".

- Further investigation is required to address the observed discrepancies in the literature. First of all, additional replications of DMA results are needed to reinforce that the differences observed in the WHMs are truly differences between samples and not due to instrumental error. Secondly, according to Nielsen and Landel (1994), to carefully examine this trend, the temperature sweep results need to be complemented with frequency sweeps.

- Using other characterization techniques for detecting homogeneity of the network. As discussed in detail in Subsection 10.3.3, ultrasonics (Zhu et al., 2011), NMR spectroscopy (Saalwachter, 2007), scattering techniques like SANS (Norisuye et al. 2005) and using fluorescence polarization methods (Leicht and Fuhrmann, 1981) could be potentially useful approaches (whole theses in themselves) to indicate homogeneity or heterogeneity of the network synthesized through controlled radical polymerization.

References

References for Chapter 2

Blau, G., Lasinski, M., Orcun, S., Hsu, S. H., Caruthers, J., Delgass, N., and Venkatasubramanian, V. (2008). High fidelity mathematical model building with experimental data: A Bayesian approach. *Computers & Chemical Engineering*, 32, 971-989.

Bois, F. Y., Fahmy T., Block J.-C., and Gatel D (1997). Dynamic modeling of bacteria in a pilot drinking-water distribution system. *Water Research*, 31, 3146-3156.

Bolstad, W. M. (2007). Introduction to Bayesian statistics. (Second Edition) Hoboken, New Jersey: John Wiley and Sons.

Box, G. E. P. and Draper, N. R. (1965). Bayesian estimation of common parameters from several responses. *Biometrika*, 52, 355.

Box, G. E. P., Hunter, J. S., & Hunter, W. G. (2005). Statistics for experimenters. (Second Edition) Hoboken, New Jersey: John Wiley & Sons.

Box, G. E. P. and Tiao, G. C. (1968). Bayesian estimation of means for random effect model. *Journal of the American Statistical Association*, 63, 174.

Box, G. E. P. and Tiao, G. C. (1965). Multi-parameter problems from a Bayesian point of view. *The Annals of Mathematical Statistics*, 36, 1468-1482.

Box, G. E. P. and Tiao, G. C. (1973). Bayesian inference in statistical analysis. Wiley-Interscience publication.

Coleman, M. C. & Block, D. E. (2006). Bayesian parameter estimation with informative priors for nonlinear systems. *AIChE Journal*, 52, 651-667.

Dube, M. A., Penlidis, A., and Reilly, P. M. (1996). A systematic approach to the study of multicomponent polymerization kinetics: The butyl acrylate/methyl methacrylate vinyl acetate

example .IV. Optimal Bayesian design of emulsion terpolymerization experiments in a pilot plant reactor. *Journal of Polymer Science Part A-Polymer Chemistry*, 34, 811-831.

Duran, M. A. and White, B. S. (1995). Bayesian-estimation applied to effective heat-transfer coefficients in a packed-bed. *Chemical Engineering Science*, 50, 495-510.

Fisher, R. A. (1926). The arrangement of field experiments. *Journal of the Ministry of Agriculture of Great Britain*, 33, 503-513.

Froment, G. F. (1975). Model discrimination and parameter estimation in heterogeneous catalysis. *AIChE Journal*, 21, 1041-1057.

Hermanto, M. W., Kee, N. C., Tan, R. B. H., Chiu, M. S., and Braatz, R. D. (2008). Robust Bayesian estimation of kinetics for the polymorphic transformation of L-glutamic acid crystals. *AIChE Journal*, 54, 3248-3259.

Hsu, S. H., Stamatis, S. D., Caruthers, J. M., Delgass, W. N., Venkatasubramanian, V., Blau, G. E., Lasinski, M. and Orcun, S. (2009). Bayesian framework for building kinetic models of catalytic systems. *Industrial & Engineering Chemistry Research*, 48, 4768-4790.

Meyer, D. L. and Collier, R. O. (1970). Bayesian statistics. Itasca, Ill., Peacock.

Montgomery, D. C. (2005). Design and analysis of experiments. (sixth edition) John Wiley & Sons, Inc.

Murphy, E. F., Gilmour, S. G., and Crabbe, M. J. C. (2004). Efficient and cost-effective experimental determination of kinetic constants and data: the success of a Bayesian systematic approach to drug transport, receptor binding, continuous culture and cell transport kinetics. *Febs Letters*, 556, 193-198.

Omidbakhsh, N., Duever, T. A., Elkamel, A., and Reilly, P. M. (2010). A Bayesian experimental design approach for assessing new product performance: an application to disinfectant formulation. *Canadian Journal of Chemical Engineering*, 88, 88-94.

Pouillot, R., Albert, I., Cornu, M., and Denis, J. B. (2003). Estimation of uncertainty and variability in bacterial growth using Bayesian inference. Application to Listeria monocytogenes. *International Journal of Food Microbiology*, 81, 87-104.

Reilly, P. M. and Blau, G. E. (1974). Use of statistical-methods to build mathematical-models of chemical reacting systems. Canadian Journal of Chemical Engineering, 52, 289-299.

Reilly, P. M. (1993). A new approach to experimentation, Technical Report, Department of Chemical Engineering, University of Waterloo, Waterloo, On, Canada.

Vivaldo-Lima, E., Penlidis, A., Wood, P. E., and Hamielec, A. E. (2006). Determination of the relative importance of process factors on particle size distribution in suspension polymerization using a Bayesian experimental design technique. *Journal of Applied Polymer Science*, 102, 5577-5586.

References for Chapter 3

Box, G. E. P. and Hunter, W. G. (1965). Sequential design of experiments for nonlinear models. In , I.B.M. Scientific Computing Symposium on Statistics (pp. 113-137).

Dube, M. A., Penlidis, A., and Reilly, P. M. (1996). A systematic approach to the study of multicomponent polymerization kinetics: The butyl acrylate/methyl methacrylate vinyl acetate example .IV. Optimal Bayesian design of emulsion terpolymerization experiments in a pilot plant reactor. *Journal of Polymer Science Part A-Polymer Chemistry*, 34, 811-831.

Hsu, S. H., Stamatis, S. D., Caruthers, J. M., Delgass, W. N., Venkatasubramanian, V., Blau, G. E., Lasinski, M., Orcun, S. (2009). Bayesian framework for building kinetic models of catalytic systems. *Industrial & Engineering Chemistry Research*, 48, 4768-4790.

Vivaldo-Lima, E., Penlidis, A., Wood, P. E., and Hamielec, A. E. (2006). Determination of the relative importance of process factors on particle size distribution in suspension polymerization using a Bayesian experimental design technique. *Journal of Applied Polymer Science*, 102, 5577-5586.

Reilly, P. M. (1993). A new approach to experimentation, Technical Report, Department of Chemical Engineering, University of Waterloo, Waterloo, On, Canada.

References for Chapter 4

Belincanta- Ximenes, B. J., Mesa, P. V. R., Lona, L. M. F., Vivaldo-Lima, E., McManus, N. T., and Penlidis, A. (2007). Simulation of styrene polymerization by monomolecular and bimolecular nitroxide-mediated radical processes over a range of reaction conditions. *Macromolecular Theory and Simulations*, 16, 194-208.

Bertin, D., Gigmes, D., Marque, S. R. A., and Tordo, P. (2011). Kinetic subtleties of nitroxide mediated polymerization. *Chemical Society Reviews*, 40, 2189-2198.

Bonilla, J., Saldivar, E., Flores-Tlacuahuac, A., Vivaldo-Lima, E., Pfaendner, R., and Tiscareno-Lechuga, F. (2002). Detailed modeling, simulation, and parameter estimation of nitroxide mediated living free radical polymerization of styrene. *Polymer Reaction Engineering Journal*, 10, 227-263.

Braunecker, W. A. and Matyjaszewski, K. (2007). Controlled/living radical polymerization: Features, developments, and perspectives. *Progress in Polymer Science*, 32, 93-146.

Dube, M. A., Penlidis, A., and Reilly, P. M. (1996). A systematic approach to the study of multicomponent polymerization kinetics: The butyl acrylate/methyl methacrylate vinyl acetate example .IV. Optimal Bayesian design of emulsion terpolymerization experiments in a pilot plant reactor. *Journal of Polymer Science Part A-Polymer Chemistry*, 34, 811-831.

Fischer, H. (2003). Criteria for livingness and control in nitroxide mediated and related radical polymerizations. In K.Matyjaszewski (Ed.), Advances in Controlled/Living Radical Polymerization (pp. 10-23). Washington, DC: American Chemical Society.

Fukuda, T., Terauchi, T., Goto, A., Ohno, K., Tsujii, Y., Miyamoto, T., Kobatake S., and Yamada b. (1996). Mechanisms and kinetics of nitroxide-controlled free radical polymerization. *Macromolecules*, 29, 6393-6398.

Georges, M., Veregin, R., Kazmaier, R., and Hamer, G. (1993). Narrow molecular weight resins by a free- radical polymerization process. *Macromolecules*, 26, 2987-2988.

Goto, A. and Fukuda, T. (1997a). Effects of radical initiator on polymerization rate and polydispersity in nitroxide-controlled free radical polymerization. *Macromolecules*, 30, 4272-4277.

Goto, A. and Fukuda, T. (1997b). Mechanism and kinetics of activation processes in a nitroxyl-mediated polymerization of styrene. *Macromolecules*, 30, 5183-5186.

Goto, A. and Fukuda, T. (2004). Kinetics of living radical polymerization. *Progress in Polymer Science*, 29, 329-385.

Greszta, D. and Matyjaszewski K. (1996). Mechanism of controlled/"living" radical polymerization of styrene in the presence of nitroxyl radicals. kinetics and simulations. *Macromolecules*, 29, 7661-7670.

Grubbs, R. B. (2011). Nitroxide-Mediated Radical Polymerization: Limitations and Versatility. *Polymer Reviews*, 51, 104-137.

Hawker, C. J., Bosman, A. W., and Harth, E. (2001). New polymer synthesis by nitroxide mediated living radical polymerization. Chem. Revs., 101, 3661-3688.

Matyjaszewski, K. (1997). Overview: Fundamentals of Controlled/Living Radical Polymerization. In K.Matyjaszewski (Ed.), Controlled Radical Polymerization (pp. 2-30). Washington, DC: American Chemical Society.

Matyjaszewski, K. and Spanswick, J. (2005). Controlled/living radical polymerization. *Materials Today*, 8, 26-33.

Moad, G. and Solomon, D. H. (2006). The Chemistry of Radical Polymerization. (Second Edition) Amsterdam: Elsevier.

Nabifar, A., McManus, N., Vivaldo-Lima, E., Lona, L. M. F., and Penlidis, A. (2008). A replicated investigation of nitroxide-mediated radical polymerization of styrene over a range of reaction conditions. *Canadian Journal of Chemical Engineering*, 86, 879-892.

Omidbakhsh, N., Duever, T. A., Elkamel, A., and Reilly, P. M. (2010). A Bayesian Experimental Design Approach for Assessing New Product Performance: An Application to Disinfectant Formulation. *Canadian Journal of Chemical Engineering*, 88, 88-94.

Roa-Luna, M., Diaz-Barber, M. P., Vivaldo-Lima, E., Lona, L. M. F., McManus, N. T., and Penlidis, A. (2007a). Assessing the importance of diffusion-controlled effects on polymerization rate and molecular weight development in nitroxide-mediated radical polymerization of styrene. *Journal of Macromolecular Science, Part A: Pure and Applied Chemistry*, 44, 193-203.

Roa-Luna, M., Nabifar, A., Diaz-Barber, M. P., McManus, N. T., Vivaldo-Lima, E., Lona, L. M. F. and Penlidis A. (2007b). Another perspective on the nitroxide mediated radical polymerization (NMRP) of styrene using 2,2,6,6-tetramethyl-1-piperidinyloxy (TEMPO) and dibenzoyl peroxide (BPO). *Journal of Macromolecular Science Part A: Pure and Applied Chemistry*, 44, 337-349.

Rutsch, W. and Cech, M. A. (2007). Effects to improve the quality of life: Color, performance and protection from Ciba Specialty Chemicals. *Chimia*, 61, 33-41.

Shipp, D. A. (2005). Living radical polymerization: controlling molecular size and chemical functionality in vinyl polymers. *Polymer Reviews*, 45, 171-194.

Solomon, D. H., Rizzardo, E., and Cacioli, P., U.S. patent 4,581,429, March 1985.

Veregin, R. P. N., Georges, M. K., Hamer, G. K., and Kazmaier, P. M. (1995). Mechanism of living free-radical polymerizations with narrow polydispersity - electron-spin-resonance and kinetic-studies. *Macromolecules*, 28, 4391-4398.

Veregin, R. P. N., Odell, P. G., Michalak, L. M., and Georges, M. K. (1996a). Molecular weight distributions in nitroxide-mediated living free radical polymerization: Kinetics of the slow equilibria between growing and dormant chains. *Macromolecules*, 29, 3346-3352.

Veregin, R. P. N., Odell, P. G., Michalak, L. M., and Georges, M. K. (1996b). The pivotal role of excess nitroxide radical in living free radical polymerizations with narrow polydispersity. *Macromolecules*, 29, 2746-2754.

Vivaldo-Lima, E., Penlidis, A., Wood, P. E., and Hamielec, A. E. (2006). Determination of the relative importance of process factors on particle size distribution in suspension polymerization using a Bayesian experimental design technique. *Journal of Applied Polymer Science*, 102, 5577-5586.

Zhang, M. and Ray, W. H. (2002). Modeling of "living" free-radical polymerization processes. I. batch, semibatch, and continuous tank reactors. *Journal of Applied Polymer Science*, 86, 1630-1662.

Zhou, M. X., McManus, N. T., Vivaldo-Lima, E., Lona, L. M. F., and Penlidis, A. (2010). Kinetics of Nitroxide Mediated Radical Polymerization of Styrene with Unimolecular Initiators. *Macromolecular Symposia*, 289, 95-107.

References for Chapter 5

Dube, M. A., Penlidis, A., and Reilly, P. M. (1996). A systematic approach to the study of multicomponent polymerization kinetics: The butyl acrylate/methyl methacrylate vinyl acetate example .IV. Optimal Bayesian design of emulsion terpolymerization experiments in a pilot plant reactor. *Journal of Polymer Science Part A-Polymer Chemistry*, 34, 811-831.

Nabifar, A., McManus, N., Vivaldo-Lima, E., Lona, L. M. F., and Penlidis, A. (2008). A replicated investigation of nitroxide-mediated radical polymerization of styrene over a range of reaction conditions. *Canadian Journal of Chemical Engineering*, 86, 879-892.

Roa-Luna, M., Nabifar, A., Diaz-Barber, M. P., McManus, N. T., Vivaldo-Lima, E., Lona, L. M. F. and Penlidis, A. (2007). Another perspective on the nitroxide mediated radical

polymerization (NMRP) of styrene using 2,2,6,6-tetramethyl-1-piperidinyloxy (TEMPO) and dibenzoyl peroxide (BPO). *Journal of Macromolecular Science Part A: Pure and Applied Chemistry*, 44, 337-349.

Veregin, R. P. N., Odell, P. G., Michalak, L. M., and Georges, M. K. (1996a). Molecular weight distributions in nitroxide-mediated living free radical polymerization: Kinetics of the slow equilibria between growing and dormant chains. *Macromolecules*, 29, 3346-3352.

Veregin, R. P. N., Odell, P. G., Michalak, L. M., and Georges, M. K. (1996b). The pivotal role of excess nitroxide radical in living free radical polymerizations with narrow polydispersity. *Macromolecules*, 29, 2746-2754.

Vivaldo-Lima, E., Penlidis, A., Wood, P. E., and Hamielec, A. E. (2006). Determination of the relative importance of process factors on particle size distribution in suspension polymerization using a Bayesian experimental design technique. *Journal of Applied Polymer Science*, 102, 5577-5586.

Zhang, M. and Ray, W. H. (2002). Modeling of "living" free-radical polymerization processes. I. batch, semibatch, and continuous tank reactors. *Journal of Applied Polymer Science*, 86, 1630-1662.

References for Chapter 6

Asua, J. M., Sudol, E. D., and El-Aasser, M. S. (1989). Radical desorption in emulsion polymerization. *Journal of Polymer Science Part A: Polymer Chemistry*, 27, 3903-3913.

Box, G. E. P., and Draper, N. R.(1969). Evolutionary Operation: A statistical method for process improvement. New York: Wiley

Dube, M. A., Penlidis, A., and Reilly, P. M. (1996). A systematic approach to the study of multicomponent polymerization kinetics: The butyl acrylate/methyl methacrylate vinyl acetate example .4. Optimal Bayesian design of emulsion terpolymerization experiments in a pilot plant reactor. *Journal of Polymer Science Part A-Polymer Chemistry*, 34, 811-831.

Dube, M. A. and Penlidis, A. (1996). Hierarchical data analysis of a replicate experiment in emulsion terpolymerization. *AIChE Journal*, 42, 1985-1994.

Hofmann, W. (1964). Nitrile Rubber. Rubber Chemistry and Technology, 37, 1-252.

Hunter, W.G. and Kittrell, J.R. (1966). Evolutionary Operation and its basic principles: a review. Technometrics, 8, 389-397.

Madhuranthakam, C. M. and Penlidis, A. (2011). Modeling uses and analysis of production scenarios for acrylonitrile-butadiene (NBR) emulsions. *Polymer Engineering & Science*, 51, 1909-1918.

Madhuranthakam, C. M. and Penlidis, A. (2012). Improved Operating Scenarios for the Production of Acrylonitrile-Butadiene Emulsions. Accepted (May 2012)), *Polymer Engineering & Science*, ms length 40 pgs.

Montgomery, D. C. (2005). Design and Analysis of Experiments. (sixth ed.) John Wiley & Sons, Inc.

Washington, I. D., Duever, T. A., and Penlidis, A. (2010). Mathematical Modeling of Acrylonitrile-Butadiene Emulsion Copolymerization: Model Development and Validation. *Journal of Macromolecular Science, Part A*, 47, 747-769.

References for Chapter 8

Benoit, D., Chaplinski, V., Braslau, R., and Hawker, C. J. (1999). Development of a universal alkoxyamine for "living" free radical polymerizations. *Journal of the American Chemical Society*, 121, 3904-3920.

Drache, M., Mandel, K., and Schmidt-Naake, G. (2007). Kinetics of nitroxide-controlled radical polymerization during the non-stationary state. *Polymer*, 48, 1875-1883.

Dube, M. A., Penlidis, A., and Reilly, P. M. (1996). A systematic approach to the study of multicomponent polymerization kinetics: The butyl acrylate/methyl methacrylate vinyl acetate

example .IV. Optimal Bayesian design of emulsion terpolymerization experiments in a pilot plant reactor. *Journal of Polymer Science Part A-Polymer Chemistry*, 34, 811-831.

Fu, Y., Cunningham, M. F., and Hutchinson, R. A. (2007). Modeling of nitroxide-mediated semi-batch radical polymerization. *Macromolecular Reaction Engineering*, 1, 243-252.

Georges, M. K., Hamer, G., Szkurhan, A. R., Kazemedah, A., and Li, J. (2002). Stable free radical polymerization process - Initiation mechanisms with benzoyl peroxide and various nitroxides. *Abstracts of Papers of the American Chemical Society*, 224, U464.

Hernandez-Ortiz, J. C., Vivaldo-Lima, E., Lona, L. M. F., McManus, N. T., and Penlidis, A. (2009). Modeling of the nitroxide-mediated radical copolymerization of styrene and divinylbenzene. *Macromolecular Reaction Engineering*, 3, 288-311.

Ide, N. and Fukuda, T. (1997). Nitroxide-controlled free-radical copolymerization of vinyl and divinyl monomers. Evaluation of pendant-vinyl reactivity. *Macromolecules*, 30, 4268-4271.

Ide, N. and Fukuda, T. (1999). Nitroxide-controlled free-radical copolymerization of vinyl and divinyl monomers. 2. Gelation. *Macromolecules*, 32, 95-99.

Matyjaszewski, K. (2002). Fundamentals of atom transfer radical polymerization (pp. 523-628). In Handbook of Radical Polymerization, K.Matyjaszewski and T. P. Davis (Eds.), Hoboken: John Wiley and Sons, Inc.

Moad, G., Rizzardo, E., and Solomon, D. H. (1981). The reaction of acyl peroxides with 2,2,6,6-tetramethylpiperidinyl-1-oxy. *Tetrahedron Letters*, 22, 1165-1168.

Nabifar, A., McManus, N., Vivaldo-Lima, E., Lona, L. M. F., and Penlidis, A. (2008). A replicated investigation of nitroxide-mediated radical polymerization of styrene over a range of reaction conditions. *Canadian Journal of Chemical Engineering*, 86, 879-892.

Roa-Luna, M., Nabifar, A., Diaz-Barber, M. P., McManus, N. T., Vivaldo-Lima, E., Lona, L. M. F., and Penlidis, A. (2007). Another perspective on the nitroxide mediated radical polymerization (NMRP) of styrene using 2,2,6,6-tetramethyl-1-piperidinyloxy (TEMPO) and

dibenzoyl peroxide (BPO). *Journal of Macromolecular Science Part A: Pure and Applied Chemistry*, 44, 337-349.

Tuinman, E., McManus, N. T., Roa-Luna, M., Vivaldo-Lima, E., Lona, L. M. F., and Penlidis, A. (2006). Controlled free-radical copolymerization kinetics of styrene and divinylbenzene by bimolecular NMRP using TEMPO and dibenzoyl peroxide. *Journal of Macromolecular Science Part A: Pure and Applied Chemistry*, 43, 1-17.

Vivaldo-Lima, E., Penlidis, A., Wood, P. E., and Hamielec, A. E. (2006). Determination of the relative importance of process factors on particle size distribution in suspension polymerization using a Bayesian experimental design technique. *Journal of Applied Polymer Science*, 102, 5577-5586.

Zetterlund, P. B., Alam, M. N., Minami, H., and Okubo, M. (2005). Nitroxide-mediated controlled/living free radical copolymerization of styrene and divinylbenzene in aqueous miniemulsion. *Macromol.Rapid Commun.*, 26, 955-960.

Zetterlund, P. B., Alam, M. N., and Okubo, M. (2006). Network formation in nitroxide-mediated radical copolymerization of styrene and divinylbenzene in miniemulsion. *Macromol.Chem.Phys.*, 207, 1732-1741.

Zhou, M. X., McManus, N. T., Vivaldo-Lima, E., Lona, L. M. F., and Penlidis, A. (2010). Kinetics of nitroxide mediated radical polymerization of styrene with unimolecular initiators. *Macromolecular Symposia*, 289, 95-107.

References for Chapter 9

Abrol, S., Kambouris, P. A., Looney, M. G., and Solomon, D. H. (1997). Studies on microgels .III. Synthesis using living free radical polymerization. *Macromolecular Rapid Communications*, 18, 755-760.

Abrol, S., Caulfield, M. J., Qiao, G. G., and Solomon, D. H. (2001). Studies on microgels. V. Synthesis of microgels via living free radical polymerization. *Polymer*, 42, 5987-5991.

Alam, M. N., Zetterlund, P. B., and Okubo, M. (2006). Network formation in nitroxide-mediated radical copolymerization of styrene and divinylbenzene in miniemulsion. *Macromolecular Chemistry and Physics*, 207, 1732-1741.

Aldabbagh, F., Zetterlund, P. B., and Okubo, M. (2008). Nitroxide-mediated precipitation polymerization of styrene in supercritical carbon dioxide: Effects of monomer loading and nitroxide partitioning on control. *European Polymer Journal*, 44, 4037-4046.

Benoit, D., Chaplinski, V., Braslau, R., and Hawker, C. J. (1999). Development of a universal alkoxyamine for "living" free radical polymerizations. *Journal of the American Chemical Society*, 121, 3904-3920.

Box, G. E. P., Hunter, J. S., & Hunter, W. G. (2005). Statistics for Experimenters. (Second Edition) Hoboken, New Jersey: John Wiley & Sons.

Dong, Z. M., Liu, X. H., Lin, Y., and Li, Y. S. (2008). Branched polystyrene with abundant pendant vinyl functional groups from asymmetric divinyl monomer. *Journal of Polymer Science Part A: Polymer Chemistry*, 46, 6023-6034.

Drache, M., Mandel, K., and Schmidt-Naake, G. (2007). Kinetics of nitroxide-controlled radical polymerization during the non-stationary state. *Polymer*, 48, 1875-1883.

Fu, Y., Cunningham, M. F., and Hutchinson, R. A. (2007). Modeling of nitroxide-mediated semi-batch radical polymerization. Macromolecular Reaction Engineering, 1, 243-252.

Fukuda, T., Terauchi, T., Goto, A., Ohno, K., Tsujii, Y., Miyamoto, T., Kobatake, S., Yamada, B. (1996). Mechanisms and kinetics of nitroxide-controlled free radical polymerization. *Macromolecules*, 29, 6393-6398.

Gao, H., Min, K., and Matyjaszewski, K. (2007). Determination of gel point during atom transfer radical copolymerization with cross-Linker. *Macromolecules*, 40, 7763-7770.

Gao, H., Li, W., and Matyjaszewski, K. (2008a). Synthesis of polyacrylate networks by ATRP: parameters influencing experimental gel points. *Macromolecules*, 41, 2335-2340.

Gao, H., Miasnikova, A., and Matyjaszewski, K. (2008b). Effect of cross-linker reactivity on experimental gel points during ATRP of monomer and cross-Linker. *Macromolecules*, 41, 7843-7849.

Georges, M. K., Hamer, G., Szkurhan, A. R., Kazemedah, A., and Li, J. (2002). Stable free radical polymerization process - Initiation mechanisms with benzoyl peroxide and various nitroxides. *Abstracts of Papers of the American Chemical Society*, 224, U464.

Goncalves, M. A., Trigo, I. M., Dias, R. C., and Costa, M. R. P. (2010). Kinetic modeling of the molecular architecture of cross-linked copolymers synthesized by controlled radical polymerization techniques. *Macromolecular Symposia*, 291-292, 239-250.

Hernandez-Ortiz, J. C., Vivaldo-Lima, E., Lona, L. M. F., McManus, N. T., and Penlidis, A. (2009). Modeling of the nitroxide-mediated radical copolymerization of styrene and divinylbenzene. *Macromolecular Reaction Engineering*, 3, 288-311.

Hernandez-Ortiz, J. C., Vivaldo-Lima, E., and Penlidis, A. (2012). Modeling of network formation in nitroxide-mediated radical copolymerization of vinyl/divinyl monomers using a multifunctional polymer molecule approach. *Macromolecular Theory and Simulations*, DOI: 10.1002/mats.201100091.

Hild, G. (1997). Interpretation of equilibrium swelling data on model networks using affine and 'phantom' network models. *Polymer*, 38, 3279-3293.

Hirano, T., Tanaka, K., Wang, H., Seno, M., and Sato, T. (2005). Effect of nitrobenzene on initiator-fragment incorporation radical polymerization of divinylbenzene with dimethyl 2,2′-azobisisobutyrate. *Polymer*, 46, 8964-8972.

Holdaway, I., Haward, R. N., and Parsons, I. W. (1978). Copolymerisation of 4,4′-divinylbiphenyl and of 4,4′-diisopropenylbiphenyl with styrene in solution. *Die Makromolekulare Chemie*, 179, 1939-1950.

Ide, N. and Fukuda, T. (1997). Nitroxide-controlled free-radical copolymerization of vinyl and divinyl monomers. Evaluation of pendant-vinyl reactivity. *Macromolecules*, 30, 4268-4271.

Ide, N. and Fukuda, T. (1999). Nitroxide-controlled free-radical copolymerization of vinyl and divinyl monomers. 2. Gelation. *Macromolecules*, 32, 95-99.

Landin, D. T. and Macosko, C. W. (1988). Cyclization and reduced reactivity of pendant vinyls during the copolymerization of methyl methacrylate and ethylene glycol dimethacrylate. *Macromolecules*, 21, 846-851.

Li, I., Howell, B. A., Matyjaszewski, K., Shigemoto, T., Smith, P. B., and Priddy, D. B. (1995). Kinetics of decomposition of 2,2,6,6-tetramethyl-1-(1-phenylethoxy)piperidine and its implications on nitroxyl-mediated styrene polymerization. *Macromolecules*, 28, 6692-6693.

Marque, S., Le Mercier, C., Tordo, P., and Fischer, H. (2000). Factors Influencing the C−O−Bond Homolysis of Trialkylhydroxylamines. *Macromolecules*, 33, 4403-4410.

McIsaac, S. L., Dube, M. A., Gao, J., and Penlidis, A. (1993). Experimental procedures for ampoule polymerization, Internal report, Department of Chemical Engineering, University of Waterloo, Waterloo, Canada.

McManus, N. T. and Penlidis, A. (1996). A kinetic investigation of styrene-ethyl acrylate copolymerization. *Journal of Polymer Science Part A-Polymer Chemistry*, 34, 237-248.

Moad, G., Rizzardo, E., and Solomon, D. H. (1981). The reaction of acyl peroxides with 2,2,6,6-tetramethylpiperidinyl-1-oxy. *Tetrahedron Letters*, 22, 1165-1168.

Mori, S. and Barth, H. G. (1999). Size Exclusion Chromatography. New York: Springer.

Mrkvicìkova, L. and Kratochvil, P. (1981). Analysis of the products of copolymerization with chain branching in the pre-gelation stage. *Journal of Polymer Science: Polymer Physics Edition*, 19, 1675-1686.

Nabifar, A., McManus, N. T., Vivaldo-Lima, E., and Penlidis, A. (2010). Kinetic aspects of styrene polymerization with an acyloxyamine. *Journal of Macromolecular Science Part A-Pure and Applied Chemistry*, 47, 496-502.

Nilsen, A. and Braslau, R. (2006). Nitroxide decomposition: Implementations towards nitroxide design for applications in living free radical polymerizations. *Journal of Polymer Science Part A-Polymer Chemistry*, 44, 697-717.

Norisuye, T., Morinaga, T., Tran-Cong-Miyata, Q., Goto, A., Fukuda, T., and Shibayama, M. (2005). Comparison of the gelation dynamics for polystyrenes prepared by conventional and living radical polymerizations: a time-resolved dynamic light scattering study. *Polymer*, 46, 1982-1994.

Odian, G. (2004). Principles of Polymerization. (4th Edition) Hoboken, New Jersey: John Wiley & Sons, Inc.

Okay, O. (1988). Formation and structural characteristics of loosely crosslinked styrene-divinylbenzene networks. *Die Makromolekulare Chemie*, 189, 2201-2217.

Patrickios, C. S. (2010). Polymer networks: recent developments. *Macromolecular Symposia*, 291-292, 1-11.

Peters, E. C., Svec, F., Fréchet, J. M. J., Viklund, C., and Irgum, K. (1999). Control of porous properties and surface chemistry in "molded" porous polymer monoliths prepared by polymerization in the presence of TEMPO. *Macromolecules*, 32, 6377-6379.

Psarreas, A., Tzoganakis, C., McManus, N., and Penlidis, A. (2007). Nitroxide-mediated controlled degradation of polypropylene. *Polymer Engineering and Science*, 47, 2118-2123.

Saka, Y., Zetterlund, P. B., and Okubo, M. (2007). Gel formation and primary chain lengths in nitroxide-mediated radical copolymerization of styrene and divinylbenzene in miniemulsion. *Polymer*, 48, 1229-1236.

Scorah, M. J., McManus, N. T., & Penlidis, A. (2004). GPC operating manual, Internal Report, Department of Chemical Engineering, University of Waterloo, Waterloo, Canada

Sobek, J., Martschke, R., and Fischer, H. (2001). Entropy control of the cross-reaction between carbon-centered and nitroxide radicals. *Journal of the American Chemical Society*, 123, 2849-2857.

Soper, B., Haward, R. N., and White, E. F. T. (1972). Intramolecular cyclization of styrene-p-divinylbenzene copolymers. *Journal of Polymer Science Part A-1: Polymer Chemistry*, 10, 2545-2564.

Tanaka, T., Suzuki, T., Saka, Y., Zetterlund, P. B., and Okubo, M. (2007). Mechanical properties of cross-linked polymer particles prepared by nitroxide-mediated radical polymerization in aqueous micro-suspension. *Polymer*, 48, 3836-3843.

Tuinman, E., McManus, N. T., Roa-Luna, M., Vivaldo-Lima, E., Lona, L. M. F., and Penlidis, A. (2006). Controlled free-radical copolymerization kinetics of styrene and divinylbenzene by bimolecular NMRP using TEMPO and dibenzoyl peroxide. *Journal of Macromolecular Science Part A: Pure and Applied Chemistry*, 43, 1-17.

Viklund, C., Nordstom, A., Irgum, K., Svec, F., and Fréchet, J. M. J. (2001). Preparation of porous poly(styrene-co-divinylbenzene) monoliths with controlled pore size distributions initiated by stable free radicals and their pore surface functionalization by grafting. *Macromolecules*, 34, 4361-4369.

Wang, A. R. and Zhu, S. (2005). Branching and gelation in atom transfer radical polymerization of methyl methacrylate and ethylene glycol dimethacrylate. *Polymer Engineering & Science*, 45, 720-727.

Yu, Q., Zeng, F., and Zhu, S. (2001). Atom transfer radical polymerization of poly(ethylene glycol) dimethacrylate. *Macromolecules*, 34, 1612-1618.

Yu, Q., Qin, Z. Q., Li, J. C., and Zhu, S. P. (2008). Diffusion-controlled atom transfer radical polymerization with crosslinking. *Polymer Engineering and Science*, 48, 1254-1260.

Zetterlund, P. B., Alam, M. N., Minami, H., and Okubo, M. (2005). Nitroxide-mediated controlled/living free radical copolymerization of styrene and divinylbenzene in aqueous miniemulsion. *Macromolecular Rapid Communications*, 26, 955-960.

Zetterlund, P. B., Saka, Y., and Okubo, M. (2009a). Gelation and hollow particle formation in nitroxide-mediated radical copolymerization of styrene and divinylbenzene in miniemulsion. *Macromolecular Chemistry and Physics*, 210, 140-149.

Zetterlund, P. B., Alam, N., and Okubo, M. (2009b). Effects of the oil-water interface on network formation in nanogel synthesis using nitroxide-mediated radical copolymerization of styrene/divinylbenzene in miniemulsion. *Polymer*, 50, 5661-5667.

Zhou, M., McManus, N. T., Vivaldo-Lima, E., Lona, L. M. F., and Penlidis, A. (2010). Kinetics of nitroxide mediated radical polymerization of styrene with unimolecular initiators. *Macromolecular Symposia*, 289, 95-107.

References for Chapter 10

Alam, M. N., Zetterlund, P. B., and Okubo, M. (2006). Network formation in nitroxide-mediated radical copolymerization of styrene and divinylbenzene in miniemulsion. *Macromolecular Chemistry and Physics*, 207, 1732-1741.

Alig, I., Nancke, K., and Johari, G. P. (1994). Relaxations in thermosets. XXVI. Ultrasonic studies of the temperature dependence of curing kinetics of diglycidyl ether of bisphenol-A with catalyst. *Journal of Polymer Science Part B: Polymer Physics*, 32, 1465-1474.

Ambler, M. R. and McIntyre, D. (1977). Randomly branched styrene/divinylbenzene copolymers. II. Solution properties and structure. *Journal of Applied Polymer Science*, 21, 2269-2282.

Bannister, I., Billingham, N. C., Armes, S. P., Rannard, S. P., and Findlay, P. (2006). Development of branching in living radical copolymerization of vinyl and divinyl monomers. *Macromolecules*, 39, 7483-7492.

Bastide, J., Leibler, L., and Prost, J. (1990). Scattering by deformed swollen gels: butterfly isointensity patterns. *Macromolecules*, 23, 1821-1825.

Brandrup, J., Immergut, E. H., Grulke, E. A., Abe, A., and Bloth, D. R. (1999). *Polymer Handbook*. (4th Ed. ed.) New York: John Wiley & Sons.

Bruinewoud, H. (2005). Thesis dissertation, Ultrasound-Induced Drug Release from Polymer Matrices, Technische Universiteit Eindhoven.

Chen, T.-F., Nguyen, K. T., Wen, S.-S. L., and Jen, C. K. (1998). Temperature measurement of polymer extrusion by ultrasonic techniques. *Measurement Science and Technology*, 10, 139.

Cheng, J. J. (2008). Mechanical and Chemical Properties of High Density Polyethylene: Effects of Microstructure on Creep Characteristics. Department of Chemical Engineering, University of Waterloo, ON, Canada.

Constable, G. S., Lesser, A. J., and Coughlin, E. B. (2003). Ultrasonic spectroscopic evaluation of the ring-opening metathesis polymerization of dicyclopentadiene. *Journal of Polymer Science Part B: Polymer Physics*, 41, 1323-1333.

Crescenzi, V., Dentini, M., Bontempo, D., and Masci, G. (2002). Hydrogels based on pullulan derivatives crosslinked via a living free-radical process. *Macromolecular Chemistry and Physics*, 203, 1285-1291.

Elliott, J. E. and Bowman, C. N. (1999). Kinetics of primary cyclization reactions in cross-linked polymers: An analytical and numerical approach to heterogeneity in network formation. *Macromolecules*, 32, 8621-8628.

Ellis, T. S., Karasz, F. E., and Brinke, G. T. (1983). The influence of thermal properties on the glass transition temperature in styrene/divinylbenzene network-Diluent systems. *Journal of Applied Polymer Science*, 28, 23-32.

Flory, P. J. (1953). Principles of Polymer Chemistry. Ithaca, N.Y.: Cornell University Press.

Franca , D. R., Jen, C. K., Nguyen, K. T., and Gendron, R. (2000). Ultrasonic in-line monitoring of polymer extrusion. *Polymer Engineering & Science*, 40, 82-94.

Gao, H., Min, K., and Matyjaszewski, K. (2007). Determination of gel point during Atom Transfer Radical Copolymerization with Cross-Linker. *Macromolecules*, 40, 7763-7770.

Gao, H., Li, W., and Matyjaszewski, K. (2008a). Synthesis of Polyacrylate Networks by ATRP: Parameters Influencing Experimental Gel Points. *Macromolecules*, 41, 2335-2340.

Gao, H., Miasnikova, A., and Matyjaszewski, K. (2008b). Effect of Cross-Linker Reactivity on Experimental Gel Points during ATRcP of Monomer and Cross-Linker. *Macromolecules*, 41, 7843-7849.

Gao, H. and Matyjaszewski, K. (2009). Synthesis of functional polymers with controlled architecture by CRP of monomers in the presence of cross-linkers: From stars to gels. *Progress in Polymer Science*, 34, 317-350.

Gao, H., Polanowski, P., and Matyjaszewski, K. (2009). Gelation in living copolymerization of monomer and divinyl cross-linker: Comparison of ATRP experiments with Monte Carlo Simulations. *Macromolecules,* 42, 5925-5932.

Ginzel, E. (1996). Based on personal communication between Professor A. Penlidis and Materials Research Institute (MRI), Waterloo, ON, Canada

Gundogan, N., Okay, O., and Oppermann, W. (2004). Swelling, elasticity and spatial inhomogeneity of poly(N,N-dimethylacrylamide) hydrogels formed at various polymer concentrations. *Macromolecular Chemistry and Physics*, 205, 814-823.

Hammouda, B. (2010). SANS from Polymers-Review of the Recent Literature. *Polymer Reviews*, 50, 14-39.

Harrison, D. J. P., Yates, W. R., and Johnson, J. F. (1985). Techniques for the analysis of cross-linked. *Journal of Macromolecular Science, Part C: Polymer Reviews, 25,* 481-549.

Horkay, F., McKenna, G. B., Deschamps, P., and Geissler, E. (2000). Neutron scattering properties of randomly cross-linked polyisoprene gels. *Macromolecules*, 33, 5215-5220.

Ide, N. and Fukuda, T. (1997). Nitroxide-controlled free-radical copolymerization of vinyl and divinyl monomers. Evaluation of pendant-vinyl reactivity. *Macromolecules*, 30, 4268-4271.

Ide, N. and Fukuda, T. (1999). Nitroxide-controlled free-radical copolymerization of vinyl and divinyl monomers. 2. Gelation. *Macromolecules*, 32, 95-99.

Kannurpatti, A. R., Anderson, K. J., Anseth, J. W., and Bowman, C. N. (1997). Use of "living" radical polymerizations to study the structural evolution and properties of highly crosslinked polymer networks. *Journal of Polymer Science Part B: Polymer Physics*, 35, 2297-2307.

Kannurpatti, A. R., Anseth, J. W., and Bowman, C. N. (1998). A study of the evolution of mechanical properties and structural heterogeneity of polymer networks formed by photopolymerizations of multifunctional (meth)acrylates. *Polymer*, 39, 2507-2513.

Landais, C. (2011). Thesis dissertation, Ultrasonic Methods for the Characterization of Complex Materials and Material Systems: Polymers, Structured Polymers, Soft Tissue and Bone. University of Nebraska - Lincoln.

Leicht, R. and Fuhrmann, J. (1981). Network formation during styrene-divinylbenzene copolymerization investigated by the fluorescence polarization method. *Polymer Bulletin*, 4, 141-148.

Li, W., Gao, H., and Matyjaszewski, K. (2009). Influence of initiation efficiency and polydispersity of primary chains on gelation during Atom Transfer Radical Copolymerization of monomer and cross-linker. *Macromolecules*, 42, 927-932.

Litvinov, V. M. and Dias, A. A. (2001). Analysis of network structure of UV-cured acrylates by ^{1}H NMR relaxation, 13C NMR spectroscopy, and dynamic mechanical experiments. *Macromolecules*, 34, 4051-4060.

Liu, R. G., Gao, X., and Oppermann, W. (2006). Dynamic light scattering studies on random cross-linking of polystyrene in semi-dilute solution. *Polymer*, 47, 8488-8494.

Mark, H. F., Bikales, N. M. O. C. G., and Menges, G. (1985). Encyclopedia of Polymer Science and Engineering. (Vol 5, Dynamic Mechanical Properties) New York, Chichester, Brisbane, Toronto, Singapore: John Wiley & Sons.

Marx, L., Eskandani, Z., and Hemery, P. (2009). Synthesis of versatile TIPNO-based alkoxyamines. *Reactive and Functional Polymers*, 69, 306-318.

Mathot, V. B. F. (1993). Calorimetry and Thermal Analysis of Polymers. Munich Vienna New York: Hanser Publishers.

Matsumoto, A., Kitaguchi, Y., and Sonoda, O. (1999). Approach to ideal network formation governed by Flory-Stockmayer gelation theory in free-radical cross-linking copolymerization of styrene with m-divinylbenzene. *Macromolecules*, 32, 8336-8339.

Menard, K. P. (2008). Dynamic Mechanical Analysis: a practical introduction. (Second Edition) Boca Raton, London, New York: CRC Press, Taylor & Francis Group.

Nguyen, N. T., Lethiecq, M., and Gerard, J. F. (1995). Glass transition characterization of homogeneous and heterogeneous polymers by an ultrasonic method. *Ultrasonics*, 33, 323-329.

Nielsen, L. E. and Landel, R. F. (1994). Mechanical properties of polymers and composites. New York: Marcel Dekker Inc.

Norisuye, T., Kida, Y., Masui, N., Tran-Cong-Miyata, Q., Maekawa, Y., Yoshida, M. and Shibayama, M. (2003). Studies on two types of built-in inhomogeneities for polymer gels: Frozen segmental concentration fluctuations and spatial distribution of cross-links. *Macromolecules*, 36, 6202-6212.

Norisuye, T., Morinaga, T., Tran-Cong-Miyata, Q., Goto, A., Fukuda, T., and Shibayama, M. (2005). Comparison of the gelation dynamics for polystyrenes prepared by conventional and

living radical polymerizations: a time-resolved dynamic light scattering study. *Polymer*, 46, 1982-1994.

O'Connor, P. J., Cutie, S. S., Smith, P. B., Martin, S. J., Sammler, R. L., Harris, W. I., Marks, M.J. and Wilson, L. (1996). ^{1}H NMR characterization of swelling in cross-linked polymer systems. *Macromolecules*, 29, 7872-7884.

Okay, O. (1988). Formation and structural characteristics of loosely crosslinked styrene-divinylbenzene networks. *Die Makromolekulare Chemie*, 189, 2201-2217.

Oral, I., Guzel, H., Ahmetli, G., and Gur, C. H. (2011). Determining the elastic properties of modified polystyrenes by sound velocity measurements. *Journal of Applied Polymer Science*, 121, 3425-3432.

Oral, I., Guzel, H., an Ahmetli, G. (2012). Ultrasonic properties of polystyrene-based composites. *Journal of Applied Polymer Science*, DOI: 10.1002/app.34926.

Painter P.C. and Coleman, M. M. (2009). Molecular Weight and Branching. In Essentials of Polymer Science and Engineering (Lancaster, Pennsylvania: DEStech Publications).

Rey, L., Galy, J., Sautereau, H., Simon, G. P., and Cook, W. D. (2004). PALS free volume and mechanical properties in dimethacrylate-based thermosets. *Polymer International*, 53, 557-568.

Saalwachter, K. (2007). Proton multiple-quantum NMR for the study of chain dynamics and structural constraints in polymeric soft materials. *Progress in Nuclear Magnetic Resonance Spectroscopy*, 51, 1-35.

Saka, Y., Zetterlund, P. B., an Okubo, M. (2007). Gel formation and primary chain lengths in nitroxide-mediated radical copolymerization of styrene and divinylbenzene in miniemulsion. *Polymer*, 48, 1229-1236.

Scorah, M. J., Dhib, R., and Penlidis, A. (2005). Branching level detection in polymers. encyclopedia of chemical processing (ECHP), S. Lee (Ed.), Taylor & Francis, pg. 251-267.

Simon, G. P., Allen, P. E. M., and Williams, D. R. G. (1991). Properties of dimethacrylate copolymers of varying crosslink density. *Polymer*, 32, 2577-2587.

Tanaka, T., Suzuki, T., Saka, Y., Zetterlund, P. B., and Okubo, M. (2007). Mechanical properties of cross-linked polymer particles prepared by nitroxide-mediated radical polymerization in aqueous micro-suspension. *Polymer*, 48, 3836-3843.

Tieghi, G., Levi, M., and Fallini, A. (1992). Characterization of crosslinked polyester resins by dynamic mechanical properties. *Polymer*, 33, 3748-3750.

Van Camp, W., Gao, H., Du Prez, F. E., and Matyjaszewski, K. (2010). Effect of crosslinker multiplicity on the gel point in ATRP. *Journal of Polymer Science Part A: Polymer Chemistry*, 48, 2016-2023.

Wang, A. R. and Zhu, S. (2005a). Branching and gelation in atom transfer radical polymerization of methyl methacrylate and ethylene glycol dimethacrylate. *Polymer Engineering & Science*, 45, 720-727.

Wang, A. R. and Zhu, S. (2005b). Control of the polymer molecular weight in atom transfer radical polymerization with branching/crosslinking. *Journal of Polymer Science Part A: Polymer Chemistry,* 43, 5710-5714.

Ward, J. H. and Peppas, N. A. (2000). Kinetic gelation modeling of controlled radical polymerizations. *Macromolecules*, 33, 5137-5142.

Ward, J. H., Shahar, A., and Peppas, N. A. (2002). Kinetics of 'living' radical polymerizations of multifunctional monomers. *Polymer*, 43, 1745-1752.

Yu, Q., Zhou, M., Ding, Y., Jiang, B., and Zhu, S. (2007). Development of networks in atom transfer radical polymerization of dimethacrylates. *Polymer*, 48, 7058-7064.

Yu, Q., Zhu, Y. S., Ding, Y. H., and Zhu, S. P. (2008). Reaction behavior and network development in RAFT radical polymerization of dimethacrylates. *Macromolecular Chemistry and Physics*, 209, 551-556.

Yu, Q., Xu, S. H., Zhang, H. W., Ding, Y. H., and Zhu, S. P. (2009). Comparison of reaction kinetics and gelation behaviors in atom transfer, reversible addition-fragmentation chain transfer and conventional free radical copolymerization of oligo(ethylene glycol) methyl ether methacrylate and oligo(ethylene glycol) dimethacrylate. *Polymer*, 50, 3488-3494.

Zetterlund, P. B., Alam, M. N., Minami, H., and Okubo, M. (2005). Nitroxide-mediated controlled/living free radical copolymerization of styrene and divinylbenzene in aqueous miniemulsion. *Macromolecular Rapid Communications*, 26, 955-960.

Zetterlund, P. B., Saka, Y., and Okubo, M. (2009a). Gelation and hollow particle formation in nitroxide-mediated radical copolymerization of styrene and divinylbenzene in miniemulsion. *Macromolecular Chemistry and Physics*, 210, 140-149.

Zetterlund, P. B., Alam, N., and Okubo, M. (2009b). Effects of the oil-water interface on network formation in nanogel synthesis using nitroxide-mediated radical copolymerization of styrene/divinylbenzene in miniemulsion. *Polymer*, 50, 5661-5667.

Zhu, S. H., Penlidis, A., Tzoganakis, C., and Ginzel, E. (2011). Ultrasonic properties and morphology of devulcanized rubber blends. *Journal of Applied Polymer Science*, DOI: 10.1002/app.35251.

Zosel, A. (1995). Mechanical properties of films from polymer latices. *Polymers for Advanced Technologies*, 6, 263-269.

References for Chapter 11

Dube, M. A., Penlidis, A., and Reilly, P. M. (1996). A systematic approach to the study of multicomponent polymerization kinetics: The butyl acrylate/methyl methacrylate vinyl acetate example .IV. Optimal Bayesian design of emulsion terpolymerization experiments in a pilot plant reactor. *Journal of Polymer Science Part A-Polymer Chemistry*, 34, 811-831.

Franceschini, G. and Macchietto, S. (2008a). Model-based design of experiments for parameter precision: State of the art. *Chemical Engineering Science*, 63, 4846-4872.

Franceschini, G. and Macchietto, S. (2008b). Novel anticorrelation criteria for model-based experiment design: Theory and formulations. *AIChE Journal*, 54, 1009-1024.

Leicht, R. and Fuhrmann, J. (1981). Network Formation During Styrene-Divinylbenzene Copolymerization Investigated by the Fluorescence Polarization Method. *Polymer Bulletin*, 4, 141-148.

Nielsen, L. E. and Landel, R. F. (1994). Mechanical Properties of Polymers and Composites. New York: Marcel Dekker Inc.

Norisuye, T., Morinaga, T., Tran-Cong-Miyata, Q., Goto, A., Fukuda, T., and Shibayama, M. (2005). Comparison of the gelation dynamics for polystyrenes prepared by conventional and living radical polymerizations: a time-resolved dynamic light scattering study. *Polymer*, 46, 1982-1994.

Reilly, P. M. (1993). A new approach to experimentation, Technical Report, Department of Chemical Engineering, University of Waterloo, Waterloo, On, Canada.

Saalwachter, K. (2007). Proton multiple-quantum NMR for the study of chain dynamics and structural constraints in polymeric soft materials. *Progress in Nuclear Magnetic Resonance Spectroscopy*, 51, 1-35.

Vivaldo-Lima, E., Penlidis, A., Wood, P. E., and Hamielec, A. E. (2006). Determination of the relative importance of process factors on particle size distribution in suspension polymerization using a Bayesian experimental design technique. *Journal of Applied Polymer Science*, 102, 5577-5586.

Zhu, S. H., Penlidis, A., Tzoganakis, C., and Ginzel, E. (2011). Ultrasonic properties and morphology of devulcanized rubber blends. *Journal of Applied Polymer Science*, DOI: 10.1002/app.35251.

APPENDICES

Appendix A. Clarification of Equations in Chapter 3

A.1. Derivation of Eq. 3.4

Consider a linear regression model below:

$$\underline{y} = \underline{X\theta} + \underline{\varepsilon} \qquad \text{Eq. A.1}$$

where:

$\underline{y}: n \times 1$ $\qquad$ $\underline{X}: n \times p$

$\underline{\theta}: p \times 1$ $\qquad$ $\underline{\varepsilon}: n \times 1$

Bayes' rule:

$$P(\theta \mid y) = \frac{P(y \mid \theta)\, P(\theta)}{P(y)} \qquad \text{Eq. A.2}$$

As mentioned in section 2.2.1 when the data y are known and the parameters θ are unknown, P(y) is constant (so there is no need to be calculated) and P(y|θ) is called the likelihood function of θ for given y and can be written as l(θ|y). Bayes' theorem can thus be rewritten as:

$$P(\theta \mid y) = c\; l(\theta \mid y) P(\theta) \qquad \text{Eq. A.3}$$

where c is a constant. Both $l(\theta \mid y)$ and $P(\theta)$ are multivariate normal probability density functions specified as per below:

$$l(\theta \mid y): N(\underline{X}\underline{\theta}, \underline{I}\sigma^2) \qquad \text{Eq. A.4}$$

$$P(\theta): N(\underline{\alpha}, \underline{U}) \qquad \text{Eq. A.5}$$

In general, a multivariate normal probability density function is specified as below:

$$\underline{z}: N(\underline{\mu}, \underline{V}) \qquad \text{Eq. A.6}$$

$$f(\underline{z}) = \overbrace{\frac{1}{(2\pi)^{n/2}\left|\underline{V}\right|^{1/2}}}^{c} \exp\left\{-\frac{1}{2}(\underline{z}-\underline{\mu})'\,\underline{V}^{-1}(\underline{z}-\underline{\mu})\right\} \qquad \text{Eq. A.7}$$

or

$$f(\underline{z}) = A\exp\left\{-\frac{1}{2}\left[\overbrace{\underline{z}'\underline{V}^{-1}}^{1}\underline{z} - \overbrace{2\underline{z}'\underline{V}^{-1}}^{2}\underline{\mu} + \overbrace{\underline{\mu}'\underline{V}^{-1}}^{3}\underline{\mu}\right]\right\} \qquad \text{Eq. A.8}$$

where $\underline{\mu}$ is the mean and $\underline{V}$ the variance. Therefore, the problem of finding the posterior distribution for θ, $\mathrm{P}(\theta \mid \mathrm{y})$, simplifies down to multiplying two multivariate normal distributions, $\mathrm{l}(\theta \mid \mathrm{y})$ and $\mathrm{P}(\theta)$.

$$\mathrm{P}(\theta \mid \mathrm{y}) \propto \frac{1}{(2\pi)^{n/2}\left|\underline{I}\,\sigma^2\right|^{1/2}} \exp\left\{-\frac{1}{2}(\underline{y}-\underline{X}\,\underline{\theta})'\,(\underline{I}\,\sigma^2)^{-1}(\underline{y}-\underline{X}\,\underline{\theta})\right\}\times$$
$$\frac{1}{(2\pi)^{n/2}\left|\underline{U}\right|^{1/2}} \exp\left\{-\frac{1}{2}(\underline{\theta}-\underline{\alpha})'\,(\underline{U})^{-1}(\underline{\theta}-\underline{\alpha})\right\} \qquad \text{Eq. A.9}$$

$$\mathrm{P}(\theta \mid \mathrm{y}) \propto \overbrace{\frac{1}{(2\pi)^{n}\left|\underline{I}\,\sigma^2\right|^{1/2}\left|\underline{U}\right|^{1/2}}}^{c} \times \qquad \text{Eq. A.10}$$
$$\exp\left[-\frac{1}{2}\left\{(\underline{y}-\underline{X}\,\underline{\theta})'\,(\underline{I}\,\sigma^2)^{-1}(\underline{y}-\underline{X}\,\underline{\theta}) + (\underline{\theta}-\underline{\alpha})'\,(\underline{U})^{-1}(\underline{\theta}-\underline{\alpha})\right\}\right]$$

$$\mathrm{P}(\theta \mid \mathrm{y}) \propto \exp\left[-\frac{1}{2}\left\{\underline{y}'(\underline{I}\,\sigma^2)^{-1}\underline{y} - \underline{\theta}'\,\underline{X}'(\underline{I}\,\sigma^2)^{-1}\underline{y} - \underline{y}'(\underline{I}\,\sigma^2)^{-1}\underline{X}\,\underline{\theta} + \underline{\theta}'\,\underline{X}'(\underline{I}\,\sigma^2)^{-1}\,\underline{X}\,\underline{\theta} + \right.\right.$$
$$\left.\left.\underline{\theta}'(\underline{U})^{-1}\underline{\theta} - \underline{\theta}'(\underline{U})^{-1}\underline{\alpha} - \underline{\alpha}'(\underline{U})^{-1}\underline{\theta} + \underline{\alpha}'(\underline{U})^{-1}\underline{\alpha}\right\}\right] \qquad \text{Eq. A.11}$$

If we show that Eq. A.11 can be in the form of Eq. A.8, then that means that $\mathrm{P}(\theta \mid \mathrm{y})$ is also a multivariate normal distribution. Rearranging Eq. A.11 we obtain:

$$P(\theta \mid y) \propto \exp\left[-\frac{1}{2} \left\{ \begin{array}{l} [\underline{\theta}' \underline{X}' (\underline{I}\sigma^2)^{-1} \underline{X}\underline{\theta} + \underline{\theta}' (\underline{U})^{-1} \underline{\theta}] - \\ [\underline{\theta}' \underline{X}' (\underline{I}\sigma^2)^{-1} \underline{y} + \underline{y}' (\underline{I}\sigma^2)^{-1} \underline{X}\underline{\theta}] - \\ [\underline{\theta}' (\underline{U})^{-1} \underline{\alpha} + \underline{\alpha}' (\underline{U})^{-1} \underline{\theta}] + \underline{y}' (\underline{I}\sigma^2)^{-1} \underline{y} + \underline{\alpha}' (\underline{U})^{-1} \underline{\alpha} \end{array} \right\} \right] \quad \text{Eq. A.12}$$

or

$$P(\theta \mid y) \propto \exp\left[-\frac{1}{2} \left\{ \overbrace{\underline{\theta}' [\underline{X}'\underline{X}/\sigma^2 + (\underline{U})^{-1}] \underline{\theta}}^{1} - \overbrace{2\, \underline{\theta}' (\underline{X}'\underline{y}/\sigma^2 + (\underline{U})^{-1} \underline{\alpha})}^{2} + \overbrace{(\underline{y}' (\underline{I}\sigma^2)^{-1} \underline{y} + \underline{\alpha}' (\underline{U})^{-1} \underline{\alpha})}^{3} \right\} \right] \quad \text{Eq. A.13}$$

Comparing Eq. A.13 with Eq. A.8, it can be concluded that $P(\theta \mid y)$ has the form of a multivariate normal distribution with:

$$\underline{V}^{-1} = (\underline{U})^{-1} + (1/\sigma^2)\, \underline{X}'\underline{X} \quad \text{Eq. A.14}$$

$$\underline{V}^{-1}\, \underline{\mu} = (\underline{U})^{-1} \underline{\alpha} + (1/\sigma^2)\, \underline{X}'\underline{y} \quad \text{Eq. A.15}$$

From Eq. A.14, the variance of the distribution $\underline{V}$ is:

$$\underline{V} = [(\underline{U})^{-1} + (1/\sigma^2)\, \underline{X}'\underline{X}]^{-1} \quad \text{Eq. A.16}$$

From Eq. A.15, the mean of the distribution $\underline{\mu}$ is:

$$\underline{\mu} = [(\underline{U})^{-1} + (1/\sigma^2)\, \underline{X}'\underline{X}]^{-1} [(\underline{U})^{-1} \underline{\alpha} + (1/\sigma^2)\, \underline{X}'\underline{y}] \quad \text{Eq. A.17}$$

In conclusion, the posterior distribution of the parameter values, $P(\theta|y)$, is a multivariate normal distribution, as claimed in Chapter 3:

$$P(\underline{\theta}|\underline{y}):N\{[\underline{U}^{-1}+(1/\sigma^2)\underline{X}'\underline{X}]^{-1}[\underline{U}^{-1}\underline{\alpha}+(1/\sigma^2)\underline{X}'\underline{y}];[\underline{U}^{-1}+(1/\sigma^2)\underline{X}'\underline{X}]^{-1}\} \quad \text{Eq. A.18}$$

A.2. More explanations for Eq. 3.5

The joint confidence region for the posterior distribution of the parameter values is described mathematically by

$$(\underline{\theta}-\hat{\theta})'\underline{V}^{-1}(\underline{\theta}-\hat{\theta})\le K \quad \text{Eq. A.19}$$

where $\hat{\theta}$ is the posterior mean, K is a constant which depends on the number of parameters and the probability level, and $\underline{V}$ is the posterior covariance matrix defined by

$$\underline{V}=[(\underline{U})^{-1}+(1/\sigma^2)\underline{X}'\underline{X}]^{-1} \quad \text{Eq. A.20}$$

In general, the objective of the design is to select experimental conditions such that the uncertainty in the estimated parameters is minimized, which can further be translated to the (hyper)volume of the joint confidence region being minimized. The (hyper)volume of such a region is

$$\frac{(\pi K)^{p/2}|\underline{V}|^{1/2}}{\Gamma(1+p/2)} \quad \text{Eq. A.21}$$

where Γ denotes the gamma function and p is the number of parameters. All the quantities in Eq. A.21 are constant except $\underline{V}$, the posterior covariance matrix. So one can say that the (hyper) volume of the joint confidence region for the parameters is proportional to $|\underline{V}|^{1/2}$. Thus,

the (hyper)volume of the posterior probability region may be minimized by choosing the experiment which minimizes $\left|\left((\underline{U})^{-1}+(1/\sigma^2)\,\underline{X}'\,\underline{X}\right)^{-1}\right|$, or maximizes

$$G=\left|(\underline{U})^{-1}+(1/\sigma^2)\,\underline{X}'\,\underline{X}\right| \qquad \text{Eq. A.22}$$

The fundamental identity rule (Mardia et al., 1988) is applied to G to provide a simplified version

$$G=\left|(\underline{U})^{-1}\right|\,\overbrace{\left|\underline{I}+(1/\sigma^2)\,\underline{X}\,U\underline{X}'\right|}^{H} \qquad \text{Eq. A.23}$$

In conclusion, the design problem is defined as choosing experiment $\underline{X}$ so as to maximize H (as in Eq. 3.5 of Chapter 3).

A.3. References

Mardia, K. V., J. T. Kent, and J. M. Bibby. 1988. Multivariate analysis. Academic Press.

Appendix B. Details of Case Study 5 of Chapter 4: Single- vs. Multi-response Scenarios

Three factors were chosen (temperature, initial concentration of the unimolecular initiator, and number-average molecular weight of the unimolecular initiator), listed in Table B.1 with their initial levels. Four runs were designed in two sequences of 2-trials each. The model initially developed for bimolecular NMRP was modified to accommodate unimolecular NMRP. Subsequently, this model was used to generate the responses for a 2^3 conventional factorial design. Values of prior $\underline{\alpha}$ and prior $\underline{U}$ for both responses are shown in Table B.2 and Table B.3. The variance for batch time was 1, whereas molecular weight had a variance of 840,000 (again the choices of variances were based on previous experience, as explained in Case Study 1 and 4, for batch time and molecular weights, respectively).

Table B.1 Selected factors and their levels in Case 5 (unimolecular NMRP, T = temperature, $[I]_0$ = initial unimolecular initiator concentration, $\overline{M}_n(I)$= average molecular weight of the unimolecular initiator)

Level	**T (°C)**	**$[I]_0$ (M)**	**$\overline{M}_n(I)$ (g/mol)**
low	120	0.03	2,200
high	140	0.05	6,200

Table B.2 Elements of initial $\underline{\alpha}$ and $\underline{U}$ for batch time response (Case 5)

Parameter	α_i	U_{ii}
Mean	10.741	67.535
T	-7.630	6.25
[I]	0.089	1.562
M_n[I]	0.739	1.562
T×[I]	-0.083	0.002
T×$M_n[I]$	-0.450	0.051
[I]×M_n[I]	0.225	0.01
T×[I]×M_n[I]	-0.091	6.25E-06

Table B.3 Elements of initial $\underline{\alpha}$ and $\underline{U}$ for molecular weight response (Case 5)

Parameter	α_i	U_{ii}
Mean	8,949	5,773,320
T	603	90,000
[I]	-1,977	1,000,000
M_n[I]	-199	9,506
T×[I]	394	22,500
$T \times M_n[I]$	442	15,625
$[I] \times M_n[I]$	437	30,625
$T \times [I] \times M_n[I]$	447	625

After implementing the Bayesian design for both responses, there happen to be four optimal 2-trial designs detected for batch time with the determinant H equal to 2689.84, and four 2-trial designs for molecular weight with the determinant H equal to 54.93. Since we were dealing with a multi-response case, it was important to check whether an optimal design for one response was nearly optimal for the other one. Hence, the optimal trials for one response were combined with the $\underline{U}$ matrix and σ^2 from the other response in order to re-evaluate the determinant H for the latter response (using Eq 3.5 of Chapter 3). For example, the optimal designs for the batch time response were each used in Eq. 3.5, along with the variance/covariance matrix ($\underline{U}$) for molecular weight, in order to recalculate the determinant H for molecular weight. All four 2-trial designs from batch time decreased the determinant value for molecular weight by 1.75%. On the other hand, using the optimal designs from molecular weight in the recalculation of the determinant H for batch time (using the $\underline{U}$ matrix for batch time) decreased the value of the determinant by 13.34%. As can be seen, using the optimal designs from batch time for the H calculation for molecular weight decreased the determinant less and hence, one of them was chosen (randomly for the sake of the example) as "the optimal design" for the first sequence of experiments.

After updating $\underline{\alpha}$ and $\underline{U}$ for batch time and molecular weight (not shown here for the sake of brevity), the next sequence of experiments was designed. There happened to be only one 2-trial design which maximized the determinant H for the molecular weight response, while for batch time there were two 2-trial experiments that corresponded to the highest H. In order to find a design that was nearly optimal for both responses, the designs from batch time were used in the H recalculations for molecular weight (using $\underline{U}_{posterior}$ from molecular weight) and vice versa

(the design from molecular weight was used in the H recalculations for batch time). Upon scrutinizing the results, again the experiments designed through batch time decreased the determinant H of the molecular weight response less dramatically. Figure B.1 shows the design that was chosen. As can be seen, in the second sequence, the concentration for the unimolecular initiator is set at the high level for both of the trials ([I] = 0.05M), while temperature and the molecular weight of the unimolecular initiator were changing from low to high level from one trial to the other.

This case shows that the Bayesian design methodology can be used in multi-response situations and, even more importantly, it can suggest experiments that are nearly optimal for all responses. In our case, batch time and a certain average molecular weight were the responses used. However, other responses like rate of polymerization or polydispersity can also be employed.

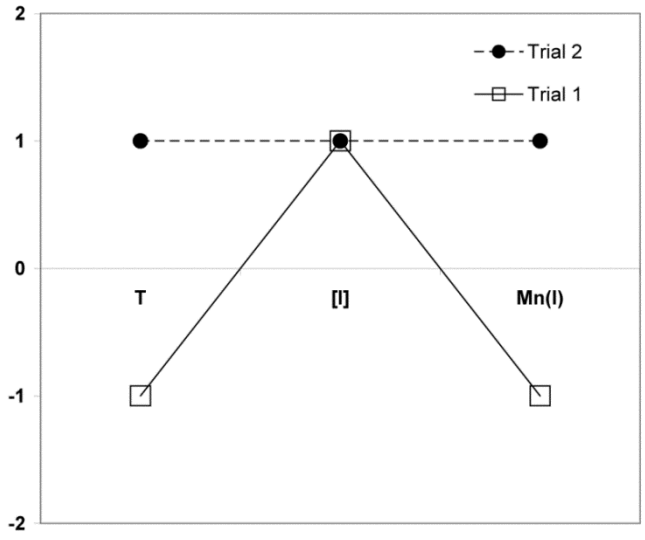

Figure B.1 Visual illustration of the second sequence of 2-trials suggested for Case 5

Appendix C. Model Equations for the Production of Acrylonitrile-Butadiene Emulsion

1. Initiator Balance

$$\frac{dN_I}{dt} = F_{I_{in}} - F_I - R_I V_a$$

$$R_I = k_1 [I]_a [Fe^{2+}]_a + 2 f k_d [I]_a$$

2. Reducing Agent Balance

$$\frac{dN_{RA}}{dt} = F_{RA_{in}} - F_{RA} - R_{RA} V_a$$

$$R_{RA} = k_2 [RA]_a [Fe^{3+}]_a$$

3. Oxidizing Agent Balance

$$\frac{dN_{Fe^{2+}}}{dt} = F_{Fe^{2+}_{in}} - F_{Fe^{2+}} - R_{Fe^{2+}} V_a$$

$$\frac{dN_{Fe^{3+}}}{dt} = F_{Fe^{3+}_{in}} - F_{Fe^{3+}} - R_{Fe^{3+}} V_a$$

$$\frac{dN_{Fe}}{dt} = F_{Fe_{in}} - F_{Fe}$$

$$R_{Fe^{2+}} = k_1 [I]_a [Fe^{2+}]_a - k_2 [RA]_a [Fe^{3+}]_a$$

$$R_{Fe^{2+}} = -R_{Fe^{3+}}$$

4. Particle Nucleation

$$\frac{dN_P}{dt} = F_{P,in} - F_P + (R_{\text{hom}} + R_{mic}) \cdot V_a \cdot N_A$$

$$R_{\text{hom}} = k_h [R^{\bullet}]_a^{\text{hom}}$$

$$R_{mic} = \rho_{des}^{mic} + \frac{k_{cm} [R^{\bullet}]_a^{mic}}{r_{mic}}$$

5. Water Balance

$$\frac{dN_w}{dt} = F_{w_{in}} - F_w$$

6. Monomer and Polymer Balances

$$\frac{dN_{m_j}}{dt} = F_{m_{jin}} - F_{m_j} - (R_{p_{j_p}} V_p + R_{p_{j_a}} V_a)$$

$$\frac{dN_{pol_j}}{dt} = F_{pol_{jin}} - F_{pol_j} + (R_{p_{j_p}} V_p + R_{p_{j_a}} V_a)$$

7. Monomer Partitioning

$$K_{m_i}^{a/p} = \frac{V_{m_i}^a / V_a}{V_{m_i}^p / V_p}$$

8. Emulsifier Balance

$$\frac{dN_{e_j}}{dt} = F_{e_{j_{in}}} - F_{e_j}$$

9. Impurities Balance

Water soluble impurities

$$\frac{dN_{Z_j}}{dt} = F_{Z_{j_{in}}} - F_{Z_j} - R_{wsi_{j_a}} V_a$$

Monomer soluble impurities

$$\frac{dN_{msi_j}}{dt} = F_{msi_{j_{in}}} - F_{msi_j} - R_{msi_{j_p}} V_p$$

10. Chain Transfer Agent Balance

$$\frac{dN_{CTA_j}}{dt} = F_{CTA_{j,in}} - F_{CTA_j} - R_{CTA_{j_p}} V_p$$

11. Molecular Weight Distribution Moments Balances

$$\frac{d}{dt}\left(V_p Q_i\right) = F_{\left(V_p Q_i\right)_{in}} - F_{V_p Q_i} + R_{V_p Q_i} V_p$$

12. Branching Average Balances

$$\frac{d}{dt}\left(V_p Q_0 \overline{BN}_i\right) = F_{\left(V_p Q_0 \overline{BN}_i\right)_{in}} - F_{V_p Q_0 \overline{BN}_i} + R_{V_p Q_0 \overline{BN}_i} V_p$$

Notation (for Appendix C)

$\overline{BN}_i$	Average number of tri- and tetra-functional branches (i = 3, 4) per chain (#/molecule)
cta_j	j^{th} chain transfer agent
e_j	j^{th} emulsifier
f	Initiation efficiency

$[i]_a$	Concentration of species i (= I, RA, Fe^{2+}, Fe^{3+}) in aqueous phase
$[I]_a$	Concentration of initiator in aqueous phase (mol/L)
I	Initiator
$F_{i_{in}}$	Total molar inflow of species *i* = I, RA, Fe, Fe^{2+}, Fe^{3+}, m_j, pol_j, w, e_j, wsi_j, msi_j, cta_j (mol/min)
Fe	Iron
F_i	Total molar outflow of species *i* = I, RA, Fe, Fe^{2+}, Fe^{3+}, m_j, pol_j, w, e_j, wsi_j, msi_j, cta_j (mol/min)
k_1,k_2	Reaction rate constants (L/mol/min)
k_{cm}	Micelle radical capture rate constant (dm/min)
k_d	Decomposition rate constant (initiator) (L/mol/min)
k_h	Homogeneous nucleation rate constant (min^{-1})
$K_{m_i}^{a/p}$	Partition coefficient of monomer i between aqueous and particle phase
m_j	j^{th} monomer
msi_j	j^{th} monomer soluble impurity
N_A	Avogadro's number (#/mol)
N_i	Total moles of species *i* = I, RA, Fe, Fe^{2+}, Fe^{3+}, m_j, pol_j, w, e_j, wsi_j, msi_j, cta_j
N_p	Number of particles (#)
pol_j	j^{th} polymer
r_{mic}	Average micelle radius (dm)
RA	Reducing agent
R_I	Rate of initiation (mol/L/min)

$R_{RA}, R_{Fe^{2+}}, R_{Fe^{3+}}$	Rates of redox ingredient consumption (mol/L/min)
R_{mic}, R_{hom}	Rate of micellar and homogeneous nucleation (#/L/min)
$[R^{\bullet}]_a^{hom}$	Concentration of radicals in the aqueous phase capable of undergoing homogeneous nucleation (mol/L)
$[R^{\bullet}]_a^{mic}$	Concentration of radicals in the aqueous phase capable of being captured by micelles (mol/L)
$R_{cta_{j_p}}$	Rate of chain transfer agent consumption (mol/L/min)
$R_{p_{j_a}}, R_{p_{j_p}}$	Rates of polymerization in aqueous and particle phases (mol/L/min)
$R_{msi_{j_p}}, R_{wsi_{j_a}}$	Rates of impurity consumption (monomer and water soluble) (mol/L/min)
$R_{V_pQ_i}$	Rate of moment generation for moments i = 0, 1, 2 (mol/L/min)
$R_{V_pQ_o\overline{BN}_i}$	Rate of $\overline{BN}_i$ generation for i = 3, 4 (mol/L/min)
V_a,V_p	Volume of aqueous and particle phase (L)
$V_{m_i}^a, V_{m_i}^p$	Volume of monomer i in aqueous and particle phase (L)
V_pQ_i	i^{th} moments of the molecular weight distribution (mol)
$V_pQ_o\overline{BN}_i$	Zeroth moments of the i^{th} (tri- and tetra-) functional branching frequency distributions (mol #/molecule)
w	water
wsi_j	j^{th} water soluble monomer
ρ_{des}^{mic}	Rate of recapture of desorbed radicals by micelles (#/L/min)

Appendix D. Hierarchical Data Analysis of a Replicated NMRP of STY/DVB

Extensive data collection and careful sample characterization through the full conversion range serve to maximize the information content of the experiments. However, in experimental data, there is always some amount of noise or variation induced by known and/or unknown disturbances. Hence, it is crucial not only to examine the trends obtained from data, but also to perform thorough assessment of the quality of the data. This can be accomplished by measuring the quantifiable uncertainties contributed by the various sources involved in the experimentation.

It is well-known that systems involving DVB as the cross-linker, involve gel materials that are difficult to deal with in the laboratory. This will introduce considerable amount of error into experimentation and subsequent analyses. Hence, when measuring polymer properties, such as molecular weights, experimental errors (from various sources) and instrumental errors are involved and it is important to identify and separate them.

As part of our comprehensive kinetic study, number- and weight-average molecular weights of the produced polymers were measured at various conversion levels using Gel Permeation Chromatography (GPC). To properly identify the sources and magnitudes of errors in measuring molecular weights, a replicated experiment was conducted and subjected to extensive characterization using a hierarchical design (Box et al., 1978). A hierarchical or nested design can be used to separate the total variation in the molecular weight measurement into parts assignable to the three sources: error associated with the GPC measurement itself (analytical error), the error related to the polymerization process/reactor (carried out under identical conditions), and the variability in the measurement corresponding to different sampling times.

D.1 Experimental Studies

To check the reproducibility of our experiments, independent polymerization runs were conducted for Exp 4 and 5 of Table 9.2. During the replicated run for Exp 4, samples were

taken out at 60 min (early steps of the reaction), 420 min (mid-range of reaction) and 480 min (gel vicinity). These times represented the 11%, 57% and 62% conversion levels for Exp 4 and corresponded to 15%, 58% and 65% conversion levels for the replicate of Exp 4. For Exp 5, samples were duplicated at 150 min (beginning of the reaction), 1020 min (gel vicinity), 1140 min (after gel point) and 1500 min (well after gel point and almost at the end of reaction). These times corresponded to 34%, 83%, 85% and 88% conversion levels for Exp 5 and represented 35%, 83%, 84% and 88% conversion levels for the replicate of Exp 5. These independent replications permitted the calculation of variability related to different batches of polymerization. The raw data tables for number- and weight-average molecular weight for both Exp 4 and 5 are shown below.

Table D.1 Raw data for number-average molecular weights for Exp 4 ([I-TIPNO] = 1 wt%, [DVB] = 1 wt%)

Time	Polymerization	GPC	Y_{tpg}	$\bar{y}_{tp}$	$\bar{y}_t$	$\bar{y}$
1 (60 min)	1	1	7,452	6,928	7,102	46,944
		2	6,404			
	2	1	6,991	7,275		
		2	7,559			
2 (420 min)	1	1	47,739	48,314	47,243	
		2	48,888			
	2	1	47,347	46,172		
		2	44,996			
3 (480 min)	1	1	129,257	111,261	86,487	
		2	93,264			
	2	1	55,645	61,714		
		2	67,783			

Table D.2 Raw data for weight-average molecular weights for Exp 4 ([I-TIPNO] = 1 wt%, [DVB] = 1 wt%)

Time	Polymerization	GPC	Y_{tpg}	$\bar{y}_{tp}$	$\bar{y}_t$	$\bar{y}$
1 (60 min)	1	1	10,640	12,208	10,492	464,318
		2	13,775			
	2	1	8,559	8,777		
		2	8,994			
2 (420 min)	1	1	282,551	283,021	278,278	
		2	283,491			
	2	1	279,493	273,535		
		2	267,576			
3 (480 min)	1	1	1,430,000	1,549,000	1,104,184	
		2	1,668,000			
	2	1	555,586	659,369		
		2	763,151			

Table D.3 Raw data for number-average molecular weights for Exp 5 ([I-TIPNO] = 2 wt%, [DVB] = 1 wt%)

Time	Polymerization	GPC	Y_{tpg}	$\bar{y}_{tp}$	$\bar{y}_t$	$\bar{y}$
1 (150 min)	1	1	7,469	7,215	7,291	52,281
		2	6,960			
	2	1	7,506	7,367		
		2	7,228			
2 (1020 min)	1	1	178,946	198,754	128,622	
		2	218,562			
	2	1	45,520	58,490		
		2	71,459			
3 (1140 min)	1	1	69,703	51,377	40,068	
		2	33,050			
	2	1	27,136	28,760		
		2	30,384			
4 (1500 min)	1	1	31,603	33,279	33,144	
		2	34,955			
	2	1	28,876	33,009		
		2	37,141			

Table D.4 Raw data for weight-average molecular weights for Exp 5 ([I-TIPNO] = 2 wt%, [DVB] = 1 wt%)

Time	Polymerization	GPC	Y_{tpg}	$\bar{y}_{tp}$	$\bar{y}_t$	$\bar{y}$
1 (150 min)	1	1	8,902	8,965	9,085	669,185
		2	9,028			
	2	1	9,016	9,205		
		2	9,393			
2 (1020 min)	1	1	3,025,000	3,094,000	2,023,738	
		2	3,163,000			
	2	1	940,622	953,477		
		2	966,331			
3 (1140 min)	1	1	867,144	717,494	475,920	
		2	567,843			
	2	1	236,698	234,346		
		2	231,994			
4 (1500 mins)	1	1	124,981	135,630	167,999	
		2	146,278			
	2	1	131,463	200,368		
		2	269,272			

D.2 Theoretical Background

Experimental values are subject to various forms of error, contributed by one or more sources. If the average of the experimental values is assumed to be the true value, the deviation from the true value can be attributed to the individual deviations caused by each source. Hence, each measurement can be represented by Eq. D.1.

$$y = \mu \pm A_a \pm B_b \pm C_c \qquad \text{Eq. D.1}$$

where μ is the mean value of y, and A_a, B_b, C_c are the quantified errors (A, B, C) associated with sources a, b, and c.

A nested hierarchical design was used to estimate the components of variance in each measurement. Three levels of the nested design were examined in this study. The lowest level was the analytical error (error associated with the measurements conducted using the GPC (G)). This was examined by performing replicate analyses. The next level was the polymerization level (P), which compared the difference between two polymerizations carried out under identical conditions).The highest level was the time (T), which examined the error associated with the measurements conducted at various times during the course of the reaction. This was also indicative of the level of conversion of the monomer.

The variance associated with each level was represented as V_G, V_P, and V_T. Each observation was then defined as y_{tp1}, y_{tp2}, …, y_{tpg}, where there were G replicated analytical tests made on the P^{th} polymerization, and T^{th} time. The averages for the P^{th} level are defined as $\bar{y}_{tp}$. The variance in the GPC measurements was calculated as in Equation 2, with V_G being an estimate of σ_G^2 having TP(G-1) degrees of freedom:

$$V_G = MS_G = \frac{SS_G}{TP(G-1)} = \frac{\sum_t^T \sum_p^P \sum_g^G \left(y_{tpg} - \bar{y}_{tp}\right)^2}{TP(G-1)} \qquad \text{Eq. D.2}$$

The variance in the polymerization reactions (V_P) was determined by calculating the averages of the values obtained for different polymerization reactions for each of the different times. These were defined as $\bar{y}_t$ in Equation 3, and V_P was calculated as follows:

$$V_P = MS_P = \frac{SS_p}{T(P-1)} = \frac{G\sum_t^T \sum_p^P \left(\bar{y}_{tp} - \bar{y}_t\right)^2}{T(P-1)} \qquad \text{Eq. D.3}$$

The variance calculated using Eq. D.3 was not an estimate of the variance in the polymerization reactions alone. Because it was calculated by pooling the averages calculated from the various GPC readings, the value of V_P was actually a combination of the variance in

the GPC measurements, as well as the variance in the polymerization reactions. The individual variance contributed by the polymerization reactions was calculated using Eq. D.4.

$$V_P = \sigma_G^2 + G\,\sigma_P^2 \qquad \text{Eq. D.4}$$

Finally, to calculate V_T Eq. D.5 was used:

$$V_T = MS_T = \frac{SS_T}{(T-1)} = \frac{PG\sum_{st}^{T}(\bar{y}_t - \bar{y})^2}{T-1} \qquad \text{Eq. D.5}$$

Again, the estimated value calculated in Eq. D.5 is an estimate of the variance contributed by each of the three factors, the GPC readings, the polymerization reactions, and the time variable. The error contributed solely by the time variable can be calculated by equating Eq. D.5 to Eq. D.6.

$$V_T = \sigma_G^2 + G\sigma_P^2 + PG\sigma_T^2 \qquad \text{Eq. D.6}$$

D.3 Hierarchical Layout

In Exp 4, the three samples taken out at 60min, 420 min and 480 min (t = 3) were reproduced in the replicated run (p = 2). For each polymerization sample two independent GPC measurements were carried out (g = 2). Thus, the design was of a 3x2x2 layout, as shown in Figure D.1.

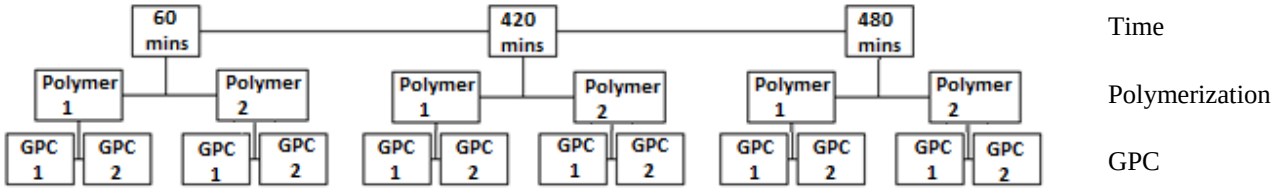

Figure D.1 Hierarchical layout for Exp 4

In Exp 5, the samples taken out at four different time intervals (t= 4; 150 min, 1020 min, 1140 min and 1500 min) were replicated in an independent polymerization run (p= 2), and for each polymerization sample two GPC measurements were carried out (g= 2). Thus, the design was of a 4x2x2 layout, as shown in Figure D.2.

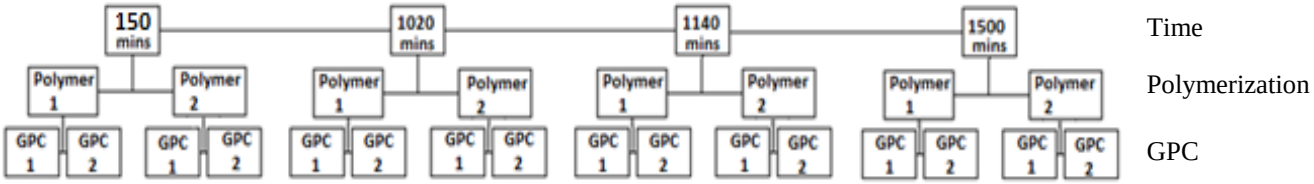

Figure D.2 Hierarchical layout for Exp 5

D.4 Results

From each of the polymerization samples, two independent GPC samples were prepared and dissolved in THF, then injected into the GPC set up and analyzed for molecular weight. The raw experimental data tables are shown in Table D.1 to Table D.4. Error analyses were performed for both number- and weight-average molecular weights (Mn and Mw). ANOVA tables were prepared to present the variance quantified for the three levels studied in this experiment. These results are summarized in Table D.5 to Table D.8.

Table D.5 ANOVA table for number-average molecular weight in Exp 4

Source	df	SS	MS	Variance Estimates
Time	2	1.26E+10	6.30E+09	1.37E+09
Polymerization	3	2.46E+09	8.20E+08	3.49E+08
GPC	6	7.26E+08	1.21E+08	1.21E+08
Total	11	1.58E+10		

Table D.6 ANOVA table for weight-average molecular weight in Exp 4

Source	df	SS	MS	Variance Estimates
Time	2	2.60E+12	1.30E+12	2.59E+11
Polymerization	3	7.92E+11	2.64E+11	1.28E+11
GPC	6	4.99E+10	8.32E+09	8.32E+09
Total	11	3.44E+12		

Table D.7 ANOVA table for number-average molecular weight in Exp 5

Source	df	SS	MS	Variance Estimates
Time	3	3.35E+10	1.12E+10	1.53E+09
Polymerization	4	2.02E+10	5.05E+09	2.41E+09
GPC	8	1.84E+09	2.30E+08	2.30E+08
Total	15	5.55E+10		

Table D.8 ANOVA table for weight-average molecular weight in Exp 5

Source	df	SS	MS	Variance Estimates
Time	3	1.02E+13	3.41E+12	5.52E+11
Polymerization	4	4.82E+12	1.20E+12	5.98E+11
GPC	8	6.44E+10	8.05E+09	8.05E+09
Total	15	1.51E+13		

Based on the ANOVA tables provided for Exp 4 (see Table D.5 and Table D.6), the analytical error associated with only the GPC measurements, was calculated to be 1.21E+08 for M_n, and 8.32E+09 for M_w. These values were calculated based on Eq. D.2. On the basis of a 95% confidence interval, and using a t-distribution, this translates into an analytical error of ±21,553 for M_n and an error of ±178,815 for M_w. This is the error solely based on the GPC measurements.

Using Eq. D.3 and Eq. D.4, the error related to polymerization was found to be 3.49E+08 and 1.28E+11 for the number- and weight-average molecular weights, respectively. This is indicative of the variability in the two polymers that were prepared, and thus, reflects the degree of inconsistency in the preparation techniques. Lastly, using Eq. D.5 and Eq. D.6, the error in the molecular weight measurements corresponding to different times (conversions) was 1.37E+09 and 2.59E+11, respectively, for number-and weight-average molecular weights (see summary Table D.9). This reflects the variance in both molecular weights as the reaction progresses (at various conversions).

Similarly, Table D.7 and Table D.8 summarize the ANOVA tables for Exp 5. In this experiment, the analytical component of the variance was found to be 2.30E+08 for M_n and 8.05E+09 for M_w. Calculations similar to those performed for Exp 4 translated in an error of

±29,709 for M_n and an error of ±175,823 for M_w, again for a 95% confidence interval. The variance associated with the polymerization component was 2.41E+09 for M_n and 5.98E+11 for M_w. Finally, the variability corresponding to different times (conversions) was 1.53E+09 and 5.52E+11 for M_n and M_w, respectively. These results are summarized in Table D.9. These results can also be presented in pictorial format, as shown in Figure D.3 and Figure D.4 below.

Table D.9 Summary of the results obtained for Exp 4 and Exp 5

	Overall Mean	**Variance in GPC** (σ_G^2)	**Variance in Polymerization** (σ_P^2)	**Variance in Time** (σ_T^2)
Exp 4				
Mn	46,944	1.21E+08	3.49E+08	1.37E+09
Mw	31,970	8.32E+09	1.28E+11	2.59E+11
Exp 5				
Mn	52,281	2.30E+08	2.41E+09	1.53E+09
Mw	669,185	8.05E+09	5.98E+11	5.52E+11

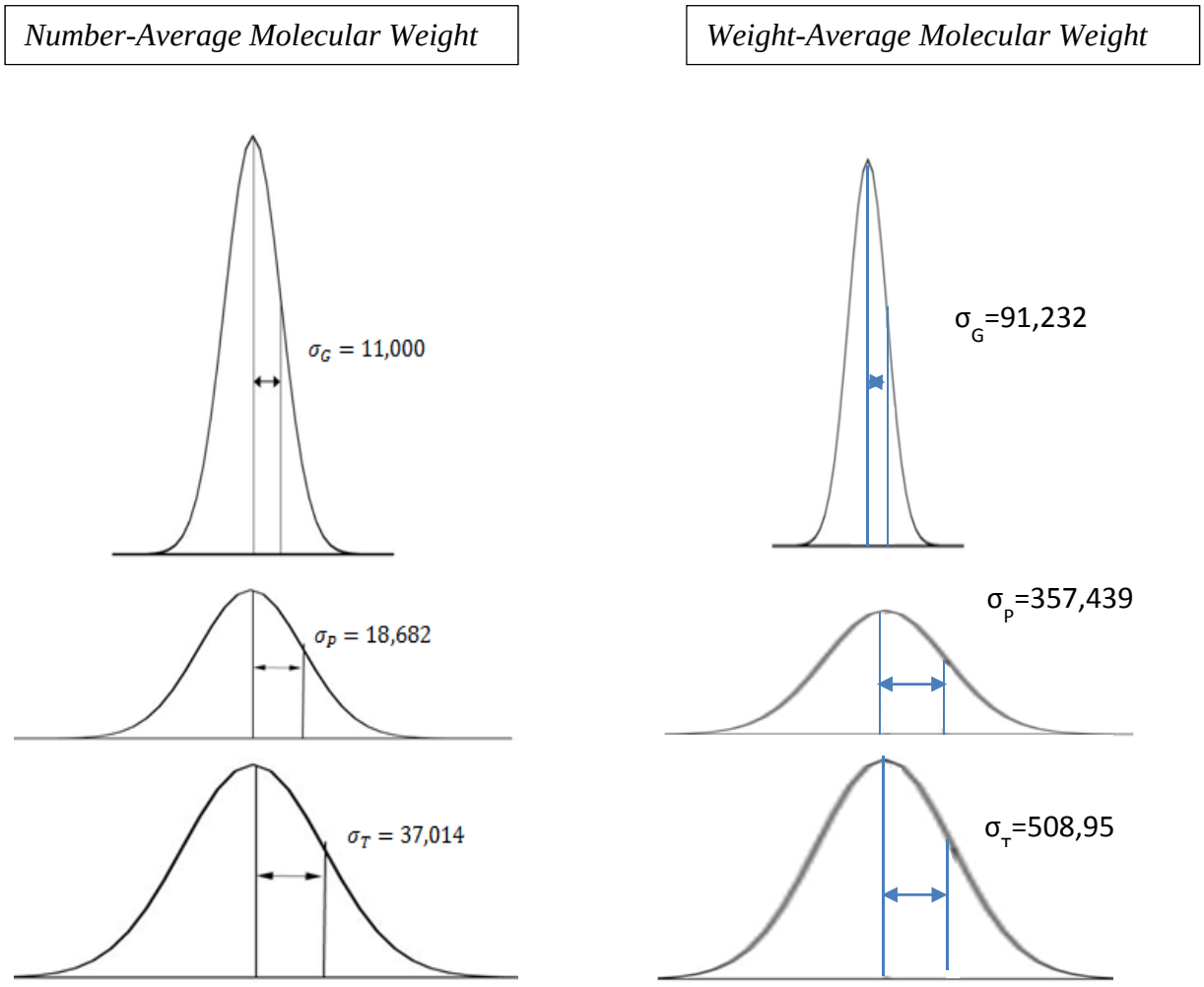

Figure D.3 Visual representation of the variances contributed by the various levels in the data collected for number- and weight-average molecular weights for Exp 4

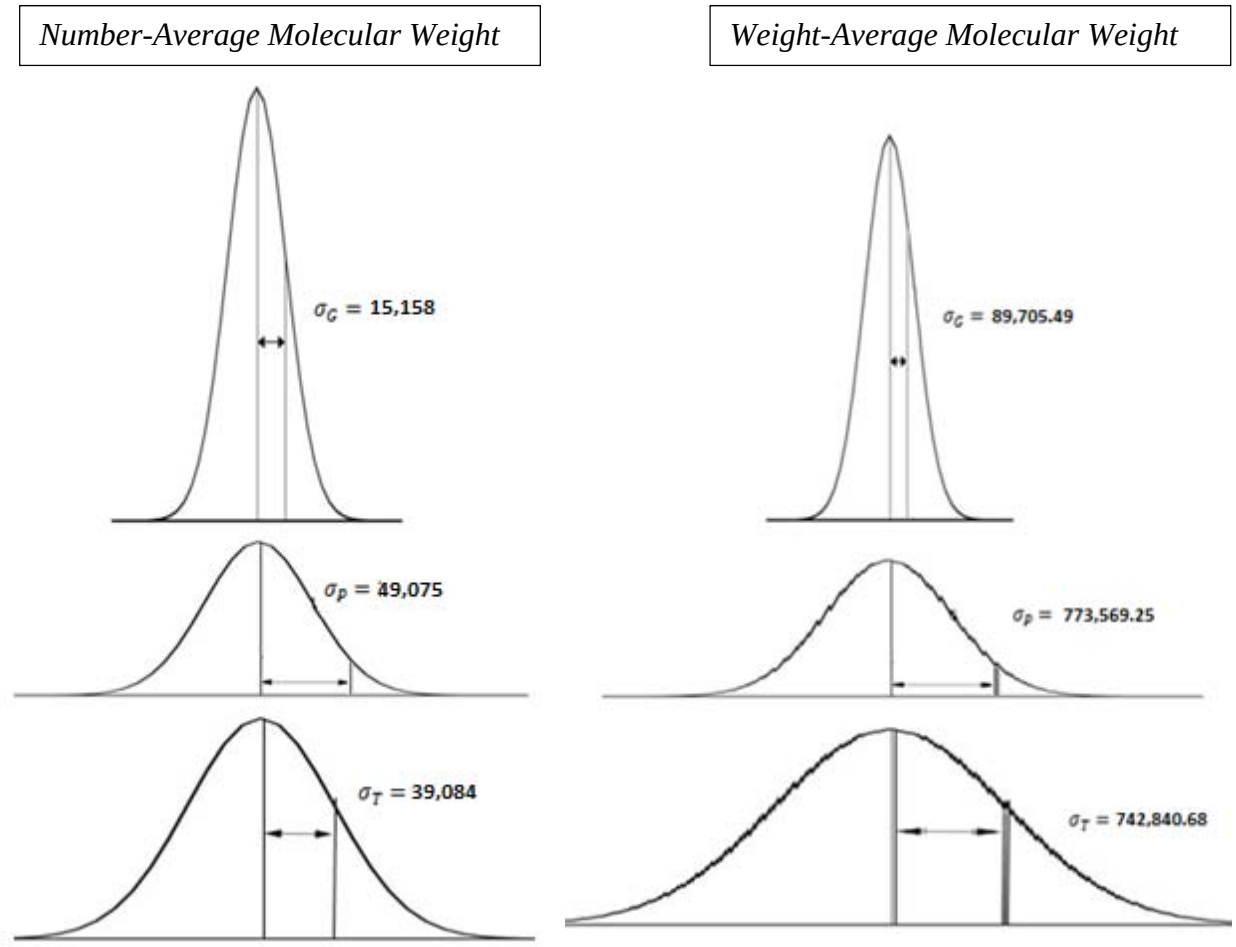

Figure D.4 Visual representation of the variances contributed by the various levels in the data collected for number- and weight-average molecular weights for Exp 5

From the above calculations, it was visible that error caused by the GPC was of the lowest magnitude when compared to the other levels, for both experiments. Hypothesis testing was also conducted to determine the impact of the different variables using an F-test. These tests were used to conclude whether or not the error was significant, by determining the validity of the null hypothesis using a 5% significance to determine whether or not it was a possibility for the error value to be zero. The hypothesis testing was conducted by using a critical value, F_c, from the F-distribution, based on the appropriate degrees of freedom, and comparing it to the observed F_{obs}. Sample calculations for M_n from Exp 4 are shown below, the calculations for the rest are analogous.

To test the significance of the contribution of variability due to different times:

$H_o: {\sigma_T}^2 = 0$

$H_1: {\sigma_T}^2 > 0$

$F_{obs} = \frac{MS_T}{MS_P} = \frac{6.30\text{E}+09}{8.20\text{E}+08} = 7.69$

$F_c = F_{2,3,0.05} = 9.55$

Therefore, since $F_{obs} < F_c$, we fail to reject the null hypothesis. This means the error associated with different polymerization times does not have a significant contribution to overall variability.

To test the significance of the contribution to variability due to different polymerizations:

$H_o: {\sigma_P}^2 = 0$

$H_1: {\sigma_P}^2 > 0$

$F_{obs} = \frac{MS_P}{MS_G} = \frac{8.20\text{E}+08}{1.21\text{E}+08} = 6.78$

$F_c = F_{3,6,0.05} = 4.76$

Therefore, since $F_{obs} > F_c$, here the null hypothesis is rejected. This means the error associated with different polymerizations does have a significant contribution to overall variability.

Similar testing was conducted for the remaining cases, summarized in Table D.10 (for variability in T) and Table D.11 (for variability in P).

Table D.10 Hypothesis testing for variability in T

Variability in T	F_c	F_{obs}	Conclusion
Exp 4, M_n	9.55	7.69	Fail to reject null
Exp 4, M_w	9.55	4.93	Fail to reject null
Exp 5, M_n	6.59	2.21	Fail to reject null
Exp 5, M_w	6.59	2.83	Fail to reject null

Table D.11 Hypothesis testing for variability in P

Variability in P	F_c	F_{obs}	Conclusion
Exp 4, M_n	4.76	6.78	Reject null
Exp 4, M_w	4.76	31.70	Reject null
Exp 5, M_n	3.84	21.96	Reject null
Exp 5, M_w	3.84	149.73	Reject null

The hypothesis testing on σ_T^2 failed to reject the null hypothesis of $\sigma_T^2 = 0$ for both Exp 4 and 5 (on both M_n and M_w). That means that the error associated with different times does not have a significant contribution to overall variability. On the other hand the null hypothesis of $\sigma_P^2 = 0$ was rejected for both Exp 4 and 5 (on both M_n and M_w). That means that there is strong evidence to conclude that the polymerization (process) error has a significant contribution to overall error.

The results obtained were compared to a previous study conducted on the error associated with GPC for a BA/MMA/VAc emulsion terpolymerization (Dube and Penlidis, 1996). In that earlier study, it had been found that the value for the variance in the GPC readings was 1.28E+08 for the number-average molecular weight, and 1.47E+08 for the weight-average molecular weight. Upon comparison (see Table D.9), the values for the variance of number-average molecular weights showed good agreement with Dube and Penlidis (1996). In contrast, the variance values for weight-average molecular weights were higher by an order of magnitude than the value obtained in Dube and Penlidis (1996). However, the good sign is that the variance values for weight-average molecular weights were very consistent variances. The differences in variances for weight-average molecular weight between this study and Dube and Penlidis (1996) could be related to the fact that the current system involves the formation of gel. At the point of formation of gel material (gelation point), the weight-average molecular weight tends to go really high. Such a system is prone to a large magnitude of error from multiple sources, namely, errors both during polymerization and GPC preparation (slight differences in the exact occurrence of the gelation point due to polymerization induction time variations; not filtering everything or filtering too much during GPC), and although one can still measure values of Mw for samples obtained in principle at the same times (at the gelation point or a bit earlier), the values may be significantly different from each other.

D.5 Conclusions

Often during experimental studies, studying the quality of the data obtained is as crucial as examining the results of the experiments themselves. In the experiments described herein, the errors in the number- and weight-average molecular weights of STY/DVB copolymers were quantified using a hierarchical design (which allows one to scrutinize the error sources associated with the various steps of replication). The experimental design consisted of three layers; replicates of GPC measurements and of polymerization reactions at various time intervals. Thus, the three layers included (from top to bottom) sampling times, polymerization process and GPC measurements.

Our analysis showed that the error associated with the GPC (analytical error) was much lower than the error associated with the other two (higher) levels. Table D.9 gives a summary of the error estimates (variances) obtained. The GPC errors in Exp 4 were ±21,553 for M_n and ±178,815 for M_w. For Exp 5, these values were ±29,709 for M_n and ±173,823 for M_w. Thus, it was also evident that the error associated with the weight-average molecular weight was much higher than that of the number-average molecular weight.

D.6 References

Box, G. E. P., W. G. Hunter, and J. S. Hunter, Statistics for Experimenters: An Introduction to Design, Data Analysis and Model Building, Wiley, Toronto (1978).

Dube, M. A., and A. Penlidis, Hierarchical Data Analysis of a Replicate Experiment in Emulsion Terpolymerization (1996), AIChE J., Vol 42, 1985-1994.

Appendix E. Error Analysis for Swelling Index and Gel Content

Determining the gel content and swelling index by Soxhlet extraction is prone to considerable error because of the nature of the procedure. In our case, the error was even higher since very small amounts of polymer were used. In order to have an estimate of error associated with gel content and swelling index. The Soxhlet extraction was repeated for several independent samples. The pooled variance for both swelling index and gel content was calculated and based on that the standard deviation and 95% confidence interval for both properties were determined. The results are summarized in Table E.1. The variance calculated from the error analysis for the gel content was 7.05×10^{-4} (corresponding to $\pm$ 1.23 error), while the variance for the swelling index was 12.23% (corresponding to $\pm$1.62 % error), as shown in the last three rows of Table E.1.

Table E.1 Error Analysis for swelling index and gel content

Sample*	Time (hr)	Conversion	Swelling Index	Gel Content	Variance (Swelling Index)	Variance (Gel Content)
3B-5	0.75	0.103	28.5755	0.7966	23.5222	0.0028
3B-5 (Rep)	0.75	0.103	35.4344	0.7222		
3B-7	1.5	0.252	6.9641	1.0006	0.0534	0.0001
3B-7 (Rep)	1.5	0.252	7.2908	0.9880		
4-10	8	0.617	54.0000	0.0011	16.4008	0.0003
4-10 (Rep)	8	0.617	48.2727	0.0245		
4-11	9	0.671	27.4761	0.4937	4.5684	0.0004
4-11 (Rep)	9	0.671	24.4534	0.5214		
4-12	15	0.798	10.8801	0.9262	3.3643	0.0000
4-12 (Rep)	15	0.798	13.4741	0.9252		
5B-1	16	0.826	0.0000	0.0000	0.0000	0.0000
5B-1 (Rep)	16	0.826	0.0000	0.0000		
5-9	17	0.834	0.0000	0.0000	0.0000	0.0000
5-9 (Rep)	17	0.834	0.0000	0.0000		
5B-3	19	0.840	26.8112	0.4571	7.2599	0.0002
5B-3 (Rep)	19	0.840	30.6217	0.4360		
5-14	27.5	0.905	16.6525	0.5888	17.4568	0.0011
5-14 (Rep)	27.5	0.905	22.5613	0.5423		

6-12 6-12 (Rep)	4 4	0.421 0.421	0.0000 0.0000	0.0000 0.0000	0.0000	0.0000
6B-1 6B-1 (Rep)	5 5	0.475 0.475	0.0000 0.0000	0.0000 0.0000	0.0000	0.0000
6-13 6-13 (Rep)	6 6	0.558 0.558	60.7333 44.2353	0.1312 0.0490	136.0926	0.0034
6B-4 6B-4 (Rep)	10 10	0.741 0.741	9.6048 8.7086	0.8959 0.8398	0.4016	0.0016
7B-2 7B-2 (Rep)	7 7	0.614 0.614	0.0000 0.0000	0.0000 0.0000	0.0000	0.0000
7-4 7-4 (Rep)	8 8	0.670 0.670	0.0000 0.0000	0.0000 0.0000	0.0000	0.0000
7-6 7-6 (Rep)	12 12	0.789 0.789	12.3122 16.1292	0.5958 0.5720	7.2846	0.0003
7-9 7-9 (Rep)	16 16	0.834 0.834	14.3643 11.9583	0.7170 0.7573	2.8946	0.0008
7-11 7-11 (Rep)	40 40	0.924 0.924	7.2898 8.6104	0.9439 0.8833	0.8719	0.0018
				Pooled Variance	12.2317	7.05×10^{-4}
				Standard Deviation	3.4974	0.0265
				Confidence Interval	1.6157	1.23%

* Based on experiment numbers in summary Table 9.2.

Appendix F. Kinetic Aspects of Styrene Polymerization with an Acyloxyamine

The evaluation of largely unstudied kinetic aspects of styrene polymerization with a (relatively new) acyloxyamine over several temperature levels are presented in this Appendix. This Appendix is heavily based on the paper published by Nabifar et al. (2010) in the Journal of Macromolecular Science, Part A: Pure and Applied Chemistry, v47, 496. The kinetic data of polymerization of STY with this acyloxyamine were contrasted with regular styrene polymerization and styrene polymerization with TEMPO.

F.1 Introduction

Hindered amines have various applications as "chemical additives". They are well-known as powerful stabilizers to protect plastics from the negative influence of light and heat. Recently, tailor-made hindered amines have been introduced with applications beyond stabilization. By adjusting the structure and the substitution pattern adjoining the functional group, these nitroxyl compounds can have a broad area of application. For example, they can be used as flame retardants, as mediators in controlled radical polymerization (CRP), and as alternatives to peroxides for degradation of polypropylene (PP) (Pfaendner, 2006)

PP degradation for production of controlled-rheology polypropylenes (CRPP) is well established and has been studied extensively (Tzoganakis et al., 1998a, b and c). This process (industrially referred to as "vis-breaking") is usually done in an extruder at elevated temperatures by adding peroxides as a source of radicals, which effect the breakdown of the chains. The most common free radical initiators used in CRPP production are mono- and di-functional peroxides. Recently, work carried out in our group studied the effect of a tetra-functional initiator in CRPP (Scorah et al., 2009) in order to investigate whether branching could also be imparted by a tetra-functional peroxide. However, a peroxide-free process is more desirable from the perspective of chemicals, handling, safety and potentially improved product quality. As a result, a relatively new hindered amine (trade name Irgatec CR76) with the structure of an acyloxyamine has been tailor-made by Ciba Specialty Chemicals (now part of BASF, however referred to as Ciba throughout the text herein) and potential uses of this

chemical in PP degradation have been described by Pfaendner (2006) and Roth et al. (2006). Aside from the preliminary proprietary Ciba evaluations, use of this radical generator as a potentially safer radical source in CRPP production was recently investigated by Psarreas et al. (2007) and the effect of processing temperature and acyloxyamine concentration on molecular weight averages, molecular weight distribution and rheological properties was reported.

In Pfaendner (2006), several potential uses of the new acyloxyamine along with other radical generators are briefly mentioned, however, detailed kinetic investigations and information in the literature are scarce. Hence, given the prior experience we have had with the acyloxyamine, described in Psarreas et al. (2007) but for a totally different application, the next logical step was to evaluate largely unstudied kinetic aspects of this new acyloxyamine for polymerization applications. In this paper, a kinetic study of styrene polymerization with the acyloxyamine (from now on simply referred to as AcAm) is presented and the results are contrasted with regular free radical styrene polymerization (as in Gao and Penlidis (1996)) and also with styrene polymerization under controlled radical conditions (as in Nabifar et al. (2009)).

F.2 Experimental

F.2.1 Reagent Purification

Styrene (Aldrich Canada Ltd., Oakville, ON) was washed three times with a 10 w/v % sodium hydroxide solution and three times with distilled water, dried over calcium chloride and distilled under vacuum. Solvents (tetrahydrofuran, ethanol, dichloromethane, and acetone) needed during experimental analysis were used as received. Both benzoyl peroxide (BPO) initiator and 2,2,6,6-tetramethyl-1-piperidinyloxy (TEMPO) controller were used as received from suppliers (ATOFINA Chemicals, King of Prussia, PA and Aldrich, respectively) without further purification.

The hindered amine (structure shown in Figure F.1) was also used as received. It is a sterically hindered N-acyloxyamine in the form of a stable concentrate with a molecular weight of 638 g/mol. It has low volatility and can be safely transported or stored at ambient temperature.

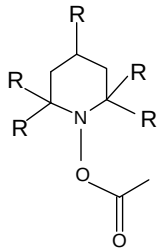

Figure F.1 Structure of acyloxyamine (AcAm)

F.2.2 Polymer Synthesis and Characterization

Experimental steps, namely, polymer synthesis (procedures and recovery of the polymer product from ampoules) and polymer characterization, carried out for the experiments reported herein, were the same as described previously in Nabifar et al. (2008, 2009), hence not reported again for the sake of brevity.

F.2.3 Summary of Experiments

Table F.1 summarizes the operating conditions of experimental runs. To investigate polymerization kinetics, runs 1 to 5 were conducted with styrene and AcAm (with the AcAm concentration being at a level typical of what is employed for peroxides). Run 1 was conducted at 120°C, while runs 2, 3, 4 and 5 were conducted at 150, 180, 210 and 230°C, in order to investigate the effect of temperature and relate to other styrene polymerization conditions.

For comparison purposes, regular (purely) thermal polymerization of styrene was conducted in the absence of initiator or AcAm at 120 and 210°C (runs 8 and 9, respectively). Experimental data for thermal polymerization of styrene at 180 and 230°C were borrowed from Gao and Penlidis (1996). For additional comparisons, runs were conducted with styrene but in the presence of TEMPO (a frequently used mediator in nitroxide-mediated radical polymerization (NMRP)), at 120 and 180°C (runs 6 and 7, respectively). The initial TEMPO concentration for these runs was as typically used in NMRP processes (Nabifar et al., 2008 and 2009).

Table F.1 Summary of experimental runs

EXP #	**Recipe**	**T (**°C)	**Initial Concentration, M**
1	STY + AcAm	120	$[AcAm]_0 = 0.036$
2		150	$[AcAm]_0 = 0.036$
3		180	$[AcAm]_0 = 0.036$
4		210	$[AcAm]_0 = 0.036$
5		230	$[AcAm]_0 = 0.036$
6	STY + TEMPO	120	$[TEMPO]_0 = 0.0396$
7		180	$[TEMPO]_0 = 0.0396$
8	STY	120	-
9		210	-

F.3 Results and Discussion

Figure F.2 shows conversion vs. time data for styrene polymerization with 0.036 M of the acyloxyamine at different temperatures (runs 1 to 5 of Table F.1). It can clearly be seen that increasing the temperature increases the rate of polymerization (as expected for any radical polymerization). Rate of polymerization is extremely fast at higher temperatures, especially at 210 and 230°C in which polymerizations are completed almost after 20-30 minutes. The insert in Figure F.2 shows the first 100 min of the reaction. It can be seen that for example, after 30 min, conversion is 6% for 120°C, 27% for 150°C, 77% for 180°C and 99% for both 210 and 230°C. Comparing further the runs at 210 and 230°C, one can see in the insert of Figure F.2 that in the first 10-15 min of the reaction, the rate of polymerization at 210°C is only slightly lower than the rate at 230°C, however, after that initial stage, the profiles of conversion vs. time for these two temperatures are overlapping. These observations suggest that at temperatures between 120 and 180°C, the profiles of conversion vs. time are affected predominantly by the change in temperature, however, at higher temperatures (above 180°C), the corresponding profiles of conversion vs. time are not significantly influenced by temperature changes.

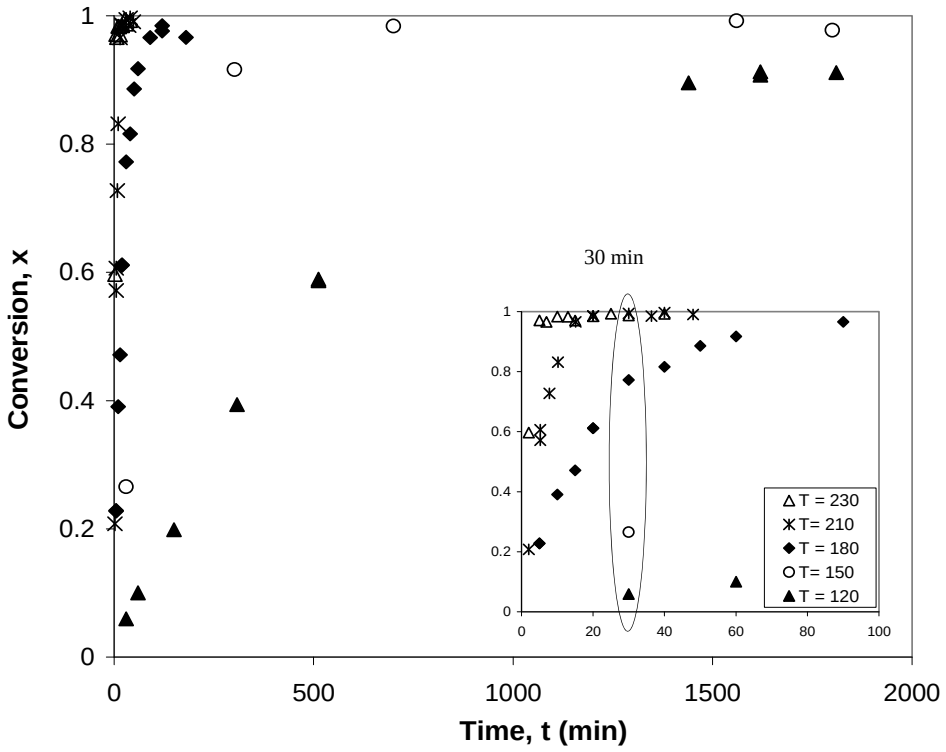

Figure F.2 Effect of temperature on rate of styrene polymerization with AcAm

Figure F.3 illustrates the corresponding number-average molecular weights and polydispersities vs. conversion. As can be seen in the upper plot, there is production of high molecular weight polymer right from the start of the reaction and molecular weights stay almost constant with conversion for all temperatures. Increasing the temperature decreases the molecular weights, a typical feature in any radical polymerization. For example, at 60% conversion, number-average molecular weight is decreasing from the order of 280,000 g/mol for 120°C to around 22,000 g/mol for 230°C. A point to note here is that the decrease in molecular weight values is less pronounced at higher temperatures. As can be seen in Figure F.3, the difference between number-average molecular weights for 210 and 230°C is not as large as the corresponding differences for the temperature range between 120 and 180°C. Independently replicated measurements for average molecular weight values were also conducted at 210°C, and as can be seen in the upper plot of Figure F.3, there is a very good agreement between the two replicated runs.

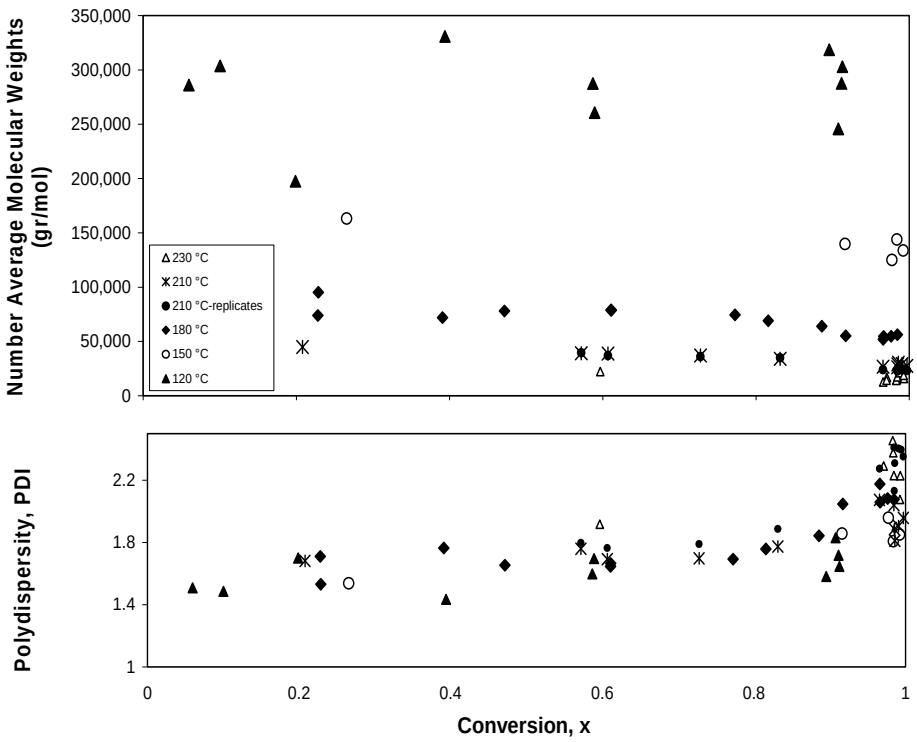

Figure F.3 Effect of temperature on number-average molecular weights and polydispersity of styrene with AcAm

The corresponding polydispersity values, shown in the lower plot, are in the range of 1.4 to 2.4, which are in the same range as values for purely thermal polymerization of styrene. At this point one can speculate that the behavior of styrene polymerization with AcAm is identical to that of regular (purely) thermal polymerization of styrene (no initiator added). To further check this, the next subsection compares experimental results of styrene with added AcAm, with experimental results and modeling simulations for thermal polymerization of styrene.

F.3.1 Comparison with Thermal Polymerization of Styrene

In this subsection styrene polymerization with AcAm is contrasted with regular thermal polymerization of styrene in order to appreciate better the effect of AcAm. At 180 and 230°C, our results with AcAm are contrasted with data from the literature (Gao and Penlidis (1996) reviewed and discussed a large number of experimental data sources on regular thermal polymerization of styrene). For further clarification, our experimental results on styrene polymerization with AcAm are selectively contrasted with model predictions for regular

(purely) thermal styrene polymerization. The modeling predictions presented herein are from a general comprehensive model developed by Jung (2008), where more details can be found.

Figure F.4 compares conversion versus time data for styrene with AcAm with the corresponding data for (purely) thermal polymerization of styrene, at 120°C (runs 1 and 8 of Table 1). As can be seen, the polymerization with AcAm is acting as regular thermal polymerization of styrene, as if they were two 'replicate' runs. Two independent replicates were analyzed for styrene polymerization with AcAm, to check for reproducibility; as can be seen, the results from the replicates are in good agreement (white triangles vs. black diamonds).

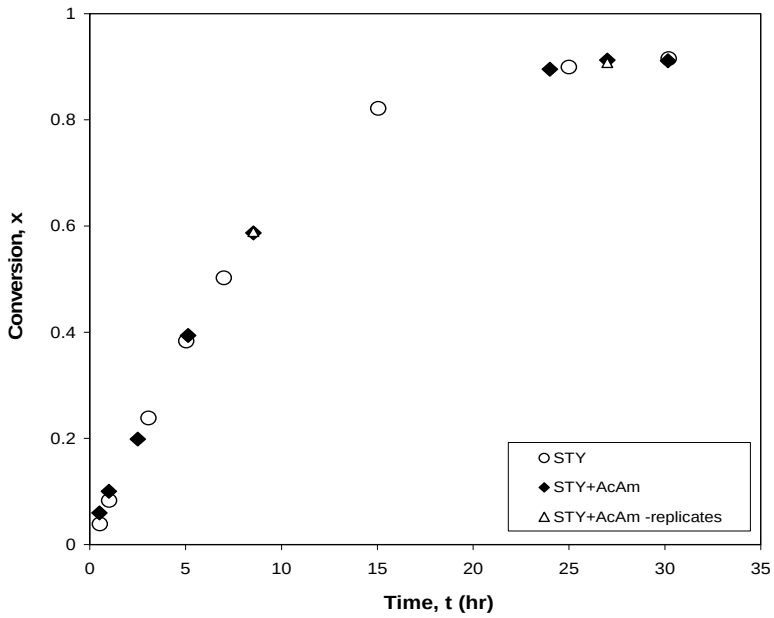

Figure F.4 Conversion vs. time data at 120°C: experimental results of styrene with AcAm vs. experimental results for thermal styrene

The corresponding comparisons for number-average molecular weights (M_n) and weight-average molecular weights (M_w) are shown in Figure F.5. The molecular weight experimental data for the run with AcAm are again almost identical with the ones from regular thermal polymerization of styrene. Figure F.5 also illustrates molecular weight model predictions for regular thermal styrene; it can be seen that model predictions capture the general behaviour, being acceptably close to the corresponding experimental results.

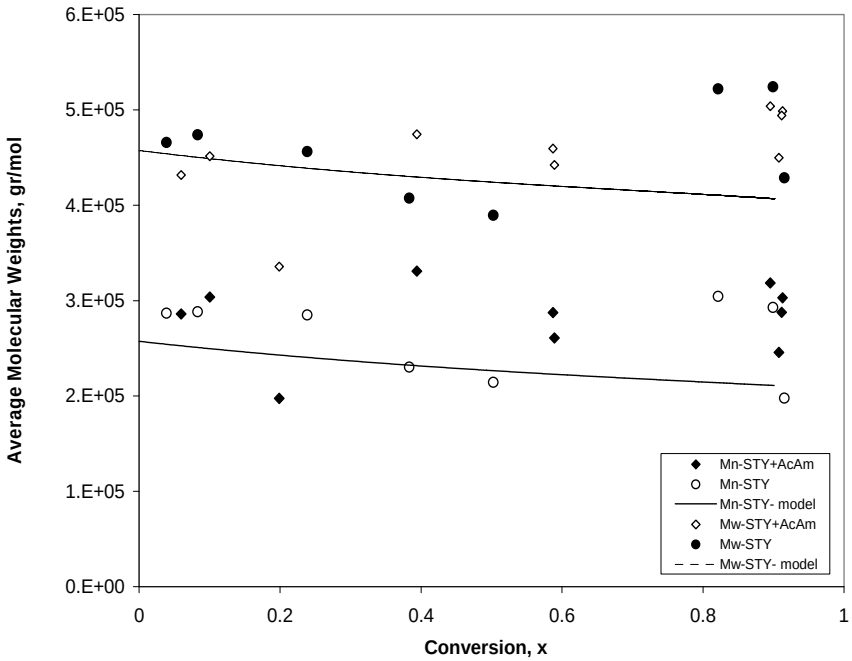

Figure F.5 Average molecular weight data at 120 °C: experimental results of styrene with AcAm vs. experimental results and model predictions for thermal styrene

Figure F.6 contrasts conversion versus time data for styrene polymerization with AcAm at 180°C, with the corresponding data for regular thermal polymerization of styrene from Arai et al. (reported in Gao and Penlidis (1996)), at 179.5°C. It can be seen that the two data sets are in excellent agreement up to about 85% conversion, after which point conversion levels for regular thermal polymerization of styrene become lower. In this case, our speculation is that since the two experiments were carried out in two different laboratories, the source of discrepancy after 85% conversion could be attributed to typical measurement error and hence one could claim that there is no significant difference between styrene polymerization with AcAm and regular thermal polymerization of styrene at this temperature level.

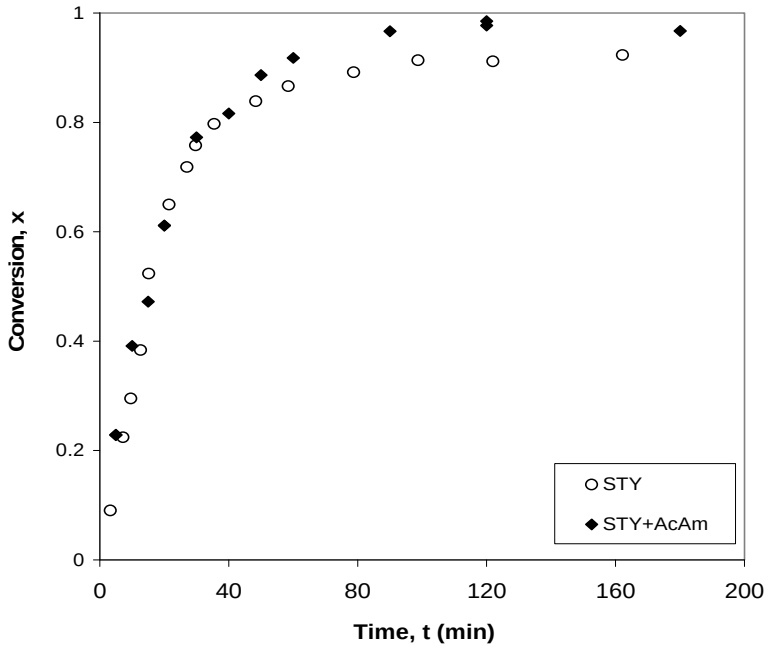

Figure F.6 Conversion vs. time data at 180°C: experimental results of styrene with AcAm vs. experimental results for thermal styrene

The corresponding comparisons for average molecular weights are shown in Figure F.7. There is excellent agreement between weight-average molecular weight data, as if again there were two independent "replicate" experiments. For number-average molecular weights, the literature data on regular thermal styrene polymerization are slightly lower than styrene polymerization with AcAm (black circles vs. open diamonds). The corresponding model predictions for styrene polymerization slightly overestimate the molecular weight experimental data for both styrene polymerization with AcAm and purely thermal polymerization of styrene. However, the predictions capture the general behavior of the molecular weights, and again they are acceptably close to the corresponding experimental results.

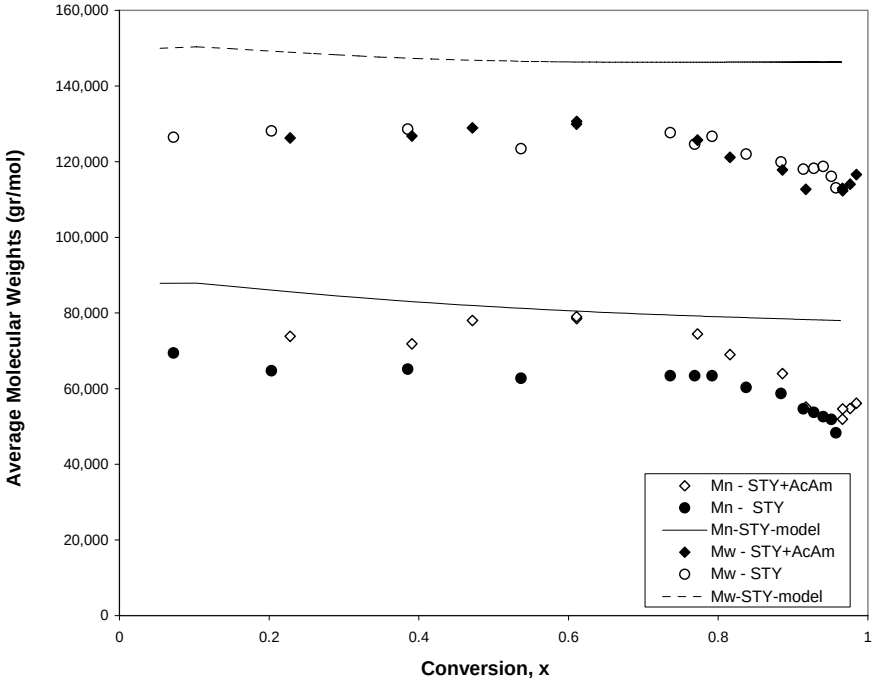

Figure F.7 Average molecular weight data at 180°C: experimental results of styrene with AcAm vs. experimental results and model predictions for thermal styrene

Figure F.8 compares conversion vs. time data for styrene polymerization with AcAm and styrene thermal polymerization at 210°C (runs 4 and 9 of Table F.1). As can be seen, the two data sets are in good agreement up to 60% conversion but after that there is a jump in conversion values for styrene with AcAm. For example, after only 15 minutes, the conversion level is 96% for styrene with AcAm, while only 83% for (purely) thermal styrene polymerization. The model predictions capture the behavior of styrene thermal polymerization almost perfectly. The observations now start suggesting that AcAm seems to have an initiator-like contribution to styrene polymerization. However, the corresponding average molecular weights in Figure F.9 do not yet reflect the expected decrease in molecular weights due to AcAm's initiator-like behavior, although one can argue that the data for styrene with AcAm are slightly lower than the ones for thermal polymerization.

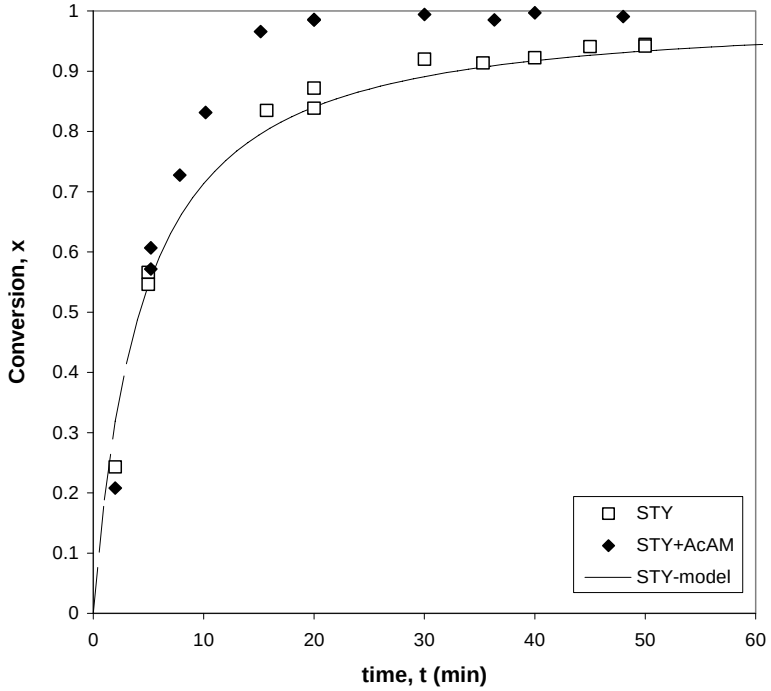

Figure F.8 Conversion vs. time data at 210°C: experimental results of styrene with AcAm vs. experimental results and model predictions for thermal styrene

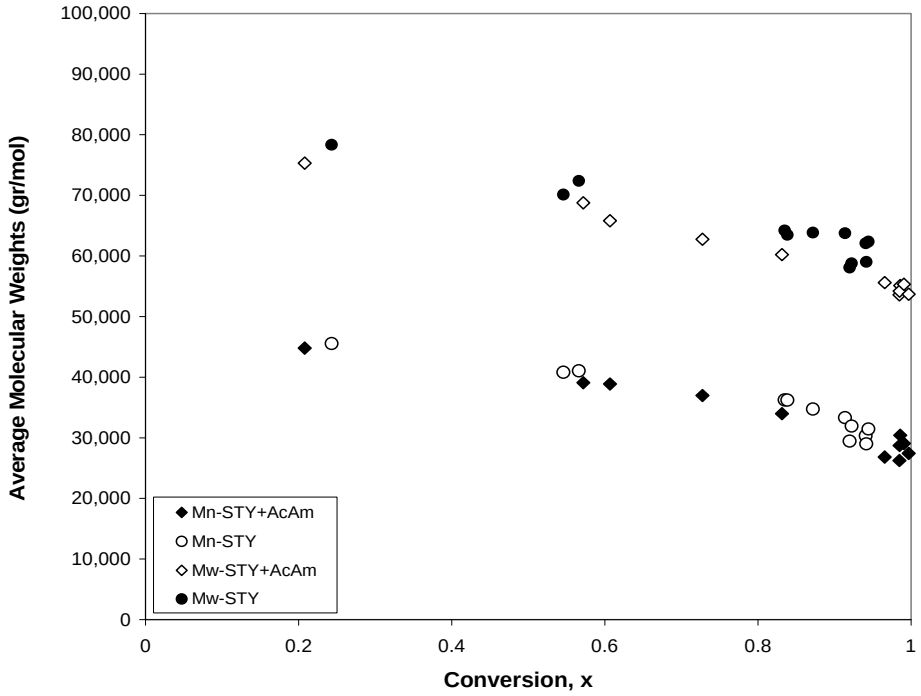

Figure F.9 Average molecular weight data at 210°C: experimental results of styrene with AcAm vs. experimental results for thermal styrene

To clarify our speculations, another experiment for styrene polymerization with AcAm was carried out at even a higher temperature (230°C; run 5 in Table F.1). Figure F.10 compares the corresponding conversion versus time data with data for styrene thermal polymerization. As can be seen, the run with AcAm is definitely faster than the purely thermal one (after only 5 min have elapsed, the run with AcAm shows 97% conversion). The model predictions follow once more the styrene thermal polymerization behavior almost perfectly. The corresponding molecular weight data are shown in Figure F.11. As can be seen, both number- and weight-average molecular weights for styrene with AcAm are lower compared to the values for purely thermal polymerization of styrene. These results show that at 230°C, AcAm again contributes as an initiator to styrene polymerization (increasing the rate of polymerization while decreasing molecular weights). This contribution had possibly started manifesting itself even at 180 and 210°C (see Figure F.6 to Figure F.9 and the discussion around them), but was not as evident at lower temperatures. According to Rutsch and Cech (2007), AcAm dissociates to aminyl and acyloxy radicals at high temperatures (more preferably at the higher temperature levels of polymer degradation operations, above 200 °C), as shown in Figure F.12, and that is why AcAm exhibits this additional initiator-like contribution at temperature levels above 180-200°C.

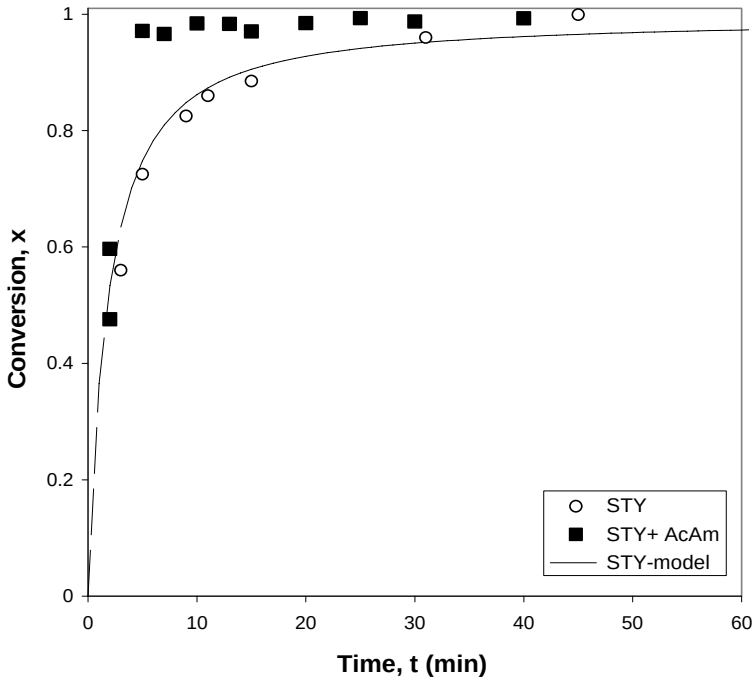

Figure F.10 Conversion vs. time data at 230°C: experimental results of styrene with AcAm vs. experimental results and model predictions for thermal styrene

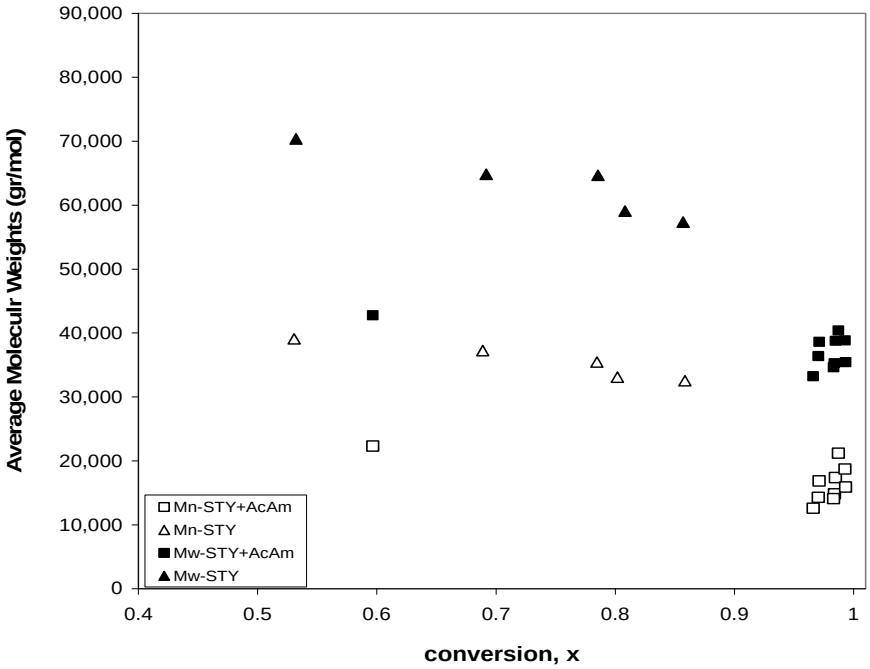

Figure F.11 Average molecular weight data at 230°C: experimental results of styrene with AcAm vs. experimental results for thermal styrene

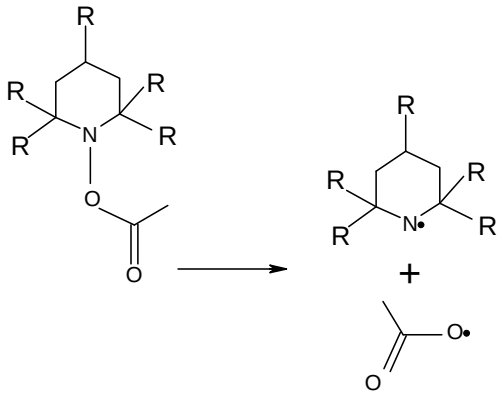

Figure F.12 Thermal cleavage of AcAm

F.3.2 Comparison with Thermal Polymerization of Styrene in the Presence of TEMPO

Figure F.13 compares conversion vs. time data for styrene polymerization with AcAm and styrene polymerization with TEMPO, at 120°C and 180°C (runs 1 and 6, and 3 and 7 of Table F.1). It can be observed that the run with AcAm is much faster than the one with TEMPO, however, the difference between polymerization rates at 180°C is not as significant as at the 120°C level. At 120°C (Figure F.13a), after 24 h, the conversion level is 90% with AcAm and

only 30% with TEMPO, while at 180°C (Figure F.13b) after 2 h, conversion is 98% with AcAm and 73% with TEMPO. Other observations for the 180°C temperature level are a plateau in conversion level for styrene polymerization with TEMPO after about 2.5 h, and a much shorter (almost negligible) induction period at the beginning of the reaction compared to the run with TEMPO at 120°C.

a) b)

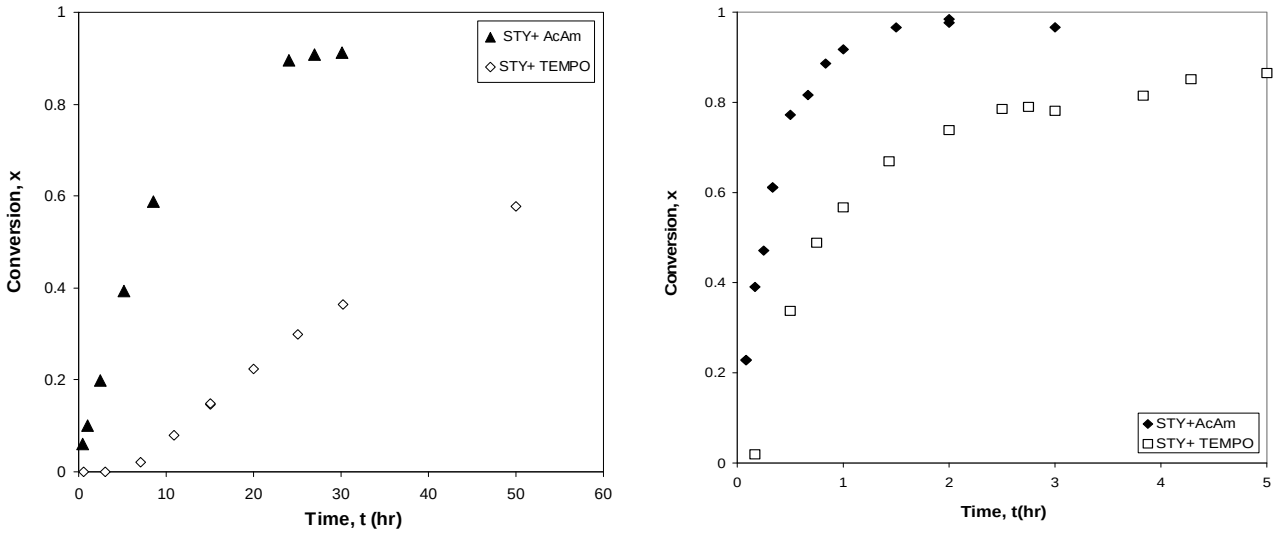

Figure F.13 Rate comparison for polymerization of styrene with AcAm and TEMPO, at a) 120°C, b) 180°C

The corresponding molecular weights for polymerization of styrene with TEMPO at 120°C are shown in Figure F.14a, showing an almost linear increase of molecular weights with conversion, typical of any controlled radical polymerization. Comparing these data with molecular weights obtained from polymerization of styrene with AcAm (Figure F.5), one can see that the molecular weights are much lower. Figure F.14b illustrates molecular weight vs. conversion for styrene polymerization with TEMPO at 180 °C. As can be seen, polymerization is not controlled at these conditions, since molecular weights are not increasing linearly with conversion. Comparing these results with styrene polymerization with AcAm (Figure F.7), one again can see that molecular weights are much lower; at 60% conversion, the number-average molecular weight is about 10,000 g/mol for styrene polymerization with TEMPO (Figure F.14a), while at the same conversion level, the molecular weight is about 78,000 g/mol for styrene with AcAm (Figure F.7).

a) b)

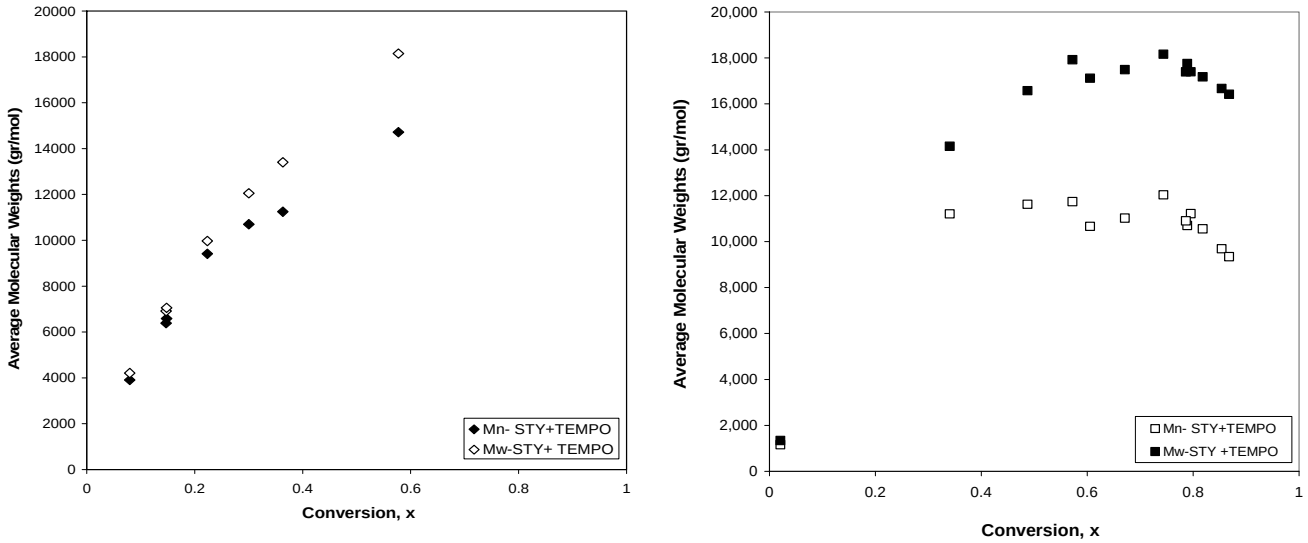

Figure F.14 Molecular weights vs. conversion for styrene with TEMPO at a) 120°C and b) 180 °C

Although styrene polymerization with TEMPO had been classified as controlled radical polymerization at lower temperatures (see Nabifar et al. (2009)), at elevated temperatures it could not be classified as controlled. However, comparing the molecular weight results to styrene polymerization with AcAm shows that the presence of TEMPO lowers the molecular weights dramatically. Radicals generated through thermal polymerization of styrene are trapped by TEMPO and the duration that the radicals are in the dormant mode is relatively long, thus causing the dramatic decrease in molecular weights. Although both AcAm and TEMPO can be categorized as hindered amines, they contribute very differently in styrene polymerization.

F.4 Conclusions

Selective kinetic investigations on styrene polymerization using an acyloxyamine over several temperature levels showed that the system behaves rather like regular (purely) thermal polymerization of styrene at temperature levels between 120-180°C, whereas at temperatures above 180-200°C AcAm seems to have an initiator-like contribution, thus increasing the rate of polymerization while decreasing molecular weights.

F.5 References

Gao, J. and Penlidis, A. (1996). A comprehensive simulator/database package for reviewing free-radical homopolymerizations. *Journal of Macromolecular Science-Reviews in Macromolecular Chemistry and Physics*, C36, 199-404.

Jung, W. (2008). Mathematical modeling of free-radical six-component bulk and solution polymerization. MASc Thesis/Dissertation, Department of Chemical Engineering, University of Waterloo.

Nabifar, A., McManus, N., Vivaldo-Lima, E., Lona, L. M. F., and Penlidis, A. (2008). A replicated investigation of nitroxide-mediated radical polymerization of styrene over a range of reaction conditions. *Canadian Journal of Chemical Engineering*, 86, 879-892.

Nabifar, A., McManus, N., Vivaldo-Lima, E., Lona, L. M. F., and Penlidis, A. (2009). Thermal polymerization of styrene in the presence of TEMPO. *Chemical Engineering Science*, 64, 304-312.

Pfaendner, R. (2006). Nitroxyl radicals and nitroxylethers beyond stabilization: radical generators for efficient polymer modification. *Comptes Rendus Chimie*, 9, 1338-1344.

Psarreas, A., Tzoganakis, C., McManus, N., and Penlidis, A. (2007). Nitroxide-mediated controlled degradation of polypropylene. *Polymer Engineering and Science*, 47, 2118-2123.

Roth, M., Pfaendner, R., Nesvadba, P., and Zink, M. O. (2006). Process for reducing the molecular weight of polypropylene. (2006) US Patent # 7,030,1960 B2.

Rutsch, W. and Cech, M. A. (2007). Effects to improve the quality of life: Color, performance and protection from Ciba Specialty Chemicals. *Chimia*, 61, 33-41.

Scorah, M. J., Zhu, S., Psareas, A., McManus, N., Dhib, R., Tzoganakis, C. and Penlidis A. (2009). Peroxide-controlled degradation of polypropylene using a tetra-functional initiator. *Polymer Engineering and Science*, 49: 1760-1766.

Tzoganakis, C., Vlachopoulos, J., and Hamielec, A. E. (1988a). Controlled Degradation of Polypropylene. *Chemical Engineering Progress*, 84, 47-49.

Tzoganakis, C., Vlachopoulos, J., & Hamielec, A. E. (1988b). Modeling of the Peroxide Degradation of Polypropylene. *International Polymer Processing*, 3, 141-150.

Tzoganakis, C., Vlachopoulos, J., & Hamielec, A. E. (1988c). Production of Controlled-Rheology Polypropylene Resins by Peroxide Promoted Degradation During Extrusion. *Polymer Engineering and Science*, 28, 170-180.

Appendix G. Complementary Data for Subsection 10.3.2

G.1 Statistical Analysis for DSC Data

Table G.1 Comparison of DSC data for 2B-10 and 3-11 of Table 10.8

Sample	Stat. indicator	ΔT_g	ΔH (W/g)	ΔC_p (J/°C.g)	Slope (W/g.°C)
2B-10		5.53	0.0634	0.3862	-0.00989
		4.91	0.0531	0.3202	-0.00991
		5.1	0.0543	0.3258	-0.00888
		5.13	0.0549	0.3310	-0.00962
	average	5.17	0.0564	0.3408	-9.58E-03
	variance	6.79E-02	2.22E-05	9.36E-04	2.31E-07
3-11		4.8	0.0582	0.3489	-0.01036
		4.64	0.0493	0.2964	-0.00955
		4.77	0.0602	0.3617	-0.01040
		4.93	0.0502	0.3022	-0.00969
	average	4.79	0.0544	0.3273	-1.00E-02
	variance	1.42E-02	3.05E-05	1.08E-03	1.95E-07
	S_p^2	4.10E-02	2.64E-05	1.01E-03	2.13E-07
	$\mathbf{t_{obs}}$	2.67*	0.55	0.60	1.30
	$\mathbf{t_{6,\ 0.025}}$ **= 2.45**	Fail to reject	Fail to reject	Fail to reject	Fail to reject

* t_{obs} for ΔT_g is slightly larger than 2.45. However, with 99% confidence, the test fails to reject H_0

G.2 Replicates for DMA measurements (see Table 10.10)

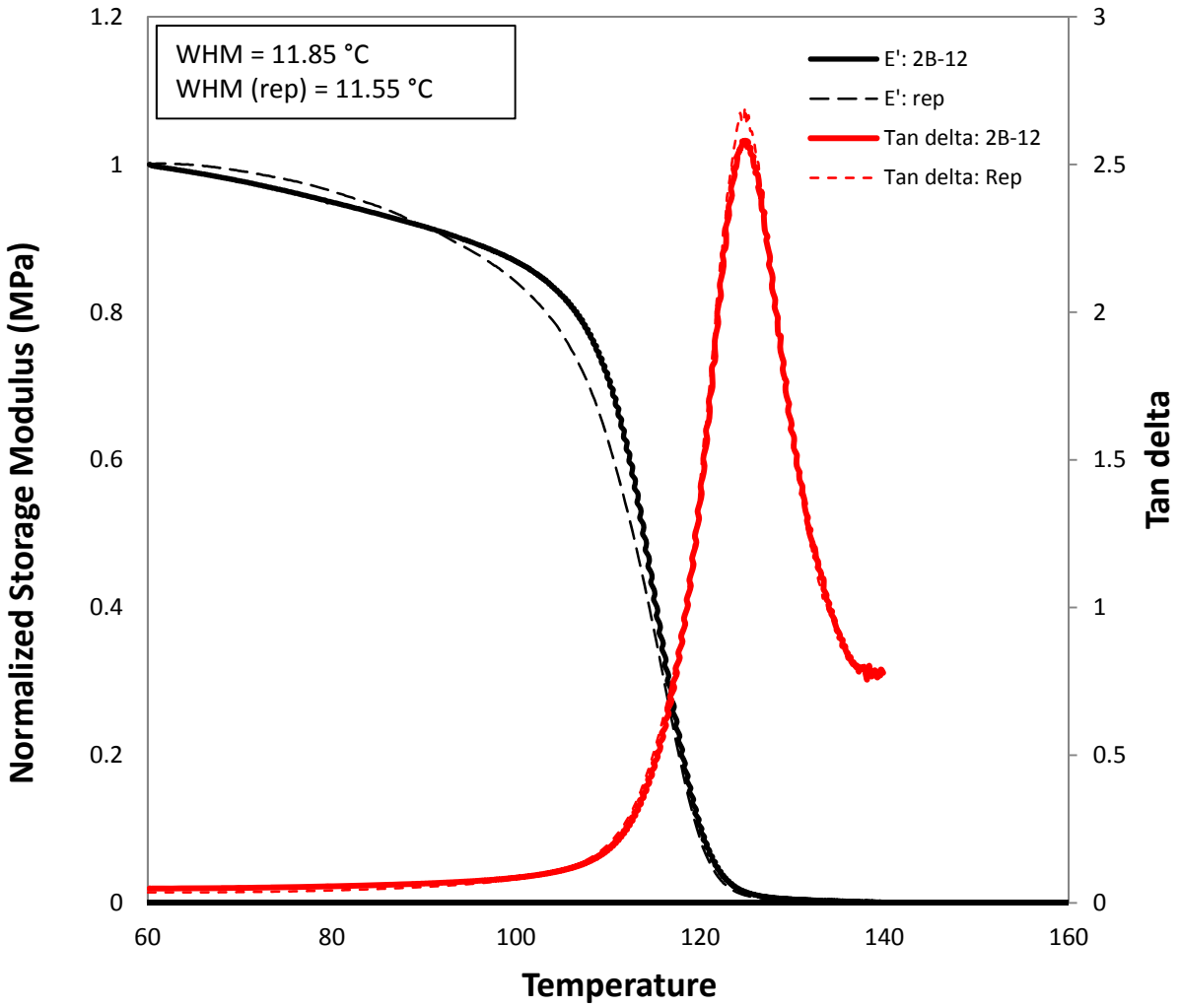

Figure G.1 Storage modulus and Tan δ for cross-linked PS at 97% conversion, synthesized through free radical polymerization with 1% DVB (sample 2B-12)

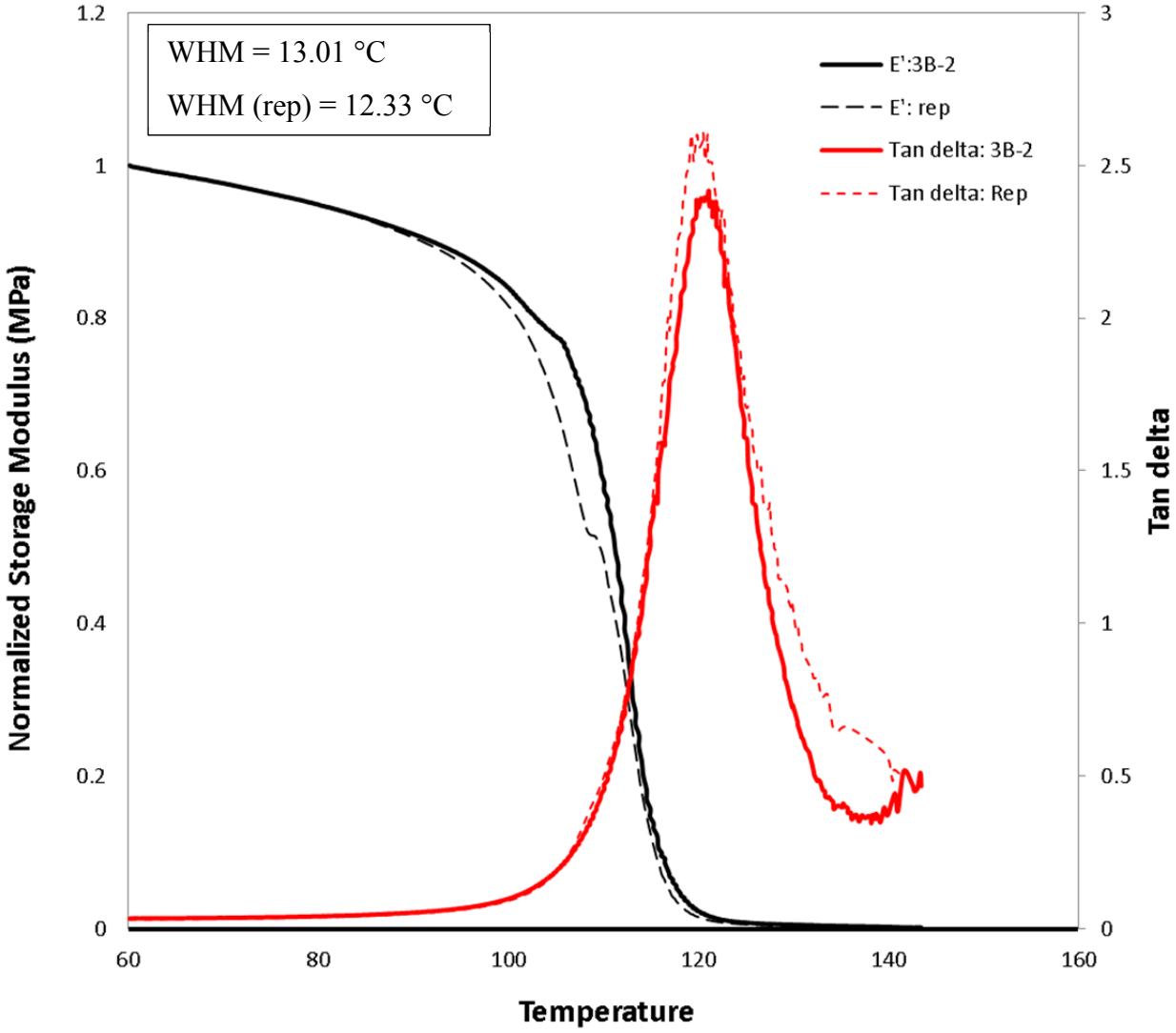

Figure G.2 Storage modulus and Tan δ for cross-linked PS at 64% conversion, synthesized through nitroxide-mediated radical polymerization with 1% DVB (sample 3B-2)

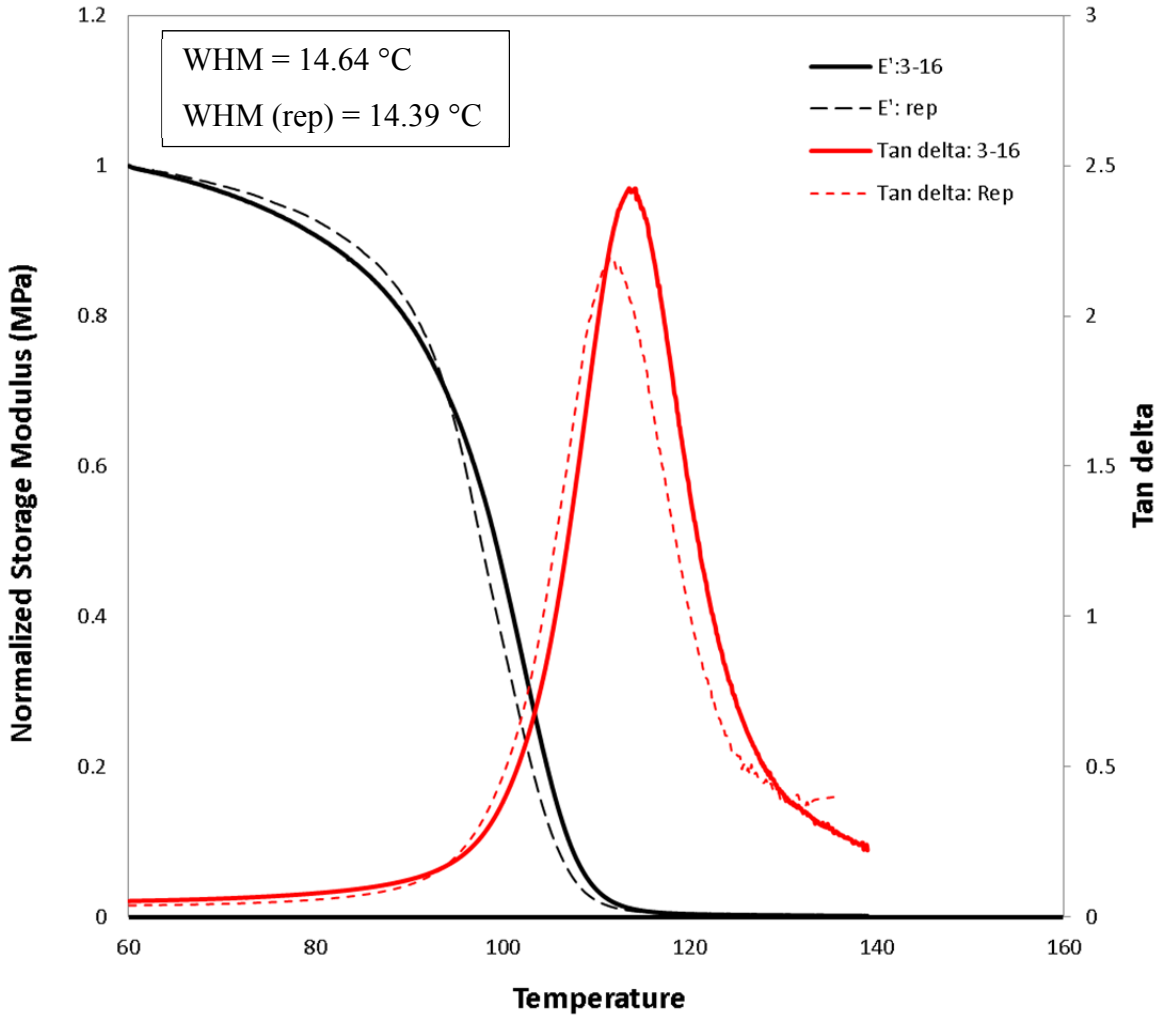

Figure G.3 Storage modulus and Tan δ for cross-linked PS at 97% conversion, synthesized through nitroxide-mediated radical polymerization with 1% DVB (sample 3-16)

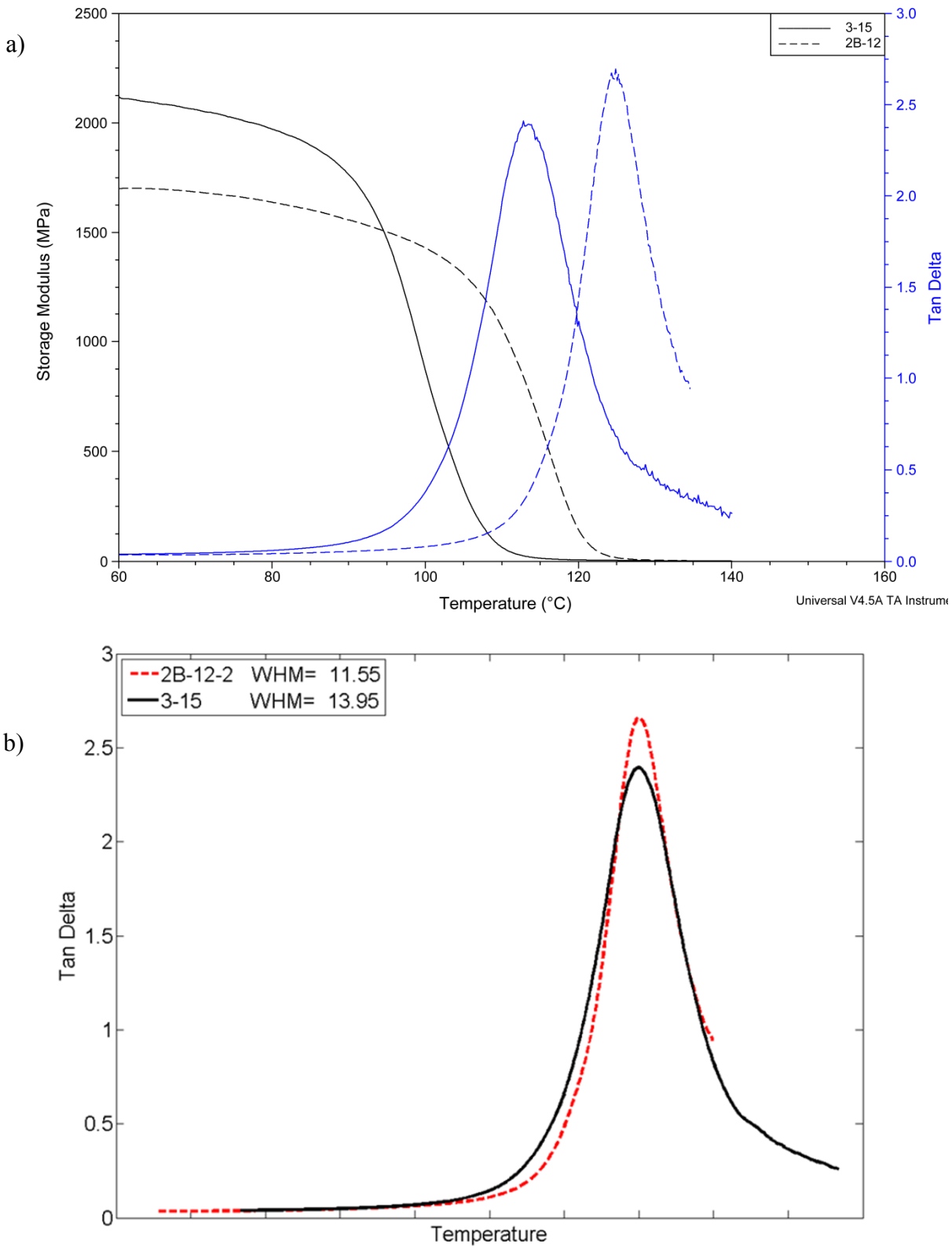

Figure G.4 Storage modulus and tan δ versus temperature for samples prepared by NMRP (3-15) and FRP (2B-12) with 1% DVB